ORCHID GENOMICS AND DEVELOPMENTAL BIOLOGY

EDITED BY: Jen-Tsung Chen and Katharina Nargar

PUBLISHED IN: Frontiers in Plant Science

frontiers Research Topics

frontiers

ISSN 1664-8714
ISBN 978-2-88963-975-5
DOI 10.3389/978-2-88963-975-5

About Frontiers

Frontiers is more than just an open-access publisher of scholarly articles: it is a pioneering approach to the world of academia, radically improving the way scholarly research is managed. The grand vision of Frontiers is a world where all people have an equal opportunity to seek, share and generate knowledge. Frontiers provides immediate and permanent online open access to all its publications, but this alone is not enough to realize our grand goals.

Frontiers Journal Series

The Frontiers Journal Series is a multi-tier and interdisciplinary set of open-access, online journals, promising a paradigm shift from the current review, selection and dissemination processes in academic publishing. All Frontiers journals are driven by researchers for researchers; therefore, they constitute a service to the scholarly community. At the same time, the Frontiers Journal Series operates on a revolutionary invention, the tiered publishing system, initially addressing specific communities of scholars, and gradually climbing up to broader public understanding, thus serving the interests of the lay society, too.

Dedication to Quality

Each Frontiers article is a landmark of the highest quality, thanks to genuinely collaborative interactions between authors and review editors, who include some of the world's best academicians. Research must be certified by peers before entering a stream of knowledge that may eventually reach the public - and shape society; therefore, Frontiers only applies the most rigorous and unbiased reviews.
Frontiers revolutionizes research publishing by freely delivering the most outstanding research, evaluated with no bias from both the academic and social point of view. By applying the most advanced information technologies, Frontiers is catapulting scholarly publishing into a new generation.

What are Frontiers Research Topics?

Frontiers Research Topics are very popular trademarks of the Frontiers Journals Series: they are collections of at least ten articles, all centered on a particular subject. With their unique mix of varied contributions from Original Research to Review Articles, Frontiers Research Topics unify the most influential researchers, the latest key findings and historical advances in a hot research area! Find out more on how to host your own Frontiers Research Topic or contribute to one as an author by contacting the Frontiers Editorial Office: researchtopics@frontiersin.org

ORCHID GENOMICS AND DEVELOPMENTAL BIOLOGY

Topic Editors:
Jen-Tsung Chen, National University of Kaohsiung, Taiwan
Katharina Nargar, Commonwealth Scientific and Industrial Research Organisation (CSIRO), Australia

Citation: Chen, J.-T., Nargar, K., eds. (2020). Orchid Genomics and Developmental Biology. Lausanne: Frontiers Media SA. doi: 10.3389/978-2-88963-975-5

Table of Contents

frontiers in Plant Science

EDITORIAL
published: 10 July 2020
doi: 10.3389/fpls.2020.01013

Editorial: Orchid Genomics and Developmental Biology

Jen-Tsung Chen[1]* *and Katharina Nargar*[2,3]

[1] Department of Life Sciences, National University of Kaohsiung, Kaohsiung, Taiwan, [2] Australian Tropical Herbarium, James Cook University, Cairns, QLD, Australia, [3] National Research Collections Australia, Commonwealth Industrial and Scientific Research Organisation (CSIRO), Canberra, ACT, Australia

Keywords: orchid, biotechnology, functional genomics, developmental biology, evolution

Editorial on the Research Topic

Orchid Genomics and Developmental Biology

Orchidaceae is the second largest family of flowering plants with more than 27,000 species inhabiting nearly every habitat worldwide. Orchids exhibit an exceptional morphological and ecological diversity, and are highly valued on the global horticultural market. Orchids possess unique morphological and physiological characteristics, such as highly reduced seeds with an immature embryo, complex flower structures such as the gynandrium and labellum, and have evolved crassulacean acid metabolism and mycoheterotrophy multiple times independently. This range of traits renders orchids prime non-model plants for studying different aspects of evolution through mechanistic studies considering gene function, physiology, and phylogenetic relationships. As summarized below, this Research Topic presents recent advances in orchid biology and consists of 12 publications in the fields of reproductive development, evolution, biotechnology, and photosynthesis.

OPEN ACCESS

Edited by:
Natalia Pabón-Mora,
University of Antioquia, Colombia

Reviewed by:
Serena Aceto,
University of Naples Federico II, Italy
Mariana Mondragón-Palomino,
University of Regensburg, Germany

***Correspondence:**
Jen-Tsung Chen
jentsung@nuk.edu.tw

Specialty section:
This article was submitted to Plant Development and EvoDevo, a section of the journal Frontiers in Plant Science

Received: *13 May 2020*
Accepted: *22 June 2020*
Published: *10 July 2020*

Citation:
Chen J-T and Nargar K (2020) Editorial: Orchid Genomics and Developmental Biology. Front. Plant Sci. 11:1013. doi: 10.3389/fpls.2020.01013

FLOWER ORGAN DEVELOPMENT

The study of transcription factors (TFs), proteins that bind to the regulatory DNA sites of specific genes and are involved in the process of transcription, is an important tool for understanding flower development in orchids. Valoroso et al. studied the expression and interaction of three myeloblastosis (MYB) TFs that are part of a regulatory module, including DIVARICATA (DIV), RADIALIS (RAD), and DIV-and-RAD-Interacting-Factor (DRIF), on flower development of the Italian orchid, *Orchis italica,* native to the Mediterranean region. The results showed higher levels of gene expression in the labellum than in lateral inner tepals of the *O. italica* flower. In addition, yeast two-hybrid analysis revealed that the *Orchis*-MYB TF OitDRIF1 interacts with OitDIV and OitRAD. Hence, the results support the hypothesis that these three MYB TFs have a crucial role in controlling zygomorphy in orchid flowers.

Lai et al. investigated the function of a SHINE-Like TF, namely PeERF1, in several *Phalaenopsis* orchids. The authors conclude that PeERF1 is crucial for the development of labellum epidermis, particularly in the formation of nanoridges.

In model plants, MADS-box TFs have been shown to play crucial roles in diverse developmental processes. Based on a comprehensive review of the literature, Teo et al. summarize reproductive developmental processes in model plants including floral transition and patterning, and discuss unique aspects of orchid floral development such as the modified ABC model and the perianth code.

An overview on orchid flower development is provided by Wang et al. summarizing recent advances in our understanding of floral induction, transition, and flowering in popular orchid genera such as *Dendrobium*, *Oncidium*, and *Phalaenopsis*. The authors propose a hypothetical pathway for flowering regulation in *P. aphrodite* under low ambient temperature, and discuss models of the orchid code and perianth code in *P. equestris* and *O.* "Gower Ramsey".

The anatomical features of reproductive organs at different developmental stages of the mycoheterotrophic orchid *Pogoniopsis schenckii* was investigated by Alves et al. The authors compared characteristics of the seed coat in *P. schenkii* to photosynthetic species of the family. *P. schenckii* was found to have a seed coat that originates from the nucellar epidermis and not from the outer integument as in the other species.

EVOLUTION

Family-wide comparative studies on plastid structure and gene loss facilitate important insights into plastid evolution in Orchidaceae. Kim et al. compared structural variation and gene content of 124 complete orchid plastomes and investigated gene loss in orchids within a phylogenomic framework. The authors provide recommendations for additional molecular studies to increase our understanding of plastome evolution, in particular in mycoheterotropic orchids.

The deceptive flowers of Lady slipper orchids (subfamily Cypripedioideae) possess a slipper shaped labellum that traps insects to facilitate pollination. Tsai et al. investigated evolutionary relationships, intrageneric classification, and historical biogeography of the Venus slipper orchids, genus *Paphiopedilum,* based on nuclear (ITS) and three plastid markers (*trnL* intron, *trnL-F*, *atpB-rbcL*) for 78 taxa. The results supported the current intrageneric classification of the genus and provide insights into biogeographic origin and the spatio-temporal evolution of the genus.

Being one of the largest flowering plant families, orchids have evolved a great variety of pollination strategies. Fernández et al. profiled and compared floral transcriptomes of two European orchid genera with different pollination strategies, the sexually deceptive *Ophrys* and *Gymnadenia* with a food-rewarding pollination strategy. Further, phylogenomic analysis was carried out based on transcriptome data to resolve evolutionary relationships within the two genera.

BIOTECHNOLOGY

In orchids, protocorm-like bodies (PLBs) induced from explants or callus *in vitro* have long been recognized to resemble somatic embryos (SEs) in some species. Based on a molecular study, Chen et al. reported that PLBs do not derive from SEs at least in *P. equestris*. Further, the authors induced SEs by overexpressing *P. aphrodite LEAFY COTYLEDON1* (*PaLEC1*) and suggested that induction of SEs may be a useful tool for clonal propagation of orchids.

Orchids rely on symbiotic relationships with fungi for seed germination and subsequent seedling growth. Sisti et al. characterized fungal communities in roots and fruits of a mycoheterotrophic orchid, *P. schenckii,* and carried out germination trials with non-mycorrhizal endophytic fungi isolated from *P. schenckii* under *in vitro* conditions. The authors observed that germination was stimulated by inoculation of *P. schenckii* seeds with the isolated non-mycorrhizal fungi.

PHOTOSYNTHESIS

The photosynthetic pathway known as crassulacean acid metabolism (CAM), found in different plant lineages including orchids, is adaptive in arid conditions due to the high water-use efficiency it confers on the plant. Ceusters et al. studied the metabolite and enzyme patterns of starch degradation in the CAM orchid *Phalaenopsis* "Edessa". Two routes of degradation were assessed: the hydrolytic route (involving cytosolic D-enzyme, plastid D-enzyme, maltase, and β-amylase), and the phosphorolytic route (involving starch phosphorylase) to compare enzyme activities as well as starch degradation rates. Ceusters et al. concluded that the phosphorolytic pathway might be the main route of starch degradation in CAM orchid *Phalaenopsis*.

CONCLUSION AND PERSPECTIVES

This Research Topic on Orchid Genomics and Developmental Biology provides only a snapshot of this exciting and growing field of research. We hope that with the rapid development of molecular tools and approaches, particularly several orchid genomes and hundreds of transcriptomes that are now available together and with high-throughput technologies and integrative multi-omics, emerging biotechnology such as CRISPR gene editing, researchers will be able to further unravel the secrets of orchid biology with emphasis on mechanistic insights into flowering regulation, flower organ development, embryo/protocorm formation and development, phylogenomics, symbiosis, and photosynthetic pathways, in the future.

We greatly appreciate the invaluable contribution of all authors and reviewers as well as the efforts of Chief Editor Neelima Roy Sinha of Frontiers in Plant Science: Plant Development and EvoDevo.

AUTHOR CONTRIBUTIONS

J-TC and KN drafted the manuscript. All authors contributed to the article and approved the submitted version.

Conflict of Interest: The authors declare that the research was conducted in the absence of any commercial or financial relationships that could be construed as a potential conflict of interest.

frontiers in Plant Science

REVIEW
published: 10 October 2019
doi: 10.3389/fpls.2019.01258

Floral Induction and Flower Development of Orchids

Shan-Li Wang[1‡], Kotapati Kasi Viswanath[2‡], Chii-Gong Tong[1], Hye Ryun An[3], Seonghoe Jang[4†], Fure-Chyi Chen[2*†]*

[1] Biotechnology Center in Southern Taiwan (BCST) of the Agricultural Biotechnology Research Center (ABRC), Academia Sinica, Tainan, Taiwan, [2] Department of Plant Industry, National Pingtung University of Science and Technology, Pingtung, Taiwan, [3] National Institute of Horticultural and Herbal Science (NIHHS), Rural Development Administration (RDA), Wanju-gun, South Korea, [4] World Vegetable Center Korea Office (WKO), Wanju-gun, South Korea

OPEN ACCESS

Edited by:
Jen-Tsung Chen,
National University of Kaohsiung, Taiwan

Reviewed by:
Lee Jeong Hwan,
Chonbuk National University, South Korea
Federico Valverde,
Institute of Plant Biochemistry and Photosynthesis (IBVF), Spain

***Correspondence:**
Seonghoe Jang
seonghoe.jang@worldveg.org
Fure-Chyi Chen
fchen@mail.npust.edu.tw

†ORCID:
Seonghoe Jang
orcid.org/0000-0001-5018-3480
Fure-Chyi Chen
orcid.org/0000-0001-5475-9248

‡These authors have contributed equally to this work

Specialty section:
This article was submitted to Plant Development and EvoDevo, a section of the journal Frontiers in Plant Science

Received: 09 May 2019
Accepted: 10 September 2019
Published: 10 October 2019

Citation:
Wang S-L, Viswanath KK, Tong C-G, An HR, Jang S and Chen F-C (2019) Floral Induction and Flower Development of Orchids. Front. Plant Sci. 10:1258. doi: 10.3389/fpls.2019.01258

Orchids comprise one of the largest, most highly evolved angiosperm families, and form an extremely peculiar group of plants. Various orchids are available through traditional breeding and micro-propagation since they are valuable as potted plants and/or cut flowers in horticultural markets. The flowering of orchids is generally influenced by environmental signals such as temperature and endogenous developmental programs controlled by genetic factors as is usual in many flowering plant species. The process of floral transition is connected to the flower developmental programs that include floral meristem maintenance and floral organ specification. Thanks to advances in molecular and genetic technologies, the understanding of the molecular mechanisms underlying orchid floral transition and flower developmental processes have been widened, especially in several commercially important orchids such as *Phalaenopsis*, *Dendrobium* and *Oncidium*. In this review, we consolidate recent progress in research on the floral transition and flower development of orchids emphasizing representative genes and genetic networks, and also introduce a few successful cases of manipulation of orchid flowering/flower development through the application of molecular breeding or biotechnology tools.

Keywords: floral transition, flower development, molecular genetics, orchids, orchid biotechnology, transgenic orchids

INTRODUCTION

The orchid family is one of the largest families of angiosperms. The flowers of Orchidaceae exhibit a high degree of speciation, with wide variations in floral features such as morphology, color, size and fragrance for attraction of pollinators (Peakall, 2007). Orchids are traded worldwide as cut flowers and potted flowering plants. The flowering of orchids can generally be divided into two steps: floral transition and flower development. In floral transition, juvenility, ambient to cool temperature and/or photoperiod are crucial in determining the time that orchids initiate flowering with respect to ontogeny and season. Although molecular and genetic approaches have made it possible to shed some light on the mechanisms underlying floral transition in model plants such as *Arabidopsis* (*Arabidopsis thaliana*) and rice (*Oryza sativa*) (He, 2009; Sun et al., 2014), orchid flowering is still not well-understood. Flower formation is initiated by activities of genes known as flowering time genes which regulate the conversion of the vegetative meristem to the floral meristem. Then, floral meristem identity genes regulate the formation of the flower. Once flowering initiates, cadastral genes which govern the whorl formation in flowers are expressed, and the structures of the whorls and

their occurrence at the right position are regulated by homeotic genes. Although extreme variation in flower morphology is found across the angiosperms, four types of relatively simple floral organs can be distinguished, namely sepals, petals, stamens and carpels (Theissen and Melzer, 2007; Heijmans et al., 2012). Based mainly on studies with *Arabidopsis*, the ABCDE model explains the establishment and maintenance of floral organ specification through an interactive network of MADS-box transcription factors. Herein, we review recent research on floral transition and flower development of a few representative orchid species from the perspective of molecular genetics. Some successful cases of the use of biotechnological tools to modulate orchid floral traits are also highlighted.

FLORAL TRANSITION OF ORCHIDS

Effect of Ambient Temperature

The Orchidaceae plants are widely distributed across the globe, thus the mechanisms of flowering control among different genera may have developed according to their natural habitats. Apostasioideae, Cypripedioideae, Vanilloideae, Epidendroideae and Orchidoideae are the subfamilies of Orchidaceae. Among these five subfamilies, the Epidendroideae is the largest containing more than 500 genera with around 20,000 species (Freudenstein and Chase, 2015). Different orchids of the Epidendroideae require different conditions of ambient temperature and photoperiod to induce flowering (Hsiao et al., 2011).

Most orchids take several years to finish the juvenile stage. *Phalaenopsis* usually reach maturity after three to five leaves. Usually, the floral spike (inflorescence) emerges from the axillary buds of the fourth node below the apical leaf whereas other axillary buds are maintained in a dormant state during the flowering season (Sakanishi et al., 1980). The mechanism of differential commitment of distinct axillary buds for flowering is unknown. At the beginning of flowering, the axillary buds are enlarged and then protrude from the base of a leaf, which takes about 3–4 weeks. After that, the bud is elongated to become a floral spike.

The flowering of several orchids is influenced by change in ambient temperature. The flowering of *Phalaenopsis* is promoted by low ambient temperature, usually less than 26 °C (Blanchard and Runkle, 2006); and can be reversed if the ambient temperature is elevated. The flowering activity of *Dendrobium* is also promoted by low ambient temperature (Campos and Kerbauy, 2004); however, flowering of some hybrid cultivars of *Dendrobium*– such as *Dendrobium* Chao Praya Smile and *Dendrobium* Madame Thong-In, are promoted by high ambient temperature. The flowering of *Miltoniopsis* and *Zygopetalum* are promoted by cool temperature 11–14 °C (Lopez et al., 2003; Lopez and Runkle, 2006). For the *Oncidium*, another popular orchid, change in ambient temperature enhances or is neutral to their flowering activity. For *Cypripedium* species, vernalization below 5 °C or subzero temperature is required for flowering (Zhang et al., 2014).

In the model plant *Arabidopsis*, flowering activity is delayed by low ambient temperature (16 °C) but promoted by vernalization. In low ambient temperature, an alternatively spliced form of FLOWERING LOCUS M (FLM), FLM-β associates with SUPPRESSOR OF VEGETATIVE PHASE (SVP) to suppress the floral integrator gene *FLOWERING LOCUS T* (*FT*) (Lee et al., 2013). The expression of *FLM* is down-regulated *via* alternative splicing coupled with nonsense-mediated decay (AS-NMD) in response to elevated temperatures (Sureshkumar et al., 2016), indicating that *FLM* plays an important role in flowering initiation by modulating thermo-sensitivity. The *FT* expression is also suppressed by a MADS-box gene *FLOWERING LOCUS C* (*FLC*). Constant expression of *FLC* prevents the winter-annual *Arabidopsis* from floral transition before winter and this repression is released by the vernalization pathway signaling (He, 2009). The vernalization pathway suppresses the *FLC* activity *via* the trimethylation of histone 3 lysine 27 (H3K9me3) of *FLC* chromatin. Vernalization is an obligatory requirement for the flowering of lily (*Lilium longiflorum*). In high ambient temperature, a fully developed floral bud is present inside the bulb. A period of prolonged cold temperature in winter is required for the switch of shoot apical meristem (SAM) to inflorescence meristem (IM). The candidate genes involved in vernalization response in lily have been elucidated using transcriptome analysis (Villacorta-Martin et al., 2015; Li et al., 2016) and several orthologs of *Arabidopsis* flowering genes were identified. Among them, *SVP* and *VERNALIZATION 1* (*VRN1*) were down- and up-regulated respectively in floral buds when the bulbs were treated with low ambient temperature. Furthermore, ectopic expression of lily *SVP* or *VRN1* in *Arabidopsis* resulted in delayed or earlier flowering, respectively.

Understanding how ambient temperature regulates the floral transition of orchids is valuable not only for the horticultural market but also for the comprehension of flowering regulation in different plant species. Using molecular genomics tools to investigate flowering in popular ornamental orchids has made it possible to identify many flowering-related genes; however, how such genes regulate flowering in an ambient temperature-dependent manner is still not clear.

Effect of Photoperiod

In *Arabidopsis* and rice, photoperiod is crucial for flowering control (He, 2009; Sun et al., 2014; Song, 2016). Under long-day conditions, *Arabidopsis FT* expression is activated in vascular tissues of leaves in a circadian rhythmic manner by the transcriptional regulator CONSTANS (CO) whose expression and activity are controlled by light signaling pathways and the circadian clock (Song, 2016). In rice, two orthologs of *FT*, *Heading date 3a* (*Hd3a*) and *RICE FLOWERING LOCUS T* (*RFT*) are mainly responsible for floral induction under short-days (SD) and LD conditions, respectively (Sun et al., 2014).

Floral initiation has been shown to be regulated by photoperiod in a few orchids. In *Doritis pulcherrima* (now *Phalaenopsis pulcherrima*), under the 30 °C/20 °C (day/night) condition, floral spikes are initiated more efficiently by 9-h light than 12-h light treatment (Wang et al., 2003). In *Miltoniopsis* orchids, SD incubation at 23 °C before shifting to cool temperature (11–14 °C) facilitates flowering (Lopez and Runkle, 2006). However, during cool temperature treatment, different

photoperiods have no significant effect on flowering suggesting that ambient temperature may play a major role in flowering of *Miltoniopsis*. On the other hand, the formation of floral spikes in *Psygmorchis pusilla* is positively correlated with the increase in day length implying that *P. pusilla* is a quantitative LD plant (Vaz et al., 2004). The effect of photoperiod on flowering seems to be various among different orchid species which have great diversity in adaptation. Furthermore, most orchids are native to tropical areas where day length does not change dramatically throughout the year. Thus, it is reasonable to anticipate that photoperiod has limited effects on flowering of orchids.

Effect of Phytohormones

The effects of phytohormones on orchid flowering have been studied (Goh and Yang, 1978). A synthetic cytokinin, 6-benzylaminopurine (BA), stimulated the flowering of monopodial (e.g., *Phalaenopsis*) and sympodial (e.g., *Dendrobium*) orchids whereas auxin suppressed the BA effect. The positive effect of BA on flowering is likely to be enhanced when combined with gibberellic acid (GA_3) although GA_3 applied alone does not have an influence on floral induction (Hew and Clifford, 1993). In *Phalaenopsis* and *Doritaenopsis*, plants sprayed with BA produced visible inflorescences 3 to 9 days earlier than those without BA treatment although the application of BA could not replace the inductive low temperature in *Phalaenopsis* (Blanchard and Runkle, 2008). Interestingly, even though GAs do not induce flowering, optimum levels of endogenous GAs in the flowering shoot tips are required for flower development in *Phalaenopsis*. Indeed, injection of GAs can rescue the blockage of flower development under high temperature (Su et al., 2001). The existence of abscisic acid (ABA) in different tissues of *Phalaenopsis* has been examined. Relatively higher level of free ABA has been detected in dormant axillary buds whereas free or bound forms of ABA were not found in floral shoots (Wang et al., 2002). In addition, exogenous application of ABA to the stem of *Phalaenopsis* inhibited the formation of floral spikes even under inductive low ambient temperature conditions implying that ABA plays an inhibitory role in orchid floral transition.

Taken together, developmental maturity and ambient temperature are likely the main endogenous and environmental factors, respectively, controlling orchid flowering together with the combined action of phytohormones. Many orchids are epiphytic plants, meaning they are adapted to face frequent periods of nutrient and water scarcity. Although this kind of orchid uses the crassulacean acid metabolism (CAM) as the strategy for carbon fixation like other CAM plants such as succulents and pineapples to adapt themselves to arid conditions (Silvera et al., 2009), flowering consumes a lot of energy. Therefore, the right timing of bud commitment for floral induction with the best physiological situation is crucial for the maintenance of the species through successful sexual propagation. In addition, most orchids have particular pollinators in the wild environment; the timing of floral transition should be consistent with the appearance of their pollinators. Thus, sensing ambient temperature seems to be a good strategy to achieve this aim if their pollinators only appear in a particular season.

Genes Involved in Flowering in *Phalaenopsis*

Based on expression analyses and functional studies with heterologous expression systems, candidate genes for flowering regulatory networks in orchids have been reported. Recently, genome-wide analyses have also been taken into consideration for the identification of Orchidaceae-specific and/or species-specific key genes controlling flowering/flower development of orchids (Huang et al., 2016; Lin et al., 2016; Wen et al., 2017).

P. aphrodite FT1 (*PaFT1*) has been isolated and functionally characterized (Jang et al., 2015). Flowering of *P. aphrodite* is induced by low ambient temperature (≤25 °C) but prohibited by high ambient temperature (≥28 °C). Moreover, photoperiod has no significant influence on flowering of *P. aphrodite*. Expression patterns of *PaFT1* reflect the flowering behavior of the orchid; its flowering is induced by low ambient temperature but not by different light regimes. Reduced expression level of *PaFT1* by virus-induced gene silencing (VIGS) methods resulted in delayed flowering under inductive low ambient temperature, while ectopic expression of *PaFT1* suppressed the late flowering phenotype caused by the induced expression of *SVP* and active *FRIGIDA* (*FRI*), a *FLC* activator, in *Arabidopsis*. Moreover, PaFT1 is able to physically interact with PaFD reminiscent of the *Arabidopsis* FT-FD module (He, 2009). *LEAFY* (*LFY*) is another floral integrator in *Arabidopsis* (He, 2009). The *LFY* gene of *P. aphrodite* (*PhapLFY*) has also been characterized (Jang, 2015). Expression of *PhapLFY* under the control of *Arabidopsis LFY* promoter rescued the abnormal floral structure of *Arabidopsis lfy* mutant and caused early heading by overexpression in rice. Recently, a *CO*-like gene, *PhalCOL* has been identified in *P. hybrida* (Wedding Promenade) (Zhang et al., 2011). *PhalCOL* has significant sequence similarity to *CO* of *Arabidopsis*. Overexpression of *PhalCOL* in tobacco caused an early-flowering phenotype suggesting the functional convergence of *CO* genes in flowering among different plant species. To discover candidate genes responsible for the flowering control of *P. aphrodite*, transcription profiles in axillary buds of plants treated with low and high ambient temperature were analyzed and compared to each other (Huang et al., 2016). The result showed that, in addition to *FT*, *LFY*, *APETALA1* (*AP1*) and *OVEREXPRESSION OF CONSTANS 1* (*SOC1*) homologs, genes involved in GA biosynthesis were also up-regulated by low ambient temperature. Another expression analysis using *Phalaenopsis* Fortune Saltzman found that transcripts of *KNOX1*, R2R3-like *MYB*, adenosine kinase 2, S-adenosylmethionine synthetase, dihydroflavonol 4-reductase, and naringenin 3-dioxygenase were accumulated at a higher level in spikes grown under warm day/cool night (28 °C/21 °C) compared with those grown at daily warm temperature (28 °C/26 °C) under natural light conditions (Li et al., 2014).

Genes Involved in Flowering in *Dendrobium*

Flowering of *D. nobile* is promoted by low ambient temperature (Campos and Kerbauy, 2004). Orthologs of *FT* and *MOTHER OF FT AND TFL1* (*MFT*), a homolog of *FT*, have been identified in *D. nobile* Lindl. (Li et al., 2012). Expression of *DnFT* is

up-regulated in leaves but down-regulated in axillary buds under low temperature treatment (12 °C/9 °C, day/night) whereas *DnMFT* expression is not affected by the low temperature treatment. Transgenic *Arabidopsis* ectopically expressing *DnFT* exhibited early flowering. In addition, an ortholog of *SOC1*, *DOSOC1* has been identified from *Dendrobium* Chao Praya Smile (Ding et al., 2013). Increased expression of *DOSOC1* was detected during floral transition. Moreover, overexpression of *DOSOC1* in both *Arabidopsis* and *Dendrobium* resulted in early-flowering phenotypes. *DOAP1*, an ortholog of *AP1* has also been identified and characterized from the orchid (Sawettalake et al., 2017). The role of *DOAP1* is similar to that of *AP1* in *Arabidopsis*. Overexpression of *DOAP1* rescued the floral defect of *ap1* mutant and resulted in early flowering in wild-type *Arabidopsis*. Differential gene expression in the SAM during *in vitro* transition from vegetative to reproductive growth has been investigated in *Dendrobium* Madame Thong-In (Yu and Goh, 2000a). Several transcription factors, including a MADS-box gene of the *AP1*/*AGL2* family, a class I *KNOX* gene and a homolog of the *Drosophila SEVEN-UP* gene were differentially expressed in vegetative and transitional SAM. The *KNOX* gene plays an important role in the function of SAM, and encodes a KNOTTED1-like homeobox (Knox) protein later designated as *DOH1* (*Dendrobium Orchid Homeobox 1*) (Yu et al., 2000). In tissue culture conditions, the expression of *DOH1* was gradually increased in the apical meristem during vegetative growth whereas it was decreased during the progress of reproductive growth. Overexpression of antisense *DOH1* resulted in early flowering in *Dendrobium*. On the other hand, *DOMADS1*, a MADS-box gene of the *AP1*/*AGL9* superfamily, was identified from the cDNA library of transitional SAM (Yu and Goh, 2000b). Expression of *DOMADS1* was up-regulated in transgenic plants harboring p*35S*: antisense *DOH1* suggesting that *DOH1* is a possible upstream repressor of *DOMADS1* in the flowering control of *Dendrobium* orchids. Recently, transcriptomes of *D. nobile* were analyzed under cold (4 °C) or exogenous cytokinin (thidiazuron) treatment (Wen et al., 2017). The results showed that *SOC1*, *LFY* and *AP1* genes were induced by both low temperature and thidiazuron treatment whereas *DnVRN1* and *FT* were induced only by cold treatment. Also, some marker genes for the GA signaling pathway were up-regulated under both low temperature and thidiazuron treatments. Further investigation is needed to uncover the cytokinin-GA signaling network in the inductive temperature condition underlying the floral transition in *Dendrobium*.

Genes Involved in Flowering in *Oncidium*

High ambient temperature (30 °C) accelerates the flowering of *Oncidium*. The flowering response to changes in ambient temperature in *Oncidium* is opposite to that of *Phalaenopsis*. The flowering promoter *FT* and repressor *TERMINAL FLOWER 1* (*TFL1*) both encode proteins belonging to phosphatidylethanolamine-binding protein (PEBP) family and have also been identified in *Oncidium* Gower Ramsey (Hou and Yang, 2009). *OnFT* was expressed in axillary buds, leaves, pseudo-bulb and flowers while *OnTFL1* was only expressed in axillary buds and pseudo-bulb. The expression of *OnFT* was regulated by photoperiod, with highest expression from the 8th to 12th hour of the light period and lowest expression at dawn. However, expression of *OnTFL1* is not influenced by photoperiod. Ectopic expression of *OnFT* resulted in an early-flowering phenotype in *Arabidopsis*, and late-flowering of *Arabidopsis ft-1* mutant was rescued by *OnFT* overexpression (Hou and Yang, 2009). On the contrary, ectopic expression of *OnTFL1* in *Arabidopsis* displayed late flowering. *OMADS1*, a homolog of *Arabidopsis AGL6* has also been identified in *Oncidium* Gower Ramsey (Hsu et al., 2003). *OMADS1* transcripts were detectable in the apical meristem and floral organs, and ectopic expression of *OMADS1* in *Arabidopsis* caused early flowering with up-regulation of *FT*, *SOC1*, *LFY* and *AP1*. Overexpression of *OMADS1* in *Oncidium* also resulted in precocious flowering (Hsu et al., 2003). Recently, ascorbate (AsA) content has been shown to play an important role in floral transition in response to thermal stress (30 °C over a 14-day period) in *Oncidium* Gower Ramsey (Chin et al., 2014). Under thermal stress conditions, the level of reactive oxygen species (ROS; e.g., H_2O_2) was significantly increased and the AsA redox ratio [AsA to dehydroascorbate (DHA, the oxidized form of AsA)] was decreased with prominent up-regulation of cytosolic ascorbate peroxidase (*cytAPX1*) expression. The oxidation of AsA to DHA by ascorbate peroxidase is the key reaction to remove H_2O_2. The report by Chin and colleagues suggests that the AsA/DHA redox ratio may act as one of the endogenous signals that induce the flowering of *Oncidium* in response to high ambient temperature. Furthermore, it has been shown that reduced GSH redox ratio caused by down-regulation of GSH metabolism-related genes such as glutathione reductase (*GR1*), γ-glutamylcysteine synthase (*GSH1*) and glutathione synthase (*GSH2*) was linked to the decrease in the AsA redox ratio for flowering of *Oncidium* orchid (Chin et al., 2016).

Genes Involved in Flowering in *Dortiaenopsis* and Other Orchids

DhFVE, a *Dortiaenopsis* ortholog of *Arabidopsis FVE*, which is a component of the autonomous flowering pathway, has been identified (Sun et al., 2012). Flowering of *Dortiaenopsis* (now *Phalaenopsis*) is promoted by low ambient temperature (22 °C/18 °C, day/night) (Luo et al., 2011) and the expression of *DhFVE* is increased in the stem during floral transition. In addition, *EARLY FLOWERING 4* (*EFL4*) family genes, *DhEFL2*, *DhEFL3* and *DhEFL4* have been identified in *Dortiaenopsis* (Chen et al., 2015). *Arabidopsis EFL4* is known to affect flowering through photoperiod perception and circadian regulation (Doyle et al., 2002). Ectopic expression of *DhEFL2*, *DhEFL3* or *DhEFL4* delayed flowering of *Arabidopsis*. Moreover, *GIGANTEA* (*GI*), an upstream activator of *CO* (Sawa et al., 2007), has been identified as *DhGI1* in *Dortiaenopsis* hybrid (Luo et al., 2011). Expression of *DhGI1* is up-regulated by low temperature and may play a role in flowering initiation in *Dortiaenopsis* hybrid. Recently, many putative flowering genes have been identified in *Cymbidium* and *Erycina* through transcriptome analyses. However, their functions still remain to be examined (Li et al., 2013; Lin et al., 2016).

A Hypothetical Model of Flowering Regulation in *P. aphrodite*

The regulatory networks of floral transition in different orchids may be divergent since the required inductive conditions are not all the same. In addition, the genetic tools for orchid research are still limited; therefore, it is time-consuming and also difficult to reveal the molecular mechanisms of flowering control in orchids. The popular ornamental orchid *P. aphrodite* has a particular requirement for floral transition, i.e., low ambient temperature, which makes this orchid an interesting target for a case-study of flowering regulation in orchids. Furthermore, a transformation system has been established in orchids including *P. aphrodite* (Hsing et al., 2016). Thus, the molecular mechanism of flowering regulation could be investigated more thoroughly.

The hypothetical gene regulatory network in flowering of *P. aphrodite* is illustrated in **Figure 1** based on the published results (data adapted from research on orchids). The expression of *PaFT1* is induced by low ambient temperature, and PaFT1 interacts with PaFD to possibly activate the downstream genes required for floral induction. Reflecting the *Arabidopsis* model, PaFT1 protein is likely transported from leaves to axillary buds to induce spiking in *Phalaenopsis* orchid. If the PaFT1 moves to dormant/juvenile buds, there must be a repressive mechanism against PaFT1 action or other unknown floral co-activators are still absent in dormant/juvenile buds. However, we cannot exclude the possibility that the pavement for the PaFT1 movement to the dormant/juvenile buds is not available. Based on the transcriptomic analyses of *Phalaenopsis* orchids, *KNOX1*, *SOC1* and *FVE* genes are induced by low ambient temperature (Sun et al., 2012; Li et al., 2014; Huang et al., 2016) although *Dendrobium KNOX1* gene is down-regulated by low ambient temperature (Yu and Goh, 2000a; Yu et al., 2000). Thus, the role of *KNOX1* in floral transition of *Phalaenopsis* needs to be further examined. In *Phalaenopsis*, *SOC1* may activate *LFY* and *AP1* during floral transition as is the case in *Arabidopsis*. Recently, *FVE* has been suggested to be an upstream activator of *SOC1* in *P. aphrodite* (Koh et al., 2018). The *CO* in *Phalaenopsis* may also activate *FT* irrespective of photoperiod (Zhang et al., 2011; Kaewphalug et al., 2017). In addition, *ELF* genes in *Phalaenopsis* may repress the *CO* activity (Doyle et al., 2002; Chen et al., 2015). Moreover, the GI-FLAVIN-BINDING, KELCH REPEAT, F BOX 1 (FKF1) and CYCLING DOF FACTOR (CDF) may also regulate the *CO* activity in *Phalaenopsis* as is also the case in *Arabidopsis* (Song, 2016). Since *SVP* and *FLM* are critical flowering regulators responding to changes in ambient temperature in *Arabidopsis*, it is also possible to anticipate that the two orthologs of *SVP* and *FLM* also act in floral induction of *Phalaenopsis* in various ways. Actually, *SVP* and *FLM* repress the expression of *FT* at low ambient temperature in *Arabidopsis* (Lee et al., 2013). Thus, the working mechanism of those orthologs in *Phalaenopsis* might be distinct from that of *Arabidopsis*. In addition, further studies are required to reveal the mechanisms underlying phytohormone-dependent flowering pathways linked to changes in ambient temperature in orchids. Even taking these findings together, it can be seen that there is a long way to go to achieve a better understanding of the flowering regulatory network in *P. aphrodite*. As one of the shortcuts to reach this goal, high throughput analyses can be applied to identify candidates involved in the floral transition of *Phalaenopsis*. Also, collection of information on flowering networks in various plant species would be very useful in the interpretation of large-scale experimental results such as omics data. Most importantly, forward or reverse genetic studies are

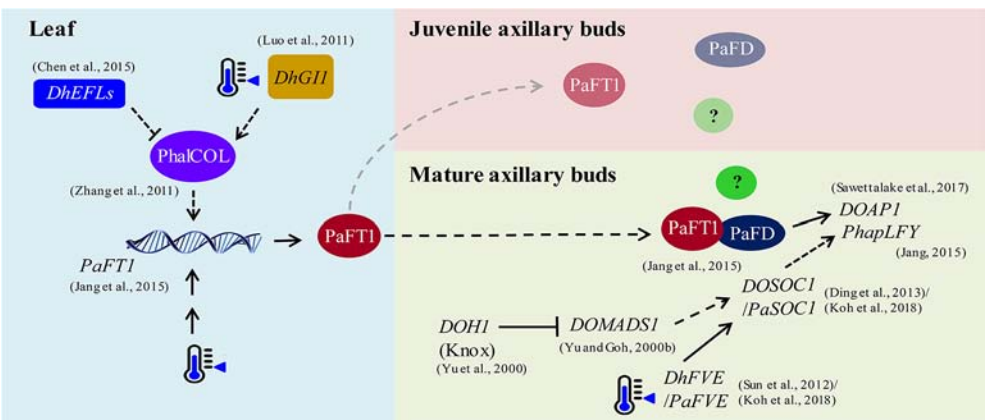

FIGURE 1 | The hypothetical flowering regulation in *P. aphrodite* under low ambient temperature. Low ambient temperature drives *PaFT1* activity in leaves and then PaFT1 protein is transported selectively to mature axillary buds or both mature and juvenile axillary buds. A complex formed by the interaction between PaFT1 and PaFD may activate downstream genes such as *AP1* required for floral meristem identity. An example of unknown factors for flowering in the meristem is presented by a green circle with a question mark inside. In juvenile axillary buds, some flowering activators required for floral induction may be absent. *PaFT1* can also be activated by *CO* pathway and the *CO* activity—*PhalCOL* (*Phalaenopsis CO Like*), here—which is likely to be regulated by *EFL* and *GI* genes. This regulation should not be dependent on photoperiod. Low ambient temperature also activates *PaFVE*. Consequently, *PaSOC1* is activated by the *PaFVE*. Moreover, the reduced expression of a KNOTTED1-like homeobox (Knox) gene may lead to the activation of *SOC1* through other MADS box genes such as *DOMADS1*. The orchid *LFY* genes such as *PhapLFY* can also be induced by *PaSOC1*. The solid lines represent pathways that have been reported in orchids and the dotted lines indicate hypothetical regulations based on studies using other plant species. References for each regulation are presented in the figure.

required for the functional confirmation of candidate genes in orchid flowering. The homologs of flowering genes in a few orchid species are listed in **Table S1**.

FLOWER DEVELOPMENT OF ORCHIDS

Floral Development of *Arabidopsis* and Monocot Plants

Floral pattern formation is one of the significant features of angiosperms, the mechanisms of which can be explained using the ABC or ABCDE model (**Figure 2A**). The identity of various floral organs is determined by MADS-box transcription factors or their complexes during flower development. According to the ABC model, in *Arabidopsis*, sepals in the first whorl are characterized by the expression of A-class genes; petals in whorl 2 are characterized by co-expression of A- and B-class genes, stamens in whorl 3 are characterized by co-expression of B- and C-class genes, and carpels in whorl 4 are determined when C-class genes are solely expressed (Jack, 2001; Theissen, 2001). The ABC model has been extended to the ABCDE model with additional functions of D- and E-class genes in floral organ identity determination (Theissen and Melzer, 2007; Heijmans et al., 2012). D-class genes are involved in ovule development while E-class genes are involved in the identity of all floral verticils. Most genes in the ABCDE model are MADS-box genes. *AP1* and *AP2* (the only non-MADS-box genes) are A-class genes; *AP3* and *PISTILLATA* (*PI*) are B-class genes. *AGAMOUS* (*AG*) is a C-class gene; *SEEDSTICK* (*STK*) is a D-class gene. The D-class genes were first identified in *Petunia*, namely *FLORAL BINDING PROTEIN 7* (*FBP7*) and *FBP11*. Finally, *SEPALLATA 1* (*SEP1*), *SEP2, SEP3* and *SEP4* formally known as *AGAMOUS-LIKE 2* (*AGL2*), *AGL4*, *AGL9* and *AGL3*, respectively, are characterized as E-class genes. According to the floral quartet model, MADS-box proteins form whorl-specific tetrameric complexes during floral organ determination. The tetrameric transcriptional factor complexes recognize specific *cis*-regulatory elements termed CArG-boxes (CC-AT rich-GG), and different complexes are postulated to function in controlling expression of different target genes (Jetha et al., 2014). Recently, a reliable and efficient two-stage approach has been developed for angiosperms MADS-Box genes classification using machine learning methods to overcome errors in phylogenetic tree construction (Chen et al., 2019).

The MADS-box genes involved in the floral development in monocot plants such as rice, maize (*Zea mays*), wheat (*Triticum aestivum*), barley (*Hordeum vulgare*) and lily have also been elucidated (Callens et al., 2018). MADS-box protein structure is conserved between diverse plants. Comparing the expressions and functions of the ABCDE MADS-box genes among different monocot plants provides the opportunity to elucidate their roles in determining the floral development during evolution.

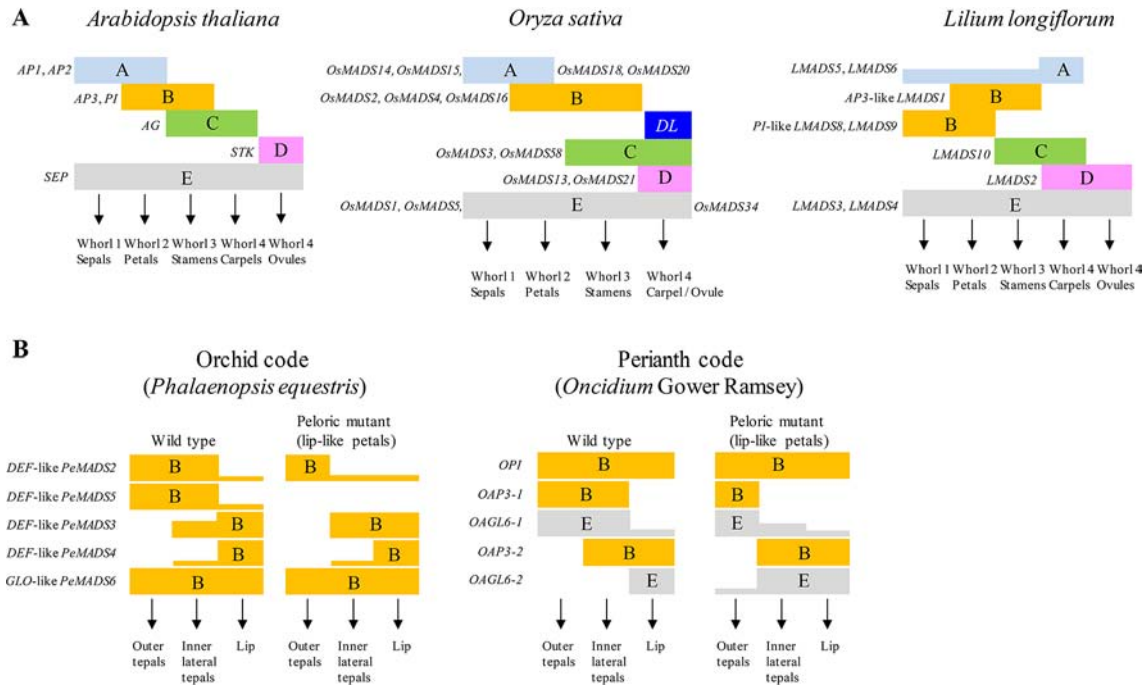

FIGURE 2 | The models of floral development in *Arabidopsis*, rice, lily and orchids. **(A)** The ABCDE model explains the floral organ identity in *Arabidopsis*, rice and lily. The floral development genes are grouped into different classes from A to E. Combinational expressions of different classes of genes determine the formation of different floral organs. Representative genes of different classes are indicated in the figures. *DL*, *DROOPING LEAF*. **(B)** The orchid code and perianth code (P code) explain the formation of perianth of orchids. In the orchid code, combinational expressions of B-class genes from different phylogenetic clades determine the morphology of orchid perianth. The expression patterns of B-class genes changed in peloric mutant are compared with that of wild type. In the P code model, combinational expressions of different B and E-class genes determine the formation sepal/petal or lip of *Oncidium* orchids.

In rice, the A-class gene, the *FUL*-like (*FRUITFULL* locus of *Arabidopsis*) *OsMADS14*, *OsMADS15*, *OsMADS18* and *OsMADS20*, are expressed to determine the whorl 1 structures of lemma and palea; co-expression of A and B-class genes, *DEF*-like (*DEFICIENS*: an *Antirrhinum* B-class gene) *SUPERWOMEN1* (*SPW1 or OsMADS16*) and *GLO*-like (*GLOBOSA*: another *Antirrhinum* B-class gene) *OsMADS2* and *OsMADS4*, determines the whorl 2 structure of lodicules (Yoshida and Nagato, 2011); co-expression of B and C-class genes, *OsMADS3* and *OsMADS58*, determines the whorl 3 structure of stamens. Another C function gene *DROOPING LEAF* (*DL*) have been identified in carpel specification and floral meristem determinacy (Shige-Hiro et al., 2019). C and D-class genes, *OsMADS13* and *OsMADS21*, are expressed to determine the whorl 4 structure of the carpel and ovule, respectively. In addition, the E-class genes, *OsMADS1*, *OsMADS5* and *OsMADS34*, are involved in the development of all four whorl structures (**Figure 2A**).

The lily has a floral character most similar to orchids, with almost identical sepals and petals. Flowers from the lily family *Liliaceae* have three sepals in whorl 1, three petals in whorl 2, six stamens in whorl 3 and three fused carpels in whorl 4. Three A-class genes from lily, *LMADS5*, *LMADS6* and *LMADS7* have been analyzed (**Figure 2A**) (Chen et al., 2008). They were all expressed in the vegetative stem and inflorescence meristem. With regard to the floral organs, *LMADS5* and *LMADS6* are mainly expressed in the carpel, whereas *LMADS7* is only expressed in the vegetative stem and inflorescence meristem. Early flowering phenotype and homeotic conversions of sepals to carpel-like and of petals to stamen-like structure were observed when they were ectopically expressed in *Arabidopsis*. For the B-class gene, mRNA of *AP3*-like *LMADS1* could be detected in all four whorls but the protein was detected only in the petal and stamen (Tzeng and Yang, 2001). The *PI*-like *LMADS8* and *LMADS9* are expressed in whorl 1 and 2 during all stages of development and are expressed in the stamen only in young flower buds (Chen et al., 2012a). The ectopic expression of *LMADS8* and *LMADS9* partially converted the sepals into petaloid structures in *Arabidopsis*. The *PI*-like gene *LFGLOA* and *LFGLOB* identified from *L.* x *formolongi* are also expressed in the first, second and third whorl of lily (Akita et al., 2008). Several C-class genes have been identified from different lilies including *LMADS10*, *LFAG1* and *LLAG1* (Benedito et al., 2004; Akita et al., 2008; Hsu et al., 2010). They are expressed in whorl 3 and 4, and ectopic expression of C-class genes in *Arabidopsis* resulted in carpel-like septal and stamen-like petal phenotypes. In addition, a double-flowered cultivar "Aphrodite" of *L.* x *formolongi* with petal-like stamen may be caused by reduction in the expression of *LFAG1* in whorl 3 (Akita et al., 2008). The lily D-class gene, *LMADS2* completely accumulated in the carpel and more specifically in the ovules (Tzeng et al., 2002). Ectopic expression of *LMADS2* in *Arabidopsis* converted the sepals into a stamen-like structure in whorl 2. *LMADS3* and *LMADS4* have been identified as E-class genes in lily (Tzeng et al., 2003). Both *LMADS3* and *LMADS4* expression are expressed in the inflorescence meristem, floral buds and all four whorls of the flower organ. Ectopic expression of *LMADS3* in *Arabidopsis* showed extremely early flowering, which was associated with up-regulation of *FT*, *SOC1*, *LUMINIDEPENDENS* and flower meristem identity gene *LFY* and *AP1*. Taken together, the different expression patterns of A- and B-class genes from that of the dicot plants such as *Arabidopsis* suggest a modified ABCDE model for flower development in lily.

Floral Organ Identity Genes in Orchids

The structure of the orchid flower has a zygomorphic nature in contrast to most plant groups leading to precise interaction with the pollinator (Cubas, 2004). Orchid flowers generally contain an outer whorl with three sepals, an inner whorl with three petals, and a single column in the center. The sepals in most orchids are enlarged and look like petals. Two of the petals are displayed in a normal shape and one becomes a highly specialized structure called the lip or labellum. The sepals and petals are usually called tepals since they are very similar in appearance. The column, also called the gynostemium, is the reproductive organ of orchids, which combines the gynoecium (female organ) and androecium (male organ). On the top of the column is the male anther which contains packets of pollen called pollinia. Many floral MADS-box genes have been identified from different orchids. According to their expression patterns and putative roles in determining the different floral organs, advanced models of flower development for orchids have been proposed. Also, these studies offer an opportunity to understand the relationships between the diverse array of floral MADS-box genes and flower development.

A-Class Genes

A- and E-class genes belong to the same *AP1*/*AGL9* superfamily group. A-function genes come from the *SQUA*-like (*SQUAMOSA*: an *Antirrhinum* A-class gene) subgroup, which can be divided into *FUL*/*AGL8*-like and *euAP1*-like clades. E-function genes come from the *SEP*-like subgroup containing *AGL9*-like and *AGL2*/*3*/*4*-like clades. *AGL6* is a member of the *AP1*/*AGL9* group between the *SQUA*-like and *SEP*-like subgroups (Purugganan et al., 1995; Chang et al., 2009). Two *AP1*-like genes, *ORAP11* and *ORAP13*, were isolated and characterized in *Phalaenopsis* Formosa Rose. Both genes are highly expressed during the early stages of floral buds and vegetative organs (Chen et al., 2007). At later stages of flower development, *ORAP11* is expressed only in the column and *ORAP13* expression is absent from all of the floral organs. *PaAP1-1* identified from *P. aphrodite* is expressed in the inner whorls of the pollinia and pedicel whereas *PaAP1-2* is expressed in the pedicel only (Su et al., 2013). This expression pattern suggests that *PaAP1-1* and *PaAP1-2* play a role in the development of the pollinia and gynoecium rather than being involved in the perianth formation like that in *Arabidopsis*. Furthermore, *PaAP2-5* is mainly expressed in whorl 1 and 2, *PaAP2-7* is specifically expressed in pollinia, and *PaAP2-11* is expressed at a low level among all floral organs. Novel functions of homeotic genes may be acquired based on the diversified expression in *Phalaenopsis* through evolutionary processes. Two *AP1*/*FUL*-like genes in *Phalaenopsis* hybrid "Athens," *PhaMADS1* and *PhaMADS2* are highly expressed in the ovary before pollination, but a low level of expression is detected in the perianth and gynostemium (Acri-Nunes-Miranda and Mondragon-Palomino, 2014). *DOMADS2* identified from

Dendrobium Madam Thong-in, and *DthyrFL1*, *DthyrFL2* and *DthyrFL3* from *D. thyrsiflorum* have been characterized as *SQUA*-like and *FUL*-like genes, respectively (Yu and Goh, 2000b; Skipper et al., 2005). The expression of *DOMADS2* could be detected in the SAM during floral transition but it was limited to the column at the later stages of flower development. Low level expression of *DthyrFL1*, *DthyrFL2* and *DthyrFL3* was observed in the vegetative tissues, but higher levels were detected in the inflorescences and ovules. The *AP1* homolog of *Oncidium* Gower Ramsey, *OMADS10* is expressed in vegetative leaves, lip and carpel of mature flowers (Chang et al., 2009). An *AP2*-like gene of *D. crumenatum*, *DcOAP2* is expressed in all floral organs (Xu et al., 2010). Weak expression of three *AP1*-like genes, *EpMADS10*, *EpMADS11* and *EpMADS12* from *Erycina pusilla* has also been observed in all floral organs (Dirks-Mulder et al., 2017). An *AP2-like* gene of *C. ensifolium*, *CeAP2*, is expressed mainly in sepals and petals with negative regulation by miR172 (Yang et al., 2015).

B-Class Genes

B-class genes in Orchidaceae have been surveyed and have 11 species characterized into four *AP3*- and two *PI*-duplicated homologs (Pan et al., 2011). *PI* homologs are uniformly expressed in all floral whorls whereas different clades of *AP3* homologs may have different expression patterns within floral organs. In *P. equestris*, four *DEF*-like genes, *PeMADS2*, *PeMADS3*, *PeMADS4* and *PeMADS5* have been identified. (Tsai et al., 2004). They are expressed in floral organs with distinct patterns. *PeMADS2* and *PeMADS5* are expressed in sepals, petals, lip and column; *PeMADS3* is expressed in petals, lip and column, whereas *PeMADS4* is expressed in lip and column only. In peloric (lip-like petal) mutant, expression of *PeMADS5* is absent from all floral organs, and expression of *PeMADS4* is extended to the lip-like petal. This indicates that, among the four *DEF*-like genes, *PeMADS4* may determine the lip formation in *Phalaenopsis*. In addition, these four *DEF*-like MADS genes are able to interact with a *GLO*-like gene *PeMADS6* (Tsai et al., 2005; Tsai et al., 2008). Ectopic expression of *PeMADS6* caused petaloid sepals in *Arabidopsis* flowers. Furthermore, these heterodimers could bind the CArG *cis*-element. A single copy of *PI*-like gene of *Phalaenopsis* hybrid, *PhPI10* has been also characterized (Guo et al., 2008). Expression of *PhPI10* is restricted to the lip of flowers. Several *AP3*-like genes *PaAP3-1*, *PaAP3-2*, *PaAP3-3* and *PaAP3-4* were identified in *P. aphrodite* and their expression was preferentially detected in sepals, petals and the lip/column (Su et al., 2013). Another *PI-like* gene, *PaPI*, has also been identified but its transcripts are detectable in all floral organs. In *Dendrobium crumenatum*, *DcOAP3A*/*B* and *DcOPI* were identified as *AP3*-like and *PI*-like genes, respectively (Xu et al., 2006). Transcripts of *DcOAP3A* and *DcOPI* are accumulated in all floral organs and their proteins form heterodimers. Abnormal flowers containing petaloid sepals were produced when *DcOPI* was overexpressed in *Arabidopsis*. In addition, the phenotypic alteration of B-function mutants has also been observed by overexpressing *DcOAP3-SRDX* repressor fusion construct implying a dominant negative effect on the B-function *via* the hetero-dimerization with its interacting partners. The *Oncidium* Gower Ramsey *AP3*-like gene, *OMADS3* is also expressed in all floral organs (Hsu and Yang, 2002). Another study characterized the B-class MADS-box genes of *Oncidium* including the *AP3*-like *OMADS3*, *OMADS5* and *OMADS9*, and *PI*-like *OMADS8* (Chang et al., 2010). *OMADS5* is expressed in sepals and petals; *OMADS9* is expressed in petals and lip; *OMADS8* is expressed in all four floral organs like *OMADS3*. In lip-like petals and lip-like sepals of peloric mutant flowers, expression of *OMADS5* is down-regulated suggesting that *OMADS5* negatively regulates the lip formation. Recently, the perianth formation in *Cymbidium goeringii* was determined through the complete analysis of expression levels of B-class genes along with co-expression of A-class and E-class genes (Xiang et al., 2018). *CgDEF1* is expressed in sepals and petals but not lip; *CgDEF3* and *CgDEF4* are highly expressed in lip and lip-like petals whereas *CgDEF2* is expressed in all floral organs. Several B-class genes have been isolated from *Habenaria* (Kim et al., 2007), *Orchis* (Salemme et al., 2011) and *Erycina* (Dirks-Mulder et al., 2017). *HrDEF* expression is exhibited in the petals and column whereas that of *HrGLO1* and *HrGLO2* is detected in all floral organs. In the petaloid-sepal mutant, expression of *HrDEF* was extended to the petaloid sepals suggesting that distinctive expression of *HrDEF* determines the differentiation of sepals and petals of *H. radiata* flowers. In *Orchis italica*, the *PI*/*GLO*-like genes *OrcPI* and *OrcPI2* are expressed in all floral organs of immature floral buds but their expression is restricted to the lip in the mature flower. In *E. pusilla*, *EpMADS13*, *EpMADS14* and *EpMADS15* are *AP3*-like genes while *EpMADS16* is a *PI*-like gene. Their expression is detectable in almost all floral organs but has diverse patterns. In *Rhynchostylis gigantea*, *RgAP3* an *AP3*-like and *RgPI* a *PI*-like genes were cloned and expression levels of *RgAP3* were noticed only in the petal and sepal, and *RgPI* was expressed in every part of the floral organs (Zhang et al., 2013).

C- and D-Class Genes

The reproductive organ, the gynostemium, is another unique floral structure in orchids in addition to the labellum. In the ABCDE model, C-class genes are important for the development of stamens and carpels, and D-class genes are required for ovule development. Both C- and D-class genes belong to the *AG* subfamily of MADS-box genes (Theissen et al., 2000; Kramer et al., 2004). In orchids, C- and D-class genes involved in the development of the gynostemium and ovule have been also identified. In *P. equestris*, *PeMADS1* and *PeMADS7* were characterized as C- and D-class genes, respectively (Chen et al., 2012b). Spatial expression analyses of *PeMADS1* and *PeMADS7* demonstrated that they are specifically expressed in the gynostemium of the flower. Development of ovules is initiated after pollination in orchids and *PeMADS1* and *PeMADS7* transcripts are accumulated in the ovules after pollination. Moreover, expression of *PeMADS1* could be detected in petals of *gynostemium-like petal* (*gylp*) mutant suggesting that *PeMADS1* functions in gynostemium development. PeMADS1 and PeMADS7 could form a homodimer or heterodimer *via* the PeMADS8, an E-class protein. Ectopic expression analyses showed that *PeMADS1* could rescue the phenotype of *AG* mutant, and *PeMADS7* in *Arabidopsis* produced characteristic

phenotypes of the D-class gene family without homeotic conversions. Another two studies also characterized C- and D-class genes in *Phalaenopsis* Hatsuyuki and *Phalaenopsis* Athens including *AG*-like *PhlAG1*, *PhaMADS8*, *PhaMADS10* and *STK*-like *PhlAG2*, *PhaMADS9* (Song et al., 2006; Acri-Nunes-Miranda and Mondragon-Palomino, 2014). Expressions of *PhlAG1* and *PhlAG2* could be detected in the lip, column and ovule, and *PhaMADS8*, *PhaMADS9* and *PhaMADS10* were specifically expressed in the gynostemium and ovary. Expression of *PhaMADS9* but not *PhaMADS8* and *PhaMADS10* is increased in the gynostemium of peloric mutants suggesting that the expression level of *STK*-like gene is crucial for gynostemium development. The C- and D-class genes in *D. crumenatum* and *D. thyrsiflorum* were also characterized; *DcOAG1* and *DthyrAG1* are C-class genes; *DcOAG2* and *DthyrAG2* are D-class genes (Skipper et al., 2006; Xu et al., 2006). *DcOAG1* is expressed in all floral organs while *DcOAG2* is mainly expressed in the ovary and in the envelope cells of pollinia. Overexpression of *DcOAG1* in *Arabidopsis* transformed the sepals and petals into carpel-like and stamen-like structures, respectively. *DthyrAG1* and *DthyrAG2* are expressed in the inflorescences and ovules after pollination, and *DthyrAG2* is believed to play more important roles in later stages of ovule development in *D. thyrsiflorum* since its expression was higher than that of *DthyrAG1* in ovules. The C- and D-class genes in *Oncidium* Gower Ramsey, namely *OMADS4* and *OMADS2* respectively, were also characterized (Hsu et al., 2010). *OMADS4* is expressed in the stamens and carpels whereas expression of *OMADS2* is restricted to the stigmatic cavity and ovary of carpels. In addition, yeast two-hybrid analyses showed that *OMADS4* and *OMADS2* are able to form homodimers by themselves or form heterodimers with each other. Ectopic expression of *OMADS4* and *OMADS2* caused only early or moderately early flowering in *Arabidopsis* without homeotic conversion of floral organs. C- and D-class genes characterized in *Cymbidium* (Wang et al., 2011b), *Orchis* (Salemme et al., 2013) and *Erycina* (Dirks-Mulder et al., 2017), include C-class genes *CeMADS1*, *CeMADS2*, *OitaAG*, *EpMADS20*, *EpMADS21* and *EpMADS22*, and D-class genes *OitaSTK* and *EpMADS23*. *CeMADS1* is only expressed in the column but *CeMADS2* is expressed in all floral organs. In the multitepal mutant whose male and female reproductive organs are replaced by a newly emerged flower, expression of *CeMADS1* is lost, suggesting that *CeMADS1* is associated with the development of the gynostemium. *O. italica OitaAG* and *OitaSTK* are also expressed in the reproductive organs in both the early and late stages. Among the *E. pusilla* MADS-box genes, *EpMADS20* is expressed in all floral organs while others, such as *EpMADS21*, *EpMADS22* and *EpMADS23* are mainly expressed in the gynostemium.

E-Class Genes

E-class genes show unique interaction with other floral organ identity genes to determine all floral organs. *Arabidopsis* has four *SEP* genes: *SEP1*, *SEP2*, *SEP3*, and *SEP4*. The flowers of a triple mutant of *sep1 sep2 sep3* consist entirely of sepal-like organs (Pelaz et al., 2000) while the quadruple mutant of *sep1 sep2 sep3 sep4* produces leaf-like organs instead of floral organs (Ditta et al., 2004). Moreover, simultaneously reduced expression of four rice *SEP*-like genes (*OsMADS1*, *OsMADS5*, *OsMADS7* and *OsMADS8*) caused the conversion of all floral organs except the lemma into leaf-like structures (Cui et al., 2010). In orchids, a number of genes belonging to the E-class have been characterized at the molecular level. A *SEP3*-like gene, *OM1* was the first E-class gene identified, from the mature flower of *Aranda* Deborah, and its expression was identified in sepals and petals (Lu et al., 1993). In *Phalaenopsis* hybrid Athens, three *SEP*-like genes *PhaMADS4*, *PhaMADS5* and *PhaMADS7* have been identified and these are expressed in the sepal, petal and labellum (Acri-Nunes-Miranda and Mondragon-Palomino, 2014). In *P. aphrodite*, *PaAGL6-1* is expressed in the lip, whereas the *PaAGL6-2* is expressed throughout all floral organs (Su et al., 2013). Four *SEP*-like genes *PeSEP1*, *PeSEP2*, *PeSEP3* and *PeSEP4* were characterized from *P. equestris* (Pan et al., 2014). These *PeSEP* genes are expressed in all floral organs and VIGS of *PeSEP3* resulted in production of leaf-like tapels. Down-regulation of *PeSEP2* expression alone by VIGS has minor effects, but silencing of both *PeSEP2* and *PeSEP3* expression caused reduced expression of B-class genes such as *PeMADS2, PeMADS3, PeMADS4, PeMADS5* and *PeMADS6* suggesting an association between *PeSEP* functions and B-class gene expression. *DOMADS1* and *DOMADS3* from *Dendrobium* Madame Thong-In are homologous genes of *SEP3* and *SEP4*, respectively, and *DcOSEP1* from *D. crumenatum* is a homolog of *SEP3* (Yu and Goh, 2000b; Xu et al., 2006). Expressions of these genes are constantly activated during floral transition and continue into the mature floral stage. Four E-class genes belonging to the *AP1*/*AGL9* superfamily, *OMADS6*, *OMADS7*, *OMADS10* and *OMADS11* have been identified from *Oncidium* Gower Ramsey (Chang et al., 2009). *OMADS6* is expressed in all floral organs except the stamen, and expression patterns of *OMADS7* and *OMADS11* are similar to that of *OMADS6*. Unlike *OMADS6*, *OMADS10* is expressed in vegetative leaves although its transcripts are specifically accumulated in the lip and carpels of mature flowers. Moreover, overexpression of *OMADS6*, *OMADS7* and *OMADS11* resulted in extremely early flowering but *OMADS10* overexpression caused moderately early flowering in *Arabidopsis*. Several *AGL6*-like genes including *EpMADS3*, *EpMADS4* and *EpMADS5* have been identified in *E. pusilla*. They are expressed in floral organs with various expression levels in distinct floral organs suggesting that multiple *AGL6*-like genes may also contribute to the development of floral organs (Dirks-Mulder et al., 2017). Seven E-class genes *CgSEP1*, *2*, *3*, *4* and *CgAGL6-1, -2, -3* were characterized in *C. goeringii* (Xiang et al., 2018). The expression level of *CgSEP1* was increased in the peloric mutant lips and decreased in the peloric mutant sepals. High expression levels of *CgSEP2* and *CgAGL6-1* could be detected in the sepals, but rarely in the lips and columns of the wild-type and the peloric mutant. An increased expression level of *CgSEP3* was noticed in peloric mutant lip-like petals and lips, but expression level of *CgSEP4* was decreased in the peloric mutant lip-like petals and lips. The expression level of *CgAGL6-2* is increased in all floral organs of the wild-type and peloric mutant, but increased level of *CgAGL6-3* could only be detected the in lip and lip-like petals of wild-type and peloric mutant. Based on expression patterns and phenotypic alterations caused by the E-class genes,

it is likely that E-class genes are required for petal, stamen, and carpel formation in both dicot and monocot plants. Of note, a recent report has shown that the greenish flower phenotype of a mutant orchid cultivar in *Habenaria radiata* is due to the absence of SEP (*HrSEP-1*) function (Mitoma and Kanno, 2018). The characterized genes of flower development in orchids are listed in **Table S2** (Aceto and Gaudio, 2011; Mondragon-Palomino, 2013; Teixeira da Silva et al., 2014).

Connective Codes for Perianth Formation

Genetic models related to the regulatory patterning formation of actinomorphic flowers in *Arabidopsis* and *Antirrhinum* are well characterized. However, orchid flowers usually have zygomorphic symmetry with a prominent, well-differentiated labellum in the inner tepals, and it is morphologically distinct from tepals of other angiosperms (Salemme et al., 2011). The perianth formation in orchids cannot be solely explained by the ABCDE model. Many divergent genes with novel functions are responsible for the regulation of perianth formation in orchids. The model "Orchid Code" has been proposed to explain how the various expression levels of duplicated *AP3*/*DEF*-like genes regulate the perianth morphogenesis in orchids (**Figure 2B**) (Mondragon-Palomino and Theissen, 2008; Mondragon-Palomino and Theissen, 2009). In this model, duplicated *DEF*-like paralogous are grouped into four clades phylogenetically and their expression patterns determine the formation of different flower organs. The development of outer tepals (sepal) is regulated by the co-expression of clade 1 (*PeMADS2*-like) and clade 2 (*PeMADS5-like* or *OMADS3*-like) genes whereas the two lateral petals are regulated by the co-expression of clade 1, clade 2 and clade 3 (*PeMADS3*-like) genes. The lip structure is regulated by the co-expression of clade 1, clade 2, clade 3 and clade 4 (*PeMADS4*-like) genes. In contrast, *GLO*-like genes form a single clade and express in all four floral whorls. In other words, the divergent *DEF*-like gene is the key that leads to the morphological diversity of the flowers in orchids. Later, the orchid code model was refined by extensive analysis of *DEF*-like genes in different subfamilies of orchids (Mondragon-Palomino and Theissen, 2011). According to this refined orchid code, four clades of *DEF*-like genes are all expressed in lateral petal and lip. However, lower expression level of clade 3 and clade 4 is displayed in lateral petal whereas lower expression level of clade 1 and clade 2 genes is displayed in the lip. Moreover, a combination of four clade genes with differential expression level may also contribute to the developments of gynostemium and ovary.

Development of different floral organs of orchids has also been proposed by a homeotic orchid tepal (HOT) model (Pan et al., 2011). Twenty-four *AP3*-like genes were identified from 11 species of orchids and grouped into four clades (*PeMADS3*-like, *PeMADS4*-like, *PeMADS2*-like and *PeMADS5*-like). Similar to the orchid code model, the sepal organ expresses *PeMADS2*-like and *PeMADS5*-like genes whereas the lateral petal expresses *PeMADS2*-like, *PeMADS5*-like and *PeMADS3*-like genes. In the lip organ, all four clade genes are expressed. In addition, the HOT model also addresses the temporal change of *PeMADS3*-like and *PeMADS4*-like expressions in different stages of inflorescence development. In the early floral organ primordial stage, they are expressed in all whorl organs. In the late floral organ primordial and floral bud stages, *PeMADS3*-like genes are restricted in petal, lip and column whereas the *PeMADS4*-like genes are restricted in the lip and column. Combinations of *PI*-like genes and other MADS-box genes also determine the identity of lip and column.

Another study also based on the expression analysis proposed a "Perianth code" (P code) hypothesis to explain the floral identity of orchids (**Figure 2B**) (Hsu et al., 2015). Two clades of *AP3*-like genes (*OAP3-1* and *AP3-2*) in *Oncidium* associate with *OPI* and different clades of O*AGL6*-like genes (E-class). Different heterotetradmers determine different organs. The SP (sepal/petal) complex (*OAP3-1*/*OAGL6-1*/*OAGL6-1*/*OPI*) specifies the sepal/petal formation whereas the L (lip) complex (*OAP3-2*/*OAGL6-2*/*OAGL6-2*/*OPI*) is exclusively required for lip formation. The P code model suggests that the diverse E-class genes are also important for development of lip structure of orchids. Diverse roles of E-class genes in floral identity have also been suggested in lily (Tzeng et al., 2003). Two *AGL2*-like genes, *LMADS3* and *LMADS4*, were identified in lily, and they were expressed in all four whorls of floral organs. Ectopic expression of *LMADS3* but bot *LMADS4* in *Arabidopsis* resulted in reduced plant size, early flowering and loss of floral determinacy. In *H. radiata*, two E-class genes (*HrSEP-1* and *HeSEP-2*) were characterized recently (Mitoma and Kanno, 2018). The expression of *HrSEP-1* is lost in a mutant cultivar "Ryokusei" that has greenish petals and a smaller lip in whorl 2, and several septaloid organs and a ventral column in whorls 3 and 4. Moreover, the expression of *HrSEP-2* is up-regulated in Ryokusei. Alternative expressions of B-class genes by silencing of E-class genes have also been revealed in *Phalaenopsis* (Pan et al., 2014). This indicates a feedback regulation between the floral identity genes may also play an important role in the development of floral organs.

All these models specify that the diverse roles of duplicated *AP3*/*DEF*-like and other floral identify genes are important for specialized flower morphogenesis, especially for the lip development of orchid flowers. This idea is supported by the recent study of whole-genome sequencing of *Apostasia shenzhenica*, a genus of Apostasioideae, which is regarded as being phylogenetically plesiomorphic in the orchid family (Zhang et al., 2017). The *Apostasia* has a radially symmetrical (actinomorphic) flower without lip and complex column structures. Comparing *A. shenzhenica* to other subfamilies of Orchidaceae, *A. shenzhenica* seems to have fewer B-class *AP3* genes.

Orchid Biotechnology

Conventional breeding efforts were initiated more than one century ago and helped propel the growth of the ornamental orchid market. In order to obtain profitable horticultural traits, successful breeding usually proceeds by preserving or selecting advantageous parents or progenies. Application of a well-controlled cultivation management system is another important factor for successful commercial orchid farming. In the worldwide market, hundreds and thousands of successful cultivars have been generated using the conventional methods through enthusiastic professional and amateur breeders. The discovery of native

tetraploid *Phalaenopsis* orchids that have better flower shapes and color intensities initiated the creation of numerous significant commercial hybrids through polyploidy breeding. Over the last two decades, a successful program to convert 20 diploid *Phalaenopsis* species to tetraploid has been developed by Chen et al. (2011). This program facilitated a breeding process that feeds the needs of the nursery business. Polyploidization can typically be achieved by introduction of colchicine in many agricultural or horticultural crops including orchids (Griesbach, 1981; Caperta et al., 2006; Azmi et al., 2016; Tuwo and Indrianto, 2016). One of the most successful product series, "Big White Flower," is comprised of tetraploid *Phalaenopsis* hybrids developed through polyploidization with the parents *Phalaenopsis* Doris. Among them, *P.* Sogo Yukidian 'V3' has been very popular in the market. At present, it is still one of the most profitable hybrids in this group. Chen et al. concluded that the importance of polyploidy to the improvement of orchid cultivars may rely on the increase in the number of sets of genes (Chen et al., 2011). The accumulation of additive genetic and heterotic effects of these genes could potentially improve the varieties possible. Currently, polyploidy is still a major technique that drives orchid breeding programs to commercial success. An alternative strategy for polyploid breeding is the phenomenon of unreduced gametes. By analyzing sporad types, Bolaños-Villegas et al. observed a certain percentage of dyads (2n gametes) and suggested the pollination from individual of these dyad may produce polyploid progeny as revealed in other plants (Bolaños-Villegas et al., 2008).

In the 1970s, the creation of recombination DNA molecules brought about revolutionary genetic engineering, also called genetic transformation, which constitutes the direct manipulation of an organism's genome using biotechnology. It is a set of technologies that is used to change genetic makeup, including the transfer of genes within and across species boundaries to produce improved or novel traits. In 2013, the blue *Phalaenopsis* orchids created by the research team of Professor Mii at Chiba University, Japan were exhibited at the 11th Asian Pacific Orchid Conference. These true-blue orchids were genetically transformed using a flavonoid 3',5'-hydroxylase gene derived from *Commelina communis* which was incorporated into the *Phalaenopsis* genome and expressed in the flowers to produce delphinidin, a blue anthocyanin pigment that is also in the flowers of delphinium (larkspur). In 2016, the white *Oncidium* orchids created by a research group from the National Taiwan University, Taiwan were exhibited at the Taiwan International Orchid Show. The genetically engineered white orchids were transformed by a flower specific promotor driving the carotenoid cleavage dioxygenase gene that degrades carotenoids, which led to white petals.

Similar to many other crops, two major transformation systems were successfully used to transport foreign genes into orchid genomes: particle bombardment and *Agrobacterium*-mediated transformation systems. The early genetic transformation studies in orchids were confined to the biolistic-mediated transformation which needed a so-called gene gun to deliver the target genes (Kuehnle and Sugii, 1992; Chia et al., 1994). The first successful genetic transformation reported using the *Agrobacterium*-mediated method was the transfer of *gus* gene into *Phalaenopsis* orchid (Belarmino and Mii, 2000). Many years later, this system also successfully transformed other genera of orchids such as *Dendrobium*, *Cymbidium* and *Oncidium* (Yu et al., 2001; Liau et al., 2003; Chin et al., 2007). Target explants for transformation using protocorms, protocorm-like bodies (PLB) and calluses have been reported so far (Belarmino and Mii, 2000; Mishiba et al., 2005; Chin et al., 2007). Usually, the genetic transformation efficiency has been low for orchid plants and the transformation process is also time-consuming. The general slow growth rate could mean the entire transformation process could take up to 2 or 3 years to reach the stage of two-leaf young plantlets. Recently, a protocol using protocorms that could shorten the transformation process to 8 months was reported for *Phalaenopsis* orchids (Hsing et al., 2016). It will be worth investigating whether a similar time frame can be achieved in other orchid genera. Genome editing, a new and revolutionary genetic engineering technology, is an approach in which a specific target DNA sequence of the genome is altered by adding, removing, or replacing DNA bases in a highly precise manner (Gaj et al., 2013). One particular tool, the CRISPR/Cas system has been developed at an accelerated pace. The application of the CRISPR/Cas system to create engineered crops or plants has yielded fruitful results for further investigation. The technology development and application have been widely reviewed (Bortesi and Fischer, 2015; Yin et al., 2017). One crucial criterion to precisely edit orchid genomes is to rely heavily on the availability of the whole genome sequence information. We predict that the combination of the genome editing technology with bioinformatics analyses will create revolutionary breeding programs for orchid research and development in the future.

PERSPECTIVES

For annual plants such as *Arabidopsis*, rice and wheat, precise control of flowering time in response to environmental cues is necessary for successful reproduction. For perennial plants like orchids, the flowering network may not be so complicated since vernalization is not required and the effect of photoperiod is limited. The changes in ambient temperature may play a more important role in the regulation of floral transition in orchids. Recently, regulations of microRNAs and anti-florigens such as *TFL1* have been shown to be involved in the flowering control of *A. alpina*, a perennial relative of *A. thaliana* (Wang et al., 2011a; Bergonzi et al., 2013). Although further investigation is required to discover whether orchid *TFL1* also plays a negative role in flowering in orchids, it is no exaggeration to say that *TFL1* may regulate the dormancy of juvenile axillary buds in the flowering season of orchids. Furthermore, regulation of *PHYTOCHROME INTERACTING FACTOR 4* (*PIF4*) *via* phytohormone pathways and sugar metabolism may also be involved (Kumar et al., 2012; Bolouri Moghaddam and Van den Ende, 2013). Flower development studies revealed that multiplicated floral homeotic genes (**Table S2**) are the basis of the specific morphology of orchids (**Figure 2**). However, how the high order complex of these proteins regulates floral organ identity needs to be further investigated. In addition, the feedback regulation between different floral homeotic genes needs further investigation to explain the floral development of orchids in detail. The A and E-class genes are involved in both

floral initiation and flower development. It will be interesting to investigate whether A and E-class genes regulate the expressions of other MADS-box genes. Finally, further advances in functional studies on key genes for flowering/flower development may rely on a breakthrough in orchid transformation technology which leads to more efficient results. Recently, the genome sequences of several orchids have been determined. Understanding of the flowering control and flower development of the CAM-using plants may provide an insightful view into plant evolution.

AUTHOR CONTRIBUTIONS

All the authors wrote and reviewed the manuscript.

FUNDING

This work was supported in part by grants from World Vegetable Center Korea Office (WKO #10000379) and core donors to the World Vegetable Center: Republic of China (ROC), UK aid from the UK government, United States Agency for International Development (USAID), Australian Center for International Agricultural Research (ACIAR), Germany, Thailand, Philippines, Korea and Japan and, a grant from the Ministry of Science and Technology, Taiwan (MOST 106-2321-B-020-002-) to F-C. C. and a grant from Council of Agriculture, Taiwan (COA 106AS-8.6.3-FD-Z1(1)) to F-C. C.

ACKNOWLEDGMENTS

The authors are grateful to Miranda Loney for English editing.

SUPPLEMENTARY MATERIAL

The Supplementary Material for this article can be found online at: https://www.frontiersin.org/articles/10.3389/fpls.2019.01258/full#supplementary-material

REFERENCES

Aceto, S., and Gaudio, L. (2011). The MADS and the beauty: genes involved in the development of orchid flowers. *Curr. Genomics* 12 (5), 342–356. doi: 10.2174/138920211796429754

Acri-Nunes-Miranda, R., and Mondragon-Palomino, M. (2014). Expression of paralogous SEP-, FUL-, AG- and STK-like MADS-box genes in wild-type and peloric *Phalaenopsis* flowers. *Front. Plant Sci.* 5, 76. doi: 10.3389/fpls.2014.00076

Akita, Y., Horikawa, Y., and Kanno, A. (2008). Comparative analysis of floral MADS-box genes between wild-type and a putative homeotic mutant in lily. *J. Hortic. Sci. Biotechnol.* 83 (4), 453–461. doi: 10.1080/14620316.2008.11512406

Azmi, T. K. K., Sukma, D., Aziz, S. A., and Syukur, M. (2016). Polyploidy induction of moth orchid (*Phalaenopsis* amabilis (L.) Blume) by colchicine treatment on pollinated flowers. *J. Agric. Sci.* 11 (2), 62. doi: 10.4038/jas.v11i2.8118

Belarmino, M. M., and Mii, M. (2000). Agrobacterium-mediated genetic transformation of a *Phalaenopsis* orchid. *Plant Cell Rep.* 19, 435–442. doi: 10.1007/s002990050752

Benedito, V. A., Visser, P. B., van Tuyl, J. M., Angenent, G. C., de Vries, S. C., and Krens, F. A. (2004). Ectopic expression of LLAG1, an AGAMOUS homologue from lily (Lilium longiflorum Thunb.) causes floral homeotic modifications in *Arabidopsis*. *J. Exp. Bot.* 55 (401), 1391–1399. doi: 10.1093/jxb/erh156

Bergonzi, S., Albani, M. C., Ver Loren van Themaat, E., Nordstrom, K. J., Wang, R., Schneeberger, K., et al. (2013). Mechanisms of age-dependent response to winter temperature in perennial flowering of Arabis alpina. *Science* 340 (6136), 1094–1097. doi: 10.1126/science.1234116

Blanchard, M. G., and Runkle, E. S. (2006). Temperature during the day, but not during the night, controls flowering of *Phalaenopsis* orchids. *J. Exp. Bot.* 57 (15), 4043–4049. doi: 10.1093/jxb/erl176

Blanchard, M. G., and Runkle, E. S. (2008). Benzyladenine promotes flowering in Doritaenopsis and *Phalaenopsis* orchids. *J. Plant Growth Regul.* 27 (2), 141–150. doi: 10.1007/s00344-008-9040-0

Bolaños-Villegas, P., Chin, S.-W., and Chen, F.-C. (2008). Meiotic chromosome behavior and capsule setting in Doritaenopsis hybrids. *J. Am. Soc. Hortic. Sci.* 133, 107–116. doi: 10.21273/JASHS.133.1.107

Bolouri Moghaddam, M. R., and Van den Ende, W. (2013). Sugars, the clock and transition to flowering. *Front. Plant Sci.* 4, 22. doi: 10.3389/fpls.2013.00022

Bortesi, L., and Fischer, R. (2015). The CRISPR/Cas9 system for plant genome editing and beyond. *Biotechnol. Adv.* 33 (1), 41–52. doi: 10.1016/j.biotechadv.2014.12.006

Callens, C., Tucker, M. R., Zhang, D., and Wilson, Z. A. (2018). Dissecting the role of MADS-box genes in monocot floral development and diversity. *J. Exp. Bot.* 69 (10), 2435–2459. doi: 10.1093/jxb/ery086

Campos, K. O., and Kerbauy, G. B. (2004). Thermoperiodic effect on flowering and endogenous hormonal status in Dendrobium (Orchidaceae). *J. Plant Physiol.* 161 (12), 1385–1387. doi: 10.1016/j.jplph.2004.07.008

Caperta, A. D., Delgado, M., Ressurreicao, F., Meister, A., Jones, R. N., Viegas, W., et al. (2006). Colchicine-induced polyploidization depends on tubulin polymerization in c-metaphase cells. *Protoplasma* 227 (2–4), 147–153. doi: 10.1007/s00709-005-0137-z

Chang, Y. Y., Chiu, Y. F., Wu, J. W., and Yang, C. H. (2009). Four orchid (Oncidium Gower Ramsey) AP1/AGL9-like MADS box genes show novel expression patterns and cause different effects on floral transition and formation in Arabidopsis thaliana. *Plant Cell Physiol.* 50 (8), 1425–1438. doi: 10.1093/pcp/pcp087

Chang, Y. Y., Kao, N. H., Li, J. Y., Hsu, W. H., Liang, Y. L., Wu, J. W., et al. (2010). Characterization of the possible roles for B class MADS box genes in regulation of perianth formation in orchid. *Plant Physiol.* 152 (2), 837–853. doi: 10.1104/pp.109.147116

Chao, Y. T., Yen, S. H., Yeh, J. H., Chen, W. C., and Shih, M. C. (2017). Orchidstra 2.0—A transcriptomics resource for the orchid family. *Plant Cell Physiol.* 58 (1), e9. doi: 10.1093/pcp/pcw220

Chen, D., Guo, B., Hexige, S., Zhang, T., Shen, D., and Ming, F. (2007). SQUA-like genes in the orchid *Phalaenopsis* are expressed in both vegetative and reproductive tissues. *Planta* 226 (2), 369–380. doi: 10.1007/s00425-007-0488-0

Chen, M. K., Hsieh, W. P., and Yang, C. H. (2012a). Functional analysis reveals the possible role of the C-terminal sequences and PI motif in the function of lily (Lilium longiflorum) PISTILLATA (PI) orthologues. *J. Exp. Bot.* 63 (2), 941–961. doi: 10.1093/jxb/err323

Chen, M. K., Lin, I. C., and Yang, C. H. (2008). Functional analysis of three lily (Lilium longiflorum) APETALA1-like MADS box genes in regulating floral transition and formation. *Plant Cell Physiol.* 49 (5), 704–717. doi: 10.1093/pcp/pcn046

Chen, W.-H., Kao, Y.-L., Tang, C.-Y., and Jean, G.-T. (2011). "Endopolyploidy in *Phalaenopsis* orchids and its application in polyploid breeding," in *Orchid Biotechnology II*. Eds. W. H. Chen and H. H. Chen (Singapore: World Scientific), 25–48. doi: 10.1142/9789814327930_0002

Chen, W., Qin, Q., Zhang, C., Zheng, Y., Wang, C., Zhou, M., et al. (2015). DhEFL2, 3 and 4, the three EARLY FLOWERING4-like genes in a Doritaenopsis hybrid regulate floral transition. *Plant Cell Rep.* 34 (12), 2027–2041. doi: 10.1007/s00299-015-1848-z

Chen, Y. T., Chang, C. C., Chen, C. W., Kuan, C. C., Wei, Y. C. (2019). MADS-box gene classification in Angiosperms by clustering and machine learning approaches. *Front. Genet.* 9, 707. doi: 10.3389/fgene.2018.00707

Chen, Y. Y., Lee, P. F., Hsiao, Y. Y., Wu, W. L., Pan, Z. J., Lee, Y. I., et al. (2012b). C- and D-class MADS-box genes from *Phalaenopsis* equestris (Orchidaceae) display functions in gynostemium and ovule development. *Plant Cell Physiol.* 53 (6), 1053–1067. doi: 10.1093/pcp/pcs048

Chia, T.-F., Chan, Y.-S., and Chua, N.-H. (1994). The firefly luciferase gene as a non-invasive reporter for Dendrobium transformation. *The Plant Journal* 6, 441–446. doi: 10.1046/j.1365-313X.1994.06030441.x

Chin, D. C., Hsieh, C. C., Lin, H. Y., and Yeh, K. W. (2016). A low glutathione redox state couples with a decreased ascorbate redox ratio to accelerate flowering in Oncidium orchid. *Plant Cell Physiol.* 57 (2), 423–436. doi: 10.1093/pcp/pcv206

Chin, D. C., Shen, C. H., SenthilKumar, R., and Yeh, K. W. (2014). Prolonged exposure to elevated temperature induces floral transition via up-regulation of cytosolic ascorbate peroxidase 1 and subsequent reduction of the ascorbate redox ratio in Oncidium hybrid orchid. *Plant Cell Physiol.* 55 (12), 2164–2176. doi: 10.1093/pcp/pcu146

Chin, D. P., Mishiba, K., and Mii, M. (2007). *Agrobacterium*-mediated transformation of protocorm-like bodies in *Cymbidium*. *Plant Cell Rep.* 26 (6), 735–743. doi: 10.1007/s00299-006-0284-5

Cubas, P. (2004). Floral zygomorphy, the recurring evolution of a successful trait. *Bioessays* 26 (11), 1175–1184. doi: 10.1002/bies.20119

Cui, R., Han, J., Zhao, S., Su, K., Wu, F., Du, X., et al. (2010). Functional conservation and diversification of class E floral homeotic genes in rice (*Oryza sativa*). *Plant J.* 61, 767–781. doi: 10.1111/j.1365-313X.2009.04101.x

Ding, L., Wang, Y., and Yu, H. (2013). Overexpression of DOSOC1, an ortholog of *Arabidopsis* SOC1, promotes flowering in the orchid *Dendrobium* Chao parya smile. *Plant Cell Physiol.* 54 (4), 595–608. doi: 10.1093/pcp/pct026

Dirks-Mulder, A., Butot, R., van Schaik, P., Wijnands, J. W., van den Berg, R., Krol, L., et al. (2017). Exploring the evolutionary origin of floral organs of Erycina pusilla, an emerging orchid model system. *BMC Evol. Biol.* 17 (1), 89. doi: 10.1186/s12862-017-0938-7

Ditta, G., Pinyopich, A., Robles, P., Pelaz, S., and Yanofsky, M. F. (2004). The *SEP4* gene of *Arabidopsis thaliana* functions in floral organ and meristem identity. *Curr. Biol.* 14, 1935–1940. doi: 10.1016/j.cub.2004.10.028

Doyle, M. R., Davis, S. J., Bastow, R. M., McWatters, H. G., Kozma-Bognar, L., Nagy, F., et al. (2002). The ELF4 gene controls circadian rhythms and flowering time in *Arabidopsis thaliana*. *Nature* 419 (6902), 74–77. doi: 10.1038/nature00954

Freudenstein, J. V., and Chase, M. W. (2015). Phylogenetic relationships in Epidendroideae (Orchidaceae), one of the great flowering plant radiations: progressive specialization and diversification. *Ann. Bot.* 115 (4), 665–681. doi: 10.1093/aob/mcu253

Gaj, T., Gersbach, C. A., and Barbas, C. F. (2013). ZFN, TALEN, and CRISPR/Cas-based methods for genome engineering. *Trends Biotechnol* 31 (7), 397–405. doi: 10.1016/j.tibtech.2013.04.004

Goh, C. J., and Yang, A. L. (1978). Effects of growth regulators and decapitation on flowering of Dendrobium orchid hybrids. *Plant Sci. Lett.* 12, 278–292. doi: 10.1016/0304-4211(78)90080-9

Griesbach, R. J. (1981). Colchicine-induced polyploidy in Phanalenopsis orchid. *Plant Cell Tissue Organ Cult.* 1, 103–107. doi: 10.1007/BF02318909

Guo, B., Zhang, T., Shi, J., Chen, D., Shen, D., and Ming, F. (2008). Cloning and characterization of a novel PI-like MADS-box gene in Phalaenopsis orchid. *DNA Seq.* 19 (3), 332–339. doi: 10.1080/10425170701606193

He, Y. (2009). Control of the transition to flowering by chromatin modifications. *Mol. Plant.* 2 (4), 554–564. doi: 10.1093/mp/ssp005

Heijmans, K., Ament, K., Rijpkema, A. S., Zethof, J., Wolters-Arts, M., Gerats, T., et al. (2012). Redefining C and D in the petunia ABC. *Plant Cell* 24 (6), 2305–2317. doi: 10.1105/tpc.112.097030

Hew, C. S., and Clifford, P. E. (1993). Plant growth regulator and orchid cut-flower industry. *Plant Growth Regul.* 13, 231–239. doi: 10.1007/BF00024843

Hou, C. J., and Yang, C. H. (2009). Functional analysis of FT and TFL1 orthologs from orchid (Oncidium Gower Ramsey) that regulate the vegetative to reproductive transition. *Plant Cell Physiol.* 50 (8), 1544–1557. doi: 10.1093/pcp/pcp099

Hsiao, Y. Y., Pan, Z. J., Hsu, C. C., Yang, Y. P., Hsu, Y. C., Chuang, Y. C., et al. (2011). Research on orchid biology and biotechnology. *Plant Cell Physiol.* 52 (9), 1467–1486. doi: 10.1093/pcp/pcr100

Hsing, H. X., Lin, Y. J., Tong, C. G., Li, M. J., Chen, Y. J., and Ko, S. S. (2016). Efficient and heritable transformation of Phalaenopsis orchids. *Bot. Stud.* 57 (1), 30. doi: 10.1186/s40529-016-0146-6

Hsu, H.-F., Hsu, W.-H., Lee, Y.-I., Mao, W.-T., Yang, J.-Y., Li, J.-Y., et al. (2015). Model for perianth formation in orchids. *Nat. Plant* 1, 1–8. doi: 10.1038/nplants.2015.46

Hsu, H. F., Hsieh, W. P., Chen, M. K., Chang, Y. Y., and Yang, C. H. (2010). C/D class MADS box genes from two monocots, orchid (*Oncidium* Gower Ramsey) and lily (*Lilium longiflorum*), exhibit different effects on floral transition and formation in Arabidopsis thaliana. *Plant Cell Physiol.* 51 (6), 1029–1045. doi: 10.1093/pcp/pcq052

Hsu, H. F., Huang, C. H., Chou, L. T., and Yang, C. H. (2003). Ectopic expression of an orchid (*Oncidium* Gower Ramsey) AGL6-like gene promotes flowering by activating flowering time genes in Arabidopsis thaliana. *Plant Cell Physiol.* 44 (8), 783–794. doi: 10.1093/pcp/pcg099

Hsu, H. F., and Yang, C. H. (2002). An orchid (Oncidium Gower Ramsey) AP3-like MADS gene regulates floral formation and initiation. *Plant Cell Physiol.* 43 (10), 1198–1209. doi: 10.1093/pcp/pcf143

Huang, J. Z., Lin, C. P., Cheng, T. C., Huang, Y. W., Tsai, Y. J., Cheng, S. Y., et al. (2016). The genome and transcriptome of Phalaenopsis yield insights into floral organ development and flowering regulation. *PeerJ* 4, e2017. doi: 10.7717/peerj.2017

Jack, T. (2001). Plant development going MADS. *Plant Mol. Biol.* 46 (5), 515–520. doi: 10.1023/A:1010689126632

Jang, S. (2015). Functional characterization of PhapLEAFY, a FLORICAULA/LEAFY Ortholog in Phalaenopsis aphrodite. *Plant Cell Physiol.* 56 (11), 2234–2247. doi: 10.1093/pcp/pcv130

Jang, S., Choi, S. C., Li, H. Y., An, G., and Schmelzer, E. (2015). Functional characterization of Phalaenopsis aphrodite flowering genes PaFT1 and PaFD. *PLoS One* 10 (8), e0134987. doi: 10.1371/journal.pone.0134987

Jetha, K., Theissen, G., and Melzer, R. (2014). *Arabidopsis* SEPALLATA proteins differ in cooperative DNA-binding during the formation of floral quartet-like complexes. *Nucleic Acids Res.* 42 (17), 10927–10942. doi: 10.1093/nar/gku755

Kaewphalug, W., Huehne, P. S., and Sriboonlert, A. (2017). Characterization of a CONSTANS-like gene from Pigeon orchid (*Dendrobium crumenatum* Swartz) and its expression under different photoperiod conditions. *Hortic. J.* 86 (2), 252–262. doi: 10.2503/hortj.MI-123

Kim, S.-Y., Yun, P.-Y., Fukuda, T., Ochiai, T., Yokoyama, J., Kameya, T., et al. (2007). Expression of a DEFICIENS-like gene correlates with the differentiation between sepal and petal in the orchid, Habenaria radiata (Orchidaceae). *Plant Sci.* 172 (2), 319–326. doi: 10.1016/j.plantsci.2006.09.009

Koh, K. W., Lee, S. H., Chen, H. K., Chang, C. Y., and Chan, M. T. (2018). Phalaenopsis flowering locus VE regulates floral organ maturation. *Plant Cell Rep.* 37 (3), 467–482. doi: 10.1007/s00299-017-2243-8

Kramer, E. M., Jaramillo, M. A., and Di Stilio, V. S. (2004). Patterns of gene duplication and functional evolution during the diversification of the AGAMOUS subfamily of MADS box genes in angiosperms. *Genetics* 166 (2), 1011–1023. doi: 10.1534/genetics.166.2.1011

Kuehnle, A. R., and Sugii, N. (1992). Transformation of Dendrobium orchid using particle bombardment of protocorms. *Plant Cell Rep.* 11 (9), 484–488. doi: 10.1007/BF00232696

Kumar, S. V., Lucyshyn, D., Jaeger, K. E., Alos, E., Alvey, E., Harberd, N. P., et al. (2012). Transcription factor PIF4 controls the thermosensory activation of flowering. *Nature* 484 (7393), 242–245. doi: 10.1038/nature10928

Lee, J. H., Ryu, H. S., Chung, K. S., Pose, D., Kim, S., Schmid, M., et al. (2013). Regulation of temperature-responsive flowering by MADS-box transcription factor repressors. *Science* 342 (6158), 628–632. doi: 10.1126/science.1241097

Li, D. M., Lu, F. B., Zhu, G. F., Sun, Y. B., Xu, Y. C., Jiang, M. D., et al. (2014). Identification of warm day and cool night conditions induced flowering-related genes in a Phalaenopsis orchid hybrid by suppression subtractive hybridization. *Genet. Mol. Res.* 13 (3), 7037–7051. doi: 10.4238/2014.February.14.7

Li, R., Wang, A., Sun, S., Liang, S., Wang, X., Ye, Q., et al. (2012). Functional characterization of FT and MFT ortholog genes in orchid (Dendrobium nobile Lindl) that regulate the vegetative to reproductive transition in *Arabidopsis*. *Plant Cell Tissue Organ Cult. (PCTOC)* 111 (2), 143–151. doi: 10.1007/s11240-012-0178-x

Li, W., Liu, X., and Lu, Y. (2016). Transcriptome comparison reveals key candidate genes in response to vernalization of Oriental lily. *BMC Genomics* 17, 664. doi: 10.1186/s12864-016-2955-0

Li, X., Luo, J., Yan, T., Xiang, L., Jin, F., Qin, D., et al. (2013). Deep sequencing-based analysis of the Cymbidium ensifolium floral transcriptome. *PLoS One* 8 (12), e85480. doi: 10.1371/journal.pone.0085480

Liau, C. H., You, S. J., Prasad, V., Hsiao, H. H., Lu, J. C., Yang, N. S., et al. (2003). Agrobacterium tumefaciens-mediated transformation of an Oncidium orchid. *Plant Cell Rep.* 21 (10), 993–998. doi: 10.1007/s00299-003-0614-9

Lin, C. S., Hsu, C. T., Liao, D. C., Chang, W. J., Chou, M. L., Huang, Y. T., et al. (2016). Transcriptome-wide analysis of the MADS-box gene family in the orchid Erycina pusilla. *Plant Biotechnol. J.* 14 (1), 284–298. doi: 10.1111/pbi.12383

Lopez, R. G., and Runkle, E. S. (2006). Temperature and photoperiod regulate flowering of potted Miltoniopsis Orchids. *Hortscience* 41, 593–597. doi: 10.21273/HORTSCI.41.3.593

Lopez, R. G., Runkle, E. S., Heins, R. D., and Whitman, C. M. (2003). Temperature and photoperiodic effects on growth and flowering of Zygopetalum redvale 'Fire Kiss' orchid. *Acta Hortic.* 624, 155–162. doi: 10.17660/ActaHortic.2003.624.20

Lu, Z. X., Wu, M., Loh, C. S., Yeong, C. Y., and Goh, C. J. (1993). Nucleotide sequence of a flower-specific MADS box cDNA clone from orchid. *Plant Mol. Biol.* 23 (4), 901–904. doi: 10.1007/BF00021545

Luo, X., Zhang, C., Sun, X., Qin, Q., Zhou, M., Paek, K. Y., et al. (2011). Isolation and characterization of a Doritaenopsis hybrid GIGANTEA gene, which possibly involved in inflorescence initiation at low temperatures. *Korean J. Hortic. Sci. Technol.* 29, 135–143.

Mishiba, K., Chin, D. P., and Mii, M. (2005). Agrobacterium-mediated transformation of Phalaenopsis by targeting protocorms at an early stage after germination. *Plant Cell Rep.* 24 (5), 297–303. doi: 10.1007/s00299-005-0938-8

Mitoma, M., and Kanno, A. (2018). The greenish flower phenotype of Habenaria radiata (Orchidaceae) is caused by a mutation in the SEPALLATA-Like MADS-Box gene HrSEP-1. *Front. Plant Sci.* 9, 831. doi: 10.3389/fpls.2018.00831

Mondragon-Palomino, M. (2013). Perspectives on MADS-box expression during orchid flower evolution and development. *Front. Plant Sci.* 4, 377. doi: 10.3389/fpls.2013.00377

Mondragon-Palomino, M., and Theissen, G. (2008). MADS about the evolution of orchid flowers. *Trends Plant Sci.* 13 (2), 51–59. doi: 10.1016/j.tplants.2007.11.007

Mondragon-Palomino, M., and Theissen, G. (2009). Why are orchid flowers so diverse? Reduction of evolutionary constraints by paralogues of class B floral homeotic genes. *Ann. Bot.* 104 (3), 583–594. doi: 10.1093/aob/mcn258

Mondragon-Palomino, M., and Theissen, G. (2011). Conserved differential expression of paralogous DEFICIENS- and GLOBOSA-like MADS-box genes in the flowers of Orchidaceae: refining the 'orchid code'. *Plant J.* 66 (6), 1008–1019. doi: 10.1111/j.1365-313X.2011.04560.x

Pan, Z. J., Chen, Y. Y., Du, J. S., Chen, Y. Y., Chung, M. C., Tsai, W. C., et al. (2014). Flower development of Phalaenopsis orchid involves functionally divergent SEPALLATA-like genes. *New Phytol.* 202 (3), 1024–1042. doi: 10.1111/nph.12723

Pan, Z. J., Cheng, C. C., Tsai, W. C., Chung, M. C., Chen, W. H., Hu, J. M., et al. (2011). The duplicated B-class MADS-box genes display dualistic characters in orchid floral organ identity and growth. *Plant Cell Physiol.* 52 (9), 1515–1531. doi: 10.1093/pcp/pcr092

Peakall, R. (2007). Speciation in the Orchidaceae: confronting the challenges. *Mol. Ecol.* 16 (14), 2834–2837. doi: 10.1111/j.1365-294X.2007.03311.x

Pelaz, S., Ditta, G. S., Baumann, E., Wisman, E., and Yanofsky, M. F. (2000). B and C floral organ identity functions require SEPALLATA MADS-box genes. *Nature* 405, 200–203. doi: 10.1038/35012103

Purugganan, M. D., Rounsley, S. D., Schmidt, R. J., and Yanofsky, M. F. (1995). Molecular evolution of flower development: diversification of the plant MADS-box regulatory gene family. *Genetics* 140 (1), 345–356.

Sakanishi, Y., Imanishi, H., and Ishida, G. (1980). Effect of temperature on growth and flowering of Phalaenopsis amabilis. *Bull. Univ. Osaka Prefect. Ser. B* 32, 1–9.

Salemme, M., Sica, M., Gaudio, L., and Aceto, S. (2011). Expression pattern of two paralogs of the PI/GLO-like locus during Orchis italica (Orchidaceae, Orchidinae) flower development. *Dev. Genes Evol.* 221 (4), 241–246. doi: 10.1007/s00427-011-0372-6

Salemme, M., Sica, M., Gaudio, L., and Aceto, S. (2013). The OitaAG and OitaSTK genes of the orchid Orchis italica: a comparative analysis with other C- and D-class MADS-box genes. *Mol. Biol. Rep.* 40 (5), 3523–3535. doi: 10.1007/s11033-012-2426-x

Sawa, M., Nusinow, D. A., Kay, S. A., and Imaizumi, T. (2007). FKF1 and GIGANTEA complex formation is required for day-length measurement in Arabidopsis. *Science* 318 (5848), 261–265. doi: 10.1126/science.1146994

Sawettalake, N., Bunnag, S., Wang, Y., Shen, L., and Yu, H. (2017). DOAP1 promotes flowering in the orchid Dendrobium Chao Praya Smile. *Front. Plant Sci.* 8, 400. doi: 10.3389/fpls.2017.00400

Shige-Hiro, S., Yukiko, Y., Suzuha, O., Wakana, T., and Hiro-, Y. H. (2019). Rice flower development revisited: regulation of carpel specification and flower meristem determinacy. *Plant Cell Physiol.* 60 (6), 1284–1295. doi: 10.1093/pcp/pcz020

Silvera, K., Santiago, L. S., Cushman, J. C., and Winter, K. (2009). Crassulacean acid metabolism and epiphytism linked to adaptive radiations in the Orchidaceae. *Plant Physiol.* 149 (4), 1838–1847. doi: 10.1104/pp.108.132555

Skipper, M., Johansen, L. B., Pedersen, K. B., Frederiksen, S., and Johansen, B. B. (2006). Cloning and transcription analysis of an AGAMOUS- and SEEDSTICK ortholog in the orchid Dendrobium thyrsiflorum (Reichb. f.). *Gene* 366 (2), 266–274. doi: 10.1016/j.gene.2005.08.014

Skipper, M., Pedersen, K. B., Johansen, L. B., Frederiksen, S., Irish, V. F., and Johansen, B. B. (2005). Identification and quantification of expression levels of three FRUITFULL-like MADS-box genes from the orchid Dendrobium thyrsiflorum (Reichb. f.). *Plant Sci.* 169 (3), 579–586. doi: 10.1016/j.plantsci.2005.04.011

Song, I. J., Nakamura, T., Fukuda, T., Yokoyama, J., Ito, T., Ichikawa, H., et al. (2006). Spatiotemporal expression of duplicate AGAMOUS orthologues during floral development in Phalaenopsis. *Dev. Genes Evol.* 216 (6), 301–313. doi: 10.1007/s00427-005-0057-0

Song, Y. H. (2016). The effect of fluctuations in photoperiod and ambient temperature on the timing of flowering: time to move on natural environmental conditions. *Mol. Cells* 39 (10), 715–721. doi: 10.14348/molcells.2016.0237

Su, C. L., Chen, W. C., Lee, A. Y., Chen, C. Y., Chang, Y. C., Chao, Y. T., et al. (2013). A modified ABCDE model of flowering in orchids based on gene expression profiling studies of the moth orchid Phalaenopsis aphrodite. *PLoS One* 8 (11), e80462. doi: 10.1371/journal.pone.0080462

Su, W. R., Chen, W. S., Koshioka, M., Mander, L. N., and Hung, L. S. (2001). Changes in gibberellin levels in the flowering shoot of *Phalaenopsis hybrida* under high temperature conditions when flower development is blocked. *Plant Physiol. Biochem.* 39, 45–50. doi: 10.1016/S0981-9428(00)01218-3

Sun, C., Chen, D., Fang, J., Wang, P., Deng, X., and Chu, C. (2014). Understanding the genetic and epigenetic architecture in complex network of rice flowering pathways. *Protein Cell* 5 (12), 889–898. doi: 10.1007/s13238-014-0068-6

Sun, X., Qin, Q., Zhang, J., Zhang, C., Zhou, M., Paek, K. Y., et al. (2012). Isolation and characterization of the FVE gene of a Doritaenopsis hybrid involved in the regulation of flowering. *Plant Growth Regul.* 68 (1), 77–86. doi: 10.1007/s10725-012-9695-1

Sureshkumar, S., Dent, C., Seleznev, A., Tasset, C., and Balasubramanian, S. (2016). Nonsense-mediated mRNA decay modulates FLM-dependent thermosensory flowering response in Arabidopsis. *Nat. Plants* 2 (5), 16055. doi: 10.1038/nplants.2016.55

Teixeira da Silva, J. A., Aceto, S., Liu, W., Yu, H., and Kanno, A. (2014). Genetic control of flower development, color and senescence of Dendrobium orchids. *Sci. Hortic.* 175, 74–86. doi: 10.1016/j.scienta.2014.05.008

Theissen, G. (2001). Development of floral organ identity: stories from the MADS house. *Curr. Opin. Plant Biol.* 4 (1), 75–85. doi: 10.1016/S1369-5266(00)00139-4

Theissen, G., Becker, A., Di Rosa, A., Kanno, A., Kim, J. T., Munster, T., et al. (2000). A short history of MADS-box genes in plants. *Plant Mol. Biol.* 42 (1), 115–149. doi: 10.1023/A:1006332105728

Theissen, G., and Melzer, R. (2007). Molecular mechanisms underlying origin and diversification of the angiosperm flower. *Ann. Bot.* 100 (3), 603–619. doi: 10.1093/aob/mcm143

Tsai, W. C., Kuoh, C. S., Chuang, M. H., Chen, W. H., and Chen, H. H. (2004). Four DEF-like MADS box genes displayed distinct floral morphogenetic roles in Phalaenopsis orchid. *Plant Cell Physiol.* 45 (7), 831–844. doi: 10.1093/pcp/pch095

Tsai, W. C., Lee, P. F., Chen, H. I., Hsiao, Y. Y., Wei, W. J., Pan, Z. J., et al. (2005). PeMADS6, a GLOBOSA/PISTILLATA-like gene in Phalaenopsis equestris involved in petaloid formation, and correlated with flower longevity and ovary development. *Plant Cell Physiol.* 46 (7), 1125–1139. doi: 10.1093/pcp/pci125

Tsai, W. C., Pan, Z. J., Hsiao, Y. Y., Jeng, M. F., Wu, T. F., Chen, W. H., et al. (2008). Interactions of B-class complex proteins involved in tepal development in Phalaenopsis orchid. *Plant Cell Physiol.* 49 (5), 814–824. doi: 10.1093/pcp/pcn059

Tuwo, M., and Indrianto, A. (2016). Improvement of orchid Vanda hybrid (Vanda limbata Blume X Vanda tricolor Lindl. var. suavis) by colchicines treatment in vitro. *Modern Appl. Sci.* 10 (11), 83. doi: 10.5539/mas.v10n11p83

Tzeng, T. Y., Chen, H. Y., and Yang, C. H. (2002). Ectopic expression of carpel-specific MADS box genes from lily and lisianthus causes similar homeotic conversion of sepal and petal in *Arabidopsis*. *Plant Physiol.* 130 (4), 1827–1836. doi: 10.1104/pp.007948

Tzeng, T. Y., Hsiao, C. C., Chi, P. J., and Yang, C. H. (2003). Two lily SEPALLATA-like genes cause different effects on floral formation and floral transition in *Arabidopsis*. *Plant Physiol.* 133 (3), 1091–1101. doi: 10.1104/pp.103.026997

Tzeng, T. Y., and Yang, C. H. (2001). A MADS box gene from lily (Lilium longiflorum) is sufficient to generate dominant negative mutation by interacting with PISTILLATA (PI) in *Arabidopsis thaliana*. *Plant Cell Physiol.* 42 (10), 1156–1168. doi: 10.1093/pcp/pce151

Vaz, A. P., Figueiredo-Ribeiro Rd Rde, C., and Kerbauy, G. B. (2004). Photoperiod and temperature effects on in vitro growth and flowering of P. pusilla, an epiphytic orchid. *Plant Physiol. Biochem.* 42 (5), 411–415. doi: 10.1016/j.plaphy.2004.03.008

Villacorta-Martin, C., Nunez de Caceres Gonzalez, F. F., de Haan, J., Huijben, K., Passarinho, P., Lugassi-Ben Hamo, M., et al. (2015). Whole transcriptome profiling of the vernalization process in Lilium longiflorum (cultivar White Heaven) bulbs. *BMC Genomics* 16, 550. doi: 10.1186/s12864-015-1675-1

Wang, R., Albani, M. C., Vincent, C., Bergonzi, S., Luan, M., Bai, Y., et al. (2011a). Aa TFL1 confers an age-dependent response to vernalization in perennial Arabis alpina. *Plant Cell* 23 (4), 1307–1321. doi: 10.1105/tpc.111.083451

Wang, S. Y., Lee, P. F., Lee, Y. I., Hsiao, Y. Y., Chen, Y. Y., Pan, Z. J., et al. (2011b). Duplicated C-class MADS-box genes reveal distinct roles in gynostemium development in Cymbidium ensifolium (Orchidaceae). *Plant Cell Physiol.* 52 (3), 563–577. doi: 10.1093/pcp/pcr015

Wang, W.-Y., Chen, W.-S., Chen, W.-H., Huang, L.-S., and Chang, P.-S. (2002). Influence of abscisic acid on flowering in Phalaenopsis hybrida. *Plant Physiol. Biochem.* 40, 97–100. doi: 10.1016/S0981-9428(01)01339-0

Wang, W.-Y., Chen, W.-S., Huang, K.-L., Huang, L.-S., Chen, W.-H., and Su, W.-R. (2003). The effects of daylength on protein synthesis and flowering in Doritis pulcherrima. *Sci. Hortic.* 97, 49–56. doi: 10.1016/S0304-4238(02)00128-0

Wen, Z., Guo, W., Li, J., Lin, H., He, C., Liu, Y., et al. (2017). Comparative transcriptomic analysis of vernalization- and cytokinin-induced floral transition in Dendrobium nobile. *Sci. Rep.* 7, 45748. doi: 10.1038/srep45748

Xiang, L., Chen, Y., Chen, L., Fu, X., Zhao, K., Zhang, J., et al. (2018). B and E MADS-box genes determine the perianth formation in Cymbidium goeringii Rchb.f. *Physiol. Plant* 162 (3), 353–369. doi: 10.1111/ppl.12647

Xu, Y., Teo, L. L., Zhou, J., Kumar, P. P., and Yu, H. (2006). Floral organ identity genes in the orchid Dendrobium crumenatum. *Plant J.* 46 (1), 54–68. doi: 10.1111/j.1365-313X.2006.02669.x

Xu, Y., Yu, H., and Kumar, P. P. (2010). Characterization of floral organ identity genes of the orchid Dendrobium crumenatum. *AsPac J. Mol. Biol. Biotechnol.* 18, 185–187.

Yang, F. X., Zhu, G. F., Wang, Z., Liu, H. L., and Huang, D. (2015). A putative miR172-targeted CeAPETALA2-like gene is involved in floral patterning regulation of the orchid Cymbidium ensifolium. *Genet. Mol. Res.* 14 (4), 12049–12061. doi: 10.4238/2015.October.5.18

Yin, K., Gao, C., and Qiu, J. L. (2017). Progress and prospects in plant genome editing. *Nat. Plants* 3, 17107. doi: 10.1038/nplants.2017.107

Yoshida, H., and Nagato, Y. (2011). Flower development in rice. *J. Exp. Bot.* 62.14, 4719–4730. doi: 10.1093/jxb/err272

Yu, H., and Goh, C. J. (2000a). Differential gene expression during floral transition in an orchid hybrid Dendrobium Madame Thong-In. *Plant Cell Rep.* 19, 926–931. doi: 10.1007/s002990000227

Yu, H., and Goh, C. J. (2000b). Identification and characterization of three orchid MADS-box genes of the AP1/AGL9 subfamily during floral transition. *Plant Physiol.* 123 (4), 1325–1336. doi: 10.1104/pp.123.4.1325

Yu, H., Yang, S. H., and Goh, C. J. (2000). DOH1, a class 1 knox gene, is required for maintenance of the basic plant architecture and floral transition in orchid. *Plant Cell* 12 (11), 2143–2160. doi: 10.1105/tpc.12.11.2143

Yu, H., Yang, S. H., and Goh, C. J. (2001). Agrobacterium -mediated transformation of a Dendrobium orchid with the class 1 knox gene DOH1. *Plant Cell Rep.* 20 (4), 301–305. doi: 10.1007/s002990100334

Zhang, G. Q., Liu, K. W., Li, Z., Lohaus, R., Hsiao, Y. Y., Niu, S. C., et al. (2017). The Apostasia genome and the evolution of orchids. *Nature* 549 (7672), 379–383. doi: 10.1038/nature23897

Zhang, J.-X., Wu, K.-L. W., Tian, L.-N., Zeng, S.-J., and Duan, J. D. (2011). Cloning and characterization of a novel CONSTANS-like gene from Phalaenopsis hybrida. *Acta Physiol. Plant* 33, 409–417. doi: 10.1007/s11738-010-0560-4

Zhang, J., Li, Z., and Xu, L. (2013). Cloning and expression analysis of B type MADS-box genes involving in floral development from Rhynchostylis gigantean. *Mol. Plant Breed.* 11, 570–574. doi: 10.3969/mpb.011.000570

Zhang, Y., Zhao, S., Liu, D., Zhang, Q., and Cheng, J. (2014). Flowering phenology and reproductive characteristics of Cypripedium macranthos (Orchidaceae) in China and their implication in conservation. *Pakistan J. Bot.* 46 (4), 1303–1308.

Conflict of Interest: The authors declare that the research was conducted in the absence of any commercial or financial relationships that could be construed as a potential conflict of interest.

frontiers in Plant Science

ORIGINAL RESEARCH
published: 01 November 2019
doi: 10.3389/fpls.2019.01359

Evolutionary Conservation of the Orchid MYB Transcription Factors DIV, RAD, and DRIF

*Maria Carmen Valoroso[1], Rómulo Sobral[2], Giuseppe Saccone[1], Marco Salvemini[1], Maria Manuela Ribeiro Costa[2] and Serena Aceto[1]**

[1] Department of Biology, University of Naples Federico II, Naples, Italy, [2] BioSystems & Integrative Sciences Institute (BioISI), Plant Functional Biology Centre, University of Minho, Campus de Gualtar, Braga, Portugal

The MYB transcription factors DIVARICATA (DIV), DIV-and-RAD-Interacting-Factor (DRIF), and the small interfering peptide RADIALIS (RAD) can interact, forming a regulatory module that controls different plant developmental processes. In the snapdragon *Antirrhinum majus*, this module, together with the TCP transcription factor CYCLOIDEA (CYC), is responsible for the establishment of floral dorsoventral asymmetry. The spatial gene expression pattern of the *OitDIV*, *OitDRIF*, and *OitRAD* homologs of *Orchis italica*, an orchid with zygomorphic flowers, has suggested a possible conserved role of these genes in bilateral symmetry of the orchid flower. Here, we have identified four *DRIF* genes of orchids and have reconstructed their genomic organization and evolution. In addition, we found snapdragon transcriptional *cis*-regulatory elements of *DIV* and *RAD* loci generally conserved within the corresponding orchid orthologues. We have tested the biochemical interactions among OitDIV, OitDRIF1, and OitRAD of *O. italica*, showing that OitDRIF1 can interact both with OitDIV and OitRAD, whereas OitDIV and OitRAD do not directly interact, as in *A. majus*. The analysis of the quantitative expression profile of these MYB genes revealed that in zygomorphic orchid flowers, the *DIV*, *DRIF1*, and *RAD* transcripts are present at higher levels in the lip than in lateral inner tepals, whereas in peloric orchid flowers they show similar expression levels. These results indicate that MYB transcription factors could have a role in shaping zygomorphy of the orchid flower, potentially enriching the underlying orchid developmental code.

Keywords: DIVARICATA, RADIALIS, DRIF, MYB, Orchidaceae

OPEN ACCESS

Edited by:
Jen-Tsung Chen, National University of Kaohsiung, Taiwan

Reviewed by:
Minsung Kim, University of Manchester, United Kingdom
Chao Bian, Beijing Genomics Institute (BGI), China

***Correspondence:**
Serena Aceto
serena.aceto@unina.it

Specialty section:
This article was submitted to Plant Development and EvoDevo, a section of the journal Frontiers in Plant Science

Received: *04 June 2019*
Accepted: *02 October 2019*
Published: *01 November 2019*

Citation:
Valoroso MC, Sobral R, Saccone G, Salvemini M, Costa MMR and Aceto S (2019) Evolutionary Conservation of the Orchid MYB Transcription Factors DIV, RAD, and DRIF. Front. Plant Sci. 10:1359. doi: 10.3389/fpls.2019.01359

INTRODUCTION

The MYB proteins DIVARICATA (DIV), RADIALIS (RAD), and DIV-and-RAD-Interacting-Factor (DRIF) are part of a regulatory module involved in distinct developmental processes of plants (Machemer et al., 2011; Raimundo et al., 2013). *DIV* and *DRIF* belong to ancient gene families that emerged in the green algae lineage, whereas the *RAD* genes are more recent as their origin can be dated back to gymnosperms (Raimundo et al., 2018). Canonical DIV transcription factors have two MYB domains (MYBI and II) (Galego and Almeida, 2002), in contrast to RAD and DRIF, both containing a single MYB domain (Corley et al., 2005; Raimundo et al., 2013). In addition to the N-terminal MYB domain, DRIF proteins share the conserved DUF3755 domain at the C-terminus, found only in this protein family and whose ability to bind WUSCHEL-RELATED HOMEOBOX

(WOX) and KNOTTED1-LIKE HOMEOBOX (KNOX) proteins has been recently described in *Populus trichocarpa* (Petzold et al., 2018). During evolution, the MYB domain has undergone successive rearrangements resulting in the acquisition of specific interaction abilities: the MYB domain of DRIF can interact with the MYBI domain of DIV or with the MYB domain of RAD (Machemer et al., 2011; Raimundo et al., 2013; Raimundo et al., 2018). In such interaction module, the small RAD proteins (less than 100 amino acids in size) have an antagonistic effect on the formation of the DIV/DRIF complex and thus have been classified as small-interfering peptides (siPEP) or microproteins (Seo et al., 2011; Staudt and Wenkel, 2011; Eguen et al., 2015).

The function of the DIV, DRIF, and RAD proteins has been described in different plant species, where they control distinct developmental processes. For example, RAD-like proteins regulate photomorphogenesis and floral transition of *Arabidopsis thaliana* (Hamaguchi et al., 2008; Li et al., 2015), DIV-like proteins are involved in sugar and hormone regulation of *Oryza sativa* (Lu et al., 2002), and the protein complexes DIV/DRIF and RAD/DRIF control cell expansion of the fruit pericarp of *Solanum lycopersicum* (Machemer et al., 2011). However, the majority of studies regarding the *DIV*, *DRIF*, and *RAD* genes focused on their role in the establishment of flower zygomorphy, an evolutionary novelty that emerged several times in flowering plants from the ancestral condition of radial symmetry (Citerne et al., 2010; Endress, 2012). The first comprehensive analysis of the molecular pathway underlying floral symmetry was conducted in the snapdragon *Antirrhinum majus* (**Figure 1**), showing that mutations of the genes *CYCLOIDEA* (*CYC*), *DIV*, and *RAD* have an effect on symmetry of the flower. The TCP transcription factor *CYC* is expressed in the dorsal part of the flower and activates the expression of *RAD* (Luo et al., 1996; Cubas et al., 1999; Luo et al., 1999; Corley et al., 2005; Costa et al., 2005) through the interaction with 5′-GGNCCC-3′ binding sites in the *RAD* promoter and intron (Costa et al., 2005). The *DIV* and *DRIF* genes are expressed both in the dorsal and ventral domains of the flower of *A. majus* (Almeida et al., 1997; Galego and Almeida, 2002; Raimundo et al., 2013). In the ventral domain, the protein complex DIV/DRIF controls downstream genes involved in the ventralization of the flower. In the dorsal domain, the siPEP RAD binds to DRIF and prevents its interaction with DIV, thus inhibiting ventralization (Raimundo et al., 2013). In addition to its ability to activate ventralization genes, the DIV/DRIF protein dimers can bind the sequence 5′-GATAA-3′ (Raimundo et al., 2013) within the *DIV* promoter, possibly autoregulating its transcriptional activity (Sengupta and Hileman, 2018).

The role of the *CYC*, *DIV*, and *RAD* genes in controlling flower bilateral symmetry outside *A. majus* has been reported in other Lamiales (Zhou et al., 2008; Preston et al., 2009; Reardon et al., 2009; Preston et al., 2011; Reardon et al., 2014; Su et al., 2017) and in Dipsacales (Howarth and Donoghue, 2009; Boyden et al., 2012), whereas only limited knowledge about these genes is available in monocots and basal angiosperms. However, a recent study suggested the recruitment of this molecular network for the establishment of floral zygomorphy before the diversification between monocots and dicots (Madrigal et al., 2019).

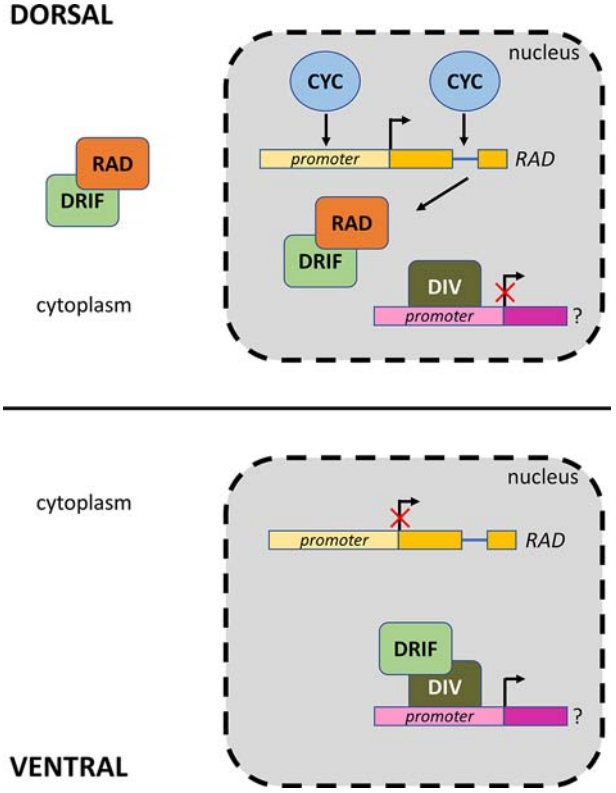

FIGURE 1 | Model of interaction of CYC, DIV, RAD, and DRIF proteins in *Antirrhinum majus* (modified from Raimundo et al., 2013). The DIV and DRIF proteins are expressed both in the dorsal and ventral parts of the flower. In the dorsal domain, the CYC protein interacts with the promoter and intron of the *RAD* gene, activating its expression. The RAD protein binds to DRIF and prevents the formation of the DIV/DRIF complex, thus inhibiting ventralization. In the ventral domain, the absence of RAD permits the formation of the DIV/DRIF complex that controls downstream genes involved in the ventralization.

Among monocots, Orchidaceae is one of the most species-rich families, adapted to many different habitats (Cozzolino and Widmer, 2005; Aceto and Gaudio, 2011). Most of the orchid species have zygomorphic flowers sharing a common organization of the perianth into three outer and three inner tepals. Zygomorphy of the orchid flower is evident in the diversified and complex morphology of the median inner tepal (labellum or lip; **Figure 2**) (Rudall and Bateman, 2002). The vast majority of studies concerning orchid flower development focused on MADS-box transcription factors (Salemme et al., 2011; Aceto et al., 2014; De Paolo et al., 2014; Cai et al., 2015; Lin et al., 2016; Zhang et al., 2016; Zhang et al., 2017; Valoroso et al., 2019), with particular attention to the *DEFICIENS* (*DEF*) and *AGAMOUS-LIKE 6* (*AGL6*) genes. The pivotal role of these genes in the evolution and formation of the orchid perianth is well explained by the "orchid code" theory and its successive modifications (Mondragon-Palomino and Theissen, 2009; Mondragon-Palomino and Theissen, 2011; Pan et al., 2011; Hsu et al., 2015; Dirks-Mulder et al., 2017). On the contrary, the MYB transcription factors are largely understudied in orchids and their potential involvement in the establishment of orchid flower

symmetry has been only recently proposed in *Orchis italica* and *Cattleya trianae* (Valoroso et al., 2017; Madrigal et al., 2019).

To date, eight *DIV*, four *RAD*, and two *DRIF* genes have been reported in *O. italica* and, among them, the corresponding homologs responsible for floral symmetry of *A. majus* have been identified (Valoroso et al., 2017). Phylogeny and genomic organization of the orchid *DIV* and *RAD* genes has also been studied (Valoroso et al., 2017; Madrigal et al., 2019), whereas a description of the *DRIF* gene family is still missing.

The aim of the present study was to expand knowledge on *DIV*, *RAD*, and *DRIF* genes of orchids and to obtain more evidence supporting their involvement in the establishment of flower zygomorphy. We firstly focused on the orchid *DRIF* genes, searching for homologs within the orchid genomes and reconstructing their phylogeny. Then, we scanned the putative promoter and intron of the *DIV* and *RAD* genes to identify known *cis*-regulatory elements conserved between orchids and snapdragon. Finally, we analyzed the interaction ability of the OitDIV, OitRAD, and OitDRIF1 proteins of *O. italica* and examined their transcript abundance in the perianth tissues of zygomorphic and peloric orchid flowers.

MATERIALS AND METHODS

Plant Material

The orchids used in this study were grown under natural light and temperature in the greenhouse of the Department of Biology of the University of Naples Federico II (Napoli, Italy). *O. italica* Poir. plants are part of the Orchidaceae collection of the Department of Biology. *Phalaenopsis equestris* (Schauer) Rchb.f. and *Phalaenopsis* Joy Fairy Tale (*Phal.* Ho's Princess Arai × *Phal.* Coral Isles) are commercially available orchids (Giulio Celandroni Orchidee, San Giuliano Terme, Pisa, Italy). *O. italica* and *P. equestris* display flower zygomorphy as the second floral whorl is clearly distinguished into two lateral inner tepals and one median inner tepal (lip) (**Figures 2A–E**). The peloric perianth of *Phalaenopsis* Joy Fairy Tale shows two lip-like structures in substitution of the lateral inner tepals, conferring radial symmetry to the flower (**Figures 2F**, **G**).

Single flowers from three different plants of each orchid were collected before (single floret length, ∼1 cm) and soon after anthesis (**Figure 2**). The perianth tissues (outer tepals, inner lateral tepals, and lip) were dissected and stored in RNA-later (Ambion) until RNA extraction.

Sequence Retrieval and Phylogenetic Analysis

In order to identify *DRIF* transcripts expressed in flower tissues of *O. italica*, the amino acid sequences corresponding to the DUF3755 domain of the known *O. italica* OitDRIF1 and two proteins (GenBank accession numbers MK834277 and MK834278, respectively) (Valoroso et al., 2017) were used as queries to scan the inflorescence transcriptome of *O. italica* (De Paolo et al., 2014) through tBLASTn searches. Using the same approach, *DRIF* homologs were searched within the transcriptomes of other orchids present in the *Orchidstra* database (Chao et al., 2017) and within the genome of *Apostasia shenzenica*, *P. equestris*, and *Dendrobium catenatum* (Cai et al., 2015; Zhang et al., 2016; Zhang et al., 2017). Recently identified *DRIF* nucleotide and amino acid sequences (Raimundo et al., 2018) were downloaded from SustainPine (http://www.scbi.uma.es/sustainpinedb/home_page), Monocots PLAZA (https://bioinformatics.psb.ugent.be/plaza/versions/plaza_v4_monocots/), NCBI (https://www.ncbi.nlm.nih.gov/), and Araport (https://www.araport.org/). The species and the corresponding accession numbers of the DRIF sequences used in the present work are listed in **Table S1**.

The amino acid sequences of the DRIF homologs identified were aligned with MAFFT (Katoh and Standley, 2013) and the resulting alignment was manually adjusted. Poorly aligned positions were removed using GBLOCKS (Talavera and Castresana, 2007) and maximum likelihood (ML) phylogenetic tree was constructed with RAxML v 8.2.10 (Stamatakis, 2014) using the default settings, with 1,000 bootstrap replicates.

Analysis of Conserved Transcription Factor Binding Sites

Approximately 3 kb noncoding sequences upstream of the translation start site of the *DIV* and *RAD* genes of the orchids *A. shenzenica*, *D. catenatum*, and *P. equestris* were downloaded from the corresponding genomes deposited at NCBI (**Table S1**). These putative promoter sequences were scanned for the presence of conserved transcription factor binding sites (TFBSs) using the *PlantPAN 3.0* database (Chow et al., 2019). The Multiple Promoter Analysis search mode was applied to identify known conserved plant TFBSs shared within each gene group of putative promoters. Specific nucleotide motifs known as TFBSs of CYC (5′-GGNCCC-3′) (Kosugi and Ohashi, 2002; Costa et al., 2005; Yang et al., 2012; Gao et al., 2015; Sengupta and Hileman, 2018) and DIV (5′-VGATAMSV-3′) (Raimundo et al., 2013; Sengupta and Hileman, 2018) of *A. majus* were searched within the orchid *RAD* and *DIV* putative promoters, respectively. In addition, the intron sequences of the *RAD* genes of *O. italica*, *P. equestris*, *D. catenatum* (Valoroso et al., 2017), and *A. shenzenica* were scanned for the presence of the CYC TFBS, as described above.

Expression Analysis

Total RNA was extracted from the perianth tissues (outer tepals, inner tepals, and lip, before and after anthesis) of *O. italica*, *P. equestris*, and *Phalaenopsis* Joy Fairy Tale using Trizol (Ambion) followed by DNase treatment. After RNA extraction and quantification, 500 ng of total RNA from each tissue were reverse-transcribed using the Advantage RT-PCR kit (Clontech) and a mix of oligo dT and random hexamer primers.

In order to validate the nucleotide sequence of the four *OitDRIF* transcripts identified in the inflorescence transcriptome of *O. italica*, specific primer pairs were designed (**Table S2**) and used to amplify the cDNA of *O. italica* inflorescence. The amplification products obtained were cloned into pSC-A-amp/kan vector (Agilent), sequenced

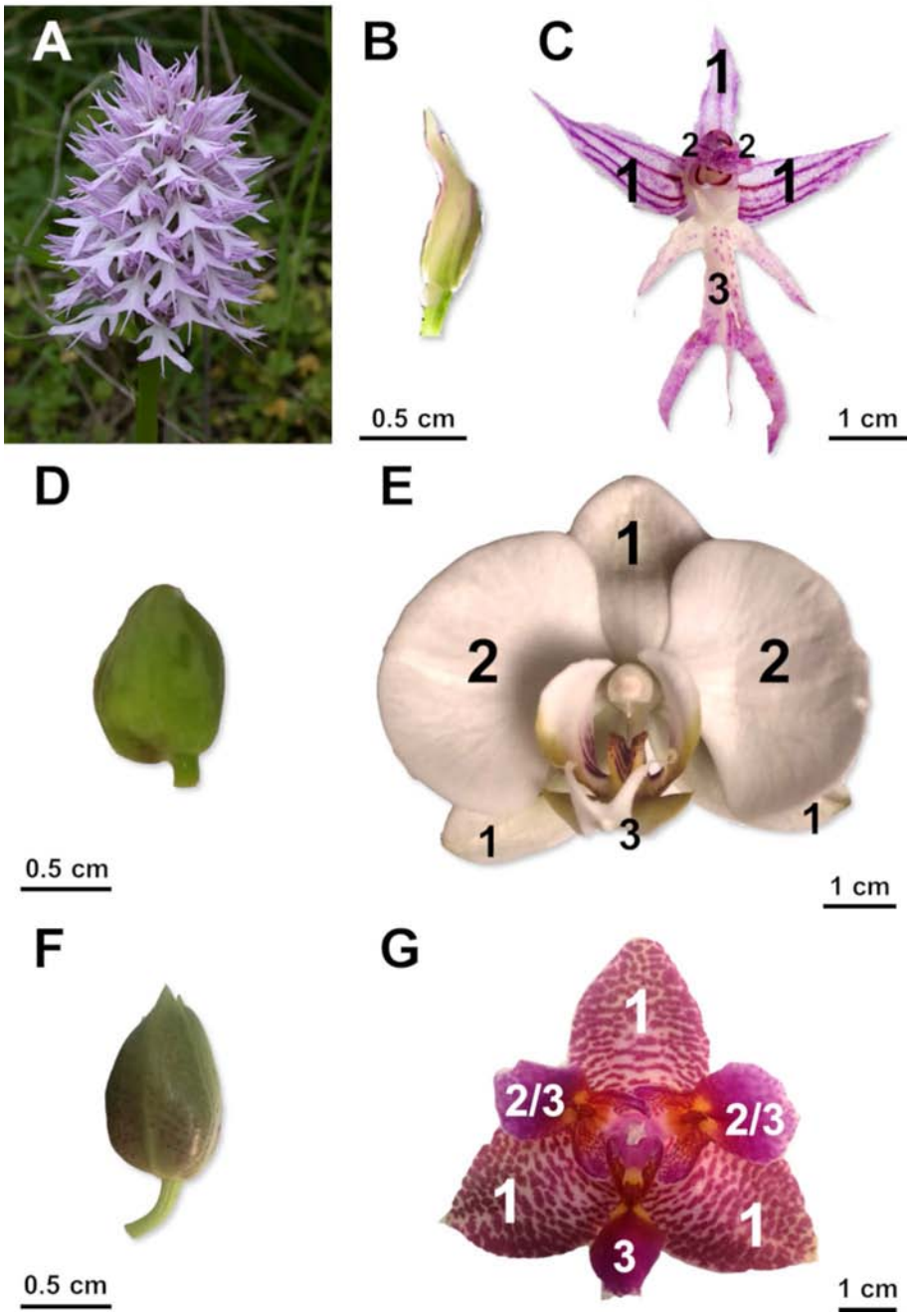

FIGURE 2 | Flowers of zygomorphic and peloric orchids. *Orchis italica* (Orchidoideae): **(A)** inflorescence; single flower before **(B)** and after **(C)** anthesis. *Phalaenopsis equestris* (Epidendroideae): flower before **(D)** and after **(E)** anthesis. *Phalaenopsis* Joy Fairy Tale: flower before **(F)** and after **(G)** anthesis. *1*, outer tepal; *2*, lateral inner tepal; *3*, lip; *2/3*, lip-like structure of *Phalaenopsis* Joy Fairy Tale.

using the T3 and T7 primers, and analyzed using an ABI 310 Automated Sequencer (Applied Biosystems). Their sequence was compared with that of the transcripts identified in the transcriptome of *O. italica*.

Relative expression of the orchid *DIV*, *RAD*, and *DRIF1* genes was evaluated by real-time PCR experiments, using 18S as reference gene, as previously described (De Paolo et al., 2015; Valoroso et al., 2017). Primer pairs are listed in the **Table S2**. Reactions were conducted in biological triplicates and technical duplicates. Mean ± SEM was calculated for each duplicate and biological triplicate. Gene relative expression level in inner lateral tepals and lip was normalized relative to outer tepals. Two-tailed *t* test was conducted to assess the statistical significance of the relative expression differences

between lateral inner tepals and lip of each species, before and after anthesis.

Yeast Two-Hybrid Analysis

The coding sequences (CDSs) of the *OitDIV* (KY089088), *OitRAD* (KY089097), and *OitDRIF1* (MK834277) homologs of *O. italica* were PCR amplified using the primer pairs listed in **Table S2** and 500 ng of cDNA of *O. italica* inflorescence. To analyse protein–protein interactions between OitDIV, OitRAD, and OitDRIF1, the GAL4-based yeast two-hybrid (Y2H) system (Matchmaker two-hybrid system; Clontech) was used. The amplified CDSs of *OitDIV*, *OitRAD*, and *OitDRIF1* were cloned into bait (pGBT9) and prey (pGAD424) vectors (Clontech). All the prey and bait recombinant vector combinations were used to transform *Saccharomyces cerevisiae* strain AH109 (Gietz et al., 1995), conducting each experiment in triplicate. Plasmid presence after double yeast transformations was checked by growing cells in Synthetic Defined (SD) medium lacking tryptophan and leucine. Protein ability to interact with each other was evaluated in SD medium lacking tryptophan, leucine, and histidine. Possible transcriptional activation activity of OitDIV, OitRAD, and OitDRIF1 proteins fused to the binding domain of GAL4 (pGBT9 vector) was verified by monitoring growth of yeast transformed cells in SD medium without histidine, in the presence of 10 mM 3-aminotriazole. Empty vectors pGBT9 or pGAD424 were transformed in combination with the recombinant vectors as negative controls.

RESULTS AND DISCUSSION

Identification and Phylogenetic Analysis of the Orchid *DRIF* Genes

To date, the *DRIF* genes of orchids have been identified only in *O. italica*, where the expression pattern of *OitDRIF1* and *OitDRIF2* was analysed in floral tissues (Valoroso et al., 2017). Evolutionary analysis has demonstrated the ancient origin of the *DRIF* genes: they have been found (together with the *DIV* genes) from green algae to angiosperms. In angiosperms, the *DRIF* homolog number in the examined species is generally five (Raimundo et al., 2018). These findings led us to search for other *DRIF* genes expressed in *O. italica*, to identify their homologs in other orchids and to verify the number of *DRIF* genes within the available genome of orchid species, currently restricted to the only subfamilies Epidendroideae and Apostasioideae.

Among plants, the DUF3755 domain is unique to DRIF proteins (Raimundo et al., 2018), and when we used it as query to identify other *DRIFs* expressed in the inflorescence transcriptome of *O. italica* we found two different transcripts, in addition to those previously identified, named *OitDRIF3* and *OitDRIF4* (accession numbers MK834279 and MK834280, respectively). All the four *OitDRIF* transcripts of *O. italica* encode for proteins containing the N-terminal MYB domain and the C-terminal DUF3755 domain. Within the genome of *P. equestris* and *D. catenatum* (both belonging to the subfamily Epidendroideae), we found four and three *DRIF* genes, respectively. In the genome of *A. shenzenica*, belonging to the basal subfamily Apostasioideae, we found three *DRIF* genes. All these orchid *DRIF* genes encode for proteins containing the MYB and the DUF3755 domain.

To cover all the five subfamilies of Orchidaceae, we scanned the transcriptomes of *Ophrys sphegodes*, belonging to the same subfamily of *O. italica* (Orchidoideae), *Cypripedium formosanum* (Cypripedioideae), and *Vanilla planifolia* (Vanilloideae) present in the database *Orchidstra* (Chao et al., 2017), a transcriptomics collection for Orchidaceae. In *C. formosanum* we found four *DRIF* transcripts, three in *O. sphegodes* and two in *V. planifolia*. Although some of them are not full-length transcripts, missing part of the N-terminus, all contain both the MYB and DUF3755 domains. The graphical view of the amino acid alignment of the orchid DRIF proteins is reported in **Figure S1**, where the consensus sequences of the MYB and DUF3755 domains are shown.

We reconstructed the genomic organization of the orchid *DRIF* genes from the assembled genomes of *P. equestris*, *D. catenatum*, and *A. shenzenica* and compared it to that of the *DRIF* genes of *A. majus*, whose genome assembly has been recently released (Li et al., 2019). Based on the exon/intron number, it is possible to divide the *DRIF* genes into two structural types: seven exons–six introns, shared by the *DRIF1-4* genes of *A. majus* and one *DRIF* gene of *A. shenzenica*, *D. catenatum*, and *P. equestris*; eight exons–seven introns, displayed by the *DRIF5-6* genes of *A. majus*, two *DRIF* genes of *A. shenzenica* and *D. catenatum*, and three of *P. equestris* (**Figure 3** and **Table S3**). Exon size is quite well conserved both among orchids and between orchids and snapdragon, whereas intron size is variable, with very large introns in orchids, reflecting a common feature of the orchid genomes due to the high number of transposable elements (Salemme et al., 2013a; Salemme et al., 2013b; Cai et al., 2015; Zhang et al., 2016; Zhang et al., 2017).

To understand the evolutionary relationships among the orchid DRIF proteins and the DRIFs of other plant species, we constructed the phylogenetic tree shown in **Figure 4**. The DRIF proteins of Tracheophyta are included in the clade I, whereas the three DRIF sequences of the moss *Physcomitrella patens* (Bryophyta) belong to the ancestral clade II, in agreement with the DRIF phylogeny recently described (Raimundo et al., 2018). Within the clade I, the orchid DRIFs (in the phylogenetic tree highlighted in different shades of pink) form three distinct groups, two belonging to the subclade Ia and one to the subclade Ib (**Figure 4**). Based on the tree topology, the orchid DRIFs seem to have originated by duplication events predating the diversification between monocots and dicots. In fact, within both subclades Ia and Ib, the orchid branches are grouped with other monocots (*O. sativa*, highlighted in green) and dicots (e.g., *A. majus* and *A. thaliana*, highlighted in different shades of blue). However, lineage-specific duplications have occurred during the evolution of DRIFs in orchids, leading to the formation of two paralog groups within the subclade Ia. In particular, an orchid-specific duplication generated the paralog groups that include, among others, OitDRIF2 and 3. The orchid homologs of DRIF1 of *A. majus* belong to the subclade Ib, where orchid-specific duplication events seem to be absent. In fact, within the subclade Ib, a single DRIF is present for each orchid species, including

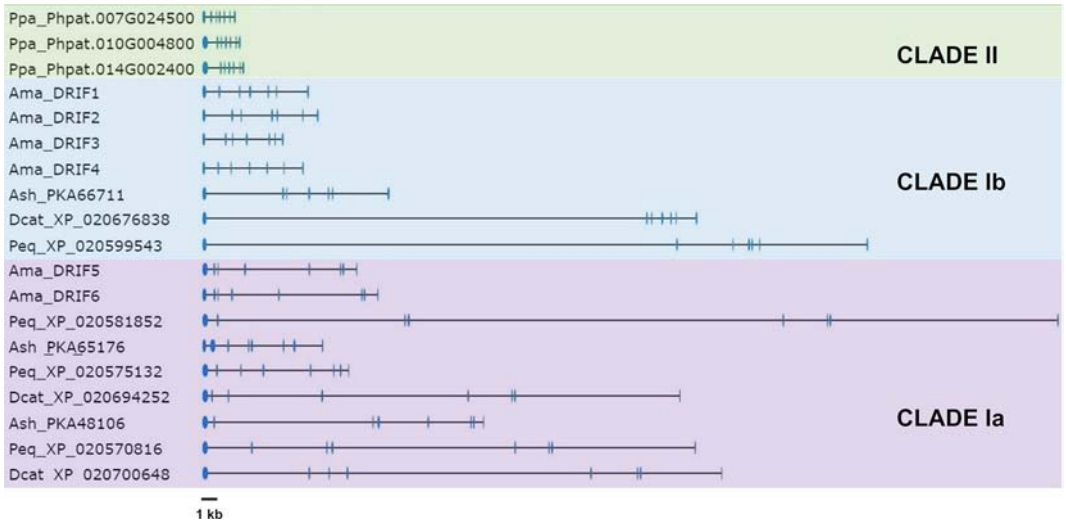

FIGURE 3 | Genomic organization of the DRIF genes of *Phalaenopsis equestris*, *Dendrobium catenatum*, *Apostasia shenzenica* (Orchidaceae), *Antirrhinum majus* (Lamiales), and *Physcomitrella patens* (Bryophyta). *Light blue boxes* and *black lines* represent exons and introns, respectively. Ama, *A. majus*; Ash, *A. shenzenica*; Dcat, *D. catenatum*; Peq, *P. equestris*; Ppa, *P. patens*. Clades Ia, Ib, and II are referred to the main groups detected in the DRIF phylogeny (see figure). The code number following the abbreviation of the species name is the accession number of the DRIF sequences deposited in public databases (**Table S1**).

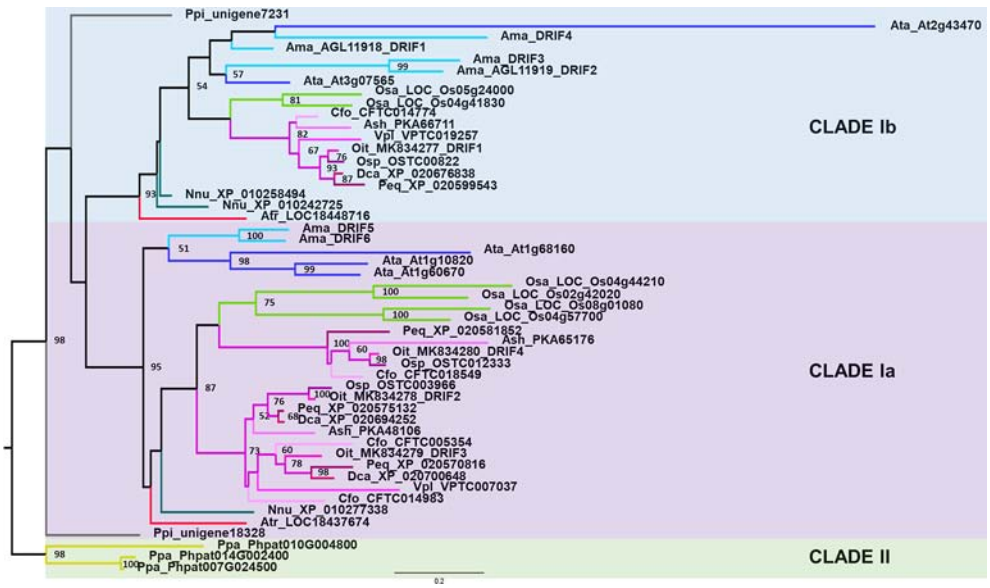

FIGURE 4 | Maximum likelihood tree of the DRIF proteins of orchids and other plant species. The *numbers above the nodes* represent the bootstrap support percentages (1,000 replicates). Bootstrap values lower than 50% are not shown. The orchid branches are highlighted in *different shades of pink*. Ama, *Antirrhinum majus* (light blue); Ata, *Arabidopsis thaliana* (*blue*); Atr, *Amborella tricopoda* (*red*); Ash, *Apostasia shenzenica*; Cfo, *Cypripedium formosanum*; Dca, *Dendrobium catenatum*; Nnu, *Nelumbo nucifera* (*dark green*); Oit, *Orchis italica*; Osa, *Oryza sativa* (*green*); Osp, *Ophrys sphegodes*; Peq, *Phalaenopsis equestris*; Ppa, *Physcomitrella patens* (*yellow*); Ppi, *Pinus pinaster* (*gray*); Vpl, *Vanilla planifolia*. The code number following the abbreviation of the species name is the accession number of the DRIF sequences deposited in public databases (**Table S1**).

OitDRIF1 of *O. italica*, and the orchid DRIF phylogeny reflects the evolutionary relationships existing within Orchidaceae: Apostasioideae, Cypripedioideae, and Vanilloideae are the most basal subfamilies, Epidendroideae and Orchidoideae the most derivates (Givnish et al., 2015). The phylogenetic relationships among DRIF proteins coincide with the division proposed based on the genomic organization of the *DRIF* loci examined, showing that the genes belonging to the subclade Ia have eight exons, whereas those belonging to the subclade Ib have seven exons. The genomic organization of the *DRIF* genes of the moss *P. patens*, belonging to the basal clade II, shows the presence of seven exons and six introns (**Figure 3** and **Table S3**).

The exon/intron structure shared by genes belonging to clade II and subclade Ib indicates that this genomic organization might be the ancestral condition and that the subclade Ia might have originated through a split of exon 7, followed by lineage-specific evolution of exon size.

Compared to the *DRIF* genomic organization, *DIV* and *RAD* genes have a significantly different structure with two exons and one intron (Valoroso et al., 2017). This difference supports the hypothesis previously proposed on the evolutionary origin of the *DIV*, *RAD*, and *DRIF* genes based on the comparison of their MYB domain (Raimundo et al., 2018). The *RAD* genes might have originated through the loss of the region of the *DIV* genes encoding for the MYBII domain. The *DIV* and *DRIF* genes might have evolved from a common ancestral gene through lineage-specific rearrangements (e.g., duplications or gene fusion events), resulting in different exon/intron organizations and acquisition of the region encoding for the MYBII (*DIV* lineage) or DUF3755 domain (*DRIF* lineage). Phylogenetic trees of the DIV and RAD proteins of orchids and other plant species are reported in **Figures S2** and **S3**, respectively. Both the DIV and RAD trees have been produced by the same approach used for the construction of the DRIF tree (see *Materials and Methods*).

Analysis of the Conserved TFBS

Some aspects of transcriptional regulation of the genes involved in floral bilateral symmetry are known for *DIV* and *RAD* of *A. majus*. In snapdragon, the expression of the *RAD* gene is activated by direct interaction of the TCP transcription factor CYC possibly through the binding to three conserved TFBSs, two located within the promoter and one within the intron of *RAD* (Costa et al., 2005). The presence of conserved CYC TFBSs within the promoter of *RAD* has been recently reported also in other Lamiales species (Sengupta and Hileman, 2018).

Within the genomic sequence upstream of the translation start site of the *RAD* gene of *P. equestris*, *D. catenatum*, and *A. shenzenica*, we found distinct conserved TFBSs (**Table S4**), among which TCP binding sites. The sequence 5′-GGNCCN-3′, very similar to the *A. majus* CYC consensus binding site 5′-GGNCCC-3′, is present in the putative *RAD* promoter of *A. shenzenica* (three sites) and *D. catenatum* (two sites) (**Table 1**). Its absence in *P. equestris* is possibly due to the lack of a complete sequence information of the upstream region (only 958 bp are currently available) of the *RAD* gene in the corresponding genomic scaffold. Within the *RAD* intron, the sequence 5′-GGNCCN-3′ is present in *D. catenatum* (four sites), *P. equestris* (one site), and *O. italica* (two sites), whereas in *A. shenzenica* it is not present. In *D. catenatum* and *P. equestris* one of the sites exactly matches the canonical CYC TFBS of *A. majus*. The presence of putative CYC target sequences within the promoter and intron of the *RAD* gene (**Table 1**) may suggest a conserved direct transcriptional regulation of *RAD* by CYC in zygomprphic orchid flowers. In *P. equestris*, *D. catenatum*, and possibly *O. italica* both promoter and intron *cis*-regulatory motifs might be necessary to activate the transcription of *RAD* in the specific spatial domain linked to zygomorphy, as in *A. majus*. The absence of these regulatory sequences within the *RAD* intron of *A. shenzenica* is in agreement with this hypothesis, *A. shenzenica* being a basal orchid species with radially symmetric perianth (Zhang et al., 2017). The putative CYC binding sequence of orchids diverged to some extent from that of *A. majus* and other Lamiales and possibly the orchid CYC protein co-evolved to recognize slightly different sequences.

In *A. majus*, two putative DIV binding sites have been identified *in silico* within the *DIV* promoter, suggesting the existence of an autoregulatory loop that maintains the transcription of *DIV*

TABLE 1 | Predicted binding sites of CYC (5′-GGNCCC-3′) and DIV (5′-VGATAMSV-3′) of *Antirrhinum majus* in the putative promoter and intron of *RAD* and in the putative promoter of *DIV*, respectively, in the orchids *Phalaenopsis equestris*, *Dendrobium catenatum*, and *Apostasia shenzenica*.

Gene	Species	Sequence	Position	Strand	Feature
RAD	*Dendrobium catenatum*	GGTCCA	−1331	+	Putative promoter
		GGTCCA	−2924	+	
	Apostasia shenzhenica	GGTCCT	−799	+	
		GGACCA	−1026	+	
		GGGCCG	−2376	+	
	Phalaenopsis equestris	**GGACCC**	1019	+	Intron
	Dendrobium catenatum	GGACCT	123	+	
		GGACCT	218	+	
		GGTCCC	789	+	
		GGACCG	809	+	
	Orchis_italica	GGCCCG	503	+	
		GGCCCG	527	+	
DIV	*Phalaenopsis equestris*	AGATAAAG	−573	−	Putative promoter
		AGATAATA	−1551	+	
		AGATAAAA	−1685	−	
	Dendrobium catenatum	**CGATAACC**	−2210	−	
	Apostasia shenzhenica	**AGATAAGA**	−739	+	
		CGATAAGA	−1008	+	
		GGATAAGA	−2898	+	

The analysis of the RAD intron was conducted also in Orchis italica. The nucleotide positions of the putative promoters are indicated with negative numbers, considering as +1 the first nucleotide of the translation start site codon ATG. The nucleotide positions of the orchid RAD introns are numbered considering as +1 the first nucleotide of the intron sequence. The binding sites exactly conserved among orchids and snapdragon are in bold.

(Sengupta and Hileman, 2018). Within the genomic sequence upstream the translation start site of the *DIV* gene of *P. equestris*, *D. catenatum*, and *A. shenzenica* many conserved TFBSs are present, among which MYB binding sites (**Table S4**). The target binding sequence of DIV of *A. majus* 5′-VGATAMSV-3′ is present in *A. shenzenica* (three sites) and *D. catenatum* (one site), whereas the three sequences found in *P. equestris* have A or T instead of C or G in the seventh position (**Table 1**). Although the DIV binding site of orchids is only partially conserved, these results suggest that also in orchids the transcriptional activity of *DIV* might be regulated by a positive feedback.

Protein Interactions and Expression Pattern

In flowering plants, the involvement of the DRIF/DIV and DRIF/RAD complexes in floral zygomorphy has been demonstrated in *A. majus* (Raimundo et al., 2013) and inferred in a few other species (Garces et al., 2016; Madrigal et al., 2019).

To date, the interaction among the DRIF, DIV, and RAD proteins in orchids has never been tested. We used the Y2H assay and found that in yeast the OitDRIF1 protein of *O. italica* can interact both with OitDIV and OitRAD, whereas OitDIV and OitRAD do not directly interact (**Figure 5**). This result is in agreement with the ancient evolutionary origin of this interaction module. In fact, the ability of the DIV and DRIF proteins to interact has evolved early, coincident with their origin in the green algae lineage. Later, with the emergence of the *RAD* genes in gymnosperms, the DRIF–RAD interaction has evolved (Raimundo et al., 2018).

To obtain evidences about the possible involvement of the orchid *DIV*, *RAD*, and *DRIF* genes in zygomorphy of orchid flowers, we examined their expression profile in the perianth tissues of *O. italica* and *P. equestris*, both with zygomorphic flower, and in a peloric *Phalaenopsis* missing the bilateral symmetry due to the presence of three lips in the second floral whorl (**Figure 2G**). **Figure 6** shows the expression levels, before and after anthesis, of the orchid *DIV*, *RAD*, and *DRIF1* genes in inner tepals and lips normalized with respect to outer tepals. In the lip of *O. italica* and *P. equestris*, the expression level of the orchid *DIV*, *RAD*, and *DRIF1* is significantly higher than in inner tepals after anthesis. This same pattern is observed before anthesis for the three genes in *P. equestris* and only for *RAD* in *O. italica*, where *OitDIV* and *OitDRIF1* are expressed at similar levels in lip and inner tepals. This expression profile is in agreement with the previous reports about the expression of these genes in *O. italica* and *C. trianae* that suggested a possible involvement of the orchid *DIV*, *RAD*, and *DRIF1* in zygomorphy of the orchid perianth (Valoroso et al., 2017; Madrigal et al., 2019). Interestingly, the expression levels of *DIV*, *RAD*, and *DRIF1* in the peloric *Phalaenopsis* are similar in the lip and in the lip-like structures present in substitution of inner tepals, both before and after anthesis. The absence of a clear morphological differentiation among the structures of the second whorl in this peloric *Phalaenopsis* is associated with similar expression levels of the three genes, in particular of *RAD*. These results support the model in which in the zygomorphic flower of *O. italica* and *P. equestris*, DIV and DRIF, expressed in all the perianth organs as in *A. majus*, can interact in inner tepals, in which *RAD* expression is lower than in lip, and control ventralization. Regardless of DIV and DRIF1 levels, in the lip, RAD competes with DIV for the binding to DRIF1 and prevents the formation of the DIV–DRIF complex, thus inhibiting ventralization (Valoroso et al., 2017). Both in *O. italica* and *P. equestris*, the levels of *RAD* are lower in inner tepals than in lip. Consequently, in inner tepals, DIV could interact with DRIF1 and activate ventralization. On the contrary, the presence of higher levels of *RAD* in lip could allow the formation of the RAD/DRIF1 complex and inhibit the interaction between DIV and DRIF1, thus preventing ventralization. In the peloric *Phalaenopsis*, there is competition between DIV and RAD also in the lip-like structures of the second whorl and consequently ventralization is suppressed. The apparent rotation of the orchid

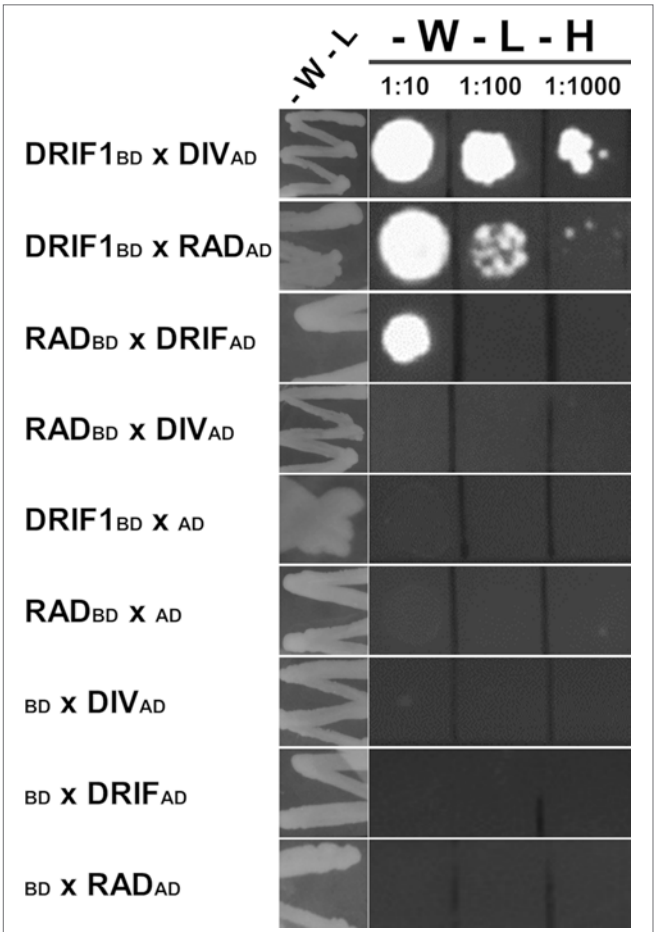

FIGURE 5 | Interactions of the OitDIV, OitDRIF1, and OitRAD proteins of *Orchis italica* in Y2H analysis. After double transformations, yeast growth in absence of tryptophan and leucine (*-W-L*) indicates the plasmid presence; yeast growth in medium lacking tryptophan, leucine, and histidine denotes a positive interaction between the two tested proteins. Double transformations conducted using one of the vectors empty are negative controls. 1:10, 1:100, and 1:1,000 indicate the dilution factor applied to the yeast inoculate. *BD*, GAL4 DNA-binding domain (pGBT9 vector); *AD*, GAL4 activation domain (pGAD424 vector). As the OitDIV protein is able to promote transcription of the reporter genes (**Figure S4**), only its fusion to the GAL4 activation domain (pGAD424 vector) is reported in combination with OitRAD or OitDRIF fused to the GAL4 binding domain.

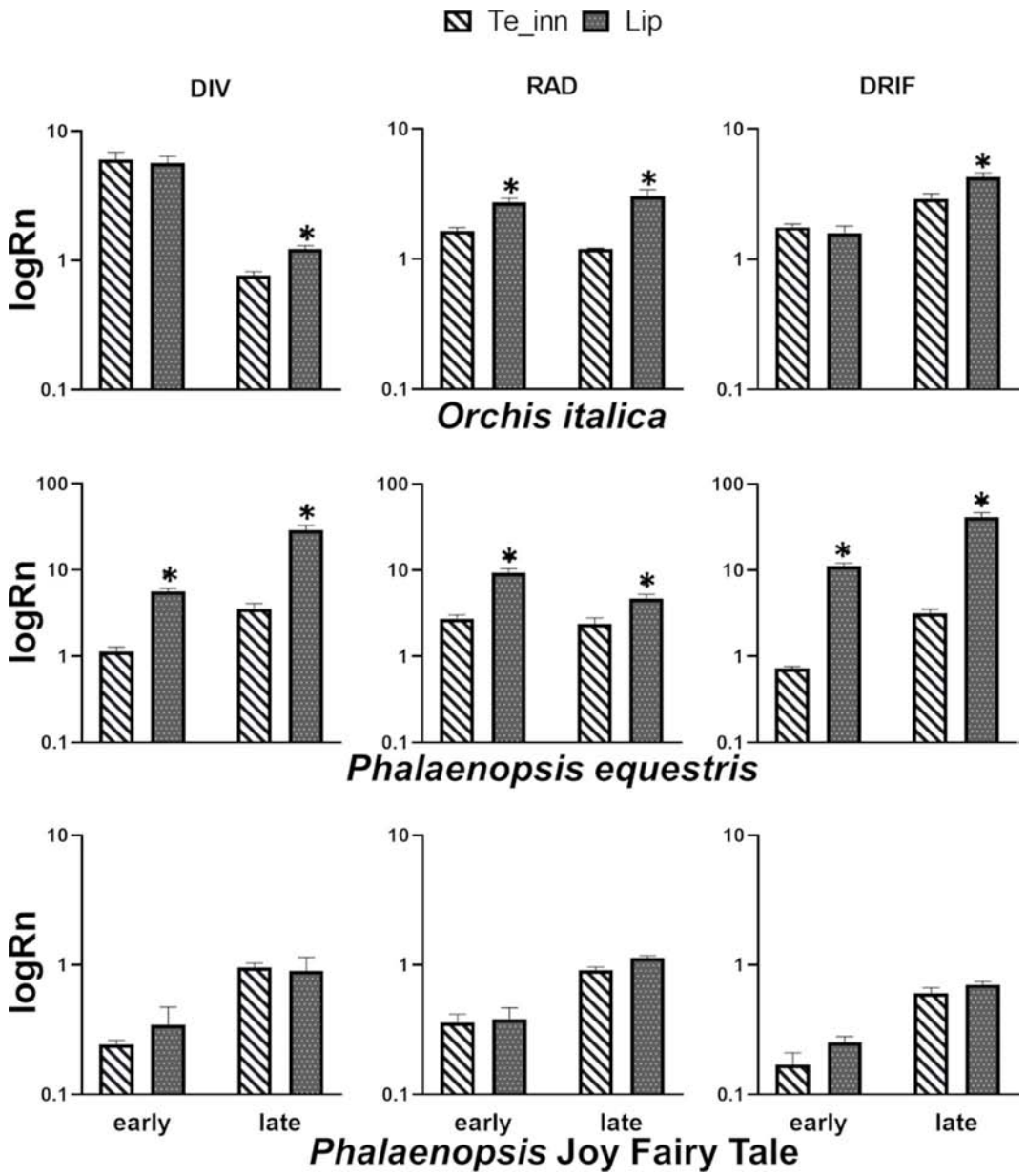

FIGURE 6 | Relative expression of the orchid *DIV*, *RAD*, and *DRIF1* genes in lateral inner tepals (*Te_inn*) and lip of *Orchis italica*, *Phalaenopsis equestris*, and *Phalaenopsis* Joy Fairy Tale. The relative expression Rn (expressed as $\log_{10}$ of the mean between technical duplicates of three biological replicates) is normalized with respect to 18S endogenous gene and outer tepal tissue. The *bars* represent SEM and the *asterisks* indicate significant difference in relative expression between lateral inner tepals and lip assessed by *t* test. *Early* and *late* indicate before and after anthesis stage, respectively.

model with respect to that of *A. majus* is due to resupination: the 180° rotation of the pedicel shifts the lip (a dorsal structure) to a ventral position during orchid flower development.

The results here obtained suggest the involvement of the orchid *DIV*, *RAD*, and *DRIF* genes in the zygomorphy of the orchid perianth and their conserved function, in addition to their conserved interaction ability, in species displaying flower zygomorphy.

Previous studies have demonstrated the role of the MADS-box genes in orchid flower development and various models have been proposed to explain the evolution and formation of the orchid perianth (Aceto and Gaudio, 2011; Salemme et al., 2013a; Acri-Nunes-Miranda and Mondragon-Palomino, 2014; Hsu et al., 2015; Dirks-Mulder et al., 2017; Valoroso et al., 2019). All these models propose interaction among different MADS-box transcription factors and attribute a crucial role to the expression levels of four *DEF* and three *AGL6* genes that permit or prevent the formation of specific protein quartets that drive the formation of specific parts of the perianth (outer tepals, inner tepals, lip) (Mondragon-Palomino and Theissen, 2009; Mondragon-Palomino and Theissen, 2011;

Pan et al., 2011; Hsu et al., 2015; Dirks-Mulder et al., 2017). Our findings suggest the existence of a second, MYB-based pathway underlying flower organ arrangement in orchids.

The very recent advances in functional genetic studies of orchids (Kui et al., 2017) open the road to investigate the potential link between these two different molecular pathways (MADS- and MYB-based) in the formation of the orchid flower and its zygomorphy and to clarify if and what kind of interaction exists, to obtain an integrated view of this complex developmental process.

DATA AVAILABILITY STATEMENT

The datasets generated for this study can be found in the NCBI nucleotide, DRIF1: MK834277, DRIF2: MK834278, DRIF3: MK834279, DRIF4: MK834280.

AUTHOR CONTRIBUTIONS

MV performed the research, analyzed the data, and participated to write the paper. RS performed the research and analyzed the data. GS, MS, and MMRC analyzed the data and participated in the paper writing process. SA designed the research, analyzed the data, and wrote the paper.

FUNDING

This study was financially supported by grant Ricerca dipartimentale 2018 from the University of Naples Federico II and by Fundação para a Ciência e Tecnologia/Ministério da Ciência, Tecnologia e Ensino Superior through national funds (Programa de Investimento e Despesas de Desenvolvimento da Administração Central) with a project grant PTDC/BIA-PLA/1402/2014 and by FCT/MCTES/PIDDAC (Portugal) under the project PEst-OE/BIA/UI4046/2014; UID/MULTI/04046/2013.

ACKNOWLEDGMENTS

We thank Prof. Giovanni Scopece for plant material and Prof. Luciano Gaudio for critical reading of the manuscript.

SUPPLEMENTARY MATERIAL

The Supplementary Material for this article can be found online at: https://www.frontiersin.org/articles/10.3389/fpls.2019.01359/full#supplementary-material

REFERENCES

Aceto, S., and Gaudio, L. (2011). The MADS and the Beauty: Genes Involved in the Development of Orchid Flowers. *Curr Genomics* 12, 342–356. doi: 10.2174/138920211796429754

Aceto, S., Sica, M., De Paolo, S., D'argenio, V., Cantiello, P., Salvatore, F., et al. (2014). The analysis of the inflorescence miRNome of the orchid Orchis italica reveals a DEF-like MADS-box gene as a new miRNA target. *PLoS One* 9, e97839. doi: 10.1371/journal.pone.0097839

Acri-Nunes-Miranda, R., and Mondragon-Palomino, M. (2014). Expression of paralogous SEP-, FUL-, AG- and STK-like MADS-box genes in wild-type and peloric Phalaenopsis flowers. *Front. Plant Sci.* 5:76. doi: 10.3389/fpls.2014.00076

Almeida, J., Rocheta, M., and Galego, L. (1997). Genetic control of flower shape in Antirrhinum majus. *Development* 124, 1387–1392.

Boyden, G. S., Donoghue, M. J., and Howarth, D. G. (2012). Duplications and expression of radialis-like genes in dipsacales. *Int. J. Plant Sci.* 173, 971–983. doi: 10.1086/667626

Cai, J., Liu, X., Vanneste, K., Proost, S., Tsai, W. C., Liu, K. W., et al. (2015). The genome sequence of the orchid Phalaenopsis equestris. *Nat. Genet* 47, 65–72. doi: 10.1038/ng.3149

Chao, Y. T., Yen, S. H., Yeh, J. H., Chen, W. C., and Shih, M. C. (2017). Orchidstra 2.0-a transcriptomics resource for the orchid family. *Plant Cell Physiol.* 58 (1):e9. doi: 10.1093/pcp/pcw220

Chow, C. N., Lee, T. Y., Hung, Y. C., Li, G. Z., Tseng, K. C., Liu, Y. H., et al. (2019). PlantPAN3.0: a new and updated resource for reconstructing transcriptional regulatory networks from ChIP-seq experiments in plants. *Nucleic Acids Res.* 47, D1155–D1163. doi: 10.1093/nar/gky1081

Citerne, H., Jabbour, F., Nadot, S., and Damerval, C. (2010). The evolution of floral symmetry. *Adv. Bot. Res.* 54 54, 85–137. doi: 10.1016/S0065-2296(10)54003-5

Corley, S. B., Carpenter, R., Copsey, L., and Coen, E. (2005). Floral asymmetry involves an interplay between TO and MYB transcription factors in Antirrhinum. *Proc. Natl. Acad. Sci. U. S. A.* 102, 5068–5073. doi: 10.1073/pnas.0501340102

Costa, M. M. R., Fox, S., Hanna, A. I., Baxter, C., and Coen, E. (2005). Evolution of regulatory interactions controlling floral asymmetry. *Development* 132, 5093–5101. doi: 10.1242/dev.02085

Cozzolino, S., and Widmer, A. (2005). Orchid diversity: an evolutionary consequence of deception? *Trends Ecol. Evol.* 20, 487–494. doi: 10.1016/j.tree.2005.06.004

Cubas, P., Lauter, N., Doebley, J., and Coen, E. (1999). The TCP domain: a motif found in proteins regulating plant growth and development. *Plant J.* 18, 215–222. doi: 10.1046/j.1365-313X.1999.00444.x

De Paolo, S., Gaudio, L., and Aceto, S. (2015). Analysis of the TCP genes expressed in the inflorescence of the orchid Orchis italica. *Sci. Rep.* 5, 16265. doi: 10.1038/srep16265

De Paolo, S., Salvemini, M., Gaudio, L., and Aceto, S. (2014). De novo transcriptome assembly from inflorescence of Orchis italica: analysis of coding and non-coding transcripts. *PLoS One* 9, e102155. doi: 10.1371/journal.pone.0102155

Dirks-Mulder, A., Butot, R., Van Schaik, P., Wijnands, J. W. P. M., Van Den Berg, R., Krol, L., et al. (2017). Exploring the evolutionary origin of floral organs of Erycina pusilla, an emerging orchid model system. *BMC Evol. Biol.* 17:89. doi: 10.1186/s12862-017-0938-7

Eguen, T., Straub, D., Graeff, M., and Wenkel, S. (2015). MicroProteins: small size - big impact. *Trends Plant Sci.* 20, 477–482. doi: 10.1016/j.tplants.2015.05.011

Endress, P. K. (2012). The immense diversity of floral monosymmetry and asymmetry across angiosperms. *Bot. Rev.* 78, 345–397. doi: 10.1007/s12229-012-9106-3

Galego, L., and Almeida, J. (2002). Role of DIVARICATA in the control of dorsoventral asymmetry in Antirrhinum flowers. *Genes Dev.* 16, 880–891. doi: 10.1101/gad.221002

Gao, Y. H., Zhang, D. Z., and Li, J. (2015). TCP1 Modulates DWF4 Expression via Directly Interacting with the GGNCCC Motifs in the Promoter Region of DWF4 in Arabidopsis thaliana. *J. Genet. Genomics* 42, 383–392. doi: 10.1016/j.jgg.2015.04.009

Garces, H. M., Spencer, V. M., and Kim, M. (2016). Control of Floret Symmetry by RAY3, SvDIV1B, and SvRAD in the Capitulum of Senecio vulgaris. *Plant Physiol.* 171, 2055–2068. doi: 10.1104/pp.16.00395

Gietz, R. D., Schiestl, R. H., Willems, A. R., and Woods, R. A. (1995). Studies on the Transformation of Intact Yeast-Cells by the Liac/S-DNA/Peg Procedure. *Yeast* 11, 355–360. doi: 10.1002/yea.320110408

Givnish, T. J., Spalink, D., Ames, M., Lyon, S. P., Hunter, S. J., Zuluaga, A., et al. (2015). Orchid phylogenomics and multiple drivers of their extraordinary diversification. *Proc. Biol. Sci.* 282:20151553. doi: 10.1098/rspb.2015.1553

Hamaguchi, A., Yamashino, T., Koizumi, N., Kiba, T., Kojima, M., Sakakibara, H., et al. (2008). A Small Subfamily of Arabidopsis RADIALIS-LIKE SANT/MYB Genes: A Link to HOOKLESS1-Mediated Signal Transduction during Early Morphogenesis. *Biosci. Biotechnol. Biochem.* 72, 2687–2696. doi: 10.1271/bbb.80348

Howarth, D. G., and Donoghue, M. J. (2009). Duplications and Expression of DIVARICATA-Like Genes in Dipsacales. *Mol. Biol. Evol.* 26, 1245–1258. doi: 10.1093/molbev/msp051

Hsu, H. F., Hsu, W. H., Lee, Y. I., Mao, W. T., Yang, J. Y., Li, J. Y., et al. (2015). Model for perianth formation in orchids. *Nat. Plants* 1:15046. doi: 10.1038/nplants.2015.46

Katoh, K., and Standley, D. M. (2013). MAFFT multiple sequence alignment software version 7: improvements in performance and usability. *Mol. Biol. Evol.* 30, 772–780. doi: 10.1093/molbev/mst010

Kosugi, S., and Ohashi, Y. (2002). DNA binding and dimerization specificity and potential targets for the TCP protein family. *Plant J.* 30, 337–348. doi: 10.1046/j.1365-313X.2002.01294.x

Kui, L., Chen, H. T., Zhang, W. X., He, S. M., Xiong, Z. J., Zhang, Y. S., et al. (2017). Building a genetic manipulation tool box for orchid biology: identification of constitutive promoters and application of CRISPR/Cas9 in the orchid, dendrobium officinale. *Front. Plant Sci.* 7:2036. doi: 10.3389/fpls.2016.02036

Li, C. N., Zhou, Y. Y., and Fan, L. M. (2015). A novel repressor of floral transition, MEE3, an abiotic stress regulated protein, functions as an activator of FLC by binding to its promoter in Arabidopsis. *Environ. Exp. Bot.* 113, 1–10. doi: 10.1016/j.envexpbot.2014.12.003

Li, M., Zhang, D., Gao, Q., Luo, Y., Zhang, H., Ma, B., et al. (2019). Genome structure and evolution of Antirrhinum majus L. *Nat. Plants* 5, 174–183. doi: 10.1038/s41477-018-0349-9

Lin, C. S., Hsu, C. T., Liao, D. C., Chang, W. J., Chou, M. L., Huang, Y. T., et al. (2016). Transcriptome-wide analysis of the MADS-box gene family in the orchid Erycina pusilla. *Plant Biotechnol J* 14, 284–298. doi: 10.1111/pbi.12383

Lu, C. A., Ho, T. H. D., Ho, S. L., and Yu, S. M. (2002). Three novel MYB proteins with one DNA binding repeat mediate sugar and hormone regulation of alpha-amylase gene expression. *Plant Cell* 14, 1963–1980. doi: 10.1105/tpc.001735

Luo, D., Carpenter, R., Copsey, L., Vincent, C., Clark, J., and Coen, E. (1999). Control of organ asymmetry in flowers of Antirrhinum. *Cell* 99, 367–376. doi: 10.1016/S0092-8674(00)81523-8

Luo, D., Carpenter, R., Vincent, C., Copsey, L., and Coen, E. (1996). Origin of floral asymmetry in Antirrhinum. *Nature* 383, 794–799. doi: 10.1038/383794a0

Machemer, K., Shaiman, O., Salts, Y., Shabtai, S., Sobolev, I., Belausov, E., et al. (2011). Interplay of MYB factors in differential cell expansion, and consequences for tomato fruit development. *Plant J.* 68, 337–350. doi: 10.1111/j.1365-313X.2011.04690.x

Madrigal, Y., Alzate, J. F., Gonzalez, F., and Pabon-Mora, N. (2019). Evolution of RADIALIS and DIVARICATA gene lineages in flowering plants with an expanded sampling in non-core eudicots. *Am J. Bot.* 106 (3): 1–18. doi: 10.1002/ajb2.1243

Mondragon-Palomino, M., and Theissen, G. (2009). Why are orchid flowers so diverse? Reduction of evolutionary constraints by paralogues of class B floral homeotic genes. *Ann. Bot.* 104, 583–594. doi: 10.1093/aob/mcn258

Mondragon-Palomino, M., and Theissen, G. (2011). Conserved differential expression of paralogous DEFICIENS- and GLOBOSA-like MADS-box genes in the flowers of Orchidaceae: refining the 'orchid code'. *Plant J.* 66, 1008–1019. doi: 10.1111/j.1365-313X.2011.04560.x

Pan, Z. J., Cheng, C. C., Tsai, W. C., Chung, M. C., Chen, W. H., Hu, J. M., et al. (2011). The duplicated B-class MADS-box genes display dualistic characters in orchid floral organ identity and growth. *Plant Cell Physiol.* 52, 1515–1531. doi: 10.1093/pcp/pcr092

Petzold, H. E., Chanda, B., Zhao, C. S., Rigoulot, S. B., Beers, E. P., and Brunner, A. M. (2018). DIVARICATA AND RADIALIS INTERACTING FACTOR (DRIF) also interacts with WOX and KNOX proteins associated with wood formation in Populus trichocarpa. *Plant J.* 93, 1076–1087. doi: 10.1111/tpj.13831

Preston, J. C., Kost, M. A., and Hileman, L. C. (2009). Conservation and diversification of the symmetry developmental program among close relatives of snapdragon with divergent floral morphologies. *New Phytol.* 182, 751–762. doi: 10.1111/j.1469-8137.2009.02794.x

Preston, J. C., Martinez, C. C., and Hileman, L. C. (2011). Gradual disintegration of the floral symmetry gene network is implicated in the evolution of a wind-pollination syndrome. *Proc. Natl. Acad. Sci. U. S. A.* 108, 2343–2348. doi: 10.1073/pnas.1011361108

Raimundo, J., Sobral, R., Bailey, P., Azevedo, H., Galego, L., Almeida, J., et al. (2013). A subcellular tug of war involving three MYB-like proteins underlies a molecular antagonism in Antirrhinum flower asymmetry. *Plant J.* 75, 527–538. doi: 10.1111/tpj.12225

Raimundo, J., Sobral, R., Laranjeira, S., and Costa, M. M. R. (2018). Successive domain rearrangements underlie the evolution of a regulatory module controlled by a small interfering peptide. *Mol. Biol. Evol.* 35, 2873–2885. doi: 10.1093/molbev/msy178

Reardon, W., Fitzpatrick, D. A., Fares, M. A., and Nugent, J. M. (2009). Evolution of flower shape in Plantago lanceolata. *Plant Mol. Biol.* 71, 241–250. doi: 10.1007/s11103-009-9520-z

Reardon, W., Gallagher, P., Nolan, K. M., Wright, H., Cardenosa-Rubio, M. C., Bragalini, C., et al. (2014). Different outcomes for the MYB floral symmetry genes DIVARICATA and RADIALIS during the evolution of derived actinomorphy in Plantago. *New Phytol.* 202, 716–725. doi: 10.1111/nph.12682

Rudall, P. J., and Bateman, R. M. (2002). Roles of synorganisation, zygomorphy and heterotopy in floral evolution: the gynostemium and labellum of orchids and other lilioid monocots. *Biol. Rev.* 77, 403–441. doi: 10.1017/S1464793102005936

Salemme, M., Sica, M., Gaudio, L., and Aceto, S. (2011). Expression pattern of two paralogs of the PI/GLO-like locus during Orchis italica (Orchidaceae, Orchidinae) flower development. *Dev. Genes Evol.* 221, 241–246. doi: 10.1007/s00427-011-0372-6

Salemme, M., Sica, M., Gaudio, L., and Aceto, S. (2013a). The OitaAG and OitaSTK genes of the orchid Orchis italica: a comparative analysis with other C- and D-class MADS-box genes. *Mol. Biol. Rep.* 40, 3523–3535. doi: 10.1007/s11033-012-2426-x

Salemme, M., Sica, M., Iazzetti, G., Gaudio, L., and Aceto, S. (2013b). The AP2-like gene OitaAP2 is alternatively spliced and differentially expressed in inflorescence and vegetative tissues of the orchid Orchis italica. *PLoS One* 8, e77454. doi: 10.1371/journal.pone.0077454

Sengupta, A., and Hileman, L. C. (2018). Novel traits, flower symmetry, and transcriptional autoregulation: new hypotheses from bioinformatic and experimental data. *Front. Plant Sci.* 9:1561. doi: 10.3389/fpls.2018.01561

Seo, P. J., Hong, S. Y., Kim, S. G., and Park, C. M. (2011). Competitive inhibition of transcription factors by small interfering peptides. *Trends Plant Sci.* 16, 541–549. doi: 10.1016/j.tplants.2011.06.001

Stamatakis, A. (2014). RAxML version 8: a tool for phylogenetic analysis and post-analysis of large phylogenies. *Bioinformatics* 30, 1312–1313. doi: 10.1093/bioinformatics/btu033

Staudt, A. C., and Wenkel, S. (2011). Regulation of protein function by 'microProteins'. *Embo Rep.* 12, 35–42. doi: 10.1038/embor.2010.196

Su, S. H., Xiao, W., Guo, W. X., Yao, X. R., Xiao, J. Q., Ye, Z. Q., et al. (2017). The CYCLOIDEA-RADIALIS module regulates petal shape and pigmentation, leading to bilateral corolla symmetry in Torenia fournieri (Linderniaceae). *New Phytol.* 215, 1582–1593. doi: 10.1111/nph.14673

Talavera, G., and Castresana, J. (2007). Improvement of phylogenies after removing divergent and ambiguously aligned blocks from protein sequence alignments. *Syst. Biol.* 56, 564–577. doi: 10.1080/10635150701472164

Valoroso, M. C., Censullo, M. C., and Aceto, S. (2019). The MADS-box genes expressed in the inflorescence of Orchis italica (Orchidaceae). *PLoS One* 14, e0213185. doi: 10.1371/journal.pone.0213185

Valoroso, M. C., De Paolo, S., Iazzetti, G., and Aceto, S. (2017). Transcriptome-Wide Identification and Expression Analysis of DIVARICATA- and RADIALIS-Like Genes of the Mediterranean Orchid Orchis italica. *Genome Biol. Evol.* 9 (6): 1418–1431. doi: 10.1093/gbe/evx101

Yang, X., Pang, H. B., Liu, B. L., Qiu, Z. J., Gao, Q., Wei, L., et al. (2012). Evolution of double positive autoregulatory feedback loops in CYCLOIDEA2 clade genes is associated with the origin of floral zygomorphy. *Plant Cell* 24, 1834–1847. doi: 10.1105/tpc.112.099457

Zhang, G. Q., Liu, K. W., Li, Z., Lohaus, R., Hsiao, Y. Y., Niu, S. C., et al. (2017). The Apostasia genome and the evolution of orchids. *Nature* 549, 379–383. doi: 10.1038/nature23897

Zhang, G. Q., Xu, Q., Bian, C., Tsai, W. C., Yeh, C. M., Liu, K. W., et al. (2016). The Dendrobium catenatum Lindl. genome sequence provides insights into polysaccharide synthase, floral development and adaptive evolution. *Sci. Rep.* 6, 19029. doi: 10.1038/srep19029

Zhou, X. R., Wang, Y. Z., Smith, J. F., and Chen, R. J. (2008). Altered expression patterns of TCP and MYB genes relating to the floral developmental transition from initial zygomorphy to actinomorphy in Bournea (Gesneriaceae). *New Phytol.* 178, 532–543. doi: 10.1111/j.1469-8137.2008.02384.x

Conflict of Interest: The authors declare that the research was conducted in the absence of any commercial or financial relationships that could be construed as a potential conflict of interest.

frontiers in Plant Science

ORIGINAL RESEARCH
published: 14 November 2019
doi: 10.3389/fpls.2019.01386

Maltose Processing and Not β-Amylase Activity Curtails Hydrolytic Starch Degradation in the CAM Orchid *Phalaenopsis*

*Nathalie Ceusters[1], Mario Frans[1], Wim Van den Ende[2] and Johan Ceusters[1,3]**

[1] KU Leuven, Department of Biosystems, Division of Crop Biotechnics, Research Group for Sustainable Crop Production & Protection, Campus Geel, Geel, Belgium, [2] KU Leuven, Department of Biology, Laboratory of Molecular Plant Biology, Leuven, Belgium, [3] UHasselt, Centre for Environmental Sciences, Environmental Biology, Diepenbeek, Belgium

OPEN ACCESS

Edited by:
Katharina Nargar, Commonwealth Scientific and Industrial Research Organisation (CSIRO), Australia

Reviewed by:
Ian Joseph Tetlow, University of Guelph, Canada
Alberto A. Iglesias, National University of the Littoral, Argentina

***Correspondence:**
Johan Ceusters
johan.ceusters@kuleuven.be

Specialty section:
This article was submitted to Plant Development and EvoDevo, a section of the journal Frontiers in Plant Science

Received: *09 August 2019*
Accepted: *08 October 2019*
Published: *14 November 2019*

Citation:
Ceusters N, Frans M, Van den Ende W and Ceusters J (2019) Maltose Processing and Not β-Amylase Activity Curtails Hydrolytic Starch Degradation in the CAM Orchid Phalaenopsis. Front. Plant Sci. 10:1386. doi: 10.3389/fpls.2019.01386

Crassulacean acid metabolism (CAM) is one of the three photosynthetic pathways in higher plants and is characterized by high water use efficiency. This mainly relies on major nocturnal CO_2 fixation sustained by degradation of storage carbohydrate such as starch to provide phosphoenolpyruvate (PEP) and energy. In contrast to C3 plants where starch is mainly degraded by the hydrolytic route, different observations suggested the phosphorolytic route to be a major pathway for starch degradation in CAM plants. To elucidate the interplay and relevant contributions of the phosphorolytic and hydrolytic pathways for starch degradation in CAM, we assessed diel patterns for metabolites and enzymes implicated in both the hydrolytic route (β-amylase, DPE1, DPE2, maltase) and the phosphorolytic route (starch phosphorylase) of starch degradation in the CAM orchid *Phalaenopsis* "Edessa." By comparing the catalytic enzyme activities and starch degradation rates, we showed that the phosphorolytic pathway is the major route to accommodate nocturnal starch degradation and that measured activities of starch phosphorylase perfectly matched calculated starch degradation rates in order to avoid premature exhaustion of starch reserves before dawn. The hydrolytic pathway seemed hampered in starch processing not by β-amylase but through insufficient catalytic capacity of both DPE2 and maltase. These considerations were further corroborated by measurements of enzyme activities in the CAM model plant *Kalanchoë fedtschenkoi* and strongly contradict with the situation in the C3 plant Arabidopsis. The data support the view that the phosphorolytic pathway might be the main route of starch degradation in CAM to provide substrate for PEP with additional hydrolytic starch breakdown to accommodate mainly sucrose synthesis.

Keywords: hydrolytic starch degradation, phosphorolytic starch degradation, DPE2, maltase, crassulacean acid metabolism, *Phalaenopsis*

INTRODUCTION

Crassulacean acid metabolism (CAM) is one of the three photosynthetic pathways present in higher plants and is characterized by an optimized water use efficiency (WUE) by taking up CO_2 predominantly at night when evapotranspiration rates are low. It is convenient to recognize four distinct phases of gas exchange in CAM plants, which are also used to describe the photosynthetic performance. Sequestration of CO_2 at night (Phase I) occurs *via* the enzyme phosphoenolpyruvate carboxylase (PEPC) with the 3-C substrate phosphoenolpyruvate (PEP) provided by the glycolytic breakdown of carbohydrate. The final 4-C product, malic acid, is stored in a large central vacuole. At the start of the next day, in Phase II, stomata will gradually close and external CO_2 is mainly fixed by ribulose-1,5-bisphosphate carboxylase-oxygenase (rubisco). Gas exchange is curtailed by stomatal closure during the middle of the day (Phase III), thereby reducing transpirational water losses and improving WUE. During this phase, malic acid exits the vacuole and decarboxylation releases CO_2 which is re-fixed by rubisco. In Phase IV stomata open again towards the end of the day and external CO_2 is mainly sequestered *via* rubisco (Osmond, 1978).

Because of the tight relationship between PEP availability and nocturnal CO_2 fixation (Dodd et al., 2003; Ceusters et al., 2019), the provision of carbon skeletons for the synthesis of PEP represents a significant sink for carbohydrate. Besides starch, also glycolysis driven by sucrose hydrolysis can attribute to PEP formation. Various studies with CAM bromeliads showed diurnal accumulation of both starch and soluble sugars followed by nocturnal decrease to fuel the dark reactions of CAM (Christopher and Holtum, 1998; Popp et al., 2003; Ceusters et al., 2008; Ceusters et al., 2009a; Ceusters et al., 2009b; Ceusters et al., 2011; Ceusters et al., 2014). Therefore, transitory starch plays a crucial role in many CAM plants. In contradiction to the starch biosynthesis pathway for which the major steps have been well characterized, the process of transitory starch breakdown in CAM has not yet been elucidated (Lloyd and Kossmann, 2015). In starch storing CAM species different modes of starch degradation might be deployed for nocturnal starch breakdown, i.e. the phosphorolytic and/or the hydrolytic route (Borland et al., 2016; Brilhaus et al., 2016). Both routes are assumed to share the same enzymes to induce the initial attack to starch granules. Glucan water dikinase (GWD) initially phosphorylates the starch granule which consists of branched amylopectin and linear amylose. Debranching enzymes limit dextrinase (LDA) and isoamylase (ISA) bring about cleavage of the branch points in amylopectin. Different enzymes are subsequently used for further processing of linear amylose into soluble sugars (Weise et al., 2011). Whilst phosphorolytic starch degradation in the chloroplast mainly delivers glucose-6-phosphate (Glc6P) for export, the export product resulting from the hydrolytic starch breakdown is maltose (Kore-eda and Kanai, 1997; Weise et al., 2004).

Several observations indicate the phosphorolytic pathway to be the main route in CAM. The facultative CAM plant *Mesembryanthemum crystallinum* (common ice plant) is able to switch from C3 to CAM under drought or salt stress and has emerged as a useful model for exploring CAM. By shifting to the CAM mode, a considerable export of Glc6P out of the chloroplast was observed whilst maltose export dramatically diminished (Neuhaus and Schulte, 1996). In addition, consistent increases in transcript abundances and in the activity of enzymes involved in the phosphorolytic route were observed when switching to CAM mode (Paul et al., 1993; Dodd et al., 2003; Cushman et al., 2008; Taybi et al., 2017). Phosphorolytic degradation of starch is mediated *via* starch phosphorylase, which releases glucose 1-phosphate (Glc1P) from the non-reducing ends of glucan chains. Subsequently, phosphoglucomutase (PGM) catalyses the conversion of Glc1P to Glc6P which is exported to the cytosol *via* the plastidic Glucose 6-Phosphate: Phosphate Translocator (GPT). GPT transcript abundance has been found to show a > 70-fold upregulation in *M. crystallinum* upon CAM induction (Haüsler et al., 2000; Cushman et al., 2008; Kore-eda et al., 2013). In C3 plants the phosphorolytic mode of starch degradation has been proposed to provide carbon solely for metabolism inside the chloroplast *via* the pentose phosphate pathway, particularly under stress conditions when photorespiration is elevated (Weise et al., 2006; Zeeman et al., 2007).

The hydrolytic route of starch degradation is mainly mediated *via* β-amylase, leading to the production of maltose. Besides maltose, a range of short malto-oligosaccharides will emerge as by-products. These require further processing by chloroplastic glucanotransferase disproportionating enzyme (DPE1) to yield glucose and a spectrum of larger, linear oligosaccharides which can further be metabolized again by β-amylase. Notwithstanding α-amylase also possesses the capacity to degrade transitory starch, no phenotype has been detected in knockout mutants of Arabidopsis (Yu et al., 2005). To reach the cytosol glucose and maltose require the dedicated transporters Maltose Excess Protein1 (MEX1) and Plastidic Glucose Transporter (pGlcT) (Niittylä et al., 2004; Smith et al., 2005; Cho et al., 2011). In Arabidopsis, the major export product out of the chloroplast has been found to be maltose and further processing in the cytosol requires a cytosolic disproportionating enzyme (DPE2), which transfers one glucose unit from maltose to an acceptor (a form of cytosolic heteroglycan) and releases the other glucose molecule (Lu and Sharkey, 2004). Based on calculations of starch breakdown in Arabidopsis wild types and DPE2 mutants, direct hydrolysis by maltase (α-glucosidase) has been considered of minor importance (Chia et al., 2004). The potential contribution of maltase in CAM plants is yet unknown. In the cytosol, cytosolic hexokinase catalyses the conversion from glucose to Glc6P, which together with the Glc6P derived from the phosphorolytic degradation, can be used for further sucrose synthesis (Borland et al., 2016).

Several studies on the common ice plant (*M. crystallinum*) demonstrated the upregulation of transcript abundances and activities of a range of starch-degrading enzymes implicated in both the hydrolytic and phosphorolytic routes of starch degradation (α-amylase, β-amylase, starch phosphorylase, and disproportionating enzyme (DPE1 and DPE2)) following CAM induction (Paul et al., 1993; Neuhaus and Schulte, 1996; Haüsler et al., 2000; Dodd et al., 2003; Cushman et al., 2008). These observations pose important questions about 1) the

relative contribution of both routes of starch degradation in CAM and 2) whether specific enzymes might be rate limiting in either phosphorolytic and hydrolytic pathways. Exploiting the phosphorolytic pathway might confer specific advantages for CAM plants as Glc6P not only functions as an allosteric activator for PEPC but its glycolytic conversion in the cytosol also provides ATP, which adds in energizing nocturnal accumulation of malate in the vacuole (Holtum et al., 2005; Weise et al., 2011; Cheung et al., 2014). However, it has recently been postulated that the use of both the hydrolytic and phosphorolytic starch degradation pathway in CAM plants might provide a means to accommodate carbohydrate partitioning between competing forces of growth and nocturnal carboxylation during the diel cycle (Borland et al., 2016). To elucidate the interplay and relevant contributions of the phosphorolytic and hydrolytic pathways for starch degradation we assessed diel *in vitro* activity patterns for enzymes implicated in either the hydrolytic route (β-amylase, DPE1, DPE2, maltase) or the phosphorolytic route (starch-phosphorylase) of starch degradation in the CAM orchid *Phalaenopsis* "Edessa." These analyses were further complemented with measurements of diel leaf gas exchange and important metabolite dynamics (starch, malic acid, sucrose, glucose, fructose, maltose, Glc6P, Glc1P). By comparing *in vitro* catalytic activities and starch degradation rates we were able to gain more insight about the relative contributions of both pathways and postulated a bottleneck limiting hydrolytic starch conversion.

MATERIALS AND METHODS

Plant Material and Sampling

Phalaenopsis "Edessa" is an obligate starch-storing CAM plant and belongs to the family of the Orchidaceae. In starch-storing CAM plants starch is the main carbohydrate to accommodate nocturnal carboxylation whilst soluble sugar storing species employ sucrose, glucose, and/or fructose. Vegetative plants of 16 weeks old were cultivated in a growth room with a constant temperature of 28°C, a relative humidity of 75% and a 12h photoperiod (zeitgeber time ZT0-ZT12) with photosynthetic photon flux density (PPFD) of 100 μmol m^{-2} s^{-1}. Watering was performed twice a week; once with a nutrient solution Peters 20N-8.7P-16.6K of 1 mS cm^{-1} and once with water. After six weeks, leaf samples (n = 5) were taken from the upper one-third of young fully expanded source leaves during a cycle of 24 h starting from 08.00 h (ZT0) every 2 h until 08.00 h the next morning (ZT24). The samples from 08.00 h (ZT0 and ZT24) were taken when the lights were turned on whilst the samples taken at 20.00 h (ZT12) were taken in the dark under green safety light.

At ZT12 samples were also taken from leaf pair six of the obligate model CAM plant *Kalanchoë fedtschenkoi* in order to provide comparison with the *Phalaenopsis* enzyme activity determinations. These plants were also grown in a growth room with a temperature of 25 °C and 19 °C during the light and dark periods respectively, with a relative humidity of 75% and a 12-h photoperiod (zeitgeber time ZT0-ZT12) with photosynthetic photon flux density (PPFD) of ~250 μmol m^{-2} s^{-1}. Plants were grown under these conditions for at least 8-10 weeks before sampling at which time all plants had around 10 to 12 leaf pairs.

All samples were immediately frozen in liquid nitrogen, powdered and stored at -80°C.

Gas Exchange Measurements

Net CO_2 exchange was measured on the youngest fully expanded leaves, using a LCi Portable Photosynthesis System (ADC BioScientific Ltd., UK; https://www.adc.co.uk/). The top part of the leaf was enclosed in a broad leaf chamber (6.25 cm2) and the incoming air was passed through a 20-l bottle to buffer short-term fluctuations in the CO_2 concentration. After six weeks, gas exchange data were collected over a 24-h period with measurements obtained at 15-min intervals (n = 3).

Chemical Analyses of Metabolites

Soluble sugars (glucose, fructose, sucrose, and maltose) were extracted using hot water (80°C), as described by Tarkowski et al. (2019), and quantified by high performance anion exchange chromatography with pulsed amperometric detection, as described by Verspreet et al. (2013).

Extraction for measurements of starch, malic acid, and phosphorylated sugars (Glc6P and Glc1P) was performed as described by Chen et al. (2002), but with modifications. Approximately 180 mg of powdered tissue was mixed with 450 μl of ice-cold 4% (v/v) $HClO_4$. The mixture was allowed to thaw slowly on ice for 30 min. The resulting suspension was then centrifuged at 4°C for 10 min at 16,200 g. The insoluble residue from the perchloric acid extraction was used to determine starch content spectrophotometrically at 340 nm as glucose equivalents (Genesys 10S UV-VIS, Thermo Scientific, USA; https://www.thermofisher.com), following digestion with a mix of amyloglucosidase (EC 3.2.1.3) and α-amylase (EC 3.2.1.1). The analyses were conducted as earlier described by Ceusters et al. (2008). The supernatant from the $HClO_4$ extraction was neutralized at 4°C with 5 M K_2CO_3, and the resulting potassium perchlorate precipitate was removed by 10 min centrifugation at 16,200 g and 4°C. Five mg activated charcoal was added to the supernatant, and after 15 min at 4°C, removed by new centrifugation. The supernatant was used for measurement of malic acid, Glc6P, and Glc1P. Malic acid was measured in a 500-μl reaction mixture (EnzytecTM code n° E1215) containing: glycylglycinebuffer, NAD, glutamate oxaloacetate transaminase (GOT, EC 2.6.1.1). Analysis was performed spetrophotometrically by determining the change in absorbance at 340 nm after adding L-malate dehydrogenase (L-MDH, EC 1.1.1.37). The phosphorylated sugars Glc6P and Glc1P were measured in a 500-μl reaction mixture containing: 100 mM HEPES-KOH, pH 7.6, 4 mM $MgCl_2$, 0.2 mM NADP and 1 unit glucose-6-phosphate dehydrogenase (G6PDH, EC 1.1.1.49) for Glc6P, then 1 unit glucose phosphate isomerase (GPI, EC 5.3.1.9) and 1 unit PGM (EC 5.4.2.2) for Glc1P (Mohanty et al., 1993). Analysis was performed spectrophotometrically by determining the change in absorbance at 340 nm.

Enzyme Activities

All extraction steps were performed by homogenizing leaf material at 4°C in extraction buffer containing: 0.3 M N-(2-hydroxyethyl)

piperazine-N′-(2-ethane sulphonic acid) (HEPES, pH 7.4), 20 mM $MgCl_2$, 1 mM EDTA, 1 mM EGTA, 4.6 mM DTT, 80 mM benzamidine, 1 mM phenylmethylsulfonyl fluoride (PMSF), and 0.1 mM Triton X-100.

The extraction of β-amylase was based on the method described by Zeeman et al. (1998), but with modifications. After extraction, the homogenate was centrifuged at 4°C for 10 min at 16,200 g. The supernatant was incubated at 30˚C for 30 min in a 250 µl reaction mixture containing 50 mM 3-(N-Morpholino) propanesulfonic acid (MOPS, pH 6.4), 5 mM EDTA, 5 mM DTT, and 15 mg ml–1 soluble potato starch. After incubation, the reaction was stopped by boiling for 5 min and maltose was hydrolyzed by incubation in a 135 µl reaction mixture, containing 74 mM 2-(N-morpholino) ethanesulfonic acid (MES, pH 6.8), and 2 units maltase (EC 3.2.1.20), for 2 h at 37˚C. The reaction was stopped by boiling for 5 min and the resulting glucose was determined in a 500 µl reaction mixture containing: 25 mM HEPES (pH 7.9), 1 mM $MgCl_2$, 1.2 mg ml^{-1} ATP, 1.0 mg ml^{-1} NAD, and 2 units hexokinase (EC 2.7.1.1). Analysis was performed spectrophotometrically (Genesys 10S UV-VIS, Thermo Scientific, USA) by determining the change in absorbance at 340 nm after adding 4 units G6PDH.

The extraction of maltase (α-glucosidase) and plastidic D-enzyme (4-α-glucanotransferase: DPE1) was based on the methods described by Kruger and ap Rees (1983) and by Takaha et al. (1993) respectively, but with modifications. After extraction, the homogenate was centrifuged at 4°C for 10 min at 16,200 g. The supernatant was incubated at 30˚C for 30 min in a 250 µl reaction mixture containing 50 mM sodium acetate (pH 5.2), 90 mM maltose for maltase and 50 mM MOPS-NaOH (pH 6.8), and 60 mM maltotriose for plastidic D-enzyme. The reaction was stopped by boiling for 1 min and 100 µl of pure extract was also boiled for 1 min as control. Subsequently glucose was determined in a 500 µl reaction mixture containing: 25 mM HEPES (pH 7.9), 1 mM $MgCl_2$, 1.2 mg ml^{-1} ATP, 1.0 mg ml^{-1} NAD and 2 units hexokinase (EC 2.7.1.1). Analysis was performed spectrophotometrically by determining the change in absorbance at 340 nm after adding 4 units G6PDH.

The extraction and assay of cytosolic D-enzyme (DPE2) was based on the method described by Chia et al. (2004), but with modifications. After extraction, the homogenate was centrifuged at 4°C for 10 min at 16,200 g. Subsequently the supernatant was desalted by passing twice through a 0.5-ml column of Sephadex G-25, equilibrated with 100 mM Tris-HCl (pH 7.5 at 4°C), 1 mM DTT, 1 mM benzamidine, and 5% (w/v) glycerol. Three series of the same samples were incubated at 30°C for 2 h. The first series for assay of glucose production contained: 31 mM MOPS (pH 7), 10% (v/v) glycerol, 2.5% (w/v) oyster glycogen, and 30 mM maltose in a 200 µl reaction mixture. The two remaining series are incubated lacking either maltose or glycogen to exclude glucose not from the reaction catalzsed by DPE2. The reaction was stopped by boiling for 2 min and analysis was performed spectrophotometrically by determining the change in absorbance at 340 nm after adding 4 units G6PDH. The activity was calculated as the difference between the amount of glucose produced in the first incubation series, and the sum of the amounts of glucose produced in the two-control series.

The extraction of starch phosphorylase (α-glucan phosphorylase) was based on the method described by Kumar and Sanwal (1982), but with modifications. After extraction, the homogenate was centrifuged at 4°C for 10 min at 16,200 g. The supernatant was incubated at 30°C for 30 min in a 200 µl reaction mixture containing 0.2 M MOPS (pH 7.1), 15 mg ml^{-1} soluble potato starch, and 16 mM phosphate mix Na_2HPO_4/KH_2PO_4. The reaction was stopped by boiling for 1 min and the supernatant was assayed in a 500 µl reaction mixture: 0.1 M HEPES (pH 7.6), 4 mM $MgCl_2$, and 1.5 mg ml^{-1} NADP. The resulting Glc1P was determined spectrophotometrically by calculating the change in absorbance at 340 nm after addition of 3 units PGM (EC 5.4.2.2) and 3 units G6PDH.

The extraction and assay of PEPC was based on the method described by Borland and Griffiths (1997). About 200 mg leaf material was homogenized in 1 ml extraction buffer at 4°C containing: 200 mM Tris-HCl (pH 8.0), 2 mM EDTA, 1 mM dithiothreitol (DTT), 2% (w/v) polyethylene glycol (PEG) 20,000, 1 mM benzamidine, and 10 mM malic acid with 240 mM $NaHCO_3$. The homogenate was centrifuged for 2 min at 16,200 g. The extract was then desalted by passing twice through a 0.5-ml column of Sephadex G-25, equilibrated with 100 mM Tris-HCl (pH 7.5 at 4°C), 1 mM DTT, 1 mM benzamidine, and 5% (w/v) glycerol. The Ki of PEPC for malic acid was estimated using different malic acid concentrations (0.25, 0.5, 2, 8, 16 mM) in a reaction mix (500 µl) containing: 65 mM Tris-HCl (pH 7.5), 5 mM $MgCl_2$, 0.2 mM NADH, 10 mM $NaHCO_3$, and 2.5 mM PEP. Production of oxaloacetate by PEPC was coupled to oxidation of NADH by the high endogenous NAD-dependent MDH activity in the extracts. The reaction was initiated by the addition of 50 µl of extract and change in absorbance at 340 nm was measured for 4 min at 25°C. Preliminary experiments confirmed a linear decrease of NADH for during at least 6 min.

Data Analyses

Where appropriate, data were analyzed using the statistical software package IBM SPSS Statistics V23. Before carrying out statistical tests, normality of the data was checked by means of the Kolmogorov-Smirnoff statistic ($p > 0.05$). Means are compared by independent sample t-test ($\alpha = 0.05$). All replicates considered in our study were independent biological replicates originating from different plants.

RESULTS

Nocturnal CO_2 Uptake and Starch Degradation

To investigate nocturnal starch degradation and the associated enzyme activities in more detail, nocturnal starch breakdown was divided into two distinct periods based on the calculated rates of breakdown (**Figure 1A**). During the first period of the night (from ZT12 to ZT20), nocturnal degradation of starch proceeded nearly linearly ($y = -20.21 x + 131.16$; $R^2 = 0.998$) with a mean rate of 67 ± 13 nmol g^{-1}FW min^{-1}, providing 32 ± 7 µmol Glc eq. g^{-1}FW which is equivalent to the provision of 64

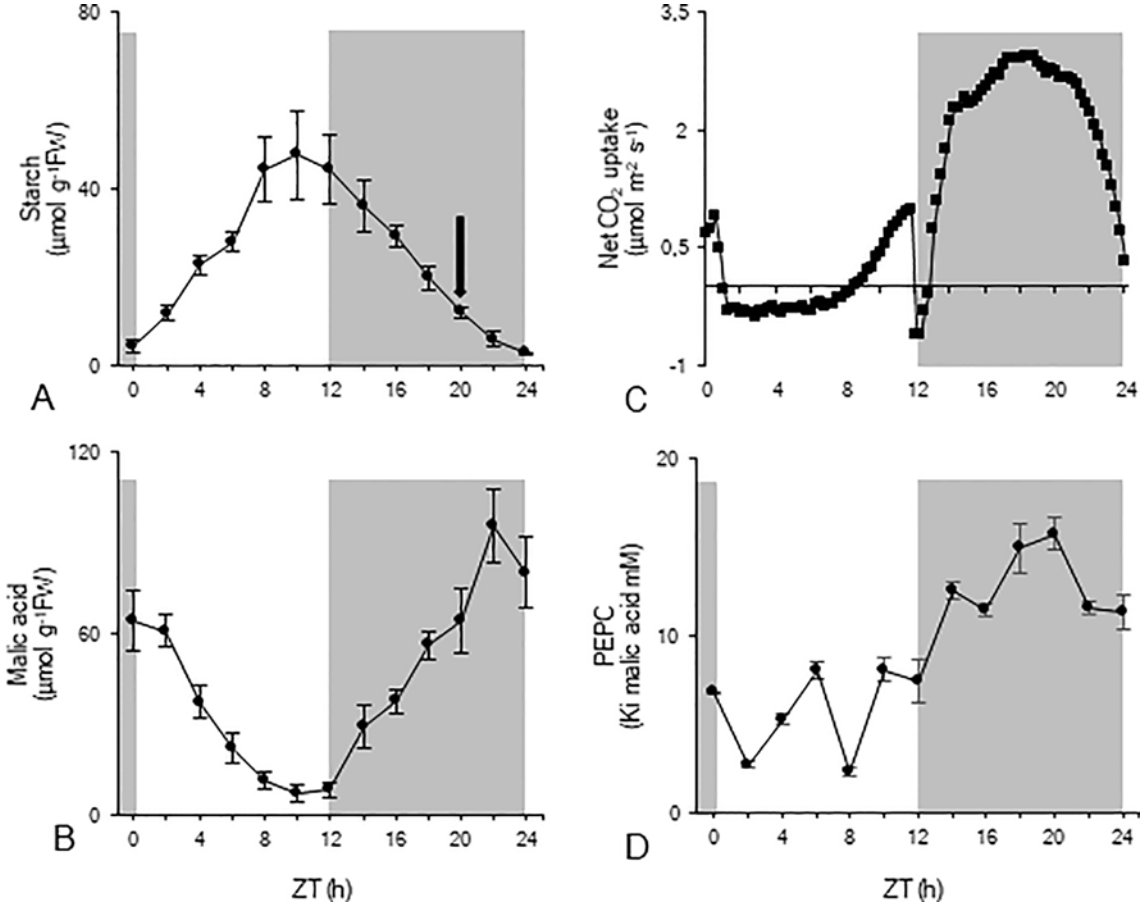

FIGURE 1 | Diel patterns of starch (µmol g^{-1}FW, **A**), malic acid (µmol g^{-1}FW, **B**), leaf gas exchange (µmol m^{-2} s^{-1}, **C**), and Ki of PEPC for malic acid (mM, **D**) for young fully developed leaves of *Phalaenopsis* 'Edessa'. The black arrow in panel **(A)** indicates the division of the nocturnal period based on the calculated starch degradation rates. The dark period is indicated in grey. Data are means ± SD (n = 5 for **A**, **B** and **D**; n = 3 for **C**).

µmol g^{-1}FW of PEP. Moving closer to dawn, from ZT20 to ZT24, nocturnal starch degradation was also linear but ($y = -11.48\ x + 40.10$; $R^2 = 0.974$) proceeded with a significantly lower rate of 38 ± 6 nmol g^{-1}FW min^{-1} and provided 9 ± 2 µmol Glc eq. g^{-1}FW which is equivalent to 18 µmol g^{-1}FW of PEP. In each of the considered periods, starch degradation provided enough substrate to sustain nocturnal malic acid synthesis (**Figure 1B**) with an initial accumulation of 56 ± 10 µmol g^{-1}FW followed by another 20 ± 7 µmol g^{-1}FW at the end of the night. In accordance, nocturnal CO_2 uptake (**Figure 1C**) was about 96 ± 8 mmol m^{-2} for the first nocturnal period and 35 ± 9 mmol m^{-2} for the second period. The pattern of leaf gas exchange showed increasing CO_2 uptake during the first three hours (ZT12 – ZT15) of the dark period whilst a decreasing CO_2 assimilation rate was noticed during the final three hours (ZT21 – ZT24) of the dark period (**Figure 1C**). Measurements of Ki PEPC for malic acid fluctuated during the day around a low mean value of 6 ± 3 mM. During the first period of the night (from ZT12 to ZT20) Ki values strongly increased to a maximum value of 16 ± 1 mM (ZT20), and slightly decreased during the second period of the night to 11 ± 1 mM (ZT24) (**Figure 1D**).

Diel Patterns of Sugars and Sugar Intermediates

The diel pattern of sucrose showed a rather stable diurnal phase followed by a significant ($p < 0.05$) nocturnal decrease to a minimum value of 3 ± 1 µmol g^{-1}FW, before rising again in the later part of the night to predusk levels (**Figure 2A**). Glucose and fructose concentrations were relatively stable during the diel cycle and fluctuated around 2 ± 1 µmol g^{-1}FW (**Figures 2B**, **C**). Leaf maltose contents remained rather stable during the photoperiod, varying around 22 ± 10 nmol g^{-1}FW, and doubled during the dark period, reaching a peak value of 47 ± 13 nmol g^{-1}FW (ZT22) (**Figure 2D**). Glc6P (**Figure 2E**) concentrations generally increased during daytime until a dramatic decrease at the day-night transition (ZT12) from 86 ± 9 nmol g^{-1}FW to 44 ± 6 nmol g^{-1}FW. After two hours in the dark, values restored again to 82 ± 6 nmol g^{-1}FW (ZT14) and remained relatively stable during the remainder of the night, until a strong decrease during the last two hours of the dark period (ZT22 – ZT24). A similar diel pattern was observed for Glc1P (**Figure 2F**). During daytime concentrations generally increased, until a dramatic decrease at the day-night transition (ZT12) from 7 ± 1 nmol g^{-1}FW to 4 ± 1 nmol g^{-1}FW. After two hours in the dark,

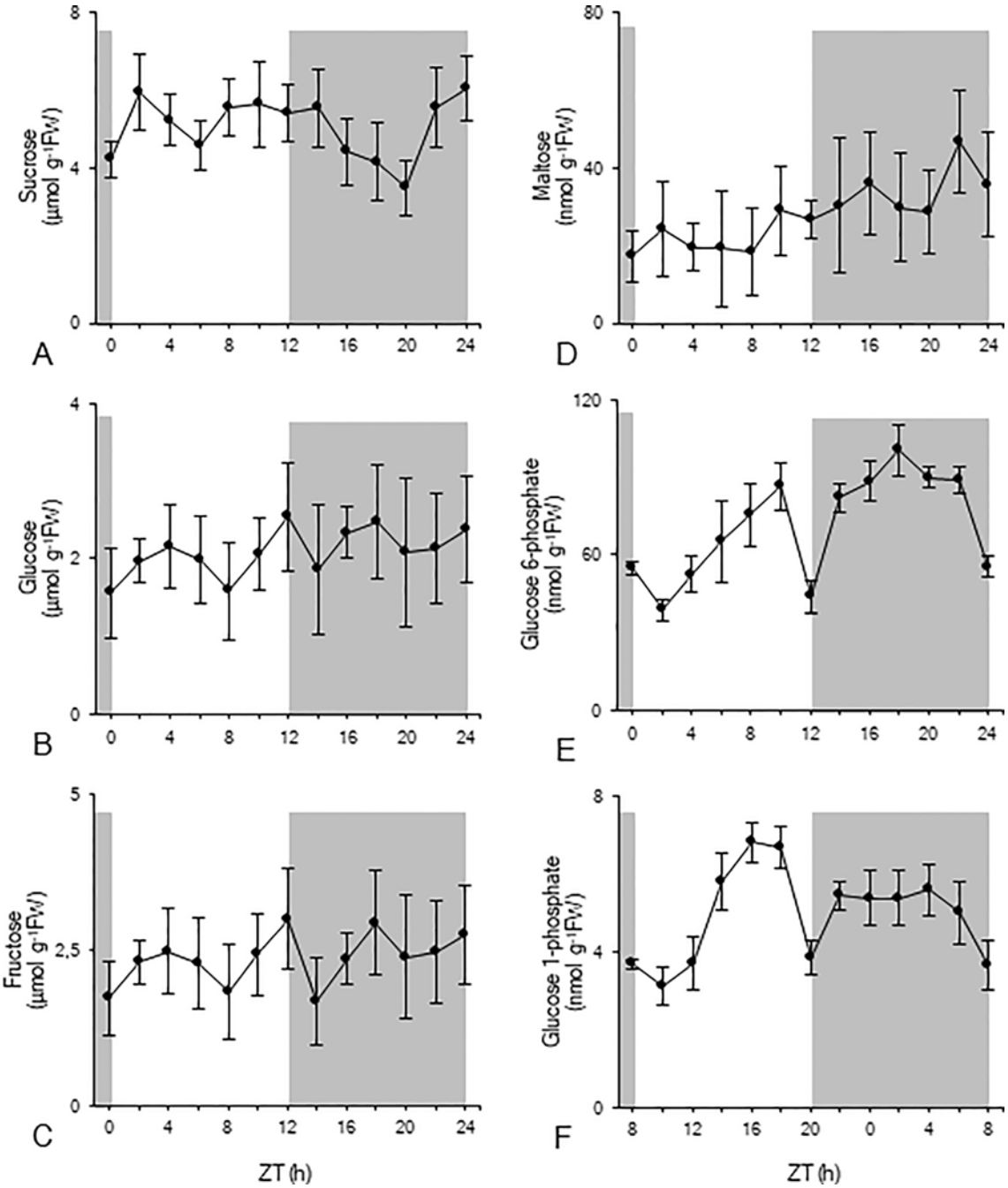

FIGURE 2 | Diel patterns of sucrose (µmol g^{-1}FW, **A**), glucose (µmol g^{-1}FW, **B**), fructose (µmol g^{-1}FW, **C**), maltose (nmol g^{-1}FW, **D**), glucose 6-phosphate (nmol g^{-1}FW, **E**), and glucose 1-phosphate (nmol g^{-1}FW, **F**) for young fully developed leaves of *Phalaenopsis* 'Edessa'. The dark period is indicated in grey. Data are means ± SD (n = 5).

values restored to 5 ± 1 nmol g^{-1}FW, and remained relatively stable during the remainder of the night, followed by a gradual decrease during the last four hours of the dark period (ZT20 – ZT24).

Diel Activity Patterns of Enzymes Implicated in Starch Degradation

In order to gain more insight into the nocturnal starch degradation process, total extractable activities of a range of enzymes implicated in starch degradation were measured over the complete diel cycle (**Figure 3**). Starch phosphorylase activity significantly ($p < 0.05$) decreased during daytime from 95 ± 15 nmol g^{-1}FW min^{-1} to 48 ± 6 nmol g^{-1}FW min^{-1} (**Figure 3A**). Compared to these daytime values, nocturnal starch phosphorylase activity was higher, fluctuating around a mean of 68 ± 8 nmol g^{-1}FW min^{-1} (**Figure 3A**). β-amylase showed the highest activity of all enzymes but without any clear pattern over the 24-h cycle (**Figure 3B**). Heavily fluctuating activities between

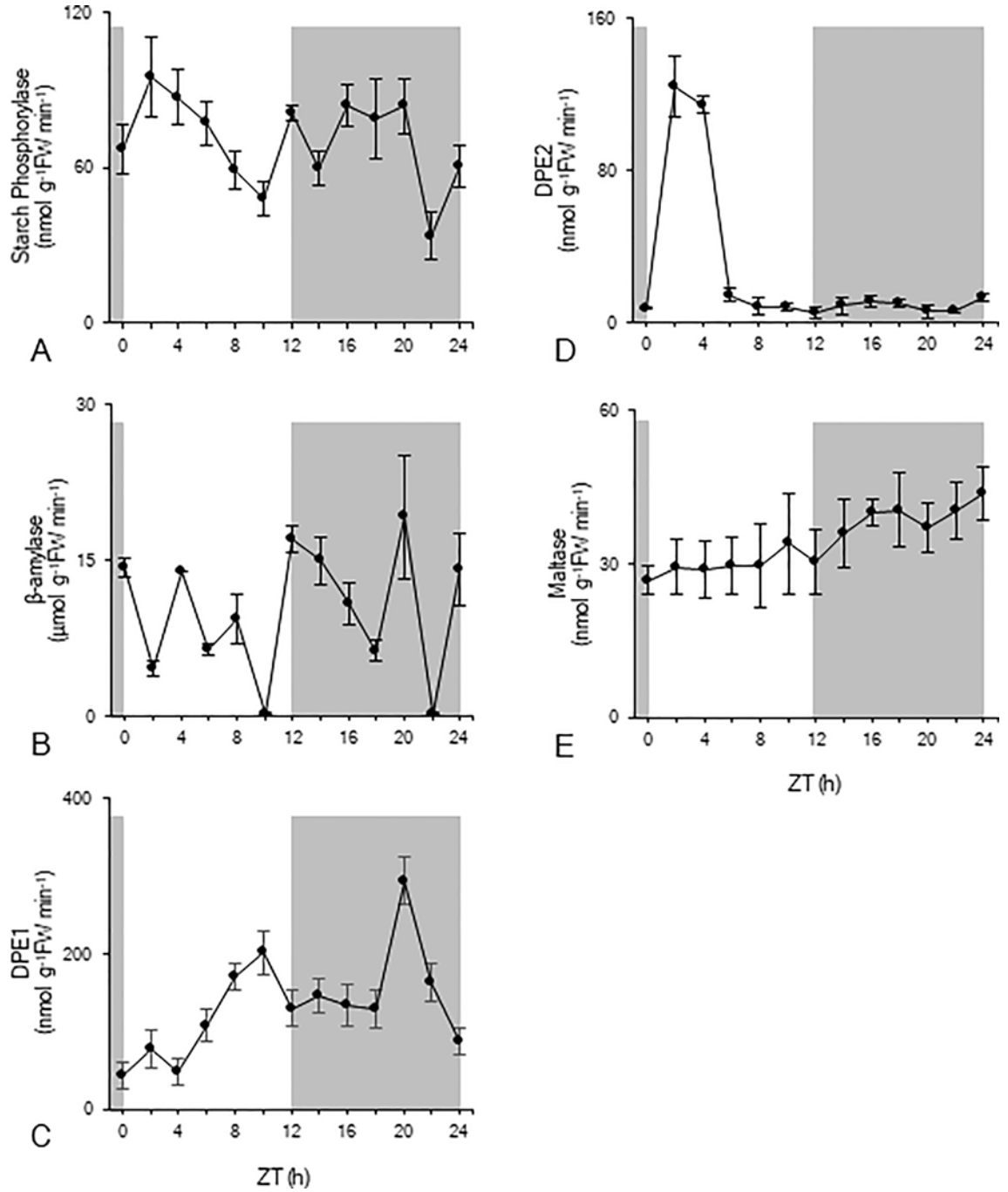

FIGURE 3 | Diel enzyme activity of starch phosphorylase (nmol g^{-1}FW min^{-1}, **A**), β-amylase (µmol g^{-1}FW min^{-1}, **B**), DPE1 (nmol g^{-1}FW min^{-1}, **C**), DPE2 (nmol g^{-1}FW min^{-1}, **D**), and maltase (nmol g^{-1}FW min^{-1}, **E**) for young fully developed leaves of *Phalaenopsis* 'Edessa'. The dark period is indicated in grey. Data are means ± SD (n = 5).

0.21 ± 0.01 µmol g^{-1}FW min^{-1} and 19 ± 6 µmol g^{-1}FW min^{-1} were observed during both day and night. The chloroplastic disproportionating enzyme (DPE1) showed an increasing activity during daytime from 44 ± 16 nmol g^{-1}FW min^{-1} (ZT0) to 200 ± 28 nmol g^{-1}FW min^{-1} (ZT10) (**Figure 3C**). Except for the observed high activity at ZT20 (317 ± 60 nmol g^{-1}FW min^{-1}), nocturnal DPE1 activity was quite stable around a mean value of 156 ± 12 nmol g^{-1}FW min^{-1}. For cytosolic disproportionating enzyme (DPE2) high activities were observed during the photoperiod at ZT2 and ZT4, i.e. 124 ± 16 nmol g^{-1}FW min^{-1} and 112 ± 4 nmol g^{-1}FW min^{-1} respectively. However, during the remainder of the day and night, the enzyme showed an overall

low activity of only 8 ± 4 nmol g^{-1}FW min^{-1} (**Figure 3D**). Maltase activity remained relatively stable during the photoperiod with a mean activity of 28 ± 8 nmol g^{-1}FW min^{-1} (**Figure 3E**). During the dark period, maltase activity significantly ($p < 0.05$) increased from a minimum activity of 30 ± 6 nmol g^{-1}FW min^{-1} (ZT12) to a maximum activity of 44 ± 5 nmol g^{-1}FW min^{-1} (ZT24).

Nocturnal Starch Degradation and Calculated Enzymatic Capacities

The nocturnal *in vitro* activities of the enzymes involved in starch degradation (starch phosphorylase, β-amylase, DPE1, DPE2, and maltase) were considered relative to the upper and lower limits of the observed starch degradation rate i.e. 67 ± 13 nmol g^{-1}FW min^{-1} from ZT12-ZT20 and 38 ± 6 nmol g^{-1}FW min^{-1} from ZT20-ZT24. Registered minimum, maximum, and mean activities were all considered for each enzyme in comparison with the calculated nocturnal starch degradation rate and symbols were used to indicate whether enzymatic capacity was theoretically sufficient (√) or insufficient (X) to meet the observed starch degradation rates (**Table 1**). These considerations indicated that even the lowest recorded values of either β-amylase or DPE1 activity were significantly higher ($p < 0.05$) than the calculated nocturnal starch degradation rates for both distinct periods. Exceeding starch degradation rates by multiples of two for DPE1 to even 6–80 for β-amylase, these particular enzymes were not rate-limiting at all in the starch degradation process. In contrast even the maximum values of DPE2 activity were far below ($p < 0.05$) the calculated nocturnal starch degradation rates for both periods and could only account for about 15% of the calculated starch degradation. Whilst maltase activity was not limiting starch degradation during the second period ($p > 0.05$) it could only account for about 50% of the calculated starch degradation during the first period of the night ($p < 0.05$). Considering the summed activity of DPE2 and maltase, it could still only account for about 65% of the calculated starch degradation during the first period of the night ($p < 0.05$). For both considered periods the calculated starch degradation rates perfectly matched the observed min-max range for starch phosphorylase activities. Only during the first nocturnal period minimum observed activities of starch phosphorylase might potentially limit starch degradation accounting for about 75% of starch breakdown ($p < 0.05$).

Starch Degradative Enzyme Activities in *Phalaenopsis* Match With Those in *Kalanchoë* But Are Clearly Different From Published Arabidopsis Values

To strengthen our study, we further compared our mean values of enzyme activities from *Phalaenopsis* with either a negative control C3 photosynthesis species such as Arabidopsis (based on published data) and a positive control CAM species such as *K. fedtschenkoi* (**Table 2**; to allow direct comparison the *Phalaenopsis* values were recalculated to mass basis). The data clearly indicated that starch phosphorylase activity in the model CAM plant *K. fedtschenkoi* could also easily accommodate the observed starch degradation whilst DPE2 + maltase fell short. These observations

TABLE 1 | Comparison between nocturnal starch degradation rate (nmol g^{-1}FW min^{-1}) and calculated nocturnal activity (minimum, maximum and mean) of starch degradative enzymes (nmol g^{-1}FW min^{-1}) in young fully developed leaves of *Phalaenopsis* 'Edessa', for both nocturnal periods.

Nocturnal starch degradation rate (nmol g^{-1}FW min^{-1})		**Period 1 67 ± 13**		**Period 2 38 ± 6**	
		Activity (nmol g^{-1}FW min^{-1})			
Starch phosphorylase	MIN	52 ± 11 *	X	33 ± 8	√
	MAX	84 ± 8 *	√	86 ± 11 *	√
	MEAN	76 ± 13	√	59 ± 23	√
β-amylase	MIN	6301 ± 1041 *	√	259 ± 48 *	√
	MAX	19167 ± 6017 *	√	19167 ± 6017 *	√
	MEAN	13661 ± 5138 *	√	11176 ± 9788 *	√
DPE1	MIN	129 ± 24 *	√	87 ± 17 *	√
	MAX	316 ± 59 *	√	316 ± 59 *	√
	MEAN	171 ± 82 *	√	186 ± 118 *	√
DPE2	MIN	4 ± 3 *	X	5 ± 3 *	X
	MAX	11 ± 3 *	X	13 ± 2 *	X
	MEAN	8 ± 3 *	X	8 ± 4 *	X
Maltase	MIN	30 ± 6 *	X	37 ± 5	√
	MAX	41 ± 7 *	X	44 ± 5	√
	MEAN	37 ± 4 *	X	40 ± 3	√
DPE2 + Maltase	MIN	36 ± 4 *	X	40 ± 8	√
	MAX	52 ± 4 *	X	56 ± 8	√
	MEAN	44 ± 8 *	X	48 ± 8	√

To investigate nocturnal starch degradation and the associated enzyme activities in more detail, the nocturnal part was divided into two distinct periods i.e. Period 1 from ZT12 to ZT20 and Period 2 from ZT20 to ZT24. Symbols are used to indicate if the enzymatic capacity is sufficient (√) of insufficient (X) to accommodate the observed starch degradation.

*Data are means ± SD (n = 5) and asteriks indicate significant differences between the calculated enzymatic activity and the nocturnal starch degradation rate of the same period at *P < 0.05 according to the independent sample t-test.*

TABLE 2 | Comparison of nocturnal starch degradation rate (nmol g^{-1}FW min^{-1}) and mean activities of starch degradative enzymes (nmol g^{-1}FW min^{-1}) in leaves of *Phalaenopsis* 'Edessa', *Kalanchoë fedtschenkoi* and *Arabidopsis thaliana*.

	CAM	CAM reference	C3 reference
	***Phalaenopsis* 'Edessa'**	***K. fedtschenkoi***	**Arabidopsis**
Starch phosphorylase	**76 ± 12**	**209 ± 38**	**40 ± 7**
β-amylase	13674 ± 5133	5293 ± 376	140 ± 27
DPE1	132 ± 8	1760 ± 209	273 ± 28
DPE2	**8 ± 4**	**31 ± 3**	**146 ± 3**
Maltase	**36 ± 4**	**43 ± 2**	**20 ± 2**
Nocturnal starch breakdown	68 ± 12	93 ± 11	~92

Data are means ± SD (n = 5). Values for Arabidopsis originate from Chia et al. (2004). Different colors have been used to indicate whether the relevant enzymatic capacities in either starch phosphorolysis (starch phosphorylase) or hydrolysis (DPE2 + maltase) are adequate (green) or inadequate (red) to accommodate the observed starch degradation.

strongly contradicted with Arabidopsis showing a completely different situation with high DPE2 activity, supporting starch hydrolysis, and insufficient starch phosphorylase activity. Moreover, high DPE2 and low starch phosphorylase activities have also been reported by Borland et al. (2016) for Arabidopsis whilst the reverse was true for *M. crystallinum* (in the CAM mode) under identical growth conditions.

DISCUSSION

Regulation of Nocturnal Starch Degradation to Avoid Premature Exhaustion of Carbohydrate

Carbohydrate availability represents a key limiting factor for CAM productivity, which makes the diel breakdown and resynthesis of a transient pool of carbohydrate a central requirement for CAM homeostasis (Borland and Dodd, 2002; Cushman et al., 2008). To account for the observed gradual decrease in starch degradation rate towards the end of the night in the leaves of *Phalaenopsis* "Edessa" we considered two starch degradation rates in our study i.e. (1) 67 ± 13 nmol g^{-1}FW min^{-1} from ZT12 to ZT20 and (2) 38 ± 6 nmol g^{-1}FW min^{-1} from ZT20 to ZT24 (**Figure 1**). Avoiding premature exhaustion of reserve carbohydrate availability before the onset of dawn is consistent with observations in the C3 plant Arabidopsis where the rate of degradation of transitory starch during the night was enhanced or declined following either shortened or lengthened photoperiods (Lu et al., 2005; Graf et al., 2010). The exact physiology behind the mechanisms that allow the plant to match starch degradation to its needs and the length of night are still exciting topics of current investigation (Fernandez et al., 2017; Flis et al., 2019). In *Phalaenopsis* "Edessa" nocturnal starch breakdown during the 4 final hours was reduced with ca. 33% and accompanied by a threefold reduction in nocturnal CO_2 fixation and malic acid accumulation (**Figure 1**). It is very reasonable that a reduced availability of carbon skeletons for PEP synthesis at the end of the night will lead to both the reduced rate and total amount of CO_2 fixed by PEPC in CAM plants. Carbohydrate limited gas exchange towards the end of the dark period is also consistent with the fact that the Ki of PEPC for malic acid showed an upward trend during the major part of the night but started to decrease during the 4 final hours (**Figure 1**). High values of Ki are indicative of phosphorylated PEPC through PEPC-kinase action, rendering PEPC less sensitive for malic acid inhibition (Nimmo et al., 1986; Borland and Griffiths, 1997; Borland et al., 1999). Expression of the kinase itself is not likely to bring about less phosphorylation towards dawn as similar declines in Phase-I CO_2 assimilation well before the onset of dawn have been noticed in other CAM plants such as *M. crystallinum*, *K. daigremontiana* and *Clusia rosea*, whilst transcript abundance of PEPC kinase remained unaffected during the second nocturnal period (Borland et al., 1998; Borland et al., 1999; Dodd et al., 2003).

The Phosphorolytic Pathway Can Accommodate the Observed Nocturnal Starch Degradation

Both the phosphorolytic and hydrolytic pathways of starch degradation are assumed to be deployed by CAM species to balance the sink demands of CAM with growth and maintenance (Borland et al., 2016). This strongly contrasts with C3 plants where starch is degraded at night *via* the hydrolytic route (Niittylä et al., 2004; Weise et al., 2004; Stitt and Zeeman, 2012), whilst phosphorolytic starch degradation mainly provides substrate for internal chloroplast metabolism (Zeeman et al., 2004; Weise et al., 2006). To increase our insights in the possible relative contributions of either pathway in the process of CAM starch degradation we compared minimum and maximum enzyme activities of a range of enzymes during the night with different rates of observed nocturnal starch degradation in leaves of the CAM orchid *Phalaenopsis* "Edessa" (**Table 1**). Starch degradation is a complex process that requires different enzymes working in sequence and/or concert and attacking different substrates. Chloroplastic starch phosphorylase could potentially account for nearly all starch degradation during the whole night with mean activities matching exactly the calculated starch breakdown and as such avoiding premature exhaustion of starch. In accordance with a decreased starch degradation during the latter part of the nocturnal period, starch phosphorylase activity also slowed down towards dawn. High levels of Glc6P were present during the major part of the night, almost three times higher compared to the observed levels of maltose (i.e. 89 ± 7 nmol g^{-1}FW and 31 ± 4 nmol g^{-1}FW respectively). This is consistent with an

important role for starch phosphorylase in starch degradation, since Glc6P is the major export product from phosphorolytic starch degradation. Glc6P is not only considered an allosteric activator of PEPC but can also easily be converted to PEP in the cytosol providing ATP by substrate-level phosphorylation and offering energetic advantages (Holtum et al., 2005; Cheung et al., 2014). According to recently developed diel flux balance models for CAM this would make a marked difference to help offset the energetic costs of running the CAM cycle (Shameer et al., 2018).

Hydrolytic Starch Degradation Is Limited by DPE2 and Maltase Activity

The other starch degrading enzymes residing in the chloroplast and belonging to the hydrolytic starch conversion pathway, i.e. β-amylase and DPE1, showed *in vitro* activities far exceeding those required for *in vivo* starch degradation by multiples of 2 to 80 (**Table 1**). Those high activities could potentially lead to complete exhaustion well before the end of the dark period without any further regulation. However, further processing of maltose, generated by degradation of starch *via* β-amylase, in the cytosol is dependent on either cytosolic disproportionating enzyme (DPE2) or maltase. DPE2 showed only very low nocturnal activities in *Phalaenopsis* and could theoretically meet only about 15% of the observed starch breakdown. Low DPE2 activities have also been reported in *M. crystallinum* and have previously been hypothesized to potentially represent a possible bottleneck in the hydrolytic starch degradation process (Borland et al., 2016). This is in marked contrast with the critical importance of DPE2 in C3 plants such as Arabidopsis where DPE2 activity, which is about 20 times higher than in *Phalaenopsis*, can easily account for the measured starch degradation (**Table 2**). Whilst maltase activities in Arabidopsis were considered of minimal importance and about seven-fold lower compared to DPE2 activity (**Table 2**), our measurements showed a four-fold higher mean maltase activity than DPE2 during the night in *Phalaenopsis* "Edessa," which was still insufficient to accommodate nocturnal starch degradation. However, it can be assumed that both enzymes, DPE2 and maltase, can act in concert to accommodate maltose processing in the cytosol. Considering the sum of both enzymatic activities, the calculated minimum, maximum, and mean activity were still significantly lower ($p < 0.05$) than required to account for the observed nocturnal starch degradation (**Table 1**). In the model CAM plant *K. fedtschenkoi* DPE2 activity was higher but still insufficient to account for the measured starch breakdown in concert with maltase, whilst β-amylase was not rate limiting (**Table 2**). The bottleneck effect of the maltose processing enzymes in regulating β-amylase mediated starch breakdown was also depicted by a significant nocturnal accumulation ($p < 0.05$) of its substrate, maltose, from 27 ± 5 nmol g^{-1}FW (ZT12) to 47 ± 13 nmol g^{-1}FW (ZT22) in *Phalaenopsis* leaves.

In conclusion we compared *in vivo* nocturnal starch degradation and *in vitro* enzyme activity measurements during the whole night in leaves of the CAM orchid *Phalaenopsis* "Edessa" to shed more light into the interplay of the phosphorolytic and hydrolytic processes of starch degradation in CAM. We showed that the phosphorolytic pathway is the major route to accommodate nocturnal starch degradation and that measured activities of starch phosphorylase perfectly matched calculated starch degradation rates in order to avoid premature exhaustion of starch reserves before dawn. The hydrolytic pathway seemed hampered in starch processing not by β-amylase but through insufficient catalytic capacity of both DPE2 and maltase. These considerations were further corroborated by measurements of enzyme activities in the CAM model plant *Kalanchoë fedtschenkoi* and strongly contradict with the situation in the C3 plant Arabidopsis. The data support the view that the phosphorolytic pathway might be the main route of starch degradation in CAM to provide substrate for PEP with additional hydrolytic starch breakdown to accommodate mainly sucrose synthesis.

DATA AVAILABILITY STATEMENT

All datasets generated for this study are included in the article/supplementary material.

AUTHOR CONTRIBUTIONS

NC, WV and JC proposed the conceptual framework for the study and performed the data collection and analysis. NC and MF performed the experimental analyses. NC and JC interpreted the data and wrote the manuscript.

FUNDING

This research was supported by the Research Fund KU Leuven.

ACKNOWLEDGMENTS

Microflor NV is acknowledged for supplying plant material. The authors also acknowledge Kim Vekemans (Geel) and Timmy Reijnders (Leuven) for assistance in the lab.

REFERENCES

Borland, A. M., and Dodd, A. N. (2002). Carbohydrate partitioning in crassulacean acid metabolism plants: reconciling potential conflicts of interest. *Funct. Plant Biol.* 29, 707–716. doi: 10.1071/PP01221

Borland, A. M., and Griffiths, H. (1997). A comparative study on the regulation of C3 and C4 carboxylation processes in the constitutive crassulacean acid metabolism (CAM) plant *Kalanchoë daigremontiana* and the C3-CAM intermediate *Clusia minor*. *Planta* 201, 368–378. doi: 10.1007/s004250050079

Borland, A. M., Guo, H. B., Yang, X., and Cushman, J. C. (2016). Orchestration of carbohydrate processing for crassulacean acid metabolism. *Curr. Opin. Plant Biol.* 31, 118–124. doi: 10.1016/j.pbi.2016.04.001

Borland, A. M., Hartwell, J., Jenkins, G. I., Wilkins, M. B., and Nimmo, H. G. (1999). Metabolite control overrides circadian regulation of phosphoenolpyruvate carboxylase kinase and CO_2 fixation in crassulacean acid metabolism. *Plant Physiol.* 121, 889–896. doi: 10.1104/pp.121.3.889

Borland, A. M., Tecsi, L., Leegood, R. C., and Walker, R. P. (1998). Inducibility of crassulacean acid metabolism (CAM) in *Clusia* species; physiological/

biochemical characterization and intercellular localization of carboxylation processes in three species which show different degrees of CAM. *Planta* 205, 342–351. doi: 10.1007/s004250050329

Brilhaus, D., Bräutigam, A., Mettler-Altmann, T., Winter, K., and Weber, A. P. M. (2016). Reversible burst of transcriptional changes during induction of crassulacean acid metabolism in *Talinum triangulare*. *Plant Physiol.* 170, 102–122. doi: 10.1104/pp.15.01076

Ceusters, J., Borland, A. M., and De Proft, M. P. (2009a). Drought adaptation in plants with crassulacean acid metabolism involved the flexible use of different storage carbohydrate pools. *Plant Signal. Behav.* 4, 212–214. doi: 10.4161/psb.4.3.7813

Ceusters, J., Borland, A. M., Godts, C., Londers, E., Croonenborghs, S., Van Goethem, D., et al. (2011). Crassulacean acid metabolism under severe light limitation: a matter of plasticity in the shadows? *J. Exp. Bot.* 62, 283–291. doi: 10.1093/jxb/erq264

Ceusters, J., Borland, A. M., Londers, E., Verdoodt, V., Godts, C., and De Proft, M. P. (2008). Diel shifts in carboxylation pathway and metabolite dynamics in the CAM bromeliad *Aechmea* 'Maya' in response to elevated CO_2. *Ann. Bot. London* 102, 389–397. doi: 10.1093/aob/mcn105

Ceusters, J., Borland, A. M., Londers, E., Verdoodt, V., Godts, C., and De Proft, M. P. (2009b). Differential usage of storage carbohydrates in the CAM bromeliad *Aechmea* 'Maya' during acclimation to drought and recovery from dehydration. *Physiol. Plantarum* 135, 174–184. doi: 10.1111/j.1399-3054.2008.01186.x

Ceusters, J., Borland, A. M., Taybi, T., Frans, M., Godts, C., and De Proft, M. P. (2014). Light quality modulates metabolic synchronization over the diel phases of crassulacean acid metabolism. *J. Exp. Bot.* 65, 3705–3714. doi: 10.1093/jxb/eru185

Ceusters, N., Luca, S., Feil, R., Claes, J., Lunn, J. E., Van den Ende, W., et al. (2019). Hierarchical clustering reveals unique features in the diel dynamics of metabolites in the CAM orchid *Phalaenopsis*. *J. Exp. Bot*. 70, 3269-3281. doi: 10.1093/jxb/erz170

Chen, L. S., Lin, Q., and Nose, A. (2002). A comparative study on diurnal changes in metabolite levels in the leaves of three crassulacean acid metabolism (CAM) species, *Ananas comosus*, *Kalanchoë daigremontiana* and *K. pinnata*. *J. Exp. Bot.* 53, 341–350. doi: 10.1093/jexbot/53.367.341

Cheung, C. Y. M., Poolman, M. G., Fell, D. A., Ratcliffe, R. G., and Sweetlove, L. J. (2014). A diel flux balance model captures interactions between light and dark metabolism during day-night cycles in C3 and crassulacean acid metabolism leaves. *Plant Physiol.* 165, 917–929. doi: 10.1104/pp.113.234468

Chia, T., Thorneycroft, D., Chapple, A., Messerli, G., Chen, J., Zeeman, S. C., et al. (2004). A cytosolic glucosyltransferase is required for conversion of starch to sucrose in Arabidopsis leaves at night. *Plant J.* 37, 853–863. doi: 10.1111/j.1365-313X.2003.02012.x

Cho, M. H., Lim, H., Shin, D. H., Jeon, J. S., Bhoo, S. H., Park, Y. I., et al. (2011). Role of the plastidic glucose translocator in the export of starch degradation products from the chloroplasts in *Arabidopsis thaliana*. *New Phytol.* 190, 101–112. doi: 10.1111/j.1469-8137.2010.03580.x

Christopher, J. T., and Holtum, J. A. M. (1998). Carbohydrate partitioning in the leaves of Bromeliaceae performing C3 photosynthesis or crassulacean acid metabolism. *Aust. J. Plant Physiol.* 25, 371–376. doi: 10.1071/PP98005

Cushman, J. C., Tillett, R. L., Wood, J. A., Branco, J. M., and Schlauch, K. A. (2008). Large-scale mRNA expression profiling in the common ice plant, *Mesembryanthemum crystallinum*, performing C3 photosynthesis and Crassulacean acid metabolism (CAM). *J. Exp. Bot.* 59, 1875–1894. doi: 10.1093/jxb/ern008

Dodd, A., Griffiths, H., Taybi, T., Cushman, J., and Borland, A. M. (2003). Integrating diel starch metabolism with the circadian and environmental regulation of Crassulacean acid metabolism in *Mesembryanthemum crystallinum*. *Planta* 216, 789–797. doi: 10.1007/s00425-002-0930-2

Fernandez, O., Ishihara, H., George, G. M., Mengin, V., Flis, A., Sumner, D., et al. (2017). Leaf starch turnover occurs in long days and in falling light at the end of the day. *Plant Physiol.* 174, 2199–2212. doi: 10.1104/pp.17.00601

Flis, A., Mengin., V., Ivakov, A. A., Mugford, S. T., Hubberten, H. M., Encke, B., et al. (2019). Multiple circadian clock outputs regulate diel turnover of carbon and nitrogen reserves. *Plant Cell Environ.* 42, 549–573. doi: 10.1111/pce.13440

Graf, A., Schlereth, A., Stitt, M., and Smith, A. M. (2010). Circadian control of carbohydrate availability for growth in Arabidopsis plants at night. *P. Natl. Acad. Sci. U.S.A.* 107, 9458–9463. doi: 10.1073/pnas.0914299107

Häusler, R. E., Baur, B., Scharte, J., Teichmann, T., Eicks, M., Fischer, et al. (2000). Plastidic metabolite transporters and their physiological functions in the inducible crassulacean acid metabolism plant *Mesembryanthemum crystallinum*. *Plant J.* 24, 285–296. doi: 10.1046/j.1365-313x.2000.00876.x

Holtum, J. A. M., Smith, J. A. C., and Neuhaus, H. (2005). Intracellular transport and pathways of carbon flow in plants with crassulacean acid metabolism. *Funct. Plant Biol.* 32, 429–449. doi: 10.1071/FP04189

Kore-eda, S., and Kanai, R. (1997). Induction of glucose 6-phosphate transport activity in chloroplasts of *Mesembryanthemum crystallinum* by the C3-CAM transition. *Plant Cell Physiol.* 38, 895–901. doi: 10.1093/oxfordjournals.pcp.a029249

Kore-eda, S., Nozawa, A., Okada, Y., Takashi, K., Azad, M. A. K., Ohnishi, J. I., et al. (2013). Characterization of the plastidic phosphate translocators in the inducible crassulacean acid metabolism plant *Mesembryanthemum crystallinum*. *Biosci. Biotech. Bioch.* 77, 1511–1516. doi: 10.1271/bbb.130174

Kruger, N. J., and ap Rees, T. (1983). Maltose metabolism by pea chloroplasts. *Planta* 158, 179–184. doi: 10.1007/BF00397712

Kumar, A., and Sanwal, G. G. (1982). Purification and physicochemical properties of starch phosphorylase from young banana leaves. *Biochemistry-US* 21, 4152–4159. doi: 10.1021/bi00260a036

Lloyd, J. R., and Kossmann, J. (2015). Transitory and storage starch metabolism: two sides of the same coin? *Curr. Opin. Biotech.* 32, 143–148. doi: 10.1016/j.copbio.2014.11.026

Lu, Y., and Sharkey, T. D. (2004). The role of amylomaltase in maltose metabolism in the cytosol of photosynthetic cells. *Planta* 218, 466–473. doi: 10.1007/s00425-003-1127-z

Lu, Y., Gehan, J. P., and Sharkey, T. D. (2005). Daylenght and circadian effects on starch degradation and maltose metabolism. *Plant Physiol.* 138, 2280–2291. doi: 10.1104/pp.105.061903

Mohanty, B., Wilson, P. M., and ap Rees, T. (1993). Effects of anoxia on growth and carbohydrate metabolism in suspension cultures of soybean and rice. *Phytochemistry* 34, 75–82. doi: 10.1016/S0031-9422(00)90785-4

Neuhaus, H. E., and Schulte, N. (1996). Starch degradation in chloroplasts isolated from C3 or CAM (crassulacean acid metabolism)-induced *Mesembryanthemum crystallinum* L. *Biochem. J.* 318, 945–953. doi: 10.1042/bj3180945

Niittylä, T., Messerli, G., Trevisan, M., Chen, J., Smith, A. M., and Zeeman, S. C. (2004). A previously unknown maltose transporter essential for starch degradation in leaves. *Science* 303, 87–89. doi: 10.1126/science.1091811

Nimmo, G. A., Nimmo, H. G., Hamilton, I. D., Fewson, C. A., and Wilkins, M. B. (1986). Purification of the phosphorylated night form and dephosphorylated day form of phosphoenolpyruvate carboxylase from *Bryophyllum fedtschenkoi*. Biochem. *J.* 239, 213–220. doi: 10.1042/bj2390213

Osmond, C. B. (1978). Crassulacean acid metabolism: A curiosity in context. *Annu. Rev. Plant Phys. Plant Mol. Biol.* 29, 379–414. doi: 10.1146/annurev.pp.29.060178.002115

Paul, M. J., Loos, K., Stitt, M., and Ziegler, P. (1993). Starch-degrading enzymes during the induction of CAM in *Mesembryanthemum crystallinum*. *Plant Cell Environ.* 16, 531–538. doi: 10.1111/j.1365-3040.1993.tb00900.x

Popp, M., Janett, H. P., Lüttge, U., and Medina, E. (2003). Metabolite gradients and carbohydrate translocation in rosette leaves of CAM and C3 bromeliads. *New Phytol.* 157, 649–656. doi: 10.1046/j.1469-8137.2003.00683.x

Shameer, S., Baghalian, K., Cheung, C. Y. M., Ratcliffe, R. G., and Sweetlove, L. J. (2018). Computational analysis of the productivity potential of CAM. *Nat. Plants* 4, 165–171. doi: 10.1038/s41477-018-0112-2

Smith, A. M., Zeeman, S. C., and Smith, S. M. (2005). Starch degradation. *Annu. Rev. Plant Biol.* 56, 73–98. doi: 10.1146/annurev.arplant.56.032604.144257

Stitt, M., and Zeeman, S. C. (2012). Starch turnover: pathways, regulation and role in growth. *Curr. Opin. Plant Biol.* 15, 282–292. doi: 10.1016/j.pbi.2012.03.016

Takaha, T., Yanase, M., Okada, S., and Smith, S. M. (1993). Disproportionating enzyme (4-alpha-glucanotransferase; EC 2.4.1.25) of potato. Purification, molecular cloning, and potential role in starch metabolism. *J. Biol. Chem.* 268, 1391–1396.

Tarkowski, L. P., Van de Poel, B., Höfte, M., and Van den Ende, W. (2019). Sweet immunity: inulin boosts resistance of lettuce (*Lactuca sativa*) against grey mold (Botrytis cinerea) in an ethylene-dependent manner. *Int. J. Mol. Sci.* 20, 1052. doi: 10.3390/ijms20051052

Taybi, T., Cushman, J. C., and Borland, A. M. (2017). Leaf carbohydrates influence transcriptional and post-transcriptional regulation of nocturnal carboxylation

and starch degradation in the facultative CAM plant, *Mesembryanthemum crystallinum*. *J. Plant Physiol.* 219, 144–154. doi: 10.1016/j.jplph.2017.07.021

Verspreet, J., Cimini, S., Vergauwen, R., Dornez, E., Locato, V., Le Roy, K., et al. (2013). Fructan metabolism in developing wheat (*Triticum aestivum* L.) kernels. *Plant Cell Physiol.* 54, 2047–2057. doi: 10.1093/pcp/pct144

Weise, S. E., van Wijk, K. J., and Sharkey, T. D. (2011). The role of transitory starch in C3, CAM and C4 metabolism and opportunities for engineering leaf starch accumulation. *J. Exp. Bot.* 62, 3109–3118. doi: 10.1093/jxb/err035

Weise, S. E., Schrader, S. M., Kleinbeck, K. R., and Sharkey, T. D. (2006). Carbon balance and circadian regulation of hydrolytic and phosphorolytic breakdown of transitory starch. *Plant Physiol.* 141, 879–886. doi: 10.1104/pp.106.081174

Weise, S. E., Weber, A. P. M., and Sharkey, T. D. (2004). Maltose is the major form of carbon exported from the chloroplast at night. *Planta* 218, 474–482. doi: 10.1007/s00425-003-1128-y

Yu, T. S., Zeeman, S. C., Thorneycroft, D., Fulton, D. C., Dunstan, H., Lue, W. L., et al. (2005). α-Amylase is not required for breakdown of transitory starch in Arabidopsis leaves. *J. Biol. Chem.* 280, 9773–9779. doi: 10.1074/jbc.M413638200

Zeeman, S. C., Delatte, T., Messerli, G., Umhang, M., Stettler, M., Mettler, T., et al. (2007). Starch breakdown: recent discoveries suggest distinct pathways and novel mechanisms. *Funct. Plant Biol.* 34, 465–473. doi: 10.1071/FP06313

Zeeman, S. C., Northrop, F., Smith, A. M., and ap Rees, T. (1998). A starch-accumulating mutant of *Arabidopsis thaliana* deficient in a chloroplastic starch-hydrolysing enzyme. *Plant J.* 15, 357–365. doi: 10.1046/j.1365-313X.1998.00213.x

Zeeman, S. C., Thorneycroft, D., Schupp, N., Chapple, A., Weck, M., Dunstan, H., et al. (2004). Plastidial α-glucan phosphorylase is not required for starch degradation in Arabidopsis leaves but has a role in the tolerance of abiotic stress. *Plant Physiol.* 135, 849–858. doi: 10.1104/pp.103.032631

Conflict of Interest: The authors declare that the research was conducted in the absence of any commercial or financial relationships that could be construed as a potential conflict of interest.

frontiers in Plant Science

REVIEW
published: 15 November 2019
doi: 10.3389/fpls.2019.01474

Dissecting the Function of MADS-Box Transcription Factors in Orchid Reproductive Development

Zhi Wei Norman Teo[1,2], *Wei Zhou*[1] *and Lisha Shen*[1]*

[1] Temasek Life Sciences Laboratory, National University of Singapore, Singapore, Singapore, [2] Department of Biological Sciences, Faculty of Science, National University of Singapore, Singapore, Singapore

The orchid family (Orchidaceae) represents the second largest angiosperm family, having over 900 genera and 27,000 species in almost all over the world. Orchids have evolved a myriad of intriguing ways in order to survive extreme weather conditions, acquire nutrients, and attract pollinators for reproduction. The family of MADS-box transcriptional factors have been shown to be involved in the control of many developmental processes and responses to environmental stresses in eukaryotes. Several findings in different orchid species have elucidated that MADS-box genes play critical roles in the orchid growth and development. An in-depth understanding of their ecological adaptation will help to generate more interest among breeders and produce novel varieties for the floriculture industry. In this review, we summarize recent findings of MADS-box transcription factors in regulating various growth and developmental processes in orchids, in particular, the floral transition and floral patterning. We further discuss the prospects for the future directions in light of new genome resources and gene editing technologies that could be applied in orchid research and breeding.

Keywords: orchid, MADS-box transcription factors, floral transition, floral patterning, development

OPEN ACCESS

Edited by:
Jen-Tsung Chen, National University of Kaohsiung, Taiwan

Reviewed by:
Adriana Garay, National Autonomous University of Mexico, Mexico
Philip Ruelens, Wageningen University & Research, Netherlands

***Correspondence:**
Lisha Shen
lisha@tll.org.sg

Specialty section:
This article was submitted to Plant Development and EvoDevo, a section of the journal Frontiers in Plant Science

Received: *02 August 2019*
Accepted: *23 October 2019*
Published: *15 November 2019*

Citation:
Teo ZWN, Zhou W and Shen L (2019) Dissecting the Function of MADS-Box Transcription Factors in Orchid Reproductive Development. Front. Plant Sci. 10:1474. doi: 10.3389/fpls.2019.01474

INTRODUCTION

The orchid family (Orchidaceae) is currently the second largest angiosperm family, having over 900 genera and 27,000 species in almost all parts of the world except Antarctica. New genera in the orchid family are being discovered at a rate of around 13 per year for over the past decade (Schuiteman, 2004; Chase et al., 2015). Nevertheless, many wild species are at the brink of extinction because of illegal trading activities (Wijnstekers, 2001; Hossain et al., 2013). Orchids have their own ecological niches through their relationships with mycorrhizal fungi, specialized pollinators and host trees (Fay and Chase, 2009). Of all the orchid species, 70% are epiphytic (growing on trees), 25% are terrestrial (growing on ground), and the remaining 5% are found on various supports such as rocks (Atwood, 1986). Thus, it is important to conserve orchid species through generating awareness and increasing our understanding on the species physiology and diversity (Cribb et al., 2003).

Being a class of valuable ornamental plants with distinct and attractive flowers, orchid is viewed as a high value commodity in the global flower cultivation and landscaping industries. They are also highly sought for as food and traditional medicine (Arditti, 1992; Bulpitt et al., 2007). Besides their great economic values, orchids are also exclusive genetic resources for studying plant developmental processes, including floral transition, floral development, flower pigmentation, and senescence, because of the specialized reproductive structures and the unique strategies for

reproduction (Yu and Goh, 2001; Gutiérrez, 2010; Da Silva et al., 2014). However, the orchid research as well as orchid breeding have been challenging due to the long vegetative developmental period before switching to flower development, and technical limitations in transformation and obtaining transgenic lines in various orchid species. Currently, to investigate the function of orchid genes, several methods are being used including the heterologous expression of gene of interest under the strong constitutive CaMV *35S* promoter in *Arabidopsis* (*Arabidopsis thaliana*) or tobacco and virus-induced gene silencing (VIGS). Sometimes, transgenic orchids are also generated to study gene function. So far, the genetic transformation of orchids using the *Agrobacterium*-mediated approach on protocorm-like bodies or rhizomes has been reported in *Cymbidium*, *Oncidium*, *Dendrobium*, *Phalaenopsis*, and other orchids (Belarmino and Mii, 2000; Yu and Goh, 2000; Chai et al., 2002; Chen, 2002; Sjahril and Mii, 2006; Shrestha et al., 2007; Zhang et al., 2010; Ding et al., 2013).

The orchids including *Phalaenopsis*, *Dendrobium*, *Cymbidium*, and *Oncidium* from the Epidendroideae subfamily are used as orchid plant models for research and biotechnology. Most of these orchids are predominantly found to be growing in tropical Asia to Australia with the exception of *Oncidium* in the West (**Table 1**). Orchids are either monopodial or sympodial in their growing habits. Monopodial orchids, such as *Phalaenopsis*, grow as a single erect "stem" with alternating leaves on opposing parts of the center. They store water in their thick leaves and roots but have no pseudobulbs. Sympodial orchids, such as *Dendrobium*, *Cymbidium*, and *Oncidium*, grow from a horizontal stem called rhizome and have pseudobulbs to store water and grow new leaves. After blooming, the plant will resume growth at axillary buds at the base of the previous pseudobulbs.

TABLE 1 | Orchid model plants and their growing characteristics.

Genus	Distribution	Branching architecture	Characteristics
Cymbidium	From the Himalayan region eastwards to Southeast Asia, China, and Australia	Sympodial	- Mostly terrestrial - Large, round pseudobulbs (stems) - Long thin leaves - Thick roots
Oncidium	South America, Central America, Mexico, and the West Indies	Sympodial	- Mostly epiphytic - Presence of column wings - Pseudobulbs with one to three leaves - Pseudobulbs having several basal bracts at the base
Dendrobium	Tropical Asia, islands of the Pacific, New Guinea, and Australia	Sympodial	- Mostly epiphytic - Generating new stems (pseudobulbs) at the base of the previous year's stems
Phalaenopsis	India, China, Southeast Asia, New Guinea, and Australia	Monopodial	- Mostly epiphytic - Long and coarse roots - Short and leafy stems - Flat flowers arranged in a flowering stem that often branches near the end

Recent findings from different orchid species have elucidated that a group of MADS-box transcription factors sharing a greatly conserved N-terminal DNA binding domain (MADS-box) exert important functions in controlling orchid growth and development, in particular, the floral transition and floral patterning. In this review, we discuss the biological roles of these MADS-box proteins and the mechanisms how they contribute to flowering and floral organ formation in orchids. We further elaborate about the prospects for research and development in light of new genome resources and gene editing technologies that could be applied in orchid research and breeding.

THE MADS-BOX PROTEIN FAMILY

In orchids and other angiosperms, there is a family of MADS-box transcription factors that have been identified to control many plant developmental processes, including floral transition, floral patterning, as well as male and female gametophyte development (Coen and Meyerowitz, 1991; Weigel and Meyerowitz, 1994; Yu and Goh, 2000; Acri-Nunes-Miranda and Mondragón-Palomino, 2014; Valoroso et al., 2019). The MADS-box family proteins are conserved in nearly all eukaryotes. The MADS-box acronym is derived from the yeast *MINICHROMOSOME MAINTENANCE 1* (*MCM1*) (Passmore et al., 1988), the *Arabidopsis AGAMOUS* (*AG*) (Yanofsky et al., 1990), the *Antirrhinum DEFICIENS* (*DEFA*) (Schwarz-Sommer et al., 1990), and the mammalian *SERUM RESPONSE FACTOR* (*SRF*) (Norman et al., 1988; Gramzow et al., 2010). All identified MADS-box proteins each contain a MADS-box domain of ~58 amino acid at the N-terminus that binds to a consensus $CC[A/T]_6GG$ sequence, termed as the "CarG-box" motif (Hayes et al., 1988; Riechmann et al., 1996). Interestingly, flowering plants (angiosperms) have more of these genes (e.g. 107 in *Arabidopsis*; 51 in *Phalaenopsis equestris*) compared to yeast (e.g. 4 in *Saccharomyces cerevisiae*) and mammals (e.g. 5 in *Homo sapiens*) (Becker and Theißen, 2003; Messenguy and Dubois, 2003; Pařenicová et al., 2003; Cai et al., 2015). The MADS-box family of genes form two major lineages, namely type I of *SRF*-like genes and type II of *MEF2*-like genes, which is resulted from an ancient event of gene duplication prior to the divergence of the kingdoms of plants and animals (Alvarez-Buylla et al., 2000). In plants, type II genes of MADS-box, also called as MIKC-type genes, feature four distinct protein domains arranged from the N-terminal end to C-terminal end. They are the highly conserved DNA binding MADS-box (M) domain, the less-conserved intervening domain (I) for conferring interaction specificity between different MADS-box transcription factors and/or other proteins, the keratin-like coiled-coil (K) domain for conferring protein–protein interactions, and a highly variable C-terminal (C) domain for regulating gene transcription or multimeric protein complexes formations (Shore and Sharrocks, 1995;

Theißen et al., 1996; Riechmann and Meyerowitz, 1997; Honma and Goto, 2001; Becker and Theißen, 2003; Hill et al., 2008).

The MIKC-type genes are specifically present in plants and many of these genes have been shown to control key processes of plant development including vegetative growth and reproductive organ development with complex cascades of events and networks (Theißen, 2001; Kaufmann et al., 2005; Adamczyk and Fernandez, 2009). Particularly, their functions in determining plant reproductive development are more remarkable as they regulate the development of consecutive reproductive processes, namely the floral transition, floral meristem specification, floral patterning, pollen growth, and development of ovules and seeds (**Figure 1**). The MADS-box genes that act in the regulation of flowering time and floral patterning in plants will be elaborated more in the latter sections (**Table 2**). The floral homeotic genes that play crucial roles in specifying reproductive floral organ identities are among the best characterized MADS-box genes. The extensive study of mutants with floral homeotic defects has resulted in the birth of the "ABCE model," which explains how the genes of A, B, C, D and E classes act jointly to determine floral organs identities (Coen and Meyerowitz, 1991; Weigel and Meyerowitz, 1994; Theissen and Saedler, 2001). All floral homeotic genes in *Arabidopsis* belong to the MADS-box family except for the A-class gene, *APETALA2* (*AP2*). In addition to determining the identities of floral organs, MADS-box proteins also regulate floral meristem specification, the process of which involves four meristem identity genes, namely *LEAFY* (*LFY*) and three MADS-box genes closely related to each other, *APETALA1* (*AP1*), *CAULIFLOWER* (*CAL*), and *FRUITFULL* (*FUL*) (Ferrándiz et al., 2000; Ng and Yanofsky, 2001). Furthermore, studies of MADS-box proteins have also demonstrated their function in seed and silique growth. For example, three MADS-box genes, *SHATTERPROOF 1* (*SHP1*), and its close homologs *SHP2* and *SEEDSTICK* (*STK*) contribute to normal growth and development of carpels and fruits (Liljegren et al., 2000; Pinyopich et al., 2003). In addition, several MADS-box genes belonging to type I, such as *PHERES 1* (*PHE1*), *AGAMOUS-LIKE 80* (*AGL80*), *DIANA* (*AGL61*), etc., are involved in embryo and seed growth (Kohler et al., 2003; Portereiko et al., 2006; Bemer et al., 2008; Colombo et al., 2008; Kang et al., 2008).

MADS-BOX PROTEINS IN ORCHID FLOWERING

The Floral Transition of Orchid

The floral transition, a developmental transition from vegetative to reproductive phase, is one of the key developmental transitions in the plant life cycle. The timing of floral transition greatly affects the success of plant reproduction. In the model plant *Arabidopsis*, the vegetative shoot apex, from which leaves are generated, is converted into the inflorescence meristem, from which flowers are generated, during the floral transition. In orchids, the length of the vegetative phase can vary from one to thirteen years between different species, but the average time for most species is between two to three years (Hew and Yong, 2004). The process of flowering is induced in the meristem of dormant axillary buds. In sympodial orchids such as *Dendrobium* and *Oncidium*, the formation of bud primordia occurs at the axils of the leaves. In the orchid *Cymbidium*, the inflorescence will be developed from the dormant axillary buds at the base of the pseudobulb. For monopodial orchids such as *Phalaenopsis* and *Vandas*, they typically have at least two dormant bud primordia at each leaf axil which can grow into inflorescences or keikis (new orchid plantlets).

With the increasing demand for whole orchids and cut flowers, modern horticulturists and breeders are learning about the flowering behavior of different species to control the time of blooming so as to maximize their economic value. Each orchid species has a time of the year when it will bloom naturally. Most orchids will grow in the abundance of sunlight and moisture during summer and bloom in the fall, winter, or spring. Significant progress has been made to determine the effects of environmental conditions, such as temperature and day length, in inducing flowering in different species (**Table 3**). Studies on *Cymbidium*, *Oncidium*, *Dendrobium*, and *Phalaenopsis* have shown that a low night temperature of 13°C and a large fluctuation of 10°C to 14°C in daily diurnal temperature are sufficient to induce flowering (Rotor, 1952; Rotor and Withner, 1959). A high day temperature of more than 28°C for 8 h or longer promotes vegetative growth and inhibit the process of flowering in *Phalaenopsis* (Blanchard and Runkle, 2006; Newton and Runkle, 2009). However, a prolonged exposure to a constant elevated temperature of 30°C induces flowering by activating the thermal stress response (Chin et al., 2014). Since orchids are likely to be shaded by leaves on trees, the length of daylight is not known to influence flowering with the exception of *Dendrobium phalaenopsis* flowering under short days (Rotor, 1952; Rotor and Withner, 1959; Lopez and Runkle, 2004). It is noteworthy to mention that flowering is an intricate process and many environmental conditions including light intensity and humidity can affect the initiation of floral spikes.

Floral Pathway Integrators

For the model plant *Arabidopsis*, the timing of floral transition is regulated by a complex system consisting of several flowering pathways—photoperiod, vernalization, thermosensory, gibberellins (GA), autonomous, and age—that perceive both environmental and endogenous flowering signals (Mouradov et al., 2002; Simpson and Dean, 2002; Blázquez et al., 2003; Boss et al., 2004; Wang et al., 2009). For environmental flowering signals, the photoperiod pathway perceives the daylength in seasonal changes; the vernalization pathway measures the period of the plant's exposure to cold; the thermosensory pathway mediates the ambient temperature effect. For endogenous flowering signals, the GA pathway promotes flowering under non-inductive photoperiod, while the autonomous pathway is a photoperiod-independent pathway that induces flowering through perceiving the internal signals at various stages of development. These genetic pathways regulate the transcription of two main integrators of floral pathways, *FLOWERING*

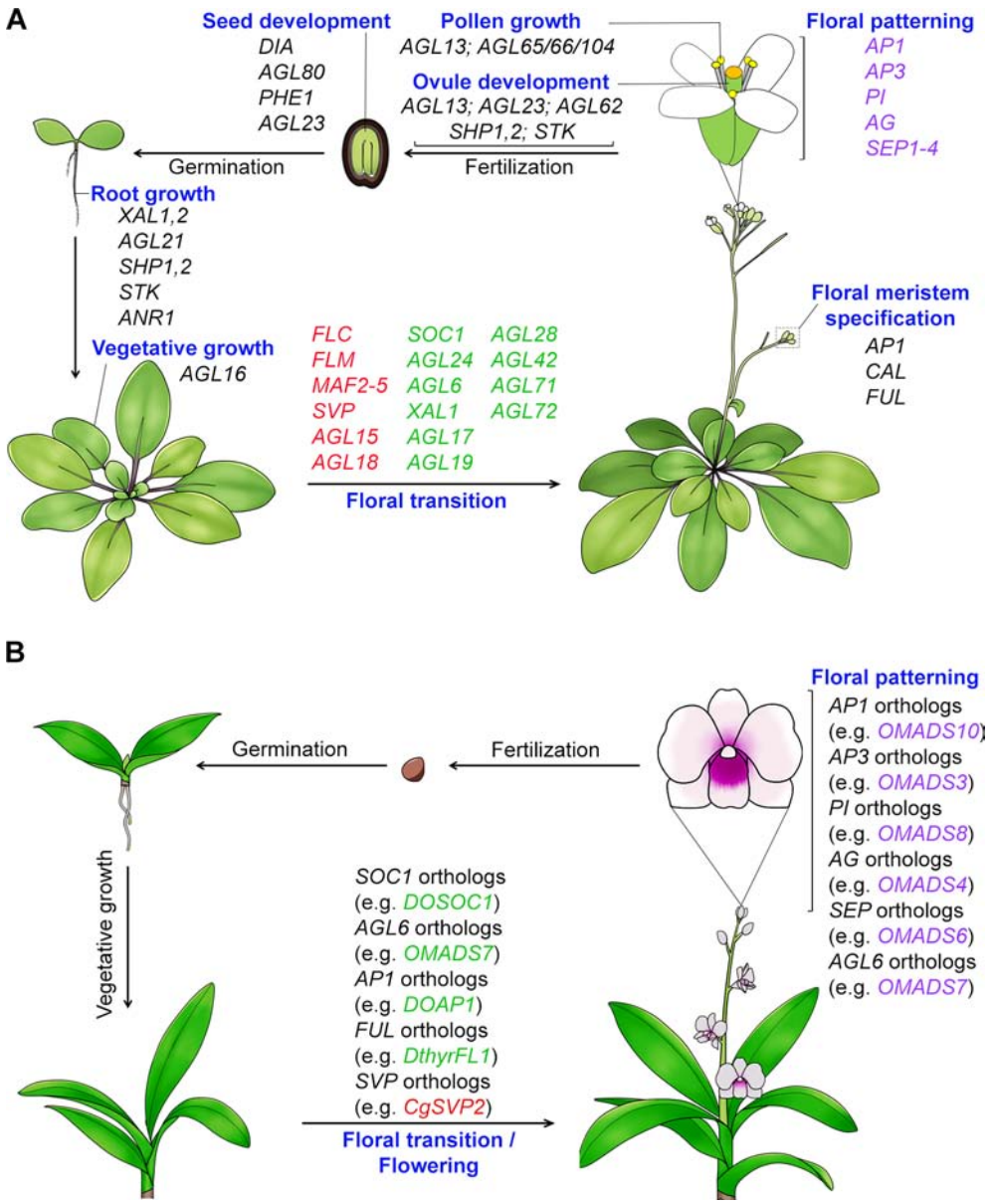

FIGURE 1 | Function of MADS-box proteins in the whole plant life cycle. **(A)** MADS-box genes regulate *Arabidopsis* development throughout its life cycle. Many MADS-box genes mediate the transition to flowering. The flowering time repressor genes, including *FLC* (Michaels and Amasino, 1999), *FLM* (Ratcliffe et al., 2001), *MAF2-5* (Ratcliffe et al., 2003; Gu et al., 2013), *SVP* (Hartmann et al., 2000; Li et al., 2008), and *AGL15/18* (Adamczyk et al., 2007), are shown in red color, whereas the flowering time promoter genes, including *SOC1* (Lee et al., 2000), *AGL24* (Yu et al., 2002), *AGL6* (Yoo et al., 2011), *XAL1/AGL12* (Tapia-Lopez et al., 2008), *AGL17* (Han et al., 2008), *AGL19* (Schonrock et al., 2006), *AGL28* (Yoo et al., 2006), and *AGL42/71/72* (Dorca-Fornell et al., 2011), are shown in green color. All the identified floral organ identity genes except *AP2* encode MADS-box transcription factors. MADS-box genes are also involved in root growth (e.g. *XAL1*, *XAL2*, *AGL21*, *ANR1, SHP1,2*, and *STK*) (Zhang and Forde, 1998; Tapia-Lopez et al., 2008; Moreno-Risueno et al., 2010; Garay-Arroyo et al., 2013; Yu et al., 2014), vegetative growth (e.g. *AGL16*'s function in stomata development) (Kutter et al., 2007), pollen maturation and tube growth (*AGL65/66/104*) (Adamczyk and Fernandez, 2009), ovule development (e.g. *AGL13*, *AGL23*, *AGL62*, *SHP1,2* and *STK*) (Liljegren et al., 2000; Pinyopich et al., 2003; Colombo et al., 2008; Kang et al., 2008; Hsu et al., 2014), and embryo and seed development (e.g. *DIA*, *AGL80*, *AGL23*, and *PHE1*) (Kohler et al., 2003; Portereiko et al., 2006; Bemer et al., 2008; Colombo et al., 2008). **(B)** Functions of MADS-box genes in orchid development. Orchid MADS-box proteins have been shown to regulate flowering and floral organ formation. *AG*, *AGAMOUS*; *AGL6*, *AGAMOUS-LIKE 6*; *AGL15*, *AGAMOUS-LIKE 15*; *AGL16*, *AGAMOUS-LIKE 16*; *AGL17*, *AGAMOUS-LIKE 17*; *AGL18*, *AGAMOUS-LIKE 18*; *AGL19*, *AGAMOUS-LIKE 19*; *AGL21*, *AGAMOUS-LIKE 21*; *AGL23*, *AGAMOUS-LIKE 23*; *AGL24*, *AGAMOUS-LIKE 24*; *AGL28*, *AGAMOUS-LIKE 28*; *AGL42*, *AGAMOUS-LIKE 42*; *AGL65*, *AGAMOUS-LIKE 65*; *AGL66*, *AGAMOUS-LIKE 66*; *AGL71*, *AGAMOUS-LIKE 71*; *AGL72*, *AGAMOUS-LIKE 72*; *AGL80*, *AGAMOUS-LIKE 80*; *AGL104*, *AGAMOUS-LIKE 104*; *ANR1*, *ARABIDOPSIS NITRATE REGULATED 1*; *AP1*, *APETALA1*; *AP3*, *APETALA3*; *CAL*, *CAULIFLOWER*; *CO*, *CONSTANS*; *DIA*, *DIANA*; *FLC*, *FLOWERING LOCUS C*; *FLM*, *FLOWERING LOCUS M*; *FT*, *FLOWERING LOCUS T*; *FUL*, *FRUITFULL*; *MAF2-5*, *MADS AFFECTING FLOWERING 2-5*; *PHE1*, *PHERES1*; *PI*, *PISTILLATA*; *SEP1-4, SEPALLATA1-4; SHP1,2*, *SHATTERPROOF1,2*; *SOC1*, *SUPPRESSOR OF OVEREXPRESSION OF CONSTANS 1*; *STK*, *SEEDSTICK*; *SVP*, *SHORT VEGETATIVE PHASE*; *XAL1*, *XAANTAL 1*; *XAL2*, *XAANTAL 2*.

TABLE 2 | A summary of MADS-box regulators involved in reproductive development in the model plant *Arabidopsis* and orchids.

***Arabidopsis* gene name**	**Function**	**Orchid species**	**Orchid orthologs**	**References**
SUPPRESSOR OF OVEREXPRESSION OF CONSTANS (*SOC1*)	Flowering promoter; FM[a] specification; floral organ patterning	*Cymbidium goeringii*	*CgSOC1*	(Yang et al., 2019)
		Dendrobium Chao Praya Smile	*DOSOC1*[b]	(Ding et al., 2013)
		Dendrobium nobile	*DnAGL19*	(Liang et al., 2012)
		Orchis italica	*Olcomp27839_SOC*	(Valoroso et al., 2019)
SHORT VEGETATIVE PHASE (*SVP*)	Flowering promoter; floral organ patterning	*C. goeringii*	*CgSVP1, CgSVP2*[b], *CgSVP3*	(Yang et al., 2019)
		O. italica	*Olcomp18466_SVP*	(Valoroso et al., 2019)
FRUITFULL (*FUL*)	Flowering promoter; FM specification; fruit development	*Dendrobium thyrsiflorum*	*DthyrFL1, DthyrFL2, DthyrFL3*	(Skipper et al., 2005)
		Phalaenopsis hybrida cv. Formosa rose	*ORAP11*, *ORAP13*	(Chen et al., 2007)
		Phalaenopsis hybrid "Athens"	*PhaMADS1, PhaMADS2*	(Acri-Nunes-Miranda and Mondragón-Palomino, 2014)
APETALA 1 (*AP1*)	FM specification; sepal and petal identity	*Cymbidium ensifolium*	*ZHLZ.comp57026*	(Yang and Zhu, 2015)
		Cymbidium faberi	*CfAP11*	(Tian et al., 2013)
		C. goeringii	*CgAP1*	(Yang et al., 2019)
		Dendrobium Chao Praya Smile	*DOAP1*[b]	(Sawettalake et al., 2017)
		Dendrobium Madame Suzie Wong	*DOMADS2*	(Yu and Goh, 2000)
		Oncidium Gower Ramsey	*OMADS10 (OAP1)*	(Chang et al., 2009; Hsu et al., 2015)
		O. italica	*Olcomp2508_AP1, Olcomp3679_AP1, Olcomp9283_AP1, Olcomp11046_AP1*	(Valoroso et al., 2019)
		Phalaenopsis aphrodite	*PaAP1-1, PaAP1-2*	(Su et al., 2013b)
APETALA3 (*AP3*)	Petal and stamen identity	*C. ensifolium*	*CeAP3, ZHLH.comp53790, ZHLZ.comp35346, ZHLZ.comp55590, ZHLZ.comp26961*	(Yang and Zhu, 2015)
		Cymbidium hybrid cultivar	*MADS1*	(Aceto and Gaudio, 2011)
		Dendrobium crumenatum	*DcOAP3A; DcOAP3B*	(Xu et al., 2006)
		Dendrobium moniliforme	*DMMADS4*	(Aceto and Gaudio, 2011)
		Gongora galeata	*GogalDEF1, GogalDEF2, GogalDEF3*	(Aceto and Gaudio, 2011)
		Habenaria radiata	*HrDEF*	(Aceto and Gaudio, 2011)
		Oncidium Gower Ramsey	*OMADS3* (*OAP3-3*)	(Hsu and Yang, 2002; Hsu et al., 2015)
			OMADS5 (*OAP3-1*), *OMADS9* (*OAP3-2*)	(Chang et al., 2010; Hsu et al., 2015)
			OMADS12 (*OAP3-4*)	(Hsu et al., 2015)
		O. italica	*Olcomp900_DEF4, Olcomp3831_DEF1, Olcomp7668_DEF3, Olcomp22604_DEF2*	(Valoroso et al., 2019)
		P. aphrodite	*PaAP3-1, PaAP3-2, PaAP3-3, PaAP3-4*	(Su et al., 2013b)
		Phalaenopsis equestris	*PeMADS2, PeMADS3 PeMADS4*	(Tsai et al., 2004)
			PeMADS5[b]	(Tsai et al., 2004; Hsieh et al., 2013a)
		Phragmipedium longifolium	*PhlonDEF1, PhlonDEF2, PhlonDEF3, PhlonDEF4*	(Aceto and Gaudio, 2011)
		Spiranthes odorata	*SpodoDEF1, SpodoDEF2, SpodoDEF3*	(Aceto and Gaudio, 2011)
		Vanilla planifolia	*VaplaDEF1, VaplaDEF2, VaplaDEF3*	(Aceto and Gaudio, 2011)
PISTILLATA (*PI*)	Petal and stamen identity	*D. crumenatum*	*DcOPI*	(Xu et al., 2006)
		Dendrobium thyrisiflorum	*DthyrPI*	(Aceto and Gaudio, 2011)
		Epipactis palustris	*EpalPI*	(Aceto and Gaudio, 2011)
		G. galeata	*GogalGLO1*	(Aceto and Gaudio, 2011)
		H. radiata	*HrGLO1, HrGLO2*	(Aceto and Gaudio, 2011)
		Oncidium Gower Ramsey	*OMADS8 (OPI)*	(Chang et al., 2009; Hsu et al., 2015; Mao et al., 2015)

(*Continued*)

TABLE 2 | Continued

Arabidopsis gene name	Function	Orchid species	Orchid orthologs	References
		O. italica	*Olcomp1173_PI, Olcomp1989_PI*	(Aceto and Gaudio, 2011; Valoroso et al., 2019)
		P. aphrodite	*PaPI-1*	(Su et al., 2013b)
		P. equestris	*PeMADS6*[b]	(Hsieh et al., 2013a, Hsieh et al., 2013b, Tsai et al., 2005; Lu et al., 2007)
		Phragmipedium longiflorum	*PhlonGLO1*	(Aceto and Gaudio, 2011)
		S. odorata	*SpodoGLO1*	(Aceto and Gaudio, 2011)
		V. planifolia	*VaplaGLO1*	(Aceto and Gaudio, 2011)
AGAMOUS (*AG*)	Stamen and carpel identity; floral meristem determinacy	*C. ensifolium*	*CeMADS1, CeMADS2, ZHLZ.comp46850, ZHLZ.comp52597, ZHLZ.comp58360, ZHLZ.comp52003, ZHLZ.comp50822*	(Wang et al., 2011; Yang and Zhu, 2015)
		D. crumenatum	*DcOAG1*	(Xu et al., 2006)
		D. thyrsiflorum	*DthyrAG1*	(Skipper et al., 2006)
		Oncidium Gower Ramsey	*OMADS4*	(Hsu et al., 2010)
		O. italica	*Olcomp1784_AG, Olcomp7958_AG, Olcomp16674_AG*	(Valoroso et al., 2019)
		P. aphrodite	*PaAG-1, PaAG-2, PaAG-3*	(Su et al., 2013b)
		P. equestris	*PeMADS1*	(Chen et al., 2012; Hsieh et al., 2013b)
		Phalaenopsis hybrid "Athens"	*PhaMADS8, PhaMADS10*	(Acri-Nunes-Miranda and Mondragón-Palomino, 2014)
		Phalaenopsis sp. "Hatsuyuki"	*PhalAG1*	(Song et al., 2006)
SEEDSTICK (*STK*)	Ovule and seed integument identity	*D. crumenatum*	*DcOAG2*	(Xu et al., 2006)
		D. thyrsiflorum	*DthyrAG2*	(Skipper et al., 2006)
		Oncidium Gower Ramsey	*OMADS2*	(Hsu et al., 2010)
		O. italica	*Olcomp3859_STK*	(Valoroso et al., 2019)
		P. aphrodite	*PaAG-4*	(Su et al., 2013b)
		P. equestris	*PeMADS7*	(Chen et al., 2012; Hsieh et al., 2013b)
		Phalaenopsis hybrid "Athens"	*PhaMADS10*	(Acri-Nunes-Miranda and Mondragón-Palomino, 2014)
		Phalaenopsis sp. "Hatsuyuki"	*PhalAG2*	(Song et al., 2006)
*SEPALLATA*s (*SEP*s)	Floral organ identity; flowering time regulation	*C. ensifolium*	*CeSEP3, ZHLZ.comp51896, ZHLZ.comp57688, ZHLZ.comp57446, ZHLZ.comp58442*	(Yang and Zhu, 2015)
		D. crumenatum	*DcOSEP1*	(Xu et al., 2006)
		Dendrobium Madame Suzie Wong	*DOMADS1, DOMADS3*	(Yu and Goh, 2000)
		Oncidium Gower Ramsey	*OMADS6 (OSEP3) OMADS11 (OSEP1)*	(Chang et al., 2009; Hsu et al., 2015)
		O. italica	*Olcomp1006_SEP, Olcomp7010_SEP*	(Valoroso et al., 2019)
		P. aphrodite	*PaSEP-1*, *PaSEP-2*, *PaSEP-3*	(Su et al., 2013b)
		P. equestris	*PeSEP1, PeSEP2*[b], *PeSEP3*[b], *PeSEP4*	(Pan et al., 2014)
		Phalaenopsis hybrid "Athens"	*PhaMADS4, PhaMADS5, PhaMADS7*	(Acri-Nunes-Miranda and Mondragón-Palomino, 2014)
AGAMOUS-LIKE 6 (*AGL6*)	Flowering promoter	*Oncidium* Gower Ramsey	*OMADS7 (OAGL6-1) OMADS1*[b] *(OAGL6-2)*	(Chang et al., 2009; Hsu et al., 2015)
		O. italica	*Olcomp1386_AGL6, Olcomp4335_AGL6, Olcomp8204_AGL6*	(Valoroso et al., 2019)
		P. aphrodite	*PaAGL6-1*, *PaAGL6-2*	(Su et al., 2013b)

[a]*FM, floral meristem.*

[b]*MADS-box genes whose function has been examined by stable or transient overexpression or silencing in orchids.*

LOCUS T (*FT*) and the MADS-box gene *SUPPRESSOR OF OVEREXPRESSION OF CONSTANS 1* (*SOC1*), which then activate the expression of *AP1* and *LFY*, two floral meristem identity genes, to start the process of floral meristem formation (**Figure 2**) (Kardailsky et al., 1999; Kobayashi et al., 1999; Blázquez and Weigel, 2000; Lee et al., 2000; Samach et al., 2000; Liu et al., 2009). Several MADS-box proteins including SOC1, AGAMOUS-LIKE 24 (AGL24), AGL6, and AGL17, promote flowering (Lee et al., 2000; Yu et al., 2002; Han et al., 2008; Yoo et al., 2011), whereas MADS-box regulators including FLOWERING LOCUS C (FLC), SHORT VEGETATIVE PHASE (SVP), MADS AFFECTING FLOWERING 1/FLOWERING

TABLE 3 | The promotive environmental factors for orchid flowering.

Genus	Temperature	Photoperiod	References
Cymbidium	- Low night temperature of 13°C - A difference of 10°C–14°C in diurnal temperature	- No known influence	(Rotor, 1952; Rotor and Withner, 1959; Goh et al., 1982; Powell et al., 1988; An et al., 2012)
Oncidium	- Low night temperature - A large difference in diurnal temperature - High constant temperature (30°C) for 2 weeks	- No known influence	(Chang and Lee, 2000; Chin et al., 2014)
Dendrobium	- Low night temperature of 13°C - 3 weeks at 13°C to 15°C	- Flowering under short days (for *Dendrobium Phalaenopsis* only)	(Rotor 1952; Rotor and Withner 1959; Goh et al., 1982; Sinoda et al., 1988; Lopez and Runkle, 2004)
Phalaenopsis	- Day temperature not higher than 28°C - Night temperature of 15°C to 18°C	- No known influence	(Tran Thanh Van, 1974; Nishimura et al., 1976; Sakanishi et al., 1980; Baker and Baker, 1996; Blanchard and Runkle, 2006; Newton and Runkle, 2009)

LOCUS M (MAF1/FLM), and MAF2/3/4/5 form various complexes to repress flowering (**Figure 2**) (Helliwell et al., 2006; Searle et al., 2006; Li et al., 2008; Gu et al., 2013; Lee et al., 2013; Pose et al., 2013; Mateos et al., 2015). Another three MADS-box transcription factors that are closely related to each other, AP1, CAL, and FUL are also involved in the activation of *LFY* in promoting flowering and floral meristem specification as the triple mutant of these genes generates leafy shoots in place of floral organs (Ferrándiz et al., 2000).

In orchids, the process of the floral transition occurs in the axillary buds where the bud primordia will develop into a more convex shape upon entering reproductive phase. Recent works have identified and examined many orthologs of flowering integrators and other MADS-box genes in orchids (**Figure 2**). As one of the major floral pathway integrator genes, *FT*, encoding a small globular protein, is transcriptionally activated by CONSTANS (CO) in companion cells in the leaf veins and the FT protein moves to the shoot apical meristem (Kardailsky et al., 1999; Kobayashi et al., 1999; An et al., 2004; Corbesier et al., 2007; Liu et al., 2012; Nakamura et al., 2014; Zhu et al., 2016). In orchids for instance, *Oncidium*, *Dendrobium*, and *Cymbidium*, the expression of *FT* orthologs was predominantly expressed in the leaves and axillary buds. In addition, the expression of *FT* orthologs has been found to be influenced by daylength in *Oncidium* and *Cymbidium*, showing a similar photoperiodic pattern like *FT* in *Arabidopsis* (Hou and Yang 2009; Huang et al., 2012). Ectopic expression of *FT* orthologs, *OnFT*, *DnFT*, *DOFT*, *CeFT*, *CgFT*, *CsFT*, and *PaFT1* from the orchids *Oncidium*,

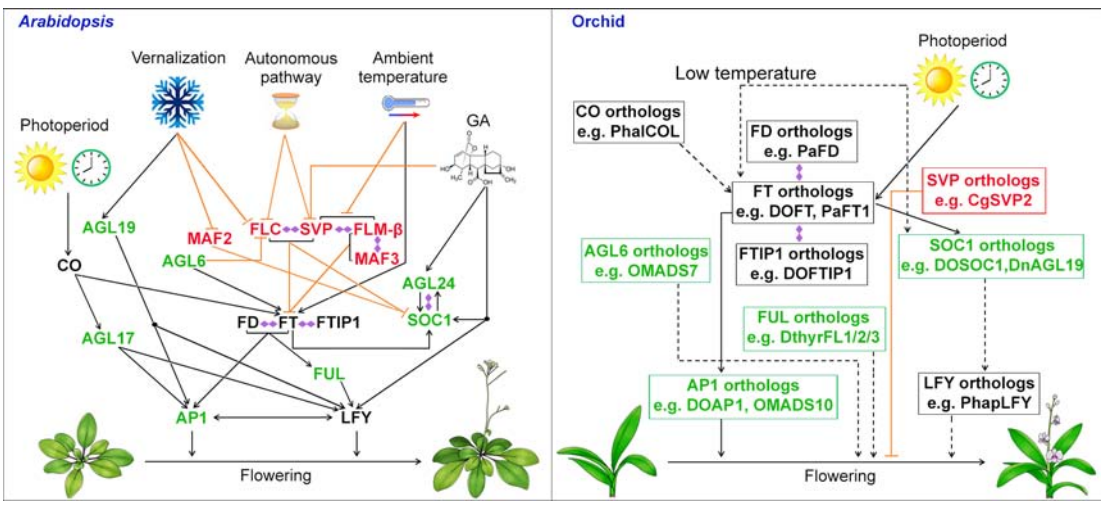

FIGURE 2 | Biological roles of MADS-box genes in controlling flowering in the model plant *Arabidopsis* and orchid. In *Arabidopsis*, the MADS-box genes including *SOC1*, *FLC*, *SVP* and *AGL24* integrates signals for flowering from environmental and endogenous cues. In orchid, orthologous genes of *SOC1*, *AGL6*, *SVP*, and *AP1* have been isolated and functionally characterized either in heterologous system (e.g. *Arabidopsis*) or orchid and shown to be involved in promoting flowering. MADS-box transcription factors that function as flowering activators and suppressors are shown in green and red, respectively, whereas other flowering regulators are shown in black. Promoting and repressive effects are indicated by black arrows and orange T bars, respectively. The dashed lines with arrows indicate possible positive regulation based on the studies using heterologous systems. Double-ended diamond arrows indicate protein–protein interactions. AGL6, AGAMOUS-LIKE 6; AGL17, AGAMOUS-LIKE 17; AGL19, AGAMOUS-LIKE 19; AGL24, AGAMOUS-LIKE 24; AP1, APETALA1; CO, CONSTANS; FLC, FLOWERING LOCUS C; FLM, FLOWERING LOCUS M; FT, FLOWERING LOCUS T; FTIP1, FT-INTERACTING PROTEIN 1; FUL, FRUITFULL; LFY, LEAFY; MAF2, MADS AFFECTING FLOWERING 2; SOC1, SUPPRESSOR OF OVEREXPRESSION OF CONSTANS 1; SVP, SHORT VEGETATIVE PHASE.

Dendrobium, *Cymbidium*, and *Phalaenopsis*, respectively, results in a precocious flowering phenotype in transgenic plants of *Arabidopsis* or tobacco (Hou and Yang, 2009; Huang et al., 2012; Li et al., 2012; Xiang et al., 2012; Jang, 2015; Wang et al., 2017). More importantly, downregulation of *DOFT* delays flowering in *Dendrobium* orchids, whereas overexpression of *DOFT* accelerates flowering in orchids (Wang et al., 2017). Interestingly, low temperature treatment specifically induces the expression of *FT* in leaves in both *Dendrobium* and *Phalaenopsis*, suggesting *FT* is the main floral inducer under floral inductive low temperature regime (Li et al., 2012; Jang et al., 2015).

MADS-Box Genes and Orchid Flowering

SOC1 encodes a MADS-box transcription factor that is a member of the *Tomato MADS-box gene 3* (*TM3*)-like genes subfamily from angiosperms and gymnosperms (Lee et al., 2000; Becker and Theißen, 2003; Cseke et al., 2003; Nakamura et al., 2005). *SOC1* expression is detected in both leaves and shoot apices and is regulated by several floral pathways (Borner et al., 2000; Lee et al., 2000; Samach et al., 2000; Moon et al., 2003). In *Dendrobium nobile*, the expression of a close *SOC1* ortholog, *DnAGL19*, has been found to be increased after vernalization (Liang et al., 2012). In the orchid *Dendrobium* Chao Praya Smile, the expression of the *SOC1* ortholog *DOSOC1* is highly detected in reproductive organs, such as inflorescence apex, pedicel, floral buds and open flowers (Ding et al., 2013). *DOSOC1* expression is upregulated in the whole seedlings upon the floral transition (Ding et al., 2013). Overexpression of *DOSOC1* shows early flowering in both *Arabidopsis* and *Dendrobium* orchids, implying the evolutionary conserved functions of *SOC1*-like genes as activators of flowering (**Figure 2**) (Ding et al., 2013). Moreover, *DOSOC1* expression is downregulated in *DOFT* knockdown *Dendrobium* orchid, whereas its expression is upregulated in *DOFT* overexpression orchid (Wang et al., 2017), indicating a conserved regulatory mechanism of *SOC1*-like genes expression. Intriguingly, *DOSOC1* overexpression in *Dendrobium* results in abnormal floral organ development with formation of immature perianth organs only, indicating the role of *DOSOC1* in maintaining the identity of floral meristem and formation floral organs (Ding et al., 2013). This is in line with the function of *SOC1*-like genes in flower development in some plant species (Liu et al., 2013; Teo et al., 2014). Additionally, another MADS-box gene *FUL* has been shown to act redundantly with *SOC1* in regulation of flowering time in *Arabidopsis* (Melzer et al., 2008). Mutations in *ful* only slightly delay flowering, while in combination with *soc1* mutants, the flowering is further delayed as compared with both single mutants. Three *FUL*-like genes have been isolated in the orchid *Dendrobium thyrsiflorum*, namely *DthyrFL1/2/3* (Skipper et al., 2005). These three genes are upregulated during orchid reproductive development, yet their involvement in orchid flowering remains unknown.

SOC1 expression is repressed by a floral repressor protein complex formed by FLC and SVP, which are also MADS-box proteins (Li et al., 2008). The orchid *SVP* orthologs have been reported in *Cymbidium* orchids, whereas no *FLC* orthologs have been isolated so far in monocots. The expression levels of *CgSVP1/2/3*, *SVP* orthologs, are greatly reduced upon cold treatment in *Cymbidium goeringii* (Yang et al., 2019). Moreover, transient overexpression of *CgSVP2* results in retarded flower bud growth, indicating its role as a repressor of flower bud formation (Yang et al., 2019). However, the involvement of *SVP* orthologs in orchid floral transition and its potential regulation of *SOC1* need further investigation.

AGL6 encodes another MADS-box transcription factor which regulates the transition to flowering in *Arabidopsis* (Yoo et al., 2011). Knockdown of *AGL6* by artificial microRNA leads to late flowering, in contrast, *agl6-1D* wherein *AGL6* is activated by the *35S* enhancer shows early flowering. Two *AGL6*-like genes, *OMADS1* (*OAGL6-2*) and *OMADS7* (*OAGL6-1*), have been found in the *Oncidium* Gower Ramsey orchid, and overexpression of either gene leads to early flowering in *Arabidopsis* (Hsu et al., 2003; Chang et al., 2009), implying a conserved function of *AGL6*-like genes in mediating flowering.

As mentioned above, AP1, a MADS-box protein, specifies the identity of floral meristem as well as sepal and petal identity (Irish and Sussex, 1990; Mandel et al., 1992; Bowman et al., 1993). In *ap1* mutants, flowers exhibit a homeotic transformation that sepals develop into bracts and petals fail to develop. By comparison, *AP1* overexpression causes early flowering and conversion of the inflorescence meristem into a determinate floral meristem (Mandel and Yanofsky, 1995). Orthologs of *AP1* have been identified and characterized in *Oncidium*, *Dendrobium*, and *Cymbidium*. The expression of *AP1* orthologs can be detected in both vegetative tissues and reproductive structures such as floral buds and pedicel (Yu and Goh, 2000; Chen et al., 2007; Chang et al., 2009; Tian et al., 2013; Sawettalake et al., 2017). Overexpression of *AP1* orthologs, such as *OMADS10* from *Oncidium* Gower Ramsey and *DOAP1* from *Dendrobium* Chao Praya Smile, causes early flowering as well as conversion of inflorescence meristems to determinate floral meristems in *Arabidopsis* (Chang et al., 2009; Sawettalake et al., 2017). Transgenic *Dendrobium* orchids overexpressing *DOAP1* also show accelerated flowering as compared to wild-type orchid and conversion of inflorescence meristems to determinate floral meristems (Sawettalake et al., 2017). In addition, *DOAP1* expression is promoted by *DOFT* in *Dendrobium* orchids, which is a conserved regulation as that in *Arabidopsis* (Wang et al., 2017). These studies suggest that orchid *AP1* orthologs have conserved functions in promoting the floral transition and determination of floral meristems.

MADS-BOX PROTEINS IN ORCHID FLORAL PATTERNING

The Orchid Flower

In angiosperms, the flowers are usually composed of four types of structures, which form two parts, namely the vegetative part and the reproductive part. While the morphology and elaboration can differ greatly among different species, the diversification of floral patterning has taken place in a relatively conserved manner

in having similar general organization of four types of structures arranged in four concentric whorls. In *Arabidopsis*, the flower consists of four concentric whorls of floral organs from the outer to inner whorls: sepals (four), petals (four), stamens (six), and two fused carpels. In orchids, the flowers are usually bilaterally symmetrical (zygomorphic) with three outer sepals, two inner petals, and a highly specialized inner median petal named lip or labellum which acts as the main pollinator attractant (**Figure 3A**). In a number of orchid species, the outer sepals and inner petals are named as tepals as they cannot be distinguished from each other morphologically. The reproductive structure gynostemium or column is composed of fused male (stamen/anther) and female (carpel/pistil) organs.

ABCE and Floral Quartet Model

Understanding the specification of the distinct floral organs through genetic study in *Arabidopsis* and *Antirrhinum majus* (snapdragon) has resulted in the birth of "ABCE model" and "floral quartet model" (**Figure 4A**) (Meyerowitz et al., 1989; Schwarz-Sommer et al., 1990; Coen and Meyerowitz, 1991; Weigel and Meyerowitz, 1994; Irish, 2010; Theißen et al., 2016). In the classical "ABC model," a combination of three gene classes specifies the four types of floral organs: sepal, petal, stamen, and carpel (Coen and Meyerowitz, 1991; Weigel and Meyerowitz, 1994). In *Arabidopsis*, the A-class genes (*AP1* and *AP2*) determine the sepal identify in the outermost whorl, A-class and B-class (*AP3* and *PI*) genes together specify petals in the second

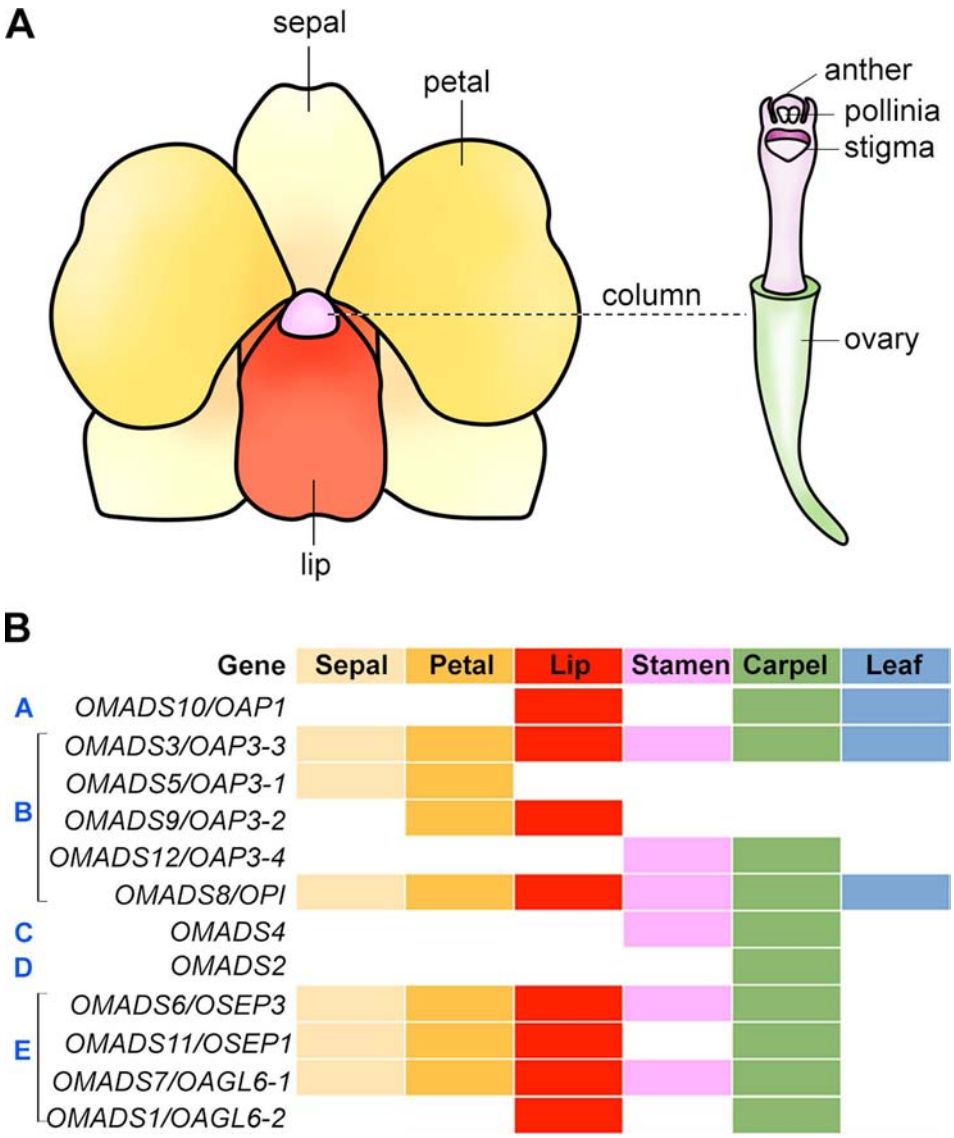

FIGURE 3 | Floral organ identity genes in orchid. **(A)** An illustration showing a typical orchid flower structure. **(B)** Expression patterns of orthologs of floral organ identity genes in orchid. The floral organs, sepal, petal, lip, stamen, carpel, and leaf are color-coded, and presence of these colors indicates detected expression in these organs. The white color indicates no expression detected. The gene expression patterns are shown based on the studies in the *Oncidium* orchid (Chang et al., 2009; Chang et al., 2010; Hsu et al., 2010; Hsu et al., 2015).

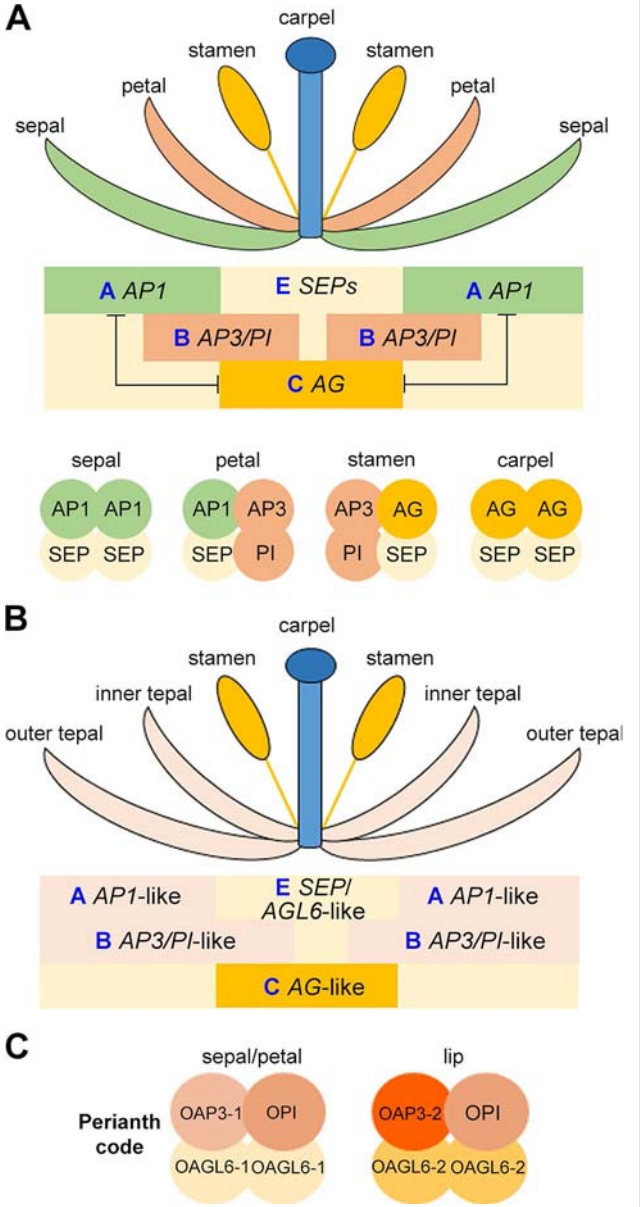

FIGURE 4 | Schematic drawing showing the ABCE model **(A)**, the modified ABC model **(B)**, and the orchid Perianth code **(C)**.

whorl, B-class and C-class (*AG*) genes determine the identity of the male reproductive organ stamen in the third whorl, and the C-class gene specifies the female reproductive organ carpel in the innermost whorl. The expression domains of A-class and C-class genes are mutually exclusive. After discovering that the E-class genes (*SEP1–4*) are essential for the determination of all of the four whorls of floral organs, the classical "ABC model" was then extended to the "ABCE model." Additionally, D-class genes (*STK* and *SHP1/2*) are needed for determining the identity of ovule (Pinyopich et al., 2003). Interestingly, except for *AP2,* all these genes belong to MADS-box gene family, and their proteins form tetrameric complexes. This was coined as the "floral quartet model" as the tetrameric complexes functions as a whole to direct the development of specific floral organs (**Figure 4A**) (Theissen and Saedler, 2001). In orchids, the study of MADS-box transcription factors related to floral patterning has been challenging as recent functional analyses have shown that these genes have functionally diversified in their own lineages, making the prediction of function on the basis of orthology difficult (Irish and Litt, 2005).

MADS-Box Genes and Orchid Floral Patterning

A-Class Genes

In orchids, there are several *AP1* orthologs isolated in *Cymbidium*, *Oncidium*, *Dendrobium*, and *Phalaenopsis* (**Table 2**). In *Dendrobium Madame Thong-In*, the *AP1* ortholog *DOMADS2* is expressed during the transitional phase and floral development (Yu and Goh, 2000). In mature flowers, *DOMADS2* is detected in the column and ovary but not in the pedicel, sepal, or petal. The differential expression pattern compared with *AP1* expression in the sepal and petal in *Arabidopsis* suggests the functional divergence of *AP1*-like genes during floral patterning. In the *Dendrobium* Chao Praya Smile orchid, the *AP1* ortholog *DOAP1* is detected at high levels in the inflorescence meristem as well as flowers. In addition, the overexpression of *DOAP1* can partially complement the *Arabidopsis ap1* mutant in restoring petal formation, suggesting *DOAP1* functions as a homeotic gene (Sawettalake et al., 2017). In *Oncidium* Gower Ramsey, the *AP1* orthologs *OMADS10* is expressed in the leaves, lip and carpel (**Figure 3B**). Overexpression of *OMADS10* induces early flowering without any floral organs defects in *Arabidopsis* (Chang et al., 2009). Two *AP1* orthologs, *PaAP1-1* and *PaAP1-2* has been isolated in the moth orchid *Phalaenopsis aphrodite* (Su et al., 2013b). *PaAP1-1* is mainly expressed in the pollinia and pedicel, whereas *PaAP1-2* is specifically expressed in the pedicel. The expression patterns of orchid *AP1* orthologs are unlike the A-class genes in *Arabidopsis* which are only present in the sepals and petals, but is somehow similar to the monocot lily *AP1* orthologs, *LMADS5/6*, which are expressed in the vegetative leaves and the innermost whorl carpel (Chen et al., 2008). This indicates the divergent function of orchid *AP1*-like genes in floral organ development.

B-Class Genes

The B-class genes are necessary for determining the identity of petals and stamens. There are two B-class genes in *Arabidopsis*, *AP3* and *PI,* analogous to the *A. majus DEFICIENS* and *GLOBOSA*, respectively. Mutations in either *AP3* or *PI* lead to similar phenotypes wherein petals and stamens are transformed into sepals and carpels, respectively (Bowman et al., 1989; Hill and Lord, 1989). Many studies have identified various numbers of B-class genes and studied their expression patterns in several orchid species (**Table 2**) (Hsu and Yang, 2002; Tsai et al., 2004; Tsai et al., 2005; Xu et al., 2006; Mondragón-Palomino and Theißen, 2008; Chang et al., 2009; Chang et al., 2010; Su et al., 2013b; Tsai et al., 2014; Hsu et al., 2015; Mao et al., 2015; Yang and Zhu, 2015). In *Dendrobium crumenatum*, the expression of *DcOAP3A* and *DcOPI* is detected in all parts of the mature flowers, but the expression of *DcOAP3B* is present in petals, lips,

anthers, and column only (Xu et al., 2006). DcOAP3A/B can form heterodimers with DcOPI. In *Oncidium* Gower Ramsey, *OMADS3* (*OAP3-3*), *OMADS5* (*OAP3-1*), *OMADS9* (*OAP3-2*), and *OMADS12* (*OAP3-4*) belong to the *AP3* lineage, while *OMADS8* (*OPI*) belongs to the *PI* lineage. *OMADS3* and *OMADS8* are expressed in both vegetative tissues and all floral organs of mature flowers (**Figure 3B**) (Chang et al., 2010). *OMADS5* is detected in both sepals and petals but not in the lip, whereas *OMADS9* is detected in the petals and lips (Chang et al., 2010). *OMADS12* is detected in the orchid reproductive floral organs including stamens and carpels, but not in the sepals, petals, and lips (Hsu et al., 2015). Overexpression of truncated *OMADS3* in *Arabidopsis* results in *ap2*-like flowers with homeotic conversion from sepals and petals to carpel-like and stamen-like organs (Hsu and Yang, 2002), while overexpression of *OMADS8,* but not *OMADS5/9,* causes the transformation of sepals to expanded petal-like structures (Chang et al., 2010). While OMADS3, OMADS5, and OMADS9 can assemble into both homodimers and heterodimers within the same group, OMADS8 can only form heterodimer with OMADS3 (Chang et al., 2010). It has been proposed that *OMADS3/5/8/9* is probably needed for the specification of sepals and petals and *OMADS3/8/9* but the absence of *OMADS5* leads to the formation of lips (Chang et al., 2010). In *P. equestris*, the MADS-box genes *PeMADS2*, *PeMADS3*, *PeMADS4,* and *PeMADS5* belong to the *AP3* lineage and *PeMADS6* belongs to the *PI* lineage. They are all expressed in lips and columns with *PeMADS2* also found in sepals and petals and *PeMADS3* in petals (Tsai et al., 2004; Tsai et al., 2005). Similarly to those B-class genes in *Dendrobium* and *Oncidium*, PeMADS2-5 interacts with PeMADS6 to form heterodimers and binds to CarG boxes on DNA (Tsai et al., 2005).

C- and D-Class Genes

In *Arabidopsis*, the C-class gene *AG* is required for the normal development of the stamens and carpels found in the third and fourth whorls, respectively. Mutations in *AG* cause the homeotic transformation of stamens and carpels into petals and sepals (Yanofsky et al., 1990). In addition, since *AG* is also necessary for floral meristem determinacy, the flowers of *ag* mutants are indeterminate and show the "flower within a flower" phenotype of sepal-petal-petal reiteration. D-class genes are required for regulating ovule identify. C and D-class genes are members of the *AG*-like family and are resulted from an ancient gene duplication event (Becker and Theißen, 2003). Both C and D-class genes have been identfied from several orchid speices (**Table 2**).

In *P. equestris*, *Phalaenopsis* sp. "Hatsuyuki," *Cymbidium ensifolium*, and *Oncidium* Gower Ramsey, the C-class genes *PeMADS1*, *PhalAG1*, *CeMADS1*, and *OMADS4,* respectively, are highly expressed in the floral buds and column in mature flowers (**Figure 3B**) (Song et al., 2006; Hsu et al., 2010; Wang et al., 2011; Chen et al., 2012). *OMADS4* in the *Oncidium* Gower Ramsey orchid is specifically detected in the stamens and carpels, similar to the expression pattern of LMADS10 from Lilium longiflorum (Hsu et al., 2010). Both *OMADS4* and *LMADS10*, when overexpressed in *Arabidopsis*, result in early flowering, whereas *LMADS10* overexpression also leads to curly leaves and floral organ conversions, indicating the probable functional diversification of the monocot C-class genes. Several C-class genes from other orchid species have broader expression pattern. For examples, the *D. crumenatum* and *D. thyrsiflorum AG* orthologs, *DcOAG1* and *DthyrAG1*, respectively, are expressed in all kinds of floral organs and are not confined to the reproductive organs (Skipper et al., 2006; Xu et al., 2006). This expression pattern is similar to the *AG* homolog from *Illicium floridanum* that is also expressed in the tepals and reproductive organs (Kim et al., 2005), suggesting the regulatory mechanisms involved in the regulation of the expression of these C-class genes have evolved independently. The ectopic expression of *DcOAG1* in *Arabidopsis* accelerates flowering with abnormal floral organs in the first and second whorls (Xu et al., 2006).

OMADS2 in the orchid *Oncidium* Gower Ramsey, a D-class gene, is specifically detected in stigmatic cavity and ovary (Hsu et al., 2010). This expression pattern is close to that of LMADS2 from *L. longiflorum*, which is exclusively present in the carpel (Tzeng et al., 2002). OMADS2 forms homodimers and heterodimers with OMADS4. Overexpression of *OMADS2* in *Arabidopsis* leads to early flowering without any floral organ converstion (Hsu et al., 2010).

E-Class Genes

The members of the *SEP* MADS-box subfamily belong to the E-class genes that are necessary for the formation of all floral organs and floral meristem determinacy in *Arabidopsis*. The triple mutant in *SEP1/2/3/4* genes produce flowers with all floral organs converted to leaf-like organs (Pelaz et al., 2000; Ditta et al., 2004). *SEP* genes are present in angiosperms, but not gymnosperms, indicating that *SEP* genes may have been important for the existence of flowers (Nam et al., 2003). In *D. crumenatum*, the *SEP* ortholog *DcOSEP1* is detected in all floral organs, similarly to *Arabidopsis SEP*s. DcOSEP1 is able to interact with the DcOAP3A-DcOPI and DcOAP3B-DcOPI heterodimers, but not with DcOAP3A and DcOPI individually, indicating that DcOSEP1 is able to form a higher order protein complex with DcOAP3A-DcOPI or DcOAP3B-DcOPI, similar to their counterparts in *Arabidopsis* (Honma and Goto, 2001; Theissen and Saedler, 2001; Xu et al., 2006). In the *Dendrobium* Madame Thong-In orchid, *DOMADS1* and *DOMADS3* encode MADS-box proteins closely related with SEP1 and SEP3, respectively. *DOMADS1* is present in all the floral organs similarly to *DcOSEP1*, while *DOMADS3* is only present in the pedicel (Yu and Goh, 2000). In the *Oncidium* Gower Ramsey orchid, *OMADS6* (*OSEP3*) and *OMADS11* (*OSEP1*) encode MADS-box proteins homologous to *SEP3* and *SEP1/2*, respectively. Both genes are highly present in the sepal, petal, lip, and carpel, with weaker and undetectable expression in stamens for *OMADS6* and *OMADS11*, respectively (**Figure 3B**) (Chang et al., 2009). Overexpression of *OMADS6* in *Arabidopsis* leads to homeotic transformation of sepals into carpelliod structures and petals into stamen-like organs (Chang et al., 2009). In *P. equestris*, the four *SEP*-like *PeSEP* genes are expressed in flower buds with the expression of *PeSEP2* higher in floral stalk and column and *PeSEP3* in petals (Pan et al., 2014). Like the SEP proteins in *D. crumenatum*, PeSEP2, PeSEP3, and PeSEP4 proteins cannot interact with the B-class proteins PeMADS2, PeMADS4, PeMADS6, or the D-class protein PeMADS7 individually, but

can form multimeric complexes with PeMADS2/6, PeMADS4/6 and PeMADS6/7. Only PeSEP1 is able to interact with PeMADS2, PeMADS4, PeMADS6, and PeMADS7 individually, and with PeMADS2/6, PeMADS4/6, and PeMADS6/7 (Pan et al., 2014). Silencing of *PeSEP3* by VIGS results in the conversion of tepal to leaf-like organ in *Phalaenopsis*, whereas silencing of *PeSEP2* does not greatly affect flower development (Pan et al., 2014), suggesting that these *PeSEPs* have divergent functions in orchid flower development.

The *AGL6*-like genes are similar to *SEP*-like genes and the *AGL6*-like gene in petunia functions like *SEP* genes in floral patterning (Rijpkema et al., 2009). It has been proposed to add *AGL6*-like genes to class-E genes. As described above, the *Arabidopsis AGL6* functions as a flowering promoter (Yoo et al., 2011). *Arabidopsis* has another *AGL6*-like gene called *AGL13*, which acts similarly to E-class *SEP* genes in specifying male and female gametophytes (Hsu et al., 2014). The orchid *Oncidium* Gower Ramsey also has two *AGL6*-like genes, *OMADS1* and *OMADS7*. *OMADS7* is expressed in all the floral organs, similar to that of E-class gene including *OMADS6* (**Figure 3B**) (Chang et al., 2009). *OMADS1* shows a different expression pattern which is in the lip and carpel, but not in other floral organs (**Figure 3B**) (Chang et al., 2009). Besides being early flowering, the flowers of *OMADS1* or *OMADS7* overexpression show homeotic transformation of sepals into carpel-like structures (Chang et al., 2009), indicating their dual roles in promoting floral transition and regulating floral organ formation. In *P. aphrodite*, the *AGL6*-like gene *PaAGL6-1* is expressed specifically in the lip, suggesting that *PaAGL6* may play an important role in lip formation (Su et al., 2013b). Subsequent studies have further revealed that the orchid *AGL6*-like genes play important roles in determining sepal/petal/lip formation (discussed in the following section). Together, *AGL6*-like genes may have diverse function in all four whorls of floral organs.

The Orchid Perianth Code

Flowers in orchids and several other monocots such as lily, the sepals and petals are morphologically similar and are also collectively called tepals. This is different from *Arabidopsis* and other dicots flowers, in which sepals and petals have distinguished morphologies. To explain this difference in perianth organs specification, the modified ABC model has been proposed, in which the expression domain of B-class genes are extended to the outermost whorl of floral organs in many orchid species (**Figure 4B**) (Van Tunen et al., 1993; Bowman, 1997; Kramer et al., 2003; Mondragón-Palomino and Theißen, 2008). In the *Oncidium* Gower Ramsey orchid, the *AP3*-like gene *OMADS3* and the *PI*-like gene *OMADS8* are detected in all perianth organs (**Figure 3B**) (Chang et al., 2010).

However, the orchid flower has a median petal called lip, which has a highly diversified morphology and acts as the main attractor of pollinators. The specification of the lip cannot be simply explained by the modified "ABC model". Several years of molecular studies of MADS-box proteins and orchid floral patterning have led to the discovery of the model of formation of perianth organs: the Perianth (P) code (**Figure 4C**) (Hsu et al., 2015). Based on this model, the two tetrameric MADS-box protein complexes, SP (sepal/petal) complex (OAP3-1/OAGL6-1/OAGL6-1/OPI) and L (lip) complex (OAP3-2/OAGL6-2/OAGL6-2/OPI), compete to promote the development of sepal/petal and lip, respectively. Different copies of B-class *AP3*-like genes (*OAP3-1* and *OAP3-2*) and *AGL6*-like genes (*OAGL6-1* and *OAGL6-2*) have different whorl-specific or whorl-biased expression patterns, providing the basis for the formation of SP and L complexes. Moreover, the relative levels of the two complexes may also determine the formation of various forms of intermediate lips or distinct lips in orchid.

CONCLUDING REMARKS AND FUTURE PERSPECTIVES

The orchid family is the second largest family of angiosperms and has delighted cultivators for their unsurpassed beauty and complexity. The study on orchids has come a long way since people began gathering and propagating them under controlled environment. Recent findings in orchids, mainly *Cymbidium*, *Oncidium*, *Dendrobium*, and *Phalaenopsis*, have revealed that MADS-box proteins play critical roles in orchid flowering and floral patterning. The unraveled molecular mechanisms underlying orchid flowering and floral development can be applied to both classical orchid breeding and targeted manipulation of orchids for desired flowering traits and floral patterns. Orchids have many MADS-box genes, for example, 51 in *P. equestris* and 63 in *Dendrobium catenatum* (Cai et al., 2015; Zhang et al., 2016), however, only several of the MADS-box genes have been characterized, and most of them are shown be involved in orchid flowering or floral development. A recent study shows that MADS-box regulators might be relevant with the development of seeds without endosperm and epiphytism in orchids (Zhang et al., 2017), but revealing the functions of MADS-box genes in other develomental processes needs more future endeavor. In addition, in this review, the comparisons of orchid MADS-box genes to *Arabidopsis* have been included as many orchid genes are named and share similar functions to their closest orthologs in *Arabidopsis*. With the increasing number of MADS-box genes being studied in model monocots such as rice, wheat, barley, maize, and lily (Callens et al., 2018), more detailed comparisons of MADS-box gene functions between orchid and other monocots can be performed and discussed in the near future.

Nowadays, the function of orchid MADS-box genes, in many cases, is studied in heterologous plant systems (e.g. *Arabidopsis* and tobacco). In only several studies, the function of MADS-box genes has been examined by using transient overexpression/knockdown in orchids by VIGS or generating transgenic orchid overexpressing or knocking down of target genes (**Table 2**). For examples, silencing of *OAGL6-2* by VIGS has been done in *Oncidium* Gower Ramsey and *Phalaenopsis amabilis* hybrid to test the Perianth code, and *DOAP1* when overexpressed in *Dendrobium* Chao Praya Smile, leads to early flowering. To better understand the function of orchid genes, there is a need for more reliable

and faster genetic transformation systems of different orchid species in orchid study and targeted orchid breeding with desired traits. Moreover, with modern genomic editing tools such as CRISPR-Cas9 (Clustered Regularly Interspaced Short Palindromic Repeats–Caspase 9), it is now possible to generate orchid mutants for *in vivo* functional characterizations (Kui et al., 2017). Indeed, CRISPR-Cas9 has been successfully used to create multiple mutants of MADS genes in the orchid *P. equestris* very recently (Tong et al., 2019).

With the advent of sequencing technologies, five orchid genomes have been released, including *Apostasia shenzhenica*, *D. catenatum*, *Dendrobium officinale*, *P. equestris*, and *Vanilla planifolia* (Cai et al., 2015; Yan et al., 2015; Zhang et al., 2016; Zhang et al., 2017; Hu et al., 2019). Moreover, the transcriptomes of several orchid species from different subfamilies are freely available in online databases, such as Orchidstra 2.0 (http://orchidstra2.abrc.sinica.edu.tw), OrchidBase 3.0 (http://orchidbase.itps.ncku.edu.tw) and OOGB (http://predictor.nchu.edu.tw/oogb) (Chang et al., 2011; Fu et al., 2011; Su et al., 2013a; Tsai et al., 2013; Chao et al., 2017; Tsai et al., 2017). Recently, the transcriptome of a Mediterranean orchid *Orchis italica* inflorescence have also been analyzed (Valoroso et al., 2019). Genome sequences and transcriptomic data have provided valuable information in aiding basic research and genomics-assisted horticultural breeding. The advent of molecular tools has allowed genomic analysis to determine the underlying mechanisms behind many morphological characteristics and developmental processes. With modern genomic editing tools available, it is now feasible to generate mutants or novel varieties in orchids. This would greatly help not only in the molecular genetic research of orchid biology, but also in generating novel orchid varieties with various desirable traits through targeted gene editing.

AUTHOR CONTRIBUTIONS

ZT and LS wrote the manuscript. WZ made the drawings of *Arabidopsis* and orchid plants. All authors read and approved of the manuscript.

FUNDING

Preparation of the review has been supported by the intramural funding from Temasek Life Sciences Laboratory and National University of Singapore.

REFERENCES

Aceto, S., and Gaudio, L. (2011). The MADS and the beauty: genes involved in the development of orchid flowers. *Curr. Genomics* 12, 342–356. doi: 10.2174/138920211796429754

Acri-Nunes-Miranda, R., and Mondragón Palomino, M. (2014). Expression of paralogous *SEP*-, *FUL*-, *AG*-and *STK*-like MADS-box genes in wild-type and peloric *Phalaenopsis* flowers. *Front. Plant Sci.* 5, 76. doi: 10.3389/fpls.2014.00076

Adamczyk, B. J., and Fernandez, D. E. (2009). MIKC* MADS domain heterodimers are required for pollen maturation and tube growth in *Arabidopsis*. *Plant Physiol.* 149, 1713–1723. doi: 10.1104/pp.109.135806

Adamczyk, B. J., Lehti-Shiu, M. D., and Fernandez, D. E. (2007). The MADS domain factors AGL15 and AGL18 act redundantly as repressors of the floral transition in *Arabidopsis*. *Plant J.* 50, 1007–1019. doi: 10.1111/j.1365-313X.2007.03105.x

Alvarez-Buylla, E. R., Pelaz, S., Liljegren, S. J., Gold, S. E., Burgeff, C., Ditta, G. S., et al. (2000). An ancestral MADS-box gene duplication occurred before the divergence of plants and animals. *Proc. Natl. Acad. Sci. U. S. A.* 97, 5328–5333. doi: 10.1073/pnas.97.10.5328

An, H., Roussot, C., Suarez-Lopez, P., Corbesier, L., Vincent, C., Pineiro, M., et al. (2004). CONSTANS acts in the phloem to regulate a systemic signal that induces photoperiodic flowering of *Arabidopsis*. *Development* 131, 3615–3626. doi: 10.1242/dev.01231

An, H. R., Kim, Y. J., and Kim, K. S. (2012). Flower initiation and development in *Cymbidium* by night interruption with potassium and nitrogen. *Hortic. Environ. Biotechnol.* 53, 204–211. doi: 10.1007/s13580-012-0023-5

Arditti, J. (1992).*Fundamentals of orchid biology*. New York: John Wiley & Sons.

Atwood, J. T. (1986). The size of the Orchidaceae and the systematic distribution of epiphytic orchids. *Selbyana*, 171–186. doi: 10.2307/41888801

Baker, M. L., and Baker, C. O. (1996).*Orchid species culture: Dendrobium*. (Portland, Oregan. USA: Timber Press)

Becker, A., and Theißen, G. (2003). The major clades of MADS-box genes and their role in the development and evolution of flowering plants. *Mol. Phylogenet. Evol.* 29, 464–489. doi: 10.1016/S1055-7903(03)00207-0

Belarmino, M., and Mii, M. (2000). *Agrobacterium*-mediated genetic transformation of a *Phalaenopsis* orchid. *Plant Cell Rep.* 19, 435–442. doi: 10.1007/s002990050752

Bemer, M., Wolters-Arts, M., Grossniklaus, U., and Angenent, G. C. (2008). The MADS domain protein DIANA acts together with AGAMOUS-LIKE80 to specify the central cell in *Arabidopsis* ovules. *Plant Cell* 20, 2088–2101. doi: 10.1105/tpc.108.058958

Blázquez, M. A., and Weigel, D. (2000). Integration of floral inductive signals in *Arabidopsis*. *Nature* 404, 889–892. doi: 10.1038/35009125

Blázquez, M. A., Ahn, J. H., and Weigel, D. (2003). A thermosensory pathway controlling flowering time in *Arabidopsis thaliana*. *Nat. Genet.* 33, 168. doi: 10.1038/ng1085

Blanchard, M. G., and Runkle, E. S. (2006). Temperature during the day, but not during the night, controls flowering of *Phalaenopsis* orchids. *J. Exp. Bot.* 57, 4043–4049. doi: 10.1093/jxb/erl176

Borner, R., Kampmann, G., Chandler, J., Gleißner, R., Wisman, E., Apel, K., et al. (2000). A MADS domain gene involved in the transition to flowering in *Arabidopsis*. *Plant J.* 24, 591–599. doi: 10.1046/j.1365-313x.2000.00906.x

Boss, P. K., Bastow, R. M., Mylne, J. S., and Dean, C. (2004). Multiple pathways in the decision to flower: enabling, promoting, and resetting. *Plant Cell* 16, S18–S31. doi: 10.1105/tpc.015958

Bowman, J. L., Smyth, D. R., and Meyerowitz, E. M. (1989). Genes directing flower development in *Arabidopsis*. *Plant Cell* 1, 37–52. doi: 10.1105/tpc.1.1.37

Bowman, J. L., Alvarez, J., Weigel, D., Meyerowitz, E. M., and Smyth, D. R. (1993). Control of flower development in *Arabidopsis thaliana* by APETALA1 and interacting genes. *Development* 119, 721–743.

Bowman, J. L. (1997). Evolutionary conservation of angiospermflower development at the molecular and genetic levels. *J. Biosci.* 22, 13. doi: 10.1007/BF02703197

Bulpitt, C. J., Li, Y., Bulpitt, P. F., and Wang, J. (2007). The use of orchids in Chinese medicine. *J. R. Soc. Med.* 100, 558–563. doi: 10.1177/0141076807100012014

Cai, J., Liu, X., Vanneste, K., Proost, S., Tsai, W. C., Liu, K. W., et al. (2015). The genome sequence of the orchid *Phalaenopsis equestris*. *Nat. Genet.* 47, 65–72. doi: 10.1038/ng.3149

Callens, C., Tucker, M. R., Zhang, D., and Wilson, Z. A. (2018). Dissecting the role of MADS-box genes in monocot floral development and diversity. *J. Exp. Bot.* 69, 2435–2459. doi: 10.1093/jxb/ery086

Chai, M., Xu, C., Senthil, K., Kim, J., and Kim, D. (2002). Stable transformation of protocorm-like bodies in *Phalaenopsis* orchid mediated by *Agrobacterium tumefaciens*. *Sci. Hortic.* 96, 213–224. doi: 10.1016/S0304-4238(02)00084-5

Chang, Y., and Lee, N. (2000). Effect of temperature on growth of pseudobulb and inflorescences development of *Oncidium* 'Gower Ramsey'. *J. Chin. Soc. Hortic. Sci.* 46, 221–230.

Chang, Y.-Y., Chiu, Y.-F., Wu, J.-W., and Yang, C.-H. (2009). Four orchid (*Oncidium* Gower Ramsey) *AP1*/*AGL9*-like MADS box genes show novel expression patterns and cause different effects on floral transition and formation in *Arabidopsis thaliana*. *Plant Cell Physiol.* 50, 1425–1438. doi: 10.1093/pcp/pcp087

Chang, Y.-Y., Kao, N.-H., Li, J.-Y., Hsu, W.-H., Liang, Y.-L., Wu, J.-W., et al. (2010). Characterization of the possible roles for B class MADS box genes in regulation of perianth formation in orchid. *Plant Physiol.* 152, 837–853. doi: 10.1104/pp.109.147116

Chang, Y.-Y., Chu, Y.-W., Chen, C.-W., Leu, W.-M., Hsu, H.-F., and Yang, C.-H. (2011). Characterization of *Oncidium* 'Gower Ramsey'transcriptomes using 454 GS-FLX pyrosequencing and their application to the identification of genes associated with flowering time. *Plant Cell Physiol.* 52 (9), 1532–1545. doi: 10.1093/pcp/pcr101

Chao, Y.-T., Yen, S.-H., Yeh, J.-H., Chen, W.-C., and Shih, M.-C. (2017). Orchidstra 2.0—A transcriptomics resource for the orchid family. *Plant Cell Physiol.* 58 (1), e9–e9. doi: 10.1093/pcp/pcw220

Chase, M. W., Cameron, K. M., Freudenstein, J. V., Pridgeon, A. M., Salazar, G., Van Den Berg, C., et al. (2015). An updated classification of Orchidaceae. *Bot. J. Linn. Soc.* 177, 151–174. doi: 10.1111/boj.12234

Chen, D., Guo, B., Hexige, S., Zhang, T., Shen, D., and Ming, F. (2007). *SQUA*-like genes in the orchid *Phalaenopsis* are expressed in both vegetative and reproductive tissues. *Planta* 226, 369–380. doi: 10.1007/s00425-007-0488-0

Chen, M. K., Lin, I. C., and Yang, C. H. (2008). Functional analysis of three lily (Lilium longiflorum) APETALA1-like MADS box genes in regulating floral transition and formation. *Plant Cell Physiol.* 49, 704–717. doi: 10.1093/pcp/pcn046

Chen, Y. Y., Lee, P. F., Hsiao, Y. Y., Wu, W. L., Pan, Z. J., Lee, Y. I., et al. (2012). C- and D-class MADS-box genes from *Phalaenopsis equestris* (Orchidaceae) display functions in gynostemium and ovule development. *Plant Cell Physiol.* 53, 1053–1067. doi: 10.1093/pcp/pcs048

Chen, L. (2002). High efficiency of *Agrobacterium* mediated transformation by using rhizome of *Cymbidium* (Orchidaceae: Maxillarieae). *Lindleyana* 17, 16–20.

Chin, D.-C., Shen, C.-H., Senthilkumar, R., and Yeh, K.-W. (2014). Prolonged exposure to elevated temperature induces floral transition *via* up-regulation of cytosolic ascorbate peroxidase 1 and subsequent reduction of the ascorbate redox ratio in *Oncidium* hybrid orchid. *Plant Cell Physiol.* 55, 2164–2176. doi: 10.1093/pcp/pcu146

Coen, E. S., and Meyerowitz, E. M. (1991). The war of the whorls: genetic interactions controlling flower development. *Nature* 353, 31. doi: 10.1038/353031a0

Colombo, M., Masiero, S., Vanzulli, S., Lardelli, P., Kater, M. M., and Colombo, L. (2008). *AGL23*, a type I MADS-box gene that controls female gametophyte and embryo development in *Arabidopsis*. *Plant J.* 54, 1037–1048. doi: 10.1111/j.1365-313X.2008.03485.x

Corbesier, L., Vincent, C., Jang, S., Fornara, F., Fan, Q., Searle, I., et al. (2007). FT protein movement contributes to long-distance signaling in floral induction of *Arabidopsis*. *Science* 316, 1030–1033. doi: 10.1126/science.1141752

Cribb, P. J., Kell, S. P., Dixon, K. W., and Barrett, R. L. (2003). "Orchid conservation: a global perspective," in *Orchid conservation.* (Kota Kinabalu: Natural History Publications), 1–24.

Cseke, L. J., Zheng, J., and Podila, G. K. (2003). Characterization of *PTM5* in aspen trees: a MADS-box gene expressed during woody vascular development. *Gene* 318, 55–67. doi: 10.1016/S0378-1119(03)00765-0

Da Silva, J.a.T., Aceto, S., Liu, W., Yu, H., and Kanno, A. (2014). Genetic control of flower development, color and senescence of *Dendrobium* orchids. *Sci. Hortic.* 175, 74–86. doi: 10.1016/j.scienta.2014.05.008

Ding, L., Wang, Y., and Yu, H. (2013). Overexpression of *DOSOC1*, an ortholog of *Arabidopsis SOC1*, promotes flowering in the orchid *Dendrobium* Chao Parya Smile. *Plant Cell Physiol.* 54, 595–608. doi: 10.1093/pcp/pct026

Ditta, G., Pinyopich, A., Robles, P., Pelaz, S., and Yanofsky, M. F. (2004). The *SEP4* gene of *Arabidopsis thaliana* functions in floral organ and meristem identity. *Curr. Biol.* 14, 1935–1940. doi: 10.1016/j.cub.2004.10.028

Dorca-Fornell, C., Gregis, V., Grandi, V., Coupland, G., Colombo, L., and Kater, M. M. (2011). The *Arabidopsis SOC1*-like genes *AGL42*, *AGL71* and *AGL72* promote flowering in the shoot apical and axillary meristems. *Plant J.* 67, 1006–1017. doi: 10.1111/j.1365-313X.2011.04653.x

Fay, M. F., and Chase, M. W. (2009). Orchid biology: from Linnaeus *via* Darwin to the 21st century. *Ann. Bot.* 104, 359–364. doi: 10.1093/aob/mcp190

Ferrándiz, C., Gu, Q., Martienssen, R., and Yanofsky, M. F. (2000). Redundant regulation of meristem identity and plant architecture by *FRUITFULL*, *APETALA1* and *CAULIFLOWER*. *Development* 127, 725–734.

Fu, C.-H., Chen, Y.-W., Hsiao, Y.-Y., Pan, Z.-J., Liu, Z.-J., and Huang, Y.-M. (2011). OrchidBase: a collection of sequences of the transcriptome derived from orchids. *Plant Cell Physiol.* 52 (2), 238–243. doi: 10.1093/pcp/pcq201

Garay-Arroyo, A., Ortiz-Moreno, E., de la Paz Sánchez, M., Murphy, A.S., García-Ponce, B., Marsch-Martínez, N., et al. (2013). The MADS transcription factor XAL2/AGL14 modulates auxin transport during Arabidopsis root development by regulating PIN expression. *EMBO J.* 32 (21), 2884–2895.

Goh, C., Strauss, M., and Arditti, J. (1982). "Flower induction and physiology in orchids," in *Orchid biology: reviews and perspectives.* (USA).

Gramzow, L., Ritz, M. S., and Theißen, G. (2010). On the origin of MADS-domain transcription factors. *Trends Genet.* 26, 149–153. doi: 10.1016/j.tig.2010.01.004

Gu, X., Le, C., Wang, Y., Li, Z., Jiang, D., Wang, Y., et al. (2013). *Arabidopsis* FLC clade members form flowering-repressor complexes coordinating responses to endogenous and environmental cues. *Nat. Commun.* 4, 1947. doi: 10.1038/ncomms2947

Gutiérrez, R. M. P. (2010). Orchids: a review of uses in traditional medicine, its phytochemistry and pharmacology. *J. Med. Plants Res.* 4, 592–638. doi: 10.5897/JMPR10.012

Han, P., Garcia-Ponce, B., Fonseca-Salazar, G., Alvarez-Buylla, E. R., and Yu, H. (2008). *AGAMOUS-LIKE 17*, a novel flowering promoter, acts in a FT-independent photoperiod pathway. *Plant J.* 55, 253–265. doi: 10.1111/j.1365-313X.2008.03499.x

Hartmann, U., Hohmann, S., Nettesheim, K., Wisman, E., Saedler, H., and Huijser, P. (2000). Molecular cloning of *SVP*: a negative regulator of the floral transition in *Arabidopsis*. *Plant J.* 21, 351–360. doi: 10.1046/j.1365-313x.2000.00682.x

Hayes, T. E., Sengupta, P., and Cochran, B. H. (1988). The human c-fos serum response factor and the yeast factors GRM/PRTF have related DNA-binding specificities. *Genes Dev.* 2, 1713–1722. doi: 10.1101/gad.2.12b.1713

Helliwell, C. A., Wood, C. C., Robertson, M., James Peacock, W., and Dennis, E. S. (2006). The *Arabidopsis* FLC protein interacts directly *in vivo* with *SOC1* and *FT* chromatin and is part of a high-molecular-weight protein complex. *Plant J.* 46, 183–192. doi: 10.1111/j.1365-313X.2006.02686.x

Hew, C. S., and Yong, J. W. (2004). The physiology of tropical orchids in relation to the industry (Singapore: World Scientific Publishing Company). doi: 10.1142/5505

Hill, J. P., and Lord, E. M. (1989). Floral development in *Arabidopsis thaliana*: a comparison of the wild type and the homeotic *pistillata* mutant. *Can. J. Bot.* 67, 2922–2936. doi: 10.1139/b89-375

Hill, K., Wang, H., and Perry, S. E. (2008). A transcriptional repression motif in the MADS factor *AGL15* is involved in recruitment of histone deacetylase complex components. *Plant J.* 53, 172–185. doi: 10.1111/j.1365-313X.2007.03336.x

Honma, T., and Goto, K. (2001). Complexes of MADS-box proteins are sufficient to convert leaves into floral organs. *Nature* 409, 525. doi: 10.1038/35054083

Hossain, M. M., Kant, R., Van, P. T., Winarto, B., Zeng, S., and Teixeira Da Silva, J. A. (2013). The application of biotechnology to orchids. *Crit. Rev. Plant Sci.* 32, 69–139. doi: 10.1080/07352689.2012.715984

Hou, C.-J., and Yang, C.-H. (2009). Functional analysis of *FT* and *TFL1* orthologs from orchid (*Oncidium* Gower Ramsey) that regulate the vegetative to reproductive transition. *Plant Cell Physiol.* 50, 1544–1557. doi: 10.1093/pcp/pcp099

Hsieh, M.-H., Lu, H.-C., Pan, Z.-J., Yeh, H.-H., Wang, S.-S., and Chen, W.-H. (2013a). Optimizing virus-induced gene silencing efficiency with *Cymbidium* mosaic virus in *Phalaenopsis* flower. *Plant Sci.* 201, 25–41. doi: 10.1016/j.plantsci.2012.11.003

Hsieh, M.-H., Pan, Z.-J., Lai, P.-H., Lu, H.-C., Yeh, H.-H., and Hsu, C.-C. (2013b). Virus-induced gene silencing unravels multiple transcription factors involved in floral growth and development in *Phalaenopsis* orchids. *J. Exp. Bot.* 64 (12), 3869–3884. doi: 10.1093/jxb/ert218

Hsu, H.-F., and Yang, C.-H. (2002). An orchid (*Oncidium* Gower Ramsey) *AP3*-like MADS gene regulates floral formation and initiation. *Plant Cell Physiol.* 43, 1198–1209. doi: 10.1093/pcp/pcf143

Hsu, H. F., Huang, C. H., Chou, L. T., and Yang, C. H. (2003). Ectopic expression of an orchid (*Oncidium* Gower Ramsey) *AGL6*-like gene promotes flowering by activating flowering time genes in *Arabidopsis thaliana*. *Plant Cell Physiol.* 44, 783–794. doi: 10.1093/pcp/pcg099

Hsu, H.-F., Hsieh, W.-P., Chen, M.-K., Chang, Y.-Y., and Yang, C.-H. (2010). C/D class MADS box genes from two monocots, orchid (*Oncidium* Gower Ramsey) and lily (*Lilium longiflorum*), exhibit different effects on floral transition and formation in *Arabidopsis thaliana*. *Plant Cell Physiol.* 51, 1029–1045. doi: 10.1093/pcp/pcq052

Hsu, W. H., Yeh, T. J., Huang, K. Y., Li, J. Y., Chen, H. Y., and Yang, C. H. (2014). *AGAMOUS-LIKE13*, a putative ancestor for the E functional genes, specifies male and female gametophyte morphogenesis. *Plant J.* 77, 1–15. doi: 10.1111/tpj.12363

Hsu, H.-F., Hsu, W.-H., Lee, Y.-I., Mao, W.-T., Yang, J.-Y., Li, J.-Y., et al. (2015). Model for perianth formation in orchids. *Nat. Plants* 1, 15046. doi: 10.1038/nplants.2015.46

Hu, Y., Resende, M. F. R., Bombarely, A., Brym, M., Bassil, E., and Chambers, A. H. (2019). Genomics-based diversity analysis of *Vanilla* species using a *Vanilla planifolia* draft genome and genotyping-by-sequencing. *Sci. Rep.* 9, 3416. doi: 10.1038/s41598-019-40144-1

Huang, W., Fang, Z., Zeng, S., Zhang, J., Wu, K., Chen, Z., et al. (2012). Molecular cloning and functional analysis of three *FLOWERING LOCUS T* (*FT*) homologous genes from Chinese *Cymbidium*. *Int. J. Mol. Sci.* 13, 11385–11398. doi: 10.3390/ijms130911385

Irish, V. F., and Litt, A. (2005). Flower development and evolution: gene duplication, diversification and redeployment. *Curr. Opin. Genet. Dev.* 15, 454–460. doi: 10.1016/j.gde.2005.06.001

Irish, V. F., and Sussex, I. M. (1990). Function of the *apetala-1* gene during *Arabidopsis* floral development. *Plant Cell* 2, 741–753. doi: 10.1105/tpc.2.8.741

Irish, V. F. (2010). The flowering of *Arabidopsis* flower development. *Plant J.* 61, 1014–1028. doi: 10.1111/j.1365-313X.2009.04065.x

Jang, S., Choi, S.-C., Li, H.-Y., An, G., and Schmelzer, E. (2015). Functional characterization of *Phalaenopsis aphrodite* flowering genes *PaFT1* and *PaFD*. *PloS One* 10, e0134987. doi: 10.1371/journal.pone.0134987

Jang, S. (2015). Functional characterization of *PhapLEAFY*, a *FLORICAULA/LEAFY* ortholog in *Phalaenopsis aphrodite*. *Plant Cell Physiol.* 56, 2234–2247. doi: 10.1093/pcp/pcv130

Kang, I. H., Steffen, J. G., Portereiko, M. F., Lloyd, A., and Drews, G. N. (2008). The AGL62 MADS domain protein regulates cellularization during endosperm development in *Arabidopsis*. *Plant Cell* 20, 635–647. doi: 10.1105/tpc.107.055137

Kardailsky, I., Shukla, V. K., Ahn, J. H., Dagenais, N., Christensen, S. K., Nguyen, J. T., et al. (1999). Activation tagging of the floral inducer. *Science* 286, 1962–1965. doi: 10.1126/science.286.5446.1962

Kaufmann, K., Melzer, R., and Theißen, G. (2005). MIKC-type MADS-domain proteins: structural modularity, protein interactions and network evolution in land plants. *Gene* 347, 183–198. doi: 10.1016/j.gene.2004.12.014

Kim, S., Koh, J., Yoo, M. J., Kong, H., Hu, Y., Ma, H., et al. (2005). Expression of floral MADS-box genes in basal angiosperms: implications for the evolution of floral regulators. *Plant J.* 43, 724–744. doi: 10.1111/j.1365-313X.2005.02487.x

Kobayashi, Y., Kaya, H., Goto, K., Iwabuchi, M., and Araki, T. (1999). A pair of related genes with antagonistic roles in mediating flowering signals. *Science* 286, 1960–1962. doi: 10.1126/science.286.5446.1960

Kohler, C., Hennig, L., Spillane, C., Pien, S., Gruissem, W., and Grossniklaus, U. (2003). The Polycomb-group protein MEDEA regulates seed development by controlling expression of the MADS-box gene *PHERES1*. *Genes Dev.* 17, 1540–1553. doi: 10.1101/gad.257403

Kramer, E. M., Di Stilio, V. S., and Schluter, P. M. (2003). Complex patterns of gene duplication in the *APETALA3* and *PISTILLATA* lineages of the Ranunculaceae. *Int. J. Plant Sci.* 164, 11. doi: 10.1086/344694

Kui, L., Chen, H., Zhang, W., He, S., Xiong, Z., Zhang, Y., et al. (2017). Building a genetic manipulation tool box for orchid biology: identification of constitutive promoters and application of CRISPR/Cas9 in the orchid, *Dendrobium officinale*. *Front. Plant Sci.* 7, 2036. doi: 10.3389/fpls.2016.02036

Kutter, C., Schob, H., Stadler, M., Meins, F. Jr., and Si-Ammour, A. (2007). MicroRNA-mediated regulation of stomatal development in *Arabidopsis*. *Plant Cell* 19, 2417–2429. doi: 10.1105/tpc.107.050377

Lee, H., Suh, S.-S., Park, E., Cho, E., Ahn, J. H., Kim, S.-G., et al. (2000). The AGAMOUS-LIKE 20 MADS domain protein integrates floral inductive pathways in *Arabidopsis*. *Genes Dev.* 14, 2366–2376. doi: 10.1101/gad.813600

Lee, J. H., Ryu, H. S., Chung, K. S., Pose, D., Kim, S., Schmid, M., et al. (2013). Regulation of temperature-responsive flowering by MADS-box transcription factor repressors. *Science* 342, 628–632. doi: 10.1126/science.1241097

Li, D., Liu, C., Shen, L., Wu, Y., Chen, H., Robertson, M., et al. (2008). A repressor complex governs the integration of flowering signals in *Arabidopsis*. *Dev. Cell* 15, 110–120. doi: 10.1016/j.devcel.2008.05.002

Li, R., Wang, A., Sun, S., Liang, S., Wang, X., Ye, Q., et al. (2012). Functional characterization of *FT* and *MFT* ortholog genes in orchid (*Dendrobium nobile Lindl*) that regulate the vegetative to reproductive transition in *Arabidopsis*. *Plant Cell Tissue Organ Cult. (PCTOC)* 111, 143–151. doi: 10.1007/s11240-012-0178-x

Liang, S., Ye, Q.-S., Li, R.-H., Leng, J.-Y., Li, M.-R., Wang, X.-J., et al. (2012). Transcriptional regulations on the low-temperature-induced floral transition in an Orchidaceae species, *Dendrobium nobile*: an expressed sequence tags analysis. *Comp. Funct. Genom.* 2012. doi: 10.1155/2012/757801

Liljegren, S. J., Ditta, G. S., Eshed, Y., Savidge, B., Bowman, J. L., and Yanofsky, M. F. (2000). *SHATTERPROOF* MADS-box genes control seed dispersal in *Arabidopsis*. *Nature* 404, 766–770. doi: 10.1038/35008089

Liu, C., Xi, W., Shen, L., Tan, C., and Yu, H. (2009). Regulation of floral patterning by flowering time genes. *Dev. Cell* 16, 711–722. doi: 10.1016/j.devcel.2009.03.011

Liu, L., Liu, C., Hou, X., Xi, W., Shen, L., Tao, Z., et al. (2012). FTIP1 is an essential regulator required for florigen transport. *PloS Biol.* 10, e1001313. doi: 10.1371/journal.pbio.1001313

Liu, C., Teo, Z. W. N., Bi, Y., Song, S., Xi, W., Yang, X., et al. (2013). A conserved genetic pathway determines inflorescence architecture in *Arabidopsis* and rice. *Dev. Cell* 24, 612–622. doi: 10.1016/j.devcel.2013.02.013

Lopez, R., and Runkle, E. (2004). "The flowering of orchids," in *Brochure*, 8 p.

Lu, H.-C., Chen, H.-H., Tsai, W.-C., Chen, W.-H., Su, H.-J., and Chang, D. C.-N. (2007). Strategies for functional validation of genes involved in reproductive stages of orchids. *Plant Physiol.* 143 (2), 558–569. doi: 10.1104/pp.106.092742

Mandel, M. A., Gustafson-Brown, C., Savidge, B., and Yanofsky, M. F. (1992). Molecular characterization of the *Arabidopsis* floral homeotic gene *APETALA1*. *Nature* 360, 273. doi: 10.1038/360273a0

Mao, W. T., Hsu, H. F., Hsu, W. H., Li, J. Y., Lee, Y. I., and Yang, C. H. (2015). The C-terminal sequence and PI motif of the orchid (*Oncidium* Gower Ramsey) *PISTILLATA* (*PI*) ortholog determine its ability to bind AP3 orthologs and enter the nucleus to regulate downstream genes controlling petal and stamen formation. *Plant Cell Physiol.* 56, 2079–2099. doi: 10.1093/pcp/pcv129

Mateos, J. L., Madrigal, P., Tsuda, K., Rawat, V., Richter, R., Romera-Branchat, M., et al. (2015). Combinatorial activities of SHORT VEGETATIVE PHASE and FLOWERING LOCUS C define distinct modes of flowering regulation in *Arabidopsis*. *Genome Biol.* 16, 31. doi: 10.1186/s13059-015-0597-1

Melzer, S., Lens, F., Gennen, J., Vanneste, S., Rohde, A., and Beeckman, T. (2008). Flowering-time genes modulate meristem determinacy and growth form in *Arabidopsis thaliana*. *Nat. Genet.* 40, 1489–1492. doi: 10.1038/ng.253

Messenguy, F., and Dubois, E. (2003). Role of MADS box proteins and their cofactors in combinatorial control of gene expression and cell development. *Gene* 316, 1–21. doi: 10.1016/S0378-1119(03)00747-9

Meyerowitz, E. M., Smyth, D. R., and Bowman, J. L. (1989). Abnormal flowers and pattern formation in floral development. *Development* 106, 209–217.

Michaels, S. D., and Amasino, R. M. (1999). *FLOWERING LOCUS C* encodes a novel MADS domain protein that acts as a repressor of flowering. *Plant Cell* 11, 949–956. doi: 10.1105/tpc.11.5.949

Mondragón-Palomino, M., and Theißen, G. (2008). MADS about the evolution of orchid flowers. *Trends Plant Sci.* 13 (2), 51–59. doi: 10.1016/j.tplants.2007.11.007

Moon, J., Suh, S. S., Lee, H., Choi, K. R., Hong, C. B., Paek, N. C., et al. (2003). The *SOC1* MADS-box gene integrates vernalization and gibberellin signals for flowering in *Arabidopsis*. *Plant J.* 35, 613–623. doi: 10.1046/j.1365-313X.2003.01833.x

Moreno-Risueno, M. A., Van Norman, J. M., Moreno, A., Zhang, J., Ahnert, S. E., and Benfey, P. N. (2010). Oscillating gene expression determines competence for periodic *Arabidopsis* root branching. *Science* 329, 1306–1311. doi: 10.1126/science.1191937

Mouradov, A., Cremer, F., and Coupland, G. (2002). Control of flowering time: interacting pathways as a basis for diversity. *Plant Cell* 14, S111–S130. doi: 10.1105/tpc.001362

Nakamura, T., Song, I.-J., Fukuda, T., Yokoyama, J., Maki, M., Ochiai, T., et al. (2005). Characterization of *TrcMADS1* gene of *Trillium camtschatcense* (*Trilliaceae*) reveals functional evolution of the *SOC1/TM3*-like gene family. *J. Plant Res.* 118, 229–234. doi: 10.1007/s10265-005-0215-5

Nakamura, Y., Andrés, F., Kanehara, K., Liu, Y.-C., Dörmann, P., and Coupland, G. (2014). *Arabidopsis* florigen FT binds to diurnally oscillating phospholipids that accelerate flowering. *Nat. Commun.* 5, 3553. doi: 10.1038/ncomms4553

Nam, J., Depamphilis, C. W., Ma, H., and Nei, M. (2003). Antiquity and evolution of the MADS-box gene family controlling flower development in plants. *Mol. Biol. Evol.* 20, 1435–1447. doi: 10.1093/molbev/msg152

Newton, L. A., and Runkle, E. S. (2009). High-temperature inhibition of flowering of *Phalaenopsis* and *Doritaenopsis* orchids. *HortScience* 44, 1271–1276. doi: 10.21273/HORTSCI.44.5.1271

Ng, M., and Yanofsky, M. F. (2001). Function and evolution of the plant MADS-box gene family. *Nat. Rev. Genet.* 2, 186–195. doi: 10.1038/35056041

Nishimura, G., Kosugi, K., and Furukawa, J. (1976). Flower bud formation in *Phalaenopsis*. *Orchid Rev.* 84, 175–179.

Norman, C., Runswick, M., Pollock, R., and Treisman, R. (1988). Isolation and properties of cDNA clones encoding SRF, a transcription factor that binds to the *c-fos serum response* element. *Cell* 55, 989–1003. doi: 10.1016/0092-8674(88)90244-9

Pan, Z. J., Chen, Y. Y., Du, J. S., Chen, Y. Y., Chung, M. C., and Tsai, W. C. (2014). Flower development of *Phalaenopsis* orchid involves functionally divergent *SEPALLATA*-like genes. *New Phytol.* 202 (3), 1024–1042. doi: 10.1111/nph.12723

Pařenicová, L., De Folter, S., Kieffer, M., Horner, D. S., Favalli, C., Busscher, J., et al. (2003). Molecular and phylogenetic analyses of the complete MADS-box transcription factor family in *Arabidopsis*: new openings to the MADS world. *Plant Cell* 15, 1538–1551. doi: 10.1105/tpc.011544

Passmore, S., Maine, G. T., Elble, R., Christ, C., and Tye, B.-K. (1988). *Saccharomyces cerevisiae* protein involved in plasmid maintenance is necessary for mating of MATα cells. *J. Mol. Biol.* 204, 593–606. doi: 10.1016/0022-2836(88)90358-0

Pelaz, S., Ditta, G. S., Baumann, E., Wisman, E., and Yanofsky, M. F. (2000). B and C floral organ identity functions require *SEPALLATA* MADS-box genes. *Nature* 405, 200. doi: 10.1038/35012103

Pinyopich, A., Ditta, G. S., Savidge, B., Liljegren, S. J., Baumann, E., Wisman, E., et al. (2003). Assessing the redundancy of MADS-box genes during carpel and ovule development. *Nature* 424, 85–88. doi: 10.1038/nature01741

Portereiko, M. F., Lloyd, A., Steffen, J. G., Punwani, J. A., Otsuga, D., and Drews, G. N. (2006). *AGL80* is required for central cell and endosperm development in *Arabidopsis*. *Plant Cell* 18, 1862–1872. doi: 10.1105/tpc.106.040824

Pose, D., Verhage, L., Ott, F., Yant, L., Mathieu, J., Angenent, G. C., et al. (2013). Temperature-dependent regulation of flowering by antagonistic FLM variants. *Nature* 503, 414–417. doi: 10.1038/nature12633

Powell, C. L., Caldwell, K., Littler, R., and Warrington, I. (1988). Effect of temperature regime and nitrogen fertilizer level on vegetative and reproductive bud development in *Cymbidium* orchids. *J. Am. Soc. Hortic. Sci.* 133, 552–556.

Ratcliffe, O. J., Nadzan, G. C., Reuber, T. L., and Riechmann, J. L. (2001). Regulation of flowering in *Arabidopsis* by an *FLC* homologue. *Plant Physiol.* 126, 122–132. doi: 10.1104/pp.126.1.122

Ratcliffe, O. J., Kumimoto, R. W., Wong, B. J., and Riechmann, J. L. (2003). Analysis of the *Arabidopsis MADS AFFECTING FLOWERING* gene family: *MAF2* prevents vernalization by short periods of cold. *Plant Cell* 15, 1159–1169. doi: 10.1105/tpc.009506

Riechmann, J. L., and Meyerowitz, E. M. (1997). MADS domain proteins in plant development. *Biol. Chem.* 378, 1079–1101.

Riechmann, J. L., Wang, M., and Meyerowitz, E. M. (1996). DNA-binding properties of *Arabidopsis* MADS domain homeotic proteins APETALA1, APETALA3, PISTILLATA and AGAMOUS. *Nucleic Acids Res.* 24, 3134–3141. doi: 10.1093/nar/24.16.3134

Rijpkema, A. S., Zethof, J., Gerats, T., and Vandenbussche, M. (2009). The petunia *AGL6* gene has a *SEPALLATA*-like function in floral patterning. *Plant J.* 60, 1–9. doi: 10.1111/j.1365-313X.2009.03917.x

Rotor, G. B., and Withner, C. L. (1959). "The photoperiodic and temperature response of orchids," in *The orchids: a scientific survey.* Ed. C. L. Withner (NY, USA: Ronald Press) 397–416.

Rotor, G. B. (1952). Daylength and temperature in relation to growth and flowering of orchids. *Cornell Expt. Sta. Bul.* 885, 3–47.

Sakanishi, Y., Imanishi, H., and Ishida, G. (1980). Effect of temperature on growth and flowering of *Phalaenopsis amabilis*. *Bull. Univ. Osaka Prefecture. Ser. B Agric. Biol.* 32, 1–9.

Samach, A., Onouchi, H., Gold, S. E., Ditta, G. S., Schwarz-Sommer, Z., Yanofsky, M. F., et al. (2000). Distinct roles of CONSTANS target genes in reproductive development of *Arabidopsis*. *Science* 288, 1613–1616. doi: 10.1126/science.288.5471.1613

Sawettalake, N., Bunnag, S., Wang, Y., Shen, L., and Yu, H. (2017). *DOAP1* promotes flowering in the orchid *Dendrobium* Chao Praya Smile. *Front. Plant Sci.* 8, 400. doi: 10.3389/fpls.2017.00400

Schonrock, N., Bouveret, R., Leroy, O., Borghi, L., Kohler, C., Gruissem, W., et al. (2006). Polycomb-group proteins repress the floral activator *AGL19* in the *FLC*-independent vernalization pathway. *Genes Dev.* 20, 1667–1678. doi: 10.1101/gad.377206

Schuiteman, A. (2004). *Devogelia* (Orchidaceae), a new genus from the Moluccas and New Guinea. *Blumea - Biodivers. Evol. Biogeogr. Plants* 49, 361–366. doi: 10.3767/000651904X484324

Schwarz-Sommer, Z., Huijser, P., Nacken, W., Saedler, H., and Sommer, H. (1990). Genetic control of flower development by homeotic genes in *Antirrhinum majus*. *Science* 250, 931–936. doi: 10.1126/science.250.4983.931

Searle, I., He, Y., Turck, F., Vincent, C., Fornara, F., Kröber, S., et al. (2006). The transcription factor FLC confers a flowering response to vernalization by repressing meristem competence and systemic signaling in *Arabidopsis*. *Genes Dev.* 20, 898–912. doi: 10.1101/gad.373506

Shore, P., and Sharrocks, A. D. (1995). The MADS-box family of transcription factors. *Eur. J. Biochem.* 229, 1–13. doi: 10.1111/j.1432-1033.1995.tb20430.x

Shrestha, B. R., Chin, D. P., Tokuhara, K., and Mii, M. (2007). Efficient production of transgenic plantls of *Vanda* through sonication-assisted *Agrobacterium*-mediated transformation of protocorm-like bodies. *Plant Biotechnol.* 24, 429–434. doi: 10.5511/plantbiotechnology.24.429

Simpson, G. G., and Dean, C. (2002). *Arabidopsis*, the Rosetta stone of flowering time? *Science* 296, 285–289. doi: 10.1126/science.296.5566.285

Sinoda, K., Suto, K., Hara, M., and Aoki, M. (1988). Effect of day and night temperature on the flowering of *Dendrobium nobile*-type cultivars. *Bull. Natl. Res. Inst. Vegetables Ornam. Plants Tea. Ser. A.* 2, 279–290.

Sjahril, R., and Mii, M. (2006). High-efficiency *Agrobacterium*-mediated transformation of *Phalaenopsis* using meropenem, a novel antibiotic to eliminate *Agrobacterium*. *J. Hortic. Sci. Biotechnol.* 81, 458–464. doi: 10.1080/14620316.2006.11512088

Skipper, M., Pedersen, K. B., Johansen, L. B., Frederiksen, S., Irish, V. F., and Johansen, B. B. (2005). Identification and quantification of expression levels of three *FRUITFULL*-like MADS-box genes from the orchid *Dendrobium thyrsiflorum* (Reichb. f.). *Plant Sci.* 169, 579–586. doi: 10.1016/j.plantsci.2005.04.011

Skipper, M., Johansen, L. B., Pedersen, K. B., Frederiksen, S., and Johansen, B. B. (2006). Cloning and transcription analysis of an *AGAMOUS*-and *SEEDSTICK* ortholog in the orchid *Dendrobium thyrsiflorum* (Reichb. f.). *Gene* 366, 266–274. doi: 10.1016/j.gene.2005.08.014

Song, I.-J., Nakamura, T., Fukuda, T., Yokoyama, J., Ito, T., Ichikawa, H., et al. (2006). Spatiotemporal expression of duplicate *AGAMOUS* orthologues during floral development in *Phalaenopsis*. *Dev. Genes Evol.* 216, 301–313. doi: 10.1007/s00427-005-0057-0

Su, C.-l., Chao, Y.-T., Yen, S.-H., Chen, C.-Y., Chen, W.-C., and Chang, Y.-C. A. (2013a). Orchidstra: an integrated orchid functional genomics database. *Plant Cell Physiol.* 54 (2), e11–e11. doi: 10.1093/pcp/pct004

Su, C.-l., Chen, W.-C., Lee, A.-Y., Chen, C.-Y., Chang, Y.-C. A., and Chao, Y.-T. (2013b). A modified ABCDE model of flowering in orchids based on gene expression profiling studies of the moth orchid Phalaenopsis aphrodite. *PloS One* 8 (11), e80462. doi: 10.1371/journal.pone.0080462

Tapia-Lopez, R., Garcia-Ponce, B., Dubrovsky, J. G., Garay-Arroyo, A., Perez-Ruiz, R. V., Kim, S. H., et al. (2008). An *AGAMOUS*-related MADS-box gene, *XAL1* (*AGL12*), regulates root meristem cell proliferation and flowering transition in *Arabidopsis*. *Plant Physiol.* 146, 1182–1192. doi: 10.1104/pp.107.108647

Teo, Z. W. N., Song, S., Wang, Y.-Q., Liu, J., and Yu, H. (2014). New insights into the regulation of inflorescence architecture. *Trends Plant Sci.* 19, 158–165. doi: 10.1016/j.tplants.2013.11.001

Theißen, G., Kim, J. T., and Saedler, H. (1996). Classification and phylogeny of the MADS-box multigene family suggest defined roles of MADS-box gene

subfamilies in the morphological evolution of eukaryotes. *J. Mol. Evol.* 43, 484–516. doi: 10.1007/BF02337521

Theißen, G., Melzer, R., and Rümpler, F. (2016). MADS-domain transcription factors and the floral quartet model of flower development: linking plant development and evolution. *Development* 143, 3259–3271. doi: 10.1242/dev.134080

Theißen, G. (2001). Development of floral organ identity: stories from the MADS house. *Curr. Opin. Plant Biol.* 4, 75–85. doi: 10.1016/S1369-5266(00)00139-4

Theissen, G., and Saedler, H. (2001). Plant biology: floral quartets. *Nature* 409, 469. doi: 10.1038/35054172

Tian, Y., Yuan, X., Jiang, S., Cui, B., and Su, J. (2013). Molecular cloning and spatiotemporal expression of an *APETALA1*/*FRUITFULL*-like MADS-box gene from the orchid *(Cymbidium faberi*). *Sheng Wu Gong Cheng Xue Bao* 29, 203–213.

Tong, C. G., Wu, F. H., Yuan, Y. H., Chen, Y. R., and Lin, C. S. (2019). High-efficiency CRISPR/Cas-based editing of Phalaenopsis orchid MADS genes. *Plant Biotechnol. J.* doi: 10.1111/pbi.13264

Tran Thanh Van, M. (1974). Methods of acceleration of growth and flowering in a few species of orchids. *Amer. Orchid Soc. Bul.* 43, 699–707.

Tsai, W.-C., Kuoh, C.-S., Chuang, M.-H., Chen, W.-H., and Chen, H.-H. (2004). Four *DEF*-like MADS box genes displayed distinct floral morphogenetic roles in *Phalaenopsis* orchid. *Plant Cell Physiol.* 45, 831–844. doi: 10.1093/pcp/pch095

Tsai, W.-C., Lee, P.-F., Chen, H.-I., Hsiao, Y.-Y., Wei, W.-J., Pan, Z.-J., et al. (2005). *PeMADS6*, a *GLOBOSA*/*PISTILLATA*-like gene in *Phalaenopsis equestris* involved in petaloid formation, and correlated with flower longevity and ovary development. *Plant Cell Physiol.* 46, 1125–1139. doi: 10.1093/pcp/pci125

Tsai, W.-C., Fu, C.-H., Hsiao, Y.-Y., Huang, Y.-M., Chen, L.-J., and Wang, M. (2013). OrchidBase 2.0: comprehensive collection of Orchidaceae floral transcriptomes. *Plant Cell Physiol.* 54 (2), e7–e7. doi: 10.1093/pcp/pcs187

Tsai, W.-C., Pan, Z. J., Hsiao, Y. Y., Chen, L.-J., and Liu, Z. J. (2014). Evolution and function of MADS-box genes involved in orchid floral development. *J. Syst. Evol.* 52, 397–410. doi: 10.1111/jse.12010

Tsai, W.-C., Dievart, A., Hsu, C.-C., Hsiao, Y.-Y., Chiou, S.-Y., and Huang, H. (2017). Post genomics era for orchid research. *Bot. Stud.* 58 (1), 61. doi: 10.1186/s40529-017-0213-7

Tzeng, T. Y., Chen, H. Y., and Yang, C. H. (2002). Ectopic expression of carpel-specific MADS box genes from lily and lisianthus causes similar homeotic conversion of sepal and petal in *Arabidopsis*. *Plant Physiol.* 130, 1827–1836. doi: 10.1104/pp.007948

Valoroso, M. C., Censullo, M. C., and Aceto, S. (2019). The MADS-box genes expressed in the inflorescence of *Orchis italica* (Orchidaceae). *PloS One* 14, e0213185. doi: 10.1371/journal.pone.0213185

Van Tunen, A. J., Eikelboom, W., and Angenent, G. C. (1993). Floral organogenesis in tulipa. *Flow. Newsl.* 16, 6.

Wang, J.-W., Czech, B., and Weigel, D. (2009). miR156-regulated SPL transcription factors define an endogenous flowering pathway in *Arabidopsis thaliana*. *Cell* 138, 738–749. doi: 10.1016/j.cell.2009.06.014

Wang, S.-Y., Lee, P.-F., Lee, Y.-I., Hsiao, Y.-Y., Chen, Y.-Y., Pan, Z.-J., et al. (2011). Duplicated C-class MADS-box genes reveal distinct roles in gynostemium development in *Cymbidium ensifolium* (Orchidaceae). *Plant Cell Physiol.* 52, 563–577. doi: 10.1093/pcp/pcr015

Wang, Y., Liu, L., Song, S., Li, Y., Shen, L., and Yu, H. (2017). DOFT and DOFTIP1 affect reproductive development in the orchid *Dendrobium* Chao Praya Smile. *J. Exp. Bot.* 68, 5759–5772. doi: 10.1093/jxb/erx400

Weigel, D., and Meyerowitz, E. M. (1994). The ABCs of floral homeotic genes. *Cell* 78, 203–209. doi: 10.1016/0092-8674(94)90291-7

Wijnstekers, W. (2001). *Evolution of Cites: a Reference to the Convention on International Trade in Endangered Species of Wild Fauna and Flora*. (London, United Kingdom: Stationery Office Books)

Xiang, L., Li, X., Qin, D., Guo, F., Wu, C., Miao, L., et al. (2012). Functional analysis of *FLOWERING LOCUS T* orthologs from spring orchid (*Cymbidium goeringii* Rchb. f.) that regulates the vegetative to reproductive transition. *Plant Physiol. Biochem.* 58, 98–105. doi: 10.1016/j.plaphy.2012.06.011

Xu, Y., Teo, L. L., Zhou, J., Kumar, P. P., and Yu, H. (2006). Floral organ identity genes in the orchid *Dendrobium crumenatum*. *Plant J.* 46, 54–68. doi: 10.1111/j.1365-313X.2006.02669.x

Yan, L., Wang, X., Liu, H., Tian, Y., Lian, J., Yang, R., et al. (2015). The genome of *Dendrobium officinale* illuminates the biology of the important traditional chinese orchid herb. *Mol. Plant* 8, 922–934. doi: 10.1016/j.molp.2014.12.011

Yang, F., and Zhu, G. (2015). Digital gene expression analysis based on *de novo* transcriptome assembly reveals new genes associated with floral organ differentiation of the orchid plant *Cymbidium ensifolium*. *PloS One* 10 (11), e0142434. doi: 10.1371/journal.pone.0142434

Yang, F., Zhu, G., Wei, Y., Gao, J., Liang, G., Peng, L., et al. (2019). Low-temperature-induced changes in the transcriptome reveal a major role of *CgSVP* genes in regulating flowering of *Cymbidium goeringii*. *BMC Genomics* 20, 53. doi: 10.1186/s12864-019-5425-7

Yanofsky, M. F., Ma, H., Bowman, J. L., Drews, G. N., Feldmann, K. A., and Meyerowitz, E. M. (1990). The protein encoded by the *Arabidopsis* homeotic gene *agamous* resembles transcription factors. *Nature* 346, 35. doi: 10.1038/346035a0

Yoo, S. K., Lee, J. S., and Ahn, J. H. (2006). Overexpression of *AGAMOUS-LIKE 28* (*AGL28*) promotes flowering by upregulating expression of floral promoters within the autonomous pathway. *Biochem. Biophys. Res. Commun.* 348, 929–936. doi: 10.1016/j.bbrc.2006.07.121

Yoo, S. K., Wu, X., Lee, J. S., and Ahn, J. H. (2011). AGAMOUS-LIKE 6 is a floral promoter that negatively regulates the *FLC*/*MAF* clade genes and positively regulates *FT* in *Arabidopsis*. *Plant J.* 65, 62–76. doi: 10.1111/j.1365-313X.2010.04402.x

Yu, H., and Goh, C. J. (2000). Identification and characterization of three orchid MADS-box genes of the *AP1*/*AGL9* subfamily during floral transition. *Plant Physiol.* 123, 1325–1336. doi: 10.1104/pp.123.4.1325

Yu, H., and Goh, C. J. (2001). Molecular genetics of reproductive biology in orchids. *Plant Physiol.* 127, 1390–1393. doi: 10.1104/pp.010676

Yu, H., Xu, Y., Tan, E. L., and Kumar, P. P. (2002). AGAMOUS-LIKE 24, a dosage-dependent mediator of the flowering signals. *Proc. Natl. Acad. Sci. U. S. A.* 99, 16336–16341. doi: 10.1073/pnas.212624599

Yu, L. H., Miao, Z. Q., Qi, G. F., Wu, J., Cai, X. T., Mao, J. L., et al. (2014). MADS-box transcription factor *AGL21* regulates lateral root development and responds to multiple external and physiological signals. *Mol. Plant* 7, 1653–1669. doi: 10.1093/mp/ssu088

Zhang, H., and Forde, B. G. (1998). An Arabidopsis MADS box gene that controls nutrient-induced changes in root architecture. *Science* 279 (5349), 407–409. doi: 10.1126/science.279.5349.407

Zhang, L., Chin, D. P., and Mii, M. (2010). *Agrobacterium*-mediated transformation of protocorm-like bodies in *Cattleya*. *Plant Cell Tissue Organ Cult. (PCTOC)* 103, 41–47. doi: 10.1007/s11240-010-9751-3

Zhang, G.-Q., Xu, Q., Bian, C., Tsai, W.-C., Yeh, C.-M., Liu, K.-W., et al. (2016). The *Dendrobium catenatum Lindl.* genome sequence provides insights into polysaccharide synthase, floral development and adaptive evolution. *Sci. Rep.* 6, 19029. doi: 10.1038/srep19029

Zhang, G.-Q., Liu, K.-W., Li, Z., Lohaus, R., Hsiao, Y.-Y., Niu, S.-C., et al. (2017). The *Apostasia* genome and the evolution of orchids. *Nature* 549, 379. doi: 10.1038/nature23897

Zhu, Y., Liu, L., Shen, L., and Yu, H. (2016). NaKR1 regulates long-distance movement of FLOWERING LOCUS T in *Arabidopsis*. *Nat. Plants* 2, 16075. doi: 10.1038/nplants.2016.75

Conflict of Interest: The authors declare that the research was conducted in the absence of any commercial or financial relationships that could be construed as a potential conflict of interest.

frontiers in Plant Science

ORIGINAL RESEARCH
published: 29 November 2019
doi: 10.3389/fpls.2019.01594

Phalaenopsis LEAFY COTYLEDON1-Induced Somatic Embryonic Structures Are Morphologically Distinct From Protocorm-Like Bodies

Jhun-Chen Chen[1,2], *Chii-Gong Tong*[1,2], *Hsiang-Yin Lin*[1,2] *and Su-Chiung Fang*[1,2]*

[1] Biotechnology Center in Southern Taiwan, Academia Sinica, Tainan, Taiwan, [2] Agricultural Biotechnology Research Center, Academia Sinica, Taipei, Taiwan

Somatic embryogenesis is commonly used for clonal propagation of a wide variety of plant species. Induction of protocorm-like-bodies (PLBs), which are capable of developing into individual plants, is a routine tissue culture-based practice for micropropagation of orchid plants. Even though PLBs are often regarded as somatic embryos, our recent study provides molecular evidence to argue that PLBs are not derived from somatic embryogenesis. Here, we report and characterize the somatic embryonic tissues induced by *Phalaenopsis aphrodite LEAFY COTYLEDON1* (*PaLEC1*) in *Phalaenopsis equestris*. We found that PaLEC1-induced somatic tissues are morphologically different from PLBs, supporting our molecular study that PLBs are not of somatic embryonic origin. The embryonic identity of PaLEC1-induced embryonic tissues was confirmed by expression of the embryonic-specific transcription factors *FUSCA3* (*FUS3*) and *ABSCISIC ACID INSENSITIVE3* (*ABI3*), and seed storage proteins *7S GLOBULIN* and *OLEOSIN*. Moreover, PaLEC1-GFP protein was found to be associated with the *Pa7S-1* and *PaFUS3* promoters containing the CCAAT element, supporting that PaLEC1 directly regulates embryo-specific processes to activate the somatic embryonic program in *P. equestris*. Despite diverse embryonic structures, PaLEC1-GFP-induced embryonic structures are pluripotent and capable of generating new shoots. Our study resolves the long-term debate on the developmental identity of PLB and suggests that somatic embryogenesis may be a useful approach to clonally propagate orchid seedlings.

Keywords: somatic embryogenesis, *Phalaenopsis* orchids, *LEAFY-COTYLEDON1*, protocorm-like-body, *Phalaenopsis equestris*

OPEN ACCESS

Edited by:
Jen-Tsung Chen,
National University of Kaohsiung, Taiwan

Reviewed by:
Sonia Gazzarrini,
University of Toronto, Canada
Guangdong Wang,
Nanjing Agricultural University, China

***Correspondence:**
Su-Chiung Fang
scfang@gate.sinica.edu.tw

Specialty section:
This article was submitted to Plant Development and EvoDevo, a section of the journal Frontiers in Plant Science

Received: *01 July 2019*
Accepted: *13 November 2019*
Published: *29 November 2019*

Citation:
Chen J-C, Tong C-G, Lin H-Y and Fang S-C (2019) Phalaenopsis LEAFY COTYLEDON1-Induced Somatic Embryonic Structures Are Morphologically Distinct From Protocorm-Like Bodies. Front. Plant Sci. 10:1594. doi: 10.3389/fpls.2019.01594

INTRODUCTION

Plant totipotency provides a means of clonally propagating a wide variety of plant species (Ikeuchi et al., 2013; Kareem et al., 2016; Radhakrishnan et al., 2017). *In vitro* regeneration bypasses the embryogenic program and directly generates seedlings with identical genetic makeup. One of the most common *in vitro* regeneration methods is somatic embryogenesis (Zimmerman, 1993; Pulianmackal et al., 2014). Somatic embryogenesis is crucial for establishing genetic transformation platforms for

many non-model plant species and for clonal propagation of numerous high-value plants. For example, somatic embryos are used as transformation materials for alfalfa, American chestnut, cassava, cotton, grapevine, maize, mango, melon, Norway spruce, papaya, rose, tea tree, and walnut (Umbeck et al., 1987; Mcgranahan et al., 1988; Robertson et al., 1992; Fitch et al., 1993; Li et al., 1996; Brettschneider et al., 1997; Trinh et al., 1998; Mondal et al., 2001; Akasaka-Kennedy et al., 2004; Chavarri et al., 2004; Li et al., 2006; Polin et al., 2006; Vergne et al., 2010). In addition, the regeneration capacity of somatic embryos has made somatic embryogenesis a common method through which to clonally propagate economically important trees or herbal plants (Joshee et al., 2007; Nordine et al., 2014; Guan et al., 2016; Kim et al., 2019).

Embryogenesis is a defined developmental program during which the zygote grows and develops into a mature embryo. Somatic embryogenesis, on the other hand, activates the embryogenesis program in the absence of gamete fusion (von Arnold et al., 2002; Braybrook and Harada, 2008; Yang and Zhang, 2010; Feher, 2015). Zygotic embryogenesis and somatic embryogenesis programs not only share similar morphogenesis and maturation phases, they also share similar if not completely identical genetic and molecular networks (Zimmerman, 1993; Mordhorst et al., 2002; Gaj et al., 2005). Moreover, ectopic expression of several key embryo-associated transcription factors (TFs) is capable of inducing the embryogenesis program in somatic tissues (Lotan et al., 1998; Hecht et al., 2001; Stone et al., 2001; Boutilier et al., 2002; Zuo et al., 2002; Harding et al., 2003; Kwong et al., 2003; Gaj et al., 2005; Wang et al., 2009), demonstrating the developmental plasticity of plant tissues.

Orchids evolve specialized developmental programs including the co-evolution of diverse floral structures and pollinators (Waterman and Bidartondo, 2008), formation of pollen dispersal units (pollinia) (Pacini and Hesse, 2002), lack of cotyledon organogenesis during embryogenesis (Kull and Arditti, 2002; Yeung, 2017), and mycorrhizal fungi-assisted seed germination (Rasmussen, 2002), and all of these developmental processes contribute to their distinct morphology and physiological characteristics. These unique developmental strategies have not only fascinated many evolutionary and plant biologists; the beauty of the resulting floral structures is also enthusiastically admired by the general public. Much effort has been put into tissue culture-based clonal propagation of elite orchids over the past decades and this technology has transformed the orchid business into a multimillion-dollar orchid biotechnology industry (Winkelmann et al., 2006; Liao et al., 2011; Hossain et al., 2013).

Generally, embryogenesis of angiosperm plants starts from morphogenesis with continuous changes in embryo morphology and establishment of shoot-root polarity followed by maturation and desiccation processes (Bentsink and Koornneef, 2008; Braybrook and Harada, 2008). One of the characteristic features that defines the somatic embryo is the formation of the embryonic cotyledons. Even though orchid embryos go through a maturation and desiccation process, they lack characteristic cotyledons (organogenesis) and fail to establish a shoot-root axis during embryogenesis (Arditti, 1992; Dressler, 1993; Burger, 1998). Instead, a tubular embryo structure with an anterior meristem is formed. Upon germination, a tubular embryo emerges as a protocorm and new leaves and roots are generated from the anterior meristem of the protocorm (Nishimura, 1981).

Protocorm-like body (PLB)-based regeneration is commonly used to produce huge amounts of orchid seedlings of elite cultivars (Arditti and Krikorian, 1996; Chen et al., 2002; Arditti, 2009; Chugh et al., 2009; Yam and Arditti, 2009; Paek et al., 2011; Yam and Arditti, 2017). For years, much effort has been devoted to develop *in vitro* protocols to induce PLB and somatic embryo development either directly or indirectly (*via* the callus tissue) from explants to improve micropropagation in *Phalaenopsis* orchids (Tokuhara and Mii, 2001; Tokuhara and Mii, 2003; Kuo et al., 2005; Chen and Chang, 2006; Gow et al., 2009; Gow et al., 2010; Pramanik et al., 2016). PLBs are often induced from somatic tissues such as protocorms, floral stalk internodes, leaves, and root tips (Chen et al., 2002; Park et al., 2002; Chen and Chang, 2004; Chen and Chang, 2006; Teixeira da Silva et al., 2006; Zhao et al., 2008; Guo et al., 2010; Paek et al., 2011). Because embryogenesis produces tubular embryos, which, upon germination, develop into protocorms, and PLBs resemble protocorms morphologically, initiation, and development of PLBs is often regarded as somatic embryogenesis (Jones and Tisserat, 1990; Begum et al., 1994; Ishii et al., 1998). However, our recent study provides molecular evidence to argue that PLBs are not somatic embryos. Instead, PLB development seems to adopt a shoot pole-related organogenesis program (Fang et al., 2016). So if PLBs are not somatic embryos, what does the somatic embryo of orchids look like? Are somatic embryos of orchid species also prolific in propagating clonal plants? To address these questions and to explore the potential of using orchid somatic embryos for clonal propagation, we generated transgenic plants overexpressing *Phalaenopsis aphrodite LEAFY COTYLEDON1* (*PaLEC1*) gene in *Phalaenopsis equestris*. *LEC1* encodes a HAP3 subunit of CCAAT-binding TF required for embryo development (Lotan et al., 1998). Moreover, ectopic expression of *LEC1* isolated from *Arabidopsis* and other plant species has been demonstrated to be a potent inducer of the somatic embryogenesis program (Lotan et al., 1998; Yazawa et al., 2004; Garcês et al., 2014; Zhu et al., 2014; Min et al., 2015; Fang et al., 2016). Consistently, we have shown that *PaLEC1* is capable of inducing somatic embryogenesis in *Arabidopsis* (Fang et al., 2016). Here, we report *PaLEC1*-induced embryonic tissues in *P. equestris* and demonstrate their embryonic identity by validation of expression of the embryonic-specific genes. To the best of our knowledge, this is the first time that somatic embryonic tissues was shown to be induced by the embryonic factor, *PaLEC1*, in the transgenic orchid plants. Our studies reveal that *PaLEC1* may be a useful tool for large scale propagation of clonal plants in orchid biotechnology.

MATERIALS AND METHODS

Plant Materials and Growth Conditions

P. equestris plants were grown and maintained in a growth chamber with alternating 12 h light (23°C)/12 h dark (18°C)

cycles. Hand pollination was conducted for each flower, as described previously (Chen and Fang, 2016).

Seeds were allowed to germinate in germination medium (0.1% tryptone, 1.8% sucrose, 2% potato, 0.75% agar, 1.08 g/l MS salt, 1X MS vitamin pH 5.7). For regeneration assay, the protocorm segments (explants) were transferred to T2 medium containing 0.1% (w/v) tryptone, 2% (w/v) sucrose, 2% (w/v) potato homogenate, 2.5% (w/v) banana homogenate, 0.01% (v/v) citric acid, 0.1% (w/v) charcoal, and 1% (w/v) agar adjusted to pH 5.5 (Chen et al., 2009) to induce PLBs.

Generation of Transgenic *Phalaenopsis equestris* Plants

Protocorms or PLBs of *P. equestris* were used for transformation. *Agrobacterium*-based transformation was conducted as described previously with slight modification (Liau et al., 2003). Briefly, protocorms or PLBs were co-cultured with *Agrobacterium tumefaciens* strain EHA105 culture (OD_{600} = ~ 0.8) containing the *35S:PaLEC1-GFP* or pH7FWG2 (vector only control) construct in the presence of 100 μM acetosyringone overnight (for protocorms) or 3 days (for PLBs) in the dark. After removing *Agrobacterium* inoculum, the infected tissues were washed four to six times with distilled water containing 40 mg/L meropenem (China Chemical & Pharmaceutical). The infected tissues were allowed to recover in New Dogashima medium (NDM) (Belarmino and Mii, 2000) containing 10 g/L maltose, 0.1 mg/L naphthaleneacetic acid (NAA), and 0.4 mg/L benzyladenine (BA) and supplemented with 40 mg/L meropenem for 1 week in the dark. All the NDM media used in this study contained 10 g/L maltose, 0.1 mg/L NAA, and 0.4 mg/L BA. The recovered tissues were then selected on NDM agar plates supplemented with 20 mg/L hygromycin and 40 mg/L meropenem at 23°C in the dark. The infected tissues were selected continuously by sub-culturing to fresh NDM plates supplemented with 20 mg/L hygromycin and 40 mg/L meropenem at 2- to 4-week intervals until new leaves emerged. The hygromycin-resistant transgenic plants were then transferred to T2 (Chen et al., 2009) medium supplemented with 20 mg/L hygromycin and 40 mg/L meropenem to encourage growth.

Deoxyribonucleic Acid Isolation and Southern Blotting

Genomic DNA from young seedlings (1 to 1.5 cm in size) of T1 transgenic plants and wild-type plants was isolated by cetyltrimethylammonium bromide (CTAB)-based method (Murray and Thompson, 1980; Saghai-Maroof et al., 1984) with some modifications. Briefly, freeze-dried tissue was ground in the presence of liquid nitrogen, resuspended in 1 g/10 ml of the CTAB extraction buffer [100 mM Tris, pH 8.0, 1.4 M NaCl, 20 mM EDTA, 2% CTAB, 0.2% (w/v) polyvinylpyrrolidone 40, and 0.2% β-mercaptoethanol], and incubated at 65°C for 60 min with occasional gentle vortexing. Equal volume of chloroform: isoamylalcohol (24:1) was then added and mixed by inversion for 15 min. Plant extract was then centrifuged at 3220 × g for 15 min at 4°C. The aqueous phase was extracted with equal volume of chloroform:isoamylalcohol (24:1) one more time. The aqueous phase was transferred to a new tube and equal volume of isopropanol was added, mixed, and incubated at -20°C overnight. DNA was precipitated by centrifugation at 3,220 × g at 4°C for 10 min. DNA was washed once with 75% ethanol followed by 99% ethanol. DNA was then resuspended in H_2O supplemented with 10 μg/ml RNase A and incubated at 37°C overnight to remove RNA. This method yielded approximately 150-350 μg per g of orchid tissue. Approximately 15 μg DNA was digested and Southern blotting and hybridization were carried out as described previously (Fang et al., 2006).

Antibody Generation and Western Blotting

To generate polyclonal antibodies specific for PaLEC1 protein, PaLEC1 peptide YLHRYRELEGDHRGSIRG (LTK BioLaboratories, Taiwan) was synthesized to generate rabbit polyclonal antisera. Polyclonal antibodies raised against PaLEC1 were affinity purified for western blotting analysis.

To prepare total protein extract, tissues were ground to a fine powder in the presence of liquid nitrogen using a pestle and mortar. One gram of ground tissues was homogenized in 1 ml 1X Urea-based protein extraction buffer (250 mM Tris-HCl, pH 6.8, 3.5% sodium dodecyl sulfate (SDS), 10% glycerol, 1 M urea) supplemented with 1X protease inhibitor cocktail (Sigma-Aldrich), 1 mM *phenylmethylsulfonyl fluoride* by vortexing. Cell debris was removed by centrifugation at 16,100 × g for 10 min at 4°C. Concentration of protein lysates was determined by Bio-Rad DC Protein Assay Kit (Bio-Rad).

Protein lysates were resolved by a standard 10% SDS-polyacrylamide gel electrophoresis (PAGE) and transferred to Immobilon-P PVDF membrane (Merck Millipore). Blots were blocked in 1 × TBST (20 mM Tris base, 150 mM NaCl, 0.1% Tween 20) supplemented with 5% non-fat milk at room temperature (RT) for 1 h and incubated with anti-GFP antibodies (Roche) diluted 1:2,000 in 1 × TBST supplemented with 5% non-fat milk at 4°C overnight. For detection of PaLEC1 and PaRbCL proteins, blots were incubated with PaLEC1 (1:2,000) and RbCL (1:5,000, Agrisera) antibodies diluted in 1 × TBST with 5% non-fat milk for 1 h at RT. Blots were washed three times for 15 min each time and then incubated with horseradish peroxidase (HRP) conjugated goat-anti-mouse-IgG (1:20,000, Jackson ImmunoResearch Laboratories), or goat-anti-rabbit-IgG (1:20,000, PerkinElmer) for 1 h at RT. After washing in 1 × TBST for 15 min three times, the blots were processed for chemiluminescence detection using Amersham ECL select Western Blotting detection reagent. The images were acquired by a ChemiDoc XRS+ imager (Bio-Rad).

Ribonucleic Acid Isolation and Quantitative Real-Time Polymerase Chain Reaction

Plant tissues (young seedlings or callus tissues) were homogenized by pestle and mortar in the presence of liquid nitrogen. RNA was isolated using RNA extraction reagent (3-Zol, MDBio) according to the manufacturer's instructions. Total RNA was treated with RNase-free DNase (Qiagen) to remove DNA followed by RNeasy column purification (Qiagen) according to the manufacturer's instructions.

Approximately 5 μg DNA-free RNA was reverse transcribed in the presence of a mixture of oligo dT and random primers (9:1 ratio) using the GoScript Reverse Transcription System (Promega) according to the manufacturer's instructions. Ten microliters of quantitative RT-PCR reaction was set up as follows: 2.5 μl of 1/20 diluted complementary DNA, 0.2 μM of primers, and 5 μl of 2X KAPA SYBR FAST master mix (KAPA Biosystems). The PCR program was used for DNA amplification: 95°C for 1 min, 40 cycles of 95°C for 5 s, and 58°C, 60°C, or 62°C for 20 s. PCR was performed in triplicate. Standard error was calculated from three technical replicates. Fold change in expression was calculated as $2^{-\triangle\triangle CT}$. A melting curve of each PCR was examined to ensure no spurious products were present. Primer pairs used for quantitative PCR are listed in **Supplementary Table S1**. A ubiquitin gene, *PaUBI* (Lin et al., 2014), was used as an internal control.

Light Microscopy

Tissues were fixed in paraformaldehyde fixative and sectioned to 10 μm in thickness using the hybrid-cut method as previously described (Chen et al., 2016). Tissues sections were then stained with hematoxylin solution and photographed on a Zeiss Axio Scope A1 microscope equipped with an Axio-Cam HRc camera (Zeiss, Germany).

Fresh tissues of transgenic plants were hand sectioned and fluorescence images were photographed on a LSM 710 Confocal Microscope (Zeiss).

Chromatin Immunoprecipitation-Polymerase Chain Reaction

Chromatin immunoprecipitation was conducted as described previously (Villar and Köhler, 2010) with slight modification. One gram of young seedling (1 to 1.5 cm in size, pooled from approximately 10 T1 seedlings) tissue was fixed in 37 ml of 1% formaldehyde and vacuum-infiltrated for 20 min. Two and half milliliters of 2 M glycine was added to stop crosslinking. Fixed tissues were then homogenized by pestle and mortar and chromatin was extracted and filtered by a 70 μM cell strainer (Biologix Group Limited) as described (Villar and Köhler, 2010). Chromatin was resuspended in 200 μl of nuclei lysis buffer (50 mM Tris-HCl, pH 8.0; 10 mM EDTA, 1% SDS, and 1X protease inhibitor cocktail) before sonication. Chromatin was then transferred to a micro TUBE-500 AFA Fiber Screw-Cap tube and sonicated for 12 min or 20 min under the condition: peak incident power 150 S; duty factor 2%, cycles per burst 200, in a Covaris S220 system (Covaris). The sheered chromatin was precleared by incubating with 40 μl protein A Magnetic Sepharose beads (Merck) at 4°C for 1.5 h. In the meantime, 5 μg PaLEC1 polyclonal antibody or histone H3 antibody (Agrisera) was incubated with protein A beads at 4°C for 1.5 h. After preclearing, protein A/antibody mix was added to each sheered chromatin sample and incubated at 4°C overnight. Magnetic beads were then washed as described (Villar and Köhler, 2010) and eluted by adding 150 μl of elution buffer (1% SDS and 0.1% $NaHCO_3$) and incubating at 65°C for 15 min. Elution was repeated one more time and elutes were pooled into a single tube. Twelve microliters of 5 M NaCl was added into 200 μl elutes and incubated at 65°C overnight. Proteins were removed by incubating with 6 μl of 2 mg/ml proteinase K, 6 μl of 0.5 M EDTA, and 12 μl of 1 M This-HCl (pH 6.5) at 45°C for 2 h. Immunoprecipated DNA was then purified by QIAquick PCR Purification Kit (Qiagen) following the manufacturer's instructions.

Twenty microliters of PCR reaction was set up as follows: 2 or 3 μl of chromatin immunoprecipitation (ChIP) DNA, 0.5 μM of primers, 2 μl of 10X PCR buffer, 3% dimethyl sulfoxide, and 1.25 unit Power Taq polymerase (Genomics, Taiwan). The PCR program was used for amplification of immunoprecipitated DNA: 95°C for 2 min, 42 cycles of 94°C for 5 s, 58–60°C for 20 s, and 72°C for 20 s. Primers used for ChIP-PCR are listed in **Supplementary Table S1**. ChIP-PCR was repeated three times using three independent biological samples.

RESULTS

Generation of Transgenic *Phalaenopsis equestris* Plants Overexpressing *PaLEC1-GFP*

To explore the possibility of inducing a somatic embryonic program in *Phalaenopsis* orchids and to investigate whether somatic embryonic potential can be utilized for micropropagation, transgenic *P. equestris* plants overexpressing the embryonic maker *PaLEC1* that has been shown to induce somatic embryogenesis in *Arabidopsis* (Fang et al., 2016) were generated. After transformation, we successfully obtained multiple independent transgenic lines carrying the *35S:PaLEC1-GFP* transgene with the hygromycin phosphotransferase (hpt) marker (**Supplementary Figure S1A**). Expression of PaLEC1-GFP was also confirmed in four out of seven independent transgenic lines by western blotting using the GFP antibody (**Supplementary Figure S1B**). However, multiple transformation attempts failed to generate transgenic plants carrying the empty pH7FWG2 vector. It is not clear why only *35S:PaLEC1-GFP* transgenic plants were obtained. Overexpression of the embryonic genes *BABYBOOM* has been reported to enhance embryogenic callus proliferation, overall transformation efficiency, and regeneration capacity in several monocot plants recalcitrant for transformation (Lowe et al., 2016). Hence, it is possible that ectopic PaLEC1 enhances transformation efficiency by increasing embryogenic callus formation and regeneration ability.

Altered Protocorm Development in Transgenic Plants Overexpressing *PaLEC1-GFP*

The *35S:PaLEC1-GFP* transgenic plants were allowed to grow in growth chamber for approximately 5 years before reaching maturity for flowering. *35S:PaLEC1-GFP* transgenic lines #1, #2, and #3 started to flower in March of 2018 and were therefore used in this study. The flowers were hand-pollinated and T1 seeds were allowed to produce in developing capsules.

Seeds were sown and allowed to germinate on medium containing hygromycin.

As expected, seeds harvested from wild-type control plants failed to grow and were arrested on hygromycin-containing plates 5 months after sowing (MAS, **Figure 1A**). T1 seeds from *35S:PaLEC1-GFP* transgenic lines #1 and #2, on the other hand, started to expand and turned green at 2 MAS (**Figure 1B**). The germinated protocorms continued to grow and produce new shoots on hygromycin-containing plates at 5 MAS (**Figure 1B**). Transgenic *35S:PaLEC1-GFP* line #3 failed to produce viable seeds and was therefore omitted from further study. Southern blotting was used to confirm independent integration of the transgene in *35S:PaLEC1-GFP* #1 and *35S:PaLEC1-GFP* #2 lines (**Supplementary Figure S1C**).

Protocorms from wild-type plants continued to develop and grow into young seedlings at approximately 80–90 days after sowing (DAS, **Figures 2A**, **B**). Instead of growing into individual seedlings, protocorms of the transgenic *35S:PaLEC1-GFP* #1 plants developed into various structures (**Figure 2A**) that did not completely resemble seedlings of wild-type seedlings at 80–90 DAS (**Table 1**). For example, approximately 25% germinated protocorms underwent uncontrolled cell division and formed unorganized callus-like structures (callus type, **Figure 2C**), which is similar to somatic embryonic calli commonly observed in other plant species (Zimmerman, 1993; Yang and Zhang, 2010; Ikeuchi et al., 2013). Around 48% of protocorms, on the other hand, developed into a fan-like structure with multiple meristems forming on the surface (multiple-meristem type, **Figure 2C**). Around 27% protocorms formed a dorsal-fin-like structure with newly emerging leaves growing from it (dorsal-fin type, **Figure 2C**). The callus-like structure was capable of acquiring meristematic fate and developed into shoots (**Supplementary Figure S2**). Even though only one shoot was developed from the dorsal-fin type structure, new shoots could occasionally emerge from the base of the dorsal-fin type structure.

Even though PaLEC1-GFP protein could not be detected in T0 *35S:PaLEC1-GFP* #2 transgenic plants, some of the germinated T1 seeds also developed into structures that were similar to those observed in *35S:PaLEC1-GFP* #1 line 80–90 DAS (**Supplementary Figure S3**). Approximately 35.2% of protocorms grew and became normal seedlings as seen for wild-type

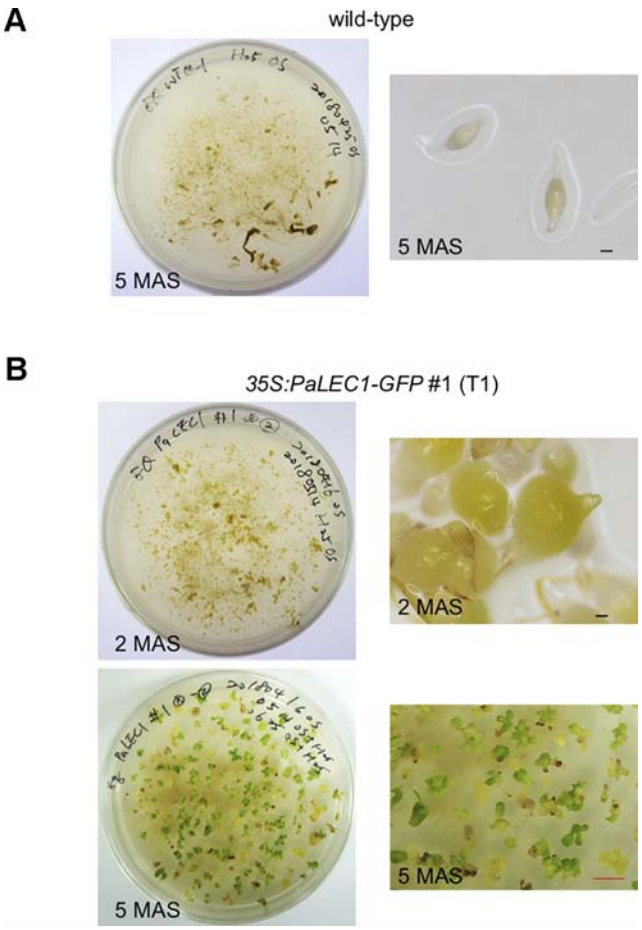

FIGURE 1 | Selection of T1 *35:PaLEC1-GFP #1* transgenic plants on hygromycin plates. **(A)** Wild-type protocorms failed to develop on hygromycin-containing medium. **(B)** *35:PaLEC1-GFP #1* protocorms continued to grow and developed into seedlings 5 months after sowing. MAS, month after sowing. Black scale bar = 100 μm. Red scale bar = 0.5 cm.

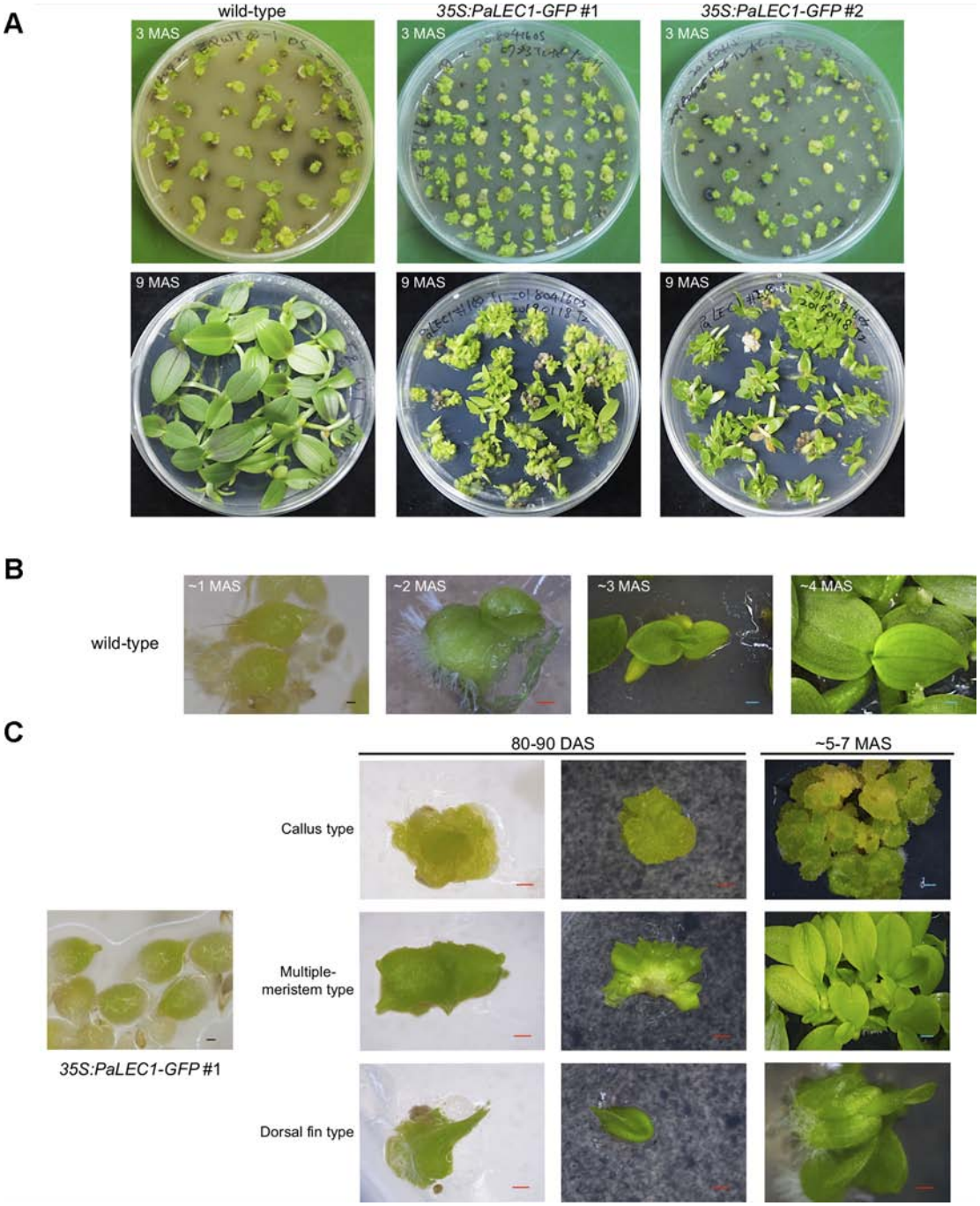

FIGURE 2 | Developmental processes of T1 *35:PaLEC1-GFP #1* transgenic plants. **(A)** Developing seedlings of wild-type plant, *35:PaLEC1-GFP #1*, and *35:PaLEC1-GFP #2* transgenic plants at 3 and 9 months after germination. **(B)** Germinated protocorms of wild-type plants developed into young seedlings at 1, 2, 3, and 4 months after germination. **(C)** Germinated protocorms of *35:PaLEC1-GFP #1* transgenic plants developed into callus-type, multiple-meristem type, and dorsal fin-like structures. MAS, month after sowing; DAS, day after sowing; Red scale bar = 500 μm. Blue scale bar = 1 mm.

protocorms (**Table 1**). Around 56.3% protocorms developed into multiple-meristem type structures and 8.5% protocorms developed into callus-like structures. No dorsal-fin type structure was observed in the T1 *35S:PaLEC1-GFP* #1 line. Quantitative RT-PCR and western blotting were conducted to validate and re-evaluate the expression of *PaLEC1-GFP* mRNA and its encoded protein in *35S:PaLEC1-GFP* #1 and *35S:PaLEC1-GFP* #2. As compared to *35S:PaLEC1-GFP* #1 seedlings, *35S:PaLEC1-GFP* #2 had much less *PaLEC1-GFP* mRNA than *35S:PaLEC1-GFP* #1 line (**Figure 3**). Because GFP monoclonal antibody may be less sensitive than polyclonal antibodies in detecting PaLEC1-GFP protein, PaLEC1 polyclonal antibodies

TABLE 1 | Different types of structures were formed from germinating protocorms of *35S:PaLEC1-GFP* transgenic lines. Number of the represented type (number) and percentage of the represented type (%) of structures are shown.

	wt		*35S:PaLEC1-GFP#1*		*35S:PaLEC1-GFP#2*	
	Number	**%**	**Number**	**%**	**Number**	**%**
Wt seedling	32	94.1%	0	0	25	35.2%
Callus-like	0	0	27	25.0%	6	8.5%
Multiple meristem-like	0	0	52	48.1%	40	56.3%
Dorsal fin-like	0	0	29	26.9%	0	0
PLB	2	5.9%	0	0	0	0
Total	34	100%	108	100%	71	100%

were generated. Similar to hygromycin-resistant T0 *35S:PaLEC1-GFP* #1 parent, PaLEC1-GFP protein was expressed in high abundance in callus-like, multiple-meristem, and dorsal-fin types of structures germinated from T1 seeds (**Figure 3**). Using the PaLEC1 polyclonal antibodies, PaLEC1-GFP protein was also detected in callus-like tissues but was barely detectable in multiple-meristem-like structures and wild-type-like seedlings of *35S:PaLEC1-GFP* #2 transgenic line (**Figure 3**), indicating PaLEC1-GFP protein was expressed but accumulated in very low abundance. We noticed that PaLEC1-induced callus tissues had a reduced amount of ribulose bisphosphate carboxylase large subunit (RbcL) protein (**Figure 3**), that is consistent with the pale-yellow appearance of PaLEC1-induced callus tissues.

To gain further structural details of the PaLEC1-induced structures, histological section and histochemical staining were conducted. As described previously (Yeung, 2017), shoot apical meristem was initiated from the apical end of a protocorm in the wild-type plants (**Figure 4**). In the *35S:PaLEC1-GFP* transgenic plants, active cell division appeared to take place on the outer cell layer (epidermal cells) of developing protocorms (early stage, **Figure 4**). Protocorms then grew into friable and unstructured cellular masses with small cells showing dense cytoplasm on the surface (late stage, **Figure 4**). As for multiple meristem-type structures, the dividing cells on the surface of developing protocorms gradually organized into the shoot apical meristems at the early stage (**Figure 4**). As development proceeded, leaf primordia started to emerge from the organized shoot apical meristems (late stage, **Figure 4**) and multiple shoots were formed.

Explants of Transgenic Plants Overexpressing *PaLEC1-GPF* Induce Tissues That Are Dissimilar to Protocorm-Like Bodies

Overexpression of *LEC1* gene is known to be a potent inducer of somatic embryos (Lotan et al., 1998; Mu et al., 2008; Horstman et al., 2017a). We were therefore interested in asking what types of somatic embryonic structures could be induced by *PaLEC1* in *P. equestris*. To do so, protocorms were used as the explants for induction of somatic embryonic tissues. As described previously (Zhao et al., 2008; Mahendran and Bai, 2012; Fang et al., 2016), cutting protocorms of wild-type plants induced green PLBs (**Figure 5**). Cutting protocorms of T1 *35S:PaLEC1-GFP* #1 transgenic line, on the other hand, induced callus-like tissues and pale yellow-green protrusions (**Figure 5**). The appearance of pale yellow-green color is consistent with a previous report stating that overexpressing *LEC1* downregulates light responsive genes in *Arabidopsis* (Junker et al., 2012). Protrusions and callus-like tissues continued to grow and develop into unorganized thick and flat tissues, which then eventually grew into multiple-meristem type structures that were capable of producing multiple shoots (**Figure 5**). Using protocorms of T1 *35S:PaLEC1-GFP* #2 line as explants also induced callus-like and multiple-meristem type structures (**Figure 5**). Taken together, we conclude that *PaLEC1*-induced tissues have the ability to establish new shoot apical meristems for shoot regeneration.

To evaluate whether PaLEC1-GFP protein was regulated post-transcriptionally as somatic embryonic calli programmed to initiate shoot formation, PaLEC1-GFP protein was monitored by western blotting. As shown in **Supplementary Figure S4**, PaLEC1-GFP protein remained stable throughout the process.

PaLEC1 Is Sufficient to Activate Embryonic Marker Genes in Seedlings of *PaLEC1-GPF* Transgenic Plants

To evaluate the embryonic identity of PaLEC1-GFP overexpressing somatic tissues, expression of previously identified embryonic-specific genes (Fang et al., 2016) were examined in T1 *35S:PaLEC1-GFP* #1 protocorm-derived young seedling tissues. Expression of the embryonic TFs *ABSCISIC ACID INSENSITITVE3-like1* (*PeABI3L1*), *PeABI3L2, BABY BOOM* (*PeBBM*), *FUSCA3* (*PeFUS3*), and *WRINKLED1* (*PeWRI1*) and seed storage proteins, *7S GLOBULIN1* (*Pe7S-1*), *Pe7S-2*, *OLEOCIN1* (*PeOLE1*), and *PeOLE2* genes were confirmed to be preferentially expressed in ovary tissues collected at 130 days after pollination (DAP) of *P. equestris* (**Figure 6**). As expected, overexpression of PaLEC1-GFP caused significant induction of embryonic TFs *PeFUS3* and *PeABI3L1*, and seed storage proteins, *Pe7S-1*, *Pe7S-2*, and *PeOLE2* genes (**Figure 6**). Overexpression of PaLEC1-GFP protein only led to mild elevation of *PeABI3L2* mRNA and did not affect expression of *PeBBM*, *PeWRI1*, and *PeOLE1* genes (**Figure 6**), suggesting that PaLEC1 activates only part of the embryonic program. Similar expression patterns were also confirmed in independently collected young seedlings and callus tissues except *PeABI3L2* whose expression was not induced in

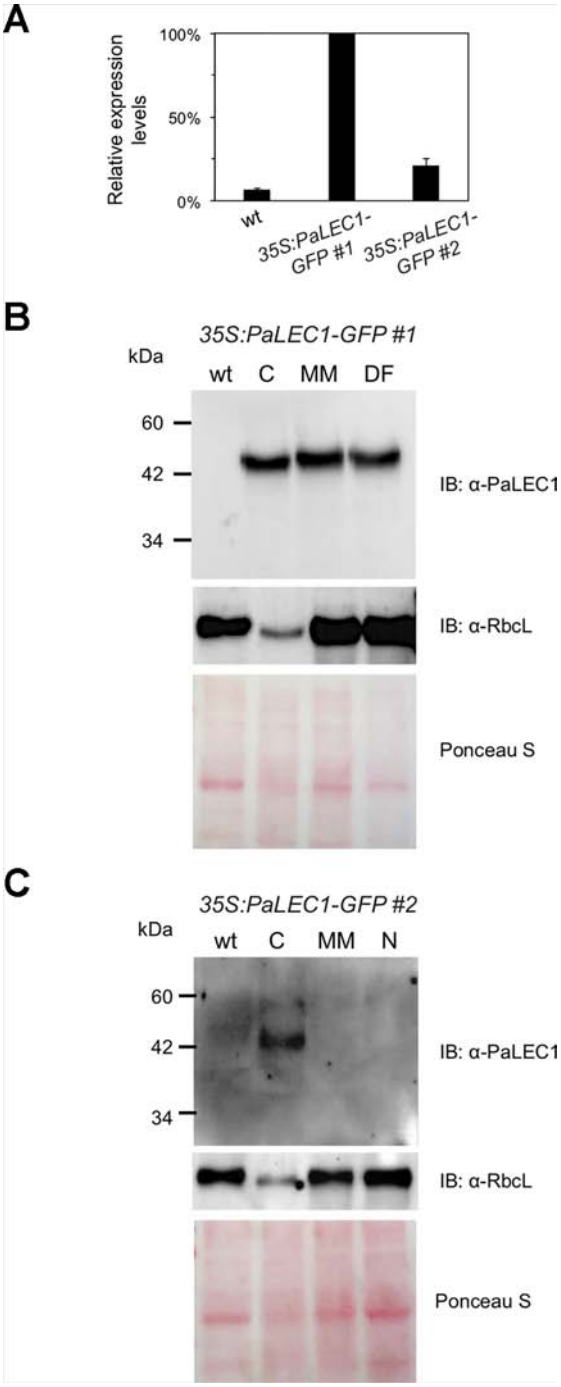

FIGURE 3 | Expression of PaLEC1-GFP protein in *35:PaLEC1-GFP* transgenic lines. **(A)** Quantitative RT-PCR analysis of expression of *PaLEC1-GFP* in wild-type (wt) and two *35:PaLEC1-GFP* transgenic lines. **(B)** Western blotting showing expression of PaLEC1-GFP and PaRbcL proteins in callus-type, multiple-meristem type, and dorsal fin-like embryonic tissues of *35:PaLEC1-GFP*#1 plants. **(C)** Western blotting showing expression of PaLEC1-GFP and PaRbcL proteins in callus-type, embryonic tissues of *35:PaLEC1-GFP*#2 plants. Blots stained with Ponceau S staining were used to visualize total loaded protein. wt, wild-type plants; C, callus-like tissues; MM, multiple meristem-like structures; DF, dorsal fin-like structures; N, normal wt-like tissues.

PaLEC1-induced callus tissues (**Supplementary Figures S5A, B**). It is likely that the moderate level of *PaLEC1-GFP* (**Supplementary Figure S5B**) in callus was not enough to induce *PeABI3L2*. Activation of *PeFUS3* was also confirmed in leaf tissues of five independent T0 *35S:PaLEC1-GFP* transgenic plants (**Supplementary Figure S6**).

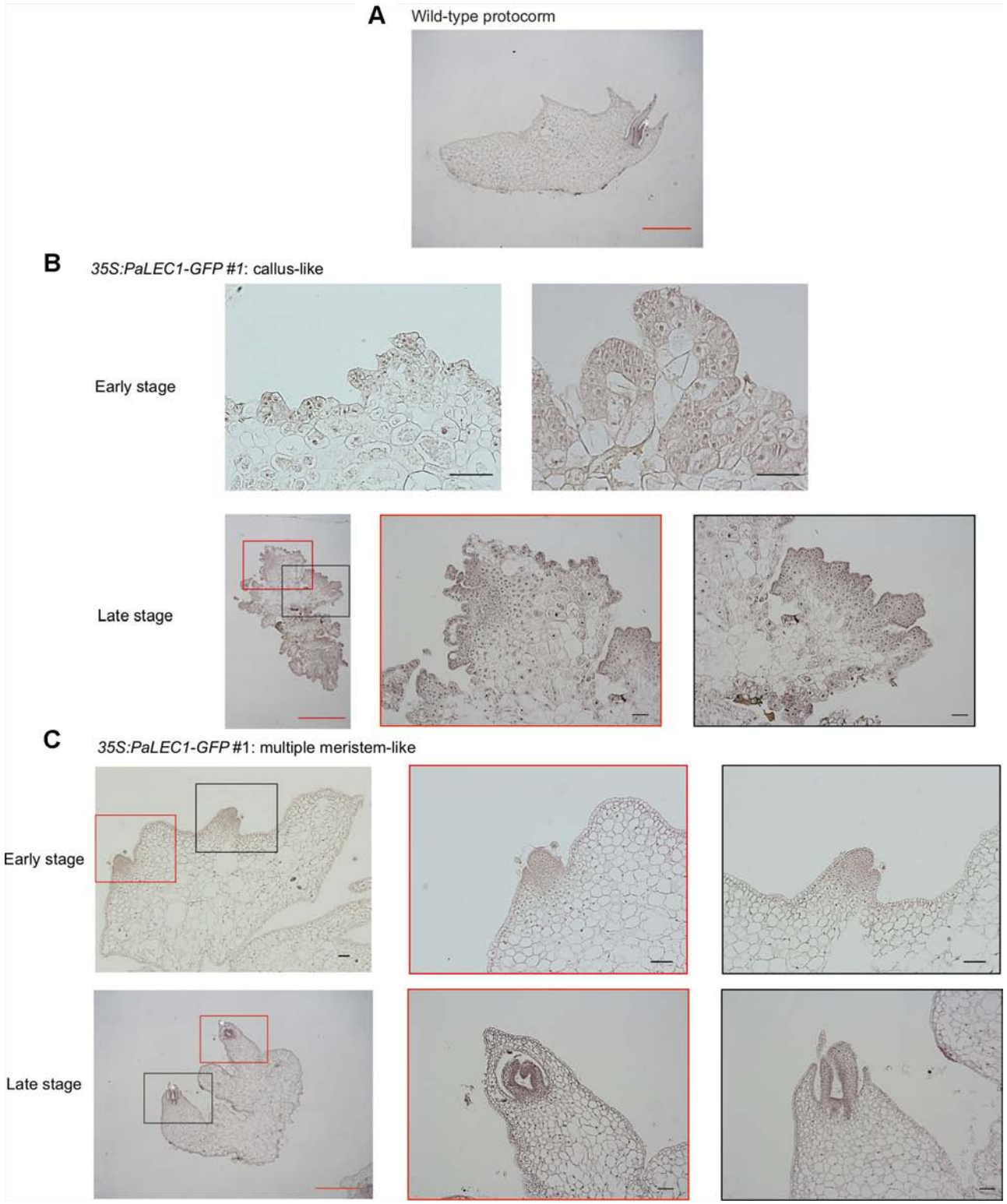

FIGURE 4 | Histological examination of embryonic tissues of *35:PaLEC1-GFP#1* transgenic plants. **(A)** Light micrograph of 10 μm longitudinal section of developing wild-type protocorm stained with hematoxylin. **(B)** Light micrograph of a 10 μm section of the early and late stages of callus-like tissues derived from protocorms of the T1 *35:PaLEC1-GFP#1* seeds. **(C)** Light micrograph of a 10 μm section of the early and late stages of multiple meristem-like tissues derived from protocorms of the T1 *35:PaLEC1-GFP#1* seeds. Shoot apical meristem (SAM) with the emerging leaf primordia are marked by a white asterisk. For panel **(B** and **C)**, low and high magnification of structures marked with red and black rectangles are shown. Red scale bar = 1 mm. Black scale bar = 100 μm.

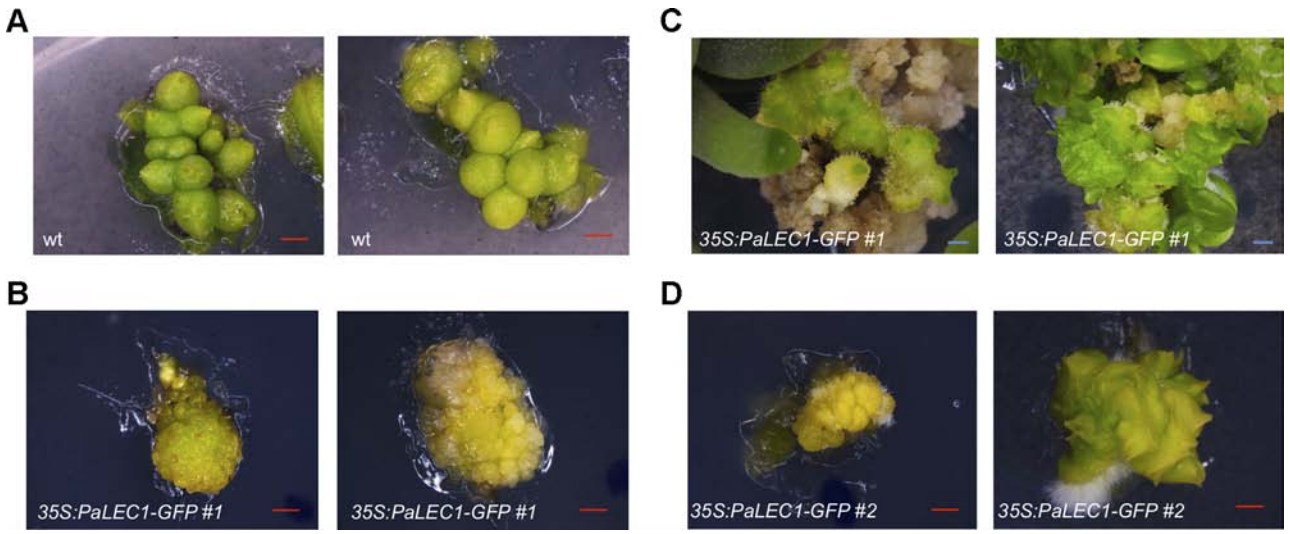

FIGURE 5 | Clonal propagation from protocorm-based explants of *35:PaLEC1-GFP#1* transgenic plants. **(A)** PLBs generated from cutting of wild-type protocorms. **(B)** Callus-like tissues produced by cutting of *35:PaLEC1-GFP#1* protocorms. **(C)** Callus-like tissues generated from *35:PaLEC1-GFP#1* grew into multiple-shoot like structures. **(D)** Callus-like and multiple shoot-like tissues produced by cutting of *35:PaLEC1-GFP#2* protocorms. For each panel, two independent clusters of tissues were photographed and showed. Red scale bar = 500 μm. Blue scale bar = 1 mm.

PaLEC1 Is Predominantly Localized in the Nucleus and Is Associated With Target Promoters Containing the CCAAT Element

Nuclear Transcription Factor-Y (NF-Y) is an evolutionarily conserved, DNA-binding, trimeric protein complex composed of NF-YA, NF-YB, and NF-YC subunits (Dolfini et al., 2012). *LEC1* encodes an atypical subunit of the (NF-YB) CCAAT-binding TF. To validate subcellular localization of PaLEC1, confocal microscopy was used to examine the localization of PaLEC1-GFP protein in transgenic plants. As predicted, PaLEC1-GFP was predominantly localized in the nuclei in the cells of the *35S:PaLEC1-GFP#1* line (**Figure 7**). The nuclear localized GFP signal was detected in all of the cells investigated in the *35S:PaLEC1-GFP#1* line. PaLEC1-GFP protein, however, was only detected in a few cells in callus tissues and was therefore much less abundant in *35S:PaLEC1-GFP#2* transgenic line (**Figure 7**), supporting the low expression level shown by western blot. Hence, PaLEC1 protein is a nuclear protein.

It has been reported that *LEC1* regulates many embryonic-specific TFs and storage proteins by directly binding to their promoters through the CCAAT DNA element (Lee et al., 2003; Gnesutta et al., 2017; Pelletier et al., 2017). To investigate whether PaLEC1 activates its targets in the same manner, we retrieved the 1 kb DNA sequences upstream of the start codon of *PeFUS3*, *PeABI3L1*, *PeABI3L2*, *PeBBM*, *PeWRI1*, *Pe7S-1*, *Pe7S*-2, *PeOLE1*, and *PeOEL2* (Cai et al., 2015) and surveyed the presence of the CCAAT element. Because of a large gap within the promoter regions of *PeABI3L2*, it was omitted from further study. Intriguingly, two to five CCAAT DNA elements were found within the 1 kb promoter sequences of *PeFUS3*, *PeABI3L1*, *Pe7S-1*, *Pe7S*-2, and *PeOLE2* (**Supplementary Figure S7**) whose expression was induced by overexpression of PaLEC1 (**Figure 6**). None or only one CCAAT element was present in promoters of *PeBBM*, *PeWRI1*, and *PeOLE1* (**Supplementary Figure S7**) whose expression was not induced in the PaLEC1 overexpressor (**Figure 6**). The correlation between the number of CCAAT elements and activation capability of PaLEC1-GFP suggests that PaLEC1-GFP protein may activate its targets in a CCAAT DNA element dosage-dependent manner.

To test whether PaLEC1-GFP binds the CCAAT element directly, ChIP using PaLEC1 antibody followed by PCR analysis was conducted. Because *PeFUS3* and *Pe7S-2* mRNAs were significantly upregulated by PaLEC1 and tandem CCAAT elements are present in their promoters (**Figure 8** and **Supplementary Figure S8**), *PeFUS3* and *Pe7S-2* were chosen for further ChIP analysis. Histone H3 antibody was used as a positive control and no antibody was included as the negative control. We found that PaLEC1-GFP protein interacted with the *PeFUS3* promoter region containing the CCAAT element but did not interact with *PeBBM* promoter that lacks the CCAAT element (**Figure 8**). Similarly, PaLEC1-GFP was found to interact with the *Pe7S-2* promoter carrying the CCAAT element but not to the *PeBBM* promoter lacking the element (**Figure 8**). These results were confirmed in three independent biological samples. Taken together, it is very likely that PaLEC1 activates *PeFUS3* and *Pe7S*-2 through binding to the CCAAT element-containing promoters.

DISCUSSION

PaLEC1 Induces Diverse Somatic Embryonic Structures

Our recent comparative transcriptome study provided evidence that PLB regeneration does not follow the somatic embryogenesis program (Fang et al., 2016) and raises a

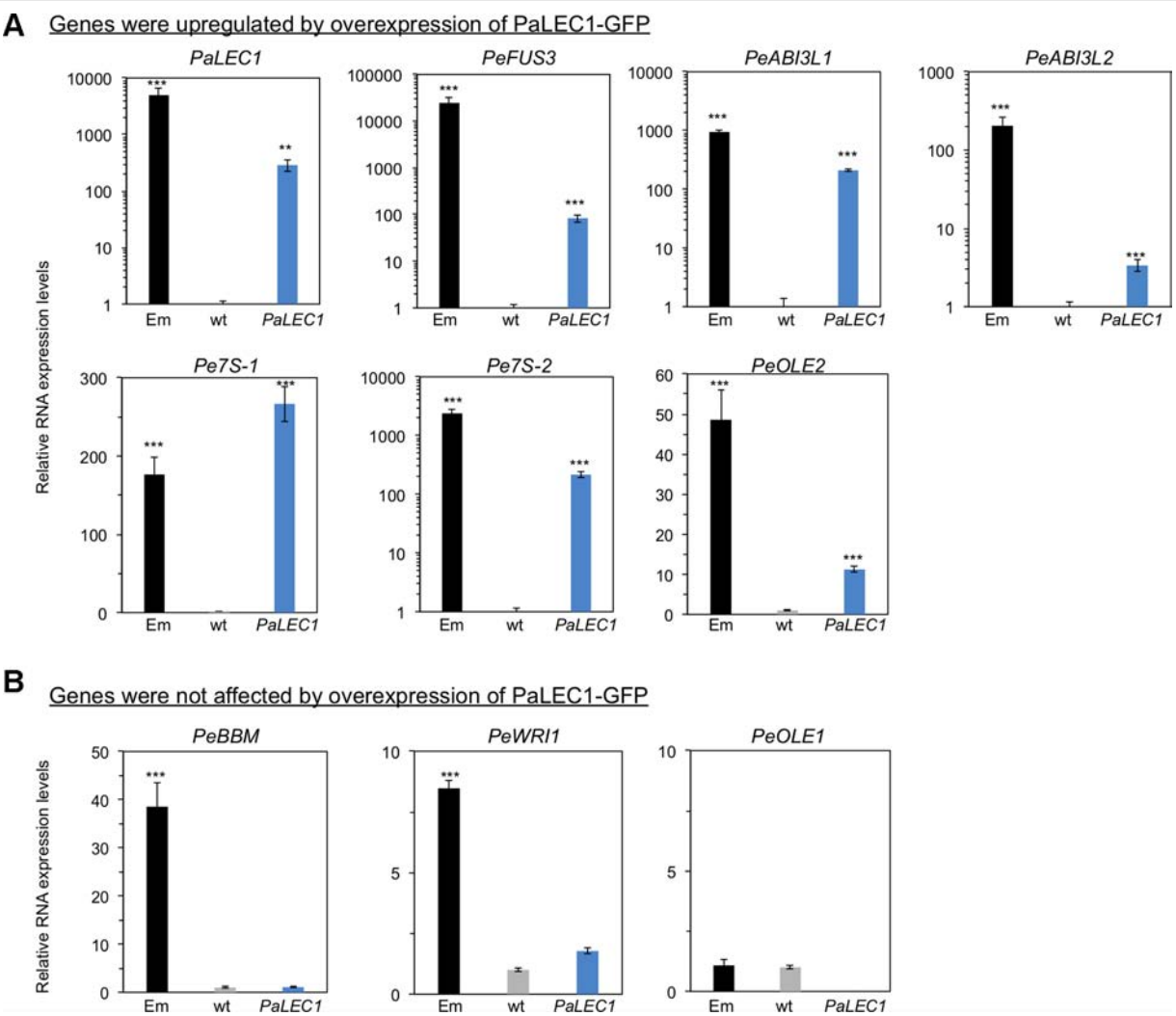

FIGURE 6 | Expression of embryonic genes in *35:PaLEC1-GFP#1* transgenic plants. **(A)** Expression of indicated embryonic genes was induced in *35:PaLEC1-GFP#1* transgenic plants. **(B)** Expression of indicated embryonic genes was not induced significantly by overexpression of PaLEC1-GFP protein. Em, zygotic embryonic tissues collected at 130 day after pollination. wt, wild-type plant. *PaLEC1*, *35:PaLEC1-GFP#1* transgenic plants. ***, $P < 0.001$; **, $P < 0.01$. Three independent biological replicates were performed.

question about the morphology and anatomy of orchid somatic embryos. In this study, overexpression of PaLEC1 was utilized to induce the somatic embryonic program in *P. equestris*. Similar to PLB induction, active cell division is a prerequisite for *PaLEC1*-induced somatic embryonic structures (**Figures 4B**, **C**). For PLB development, the polarized growth of proliferating cells gives rise to small protuberances with a distinct gradient of cell size, with the smaller cells occupying the future shoot pole and larger and vacuolated cells forming the base of the structure (Lee et al., 2013). For *PaLEC1*-induced somatic embryonic tissues, on the other hand, diverse types of somatic embryonic structures were formed from protocorms or explants of the two *35S:PaLEC1-GFP* transgenic lines regardless of the large difference in the amounts of PaLEC1-GFP protein accumulated. The most common type (~50% in both transgenic lines) was tissue clusters containing multiple shoot apical meristems (multiple-meristem type). For this type of regeneration, multiple meristems were initiated directly from developing protocorms and establishment of unorganized callus tissue did not seem to be a prerequisite. It is important to note that this type of regeneration is very different from direct shoot regeneration during which leaf primordia are generated directly (Košir et al., 2004; Wu and Chen, 2008; Yam and Arditti, 2017). In addition to producing multiple meristems for shoot regeneration, new shoots could also be produced indirectly from callus-type tissue (**Supplementary Figure S2**). The frequency of obtaining the callus-type tissue was higher in the strong *PaLEC1-GFP* overexpressors than in the weak ones (**Table 1**), indicating formation of the embryonic callus may be PaLEC1 dosage-dependent. Dosage-dependent induction of somatic embryogenesis has also been reported for *Arabidopsis* BBM and PLT2 (Horstman et al., 2017b). Intriguingly, the fin-like structure was only observed in the

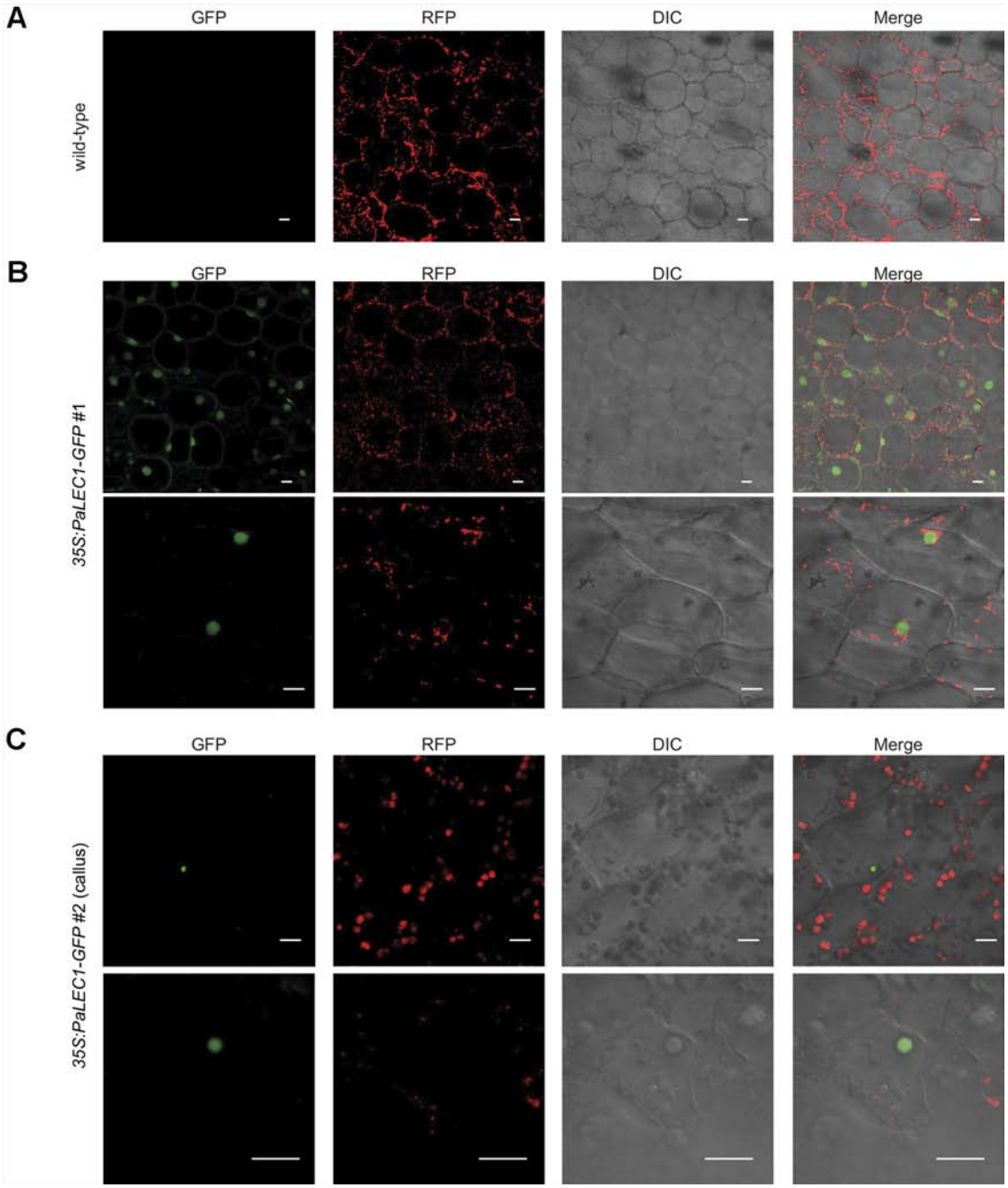

FIGURE 7 | Nuclear localization of PaLEC1-GFP. **(A)** No GFP signal was detected in wild-type plants. **(B)** PaLEC1-GFP was detected in nuclei of cells in roots of *35:PaLEC1-GFP#1* transgenic line. Nuclear localization of PaLEC1-GFP was confirmed in multiple (more than three) independent seedlings. **(C)** PaLEC1-GFP was detected in very few nuclei within callus cells of *35:PaLEC1-GFP#2* transgenic line. This sparsely distribution of nuclear PaLEC1-GFP signal was confirmed in multiple (more than three) protocorm-derived callus tissues. Photos with lower magnification are shown in the upper panel in panels **(B** and **C)**. Photos with higher magnification are shown in the bottom panel in panels **(B** and **C)**. GFP, photographs taken in the GFP channel. RFP, photographs taken in the RFP channel. DIC, differential interference contrast images. Merge, differential interference contrast images of cells superimposed with PaLEC1 (GFP) and chloroplast (RFP) channels. Scale bar = 20 μm.

strong overexpressor (*PaLEC1-GFP #1*) and normal protocorm-derived seedlings were only observed in the weak overexpressor (*PaLEC1-GFP #2*). Taken together these results indicate that *PaLEC1*-induced embryonic tissues were morphologically distinct from PLBs. Regardless of the type of structures induced by PaLEC1, all embryonic structures documented here are totipotent and capable of generating clonal orchid seedlings.

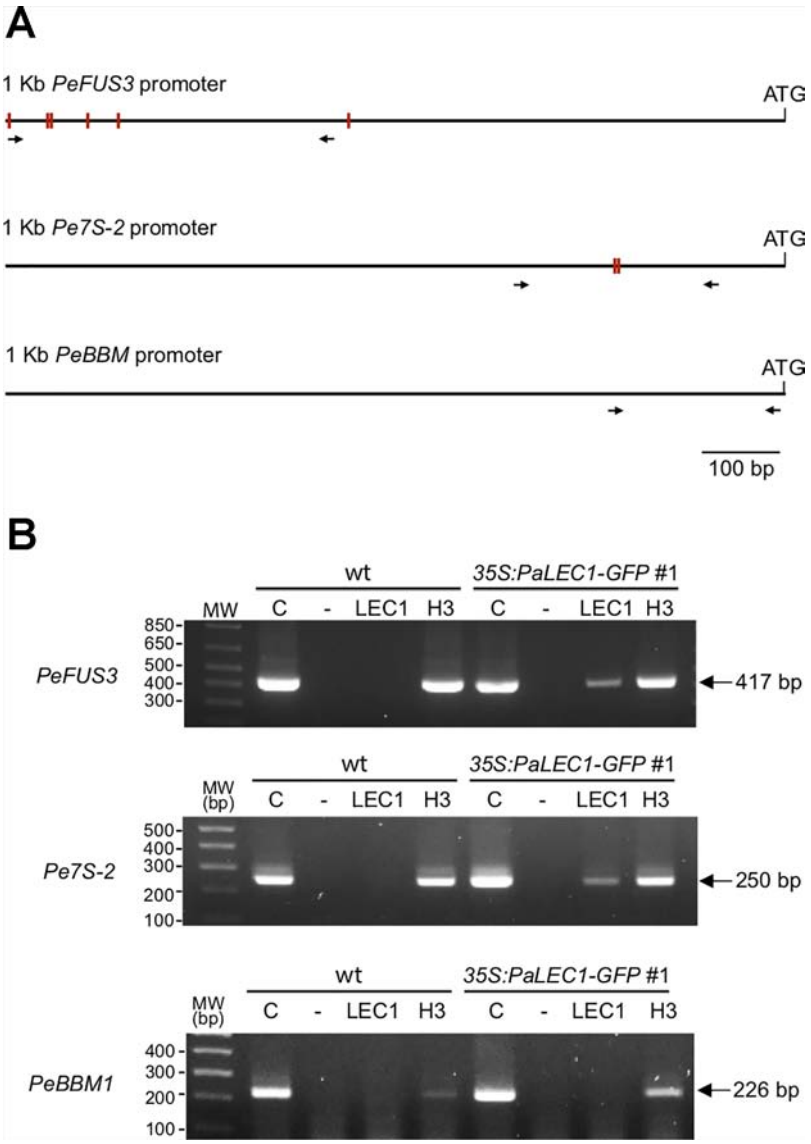

FIGURE 8 | Interaction between PaLEC1-GFP protein and the CCAAT element containing promoters. **(A)** Schematic representation of distribution of the CCAAT elements (red rectangles) in 1 kb upstream of the start codon of *PeFUS3* and *Pe7S-2* genomic DNAs. No CCAAT element was found in 1 Kb promoter region of *PeBBM*. Primers used for PCR reactions were shown as black arrows. **(B)** PCR of chromatin immunoprecipitation isolated DNA fragments to confirm interaction between PaLEC1-GFP protein and the CCAAT-containing promoters of the indicated genes. C, total cell lysate; "-", no antibody control; PaLEC1, PaLEC1 antibody precipitated chromatin; H3, histone H3 antibody precipitated chromatin. The amplified PCR fragments were verified by DNA sequencing. The same result was validated in two other independent biological samples (**Supplementary Figure S8**).

PaLEC1 Activates Part of the Embryonic Program

The embryonic identity of PaLEC1-induced embryonic tissues was verified by expression of embryonic TFs, *PeFUS3*, *PeABI3L1*, *PeABI3L2*, as well as seed storage proteins *Pe7S-1*, and *Pe7S-2*. In *Arabidopsis*, *FUS3*, *ABI3*, and *WRI1* are reported to be the direct targets of LEC1 (Pelletier et al., 2017). However, overexpression of PaLEC1 failed to induce *PeWRI1*. *LEC1* is reported to directly activate *WRI1* or indirectly acts through upregulation of *FUS3* and *LEC2* (Baud et al., 2007; Mu et al., 2008; Shen et al., 2010; Wang and Perry, 2013; Pelletier et al., 2017). Despite a high level of PaLEC1 protein and elevation of *PeFUS3* mRNA in *35S:PaLEC1-GFP*#1 transgenic line, we did not observe induction of *PeWRI1*, suggesting a PaLEC1-independent pathway is required to induce *PeWRI1* in *Phalaenopsis* orchids. Similar to *Arabidopsis* on the other hand, PaLEC1 cannot activate *PeBBM* and only induces a subset of storage proteins (West et al., 1994; Pelletier et al., 2017). In *Arabidopsis*, *BBM* acts upstream of the LEC1-FUS3-ABI3-LEC2 network to induce the somatic embryogenesis program (Horstman et al., 2017b).

Whether a similar regulatory module exists in *Phalaenopsis* orchids remains to be tested. Taken together, despite being a potent inducer of somatic embryogenesis in *Phalaenopsis* orchids, the PaLEC1-dependent regulatory network is similar but not identical to that reported in *Arabidopsis*.

LEC1 belongs to a distinct subgroup of the NF-YB family that is diverged from non-*LEC1*-type NF-YB genes in non-seed vascular plants (Xie et al., 2008). It has been proposed that LEC1-type NF-YB is recruited into a seed-specific regulatory network during evolution. Similar to *Arabidopsis* LEC1-type NF-YB TFs (Calvenzani et al., 2012; Laloum et al., 2013), PaLEC1 also binds to the CCAAT-containing promoters of its downstream genes, *PeFUS3* and *Pe7S-2*. Therefore, PaLEC1 is very likely to regulate its targets by directly acting through binding of the CCAAT DNA element. Even though one CCAAT element was present in the 1 kb promoters of *PeWRI1* and *PeOLE1* genes (**Supplementary Figure S4**), *PeWRI1* and *PeOLE1* mRNAs were not activated by overexpression of PaLEC1-GFP protein, indicating the CCAAT DNA element may not be sufficient for PaLEC1 binding. This notion is supported by studies of *Arabidopsis* and soybean that the G-box (CACGTG), abscisic acid response element (ABRE)-like (C/G/T)ACGTG(G/T)(A/C), and RY (CATGCA) motifs are significantly overrepresented in LEC1 target genes (Pelletier et al., 2017). The involvement of G-box, ABRE-like, and RY motifs in PaLEC1 functions remain to be determined.

In conclusion, our study of PaLEC1-induced somatic embryogenesis has demonstrated that somatic tissues of *Phalaenopsis* orchids do not resemble PLB, a result that is consistent with our previous comparative transcriptome studies. In addition to confirming the role of PaLEC1 in activating the somatic embryonic program, we obtained evidence supporting a direct role for PaLEC1 in controlling its targets and revealed the potential of PaLEC1-induce somatic embryonic tissues for orchid propagation. Conservation of the developmental processes and gene regulatory networks controlled by PaLEC1 is consistent with the notion that LEC1 is a major regulator of embryogenesis.

DATA AVAILABILITY STATEMENT

All datasets generated for this study are included in the article/ **Supplementary Material**.

AUTHOR CONTRIBUTIONS

S-CF designed the experiments, coordinated the studies, and wrote the manuscript. J-CC maintained and characterized transgenic orchid plants, and developed the ChIP protocol. J-CC and H-YL carried out the molecular biology experiments. C-GT developed and coordinated the orchid transformation process. All the authors have read and approved the final manuscript.

FUNDING

This work was supported by the Innovative Translational Agricultural Research Grants (to S-CF); and in part by a grant (to S-CF) from the Biotechnology Center in Southern Taiwan, Academia Sinica.

ACKNOWLEDGMENTS

We thank Dr. Yao-Cheng Lin for his assistance with bioinformatics, Ms. Miao-Ju Wei for her technical support during the initial work on transgenic orchid plants, the Confocal Microscopy Core, and Greenhouse Core Facilities for their supporting services, and Ms. Miranda Loney for English editing.

SUPPLEMENTARY MATERIAL

The Supplementary Material for this article can be found online at: https://www.frontiersin.org/articles/10.3389/fpls.2019.01594/full#supplementary-material

REFERENCES

Akasaka-Kennedy, Y., Tomita, K. O., and Ezura, H. (2004). Efficient plant regeneration and *Agrobacterium*-mediated transformation via somatic embryogenesis in melon (*Cucumis melo* L.). *Plant Sci.* 166 (3), 763–769. doi: 10.1016/j.plantsci.2003.11.020

Arditti, J., and Krikorian, A. D. (1996). Orchid micropropagation: the path from laboratory to commercialization and an account of several unappreciated investigators. *Bot. J. Linean Soc.* 122 (3), 183–241. doi: 10.1111/j.1095-8339.1996.tb02073.x

Arditti, J. (1992). *Fundamentals of orchid biology* (New York: John Wiley & Sons).

Arditti, J. (2009). *Micropropagation of Orchid* (Oxford, UK: Wiley-Blackwell).

Baud, S., Mendoza, M. S., To, A., Harscoet, E., Lepiniec, L., and Dubreucq, B. (2007). WRINKLED1 specifies the regulatory action of LEAFY COTYLEDON2 towards fatty acid metabolism during seed maturation in *Arabidopsis*. *Plant J.* 50 (5), 825–838. doi: 10.1111/j.1365-313X.2007.03092.x

Begum, A. A., Tamaki, M., Tahara, M., and Kako, S. (1994). Somatic embryogenesis in *Cymbidium* through i*n vitro* culture of inner tissue of protocorm-like bodies. *J. Jpn Soc. Hortic. Sci.* 63 (2), 419–427. doi: 10.2503/jjshs.63.419

Belarmino, M. M., and Mii, M. (2000). *Agrobacterium*-mediated genetic transformation of a *Phalaenopsis* orchid. *Plant Cell Rep.* 19 (5), 435–442. doi: 10.1007/s002990050752

Bentsink, L., and Koornneef, M. (2008). Seed dormancy and germination. *Arabidopsis Book* 6, e0119. doi: 10.1199/tab.0119

Boutilier, K., Offringa, R., Sharma, V. K., Kieft, H., Ouellet, T., Zhang, L., et al. (2002). Ectopic expression of BABY BOOM triggers a conversion from vegetative to embryonic growth. *Plant Cell* 14 (8), 1737–1749. doi: 10.1105/tpc.001941

Braybrook, S. A., and Harada, J. J. (2008). LECs go crazy in embryo development. *Trends In Plant Sci.* 13 (12), 624–630. doi: 10.1016/j.tplants.2008.09.008

Brettschneider, R., Becker, D., and Lorz, H. (1997). Efficient transformation of scutellar tissue of immature maize embryos. *Theor. Appl. Genet.* 94 (6-7), 737–748. doi: 10.1007/s001220050473

Burger, W. C. (1998). The question of cotyledon homology in angiosperms. *Bot. Rev.* 64 (4), 356–371. doi: 10.1007/BF02857623

Cai, J., Liu, X., Vanneste, K., Proost, S., Tsai, W. C., Liu, K. W., et al. (2015). The genome sequence of the orchid *Phalaenopsis equestris*. *Nat. Genet.* 47 (1), 65–72. doi: 10.1038/ng.3149

Calvenzani, V., Testoni, B., Gusmaroli, G., Lorenzo, M., Gnesutta, N., Petroni, K., et al. (2012). Interactions and CCAAT-binding of *Arabidopsis thaliana* NF-Y subunits. *PloS One* 7 (8), e42902. doi: 10.1371/journal.pone.0042902

Chavarri, M., Vegas, A., Zambrano, A. Y., and Demey, J. R. (2004). Transformation of mango somatic embryos by biobalistics. *Interciencia* 29 (5), 261–266.

Chen, J. T., and Chang, W. C. (2004). Induction of repetitive embryogenesis from seed-derived protocorms of *Phalaenopsis amabilis* var. *formosa Shimadzu*. *In Vitro Cell Dev. Biol. Plant* 40 (3), 290–293. doi: 10.1079/IVP2003527

Chen, J., and Chang, W. (2006). Direct somatic embryogenesis and plant regeneration from leaf explants of *Phalaenopsis amabilis*. *Biol. Plantarum* 50 (2), 169–173. doi: 10.1007/s10535-006-0002-8

Chen, J. C., and Fang, S. C. (2016). The long pollen tube journey and i*n vitro* pollen germination of *Phalaenopsis* orchids. *Plant Reprod.* 29 (1-2), 179–188. doi: 10.1007/s00497-016-0280-z

Chen, L. R., Chen, J. T., and Chang, W. C. (2002). Efficient production of protocorm-like bodies and plant regeneration from flower stalk explants of the sympodial orchid *Epidendrum radicans*. *In Vitro Cell Dev. Biol. Plant* 38 (5), 441–445. doi: 10.1079/IVP2002315

Chen, W.-H., Kao, Y.-L., and Tang, C.-Y. (2009). *Method for producing polyploid plants of orchids* (USA patent application).

Chen, T. K., Yang, H. T., Fang, S. C., Lien, Y. C., Yang, T. T., and Ko, S. S. (2016). Hybrid-Cut: an improved sectioning method for recalcitrant plant tissue samples. *J. Vis Exp.* (117), e54754. doi: 10.3791/54754

Chugh, S., Guha, S., and Rao, I. U. (2009). Micropropagation of orchids: a review on the potential of different explants. *Sci. Hortic.* 122 (4), 507–520. doi: 10.1016/j.scienta.2009.07.016

Dolfini, D., Gatta, R., and Mantovani, R. (2012). NF-Y and the transcriptional activation of CCAAT promoters. *Crit. Rev. Biochem. Mol. Biol.* 47 (1), 29–49. doi: 10.3109/10409238.2011.628970

Dressler, R. L. (1993). *Phylogeny and classification of the orchid family* (Portland, Oregon: Dioscorides Press).

Fang, S. C., de los Reyes, C., and Umen, J. G. (2006). Cell size checkpoint control by the retinoblastoma tumor suppressor pathway. *PloS Genet.* 2 (10), e167. doi: 10.1371/journal.pgen.0020167

Fang, S. C., Chen, J. C., and Wei, M. J. (2016). Protocorms and protocorm-like bodies are molecularly distinct from zygotic embryonic tissues in *Phalaenopsis aphrodite*. *Plant Physiol.* 171 (4), 2682–2700. doi: 10.1104/pp.16.00841

Feher, A. (2015). Somatic embryogenesis - Stress-induced remodeling of plant cell fate. *Biochim. Biophys. Acta* 1849 (4), 385–402. doi: 10.1016/j.bbagrm.2014.07.005

Fitch, M. M., Manshardt, R. M., Gonsalves, D., and Slightom, J. L. (1993). Transgenic papaya plants from *Agrobacterium*-mediated transformation of somatic embryos. *Plant Cell Rep.* 12 (5), 245–249. doi: 10.1007/BF00237128

Gaj, M. D., Zhang, S., Harada, J. J., and Lemaux, P. G. (2005). Leafy cotyledon genes are essential for induction of somatic embryogenesis of *Arabidopsis*. *Planta* 222 (6), 977–988. doi: 10.1007/s00425-005-0041-y

Garcês, H. M., Koenig, D., Townsley, B. T., Kim, M., and Sinha, N. R. (2014). Truncation of LEAFY COTYLEDON1 protein is required for asexual reproduction in *Kalanchoë daigremontiana*. *Plant Physiol.* 165 (1), 196–206. doi: 10.1104/pp.114.237222

Gnesutta, N., Saad, D., Chaves-Sanjuan, A., Mantovani, R., and Nardini, M. (2017). Crystal structure of the *Arabidopsis thaliana* L1L/NF-YC3 histone-fold dimer reveals specificities of the LEC1 Family of NF-Y subunits in plants. *Mol. Plant* 10 (4), 645–648. doi: 10.1016/j.molp.2016.11.006

Gow, W. P., Chen, J. T., and Chang, W. C. (2009). Effects of genotype, light regime, explant position and orientation on direct somatic embryogenesis from leaf explants of *Phalaenopsis* orchids. *Acta Physiol. Plant* 31 (2), 363–369. doi: 10.1007/s11738-008-0243-6

Gow, W. P., Chen, J. T., and Chang, W. C. (2010). Enhancement of direct somatic embryogenesis and plantlet growth from leaf explants of *Phalaenopsis* by adjusting culture period and explant length. *Acta Physiol. Plant* 32 (4), 621–627. doi: 10.1007/s11738-009-0438-5

Guan, Y., Li, S. G., Fan, X. F., and Su, Z. H. (2016). Application of somatic embryogenesis in woody plants. *Front. Plant Sci.* 7, 938. doi: 10.3389/fpls.2016.00938

Guo, W. L., Chang, Y. C. A., and Kao, C. Y. (2010). Protocorm-like Bodies initiation from root tips of *Cyrtopodium paranaense* (Orchidaceae). *HortScience* 45 (9), 1365–1368. doi: 10.21273/HORTSCI.45.9.1365

Harding, E. W., Tang, W., Nichols, K. W., Fernandez, D. E., and Perry, S. E. (2003). Expression and maintenance of embryogenic potential is enhanced through constitutive expression of *AGAMOUS-Like 15*. *Plant Physiol.* 133 (2), 653–663. doi: 10.1104/pp.103.023499

Hecht, V., Vielle-Calzada, J. P., Hartog, M. V., Schmidt, E. D., Boutilier, K., Grossniklaus, U., et al. (2001). The *Arabidopsis SOMATIC EMBRYOGENESIS RECEPTOR KINASE 1* gene is expressed in developing ovules and embryos and enhances embryogenic competence in culture. *Plant Physiol.* 127 (3), 803–816. doi: 10.1104/pp.010324

Horstman, A., Bemer, M., and Boutilier, K. (2017a). A transcriptional view on somatic embryogenesis. *Regenerat. (Oxf.)* 4 (4), 201–216. doi: 10.1002/reg2.91

Horstman, A., Li, M., Heidmann, I., Weemen, M., Chen, B., Muino, J. M., et al. (2017b). The BABY BOOM transcription factor activates the LEC1-ABI3-FUS3-LEC2 network to induce somatic embryogenesis. *Plant Physiol.* 175 (2), 848–857. doi: 10.1104/pp.17.00232

Hossain, M. M., Kant, R., Van, P. T., Winarto, B., Zeng, S. J., and da Silva, J. A. T. (2013). The application of biotechnology to orchids. *Crit. Rev. Plant Sci.* 32 (2), 69–139. doi: 10.1080/07352689.2012.715984

Ikeuchi, M., Sugimoto, K., and Iwase, A. (2013). Plant callus: mechanisms of induction and repression. *Plant Cell* 25 (9), 3159–3173. doi: 10.1105/tpc.113.116053

Ishii, Y., Takamura, T., Goi, M., and Tanaka, M. (1998). Callus induction and somatic embryogenesis of *Phalaenopsis*. *Plant Cell Rep.* 17 (6), 446–450. doi: 10.1007/s002990050423

Jones, D., and Tisserat, B. (1990). Clonal propagation of orchids. *Methods Mol. Biol.* 6, 181–191. doi: 10.1385/0-89603-161-6:181

Joshee, N., Biswas, B. K., and Yadav, A. K. (2007). Somatic embryogenesis and plant development in *Centella asiatica* L., a highly prized medicinal plant of the tropics. *HortScience* 42 (3), 633–637. doi: 10.21273/HORTSCI.42.3.633

Junker, A., Monke, G., Rutten, T., Keilwagen, J., Seifert, M., Thi, T. M., et al. (2012). Elongation-related functions of LEAFY COTYLEDON1 during the development of *Arabidopsis thaliana*. *Plant J.* 71 (3), 427–442. doi: 10.1111/j.1365-313X.2012.04999.x

Kareem, A., Radhakrishnan, D., Sondhi, Y., Aiyaz, M., Roy, M. V., Sugimoto, K., et al. (2016). De novo assembly of plant body plan: a step ahead of Deadpool. *Regenerat. (Oxf.)* 3 (4), 182–197. doi: 10.1002/reg2.68

Kim, J. Y., Adhikari, P. B., Ahn, C. H., Kim, D. H., Kim, Y. C., Han, J. Y., et al. (2019). High frequency somatic embryogenesis and plant regeneration of interspecific ginseng hybrid between *Panax ginseng* and *Panax quinquefolius*. *J. Ginseng Res.* 43 (1), 38–48. doi: 10.1016/j.jgr.2017.08.002

Košir, D., Škof, S., and Luthar, Z. (2004). Direct shoot regeneration from nodes of *Phalaenopsis* orchids. *Acta Agriu. Slovenica* 83, 233–242.

Kull, T., and Arditti, J. (2002). *Orchid biology reviews and perspectives* (Dordrecht; London: Kluwer Academic Publishers). doi: 10.1007/978-94-017-2500-2

Kuo, H. L., Chen, J. T., and Chang, W. C. (2005). Efficient plant regeneration through direct somatic embryogenesis from Leaf explants of *Phalaenopsis* 'Little Steve'. *In Vitro Cell Devl. Biol. Plant* 41 (4), 453–456. doi: 10.1079/IVP2005644

Kwong, R. W., Bui, A. Q., Lee, H., Kwong, L. W., Fischer, R. L., Goldberg, R. B., et al. (2003). LEAFY COTYLEDON1-LIKE defines a class of regulators essential for embryo development. *Plant Cell* 15 (1), 5–18. doi: 10.1105/tpc.006973

Laloum, T., De Mita, S., Gamas, P., Baudin, M., and Niebel, A. (2013). CCAAT-box binding transcription factors in plants: Y so many? *Trends Plant Sci.* 18 (3), 157–166. doi: 10.1016/j.tplants.2012.07.004

Lee, H., Fischer, R. L., Goldberg, R. B., and Harada, J. J. (2003). *Arabidopsis* LEAFY COTYLEDON1 represents a functionally specialized subunit of the CCAAT binding transcription factor. *Proc. Natl. Acad. Sci. U.S.A.* 100 (4), 2152–2156. doi: 10.1073/pnas.0437909100

Lee, Y. I., Hsu, S. T., and Yeung, E. C. (2013). Orchid protocorm-like bodies are somatic embryos. *Am. J. Bot.* 100 (11), 2121–2131. doi: 10.3732/ajb.1300193

Li, H. Q., Sautter, C., Potrykus, I., and PuontiKaerlas, J. (1996). Genetic transformation of cassava (*Manihot esculenta* Crantz). *Nat. Biotech.* 14 (6), 736–740. doi: 10.1038/nbt0696-736

Li, Z. T., Dhekney, S., Dutt, M., Van Aman, M., Tattersall, J., Kelley, K. T., et al. (2006). Optimizing *Agrobacterium*-mediated transformation of grapevine. *In Vitro Cell Dev. Biol. Plant* 42 (3), 220–227. doi: 10.1079/IVP2006770

Liao, Y. J., Tsai, Y. C., Sun, Y. W., Lin, R. S., and Wu, F. S. (2011). *In vitro* shoot induction and plant regeneration from flower buds in *Paphiopedilum* orchids. *In Vitro Cell Dev. Biol. Plant* 47 (6), 702–709. doi: 10.1007/s11627-011-9370-7

Liau, C. H., You, S. J., Prasad, V., Hsiao, H. H., Lu, J. C., Yang, N. S., et al. (2003). *Agrobacterium tumefaciens*-mediated transformation of an *Oncidium* orchid. *Plant Cell Rep.* 21 (10), 993–998. doi: 10.1007/s00299-003-0614-9

Lin, H. Y., Chen, J. C., Wei, M. J., Lien, Y. C., Li, H. H., Ko, S. S., et al. (2014). Genome-wide annotation, expression profiling, and protein interaction studies of the core cell-cycle genes in *Phalaenopsis aphrodite*. *Plant Mol. Biol.* 84 (1-2), 203–226. doi: 10.1007/s11103-013-0128-y

Lotan, T., Ohto, M., Yee, K. M., West, M. A., Lo, R., Kwong, R. W., et al. (1998). *Arabidopsis* LEAFY COTYLEDON1 is sufficient to induce embryo development in vegetative cells. *Cell* 93 (7), 1195–1205. doi: 10.1016/S0092-8674(00)81463-4

Lowe, K., Wu, E., Wang, N., Hoerster, G., Hastings, C., Cho, M. J., et al. (2016). Morphogenic regulators *Baby boom* and *Wuschel* improve monocot transformation. *Plant Cell.* 28 (9), 1998–2015. doi: 10.1105/tpc.16.00124

Mahendran, G., and Bai, V. N. (2012). Direct somatic embryogenesis and plant regeneration from seed derived protocorms of *Cymbidium bicolor* Lindl. *Sci. Hortic.* 135, 40–44. doi: 10.1016/j.scienta.2011.12.003

Mcgranahan, G. H., Leslie, C. A., Uratsu, S. L., Martin, L. A., and Dandekar, A. M. (1988). *Agrobacterium*-mediated transformation of salnut somatic embryos and regeneration of transgenic plants. *Nat. Biotech.* 6 (7), 800–804. doi: 10.1038/nbt0788-800

Min, L., Hu, Q., Li, Y., Xu, J., Ma, Y., Zhu, L., et al. (2015). LEAFY COTYLEDON1-CASEIN KINASE I-TCP15-PHYTOCHROME INTERACTING FACTOR4 network regulates somatic embryogenesis by regulating auxin homeostasis. *Plant Physiol.* 169 (4), 2805–2821. doi: 10.1104/pp.15.01480

Mondal, T. K., Bhattacharya, A., Ahuja, P. S., and Chang, P. K. (2001). Transgenic tea [*Camellia sinensis* (L.) O. Kuntze cv. Kangra Jat] plants obtained by *Agrobacterium*-mediated transformation of somatic embryos. *Plant Cell Rep.* 20 (8), 712–720. doi: 10.1007/s002990100382

Mordhorst, A. P., Hartog, M. V., El Tamer, M. K., Laux, T., and de Vries, S. C. (2002). Somatic embryogenesis from *Arabidopsis* shoot apical meristem mutants. *Planta* 214 (6), 829–836. doi: 10.1007/s00425-001-0700-6

Mu, J., Tan, H., Zheng, Q., Fu, F., Liang, Y., Zhang, J., et al. (2008). *LEAFY COTYLEDON1* is a key regulator of fatty acid biosynthesis in *Arabidopsis*. *Plant Physiol.* 148 (2), 1042–1054. doi: 10.1104/pp.108.126342

Murray, M. G., and Thompson, W. F. (1980). Rapid isolation of high molecular weight plant DNA. *Nucleic Acids Res.* 8 (19), 4321–4325. doi: 10.1093/nar/8.19.4321

Nishimura, G. (1981). Comparative morphology of *Cattleya* and *Phalaenopsis* (Orchidaceae) seedlings. *Bot. Gazette* 142 (3), 360–365. doi: 10.1086/337235

Nordine, A., Tlemcani, C. R., and El Meskaoui, A. (2014). Regeneration of plants through somatic embryogenesis in *Thymus hyemalis* Lange, a potential medicinal and aromatic plant. *In Vitro Cell Dev. Biol. Plant* 50 (1), 19–25. doi: 10.1007/s11627-013-9577-x

Pacini, E., and Hesse, M. (2002). Types of pollen dispersal units in orchids, and their consequences for germination and fertilization. *Ann. Bot.* 89 (6), 653–664. doi: 10.1093/aob/mcf138

Paek, K. Y., Hahn, E. J., and Park, S. Y. (2011). Micropropagation of *Phalaenopsis* orchids via protocorms and protocorm-like bodies. *Methods Mol. Biol.* 710, 293–306. doi: 10.1007/978-1-61737-988-8_20

Park, S. Y., Yeung, E. C., Chakrabarty, D., and Paek, K. Y. (2002). An efficient direct induction of protocorm-like bodies from leaf subepidermal cells of *Doritaenopsis* hybrid using thin-section culture. *Plant Cell Rep.* 21 (1), 46–51. doi: 10.1007/s00299-002-0480-x

Pelletier, J. M., Kwong, R. W., Park, S., Le, B. H., Baden, R., Cagliari, A., et al. (2017). LEC1 sequentially regulates the transcription of genes involved in diverse developmental processes during seed development. *Proc. Natl. Acad. Sci. U.S.A.* 114 (32), E6710–E6719. doi: 10.1073/pnas.1707957114

Polin, L. D., Liang, H. Y., Rothrock, R. E., Nishii, M., Diehl, D. L., Newhouse, A. E., et al. (2006). *Agrobacterium*-mediated transformation of American chestnut (*Castanea dentata* (Marsh.) Borkh.) somatic embryos. *Plant Cell Tiss. Org. Cult.* 84 (1), 69–78. doi: 10.1007/s11240-005-9002-1

Pramanik, D., Rachmawati, F., and Winarto, B. (2016). Propagation of *Phalaenopsis* 'Puspa Tiara Kencan'?™ via somatic embryogenesis. *Acta Hortic.* (1113), 21–26. doi: 10.17660/ActaHortic.2016.1113.3

Pulianmackal, A. J., Kareem, A. V., Durgaprasad, K., Trivedi, Z. B., and Prasad, K. (2014). Competence and regulatory interactions during regeneration in plants. *Front. Plant Sci.* 5, 142. doi: 10.3389/fpls.2014.00142

Radhakrishnan, D., Kareem, A., Durgaprasad, K., Sreeraj, E., Sugimoto, K., and Prasad, K. (2017). Shoot regeneration: a journey from acquisition of competence to completion. *Curr. Opin. Plant Biol.* 41, 23–31. doi: 10.1016/j.pbi.2017.08.001

Rasmussen, H. N. (2002). Recent developments in the study of orchid mycorrhiza. *Plant Soil* 244 (1-2), 149–163. doi: 10.1023/A:1020246715436

Robertson, D., Weissinger, A. K., Ackley, R., Glover, S., and Sederoff, R. R. (1992). Genetic transformation of Norway Spruce (*Picea abies* (L) Karst) using somatic embryo explants by microprojectile bombardment. *Plant Mol. Biol.* 19 (6), 925–935. doi: 10.1007/BF00040525

Saghai-Maroof, M. A., Soliman, K. M., Jorgensen, R. A., and Allard, R. W. (1984). Ribosomal DNA spacer-length polymorphisms in barley: mendelian inheritance, chromosomal location, and population dynamics. *Proc. Natl. Acad. Sci. U.S.A.* 81 (24), 8014–8018. doi: 10.1073/pnas.81.24.8014

Shen, B., Allen, W. B., Zheng, P., Li, C., Glassman, K., Ranch, J., et al. (2010). Expression of *ZmLEC1* and *ZmWRI1* increases seed oil production in maize. *Plant Physiol.* 153 (3), 980–987. doi: 10.1104/pp.110.157537

Stone, S. L., Kwong, L. W., Yee, K. M., Pelletier, J., Lepiniec, L., Fischer, R. L., et al. (2001). *LEAFY COTYLEDON2* encodes a B3 domain transcription factor that induces embryo development. *Proc. Natl. Acad. Sci. U.S.A.* 98 (20), 11806–11811. doi: 10.1073/pnas.201413498

Teixeira da Silva, J. A., Singh, N., and Tanaka, M. (2006). Priming biotic factors for optimal protocorm-like body and callus induction in hybrid *Cymbidium* (Orchidaceae), and assessment of cytogenetic stability in regenerated plantlets. *Plant Cell Tissue Organ Cult.* 84 (2), 135–144. doi: 10.1007/s11240-005-9003-0

Tokuhara, K., and Mii, M. (2001). Induction of embryogenic callus and cell suspension culture from shoot tips excised from flower stalk buds of *Phalaenopsis* (Orchidaceae). *In Vitro Cell Dev. Biol. Plant* 37 (4), 457–461. doi: 10.1007/s11627-001-0080-4

Tokuhara, K., and Mii, M. (2003). Highly-efficient somatic embryogenesis from cell suspension cultures of *Phalaenopsis* orchids by adjusting carbohydrate sources. *In Vitro Cell Dev. Biol. Plant* 39 (6), 635–639. doi: 10.1079/IVP2003466

Trinh, T. H., Ratet, P., Kondorosi, E., Durand, P., Kamate, K., Bauer, P., et al. (1998). Rapid and efficient transformation of diploid *Medicago truncatula* and *Medicago sativa ssp falcata* lines improved in somatic embryogenesis. *Plant Cell Rep.* 17 (5), 345–355. doi: 10.1007/s002990050405

Umbeck, P., Johnson, G., Barton, K., and Swain, W. (1987). Genetically transformed cotton (*Gossypium Hirsutum*-L) Plants. *Nat. Biotech.* 5 (3), 263–266. doi: 10.1038/nbt0387-263

Vergne, P., Maene, M., Gabant, G., Chauvet, A., Debener, T., and Bendahmane, M. (2010). Somatic embryogenesis and transformation of the diploid *Rosa chinensis* cv Old Blush. *Plant Cell Tiss. Org. Cult.* 100 (1), 73–81. doi: 10.1007/s11240-009-9621-z

Villar, C. B., and Köhler, C. (2010). Plant chromatin immunoprecipitation. *Methods Mol. Biol.* 655, 401–411. doi: 10.1007/978-1-60761-765-5_27

von Arnold, S., Sabala, I., Bozhkov, P., Dyachok, J., and Filonova, L. (2002). Developmental pathways of somatic embryogenesis. *Plant Cell Tiss. Org. Cult.* 69 (3), 233–249. doi: 10.1023/A:1015673200621

Wang, F., and Perry, S. E. (2013). Identification of direct targets of FUSCA3, a key regulator of *Arabidopsis* seed development. *Plant Physiol.* 161 (3), 1251–1264. doi: 10.1104/pp.112.212282

Wang, X., Niu, Q. W., Teng, C., Li, C., Mu, J., Chua, N. H., et al. (2009). Overexpression of *PGA37/MYB118* and *MYB115* promotes vegetative-to-embryonic transition in *Arabidopsis*. *Cell Res.* 19 (2), 224–235. doi: 10.1038/cr.2008.276

Waterman, R. J., and Bidartondo, M. I. (2008). Deception above, deception below: linking pollination and mycorrhizal biology of orchids. *J. Exp. Bot.* 59 (5), 1085–1096. doi: 10.1093/jxb/erm366

West, M., Yee, K. M., Danao, J., Zimmerman, J. L., Fischer, R. L., Goldberg, R. B., et al. (1994). *LEAFY COTYLEDON1* is an essential regulator of late embryogenesis and cotyledon identity in *Arabidopsis*. *Plant Cell* 6 (12), 1731–1745. doi: 10.1105/tpc.6.12.1731

Winkelmann, T., Geier, T., and Preil, W. (2006). Commercial *in vitro* plant production in Germany in 1985-2004. *Plant Cell Tiss. Org. Cult.* 86 (3), 319–327. doi: 10.1007/s11240-006-9125-z

Wu, H.-H., and Chen, F.-C. (2008). Effect of plant growth regulators on shoot multiplication from flower stalk nodal buds of *Phalaenopsis* and *Doritaenopsis*. *J. Taiwan Soc Hortic. Sci.* 54 (2), 151–159.

Xie, Z., Li, X., Glover, B. J., Bai, S., Rao, G. Y., Luo, J., et al. (2008). Duplication and functional diversification of HAP3 genes leading to the origin of the seed-developmental regulatory gene, *LEAFY COTYLEDON1* (*LEC1*), in nonseed plant genomes. *Mol. Biol. Evol.* 25 (8), 1581–1592. doi: 10.1093/molbev/msn105

Yam, T. W., and Arditti, J. (2009). History of orchid propagation: a mirror of the history of biotechnology. *Plant Biotechnol. Rep.* 3 (1), 1–56. doi: 10.1007/s11816-008-0066-3

Yam, T. W., and Arditti, J. (2017). *Micropropagation of Orchids, Third Edition* (Chichester, West Sussex, UK: John Wiley & Sons Ltd.). doi: 10.1002/9781119187080

Yang, X. Y., and Zhang, X. L. (2010). Regulation of somatic embryogenesis in higher plants. *Crit. Rev. Plant Sci.* 29 (1), 36–57. doi: 10.1080/07352680903436291

Yazawa, K., Takahata, K., and Kamada, H. (2004). Isolation of the gene encoding carrot *LEAFY COTYLEDON1* and expression analysis during somatic and zygotic embryogenesis. *Plant Physiol. Biochem.* 42 (3), 215–223. doi: 10.1016/j.plaphy.2003.12.003

Yeung, E. C. (2017). A perspective on orchid seed and protocorm development. *Bot. Stud.* 58 (1), 33. doi: 10.1186/s40529-017-0188-4

Zhao, P., Wu, F., Feng, F.-S., and Wang, W.-J. (2008). Protocorm-like body (PLB) formation and plant regeneration from the callus culture of *Dendrobium candidum* Wall ex Lindl. *In Vitro Cell Dev. Biol. Plant* 44 (3), 178–185. doi: 10.1007/s11627-007-9101-2

Zhu, S. P., Wang, J., Ye, J. L., Zhu, A. D., Guo, W. W., and Deng, X. X. (2014). Isolation and characterization of *LEAFY COTYLEDON 1-LIKE* gene related to embryogenic competence in *Citrus sinensis*. *Plant Cell Tiss. Org. Cult.* 119 (1), 1–13. doi: 10.1007/s11240-014-0509-1

Zimmerman, J. L. (1993). Somatic embryogenesis: a model for early development in higher plants. *Plant Cell* 5 (10), 1411–1423. doi: 10.1105/tpc.5.10.1411

Zuo, J., Niu, Q. W., Frugis, G., and Chua, N. H. (2002). The *WUSCHEL* gene promotes vegetative-to-embryonic transition in *Arabidopsis*. *Plant J.* 30 (3), 349–359. doi: 10.1046/j.1365-313X.2002.01289.x

Conflict of Interest: The authors declare that the research was conducted in the absence of any commercial or financial relationships that could be construed as a potential conflict of interest.

frontiers in Plant Science

ORIGINAL RESEARCH
published: 29 November 2019
doi: 10.3389/fpls.2019.01589

The Role of Non-Mycorrhizal Fungi in Germination of the Mycoheterotrophic Orchid *Pogoniopsis schenckii* Cogn.

Laís Soêmis Sisti[1], Denisele Neuza Aline Flores-Borges[1], Sara Adrián López de Andrade[2], Samantha Koehler[3], Maria Letícia Bonatelli[4] and Juliana Lischka Sampaio Mayer[1]**

[1] Laboratory of Plant Anatomy, Department of Plant Biology, Institute of Biology, State University of Campinas, Campinas, Brazil, [2] Laboratory of Plant Molecular Physiology, Department of Plant Biology, Institute of Biology, State University of Campinas, Campinas, Brazil, [3] Laboratory of Plant Taxonomy, Department of Plant Biology, Institute of Biology, State University of Campinas, Campinas, Brazil, [4] Laboratory of Genetics of Microorganisms, Department of Genetics, College of Agriculture "Luiz de Queiroz," University of São Paulo, Piracicaba, Brazil

OPEN ACCESS

Edited by:
Jen-Tsung Chen, National University of Kaohsiung, Taiwan

Reviewed by:
Kei Hiruma, Nara Institute of Science and Technology (NAIST), Japan
Pablo Delgado-Sánchez, Universidad Autónoma de San Luis Potosí, Mexico

***Correspondence:**
Laís Soêmis Sisti
laisoemis@hotmail.com
Juliana Lischka Sampaio Mayer
mjimayer@yahoo.com.br

Specialty section:
This article was submitted to Plant Development and EvoDevo, a section of the journal Frontiers in Plant Science

Received: *25 July 2019*
Accepted: *12 November 2019*
Published: *29 November 2019*

Citation:
Sisti LS, Flores-Borges DNA, Andrade SALd, Koehler S, Bonatelli ML and Mayer JLS (2019) The Role of Non-Mycorrhizal Fungi in Germination of the Mycoheterotrophic Orchid Pogoniopsis schenckii Cogn. Front. Plant Sci. 10:1589. doi: 10.3389/fpls.2019.01589

Endophytic fungi are those that inhabit within organs and tissues without causing damage, while mycorrhizal fungi develop hyphal complexes called pelotons within cortical cells of orchid roots. Although abundant and frequent in all plant organs, the role of endophytic fungi has been neglected in relation to orchid's early development. *Pogoniopsis schenckii* Cogn. is an aclorophyllated and mycoheterotrophic (MH) orchid. This study aimed at i) investigating the endophytic fungal community in organs of *P. schenckii* and its mycorrhizal fungi associated; ii) evaluating the ability of isolated fungus in the *in vitro* germination of the seeds of the species, and iii) describing the development of *P. schenckii* protocorm, analyzing the ultrastructure of the infected cells. Six genera of fungi were isolated and identified through the partial sequencing of the internal transcribed spacer region, all belonging to the phylum Ascomycota. Also, Tulasnellaceae was identified through uncultured technique as potentially mycorrhizal in this MH orchid. Some isolates of the genera *Trichoderma*, *Fusarium*, and especially *Clonostachys* presented germinative potential on *P. schenckii* seeds, causing rupture of the external tegument. The protocorms showed complete absence of peloton formation, but fungal hyphae were clearly observed within living cells. This is the first report of germination of a MH and aclorophyllated orchid species stimulated by the presence of non-mycorrhizal endophytic fungi isolated from fruits and roots of the same species.

Keywords: endophytic fungi, symbiotic germination, plant anatomy, aclorophyllated plant, ultrastructure, protocorm, Orchidaceae, Tulasnellaceae

INTRODUCTION

Mycoheterotrophic (MH) plants evolved independently in several locations and represent one of the most extreme forms of mycorrhizal dependence (Leake, 1994). These plants remain aclorophyllated throughout their life cycle and are totally dependent on their mycorrhizal partners for their survival (Peterson et al., 2004). There are approximately 235 MH species within the Orchidaceae family (Merckx, 2013). One of the main characteristics of mycorrhizal orchids is the formation of a hyphal complex, also called peloton, which develops within the parenchyma cells of the roots and rhizomes

of such plants (Peterson et al., 2004; Rasmussen and Rasmussen 2009). During the germination in *Orchidaceae*, the embryo swells and promotes the seed coat rupture, thus forming a cone-shaped structure (Arditti, 1967), also known as protocorm (Bernard, 1909, qt. in Leroux et al., 1997). This structure is considered an intermediate phase between the embryo and the seedling (Leroux et al., 1997). After seed coating rupture, absorbent trichomes appear, the protocorm increases in size, the apical meristem is installed, and the first leaves are formed, all that followed by the development of adventitious root (Arditti, 1967; Harrison, 1977).

Under natural conditions, even photosynthetic orchids undergo a phase of mycorrhizal fungi dependence at their early stages of growth and development, not being able to germinate in their absence (McKendrick et al., 2000; Leake et al., 2004). Some species of green orchids can be germinated *in vitro,* in an asymbiotic way, if soluble carbohydrates and other organic compounds are supplied (Rasmussen and Rasmussen, 2009). Otherwise, it is necessary to establish a symbiotic association with an appropriate fungal partner and a complex carbohydrate source (Zettler, 1997; Peterson et al., 2004). During the symbiotic germination, anatomical analyzes allows the observation of pelotons in protocorm cells of MH species, and transmission electron microscopy is important to investigate and confirm that plant cells containing hyphae remain alive and with intact organelles, ensuring that the association with the fungus is not harmful to the plant. In addition, the latter allows verifying if the hyphae have clamp connections, dolipores, and parenthesomes, typical characteristics of Basidiomycota. As described by Roy et al. (2009), in MH orchid *Epipogium aphyllum*, the authors observed, in electron micrographs, the presence of clamp connections, dolipores, and parenthesomes, and confirmed the identification of *Inocybe*, a basidiomycetous symbiont, by means of molecular techniques.

Orchids can relate to a great diversity of fungal taxa and combine it with different nutritional strategies (Rasmussen, 2002; Peterson et al., 2004). Photosynthetic orchid species are generally associated with rhizoctonia-like fungi group belonging to the families Ceratobasidiaceae, Tulasnellaceae, and Sebacinaceae (Otero et al., 2002; Rasmussen, 2002). However, the heterotrophic species of temperate regions often associate with ectomycorrhizal basidiomycetes, as those of the families Thelephoraceae and Russulaceae (Julou et al., 2005; Roy et al., 2009). In addition, MH species from tropical regions appear to exhibit greater diversity in their symbiotic associations and less degree of specificity when compared with species from temperate regions, associating with predominantly saprophytic fungi (Martos et al., 2009; Selosse et al., 2010). It has been shown in a study by Yagame et al. (2007), which revealed the association of the Asiatic orchid *Epipogium roseum* with saprophytic fungi belonging to *Psathyrella* or *Coprinus* in Coprinaceae, isolated from root and rhizome. Even though most MH species belong to tropical regions, most of the studies include species belonging to temperate regions as models (Selosse et al., 2010).

Although mycorrhizal associations with orchids are predominantly related to the fungi of the phylum Basidiomycota, groups of Ascomycota have already been described forming such association. In a previous work by Selosse et al. (2004), it was possible to verify the formation of pelotons by fungi belonging to the order Pezizales, previously identified as ascomycetes, present in root cells of the green *Epipactis microphylla*, analyzed by light and transmission electron microscopy. According to the authors, an endophyte was found forming this association with the orchid, and it belongs to a fungal group known as ectomycorrhizal in tree roots. Endophytic microorganisms, unlike pathogens, do not cause damage to the host and are known for establishing beneficial or neutral associations with plants (Petrini, 1991). They inhabit the internal part of organs and tissues of plants, and can confer protection against pathogens, or cause the production of plant growth factors (Azevedo, 1998; Ma et al., 2015). Although their role in orchids is rarely addressed, non-mycorrhizal endophytic fungi can be found in all organs of the plant, encompassing more than 110 genera, predominantly belonging to the phylum *Ascomycota* (Ma et al., 2015).

The genus *Pogoniopsis* belongs to the subfamily Vanilloideae, Pogoniae tribe (Cameron, 2009). It is composed only of two species, *Pogoniopsis schenckii* Cogn. and *Pogoniopsis nidusavis* Rchb.f. & Warm., and both are MH. Both develop under organic matter in dense tropical and subtropical forests, are aclorophyllated, and have a pale-yellow coloration. The plants of the genus have short and fasciculate roots, with bracts that cover the floral stem. *P. schenckii* is a poorly-known species, with collections described in several states of Brazil (Bittencourt and de Gasper, 2016). Despite being widely distributed, it is considered a rare species, and it is included in the Red List of the Threatened Flora of Paraná State (1995), and classified as a vulnerable species by the Red List of Threatened Flora of São Paulo State, both in Brazil (2004) (CNCFlora, 2012). In addition, in a recent study, projections on future climate changes indicated that with global warming, the species *P. schenckii* could have its ideal niche reduced by up to 30% of its current extent (Kolanowska et al., 2017), severely compromising its survival. Therefore, studies to understand its germination and biology, as well as strategies to enable its establishment *in vitro,* can be of great value for the conservation of populations of this species.

In a previous analysis, it was possible to observe the presence of fungal hyphae inside the mature fruits of *P. schenckii* (data not shown), and this finding promoted the hypothesis that these fungi could be related to the germination of the species, in addition to those present in the roots. Moreover, there is lack of studies on the endophytic fungi present in other organs of MH orchids and not only in the roots, especially when dealing with their function for germination of these plants (Ma et al., 2015). Therefore, other organs of the species (floral stem and fruits) were also included in the studies of isolation and identification of fungi in order to test such hypothesis. This work was generally aimed at i) investigating the endophytic fungal community of *P. schenckii* and the non-cultivable mycorrhizal fungi present in their roots; ii) evaluating the role of these fungi in germination of the seeds of *P. schenckii*, and iii) monitoring the development of the protocorm after germination.

MATERIAL AND METHODS

Vegetal Sampling Collection

Roots, fruits, and floral stems samples of *P. schenckii* were collected from three populations located at three trails: *Trilha do Poço do*

Pito (TPP), *Trilha do Pirapitinga* (TP), and *Trilha do Garcez* (TG) (**Figure 1**). All trails belong to the Santa Virgínia Nucleus (SVN), located in the Serra do Mar State Park, in the outskirts of the municipalities of São Luiz do Paraitinga and Natividade da Serra, São Paulo State, Brazil. Access to the study area and collection permission was authorized by COTEC through permission (291/2018 D83/2018 PM) and São Paulo State Environment Secretariat (SMA) permission 260108 – 005.510/2014.

Isolation of Fungi and Analysis of Frequency of Isolation

In order to investigate the community of endophytic and mycorrhizal fungi of *P. schenckii*, roots, floral stems, and fruit portions of the three populations were isolated according to the methodology described by Araújo et al. (2001). Healthy plant samples were washed in running water, and then washed for 1 min with 70% ethanol solution, followed by a 3 or 5 min commercial sodium hypochlorite (2% active chlorine) washing, and a 30 s 70% alcohol washing. Finally, two washes were performed in autoclaved distilled water, and an aliquot of the water from the last wash was plated in commercial PDA (potato dextrose agar) medium to verify the efficacy of surface disinfection. After, fragments of about 5 mm were sectioned and inoculated in PDA with addition of ampicillin (75 μg/ml) and left to grow at room temperature in the dark for 5 days. After the incubation period, the grown hyphae were striated in WA (water agar: 7 g/L agar) and kept at room temperature and in the dark. After 3 days, fragments of the WA containing the grown fungal mycelium were inoculated at the center of PDA plates and incubated for 7 days under the same conditions previously described. The isolated fungi were placed in mineral oil and stored.

In order to calculate the frequency of isolation (FI) of fungi, the calculation described in Araújo et al. (2014) was performed, which consists in evaluating the number of plant fragments that presented fungal growth in relation to the total number of fragments sampled.

Total Deoxyribonucleic Acid Extraction and Identification of Isolated Fungi

For identification of the isolated fungi, the methodology of total fungal DNA extraction described in Raeder and Broda (1985), with modifications by Araújo et al. (2014), was used. The fungi were inoculated in PDA and grown for approximately 10 days at room temperature. The grown fungal mycelium was scraped from the surface of the culture medium, crushed in liquid nitrogen, and approximately 200 mg of the crushed mycelium was transferred to a 2 ml tube. Then, 1 ml of extraction buffer (1% SDS, 25 mM EDTA, 250 mM NaCl, and 200 mM Tris-HCl [pH 8.0]) was added to the tube, vortexed, and incubated at 65°C for 20 min. The solution was centrifuged at 10,000 xg for 10 min at 4°C and the supernatant was transferred to a new tube containing 800 μl of phenol. The suspension was homogenized by inversion and centrifuged at 10,000 x*g* for 10 min at 4°C. The supernatant was transferred to a new tube and 400 μl phenol and 400 μl chloroform (1:1) were added. The solution was homogenized by inversion and centrifuged at 10,000 x*g* for 10 min at 4°C. The upper phase was transferred to a new tube containing 800 μl of chloroform, homogenized by inversion, and centrifuged at 10,000 xg for 10 min at 4°C. The supernatant was transferred to a new tube and 450 μl of isopropanol was added. The solution was homogenized by inversion, incubated for 5 min at room temperature and centrifuged at 10,000 x*g* for 5 min at 4°C. The supernatant was discarded and the precipitate (DNA) was washed with 500 μl of 80% ethanol and centrifuged at 10,000 xg for 5 min at 4° C. Then, the ethanol was discarded, the DNA was dried at 37°C for 30 min and finally resuspended in 40 μl of deionized distilled autoclaved water and kept in a refrigerator overnight. The DNA suspension was quantified in a spectrophotometer (NanoDrop 2000c, Thermo Scientific) and stored in a freezer at −20°C.

For amplification of the fragment of interest, amplification of the ITS1-5,8S-ITS2 region was performed using the primers ITS1 (5'-TCCGTACCTCAACCTGCGG-3') and ITS4

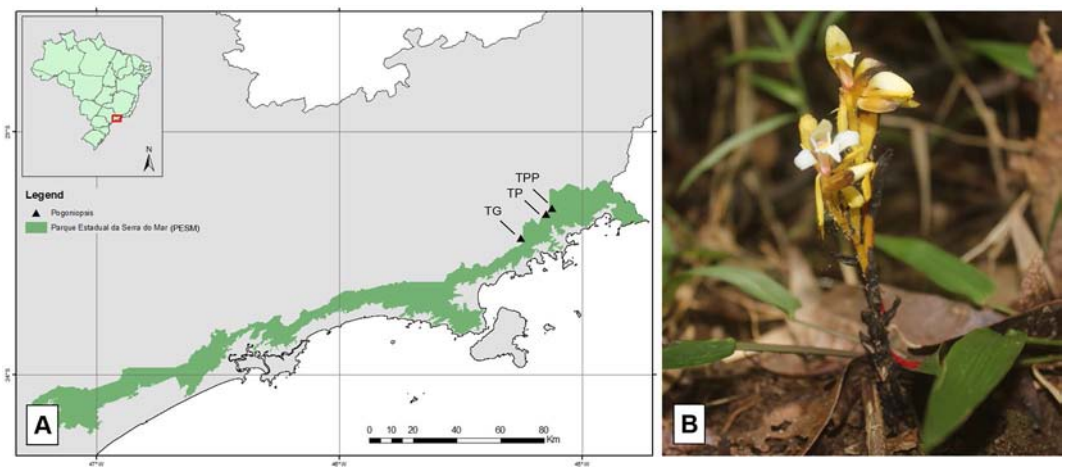

FIGURE 1 | Representation of the Serra do Mar State Park **(A)** (in green) and location of the trials (triangles) where *Pogoniopsis schenckii* **(B)** individuals were collected.

(5'-TCCTCCGCTTATTGATATGC-3') (White et al., 1990). Polymerase chain reaction (PCR) was performed with 3.7 mM $MgCl_2$, 1 mM of each deoxynucleoside triphosphate, 0.4 μM of each primer, 2.5 U of Taq DNA polymerase, 1 X buffer, 5 ng DNA in a final volume of 50 μl. The ITS1-5.8S-ITS2 region of recombinant DNA (rDNA) was amplified by 24 cycles of PCR reaction with initial denaturation of 4 min at 94°C, followed by 24 cycles of 30 s at 94°C, 1 min at 55°C; 30 s at 72°C, and a final extension of 7 min at 72°C in thermal cycler (Peltier Thermal Cycler 200, MJ Research). The reaction product was analyzed by using agarose gel (1% w/v) along with the 1 Kb/100 pb DNA molecular weight marker (Invitrogen). Amplified (400 pb) rDNA ITS1-5, 8S-ITS2 region fragments were sequenced at the company Macrogen (Seoul, South Korea) and the sequences obtained were used for phylogenetic identification on the NCBI (National Center for Biotechnology Information—www.ncbi.nlm.nih.gov) database through Blastn.

A phylogenetic tree was built using the MEGA 10.0 program (Kumar et al., 2018). The alignment was made with MUSCLE default settings. The evolutionary history was inferred according to the neighbor-joining method (Saitou and Nei, 1987), considering bootstrap test (1,000 replicates) (Felsenstein, 1985), and the evolutionary distances were computed using the Jukes-Cantor method (Jukes and Cantor, 1969) (**Figure 2**). Sequences were deposited in GenBank under the accession numbers MN611256 to MN611298.

Total Root Deoxyribonucleic Acid Extraction and Identification of Basidiomycetes

Roots of *P. schenckii.* were used order to investigate the presence of Basidiomycetes that could not be cultivated. For this purpose, DNA extractions were made from root samples of TPP and TP populations, which were collected and promptly stored at −80°C. The methodology used was described in (Tel-Zur et al., 1999), with modifications. In this procedure, the samples were macerated and placed in a microtube, and then 1.5 ml of sorbitol (0,35 M sorbitol, 100 mM Tris-HCl, 5 mM EDTA) was added. The samples were vortexed, incubated in the refrigerator for 20 min, and centrifuged for 10 min at 10,000 x*g* at 4°C. The supernatant is discarded and 800 μl of cetyl trimethylammonium bromide and 30 μl of sakosyl 30% were added. The samples were then vortexed and incubated at 65°C for 1 h. Then 600 μl of chloroform-isoamyl alcohol was added and the samples were vortexed again and centrifuged for 10 min at 10,000 x*g*. The supernatant was placed in a new microtube with 30 μl of ammonia acetate and 500 μl of isopropanol, and the samples were incubated at −20°C overnight. In the next day, samples were

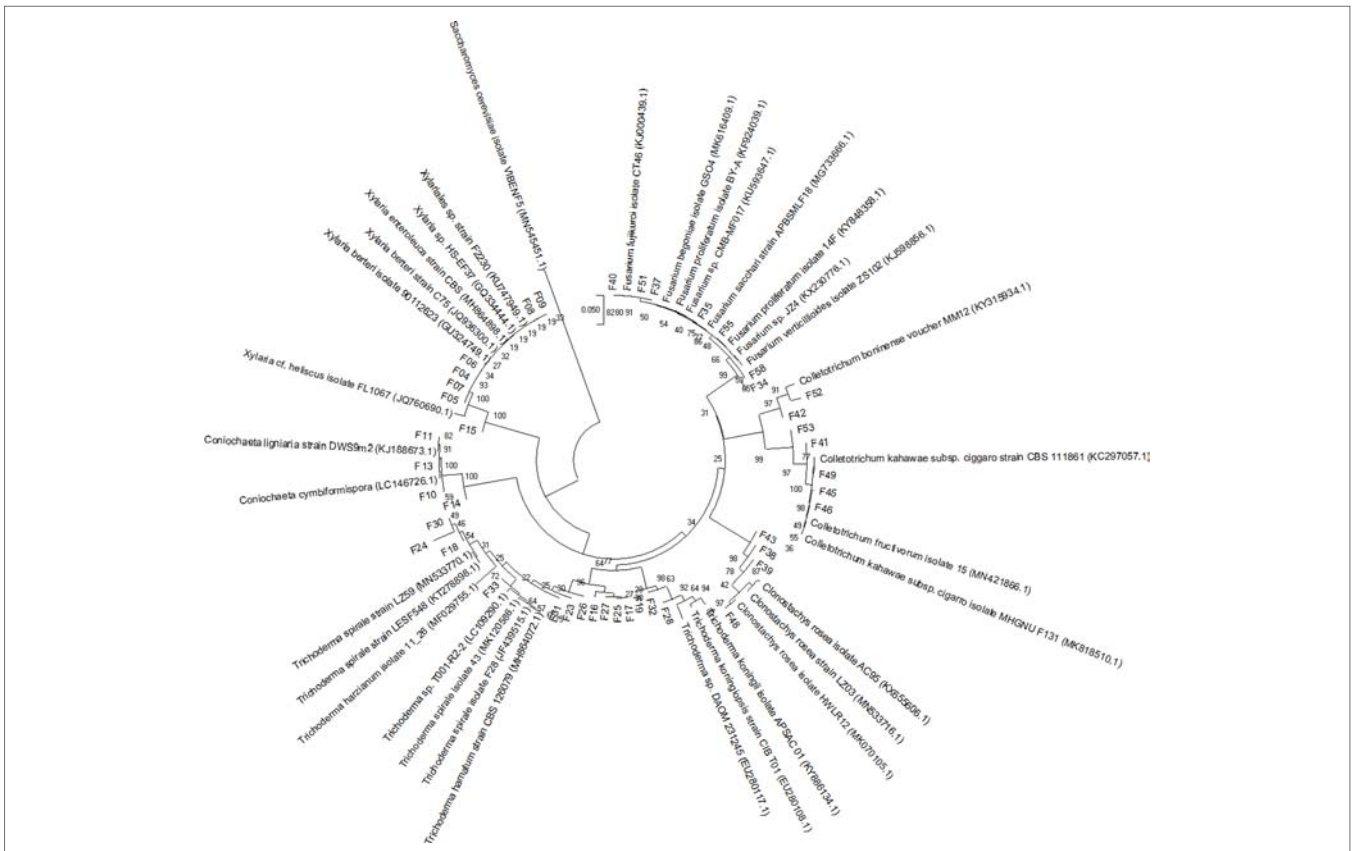

FIGURE 2 | Neighbor-joining tree, based on Jukes and Cantor's model, obtained from the analysis of recombinant DNA internal transcribed spacer sequences of 42 fungi isolated from *Pogoniopsis schenckii*. Reference sequences from GenBank were used to compare the relationships among the isolates. The Basidiomycota *Saccharomyces cerevisiae* (MN545451.5) was used as the out-group. Bootstrap values (n = 1,000 replicates) are shown at the intersections.

centrifuged at 15,000 x*g* for 30 min at 4°C. The supernatant was discarded, 500 µl of 70% ethanol were added and centrifuged for 10 min at 15,000 x*g* at room temperature. The supernatant was discarded again, the samples were incubated at 65°C for 30 min, 50 µl of deionized distilled water is added, and the samples were incubated at 37°C for 2 h. The extraction products were analyzed with 1% agarose gel with the 1 kb molecular weight marker.

The amplification of the region of interest was performed through the primers ITS1-OF and ITS4-OF (Taylor and McCormick, 2008) and following the methodology indicated by the authors. An aliquot of the product of this first reaction was used in a second reaction for the primers ITS4-tul and ITS1, according to their recommendation. The amplified samples were sequenced at the company Macrogen (South Korea) and the sequences obtained were used for phylogenetic identification on the NCBI (National Center for Biotechnology Information—www.ncbi.nlm.nih.gov) database through Blastn.

Symbiotic, Asymbiotic, and *In Situ* Germination

For symbiotic germination trials, fruits from two isolated populations of *P. schenckii* were superficially disinfected according to the methodology described in Pereira et al. (1993) and Araújo et al. (2001). After disinfection, the fruits were sectioned and the seeds removed. The seeds were disinfested by immersion in sodium hypochlorite (1% active chlorine) for 7 min and washed three times with autoclaved distilled water. The seeds were inoculated on filter paper fragments arranged on plates containing OMA-oatmeal agar (2 or 4 g/L oat flour and 7 g/L agar [pH 6.0]), as suggested by Zettler (1997). Each plate was inoculated with the mycelium of fungal representatives isolated from root or fruit of *P. schenckii*; the plates were sealed and incubated in the dark at room temperature. For control purposes, plaques with seeds were maintained in the same culture medium without inoculation of fungi. The seeds were transferred monthly to new plates with oat meal agar and analyzed periodically, and the development of the protocorm was classified in phases, according to their size.

For the asymbiotic germination, the same methodology of disinfestation of the seeds described for the symbiotic germination trial was used. The culture medium used was the MS, proposed by Murashige and Skoog (1962), with modifications. The concentration of micro and macro-nutrients was reduced by half and the medium supplemented with 30 g/L sucrose and 0.5 mg/L nicotinic acid, 0.5 mg/L pyridoxine HCl, 0.1 mg/L thiamine HCl, 2.0 mg/L glycine, and 100 mg/L myo-inositol (pH 6.0). The plates were sealed, incubated in the dark in a growth chamber at 27°C, and analyzed periodically.

For the *in situ* germination trial, a methodology proposed by Rasmussen and Whigham (1993) was used. Several mature fruits of a population of *P. schenckii* were placed in small packages made of nylon, whose pores allow the passage of water and nutrients and soil bacteria and hyphae of filamentous fungi. After being properly sealed, the packages were tied to a stake fixed to the ground and buried superficially under litter in the TPP site, near the same population of plants of their origin. The fruits buried were monitored and recovered periodically for seed germination analysis.

Anatomical, Ultrastructure, and Surface Analysis

Samples of protocorms at different stages, as well as samples of buried field structures, were fixed with 2.5% glutaraldehyde in 3% sodium cacodylate buffer (pH 7.25) for 24 h at 4°C. Post-fixation was performed with 1% aqueous osmium tetroxide (OsO_4) overnight. The samples were then washed three times in distilled water and dehydrated in a rising ethyl series. After dehydration, the samples were soaked in hydrophilic acrylic resin LR White® Hard Grade (EMS) and polymerized in gelatin capsules in an oven at 60°C for 12 h. The ultrafine sections were contrasted with uranyl acetate (Watson, 1958) and lead citrate (Reynolds, 1963) and examined under a Philips EM 100 transmission electron microscope operated at 60 Kv in the Laboratory of Electron Microscopy of the Institute of Biology of UNICAMP.

For analyzes of the anatomical structures of the protocorms, as well as in the transmission electron microscopy analysis, samples of different sizes were processed, ultrafine sections were stained with 0.05% toluidine blue (Sakai, 1973) in phosphate and citrate buffer pH 4.5, and analyzed under a light microscope. To record the results, the images were captured using an Olympus DP71 video camera coupled to an Olympus BX 51 microscope.

To investigate the surface of the samples, protocorms in different phases and fixed in solution of Karnovsky (Karnovsky, 1965) were used. After fixation, the samples were dehydrated in ethyl series and dried by the CO_2 critical point method in a Balzers CPD 030 Critical Point Dryer. The material was then mounted on metal supports and covered with colloidal gold for 220 s with a Bal-Tec SCD 050 Sample Sputter Coater. The analysis and electromicrographic recording were performed using a LEO VP 435 scanning electron microscope at 20 kV, at the Institute of Biology of UNICAMP.

RESULTS

Isolation and Identification of Fungal Community From *Pogoniopsis schenckii* Organs

Thirty-three fungi were isolated from the roots, 19 from the fruits, and 16 from the floral stems of *P. schenckii*. The fungal isolates were purified and stored, totalizing 68 fungi from all populations and different plant organs (**Figure 3**). None of the surface disinfestation methodologies generated fungal contamination in the water of the last wash. Forty-two isolates were identified, all belonging to the phylum Ascomycota. Among the fungi isolated from the roots, the genera *Xylaria* and *Coniochaeta* were found as endophytic in *P. schenckii* individuals from TG population, and only the genus *Trichoderma* were isolated from individuals of TP and TPP populations. As for floral stem and fruit portions of TP and TPP individuals, the genera *Fusarium, Clonostachys*, and *Colletotrichum* were reported in both organs. Further details on isolation and identification of the fungal community can be found in **Supplementary Table 1**.

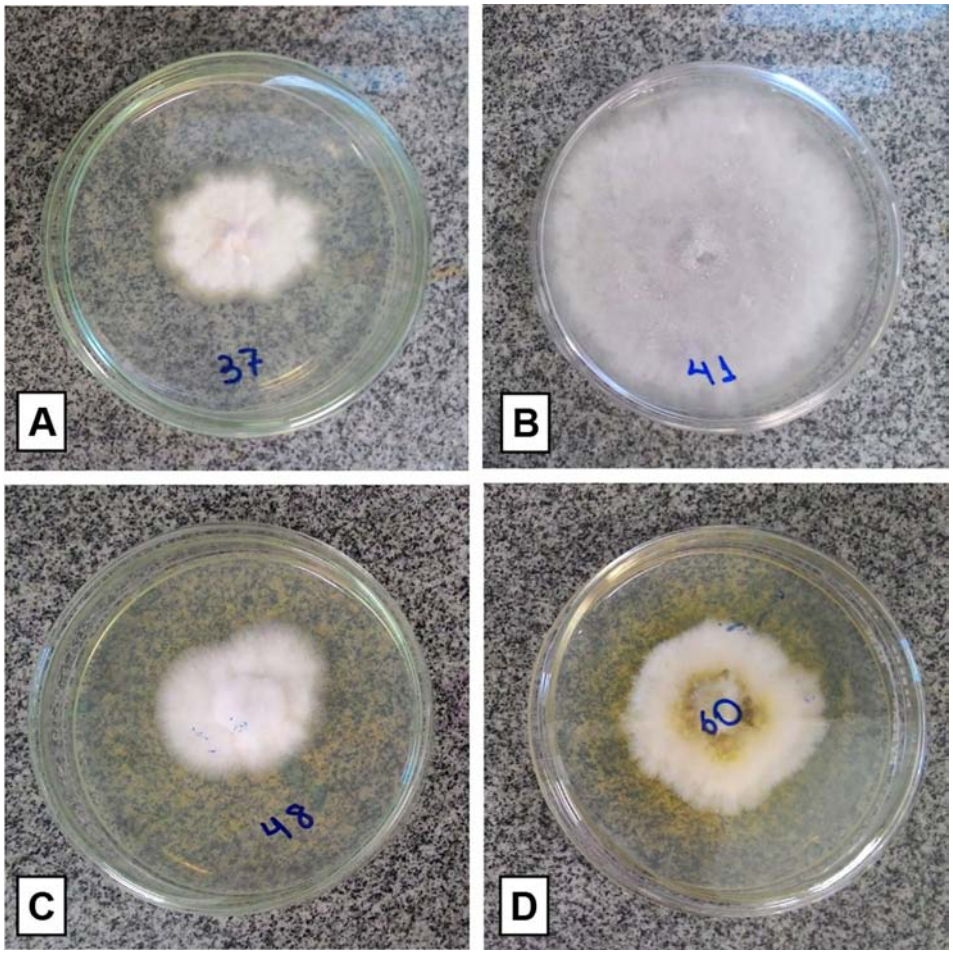

FIGURE 3 | Isolated fungal representatives of different organs of *Pogoniopsis schenckii*. *Fusarium* sp. and *Colletotrichum* sp., respectively, isolated from fruit **(A**, **B)**. *Clonostachys* sp., both isolated from floral stem **(C**, **D)**.

A total of three isolation procedures were carried out at different stages of plant development. Initially, the plant material used for the isolation were root portions of two populations of *P. schenckii*, TG, and TP, through the modified surface disinfestation methodology of Pereira et al. (1993) and Araújo et al. (2001), aiming at increasing the efficiency of disinfestation (5 min in hypochlorite). However, this first trial resulted in the isolation of 15 fungi only from TG population, with isolation frequency (IF) of 12.5%. Therefore, in a second isolation, the authors' methodology was used without modification (3 min in hypochlorite) for isolating fungi from the roots of the plant. In this experiment, FI of 38.8 and 41.6% were obtained for TPP population and TP population, respectively, both located in the SVN, and a total of 18 fungi were isolated from the *P. schenckii* populations. Due to the higher IF obtained in the second experiment, the unmodified methodology was adopted for a third isolation round. In this isolation, fruit and floral stem portions of NSV individuals were used without discriminating the populations, obtaining 100% IF for both organs.

Identification of Non-Cultured Root Basidiomycetes

Identification of the sequences obtained from the roots of *P. schenckii* with the specific primers ITS4-tul and ITS1 revealed the presence of the fungus from genus *Tulasnella*, belonging to family Tulasnellaceae and Basidiomycota phylum.

Germination Trials

In a first trial, beginning in April 2016, a total of 18 fungal representatives isolated from the roots and 13 fungi from the fruits of *P. schenckii* were selected according to their morphology to be inoculated in seeds of TP and TPP populations. After about 20 days of plate incubation, it was possible to observe the external seed coat rupture of both populations in the presence of two fungal isolates from the roots of five from the fruits. At 40 days of experiment, two other fungi, one of root and another of fruit, were able to cause the external seed coat rupture of both populations. However, among the total of nine fungi, three isolates of root, and six of fruit, only the isolates F38 and F39

caused visible changes in the development of the protocorms after the external tegument rupture, both fungi of fruits of *P. schenckii*. The experiment exceeded 15 months, presenting minimal changes only in the size of the protocorms, under magnifying glass. Among the fungi that showed to be effective in germination, they comprise the genera *Trichoderma* sp. (F16, F25, and F32), *Fusarium* sp. (F34, F37, and F40) and *Clonostachys* sp. (F38, F39, and F43).

The mature seeds of *P. schenckii* had a rounded shape and they were slightly tapered at one end. Its external tegument is extremely rigid and dark brown in color (**Figure 4A**). At the initial stage of germination, the seed underwent a slight swelling accompanied by the whitening of the external tegument, almost imperceptible changes. After this stage, the testa rupture occurred (**Figures 4A**, **B**), and the protocorm began to increase in size (**Figures 4C–E**), at a very slow growth rate, assuming a slightly elongated shape (**Figure 4F**).

No changes were observed in the seeds during the whole period of incubation of the asymbiotic germination plates in MS medium, which took about 15 months, suggesting the inefficiency of germination in the absence of fungi and under such cultivation conditions. The same occurred with the sowing and seed recovery trials *in situ*, which did not demonstrate efficacy in the germination of seeds of *P. schenckii* either.

Anatomical, Ultrastructure, and Surface Analysis

Due to its ability to cause changes in protocorm development after external tegument rupture, different stages of seed development incubated with the isolate F38 (*Clonostachys* sp.) were analyzed by scanning electron microscopy. The seeds have an oval shape and a wavy external tegument. At their initial germination stage, it is possible to observe the proliferation of fungal hyphae exclusively in the funicular region of the seeds (**Figure 5A**). Then, the seeds increase in size and the external tegument ruptures (**Figures 5B–D**). The protocorm is exposed, fully covered by hyphae and the development of tector trichomes begins (**Figures 5E, F**). In this phase, the protocorm continues to increase in size, taking an elongated form, and scarce tector trichomes can be observed

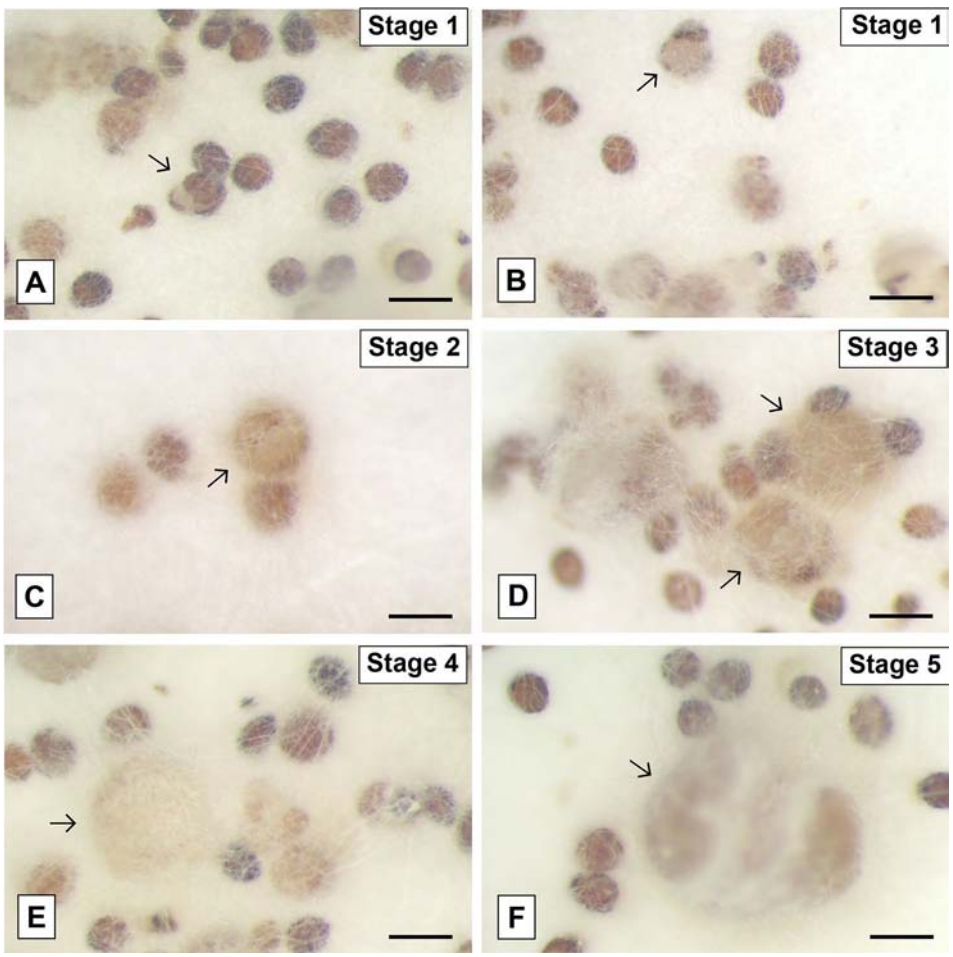

FIGURE 4 | *Pogoniopsis schenckii* seeds inoculated with the fungal isolate of the genus *Clonostachys* (F38) isolated from *P. schenckii* at different stages of the germination. Seeds showing swelling and rupture of the external tegument **(A**, **B)** and subsequent growth and development of the protocorms (arrows) after testa rupture **(C**–**F)**. Scale bar—200 μm.

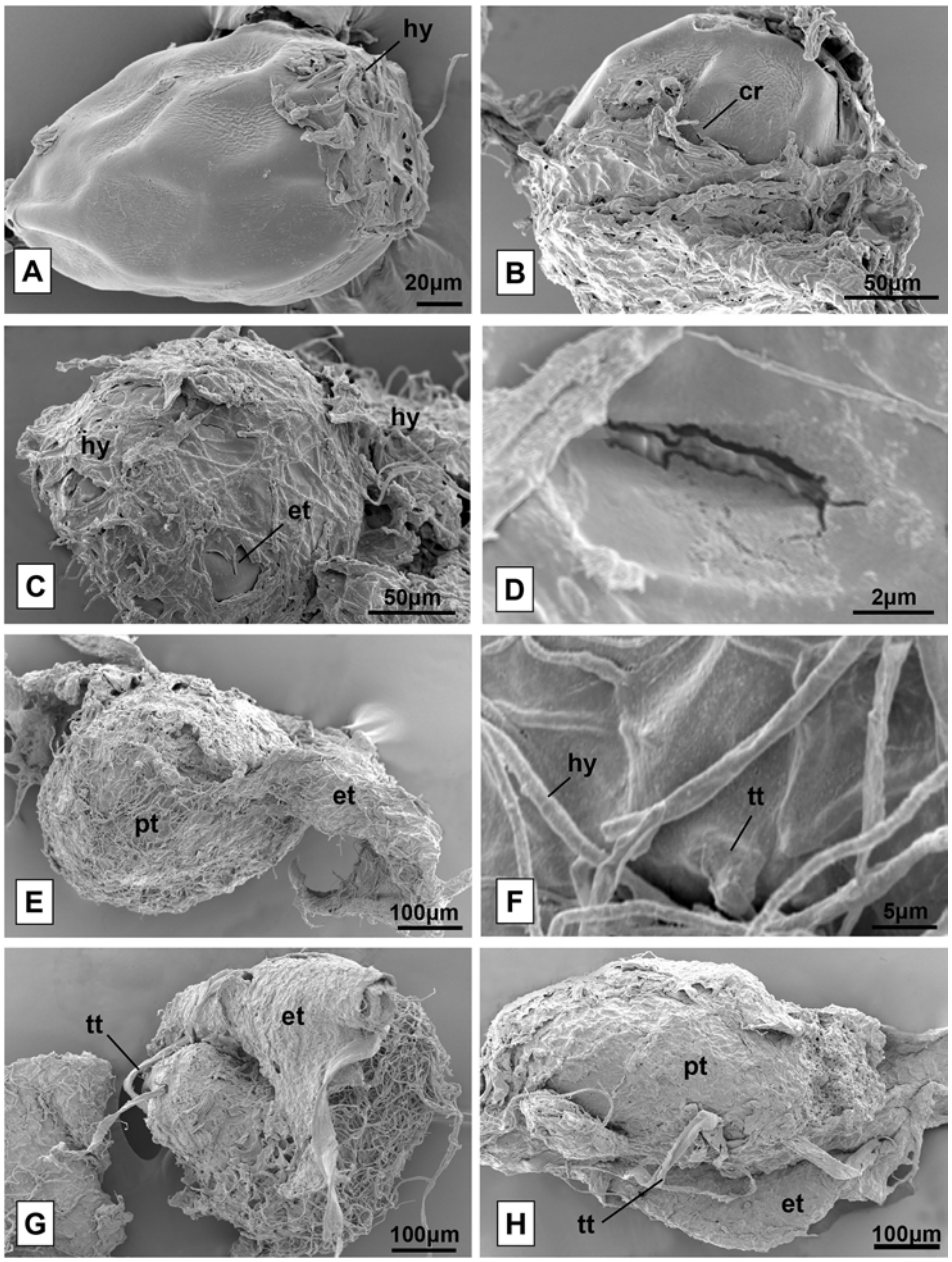

FIGURE 5 | Seeds of *Pogoniopsis schenckii* in co-culture with the isolate F38, under scanning electron microscopy. Seed of *P. schenckii* being infected by fungal hyphae **(A)**. Seeds with cracked external tegument **(B**, **C)** and crack detail **(D)**. Completely cracked external tegument and protocorm exposed and covered by hyphae **(E)** and detail of the beginning of tector trichome formation **(F)**. View of the surface of protocorms and tector trichomes already formed **(G**, **H)**. hy, hyphae; cr, crack; et, external tegument; pt, protocorm; tt, tector trichome.

(**Figures 5G**, **H**). The hyphae growth allowed only partial visualization of the vast majority of protocorms, making it difficult to analyze the samples and collect data.

The light microscopic analysis of the seeds with the onset of external tegument rupture allowed observing that the plant cells were alive and intact. However, no evidence was found of the formation of pelotons or even the growth of hyphae within the cells at this early stage of germination. The living cells have numerous vacuoles widely distributed in their interior and a large mass of fungal hyphae was also observed on the surface of the tegument (**Figure 6A**).

It was possible to verify the presence of intact plant cells through the analysis of transmission electron microscopy of protocorms resulting from the trials of symbiotic germination at different stages of development. As observed in light microscopy, the surface of the protocorm is covered by a mass of fungal hyphae, and fragments of the ruptured external tegument were found (**Figures 6B**, **C**). The cells of the observed protocorm

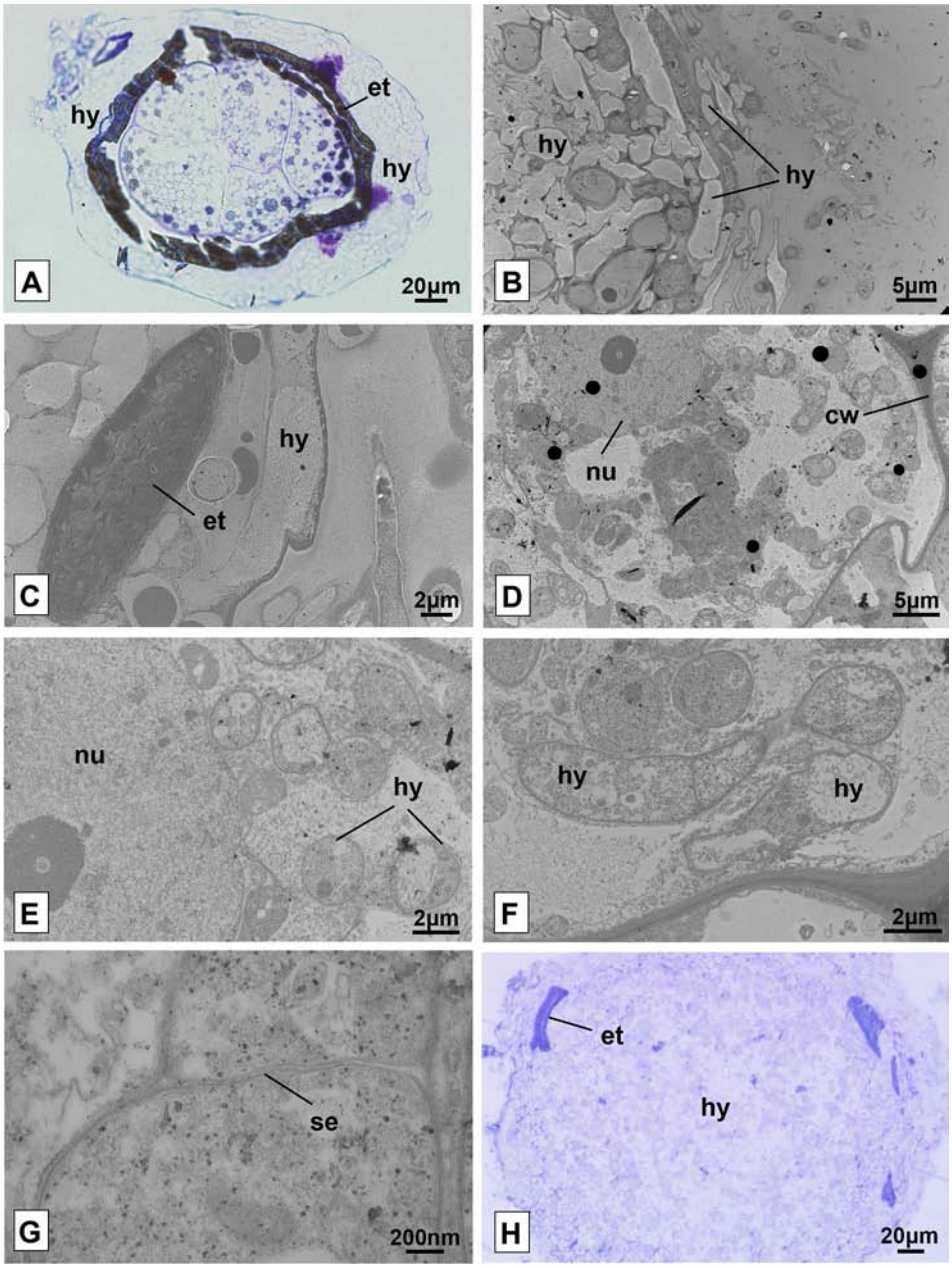

FIGURE 6 | Seeds and protocorms of *Pogoniopsis schenckii* under light and transmission electron microscopy. Seeds showing live cells at stage 1, external tegument scarification, and massive growth of hyphae on its surface after 20 days in co-culture with the isolate F38 **(A)**. Overview of the periphery of the protocorm covered by hyphae **(B)** and detail of fragment of the external integument cracked **(C)**. Integral cell of the protocorm **(D)** and, in detail, cell with evidenced nucleus and hyphae in transverse section **(E)**. Hyphae in longitudinal and transverse section **(F)** and fungal cell septum detail **(G)**. Mass entanglement of hyphae growing from inside the protocorms after phase 5 **(H)**. hy, hyphae; et, external tegument; nu, nucleus; cw, cell wall; se, septum.

had the nucleus and cell wall intact and fungal structures were found occupying much of the interior of the cells, being several times smaller than the first ones (**Figures 6D**, **E**). The hyphae, surrounded by the membrane of the plant cell (**Figure 6E**), presented several structures with distinct patterns, and some hyphae were filled with dense cytoplasmic content and others with little dense content (**Figure 6F**). It was possible to note the absence of clamp connections, dolipores and parenthesomes in the hyphae found (**Figure 6G**). No formation of pelotonswas observed by the fungal isolate of the genus *Clonostachys*.

After phase 5, the growth of the protocorm was no longer observed, which started being degraded by the fungi. Instead, a cluster of fungal hyphae was found occupying the entire interior of the protocorm and expanding beyond the external tegument of the seeds, forming massive structures (**Figure 6H**). It is believed that at some point in development, protocorm structures were degraded and

absorbed by the inoculated fungus, even on plates where protocorms were transferred to new culture media on a monthly basis.

DISCUSSION

Endophytic and Mycorrhizal Community

The community of endophytic cultivable fungi of the MH species *P. schenckii* was characterized for the first time. All the fungi isolated from root, floral stem, and fruit belong to the phylum *Ascomycota* and were grouped in the taxon Sordariomycetes (Ma et al., 2015). The genera *Xylaria* and *Coniochaeta*, reported for TG population roots, were not found in the plants of TPP and TP populations, which presented only the presence of the genus *Trichoderma*. It is interesting to note that TG population is miles away from the other two, and there is a road separating them geographically. As for floral stem and fruit, the genera found were the same for the two organs, and the genera *Fusarium*, *Clonostachys*, and *Colletotrichum* were isolated. According to Ma et al. (2015), the diversity of non-mycorrhizal endophytic fungi of orchids would be more related to the locality of the orchid collection than to other factors, and it may vary from population to population to the detriment of the geographical differences between them.

The genera *Xylaria*, *Trichoderma*, and *Fusarium* are non-mycorrhizal endophytes often found in association with orchids (Ma et al., 2015). The taxon *Xylariaceae* has been repeatedly found in *Dendrobium* sp. (Yuan et al., 2009; Chen et al., 2011; Chen et al., 2013), and *Xylaria* sp. has also been reported in the green orchid *Anoectochilus setáceus,* from which it was possible to extract an important antibacterial compound (Ratnaweera et al., 2014). Antimicrobial properties have also been observed in *Trichoderma* sp., associated with Cupressaceae (Mahdieh and Soltani, 2014). The abundance of compounds with pharmacological properties found in orchids may have the production, to some extent, related to the great diversity of fungal metabolites present in their tissues, which would represent a benefit to the plant in this association (Ma et al., 2015). The production of metabolites by the endophytic fungi isolated from *P. schenckii* was not investigated in this work, and it is a point to be explored. To our best knowledge, *Coniochaeta* was reported only once in recent work by Lee and Eom (2017), associated with a native orchids from Korea, *Coniochaeta mutabilis*.

Some plant pathogens may appear as asymptomatic endophytes in orchids, such as *Trichoderma*, related to diseases in cotton (Lutfunnessa and Shamsi, 2011), and *Fusarium* (Pecoraro et al, 2013). Although some species of *Colletotrichum* have already been listed as pathogens in orchids such as *Oncidium flexuosum*, *Bulbophyllum cylindraceum* and *Coelogyne cristata* (Tao et al., 2013), they have also been found in healthy tissues of *Lepanthes* and *Dendrobium* (Bayman et al., 1997; Chen et al., 2011) as in *P. schenckii.* In this study, the isolations were only performed in tissues and organs of healthy plants, without any apparent disease.

Differently from what is expected from tropical MH orchids, *P. schenckii* is associated with *Tulasnella* sp., belonging to the groups frequently found for green orchids from temperate regions (Rasmussen, 2002; Rasmussen et al., 2015). Fungi belonging to *Tulasnellaceae* have also been reported previously associated with two orchids of the genus *Neottia* (Těšitelová et al., 2015). For green orchids from the Atlantic Forest, there were identification of fungi belonging to the orders *Sebacinales* and *Cantharellales,* described in Oliveira et al. (2014), in addition to the genera *Ceratorhiza* and *Ephulorhiza* reported in a conservation study conducted by Pereira et al. (2005). The methodology used for the molecular identification of the DNA extracted from the roots of *P. schenckii* is quite specific for *Tulasnellaceae*, bringing into question the fact that other species of fungi may be related to this orchid besides the one reported in the present study. This analysis represented a brief investigation to verify the presence of this taxon, known as being a rhizoctonia associated with the roots of *P. schenckii,* considering the absence of mycorrhizal fungi in the isolation trials by means of culture.

Some genera of mycorrhizal fungi may not be able to grow in culture medium or be isolated through conventional techniques, which may explain their absence among the isolated fungi of *P. schenckii*. In their work, Zelmer et al. (1996) had reported the difficulty of isolating mycorrhizal fungi in *Cypripedium acaule* and *Malaxis monophyllos* and, despite the presence of pelotons in root tissues, no mycorrhizal fungi were isolated in their work. For *P. schenckii*, the absence of typical pelotons was also confirmed for the root cells and subterranean system of the species (unpublished data—Flores-Borges, D.N.A). Although the presence of degraded pelotons cannot be discarded. Moreover, no hyphae were observed with clamp connections, dolipores or parenthesomes, typical characteristics of Basidiomycota (Roy et al., 2009), in fungi of roots (unpublished data—Flores-Borges, DNA), as well as of fruits of *P. schenckii* (unpublished data—Alves, MF). Among the difficult cultivable fungi, there are those not related to rhizoctonia (Zelmer et al., 1996). It was not true for the fungus found in this work, *Tulasnella* sp., which, despite being closely related as the group, as well as Ceratobasidiaceae and Sebacinales, was not possible to be verified by means of the culture dependent identification methodology employed in this study. The PDA medium is very nutrient rich and greatly favors the development of fast-growing fungi, which can lead to the non-development of slower-growing fungi such as Tulasnellaceae (Zettler and Corey, 2018).

Germination Trials

Regarding the fungi tested, three genera were able to cause seed germination of *P. schenckii*, namely: *Trichoderma*, *Fusarium*, and *Clonostachys*. Among these, only the genus *Clonostachys* stimulated the development of the protocorm beyond the seed testa rupture. *Fusarium* has previously been reported in the literature as being able to cause seed germination of three green orchids, *Cypripedium reginae*, *Cypripedium parviflorum*, and *Platanthera grandiflora* (Vujanovic et al., 2000), and a century earlier, by Bernard (1900, 1903, 1904), qt. in Vujanovic et al. (2000). Other taxa of Ascomycota have also been related to the germination of terrestrial orchid seeds belonging to Neottieae and Orchideae tribes (Rasmussen et al., 2015). According to Vujanovic et al. (2000), *Fusarium* would be able to produce structures very similar to the shape and distribution of monilioid cells, typical of rhizoctonia, and easily confused with them. As far as it is known, there are no reports in the literature about the germination of orchids by fungi of the genus *Trichoderma* or *Clonostachys*.

In preliminary studies by Yagame et al. (2007), it was not possible to induce the germination of the aclorophyllated orchid *E. roseum* through symbiotic germination in oat meal agar medium despite the use of a mycorrhizal fungus, due to the excessive growth of the fungi in the culture medium, as also reported in the first trials with *P. schenckii*. In subsequent trials, altering oat concentration of the culture medium as well as its renewal by means of periodic transfers of the seeds and protocorms to new plates, it was enough to solve this obstacle. The germination methodology initially cited in this paragraph has been successfully used for several species of green orchids (Stewart and Kane, 2007; Steinfort et al., 2010; Pereira et al., 2015) and, in some cases, for MH ones (Bruns and Read, 2000). The methodology used may not have been adequate to meet the requirements necessary for the complete development of protocorm and establishment of the seedling of this species, or the association with other mycorrhizal fungal taxa may be necessary for this to occur. It is not clear what prevented the later development of the protocorm of *P. schenckii* beyond that reached in this work, and further studies are necessary.

In *in situ* germination experiments by Rasmussen and Whighan (1993), none of the five terrestrial orchid species germinated before 6 months of experiment; two of them, *Liparis liliifolia* and *Tipularia discolor*, were not able to germinate in the 12 months from the beginning of their experiment, and the seeds of *P. schenckii* did not germinate in a period of 18 months. During this period, the seeds remained intermixed by hyphae within the fruits, but without presenting increase in volume or testa rupture (data not shown). As expected, the asymbiotic germination of *P. schenckii* also did not produce results and, to date, no MH orchid species have been able to germinate in the absence of mycorrhizal fungi (Bruns and Read, 2000; McKendrick et al. 2002; Leake et al., 2004; Yagame et al., 2007). Although the *in vitro* symbiotic germination assays show only the initial development of protocorms of *P. schenckii*, and their development is not possible until the establishment of the seedling, this is probably the first report of the germination of a species of heterotrophic and aclorophyllated orchid that is stimulated by the presence of non-mycorrhizal endophytic fungi isolated from roots and, specifically, from fruits.

Protocorm Development

The mycorrhizal interactions within the Orchidaceae family occur from the association between specific fungal taxa of the phylum Basidiomycota and the orchids (Peterson et al., 2004). This interaction can be verified by the ability of the fungus to cause germination of the plant seeds, besides of its capacity to form pelotons inside the living cells of the plant (Peterson et al., 2004; Rasmussen and Rasmussen, 2009). In this study, despite of causing the germination of the seeds of *P. schenckii,* the formation of pelotons in the cells of the protocorm was not observed for the isolate F38, of the genus *Clonostachys*, being that this fungus does not belong to a taxa known as mycorrhizal. Therefore, the interaction between both cannot be classified as mycorrhizal. However, MH orchids are not known to be able to germinate or even develop independently from a mycorrhizal fungus (Rasmussen and Rasmussen, 2009), and even less in the form of culture to which the seeds of *P. schenckii* were submitted, in culture medium with complex carbon sources (Zettler, 1997). Therefore, it is assumed that some degree of interaction between some of the tested fungal isolates and the orchid protocorms has occurred that seed germination and initial protocorm development was stimulated, although it is not of mycorrhizal nature.

CONCLUSION

Identifying fungal endophytes from MH orchids is a key step in understanding species interactions in tropical conditions. All the endophytic fungi present in the roots of *P. schenckii* belonged to the phylum Ascomycota and varied in the detriment of the geographic distance of the populations, as commonly observed for the endophytes of other orchids. The methodology employed for fungal isolation was not able to isolate potentially mycorrhizal fungi from the Tulasnellaceae, found by other means, as well as no other taxon of Basidiomycota.

Differently from what is observed for most of the MH species of tropical regions, *P. schenckii* is associated with fungi commonly found in green orchids. Three different genera of isolated non-mycorrhizal fungi were able to induce the germination of the seeds of the species under the asymbiotic condition and one of them, *Clonostachys* sp., in addition to the external tegument rupture, promoted the initial development of the protocorm. *P. schenkii* protocorms in co-culture with this isolate showed fungal hyphae within living plant cells, but without the formation of typical mycorrhizal pelotons.

P. schenckii was not able to germinate in the absence of fungi or in seeding and seed recovery trials *in situ*. This is the first report of stimulation of the germination of the MH orchid species in the presence of non-mycorrhizal endophytic fungi isolated from above and belowground organs of this orchid species.

DATA AVAILABILITY STATEMENT

All datasets for this study are included in the article/ **Supplementary Material**.

AUTHOR CONTRIBUTIONS

JM and LS initiated and designed the study. LS carried the anatomical analysis, analysis of scanning microscopy, isolation and analysis of fungi, germination trials and writing the manuscript. MB and LS developed the phylogenetic tree. DF-B carried transmission microscopy and SA and SK assisted molecular analysis of fungi and contributed to the drafts. MB and JM supervised the work and assisted and interpreted of the results.

FUNDING

This work was financed by the São Paulo Research Foundation (FAPESP—2015/26479-6), and the National

Council for Scientific and Technological Development (CNPq - 447453/2014-9; 310184/2016-9). We thank CNPq and the Coordination for the Improvement of Higher Education Personnel (CAPES) for the master's degree scholarships to the first author and doctoral scholarship to the second author, respectively. This study was funded in part by CAPES—Finance Code 001.

ACKNOWLEDGMENTS

We thank the Instituto Florestal (Parque Estadual da Serra do Mar, Núcleo Santa Virginia and Núcleo Picinguaba) for the development of the study on a protected public land. We also thank the Laboratory of Electron Microscopy (LME) of Unicamp for assisting in the preparation of samples and microscope analysis. The authors also thank Espaço da Escrita—Pró-Reitoria de Pesquisa—UNICAMP—for the language services provided.

SUPPLEMENTARY MATERIAL

The Supplementary Material for this article can be found online at: https://www.frontiersin.org/articles/10.3389/fpls.2019.01589/full#supplementary-material

REFERENCES

Araújo, W. L., Maccheroni, W.Jr., Aguilar-Vildoso, C. I., Barroso, P. A., Saridakis, H. O., and Azevedo, J. L. (2001). Variability and interactions between endophytic bacteria and fungi isolated from leaf tissues of citrus rootstocks. *Can. J. Microbiol.* 47 (3), 229–236. doi: 10.1139/w00-146

Araújo, W. L., Quecine, M. C., Lacava, P. T., Aguilar-Vildoso, C. I., Marcon, J., Lima, A. O. S., et al. (2014). *Micro-organismos Endofíticos: Aspectos Teóricos e Práticos de Isolamento e Caracterização* (Santarém: UFOPA, PA, Brazil).

Arditti, J. (1967). Factors affecting the germination of orchid seeds. *Bot. Rev.* 33 (1), 1–97. doi: 10.1007/BF02858656

Azevedo, J. L. (1998). Microrganismos endofíticos. *Ecologia microbiana*, 117–137. In: I.S. Melo and J. L. Azevedo (eds.). Ecology Microbial. Jaguariúna, Embrapa-CNPMA

Bayman, P., Lebron, L. L., Tremblay, R. L., and Lodge, D. J. (1997). Variation in endophytic fungi from roots and leaves of Lepanthes (Orchidaceae). *New Phytol.* 135 (1), 143–149. doi: 10.1046/j.1469-8137.1997.00618.x

Bittencourt, F., and de Gasper, A. (2016). First record of Pogoniopsis Rchb. (Orchidaceae: Triphorinae) in Santa Catarina state, southern Brazil. Check List, 12, 1. doi: 10.15560/12.6.1990

Bruns, T. D., and Read, D. J. (2000). In vitro germination of nonphotosynthetic, myco-heterotrophic plants stimulated by fungi isolated from the adult plants. *New Phytol.* 148 (2), 335–342. doi: 10.1046/j.1469-8137.2000.00766.x

Cameron, K. M. (2009). On the value of nuclear and mitochondrial gene sequences for reconstructing the phylogeny of vanilloid orchids (Vanilloideae, Orchidaceae). *Ann. Bot.* 104 (3), 377–385. doi: 10.1093/aob/mcp024

Chen, J., Hu, K. X., Hou, X. Q., and Guo, S. X. (2011). Endophytic fungi assemblages from 10 Dendrobium medicinal plants (Orchidaceae). *World J. Microbiol. Biotechnol.* 27 (5), 1009–1016. doi: 10.1007/s11274-010-0544-y

Chen, J., Zhang, L. C., Xing, Y. M., Wang, Y. Q., Xing, X. K., Zhang, D. W., et al. (2013). Diversity and taxonomy of endophytic xylariaceous fungi from medicinal plants of Dendrobium (Orchidaceae). *PloS One* 8 (3), e58268. doi: 10.1371/journal.pone.0058268

CNCFlora. (2012). Pogoniopsis schenckii in Lista Vermelha da flora brasileira versão. 2 Centro Nacional de Conservação da Flora. Disponível em <http://cncflora.jbrj.gov.br/portal/pt-br/profile/Pogoniopsis schenckii>. Acesso em .

Felsenstein, J. (1985). Confidence limits on phylogenies: an approach using the bootstrap. *Evolution* 39, 783–791. doi: 10.1111/j.1558-5646.1985.tb00420.x

Harrison, C. R. (1977). Ultrastructural and histochemical changes during the germination of Cattleya aurantiaca (Orchidaceae). *Bot. Gaz.* 138 (1), 41–45. doi: 10.1086/336896

Jukes, T. H., and Cantor, C. R. (1969). "Evolution of protein molecules," in *Mammalian Protein Metabolism*. Ed. H. N. Munro (New York: Academic Press), 21–132. doi: 10.1016/B978-1-4832-3211-9.50009-7

Julou, T., Burghardt, B., Gebauer, G., Berveiller, D., Damesin, C., and Selosse, M. A. (2005). Mixotrophy in orchids: insights from a comparative study of green individuals and nonphotosynthetic individuals of Cephalanthera damasonium. *New Phytol.* 166 (2), 639–653. doi: 10.1111/j.1469-8137.2005.01364.x

Karnovsky, M. J. (1965). A formaldehyde-glutaraldehyde fixative of high osmolality for use in eletron microscopy. *J. Cell. Biol.* 27, 137–138.

Kolanowska, M., Kras, M., Lipińska, M., Mystkowska, K., Szlachetko, D. L., and Naczk, A. M. (2017). Global warming not so harmful for all plants-response of holomycotrophic orchid species for the future climate change. *Sci. Rep.* 7 (1), 12704. doi: 10.1038/s41598-017-13088-7

Kumar, S., Stecher, G., Li, M., Knyaz, C., and Tamura, K. (2018). MEGA X: molecular evolutionary genetics analysis across computing platforms. *Mol. Biol. Evol.* 35, 1547–1549. doi: 10.1093/molbev/msy096

Leake, J. R., McKendrick, S. L., Bidartondo, M., and Read, D. J. (2004). Symbiotic germination and development of the myco-heterotroph Monotropa hypopitys in nature and its requirement for locally distributed Tricholoma spp. *New Phytol.* 163 (2), 405–423. doi: 10.1111/j.1469-8137.2004.01115.x

Leake, J. R. (1994). The biology of myco-heterotrophic ('saprophytic') plants. *New Phytol.* 127 (2), 171–216. doi: 10.1111/j.1469-8137.1994.tb04272.x

Lee, B. H., and Eom, A. H. (2017). Five species of endophytic fungi isolated from roots of native orchid plants from Korea. *Korean J. Mycol.* 45 (4), 355–361. doi: 10.4489/KJM.20170041

Leroux, G., Barabé, D., and Vieth, J. (1997). Morphogenesis of the protocorm of Cypripedium acaule (Orchidaceae). *Plant Syst. Evol.* 205 (1–2), 53–72. doi: 10.1007/BF00982797

Lutfunnessa, R. J. F., and Shamsi, S. (2011). Fungal diseases of cotton plant Gossypium hirsutum L. @ in Bangladesh. Dhaka University. *J. Biol. Sci.* 20 (2), 139–146. doi: 10.3329/dujbs.v20i2.8974

Ma, X., Kang, J., Nontachaiyapoom, S., Wen, T., and Hyde, K. D. (2015). Non-mycorrhizal endophytic fungi from orchids. *Curr. Sci.* 109, 72–87.

Mahdieh, S. H. M. and Soltani, J. (2014). Bioactivity of endophytic Trichoderma fungal species from the plant family Cupressaceae. *Ann. Microbiol.* 64 (2), 753–761.

Martos, F., Dulormne, M., Pailler, T., Bonfante, P., Faccio, A., Fournel, J., et al. (2009). Independent recruitment of saprotrophic fungi as mycorrhizal partners by tropical achlorophyllous orchids. *New Phytol.* 184 (3), 668–681. doi: 10.1111/j.1469-8137.2009.02987.x

McKendrick, S. L., Leake, J. R., Taylor, D. L., and Read, D. J. (2000). Symbiotic germination and development of myco-heterotrophic plants in nature: ontogeny of Corallorhiza trifida and characterization of its mycorrhizal fungi. *New Phytol.* 145 (3), 523–537. doi: 10.1046/j.1469-8137.2000.00603.x

McKendrick, S. L., Leake, J. R., Taylor, D. L., and Read, D. J. (2002). Symbiotic germination and development of the myco-heterotrophic orchid Neottia nidus-avis in nature and its requirement for locally distributed Sebacina spp. *New Phytol.* 154 (1), 233–247. doi: 10.1046/j.1469-8137.2002.00372.x

Merckx, V. (2013). *Mycoheterotrophy: the biology of plants living on fungi* (New York, NY: Springer Science and Business Media). doi: 10.1007/978-1-4614-5209-6

Murashige, T., and Skoog, F. (1962). A revised medium for rapid growth and bio assays with tobacco tissue cultures. *Physiol. Plant.* 15 (3), 473–497. doi: 10.1111/j.1399-3054.1962.tb08052.x

Oliveira, S. F., Bocayuva, M. F., Veloso, T. G. R., Bazzolli, D. M. S., da Silva, C. C., Pereira, O. L., et al. (2014). Endophytic and mycorrhizal fungi associated with

roots of endangered native orchids from the Atlantic Forest, Brazil. *Mycorrhiza* 24 (1), 55–64. doi: 10.1007/s00572-013-0512-0

Otero, J. T., Ackerman, J. D., and Bayman, P. (2002). Diversity and host specificity of endophytic Rhizoctonia-like fungi from tropical orchids. *Am. J. Bot.* 89 (11), 1852–1858. doi: 10.3732/ajb.89.11.1852

Pecoraro, L., Girlanda, M., Kull, T., Perini, C., and Perotto, S. (2013). Fungi from the roots of the terrestrial photosynthetic orchid Himantoglossum adriaticum. *Plant Ecol. Evol.* 146 (2), 145–152. doi: 10.5091/plecevo.2013.782

Pereira, J. O., Azevedo, J. L., and Petrini, O. (1993). Endophytic fungi of Stylosanthes: a first report. *Mycologia* 85 (3), 362–364.

Pereira, O. L., Kasuya, M. C. M., Borges, A. C., and Araújo, E. F. D. (2005). Morphological and molecular characterization of mycorrhizal fungi isolated from neotropical orchids in Brazil. *Can. J. Bot.* 83 (1), 54–65. doi: 10.1139/b04-151

Pereira, M. C., Rocha, D. I., Veloso, T. G. R., Pereira, O. L., Francino, D. M. T., Meira, R. M. S. A., et al. (2015). Characterization of seed germination and protocorm development of Cyrtopodium glutiniferum (Orchidaceae) promoted by mycorrhizal fungi Epulorhiza spp. *Acta Botanica Brasilica* 29 (4), 567–574. doi: 10.1590/0102-33062015abb0078

Peterson, R. L., Massicotte, H. B., and Melville, L. H. (2004). *Mycorrhizas: anatomy and cell biology* (Canada: NRC Research Press).

Petrini, O. (1991). Fungal endophytes of tree leaves. In: Andrews J. H. Hirano S. S. editors. *Microbial ecology of leaves*. (New York: Springer). 179–197. doi: 10.1007/978-1-4612-3168-4_9

Raeder, U., and Broda, P. (1985). Rapid preparation of DNA from filamentous fungi. *Lett. In Appl. Microbiol.* 1 (1), 17–20. doi: 10.1111/j.1472-765X.1985.tb01479.x

Rasmussen, H. N., and Rasmussen, F. N. (2009). Orchid mycorrhiza: implications of a mycophagous life style. *Oikos* 118 (3), 334–345. doi: 10.1111/j.1600-0706.2008.17116.x

Rasmussen, H. N., and Whigham, D. F. (1993). Seed ecology of dust seeds in situ: a new study technique and its application in terrestrial orchids. *Am. J. Bot.* 80 (12), 1374–1378. doi: 10.1002/j.1537-2197.1993.tb15381.x

Rasmussen, H. N., Dixon, K. W., Jersáková, J., and Těšitelová, T. (2015). Germination and seedling establishment in orchids: a complex of requirements. *Ann. Bot.* 116 (3), 391–402. doi: 10.1093/aob/mcv087

Rasmussen, H. N. (2002). Recent developments in the study of orchid mycorrhiza. *Plant Soil* 244 (1-2), 149–163. doi: 10.1023/A:1020246715436

Ratnaweera, P. B., Williams, D. E., de Silva, E. D., Wijesundera, R. L., Dalisay, D. S., and Andersen, R. J. (2014). Helvolic acid, an antibacterial nortriterpenoid from a fungal endophyte, Xylaria sp. of orchid Anoectochilus setaceus endemic to Sri Lanka. *Mycology* 5 (1), 23–28. doi: 10.1080/21501203.2014.892905

Reynolds, E. S. (1963). The use of lead citrate at high pH as an electron-opaque stain in electron microscopy. *J. Cell Biol.* 17 (1), 208. doi: 10.1083/jcb.17.1.208

Roy, M., Watthana, S., Stier, A., Richard, F., Vessabutr, S., and Selosse, M. A. (2009). Two mycoheterotrophic orchids from Thailand tropical dipterocarpacean forests associate with a broad diversity of ectomycorrhizal fungi. *BMC Biol.* 7 (1), 51. doi: 10.1186/1741-7007-7-51

Saitou, N., and Nei, M. (1987). The neighbor-joining method: A new method for reconstructing phylogenetic trees. *Mol. Biol. Evol.* 4, 406–425. doi: 10.1093/oxfordjournals.molbev.a040454

Sakai, W. S. (1973). Simple method for differential staining of paraffin embedded plant material using toluidine blue O. *Stain Technol.* 48 (5), 247–249. doi: 10.3109/10520297309116632

Selosse, M. A., Faccio, A., Scappaticci, G., and Bonfante, P. (2004). Chlorophyllous and achlorophyllous specimens of Epipactis microphylla (Neottieae, Orchidaceae) are associated with ectomycorrhizal septomycetes, including truffles. *Microb. Ecol.* 47 (4), 416–426. doi: 10.1007/s00248-003-2034-3

Selosse, M. A., Martos, F., Perry, B., Maj, P., Roy, M., and Pailler, T. (2010). Saprotrophic fungal symbionts in tropical achlorophyllous orchids: finding treasures among the 'molecular scraps'? *Plant Signaling Behav.* 5 (4), 349–353.

Steinfort, U., Verdugo, G., Besoain, X., and Cisternas, M. A. (2010). Mycorrhizal association and symbiotic germination of the terrestrial orchid Bipinnula fimbriata (Poepp.) Johnst (Orchidaceae). Flora-Morphology, Distribution. *Funct. Ecol. Plants* 205 (12), 811–817. doi: 10.1016/j.flora.2010.01.005

Stewart, S. L., and Kane, M. E. (2007). Symbiotic seed germination and evidence for in vitro mycobiont specificity in Spiranthes brevilabris (Orchidaceae) and its implications for species-level conservation. *In Vitro Cell. Dev. Biology-Plant* 43 (3), 178–186. doi: 10.1007/s11627-006-9023-4

Taylor, D. L., and McCormick, M. K. (2008). Internal transcribed spacer primers and sequences for improved characterization of basidiomycetous orchid mycorrhizas. *New Phytol.* 177 (4), 1020–1033.

Těšitelová, T., Kotilínek, M., Jersáková, J., Joly, F. X., Košnar, J., Tatarenko, I., et al. (2015). Two widespread green Neottia species (O rchidaceae) show mycorrhizal preference for S ebacinales in various habitats and ontogenetic stages. *Mol. Ecol.* 24 (5), 1122–1134. doi: 10.1111/mec.13088

Tao, G., Liu, Z. Y., Liu, F., Gao, Y. H., and Cai, L. (2013). Endophytic Colletotrichum species from Bletilla ochracea (Orchidaceae), with descriptions of seven new speices. *Fungal Diversity* 61 (1), 139–164. doi: 10.1007/s13225-013-0254-5

Tel-Zur, N., Abbo, S., Myslabodski, D., and Mizrahi, Y. (1999). Modified CTAB procedure for DNA isolation from epiphytic cacti of the genera Hylocereus and Selenicereus (Cactaceae). *Plant Mol. Biol. Rep.* 17 (3), 249–254. doi: 10.1023/A:1007656315275

Vujanovic, V., St-Arnaud, M., Barabé, D., and Thibeault, G. (2000). Viability testing of orchid seed and the promotion of colouration and germination. *Ann. Bot.* 86 (1), 79–86. doi: 10.1006/anbo.2000.1162

Watson, M. L. (1958). Staining of tissue sections for electron microscopy with heavy metals. *J. Cell Biol.* 4 (4), 475–478. doi: 10.1083/jcb.4.4.475

White, T. J., Bruns, T., Lee, S. J. W. T., and Taylor, J. L. (1990). Amplification and direct sequencing of fungal ribosomal RNA genes for phylogenetics. *PCR protocols: a guide to methods and applications* 18 (1), 315–322. doi: 10.1016/B978-0-12-372180-8.50042-1

Yagame, T., Yamato, M., Mii, M., Suzuki, A., and Iwase, K. (2007). Developmental processes of achlorophyllous orchid, Epipogium roseum: from seed germination to flowering under symbiotic cultivation with mycorrhizal fungus. *J. Plant Res.* 120 (2), 229–236. doi: 10.1007/s10265-006-0044-1

Yuan, Z. L., Chen, Y. C., and Yang, Y. (2009). Diverse non-mycorrhizal fungal endophytes inhabiting an epiphytic, medicinal orchid (Dendrobium nobile): estimation and characterization. *World J. Microbiol. Biotechnol.* 25 (2), 295. doi: 10.1007/s11274-008-9893-1

Zelmer, C. D., Cuthbertson, L., and Currah, R. S. (1996). Fungi associated with terrestrial orchid mycorrhizas, seeds and protocorms. *Mycoscience* 37 (4), 439. doi: 10.1007/BF02461001

Zettler, L. W., and Corey, L. L. (2018). "Orchid Mycorrhizal Fungi: Isolation and Identification Techniques," in *Orchid Propagation: From Laboratories to Greenhouses-Methods and Protocols* (New York, NY: Humana Press), 27–59. doi: 10.1007/978-1-4939-7771-0_2

Zettler, L. W. (1997). Terrestrial orchid conservation by symbiotic seed germination: techniques and perspectives. *Selbyana* 18 (2), 188–194. Retrieved from www.jstor.org/stable/41760433

Conflict of Interest: The authors declare that the research was conducted in the absence of any commercial or financial relationships that could be construed as a potential conflict of interest.

frontiers in Plant Science

ORIGINAL RESEARCH
published: 29 November 2019
doi: 10.3389/fpls.2019.01553

A Phylogenomic Analysis of the Floral Transcriptomes of Sexually Deceptive and Rewarding European Orchids, *Ophrys* and *Gymnadenia*

Laura Piñeiro Fernández [1,2], Kelsey J. R .P. Byers [2,3], Jing Cai [2,4], Khalid E. M. Sedeek [2,5,6], Roman T. Kellenberger [2,7], Alessia Russo [1,2,8], Weihong Qi [9], Catharine Aquino Fournier [9] and Philipp M. Schlüter [1]**

[1] Institute of Botany, University of Hohenheim, Stuttgart, Germany, [2] Department of Systematic and Evolutionary Botany, University of Zurich, Zurich, Switzerland, [3] Department of Zoology, University of Cambridge, Cambridge, United Kingdom, [4] Center for Ecological and Environmental Sciences, Northwestern Polytechnical University, Xi'an, China, [5] Laboratory for Genome Engineering and Synthetic Biology, Division of Biological Sciences, King Abdullah University of Science and Technology, Thuwal, Saudi Arabia, [6] Agricultural Genetic Engineering Research Institute (AGERI), Agriculture Research Centre, Giza, Egypt, [7] Department of Plant Sciences, University of Cambridge, Cambridge, United Kingdom, [8] Department of Plant and Microbial Biology, University of Zurich, Zurich, Switzerland, [9] Functional Genomics Centre Zurich, Zurich, Switzerland

OPEN ACCESS

Edited by:
Jen-Tsung Chen,
National University of Kaohsiung, Taiwan

Reviewed by:
Ashley N. Egan,
Aarhus University, Denmark
Alejandra Vázquez-Lobo,
Universidad Autónoma del Estado de Morelos, Mexico

***Correspondence:**
Laura Piñeiro Fernández
laura.pineiro@systbot.uzh.ch
Philipp M. Schlüter
philipp.schlueter@uni-hohenheim.de

Specialty section:
This article was submitted to Plant Systematics and Evolution, a section of the journal Frontiers in Plant Science

Received: 20 July 2019
Accepted: 07 November 2019
Published: 29 November 2019

Citation:
Piñeiro Fernández L, Byers KJRP, Cai J, Sedeek KEM, Kellenberger RT, Russo A, Qi W, Aquino Fournier C and Schlüter PM (2019) A Phylogenomic Analysis of the Floral Transcriptomes of Sexually Deceptive and Rewarding European Orchids, Ophrys and Gymnadenia. Front. Plant Sci. 10:1553. doi: 10.3389/fpls.2019.01553

The orchids (Orchidaceae) constitute one of the largest and most diverse families of flowering plants. They have evolved a great variety of adaptations to achieve pollination by a diverse group of pollinators. Many orchids reward their pollinators, typically with nectar, but the family is also well-known for employing deceptive pollination strategies in which there is no reward for the pollinator, in the most extreme case by mimicking sexual signals of pollinators. In the European flora, two examples of these different pollination strategies are the sexually deceptive genus *Ophrys* and the rewarding genus *Gymnadenia*, which differ in their level of pollinator specialization; *Ophrys* is typically pollinated by pseudo-copulation of males of a single insect species, whilst *Gymnadenia* attracts a broad range of floral visitors. Here, we present and describe the annotated floral transcriptome of *Ophrys iricolor*, an *Andrena*-pollinated representative of the genus *Ophrys* that is widespread throughout the Aegean. Furthermore, we present additional floral transcriptomes of both sexually deceptive and rewarding orchids, specifically the deceptive *Ophrys insectifera*, *Ophrys aymoninii*, and an updated floral transcriptome of *Ophrys sphegodes,* as well as the floral transcriptomes of the rewarding orchids *Gymnadenia conopsea, Gymnadenia densiflora, Gymnadenia odoratissima*, and *Gymnadenia rhellicani* (syn. *Nigritella rhellicani*). Comparisons of these novel floral transcriptomes reveal few annotation differences between deceptive and rewarding orchids. Since together, these transcriptomes provide a representative sample of the genus-wide taxonomic diversity within *Ophrys* and *Gymnadenia* (Orchidoideae: Orchidinae), we employ a phylogenomic approach to address open questions of phylogenetic relationships within the genera. Specifically, this includes the controversial placement of *O. insectifera* within the *Ophrys* phylogeny and the placement of "*Nigritella*"-type morphologies within the phylogeny of *Gymnadenia*. Whereas in *Gymnadenia*, several

conflicting topologies are supported by a similar number of gene trees, a majority of *Ophrys* gene topologies clearly supports a placement of *O. insectifera* as sister to a clade containing *O. sphegodes*.

Keywords: phylogenomics, orchids, *Ophrys*, *Gymnadenia*, transcriptome, pollination strategy

INTRODUCTION

Orchidaceae and Asteraceae constitute the largest families of flowering plants. Over 800 orchid genera and 25,000 species have been described, with an average rate of 500 species and 13 genera described per year (Cribb et al., 2003; Chase et al., 2015). Orchids have colonized a great variety of geographical ranges, from Scandinavia to Tierra del Fuego (Antonelli et al., 2009; Domínguez and Bahamonde, 2013), although the vast majority of species occur in tropical and neotropical areas (Dressler, 1993). The key to their success has variously been hypothesized to reside in their epiphytic habitat (for tropical orchids) or in their high level of pollinator specialization (Gravendeel et al., 2004; Cozzolino and Widmer, 2005). About two thirds of orchid species present rewards to their visitors, in most cases, nectar (Dafni and Ivri, 1979; Bell et al., 2009; Johnson et al., 2013). These rewarding species are commonly generalized in their pollination, attracting a wide range of pollinators (Brantjes, 1981; Claessens and Kleynen, 2017). However, the ability to produce nectar is missing in one third of species across the family. Instead, they have developed alternative mechanisms based on deception (Ackerman, 1986; Jersáková et al., 2006; Schiestl and Schlüter, 2009; Johnson and Schiestl, 2016). Some of these mechanisms target generalist pollinators, e.g., food deception, where orchids attract pollinators by advertising floral cues that resemble those from rewarding plants (Salzmann et al., 2007; Braunschmid et al., 2017). On the other hand, orchids have also developed mechanisms such as sexual deception to attract highly specialized pollinators. Sexually deceptive flowers produce chemical signals that mimic the sexual pheromones of pollinators, and thus, lead the pollinators to "pseudo-copulate" with the flowers (Kullenberg and Bergström, 1976; Paulus and Gack, 1990; Schiestl et al., 1999). Examples of such behaviour occur in the Australian *Chiloglottis* spp. (Mant et al., 2002; Schiestl et al., 2003), or the recently discovered sexually deceptive *Caladenia abbreviata* (Phillips and Peakall, 2018).

In the European flora, one can find representatives of the aforementioned pollination strategies in the sexually deceptive genus *Ophrys* and the rewarding genus *Gymnadenia,* both within the subtribe Orchidinae (subfamily Orchidoideae) (Inda et al., 2012). Orchids from the Mediterranean genus *Ophrys* attract male pollinators by means of sexual deception (Paulus and Gack, 1990; Ayasse et al., 2000; Schiestl et al., 2000). Attractiveness to pollinators in the genus is highly species-specific, that is, each *Ophrys* species normally attracts a single pollinator species (Paulus and Gack, 1990; Paulus, 2018) by releasing chemicals (for solitary bees, mostly alkenes) mimicking the female sex pheromones (Schiestl et al., 2000; Schlüter and Schiestl, 2008; Xu et al., 2012). This high specificity acts as a pre-zygotic barrier and facilitates reproductive isolation between orchid species (Xu et al., 2011; Xu et al., 2012; Paulus, 2018). *Ophrys* is a recently diverged genus (crown age estimated ca. 5 Ma) with ancestral wasp pollination (Breitkopf et al., 2015), but extant species are commonly pollinated by solitary bees, e.g. *Eucera* or *Andrena* (Paulus and Gack, 1990; Gaskett, 2011). Successful floral isolation and species divergence in the genus may easily be achieved by shifts between similar pollinators, where small changes in genes involved in the pheromone profiles can lead to attraction of new, related pollinators (Schlüter et al., 2011; Sedeek et al., 2014; Schlüter, 2018). For instance, after two independent shifts to (mostly) *Andrena* solitary bee pollination (Breitkopf et al., 2015), two parallel adaptive radiations have taken place simultaneously within the last ca. 1 Ma, yielding two major clades, the *Ophrys sphegodes* and the *Ophrys fusca* species complexes. In line with its recent radiation, a large amount of genetic polymorphism is shared across closely related species within the *O. sphegodes* complex, which has been attributed to common ancestry rather than independent mutations or recent hybridization, although a hybridization event *prior* to radiation seems distinctly possible (Sedeek et al., 2014; Roma et al., 2018; Cozzolino et al., 2019). Coalescence theory predicts that in the case of a radiation, the time of coalescence of these polymorphic alleles will often predate the split of species (Takahata, 1989). Yet, or maybe because of this, phylogenetic relationships within *Ophrys* remain controversial, with different markers in the genome potentially painting different pictures of relationships (Cozzolino et al., 2019). Phylogenetically, the ca. 10 main *Ophrys* lineages are split into three major clades (where clade α includes *Ophrys insectifera*, β includes the *O. fusca s.l.* lineage and γ includes the *O. sphegodes s.l.* lineage) and the relationships among major lineages within these clades are relatively clear, although one major question remains unclear. In particular, the placement of the wasp-pollinated *O. insectifera* L. (clade α) within the *Ophrys* phylogeny has been suggested to be either the earliest-branching lineage [topology: $(\alpha,(\beta,\gamma))$] or more closely related to the *O. sphegodes* lineage [topology: $(\beta,(\alpha,\gamma))$] (cf. e.g. Breitkopf et al., 2015; Bateman et al., 2018b, and references therein).

The Eurasian genus *Gymnadenia* is characterized by fragrant, purple to white, resupinate flowers that mainly attract diurnal and nocturnal Lepidoptera species offering nectar as a reward. Although they attract a wide range of Lepidoptera, and some species are found in sympatry, pollinator overlap is minimal between most species (Vöth, 2000; Huber et al., 2005; Claessens and Kleynen, 2011) and strong pollinator-mediated reproductive isolation has been reported between the putative sister species *G. odoratissima* (L.) Richard and *Gymnadenia conopsea* (L.) Brown (Sun et al., 2015). The latter species is strongly genetically differentiated from the morphologically similar taxon *G.*

densiflora (Wahlenberg) Dietrich (Stark et al., 2011). Finally, the Alpine *G. rhellicani* (Teppner & E. Klein) Teppner & E. Klein (syn. *Nigritella rhelliani*) represents a morphologically distinct lineage within the genus, characterized by extremely dense inflorescences, generally dark red and without resupination, i.e. the labellum remains pointing upwards as opposed to rotated downwards as in other *Gymnadenia* species. The former genus *Nigritella* was merged into *Gymnadenia* only following molecular phylogenies (Hedrén et al., 2000). Previous phylogenetic analysis have shown that *Gymnadenia odoratissima* is sister to *Gymnadenia conopsea*, and *Gymnadenia densiflora* forms a clade with *Gymnadenia rhellicani* (Bateman et al., 2003; Sun et al., 2015). However, these relationships remain contentious, since other studies support a sister-group relationship among *Nigritella* and the "classical" genus *Gymnadenia* (Hedrén et al., 2000; Brandrud et al., 2019). Hence, further attention is warranted, especially to clarify the position of *Nigritella*. The age of the most recent common ancestor shared among all *Gymnadenia/Nigritella* species is estimated to be around 2.5–3 Ma (Inda et al., 2012).

Due to the high taxonomic complexity of Orchidaceae, reconstructing phylogenetic patterns to understand relationships in the family remains challenging. In the last decades, phylogenetic studies in orchids moved from a morphological (Chittka and Menzel, 1992; Gravendeel et al., 2004) to a molecular approach aiming to provide a better insight into orchid relationships (Cameron et al., 1999; Stark et al., 2011; Inda et al., 2012; Breitkopf et al., 2015; Givnish et al., 2015; Bateman et al., 2018a). Previously, the focus of these analyses was at the level of using few genetic markers, e.g. ITS, to reconstruct phylogenies. However, this approach can be problematic as some markers are chosen by their relevance or suitability in a certain taxonomic group, even though they could present low resolution for certain taxonomic groups (Capella-Gutiérrez et al., 2014). Moreover, this approach generally focuses on estimating one coherent tree (e.g. by concatenating sequences), which ignores the fact that different loci can have different phylogenetic histories. Especially when dealing with recently diverged groups with incomplete lineage sorting (Pamilo and Nei, 1988), a genomic approach focusing on understanding patterns on different gene genealogies, may allow the quantification of the different phylogenetic scenarios and thus, be more informative on the evolutionary history of a group (Pease and Hahn, 2015; Pease et al., 2016). Orthologous genes, described as homologous genes that originated from a common ancestral gene as a result of the speciation process (Fitch, 1970), tend to retain the original function from the common ancestor over evolutionary time (Jensen, 2001). Thus, groups of orthologous genes within gene families, together with a genome-wide approach, are perfect candidates to resolve orchid phylogeny and effectively clarify their relationships in an evolutionary framework (Li et al., 2003; Deng et al., 2015).

Here, we present the novel floral transcriptome of the Mediterranean sexually deceptive orchid *Ophrys iricolor* Desf., a representative of the genus *Ophrys* in the Aegean area, which is considered to be a member of the *O. fusca* group (clade β) and represents the evolutionarily distinct abdomen-pollinated members of the genus (previous section *Pseudophrys*) (Schlüter et al., 2009). In addition, we present several floral transcriptomes of both rewarding and deceptive orchids of the subtribe Orchidinae, particularly the rewarding orchids *G. conopsea, G. densiflora, G. odoratissima*, and *G. rhellicani*, together with the sexually deceptive *O. insectifera*, *Ophrys aymoninii* (Breistroffer) Buttler, and finally, an updated transcriptome of *O. sphegodes s.l.* (Sedeek et al., 2013). Using a set of orthologous genes, we employ a genome-wide approach to phylogenetic analysis of these novel floral transcriptomes together with published orchid transcriptomic/genomic data, to compare the transcriptomes of deceptive and rewarding orchids. Furthermore, as these transcriptomes cover the genus-wide taxonomic diversity within *Ophrys* and *Gymnadenia*, our objectives are to elucidate (1) the placement of the *O. insectifera* complex within the three major clades in the *Ophrys* phylogeny, (2) the placement of the morphologically distinct *G. rhellicani* (and presumably other members of subgenus *Nigritella*) within the phylogeny of *Gymnadenia* and (3) whether there is evidence of introgression due to shared pollinators in distinct *Ophrys* lineages.

MATERIAL AND METHODS

Plant Material

The novel *Ophrys iricolor s.l.* (*O. iricolor s.s.* and *Ophrys mesaritica* H.F. Paulus, C. Alibertis & A. Alibertis) cross-species transcriptome is presented here. Data from the putative sister species *O. iricolor s.s.* and *O. mesaritica* (Schlüter et al., 2009) were assembled into a single transcriptome due to expected high levels of allele sharing among the group, as seen in the *O. sphegodes* complex (Sedeek et al., 2013; Sedeek et al., 2014). Sample size (*Ophrys iricolor s.l.,* N = 16 biological replicates; *O. sphegodes s.l.,* N = 37) and provenance are listed in **Table 1**. The previously published cross-species *O. sphegodes s.l.* (*O. exaltata* subsp. *archipelagi* (Gölz & H.R. Reinhard) Del Prete, *O. garganica* Nelson ex O. & E. Danesch, and *O. sphegodes* Miller) transcriptome (Sedeek et al., 2013) is here updated with data from additional samples, including from *O. incubacea* Bianca (samples from Sedeek et al., 2014) within the same species complex that is characterized by the aforementioned high levels of allele and transcript sharing among species (Sedeek et al., 2013; Sedeek et al., 2014) and is hence covered in a single cross-species transcriptome assembly. Additionally, *O. insectifera* and *O. aymoninii* transcriptomes are also presented here. Data from *O. insectifera* and *O. aymoninii* (collected in Gervasi et al., 2017), were assembled into separate transcriptomes because these species are pollinated by different types of pollinators (*O. insectifera* is wasp-pollinated, while *O. aymoninii* is *Andrena*-pollinated) and the assumption of high levels of within-group allele sharing cannot be made. Finally, sampled flowers from the clearly distinct species *G. conopsea, G. densiflora, G. odoratissima* and *G. rhellicani* (from Kellenberger et al., 2019) were used to create individual transcriptome assemblies for these species to complement the published cross-species *Gymnadenia* transcriptome assembly (N = 10,

TABLE 1 | Statistics of transcriptomic data for each species/assembly.

Assembly	*O. iricolor s.l.* complex	*O. sphegodes s.l.* complex v.2	*O. insectifera*	*O. aymoninii*	*Gymnadenia* spp. cross-species assembly[3]	*G. conopsea*	*G. densiflora*	*G. odoratissima*	*G. rhellicani*
Number of biological samples[1]	16 (I: 8, M: 8)[a,b]	37 (E: 9, G: 10, I: 8, S: 10)[c,d,e]	1	1	10 (C: 1; D: 2; O: 1; R: 6)[f]	1	2	1	6
Sample origin[2]	this study: Crete, Greece[g]	R1, R2	R3	R3	R4	R4	R4	R4	R4
Assembly[2]	this study	v1: R5, v2: this study	this study	this study	R4	this study[h]	this study[h]	this study[h]	this study[h]
Illumina Technology	HiSeq 2000 (PE100)	HiSeq 2000 (PE100)	HiSeq 2000 (PE100)	HiSeq 2000 (PE100)	HiSeq 2500 (PE125)	HiSeq 2500 (PE125)	HiSeq 2500 (PE125)	HiSeq 2500 (PE125)	HiSeq 2500 (PE125)
Number of PE reads	493 522 864	1 340 285 065	43 629 062	41 727 306	191 906 267	8 364 102	45 753 532	21 459 264	116 329 369
Sequenced bases (Gbp)	98.7	268.1	8.7	8.3	48.0	2.1	11.4	5.4	29.1
Number contigs	131 528	547 360	81 951	66 505	589 218	100 467	255 230	144 454	430 600
GC%	42.41	41.41	44.76	44.97	44.22	46.45	45.37	44.10	44.08
N50 length	1018	973	1107	1200	553	1152	1295	1126	826
SRA accessions	PRJNA574279	PRJNA574279	PRJNA574279	PRJNA574279	PRJNA504609	PRJNA504609	PRJNA504609	PRJNA504609	PRJNA504609
TSA accession number	GHXI00000000	GHXJ00000000	GHWX00000000	GHWW00000000	figshare: 7314731[i]	GHXG00000000	GHXE00000000	GHXF00000000	GHXH00000000

[1]*Generally, for Ophrys, one biological sample refers to one fresh, anthetic unpollinated flower labellum of one plant individual collected in the field, except as detailed under note* [d] *for O. sphegodes s.l. v.2, or, for Gymnadenia, to a small number of anthetic flowers;*

[2]*References are R1:* Schlüter et al. (2011), *R2:* Sedeek et al. (2014), *R3:* Gervasi et al. (2017), *R4:* Kellenberger et al. (2019), *R5:* Sedeek et al. (2013);

[3]*Raw sequencing data for this column represents the sum of data from all Gymnadenia samples;*

[a]*Species are I: O. iricolor, M: O. mesaritica;* [b]*one O. iricolor sample failed to produce results;* [c]*species are E: O. exaltata subsp. archipelagi, G: O. garganica, I: O. incubacea, S: O. sphegodes;* [d]*for O. exaltata, O. garganica and O. sphegodes, one sample each was derived from labella at bud stage (same biological individuals as used for open flowers), and one sample each of these species was field-collected whereas the remaining samples were grown under greenhouse conditions (*Schlüter et al., 2011*);* [e]*for O. incubacea, 3 were sampled under greenhouse conditions and 5 were collected in the field and were added in a second sequencing batch;* [f]*species are C: G. conopsea, D: G. densiflora, O: G. odoratissima, R: G. rhellicani;* [g]*O. mesaritica was sampled at Pirgos, Crete (28 February 2013; accessions PMS540 A,D,K,N,O,Q,R,T) and O. iricolor at Kato Chorio, Crete (8 April 2013; accessions PMS558 E, I), Vasiliki, Crete (9 April 2013; PMS560 A, C) and at Jouchtas, Crete (10 April 2013; PMS561 A, I, H, O), all under permit number 125001/95 issued on 28 January 2013 by the Hellenic Republic Ministry Of The Environment, Energy & Climate Change, Athens, Greece.* [h]*Raw sequencing data published by* Kellenberger et al. (2019). [i]*Figshare rather than TSA identifier.*

Table 1) (Kellenberger et al., 2019). As far as it was possible to ascertain pollination status (not always possible for *Gymnadenia* flowers), all samples used in this study were from unpollinated flowers of diploid individuals. Flowers were flash-frozen and stored at -80°C until RNA extraction was conducted as detailed by Kellenberger et al. (2019). Since polyploids are known from *Gymnadenia* and (occasionally) *Ophrys* and to ensure that all samples sequenced were diploid, ploidy levels of *O. iricolor* and *O. mesaritica* were checked *via* flow cytometry of pollinia as described by Xu et al. (2011) using a Cell Lab Quanta™ SC-MPL flow cytometer (Beckman Coulter, Fullerton, Canada). *Phaseolus coccineus* "Scarlett Emperor" (sativa Rheinau SG, Switzerland) leaf material was used as internal standard. Ploidy levels were previously described for *O. sphegodes s.l.* (Sedeek et al., 2014), *O. insectifera* and *O. aymoninii* (Gervasi et al., 2017) and the four *Gymnadenia* species (Kellenberger et al., 2019) used in this study, including all sequenced individuals.

RNA Extraction, Library Preparation and Sequencing

Total RNA was extracted separately for each biological individual and tissue with TRIzol reagent (Thermo Fisher Scientific, Massachusetts) according to the manufacturer's protocol followed by a purification step using Qiagen RNeasy MinElute Cleanup Kit (Qiagen, Netherlands). Quality of the isolated RNA was determined with a Qubit® (1.0) Fluorometer (Life Technologies, California, USA) and a Bioanalyzer 2100 (Agilent, Waldbronn, Germany). Paired-end sequencing was performed on the Illumina HiSeq 2000 or 2500 platforms (Illumina, Inc, California, USA) for *Ophrys* and *Gymnadenia* samples (**Table 1**), generating separate files for each biological sample.

Transcriptome Assemblies and Functional Annotation

Individual reads were first aligned to PhiX Control library (Illumina) sequences using bowtie2 v2.2.4 (Langmead and Salzberg, 2012) to remove sequencing control reads. Filtered reads were trimmed using Trimmomatic v. 0.36 (Bolger et al., 2014) to remove any Illumina adapters. Surviving reads were then de-novo assembled to transcripts using Trinity r20140717/ v. 2.0.618 (Grabherr et al., 2011). In the case of *O. sphegodes*, where a previous assembly based on 454, Solexa and Sanger data was available (Sedeek et al., 2013), additional Illumina HiSeq reads were assembled with Trinity as described above and then merged with the published assembly using cd-hit-est (Li and Godzik, 2006; Fu et al., 2012) (95% sequence identity threshold with full length alignment coverage for the shorter sequence). Protein coding regions were analysed using TransDecoder r20140704 (http://transdecoder.github.io) (Haas et al., 2013). The assembled contigs were annotated with the standard Trinotate annotation pipeline (https://trinotate.github.io/) (Grabherr et al., 2011) against Swissprot (Boeckmann et al., 2003), Pfam (Finn et al., 2014), TmHMM (Krogh et al., 2001), Gene Ontology (Ashburner et al., 2000) and SignalP (Petersen et al., 2011). Due to high levels of overlap among the four single-species *Gymnadenia* transcriptomes (**Figure S1B**), we annotated only the cross-species *Gymnadenia* transcriptome from all four species. For purposes of comparison, we also updated the annotation of the previously published, updated (v.2) transcriptome of *O. sphegodes* (Sedeek et al., 2013) with Trinotate. Finally, to estimate the completeness of the transcriptomes, we performed a BUSCO v3.1.0 assessment (Simão et al., 2015) with the lineage databases embryophyta_odb10 and liliopsida_odb10 (**Figures 1A**, **B**).

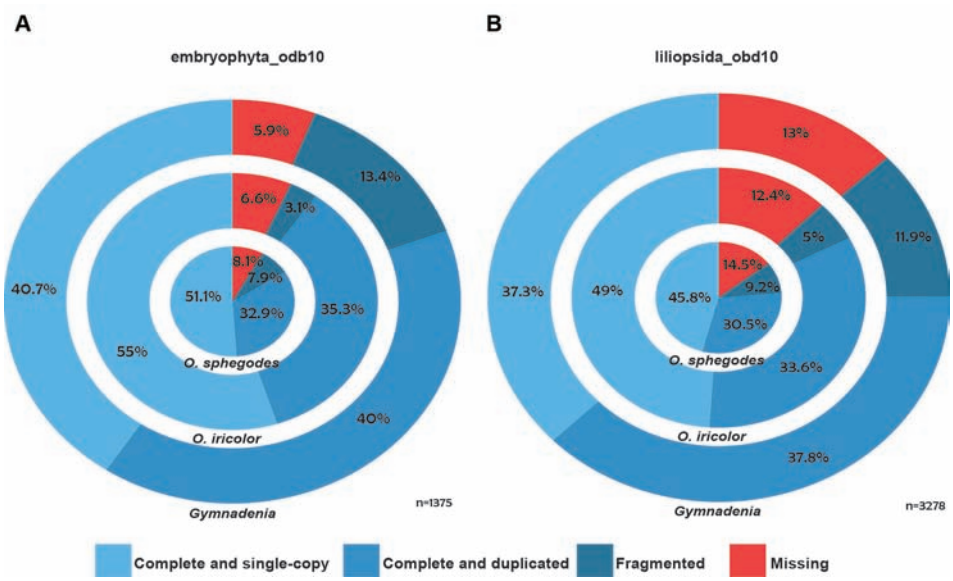

FIGURE 1 | BUSCO assessment. Concentric circles show the BUSCO assessment of *O. sphegodes* v.2, *O. iricolor* and cross-species *Gymnadenia* spp. transcriptomes (from inside to outside), where the first three (blue) categories together are taken as an estimation of transcriptome "completeness". **(A)** BUSCO results with embryophyta_odb10 and **(B)** the larger liliopsida_odb10 databases.

Phylogenomic Analysis

OrthoMCL v2.0.9 (Li et al., 2003) was used under the MySQL v14.14 server to identify orthologous groups based on annotated coding sequences (CDS) (where no annotated CDS were available, they were derived by TransDecoder as above) of 15 members of the Orchidaceae family including the above described *Ophrys* and the four *Gymnadenia* single-species transcriptome assemblies together with the transcriptomes/genomes of *Apostasia shenzhenica* and *Phalaenopsis equestris* (Zhang et al., 2017), *Dactylorhiza fuchsii* (Balao et al., 2017), *Chiloglottis trapeziformis* (Wong et al., 2017), *Dendrobium catenatum* (Zhang et al., 2016), and *Platanthera clavellata* and *Goodyera pubescens* (retrieved from the 1KP project; http://www.onekp.com/). Following the TranslatorX pipeline (Abascal et al., 2010), sequences were aligned using Mafft v7.407 (Katoh and Standley, 2013). To construct phylogenetic trees, a pipeline as described in Xu et al. (2017) was followed. In brief, poorly aligned sequences were removed using trimal v1.2 (Capella-Gutiérrez et al., 2009). Selection of the best-fit models of nucleotide substitution was performed with jModelTest 2.1.10 (Santorum et al., 2014), with parameters: -f -i -g 4 -a -AIC -s 3. This allowed the inclusion of models with unequal base frequencies, a proportion invariable sites, rate variation among sites and set 4 categories, model-averaged phylogeny for each active criterion. Moreover, it used AIC (Akaike Information Criterion) for model selection and accounted for 3 substitution schemes. Maximum likelihood trees of the best-fit models were calculated with phyML 3.3 (Guindon and Gascuel, 2003). For each taxonomically fully sampled orthologous group, tree topologies from *Ophrys* and *Gymnadenia* single-copy gene branches were extracted. In addition, we also extracted topologies where one *Ophrys* species was missing. The extraction of tree topologies was automated with an in-house R script. Moreover, for both *Ophrys* and *Gymnadenia*, we extracted topologies where gene duplications happened only within a monophyletic group of a given species. In the latter case, all but one of the duplicate tips was dropped from the phylogeny (keep.tip function from the package ape for R v3.5.0) (R Core Team, 2001). After retrieving (rooted) topologies of target groups, we compared these topologies with Robinson-Foulds distances, where a distance of 0 indicates that topologies are in full agreement with each other (Robinson and Foulds, 1981), using the package phytools (Revell, 2012) for R. Tree visualization was performed using the Bioconductor package Ggtree (Yu et al., 2017) for R. Finally, we compared the annotation, particularly the GO Plant Slim terms, of the different topologies observed for *Ophrys* and *Gymnadenia*.

RESULTS

Transcriptome Assemblies and Functional Annotation

All *Ophrys* individuals were diploid (**Figure S2** for *O. iricolor s.l.*), consistent with previous studies (Xu et al., 2011; Sedeek et al., 2014). After sequencing, a total of 493.5 million paired-end (PE) reads from *O. iricolor* and 191.9 million from *Gymnadenia* were produced (**Table 1**). All the raw sequencing data (totalling 431.8 Gbp from 2111 million PE reads) are available in the Sequence Read Archive (SRA) of the National Center for Biotechnology Information (NCBI) under the accession numbers in **Table 1**. We successfully produced 131,528 and 589,218 contigs (**Table 1**) for *O. iricolor* and for the *Gymnadenia* cross-species assembly, respectively, corresponding to 88,664 and 174,633 Coding Sequences (CDSes) (**Table 2**). The remaining sequences did not match any known gene from the databases queried. The annotation tables can be downloaded from figshare (links in **Table 2**). Based on the three main Gene Ontology categories (biological process, cellular component, and molecular function), we compared the 14 most common GO Plant Slim terms (Clark et al., 2005) in the *Gymnadenia* spp. cross-species, *O. iricolor* and the updated *O. sphegodes* transcriptomes (**Table 1**, **Figure 2**). To avoid overrepresentation of general terms such as "metabolic" or "cellular" processes, we omitted the first 7, 3, and 3 terms for Biological Process, Cellular Component and Molecular Function, respectively. Overall, the three transcriptomes are very similar in GO terms. The main differences between *O. sphegodes* and *O. iricolor* are the lack of terms related to "response to endogenous stimulus" in *O. iricolor*, and the presence of terms related to "vacuole" in *O. sphegodes* (**Figures 2A, B**). On the other hand, the *Gymnadenia* transcriptome differs from the *Ophrys* transcriptome by showing a high number of genes related to "nucleus" processes and an absence of those related to "membrane" processes (**Figure 2B**). Finally, BUSCO assessments with the embryophyta lineage database indicated that the completeness of the transcriptomes was 93.4, 91.9, and 94.1% for *O. iricolor*, *O. sphegodes* v.2, and cross-species *Gymnadenia* transcriptomes, respectively (**Figure 1A**). These results therefore suggest a reasonably high assembly quality of our floral transcriptomes, especially when compared with fully sequenced orchid genomes (encoding the transcripts of all tissues), i.e. the *Apostasia* genome with a 93.62% completeness, 94.45% in *Phalaenopsis equestris* and 95.49% in *Dendrobium catenatum* (all using the embryophyta database) (Zhang et al., 2017). Also, with 87.6, 85.5, and 87% for the larger BUSCO liliopsida lineage database (**Figure 1B**), for *O. iricolor*, *O.*

TABLE 2 | Annotation statistics.

Annotation	*O. iricolor s.l.*	*O. sphegodes s.l.* v2	*Gymnadenia* cross-species
CDSes	88,664	167,997	174,633
BLASTX	51,706	83,722	193,416
BLASTP	75,825	126,548	275,242
Pfam	52,288	84,592	195,443
SignalP	55,429	88,779	207,377
EggNOG	57,652	92,178	211,305
KEGG	54,457	85,892	201,018
TmHMM	75,781	89,813	208,338
Gene Ontology	30,098	79,238	129,578
Figshare identifier	10.6084/m9.figshare.9944015	10.6084/m9.figshare.9944018	10.6084/m9.figshare.9944006

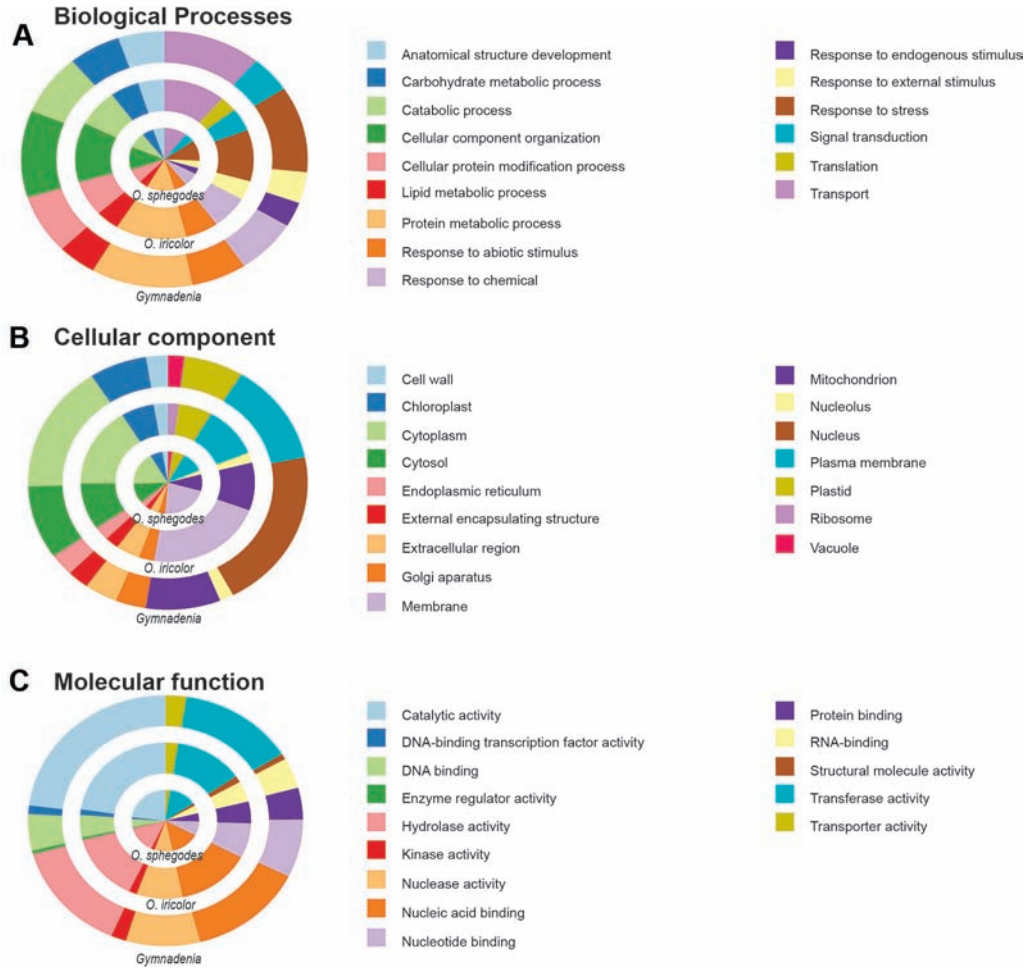

FIGURE 2 | GO Plant Slim functional annotation. GO Plant Slim annotation of the three transcriptomes for the most common **(A)** Biological Process, **(B)** Cellular Component and **(C)** Molecular Function terms.

sphegodes v.2 and cross-species *Gymnadenia* transcriptomes, respectively, our transcriptomes appear relatively complete with respect to monocot-specific genes.

Phylogenomic Analysis

Overall, we found the 15 orchid species included in this study to share a total of 1,749 gene families. From these gene family phylogenies, 226 contain *Ophrys* monophyletic groups with no gene duplications sampled from *all Ophrys* species and 160 contain *Gymnadenia* monophyletic groups with no gene duplications sampled from *all Gymnadenia* species separately. In addition, 116 contain informative topologies with one *Ophrys* species missing; and 153 and 318 topologies contain gene duplications (or alleles) within single-species monophyletic groups for *Ophrys* and *Gymnadenia*, respectively. For *Ophrys* and *Gymnadenia*, we found 5 and 6 of the 15 possible rooted topologies for four taxa, respectively. In *Ophrys,* the most common topology (77% of the trees) suggests that *O. insectifera s.l.* (with *O. aymoninii*) is not the basalmost clade, but instead places it in a clade with *O. sphegodes,* whereas *O. iricolor* takes the basal position (**Figures 3A**, **B**). This is also evident from the consensus tree over all orthologous gene groups (**Figure 3C**) and from all (100%) of the trees missing one *Ophrys* species (**Figure 3B**). In the case of *Gymnadenia*, the distribution of topologies is more even. Yet, the most common topology, supported by 33% of the trees, places *G. rhellicani* at the basal position in the *Gymnadenia* tree (**Figure 4**). Overall, a total of 48% of evaluated *Gymnadenia* genes show a topology that places *G. rhellicani* as a sister to all other species. Also, strikingly, only 33% of gene topologies support a sister-species relationship among *G. conopsea* and *G. odoratissima*. We compared the GO annotations of each topology in *Ophrys* and *Gymnadenia*, but despite some annotation differences between topologies, there is no clear pattern with respect to putatively pollinator-relevant features (**Figures S3** and **S4**). Although not significant, the two most common *Ophrys* topologies also show the highest average branch length (**Figure S5A**), whereas two less common topologies have the longest branch lengths in *Gymnadenia* (**Figure S5B**, non-significant); these are not united by a common phylogenetic theme (e.g. with respect to *G. rhellicani*).

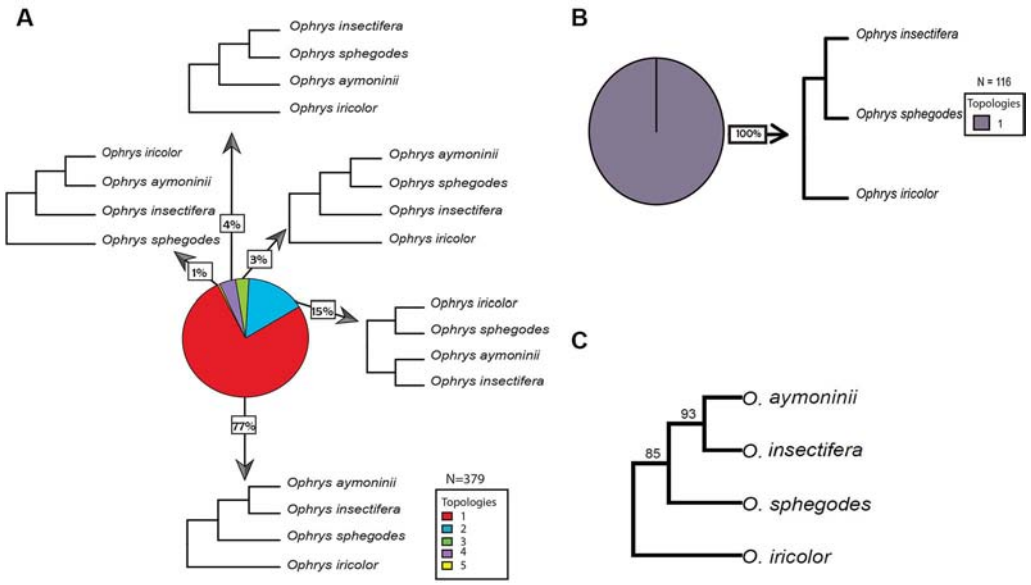

FIGURE 3 | Distribution of gene tree topologies in *Ophrys*. Proportions of rooted orthologous gene tree topologies (shown without branch lengths) for *Ophrys*. **(A)** overview of four-species *Ophrys* topologies; **(B)** three-species *Ophrys* topology; **(C)** majority-rule consensus tree from all individual 4-species gene trees, where numbers above branches indicate the percentage of individual gene trees supporting a group.

DISCUSSION

This study provides significant new transcriptome sequence resources aimed to improve our knowledge about the highly complex Orchidaceae family. Specifically, we present novel floral transcriptomes of several members of the subtribe Orchidinae of the Orchidoideae subfamily, covering both sexually deceptive and rewarding orchids. Overall, there were no striking differences between sexually deceptive and rewarding orchids when comparing the most common annotation terms based on Gene Ontology categories. This is not a surprise, because the GO Slim categories approach, although providing a large vocabulary to describe the functional categories, also suffers from a lack of clarity and too broad definitions, resulting in only a vague overview of molecular biology (Smith et al., 2003). At the same time, the phylogenetic proximity of *Ophrys* and *Gymnadenia* provides a plausible explanation for the lack of strong differentiation in terms of GO categories and suggests that differences in pollination strategy do not require fundamental changes in the genome-wide repertoire of florally expressed genes. This is in line with the phylogenetic lability of pollination strategies reported within the Orchidinae (Inda et al., 2012).

However, clear differences between *Ophrys* and *Gymnadenia* are apparent in terms of the transcriptome-wide distribution of gene tree topologies. For phylogeny reconstructions, rather than concatenating sequences, we evaluated multiple gene family trees separately. Trees derived from concatenated sequences do not reveal discrepancies between individual genes that are expected under a standard coalescent process, i.e., the more recent a species split is, the more tree topologies are expected due to incomplete lineage sorting (Takahata, 1989). Disagreement between gene trees and species trees has been observed in an increasing number of studies suggesting that the combination of a large amount of ancestral polymorphism and post-speciation gene flow between taxa can lead to large systematic differences between gene and species trees (Green et al., 2010; Novikova et al., 2016; Filiault et al., 2018; Malinsky et al., 2018).

Interestingly, the two most common gene tree topologies recovered for *Ophrys* reflect previous published phylogenetic reconstructions, our topologies 1 and 2 (**Figure 3**) corresponding to the phylogenies published most recently by Bateman et al. (2018b) and Breitkopf et al. (2015), respectively. Breitkopf et al.'s reconstruction suggested the *O. insectifera* group (clade α, including *O. aymoninii*) as the basal clade on the tree. By contrast, the phylogenetic reconstruction by Bateman et al. places *O. insectifera* closer to the *O. sphegodes* group, whereas a lineage containing the *O. fusca* complex (clade β, here represented by *O. iricolor*) is the earliest diverged. Our results, with a consensus of 85% of gene topologies, overwhelmingly support the inner placement of *O. insectifera*, rather than a basal position (**Figure 3C**). However, with the wasp-pollinated *O. insectifera* sister to the clade containing *O. sphegodes* and the wasp-pollinated *O. speculum* sister to the clade containing *O. iricolor/O. fusca*, the phylogeny's implication for the ancestral mode of pollination remains unchanged; the inference of ancestral wasp pollination in the genus *Ophrys* (Breitkopf et al., 2015) therefore seems unaffected by our findings. Nevertheless, it is striking that we found no strong evidence for discordant phylogenies throughout the genome.

Since the *O. insectifera*-group member *O. aymoninii*, a narrow endemic in southern France, is *Andrena*-pollinated (Paulus and Gack, 1990; Gervasi et al., 2017), phylogenies placing *O. aymoninii* together with the other *Andrena*-

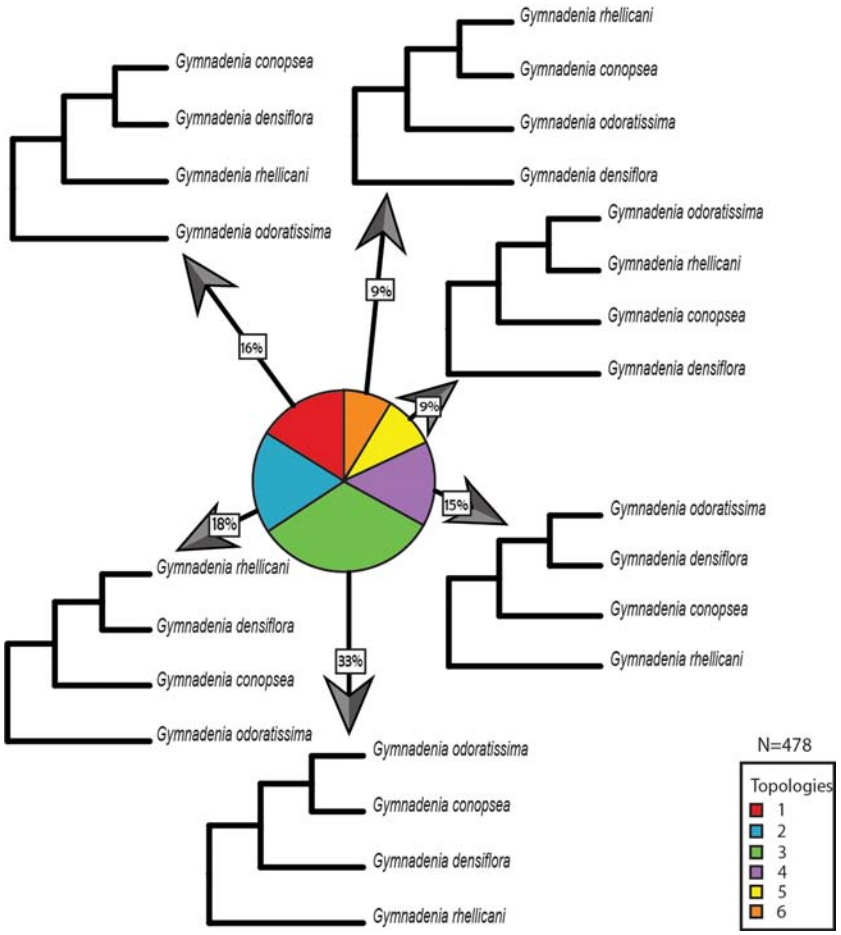

FIGURE 4 | Distribution of gene tree topologies in *Gymnadenia*. Proportions of rooted orthologous gene tree topologies (shown without branch lengths) for *Gymnadenia*.

pollinated linages, *O. sphegodes* and/or *O. iricolor* could be (but need not be) an indication of hybridization and introgression via *Andrena* pollinators. Although our analysis recovers phylogenies (**Figure 3A**, topologies 3 and 5) consistent with this hypothesis, with only 4% of the gene trees overall, support for pollinator-mediated introgression is weak at best.

Unlike *Ophrys* with a clearly predominant phylogeny across the transcriptome, *Gymnadenia* presents a much less clear picture of species relationships. The sister relationship between *G. conopsea* and *G. odoratissima* has been supported in several previous studies (e.g. Bateman et al., 2003; Sun et al., 2015) including by a recent genome-wide RAD-Seq (concatenated) SNP data set (Brandrud et al., 2019). This relationship is here supported by the most common topology in the transcriptome (**Figure 4**, topology 3). Yet this is also the *only* topology that supports this relationship, accounting for only 33% of orthologous gene groups evaluated. We must therefore conclude that, from a genomic perspective, the sister relationship of *G. conopsea* and *G. odoratissima* is not beyond doubt.

The genus *Gymnadenia* now typically includes its former sister genus *Nigritella* as a subgenus. Initial hypotheses built on morphological data (Wucherpfennig, 2002), anthocyanin pigments (Strack et al., 1989), or AFLP markers (Ståhlberg, 1999) suggested the separation of the two genera. Early molecular phylogenies (usually based solely on ITS) typically sampled only *G. conopsea*, *G. odoratissima*, and a single member of *Nigritella*, which was generally the outgroup to the sister *Gymnadenia* species (Hedrén et al., 2000). When additional species were sampled and added to this basic phylogeny, *G. densiflora* (or, depending on the sampling, *G. borealis*) was shown to be the sister taxon to members of *Nigritella*, arguing for combining the genera (Pridgeon et al., 1997; Bateman et al., 1997; Bateman et al., 2003; Stark et al., 2011; Efimov, 2013). Addition of three nuclear genes did not change this topology (Rey, 2011; Sun et al., 2015). Interestingly, where authors considered multiple phylogenetic methods, conflict seems to arise in tree construction, with parsimony showing *Nigritella* as the outgroup to *G. conopsea*/*G. densiflora*/*G. odoratissima*/*G. borealis*, while Bayesian and maximum likelihood analyses demonstrate a sister relationship between *Nigritella* and either *G. borealis* or *G. densiflora* (Rey, 2011; Inda et al., 2012). In a major upgrade to the generic phylogeny, Brandrud et al. (2019) performed RAD-Seq, with contrasting results to the ITS-based

phylogenies. Their phylogeny shows four *Nigritella* species as the outgroup to five *Gymnadenia* species, with no sister relation between *G. densiflora* and *Nigritella*, and the relevant nodes show high support.

Given the often contradictory results of earlier circumscription attempts, it is perhaps not too surprising that the different *Gymnadenia* gene topologies are relatively evenly distributed and that we see no single *Gymnadenia* phylogeny standing out as the best supported tree. However, the most common gene tree topology shows *G. rhellicani* as the outgroup to the other three sampled species (**Figure 4**, topology 3), in agreement with the recent RAD-Seq-based concatenated SNP analysis by Brandrud et al. (2019). Nonetheless, overall support for versus against a basal position of *G. rhellicani* is equivocal, at 48% of gene trees for (topologies 3 and 4) versus 52% against a basal position. The prevalence of other supported topologies (generally with *G. odoratissima* rather than *G. rhellicani* as the outgroup) suggests a complex population genetic history within the genus, perhaps partially due to gene exchange and incomplete lineage sorting. Neither gene annotation (**Figure S4**) nor average gene tree branch lengths (**Figure S5**) for topologies with basal *G. rhellicani* placement stand out as an indication of adaptive processes. Although *Gymnadenia* and *Nigritella* have produced one stable hybrid offspring, the apomict *G. runei* (Teppner and Klein, 1989) and other hybrids may be found, some dispute about their frequency exists (Claessens and Kleynen, 2011; Brandrud et al., 2019). Taken together, our analysis of *Gymnadenia* hints at a complex relationship among species that we are only beginning to understand. Whether this apparently more complicated pattern of genome-wide relationships in *Gymnadenia* as compared to *Ophrys* is due to the difference in pollination systems is currently unclear, although *Gymnadenia*'s less specialized pollination strategy would certainly present more opportunities for hybridization.

Using multiple gene family trees instead of one concatenated tree has proven to be a useful approach (Boussau et al., 2013; One Thousand Plant Transcriptomes Initiative, 2019). Concatenation of sequences implies that loci with a larger number of phylogenetically informative sites can bias the inference such that it may not be representative of patterns of unlinked genes throughout the genome. Also, such an approach holds no explicit information about the specific other topologies that may be useful for disentangling more complex evolutionary patterns of relationships throughout the genome, as would clearly be of interest in cases such as *Gymnadenia*. This problem is likely to be more severe in phylogenies of closely related species where excessive incomplete linage sorting may be expected and where a more sophisticated coalescent-based analysis may be valuable. Additionally, a consensus tree of individual gene trees (e.g. **Figure 3C**) is informative of the proportions of those genes in the genome that support a certain species relationship. Moreover, it is important to note that unlike a bootstrap pseudoreplicate approach, this allows for real quantification of proportions of independently segregating loci and/or functional genes and is thus more biologically meaningful. So far, our analysis only covers a small part of the genome. However, given a high-quality genome reference, future integration of this approach along chromosomes may be able to reconstruct the ancestry of individual chromosomal fragments and thereby shed light on the detailed evolutionary patterns and the role of selection (see Filiault et al., 2018) in shaping lineage divergence. The significant new sequence resources provided in this study may be a first step towards realizing this goal for European orchids in the future.

DATA AVAILABILITY STATEMENT

The datasets analysed for this study can be found in the NCBI accessions PRJNA574279 and PRJNA504609, and as indicated in **Table 1** and **2**.

AUTHOR CONTRIBUTIONS

Designed the project: PS. Drafted the manuscript: LP, with assistance from PS, KB, and RK. Revised the manuscript: all authors. Extracted material and prepared the libraries: JC, KS, and RK. Sequenced and processed the raw data: WQ, CA. Assembled and annotated the transcriptomes: LP, KB, JC, AR, and WQ. Conducted phylogenomic analysis: LP. Interpreted the results: LP, KB, RK, and PS. Acquired funding: KB, RK, and PS.

FUNDING

This work was financially supported by the Swiss National Science Foundation (SNF) (31003A_155943 to PS). Additional support came from the University of Zurich Research Priority Programme "Evolution in Action" (PS/AR and F. Schiestl/RK), a University of Zurich Forschungskredit grant to RK, a PLANT FELLOWS Postdoctoral Fellowship grant to KB (European Union: FP7-PEOPLE-2010-COFUND Proposal 267243), and several travel grants from the Georges & Antoine Claraz Foundation Zurich (to LP, RK, KB, and PS).

ACKNOWLEDGMENTS

We wish to thank Kriton Kalantidis, University of Crete, for access to his lab and support during sampling. We thank Karin Gross, Danae Laina and Daniel Gervasi for help with field work and sample collection, Shuqing Xu for sharing his scripts, and Florian Schiestl for support and sharing data. We also thank our funding sources as well as members of the Schlüter and Schiestl labs for assistance and helpful discussions.

SUPPLEMENTARY MATERIAL

The Supplementary Material for this article can be found online at: https://www.frontiersin.org/articles/10.3389/fpls.2019.01553/full#supplementary-material

REFERENCES

Abascal, F., Zardoya, R., and Telford, M. J. (2010). TranslatorX: multiple alignment of nucleotide sequences guided by amino acid translations. *Nucleic Acids Res.* 38, 7–13. doi: 10.1093/nar/gkq291

Ackerman, J. D. (1986). Mechanisms and evolution of food-deceptive pollination system in orchids. *Lindleyana* 1, 108–113.

Antonelli, A., Dahlberg, C. J., Carlgren, K. H. I., and Appelqvist, T. (2009). Pollination of the lady's slipper orchid (*Cypripedium calceolus*) in Scandinavia - Taxonomic and conservational aspects. *Nord. J. Bot.* 27, 266–273. doi: 10.1111/j.1756-1051.2009.00263.x

Ashburner, M., Ball, C. A., Blake, J. A., Botstein, D., Butler, H., Cherry, J. M., et al. (2000). Gene Ontology: tool for the unification of biology. *Nat. Genet.* 25, 25. doi: 10.1038/75556

Ayasse, M., Schiestl, F. P., Paulus, H. F., Löfstedt, C., Hansson, B., Ibarra, F., et al. (2000). Evolution of reproductive strategies in the sexually deceptive orchid *Ophrys sphegodes*: how does flower-specific variation of odor signals influence reproductive success? *Evolution* 54, 1995–2006. doi: 10.1111/j.0014-3820.2000.tb01243.x

Balao, F., Trucchi, E., Wolfe, T. M., Hao, B. H., Lorenzo, M. T., Baar, J., et al. (2017). Adaptive sequence evolution is driven by biotic stress in a pair of orchid species (*Dactylorhiza*) with distinct ecological optima. *Mol. Ecol.* 26, 3649–3662. doi: 10.1111/mec.14123

Bateman, R. M., Pridgeon, A. M., and Chase, M. W. (1997). Phylogenetics of subtribe Orchidinae (Orchidoideae, Orchidaceae) based on nuclear ITS sequences. 2. Infrageneric relationships and reclassification to achieve monophyly of *Orchis* sensu stricto. *Lindleyana* 12, 113–141.

Bateman, R. M., Hollingsworth, P. M., Preston, J., Yi-Bo, L., Pridgeon, A. M., and Chase, M. W. (2003). Molecular phylogenetics and evolution of Orchidinae and selected Habenariinae (Orchidaceae). *Bot. J. Linn. Soc.* 142, 1–40. doi: 10.1046/j.1095-8339.2003.00157.x

Bateman, R. M., Murphy, A. R. M., Hollingsworth, P. M., Hart, M., Denholm, I., and Rudall, P. J. (2018a). Molecular and morphological phylogenetics of the digitate-tubered clade within subtribe Orchidinae s.s. (Orchidaceae: Orchideae). *Kew Bull.* 73, 54. doi: 10.1007/s12225-018-9782-1

Bateman, R. M., Sramkó, G., and Paun, O. (2018b). Integrating restriction site-associated DNA sequencing (RAD-seq) with morphological cladistic analysis clarifies evolutionary relationships among major species groups of bee orchids. *Ann. Bot.* 121, 85–105. doi: 10.1093/aob/mcx129

Bell, A. K., Roberts, D. L., Hawkins, J. A., Rudall, P. J., Box, M. S., and Bateman, R. M. (2009). Comparative micromorphology of nectariferous and nectarless labellar spurs in selected clades of subtribe Orchidinae (Orchidaceae). *Bot. J. Linn. Soc.* 160, 369–387. doi: 10.1111/j.1095-8339.2009.00985.x

Boeckmann, B., Bairoch, A., Apweiler, R., Blatter, M.-C., Estreicher, A., Gasteiger, E., et al. (2003). The SWISS-PROT protein knowledge base and its supplement TrEMBL in 2003. *Nucleic Acids Res.* 31, 365–370. doi: 10.1093/nar/gkg095

Bolger, A. M., Lohse, M., and Usadel, B. (2014). Trimmomatic: a flexible trimmer for Illumina sequence data. *Bioinformatics* 30, 2114–2120. doi: 10.1093/bioinformatics/btu170

Boussau, B., Szöllosi, G. J., Duret, L., Gouy, M., Tannier, E., and Daubin, V. (2013). Genome-scale coestimation of species and gene trees. *Genome Res.* 23, 323–330. doi: 10.1101/gr.141978.112

Brandrud, M. K., Paun, O., Lorenz, R., Baar, J., and Hedrén, M. (2019). Restriction-site associated DNA sequencing supports a sister group relationship of *Nigritella* and *Gymnadenia* (Orchidaceae). *Mol. Phylogenet. Evol.* 136, 21–28. doi: 10.1016/j.ympev.2019.03.018

Brantjes, N. B. M. (1981). Ant, bee and fly pollination in *Epipactis palustris* (L.) Crantz (Orchidaceae). *Acta Botanica Neerl.* 30, 59–68. doi: 10.1111/j.1438-8677.1981.tb00387.x

Braunschmid, H., Mükisch, B., Rupp, T., Schäffler, I., Zito, P., Birtele, D., et al. (2017). Interpopulation variation in pollinators and floral scent of the lady's-slipper orchid *Cypripedium calceolus* L. *Arthropod-Plant Interact.* 11, 363–379. doi: 10.1007/s11829-017-9512-x

Breitkopf, H., Onstein, R. E., Cafasso, D., Schlüter, P. M., and Cozzolino, S. (2015). Multiple shifts to different pollinators fuelled rapid diversification in sexually deceptive *Ophrys* orchids. *New Phytol.* 1, 377–389. doi: 10.1111/nph.13219

Cameron, K. M., Chase, M. W., Whitten, W. M., Kores, P. J., Jarrell, D. C., Albert, V. A., et al. (1999). A phylogenetic analysis of the Orchidaceae: Evidence from *rbcL* nucleotide sequences. *Am. J. Bot.* 86, 208–224. doi: 10.2307/2656938

Capella-Gutiérrez, S., Silla-Martínez, J. M., and Gabaldón, T. (2009). TrimAl: a tool for automated alignment trimming in large-scale phylogenetic analyses. *Bioinformatics* 25, 1972–1973. doi: 10.1093/bioinformatics/btp348

Capella-Gutiérrez, S., Kauff, F., and Gabaldón, T. (2014). A phylogenomics approach for selecting robust sets of phylogenetic markers. *Nucleic Acids Res.* 42, e54. doi: 10.1093/nar/gku071

Chase, M. W., Cameron, K. M., Freudenstein, J. V., Pridgeon, A. M., Salazar, G., Berg, C., et al. (2015). An updated classification of Orchidaceae. *Bot. J. Linn. Soc.* 177, 151–174. doi: 10.1111/boj.12234

Chittka, L., and Menzel, R. (1992). The evolutionary adaptation of flower colours and the insect pollinators' colour vision. *J. Comp. Physiol. A Neuroethology Sens. Neural Behav. Physiol.* 171, 171–181. doi: 10.1007/BF00188925

Claessens, J., and Kleynen, J. (2011). *The Flower of the European Orchid: Form and Function*, Claessens and Kleynen.

Claessens, J., and Kleynen, J. (2017). The Pollination of European Orchids Part 6: nectar as attractant: *Gymnadenia conopsea* and *Neottia ovata*. *J. Hardy Orchid Soc.* 14, 110–136.

Clark, J. I., Brooksbank, C., and Lomax, J. (2005). It's all GO for plant scientists. *Plant Physiol.* 138, 1268–1279. doi: 10.1104/pp.104.058529

Cozzolino, S., and Widmer, A. (2005). Orchid diversity: An evolutionary consequence of deception? *Trends Ecol. Evol.* 20, 487–494. doi: 10.1016/j.tree.2005.06.004

Cozzolino, S., Roma, L., Schlüter, P. M., and Scopece, G. (2019). Different filtering strategies of Genotyping-By-Sequencing data provide complementary resolutions of species boundaries and relationships in a clade of sexually deceptive orchids. *J. Syst. Evol.* in press. doi: 10.1111/jse.12493

Cribb, P. J., Kell, S. P., Dixon, K. W., and Barrett, R. L. (2003). "Orchid conservation: a global perspective," in Dixon, K. W., Kell, S. P., Barrett, R. L., and Cribb, P. J. (eds.) *Orchid Conservation*, (Kinabalu, Malaysia: Natural History Publications, Kota). p. 1–24.

Dafni, A., and Ivri, Y. (1979). Pollination ecology of, and hybridization between, *Orchis coriophora* L. and *O. collina* Sol. ex Russ. (Orchidaceae) in Israel. *New Phytol.* 83, 181–187. doi: 10.1111/j.1469-8137.1979.tb00740.x

Deng, H., Zhang, G. Q., Lin, M., Wang, Y., and Liu, Z. J. (2015). Mining from transcriptomes: 315 single-copy orthologous genes concatenated for the phylogenetic analyses of Orchidaceae. *Ecol. Evol.* 5, 3800–3807. doi: 10.1002/ece3.1642

R Core Team. (2018). *R: A Language and Environment for Statistical Computing*, R Foundation for Statistical Computing: Vienna, Austria. https://www.R-project.org/.

Domínguez, E., and Bahamonde, N. (2013). *Gavilea araucana* (Phil.) M. N. Correa: first record of an orchid for Chile on *Sphagnum* peatland in Magallanes. *Biodiv. J.* 4, 125–128.

Dressler, R. L. (1993). *Phylogeny and Classification of the Orchid Family*. Cambridge, UK: Cambridge University Press.

Efimov, P. G. (2013). Sibling species of fragrant orchids (*Gymnadenia*: Orchidaceae, Magnoliophyta) in Russia. *Russian J. Genet.* 49, 299–309. doi: 10.1134/S102279541302004X

Filiault, D. L., Ballerini, E. S., Mandáková, T., Aköz, G., Derieg, N. J., Schmutz, J., et al. (2018). The *Aquilegia* genome provides insight into adaptive radiation and reveals an extraordinarily polymorphic chromosome with a unique history. *eLife* 7, e36426. doi: 10.7554/eLife.36426

Finn, R. D., Bateman, A., Clements, J., Coggill, P., Eberhardt, R. Y., Eddy, S. R., et al. (2014). Pfam: The protein families database. *Nucleic Acids Res.* 42, 138–141. doi: 10.1093/nar/gkt1223

Fitch, W. M. (1970). Distinguishing homologous from analogous proteins. *Syst. Zool.* 19, 99. doi: 10.2307/2412448

Fu, L., Niu, B., Zhu, Z., Wu, S., and Li, W. (2012). CD-HIT: accelerated for clustering the next-generation sequencing data. *Bioinformatics* 28, 3150–3152. doi: 10.1093/bioinformatics/bts565

Gaskett, A. C. (2011). Orchid pollination by sexual deception: Pollinator perspectives. *Biol. Rev.* 86, 33–75. doi: 10.1111/j.1469-185X.2010.00134.x

Gervasi, D. D. L., Selosse, M. A., Sauve, M., Francke, W., Vereecken, N. J., Cozzolino, S., et al. (2017). Floral scent and species divergence in a pair of sexually deceptive orchids. *Ecol. Evol.* 7, 6023–6034. doi: 10.1002/ece3.3147

Givnish, T. J., Spalink, D., Ames, M., Lyon, S. P., Hunter, S. J., Zuluaga, A., et al. (2015). Orchid phylogenomics and multiple drivers of their extraordinary diversification. *Proc. Roy. Soc. B. Biol. Sci.* 282, 20151553. doi: 10.1098/rspb.2015.1553

Grabherr, M. G., Haas, B. J., Yassour, M., Levin, J. Z., Thompson, D. A., Amit, I., et al. (2011). Full-length transcriptome assembly from RNA-Seq data without a reference genome. *Nat. Biotechnol.* 29, 644–652. doi: 10.1038/nbt.1883

Gravendeel, B., Smithson, A., Slik, F. J. W., and Schuiteman, A. (2004). Epiphytism and pollinator specialization: Drivers for orchid diversity? *Phil. Trans. Roy. Soc. B. Biol. Sci.* 359, 1523–1535. doi: 10.1098/rstb.2004.1529

Green, R. E., Krause, J., Briggs, A. W., Maricic, T., Stenzel, U., Kircher, M., et al. (2010). A draft sequence of the Neandertal genome. *Science* 328, 710–722. doi: 10.1126/science.1188021

Guindon, S., and Gascuel, O. (2003). A simple, fast, and accurate algorithm to estimate large phylogenies by maximum likelihood. *Syst. Biol.* 52, 696–704. doi: 10.1080/10635150390235520

Haas, B. J., Papanicolaou, A., Yassour, M., Grabherr, M., Blood, P. D., Bowden, J., et al. (2013). De novo transcript sequence reconstruction from RNA-seq using the Trinity platform for reference generation and analysis. *Nat. Protoc.* 8, 1494–1512. doi: 10.1038/nprot.2013.084

Hedrén, M., Klein, E., and Teppner, H. (2000). Evolution of polyploids in the European orchid genus *Nigritella*: evidence from allozyme data. *Phyton* 40, 239–275.

Huber, F. K., Kaiser, R., Sauter, W., and Schiestl, F. P. (2005). Floral scent emission and pollinator attraction in two species of *Gymnadenia* (Orchidaceae). *Oecologia* 142, 564–575. doi: 10.1007/s00442-004-1750-9

Inda, L. A., Pimentel, M., and Chase, M. W. (2012). Phylogenetics of tribe Orchideae (Orchidaceae: Orchidoideae) based on combined DNA matrices: inferences regarding timing of diversification and evolution of pollination syndromes. *Ann. Bot.* 110, 71–90. doi: 10.1093/aob/mcs083

Jensen, R. A. (2001). Orthologs and paralogs - we need to get it right. *Genome Biol.* 2, interactions 1002.1–1002.3. doi: 10.1186/gb-2001-2-8-interactions 1002

Jersáková, J., Johnson, S. D., and Kindlmann, P. (2006). Mechanisms and evolution of deceptive pollination in orchids. *Biol. Rev.* 81, 219–235. doi: 10.1017/S1464793105006986

Johnson, S. D., and Schiestl, F. P. (2016). *Floral Mimicry*. Oxford, UK.: Oxford University Press.

Johnson, S. D., Hobbhahn, N., and Bytebier, B. (2013). Ancestral deceit and labile evolution of nectar production in the African orchid genus *Disa*. *Biol. Lett.* 9, 20130500. doi: 10.1098/rsbl.2013.0500

Katoh, K., and Standley, D. M. (2013). MAFFT multiple sequence alignment software version 7: improvements in performance and usability. *Mol. Biol. Evol.* 30, 772–780. doi: 10.1093/molbev/mst010

Kellenberger, R. T., Byers, K. J. R. P., De Brito Francisco, R. M., Staedler, Y. M., LaFountain, A. M., Schönenberger, J., et al. (2019). Emergence of a floral colour polymorphism by pollinator-mediated overdominance. *Nat. Commun.* 10, 63. doi: 10.1038/s41467-018-07936-x

Krogh, A., Larsson, È., Heijne, G. V., and Sonnhammer, E. L. L. (2001). Predicting transmembrane protein topology with a hidden Markov model: application to complete genomes. *J. Mol. Biol.* 305, 567–580. doi: 10.1006/jmbi.2000.4315

Kullenberg, B., and Bergström, G. (1976). The pollination of *Ophrys* orchids. *Botaniska Notiser* 29, 11–19.

Langmead, B., and Salzberg, S. L. (2012). Fast gapped-read alignment with Bowtie 2. *Nat. Methods* 9, 357–359. doi: 10.1038/nmeth.1923

Li, W., and Godzik, A. (2006). Cd-hit: a fast program for clustering and comparing large sets of protein or nucleotide sequences. *Bioinformatics* 22, 1658–1659. doi: 10.1093/bioinformatics/btl158

Li, L., Stoeckert, C. J.Jr., and Roos, D. S. (2003). OrthoMCL: Identification of ortholog groups for eukaryotic genomes. *Genome Res.* 13, 2178–2189. doi: 10.1101/gr.1224503

Malinsky, M., Svardal, H., Tyers, A. M., Miska, E. A., Genner, M. J., Turner, G. F., et al. (2018). Whole-genome sequences of Malawi cichlids reveal multiple radiations interconnected by gene flow. *Nat. Ecol. Evol.* 2, 1940–1955. doi: 10.1038/s41559-018-0717-x

Mant, J. G., Schiestl, F. P., Peakall, R., and Weston, P. H. (2002). A phylogenetic study of pollinator conservatism among sexually deceptive orchids. *Evolution* 56, 888–898. doi: 10.1554/0014-3820(2002)056[0888:apsopc]2.0.co;2

Novikova, P. Y., Hohmann, N., Nizhynska, V., Tsuchimatsu, T., Ali, J., Muir, G., et al. (2016). Sequencing of the genus *Arabidopsis* identifies a complex history of nonbifurcating speciation and abundant trans-specific polymorphism. *Nat. Genet.* 48, 1077–1082. doi: 10.1038/ng.3617

One Thousand Plant Transcriptomes Initiative. (2019). One thousand plant transcriptomes and the phylogenomics of green plants. *Nature* 574, 679–685. doi: 10.1038/s41586-019-1693-2

Pamilo, P., and Nei, M. (1988). Relationships between gene trees and species trees. *Mol. Biol. Evol.* 5, 568–583. doi: 10.1093/oxfordjournals.molbev.a040517

Paulus, H. F., and Gack, C. (1990). Pollinators as prepollinating isolation factors: Evolution and speciation in *Ophrys* (Orchidaceae). *Isr. J. Bot.* 39, 43–79.

Paulus, H. F. (2018). Pollinators as isolation mechanisms: field observations and field experiments regarding specificity of pollinator attraction in the genus *Ophrys* (Orchidaceae und Insecta, Hymenoptera, Apoidea). *Entomol. Generalis* 37, 261–316. doi: 10.1127/entomologia/2018/0650

Pease, J. B., and Hahn, M. W. (2015). Detection and polarization of introgression in a five-taxon phylogeny. *Syst. Biol.* 64, 651–662. doi: 10.1093/sysbio/syv023

Pease, J. B., Haak, D. C., Hahn, M. W., and Moyle, L. C. (2016). Phylogenomics reveals three sources of adaptive variation during a rapid radiation. *PloS Biol.* 14, e1002379. doi: 10.1371/journal.pbio.1002379

Petersen, T. N., Brunak, S., and Nielsen, H. (2011). SignalP 4.0: discriminating signal peptides from transmembrane regions. *Nat. Methods* 8, 785. doi: 10.1038/nmeth.1701

Phillips, R. D., and Peakall, R. (2018). Breaking the rules: discovery of sexual deception in *Caladenia abbreviata* (Orchidaceae), a species with brightly coloured flowers and a non-insectiform labellum. *Aust. J. Bot.* 66, 95–100. doi: 10.1071/BT17151

Pridgeon, A. M., Bateman, R. M., Cox, A. V., Hapeman, J. R., and Chase, M. W. (1997). Phylogenetics of subtribe Orchidinae (Orchidoideae, Orchidaceae) based on nuclear ITS sequences. 1. Intergeneric relationships and polyphyly of *Orchis* sensu lato. *Lindleyana* 12, 89–109.

Revell, L. J. (2012). Phytools: an R package for phylogenetic comparative biology (and other things). *Meth. Ecol. Evol.* 3, 217–223. doi: 10.1111/j.2041-210X.2011.00169.x

Rey, M. (2011). Speciation in *Gymnadenia* (Orchidaceae): a phylogenetic reconstruction and underlying ecological processes. (master thesis) University of Zürich, Supervisor Florian P. Schiestl.

Robinson, D. F., and Foulds, L. R. (1981). Comparison of phylogenetic trees. *Math. Biosci.* 53, 131–147. doi: 10.1016/0025-5564(81)90043-2

Roma, L., Cozzolino, S., Schlüter, P. M., Scopece, G., and Cafasso, D. (2018). The complete plastid genomes of *Ophrys iricolor* and *O. sphegodes* (Orchidaceae) and comparative analyses with other orchids. *PloS One* 13, e0204174. doi: 10.1371/journal.pone.0204174

Salzmann, C. C., Nardella, A. M., Cozzolino, S., and Schiestl, F. P. (2007). Variability in floral scent in rewarding and deceptive orchids: the signature of pollinator-imposed selection? *Ann. Bot.* 100, 757–765. doi: 10.1093/aob/mcm161

Santorum, J. M., Darriba, D., Taboada, G. L., and Posada, D. (2014). Jmodeltest.org: selection of nucleotide substitution models on the cloud. *Bioinformatics* 30, 1310–1311. doi: 10.1093/bioinformatics/btu032

Schiestl, F. P., and Schlüter, P. M. (2009). Floral isolation, specialized pollination, and pollinator behavior in orchids. *Annu. Rev. Entomol.* 54, 425–446. doi: 10.1146/annurev.ento.54.110807.090603

Schiestl, F. P., Ayasse, M., Paulus, H. F., Löfstedt, C., Hansson, B. S., Ibarra, F., et al. (1999). Orchid pollination by sexual swindle. *Nature* 399, 421–421. doi: 10.1038/20829

Schiestl, F. P., Ayasse, M., Paulus, H. F., Löfstedt, C., Hansson, B. S., Ibarra, F., et al. (2000). Sex pheromone mimicry in the early spider orchid (*Ophrys sphegodes*): patterns of hydrocarbons as the key mechanism for pollination by sexual deception. *J. Comp. Physiol.* 186, 567–574. doi: 10.1007/s003590000112

Schiestl, F. P., Peakall, R., Mant, J. G., Ibarra, F., Schulz, C., Franke, S., et al. (2003). The chemistry of sexual deception in an orchid-wasp pollination system. *Science* 302, 437–438. doi: 10.1126/science.1087835

Schlüter, P. M., and Schiestl, F. P. (2008). Molecular mechanisms of floral mimicry in orchids. *Trends Plant Sci.* 13, 228–235. doi: 10.1016/j.tplants.2008.02.008

Schlüter, P. M., Ruas, P. M., Kohl, G., Ruas, C. F., Stuessy, T. F., and Paulus, H. F. (2009). Genetic patterns and pollination in *Ophrys iricolor* and *O. mesaritica* (Orchidaceae): Sympatric evolution by pollinator shift. *Bot. J. Linn. Soc.* 159, 583–598. doi: 10.1111/j.1095-8339.2009.00957.x

Schlüter, P. M., Xu, S., Gagliardini, V., Whittle, E., Shanklin, J., Grossniklaus, U., et al. (2011). Stearoyl-acyl carrier protein desaturases are associated with floral isolation in sexually deceptive orchids. *Proc. Natl. Acad. Sci.* 108, 5696–5701. doi: 10.1073/pnas.1013313108

Schlüter, P. M. (2018). The magic of flowers or: speciation genes and where to find them. *Am. J. Bot.* 105, 1957–1961. doi: 10.1002/ajb2.1193

Sedeek, K. E. M., Qi, W., Schauer, M. A., Gupta, A. K., Poveda, L., Xu, S., et al. (2013). Transcriptome and proteome data reveal candidate genes for pollinator attraction in sexually deceptive orchids. *PloS One* 8, e64621. doi: 10.1371/journal.pone.0064621

Sedeek, K. E. M., Scopece, G., Staedler, Y. M., Schönenberger, J., Cozzolino, S., Schiestl, F. P., et al. (2014). Genic rather than genome-wide differences between sexually deceptive *Ophrys* orchids with different pollinators. *Mol. Ecol.* 23, 6192–6205. doi: 10.1111/mec.12992

Simão, F. A., Waterhouse, R. M., Ioannidis, P., Kriventseva, E. V., and Zdobnov, E. M. (2015). BUSCO: assessing genome assembly and annotation completeness with single-copy orthologs. *Bioinformatics* 31, 3210–3212. doi: 10.1093/bioinformatics/btv351

Smith, B., Williams, J., and Steffen, S. (2003). The ontology of the Gene Ontology. *AMIA Annu. Symp. Proc.* 2003, 609.

Ståhlberg, D. (1999). *Polyploid evolution in the European orchid genus Nigritella: evidence from DNA fingerprinting*, (master thesis) Lund University, Supervisor Mikael Hedrén.

Stark, C., Michalski, S. G., Babik, W., Winterfeld, G., and Durka, W. (2011). Strong genetic differentiation between *Gymnadenia conopsea*, and *G. densiflora* despite morphological similarity. *Plant Syst. Evol.* 293, 213–226. doi: 10.1007/s00606-011-0439-x

Strack, D., Busch, E., and Klein, E. (1989). Anthocyanin patterns in european orchids and their taxonomic and phylogenetic relevance. *Phytochemistry* 28, 2127–2139. doi: 10.1016/S0031-9422(00)97931-7

Sun, M., Schlüter, P. M., Gross, K., and Schiestl, F. P. (2015). Floral isolation is the major reproductive barrier between a pair of rewarding orchid sister species. *J. Evol. Biol.* 28, 117–129. doi: 10.1111/jeb.12544

Takahata, N. (1989). Gene genealogy in three related populations: consistency probability between gene and population trees. *Genetics* 122, 957–966.

Teppner, H., and Klein, E. (1989). *Gymnigritella runei* spec. nova (Orchidaceae-Orchideae) aus Schweden. *Phyton* 29, 161–173.

Vöth, W. (2000). *Gymnadenia*, *Nigritella* und ihre Bestäuber. *J. Europäischer Orchideen* 32, 547–573.

Wong, D. C. J., Amarasinghe, R., Rodriguez-Delgado, C., Eyles, R., Pichersky, E., and Peakall, R. (2017). Tissue-specific floral transcriptome analysis of the sexually deceptive orchid *Chiloglottis trapeziformis* provides insights into the biosynthesis and regulation of its unique UV-B dependent floral volatile, chiloglottone 1. *Front. Plant Sci.* 8, 1260. doi: 10.3389/fpls.2017.01260

Wucherpfennig, W. (2002). *Nigritella*: Gattung oder Untergattung? *Jber. Naturwiss. Ver. Wuppertal* 55, 46–61.

Xu, S., Schlüter, P. M., Scopece, G., Breitkopf, H., Gross, K., Cozzolino, S., et al. (2011). Floral isolation is the main reproductive barrier among closely related sexually deceptive orchids. *Evolution* 65, 2606–2620. doi: 10.1111/j.1558-5646.2011.01323.x

Xu, S., Schlüter, P. M., and Schiestl, F. P. (2012). Pollinator-driven speciation in sexually deceptive orchids. *Int. J. Ecol.* 2012, 285081. doi: 10.1155/2012/285081

Xu, S., Brockmöller, T., Navarro-Quezada, A., Kuhl, H., Gase, K., Ling, Z., et al. (2017). Wild tobacco genomes reveal the evolution of nicotine biosynthesis. *Proc. Natl. Acad. Sci.* 114, 6133–6138. doi: 10.1073/pnas.1700073114

Yu, G., Smith, D. K., Zhu, H., Guan, Y., and Lam, T. T. (2017). GGTREE: an R package for visualization and annotation of phylogenetic trees with their covariates and other associated data. *Meth. Ecol. Evol.* 8, 28–36. doi: 10.1111/2041-210X.12628

Zhang, G. Q., Xu, Q., Bian, C., Tsai, W., and Yeh, C. (2016). The *Dendrobium catenatum* Lindl. genome sequence provides insights into polysaccharide synthase, floral development and adaptive evolution. *Sci. Rep.* 6, 19029. doi: 10.1038/srep19029

Zhang, G. Q., Liu, K. W., Li, Z., Lohaus, R., Hsiao, Y. Y., Niu, S. C., et al (2017). The *Apostasia* genome and the evolution of orchids. *Nature* 549, 379–383. doi: 10.1038/nature23897

Conflict of Interest: The authors declare that the research was conducted in the absence of any commercial or financial relationships that could be construed as a potential conflict of interest.

frontiers in Plant Science

ORIGINAL RESEARCH
published: 29 November 2019
doi: 10.3389/fpls.2019.01447

First Record of Ategmic Ovules in Orchidaceae Offers New Insights Into Mycoheterotrophic Plants

Mariana Ferreira Alves, Fabio Pinheiro, Marta Pinheiro Niedzwiedzki and Juliana Lischka Sampaio Mayer**

Departamento de Biologia Vegetal, Instituto de Biologia, Universidade Estadual de Campinas, São Paulo, Brazil

The number of integuments found in angiosperm ovules is variable. In orchids, most species show bitegmic ovules, except for some mycoheterotrophic species that show ovules with only one integument. Analysis of ovules and the development of the seed coat provide important information regarding functional aspects such as dispersal and seed germination. This study aimed to analyze the origin and development of the seed coat of the mycoheterotrophic orchid *Pogoniopsis schenckii* and to compare this development with that of other photosynthetic species of the family. Flowers and fruits at different stages of development were collected, and the usual methodology for performing anatomical studies, scanning microscopy, and transmission microscopy following established protocols. *P. schenckii* have ategmic ovules, while the other species are bitegmic. No evidence of integument formation at any stage of development was found through anatomical studies. The reduction of integuments found in the ovules could facilitate fertilization in this species. The seeds of *P. schenckii*, *Vanilla planifolia*, and *V. palmarum* have hard seed coats, while the other species have seed coats formed by the testa alone, making them thin and transparent. *P. schenckii,* in contrast to the other species analyzed, has a seed coat that originates from the nucellar epidermis, while in other species, the seed coat originates from the outer integument.

Keywords: anatomy, integument, Epidendroideae, saprophytic, Vanilloideae

OPEN ACCESS

Edited by:
Jen-Tsung Chen, National University of Kaohsiung, Taiwan

Reviewed by:
David Smyth, Monash University, Australia
Dennis William Stevenson, New York Botanical Garden, United States

****Correspondence:***
Mariana Ferreira Alves
marianafealves@gmail.com
Juliana Lischka Sampaio Mayer
jimayer@yahoo.com.br

Specialty section:
This article was submitted to Plant Development and EvoDevo, a section of the journal Frontiers in Plant Science

Received: *05 July 2019*
Accepted: *17 October 2019*
Published: *29 November 2019*

Citation:
Alves MF, Pinheiro F, Niedzwiedzki MP and Mayer JLS (2019) First Record of Ategmic Ovules in Orchidaceae Offers New Insights Into Mycoheterotrophic Plants. Front. Plant Sci. 10:1447. doi: 10.3389/fpls.2019.01447

INTRODUCTION

Flowers are highly variable structures, resulting in a great morphological diversity and a variety of adaptive processes in angiosperms (Endress, 1994; Friis et al., 2011). Variations in flower size and number of whorls, besides the presence or absence of fused floral parts, are caused by differences that occur during the development of floral organs. Plants exhibit open organization, which means that their organs are generally exposed, and that they do not have any organ or parts of organs internalized, with the exception of carpels (Endress, 2015). In turn, carpels can be free or united, becoming curved during their initial development, with edges getting closed or sealed when they are fully developed (Endress, 2006). While most floral organs are exposed, mainly due to the action of pollinating agents (e.g., animals, wind, and water), ovules are completely enclosed in the carpel a condition known as angiospermy (Endress, 2006).

Ovules are female reproductive structures that develop in the seeds (Bouman, 1984; Endress, 2011). Despite their relatively stable basic structure, ovules have a wide diversity of form, varying in terms of

their position in the ovary, size, curvature, number and thickness of integument, funiculus length, and degree of vascularization (Endress, 2011). For angiosperms, there are records of bitegmic, unitegmic, and ategmic species (Bouman, 1984; Endress, 2011). Although most angiosperms are bitegmic, variation in the number and thickness of integuments can be observed at different taxonomic levels, such as in families and genera. For example, in Olacaceae, there are described bitegmic, unitegmic, and ategmic species (Brown et al., 2010). In Melastomataceae, ovules are bitegmic; however, in species of the same genus, the number of the outer integument layers can vary from two to many (Caetano et al., 2018).

Previous studies have described the main function of integuments as the delimitation of the micropyle, and protection to the embryo sac and embryo (Herrero, 2001); however, they may also have other functions in species of different families. For example, the inner epidermis of the inner integument can function as a secretory tissue, playing a role in the nutrition of the embryonic sac. This layer of cells is known as integumentary tapetum (Kapil and Tiwari, 1978). Another hypothesis is that the number of integument layers could be related to the fruit type and seed dispersal mode. A study performed with several species of Melastomataceae tried to confirm if there was a relationship between ovules with multiseriate outer integument and fleshy fruits (Caetano et al., 2018). The data obtained did not confirm this relation; however, ancestral state reconstruction shows a tendency for ovules with multiseriate outer integument to occur in fleshy fruit clades. Recent studies conducted with *Arabidopsis* show that the number of ovule integument layers is related to gene and hormone expression (Bencivenga et al., 2012; Gomez et al., 2016; Coen and Magnani, 2018) and may be responsible for the seed coat diversity observed in angiosperms. After fertilization, the integument layers go through different pathways to establish a protective barrier for the embryo (Windsor et al., 2000). There is an immense diversity in seed structure, such as size, color, texture, and shape; this diversity is related to dispersal and germination strategies (Boesewinkel and Bouman, 1984), and may have been initially determined by the arrangement and number of ovule integuments.

In most angiosperms, the formation of ovules is complete when anthesis starts. In Orchidaceae, however, a different pattern is observed, where in the development of ovules and their respective placental proliferation are conditioned to the pollination event (Swamy, 1949a). In general, orchids have low reproductive success because of low pollination rates (Cozzolino and Widmer, 2005). Thus, ovules will be produced only if there is guaranteed seed formation, in order to prevent unnecessary energy expenditure (Arditti, 1992). The formation of the integuments in orchids occurs simultaneously with the formation of the embryonic sac. To date, in most species studied, the embryonic sac is bitegmic (Swamy, 1949a; Yeung and Law, 1997; Mayer et al., 2011). However, four unitegmic species, which are all mycoheterotrophic, have been described in previous studies (Abe, 1976; Arekal and Karanth, 1981; Krawczyk et al., 2016; Li et al., 2016).

Mycoheterotrophic plants are aclorophyllated and are completely dependent on carbon available through their association with fungi throughout their life cycle (Leake, 1994). Recent phylogeny using plastid and mitochondrial genomes in Orchidaceae show that mycoheterotrophic species evolved several times independently (Li et al., 2019). In the family, 235 species with this condition are described (Merckx et al., 2013), and little is known about the reproductive process of these species. Owing to the importance of the seed coat in the life cycle of plants, and because it is considered a stable characteristic, understanding its structure and development can reveal information relevant to its functional aspects, such as dispersal and seed germination (Bouman, 1984; Windsor et al., 2000; Endress, 2011). Thus, the objective of this work was to analyze the origin and development of the seed coat of the mycoheterotrophic orchid *Pogoniopsis schenckii* Cogn, and to compare this development with that of other species in the family that have chlorophyll and present different mechanisms of seed dispersal, *Polystachya estrellensis* Rchb.f., *Elleanthus brasiliensis* Rchb.f., *Isochilus linearis* (Jacq) Barb.Rodr., and *Cleistes libonii* (Rchb. f.) Schltr.—species that exhibit anemochory, and *Vanilla planifolia* Jacks. ex Andrews and *Vanilla palmarum* (Salzm ex. Lindl.) Lindl.—species showing evidence of zoochory (Cribb, 1999). *Pogoniopsis schenckii* is an endemic mycoheterotrophic species found in the Brazilian Atlantic Forest. Prior studies indicate a tendency of reduction in the number of integuments in species of mycoheterotrophic plants, including orchids (Abe, 1976; Arekal and Karanth, 1981; Maas and Ruyters, 1986; Bouman et al., 2002; Endress, 2011; Krawczyk et al., 2016; Li et al., 2016). Thus, our hypothesis is that *P. schenckii* also exhibits reduction in the number of integuments, leading to a greater exposure of the ovule and simplification of the seed coat involving the embryo, which may facilitate the penetration of fungal hyphae. In this context, structural information on the reproductive organs of mycoheterotrophic species, especially *P. schenckii*, can contribute to the elucidation of processes related to the symbiosis between fungi and mycoheterotrophic species. In addition, since the mode of seed dispersal of *P. schenckii* is not known, characterization of the stages of development of its seeds can contribute to the understanding of the ecological interactions involved in the dispersal and colonization of new habitats.

MATERIAL AND METHODS

Species Studied and Literature Review

Pogoniopsis schenckii Cogn. -Epidendroideae- is aclorophyllated and remains underground for almost its entire life cycle. During its reproductive phase, a floral stem appears above ground level; afterwards, flowers and fruits develop. *Polystachya estrellensis* Rchb. f., *Elleanthus brasiliensis* Rchb. f., *Isochilus linearis* (Jacq) Barb. Rodr., belonging to the subfamily Epidendroideae, and *Cleistes libonii* (Rchb. f.) Schltr., *Vanilla planifolia* Jacks. ex Andrews, and *Vanilla palmarum* (Salzm ex. Lindl.) Lindl., belonging to the subfamily Vanilloideae, are photosynthetic species that are found in all Brazilian regions, and in different phytogeographical domains, such as the Cerrado, Atlantic Forest, and Amazon. Voucher specimens were deposited at the Herbarium of the University of Campinas (HUEC), Campinas, São Paulo, Brazil, and the registration numbers are: 196921, 205027, 161354, 197343, 205047, 205028, and 20502.

A literature review was carried out to verify the number of species that developed bitegmic ovules, and the number of species that

developed unitegmic ovules. The following keywords were used to search publication databases: embryo development in Orchidaceae, embryology in Orchidaceae, and integuments in Orchidaceae.

Anatomic Analyses

To analyze the integument development freshly opened flowers off all species were collected. For *E. brasilliensis* and *V. palmarum* fruits from natural pollinations at different developmental stages were collected. For *P. schenckii* freshly opened flowers were marked and monitored. For the other species we carried out experimental self-pollination in flowers during the first day of anthesis. The flowers were then monitored and fruits at different stages of development were collected with 15, 20, 25, 30, 60, and 90 opening flower/days after pollination. All material was fixed in Karnovsky (Karnovsky, 1965), dehydrated in serial dilutions of ethanol, and were infiltrated with hydroxyethylmethacrylate (Gerrits and Smid, 1983). The samples were sectioned at 4 μm thickness using a Leica RM2245 rotary microtome, stained with Toluidine Blue 0.05% in phosphate buffer, pH 4.5 (Sakai, 1973), and mounted using Entellan® synthetic resin (Merck®). The slides were analyzed under an Olympus BX51 optical microscope and photographed with an Olympus DP71 digital camera.

Scanning Electron Microscopy

Botanical material was fixed in Karnovsky's solution (Karnovsky, 1965), dehydrated using a serial dilution of ethanol and critical point dried under carbon dioxide (CO_2) in a Balzers model CPD 030 Critical Point Dryer. The material was then mounted on metal supports and coated with colloidal gold for 220 s on the Bal-Tec model SCD 050 equipment. Analysis and electron micrograph recordings were performed using a LEO VP 435 scanning electron microscope at 20 kV, at the Institute of Biology/UNICAMP.

Transmission Electron Microscopy

To analyze the changes occurring during the development of *P. schenckii* seed coat, ovules, and seeds at different stages of development were fixed using 2.5% glutaraldehyde in 0.2 M sodium cacodylate buffer, pH 7.25, for 24 h (Mc Dowel and Trump, 1976). Post-fixation was performed with 1.0% osmium tetroxide (OsO4) in sodium cacodylate buffer for 12 h in the dark (Gabriel, 1982). The material was dehydrated in a series of increasing concentrations of acetone solution and soaked in LR White® resin according to the manufacturer's instructions. The ultrafine sections were prepared with Leica ultramicrotome using diamond knife. The ultrafine sections were contrasted with uranyl acetate (Bozzola and Russel, 1998) and lead citrate (Hanaich et al., 1986), examined under a Philips EM 100 transmission electron microscope at 80 kV, and documented with Eastman Kodak 5302 (35 mm) film.

RESULTS

Literature review showed that 97 species of orchids of different subfamilies, 2 species of Vanilloideae, 8 species of Cypripedioideae, 31 species of Orchidoideae, and 56 species of Epidendroideae, had been evaluated till date. Regarding these species, 93 presented bitegmic ovules, and 4 presented unitegmic ovules (**Table 1** and **Supplementary Table 1**). With the 6 new species included in this study, a total of 103 species have been evaluated in terms of the type of ovule integuments.

All species analyzed in this study are teninucellate and bitegmic, except for *P. schenckii* (**Figures 1A–J**), which has an ategmic ovule. *P. schenckii* is the first species within Orchidaceae possessing this characteristic. There is no growth of integuments at any stage of development (**Figures 1A**, **B**, **I**, **J**). The embryonic sac is only covered by the nucellar epidermis, which exhibit cells with high metabolism, thin walls, and evident nucleus (**Figures 1A**, **B**, **E**, **F**). Owing to the absence of integuments, there is no micropyle formation in the ovule of the species (**Figures 1B**, **I**, **J**, **K**).

In other species, the development of integuments occurs from periclinal divisions in the epidermal cells located at the base of the ovules, which is seen in both the subfamily Epidendroideae (**Figures 2A–P**) and in the subfamily Vanilloideae (**Figures 3A–Q**). During ovule development, the inner integument grows and recovers the nucellar epidermis. In *P. estrellensis*, *E. brasiliensis*, *I. linearis,* and *C. libonii*, the outer integument grows and covers the inner integument (**Figures 2A–D, G–L, M–O** and **3A–E**). In *P. estrellensis*, the outer integument has three layers (**Figure 2C**). The initial development of the integuments in *V. planifolia* and *V. palmarum* show that the outer integument also has three layers (**Figure 3P**). In other species, the outer integument has two layers, and in all the species analyzed, the inner integument has two layers (**Figures 2M** and **3B**).

After fertilization, changes are observed in the integument of all species. In *P. schenckii* (i.e., about 25 days after the floral opening), the seed coat becomes hard and forms from the nucellar epidermis itself (**Figures 1C**, **D**, **G**, **H**, **L**). It is possible to observe that during development of the seed coat there is an accumulation of substances that confers the cytoplasm a dense aspect (**Figures 1G, H**). When mature, the seed presents a brown-colored integument (**Figure 4A**). In *P. estrellensis*, *E. brasiliensis,* and *I. linearis*, the inner integument is fully absorbed, and the outer integument undergoes elongation. In the outer integument, the inner layer is absorbed, and the outer layer gives rise to the seed testa, which, when mature, is impregnated with lignin and surrounds the embryo (**Figures 2D–F, P** and **4B–D**). In *C. libonii*, at the beginning of seed development (i.e., about 40 days after fertilization), the inner layer of the inner integument begins to possess a dense cytoplasm and an evident nucleus (**Figures 3E**, **F**). Sixty days after fertilization, it is possible to observe the presence of a natural yellow-colored secretion surrounding the embryo (**Figures 3G**, **H** and **4E**). In the mature seed, only the outer tegument and this secreted layer that covers the embryo remain as coat, whereas the inner layer of the internal integument is reabsorbed (**Figures 2E**, **P** and **4E**). This substance is probably secreted by the cells of the inner layer of the inner integument. In *V. planifoli*a and *V. palmarum*, the mature seed has a hard dark-colored coat (**Figures 3M**, **Q** and **4F**, **G**).

DISCUSSION

For the first time the presence of ategmic ovules, as observed in *P. schenckii*, are described in Orchidaceae. Bitegmic ovules are commonly in orchids (Swamy, 1949a), but a reduction in ovule integuments are commonly observed in mycoheterotrophic

TABLE 1 | List of the type of integuments in species of Orchidaceae.

Species	Subfamily	Integument	Reference
Cleistes libonii (Rchb. f.) Schltr.	Vanilloideae	Biteg	Present study
Vanilla palmarum (Salzm ex. Lindl.) Lindl.	Vanilloideae	Biteg	Present study
Vanilla planifolia Jacks. ex Andrews	Vanilloideae	Biteg	Nishimura and Yukawa, 2010
Vanilla imperialis Kraenzl.	Vanilloideae	Biteg	Kodahl et al., 2015
Paphiopedilum delenatii Guillaumin	Cypripedioideae	Biteg	Lee and Yeung, 2012
Cypripedium cordigerum D. Don	Cypripedioideae	Biteg	Sood and Mohana Rao, 1988
Cypripedium spectabile (C. hirsutum Mill.)	Cypripedioideae	Biteg	Swamy, 1945
Cypripedium parviflorum Salisb.	Cypripedioideae	Biteg	Pace, 1907
Cypripedium pubenscens (Willd.)	Cypripediodeae	Biteg	Pace, 1907
Cypripedium formosanum Haiata	Cypripediodeae	Biteg	Lee et al., 2005
Cypripedium macranthos Sw.	Cypripediodeae	Biteg	Zeng et al., 2014
Cypripedium japonicum Thunb.	Cypripediodeae	Biteg	Liu et al., 2012
Amitostigma kinoshitae (Makino) Schltr.	Orchidoideae	Biteg	Abe, 1977
Zeuxine gracilis (Breda) Blume	Orchidoideae	Biteg	Gurudeva, 2011
Zeuxine sulcata Lindl.	Orchidoideae	Biteg	Swamy, 1946a
Orchis aristata Fisher	Orchidoideae	Biteg	Abe, 1972
Platanthera tipuloides Lindl. var. nipponica (Makino) Ohwi	Orchidoideae	Biteg	Abe, 1972
Platanthera chlorantha Custer (Rchb.)	Orchidoideae	Biteg	Abe, 1972
Platanthera sachalinensis Fr. Schm.	Orchidoideae	Biteg	Abe, 1972
Peristylus spiralis A. Rich	Orchidoideae	Biteg	Swamy, 1949a
Peristylus stocksii Krzl.	Orchidoideae	Biteg	Swamy, 1949a
Dactylohiza maculata (L.) Vermln.	Orchidoideae	Biteg	Fredrikson et al., 1988
Herminium monorchis (L.) R. Br.	Orchidoideae	Biteg	Fredrikson, 1990
Spiranthes australis Lindl.	Orchidoideae	Biteg	Maheshwari and Naraynaswami, 1951
Spiranthes sinensis (Pers.) Ames	Orchidoideae	Biteg	Lu-Han et al., 2016
Habenaria platyphylla Spr.	Orchidoideae	Biteg	Swamy, 1946b
Habenaria rariflora A. Rich.	Orchidoideae	Biteg	Swamy, 1946b
Habenaria longicalcarata A. Rich.	Orchidoideae	Biteg	Swamy, 1946b
Habenaria decipiens Wight.	Orchidoideae	Biteg	Swamy, 1946b
Habenaria plantagenea Lindl.	Orchidoideae	Biteg	Swamy, 1946b
Habenaria longicornu Lindl.	Orchidoideae	Biteg	Swamy, 1946b
Habenaria marginata Coleb.	Orchidoideae	Biteg	Swamy, 1946b
Habenaria heyeneana Lindl.	Orchidoideae	Biteg	Swamy, 1946b
Habenaria viridiflora R. Br.	Orchidoideae	Biteg	Swamy, 1946b
Habenaria densa Wall.	Orchidoideae	Biteg	Mohana Rao and Sood, 1979
Habenaria galeandra Hook. f.	Orchidoideae	Biteg	Sood, 1986
Habenaria elisabethae Duthie	Orchidoideae	Biteg	Sood, 1986
Habenaria edgeworthii Hook. f. ex. Collett	Orchidoideae	Biteg	Sood, 1986
Habenaria radiata (Thunb.) Spreng.	Orchidoideae	Biteg	Abe, 1972
Habenaria sagittifera (Reichb.) f.	Orchidoideae	Biteg	Abe, 1972
Goodyera repens (L.) R. Br.	Orchidoideae	Biteg	Sood, 1988
Myrmechis japonica (Reichb. f.) Br.	Orchidoideae	Biteg	Abe, 1972
Gymnadenia camtschatica Miyabe et Kudo	Orchidoideae	Biteg	Abe, 1972
Pogoniopsis schenckii Cogn.	Epidendroideae	Ateg	Present study
Polystachya estrelensis Rchb.f.	Epidendroideae	Biteg	Present study
Isochilus linearis (Jacq) Barb. Rodr.	Epidendroideae	Biteg	Present study
Elleanthus brasiliensis Rchb. f.	Epidendroideae	Biteg	Present study
Coelogyne breviscapa Lindl.	Epidendroideae	Biteg	Swamy, 1949a
Coelogyne odorotissima Lindl.	Epidendroideae	Biteg	Swamy, 1949a
Calypso bulbosa L.	Epidendroideae	Biteg	Law and Yeung, 1989
Spathoglotis plicata Bl.	Epidendroideae	Biteg	Swamy, 1949a
Geodorum densiflorum Schlechter.	Epidendroideae	Biteg	Swamy, 1949a
Oncidium flexuosum Sims	Epidendroideae	Biteg	Mayer et al., 2011
Cymbidium sinense (Andr.) Willd.	Epidendroideae	Biteg	Yeung, 1996
Eulophia nuda Lindl	Epidendroideae	Biteg	Swamy, 1949a
Geodorum densiflorum Schlechter.	Epidendroideae	Biteg	Swamy, 1949a
Bulbophyllum mysorense J. J. Smith.	Epidendroideae	Biteg	Swamy, 1949a
Bulbophyllum neilgherrense Wt. Ic. t.	Epidendroideae	Biteg	Swamy, 1949a
Dendrobium barbatulum Lindl.	Epidendroideae	Biteg	Swamy, 1949a
Dendobrium haemoglossum Thw.	Epidendroideae	Biteg	Swamy, 1949a
Dendobrium microbulbon A. Rich.	Epidendroideae	Biteg	Swamy, 1949a
Dendobrium graminifolium Wt. Ic. t.	Epidendroideae	Biteg	Swamy, 1949a
Epidendrum variegatum Hook	Epidendroideae	Biteg	Sharp, 1912

(Continued)

TABLE 1 | Continued

Species	Subfamily	Integument	Reference
Epidendrum ibaguense Lindl.	Epidendroideae	Biteg	Yeung and Law, 1989
Gastrodia elata Blume	Epidendroideae	Uniteg	Abe, 1976; Li et al., 2016
Gastrodia nantoensis	Epidendroideae	Uniteg	Li et al., 2016
Microstylis cylindrostachya Reichb. F	Epidendroideae	Biteg	Sood, 1985
Microstylis wallichii Lindl.	Epidendroideae	Biteg	Sood and Mohana Rao, 1986
Malaxis saprophyta (King & Panting) Tang & F.T. Wang	Epidendroideae	Biteg	Sood, 1992
Oberonia iridiflora var. *denticulata* Hook	Epidendroideae	Biteg	Swamy, 1949a
Epipactis atrorubens (Hoffm.) Besser	Epidendroideae	Biteg	Fredrikson, 1992
Epipactis helleborine (L.) Crantz	Epidendroideae	Biteg	Fredrikson, 1992
Epipactis palustris (L.) Crantz	Epidendroideae	Biteg	Fredrikson, 1992
Epipogium aphyllum Sw.	Epidendroideae	Uniteg	Krawczyk et al., 2016
Epipogium roseum (D. Don) Lindl.	Epidendroideae	Uniteg	Arekal and Karanth, 1981
Rhynchostylis retusa Blume	Epidendroideae	Biteg	Swamy, 1949a
Diplocentrum recurvum Lindl.	Epidendroideae	Biteg	Swamy, 1949a
Diplocentrum conjestrum Wt. Ic. t.	Epidendroideae	Biteg	Swamy, 1949a
Luisia teretrifolia Gaud	Epidendroideae	Biteg	Swamy, 1949a
Luisia teunifolia Bl.	Epidendroideae	Biteg	Swamy, 1949a
Cottonia peduncularis Wt. Ic. t.	Epidendroideae	Biteg	Swamy, 1949a
Saccolabium filiforme Lindl.	Epidendroideae	Biteg	Swamy, 1949a
Saccolabium jerdonianum Reichb.	Epidendroideae	Biteg	Swamy, 1949a
Saccolabium gracile Lindl.	Epidendroideae	Biteg	Swamy, 1949a
Saccolabium pulchellum Fisher.	Epidendroideae	Biteg	Swamy, 1949a
Saccolabium matsuran Makino	Epidendroideae	Biteg	Abe, 1972
Vanda spathulata Spreng	Epidendroideae	Biteg	Swamy, 1949a
Aerides cylindricum Lindl.	Epidendroideae	Biteg	Swamy, 1949a
Aerides ringens Fisher.	Epidendroideae	Biteg	Swamy, 1949a
Phalaenopsis sp.	Epidendroideae	Biteg	Zhang and O'Neill, 1993
Phalaenopsis amabilis var. *formosa* Shimadzu	Epidendroideae	Biteg	Lee et al., 2008
Eleorchis japonica (A. Gray) F Maekawa	Epidendroideae	Biteg	Abe, 1972
Bletia shepherdii Hook.	Epidendroideae	Biteg	Sharp, 1912
Phaius grandifolius Lour.	Epidendroideae	Biteg	Sharp, 1912
Phaius minor Blume	Epidendroideae	Biteg	Abe, 1972
Phaius tankervilliae (Aiton) Bl.	Epidendroideae	Biteg	Dong-mei et al., 2006
Calanthe anistrifera Reichb. f.	Epidendroideae	Biteg	Abe, 1972
Calanthe discolor Lindl.	Epidendroideae	Biteg	Abe, 1972
Calanthe torifera Schltr.	Epidendroideae	Biteg	Abe, 1972
Ephippianthus schmidtii	Epidendroideae	Biteg	Abe, 1972
Liparis paradoxa Reichb.	Epidendroideae	Biteg	Sood, 1989
Liparis rostrata Reichb. f.	Epidendroideae	Biteg	Sood, 1989
Acianthera johannensis (Barb Rodr) Pridgeon & M.W. Chase	Epidendroideae	Biteg	Duarte et al., 2019

Ateg, ategmic ovules; biteg, bitegmic ovules; uniteg, unitegmic ovules.

species, which are unitegmic (Tohda, 1967; Abe, 1976; Arekal and Karanth, 1981; Krawczyk et al., 2016; Li et al., 2016). Anatomical analyses show that the ovules of *P. schenckii* develop normally, and that there is no evidence of development of integument in the ovules of the species at all time points. In this way, the nucellar epidermis is responsible for surrounding the embryo sac, and in the mature seed, for surrounding the embryo. This result differs from the pattern found in other species analyzed in this study, which had seed coats originating from the outer integument.

Reduction of integuments occurs independently in different groups. They have been described in mycoheterotrophic species of Gentianales (Gentianaceae), parasite species of Santalales (Balanophoraceae, Loranthaceae, Olacaeae, and Santalaceae), and in a photosynthetic species of Aquifoliales (Cardiopteridaceae) (Maas and Ruyters, 1986; Bouman et al., 2002; Brown et al., 2010; Polli et al., 2016; Sato and Maria Gonzalez, 2016; Suaza-Gaviria et al., 2016; Tobe, 2016; Gonzalez et al., 2019). Molecular studies show that in ategmic ovules of Santalales, the genes associated with the expression of the integument are expressed in the periphery of the ovary, and that the reduction found in these species is the result of the fusion between the integument and the nucellus (Brown et al., 2010). In *P. schenckii*, the reduction of integuments leads to a total loss of the micropyle. However, this structural reduction does not seem to compromise reproduction, since the synergids continue to secrete substances for pollen tube attraction. The absence of integuments could facilitate the penetration of the synergids (**Figure 1B**) and subsequent fertilization. Mycoheterotrophic orchids have ovules with simpler structures, and the absence of a distinct micropyle is common in unitegmic species (Tohda, 1967; Abe, 1976; Arekal and Karanth, 1981; Li et al., 2016). The micropyle is responsible for directing the pollen tube; moreover, both the micropyle and secretions released by the synergid that promotes pollen tube attraction facilitate fertilization (Cheung and Wu, 2001; Okuda et al., 2009; Chen and Fang, 2016).

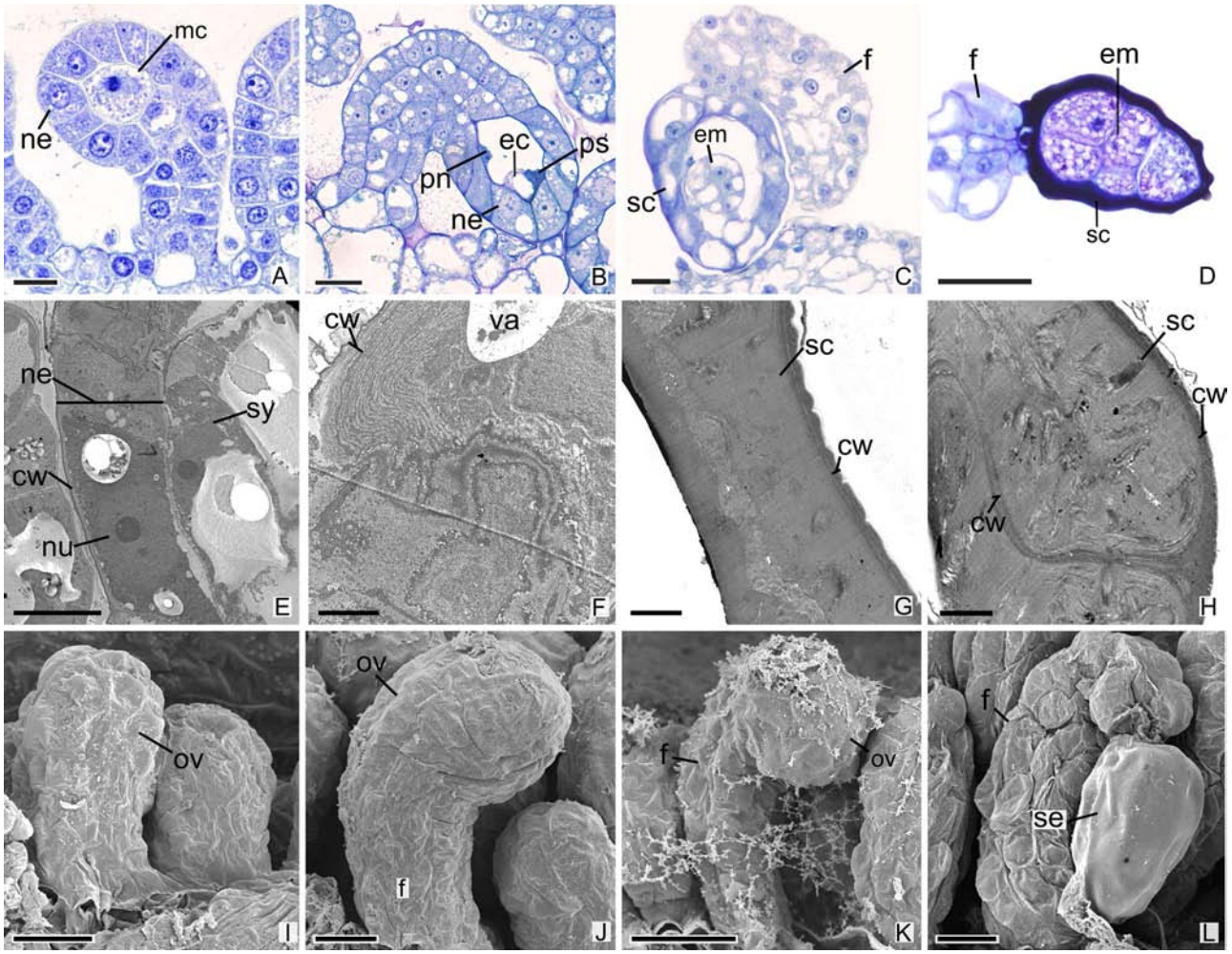

FIGURE 1 | Longitudinal sections of ovules and seeds of *Pogoniopsis schenckii*. **(A)** Megaspore mother cell. Note that there is no formation of integuments. **(B)** Penetrated synergid, egg cell, and polar nuclei. **(C)** Young seed. **(D)** Embryo with five cells. **(E–H)** Transmission microscopy electromyography. **(E)** Embryo sac and nucellar epidermis. **(F)** Details of the nucellar epidermis which presents cells with thin walls and evident nucleus. **(G)** Seed coat that originates from the nucellar epidermis. **(H)** Details of the hard seed coat. Note their accumulation of substances that confers the cytoplasm a dense aspect. **(I–L)** Scanning microscopy electromyography. **(I–K)** Ovule in development. Note that there is no formation of integuments. **(L)** Seed. cw, cell wall; ec, egg cell; em, embryo; f, funiculus; mc, megaspore mother cell; ov, ovule; ne, nucellar epidermis; nu, nuclei; pn, polar nuclei; ps, penetrated synergid; sc, seed coat; se, seed; sy, synergid; va, vacuolo. Scale bars A, C, I = 20 μm; B, D, K, L = 50 μm; E, J = 10 μm; F–H = 2 μm.

The differentiation of ovules in the species studied occurred after the stimulation of pollination, and the development of the integuments in *P. estrellensis*, *I. linearis*, *E. brasiliensis*, *C. libonii, V. planifolia,* and *V. palmarum* occurs simultaneously with the events of the megasporogenesis, as observed in other species of the family (Swamy, 1949a; Sood, 1985; Sood, 1986; Sood and Rao, 1986; Mayer et al., 2011; Li et al., 2016; Duarte et al., 2019). In most orchids, the outer integument has two layers of cells (Swamy 1949a; Wirth and Withner, 1959). However, in *P. estrellensis,* the outer integument was observed to have three layers, and the *Vanilla* species presented ovules with outer integuments that had three to four layers of cells in *V. imperialli*s, and four to six layers of cells in *V. planifolia* (Swamy, 1947; Nishimura and Yukawa, 2010; Kodahl et al., 2015). It is believed that the outer multiseriate integument in *Vanilla* would be related to the larger size of the seed found in the species of the genus (Kodahl et al., 2015).

Of all species analyzed, *P. schenckii*, *V. planifolia,* and *V. palmarum* have seeds with hard coat. Preliminary results show that in *P. schenckii*, dispersal in the species is very restricted (personal data). It was found to not be related to anemochory; moreover, dispersal by animals was not observed. Based on this, it seems that the hard coat has other unknown functions. Population genetics studies have been conducted, seeking to understand how this restricted dispersal can affect the dynamics of the populations of the species (Alves, unpublished data). Besides the hard coat *P. schenckii* presents seed with a large funiculus, differing from the other analyzed species. Preliminary analyzes show that the funiculus assists in the penetration of fungal hyphae after dispersion (personal

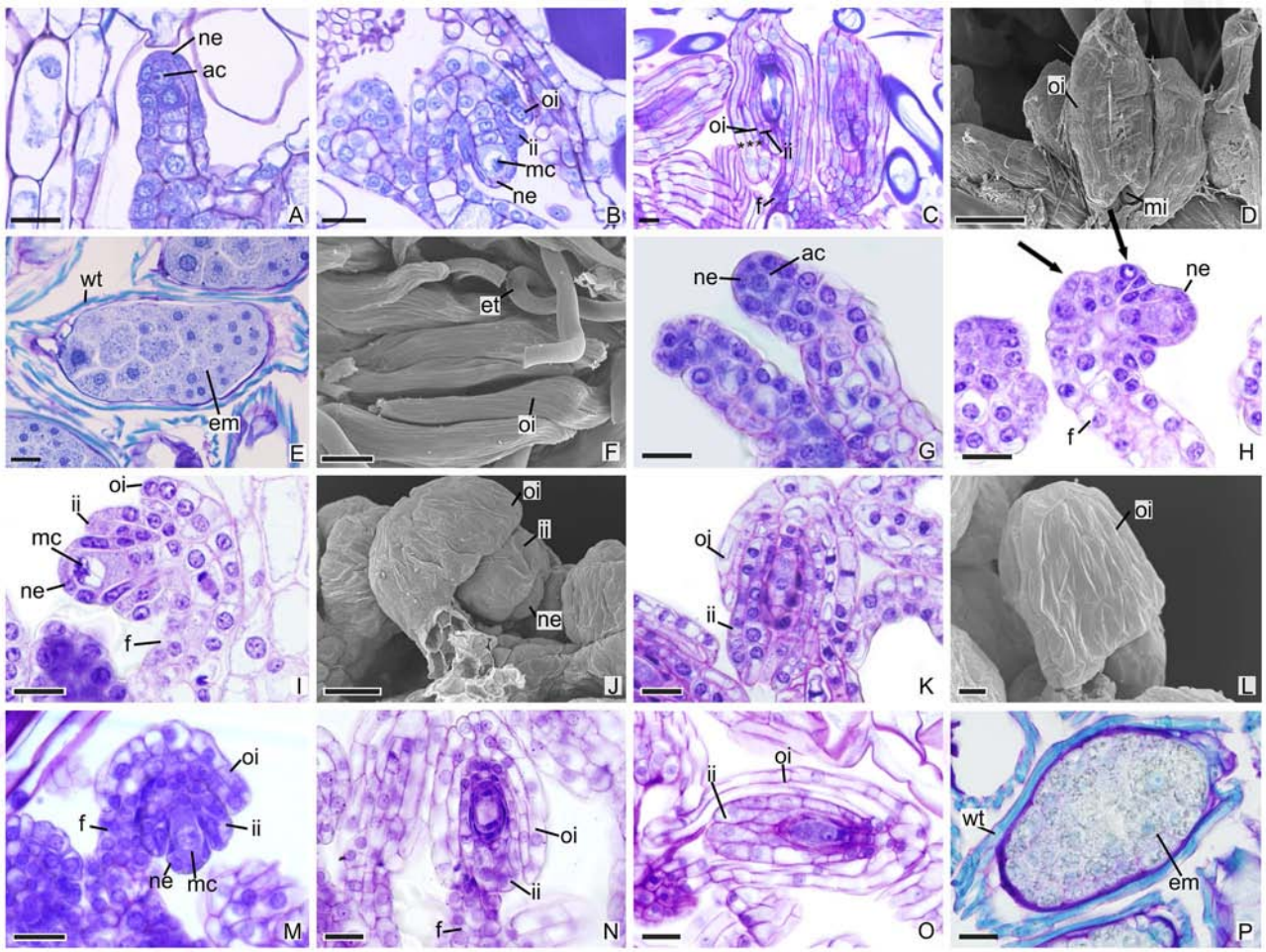

FIGURE 2 | Longitudinal sections of ovules and seeds of Epidendroideae species. **(A–F)** Ovules and seeds of *Polystachya estrellensis*. **(D, F)** Scanning microscopy electromyography. **(A)** Differentiation of the initial archesporial cell. **(B)** Megaspore mother cell and formation of integuments. **(C)** Embryo sac. *indicates the outer integument with three layers. **(D)** Embryo sac. **(E, F)** Seed. **(G–L)** Ovules of *Elleanthus brasiliensis*. **(J, L)** Scanning microscopy electromyography. **(G)** Differentiation of the initial archesporial cell. **(H)** Formation of integuments indicated by arrows. **(I)** Megaspore mother cell. **(J–K)** Formation of integuments. **(L)** Embryo sac with the outer integument developed. **(M–P)** Ovules and seeds of *Isochilus linearis*. **(M)** Megaspore mother cell and formation of integuments. **(N, O)** Embryo sac with the integuments developed. P. Seed. ac, initial archesporial cell; em, embryo; f, funiculus; ii, inner integument; mc, megaspore mother cell; mi, micropyle; ne, nucellar epidermis; oi, outer integument; wt, wall thickening. Scale bars A–C; E; G-K; M-P = 20 μm; D, F = 50 μm; L = 10 μm.

data). Seeds with hard coat have also been described for other mycoheterotrophic orchids. For *Cyrtosia japonica*, seeds with coats originating from the outer integument and inner integument (Yang and Lee, 2014) are registered. In *C. japonica*, the seed presents an outer integument with four layers, and the outermost layer later becomes sclerified (Yang and Lee, 2014). It is suggested that the observed lignification protects the embryo when it passes through the alimentary tract of its dispersers (Rodolphe et al., 2011; Yang and Lee, 2014). In *Yonia japonica,* the seed also presents a lignified coat; however, the fruits and seeds of the species are dispersed by insects (Suetsugu, 2018). Similar to *Cyrtosia,* it is believed that the lignified seed coat in *Y. japonica* is an adaptation that protects the seed during digestion (Suetsugu, 2018).

It is assumed that *V. planifolia* and *V. palmarum* undergo endozoochory dispersal (Cribb, 1999; Kodahl et al., 2015). In these species, as in others belonging to Vanilloideae, seeds with hard coats exist as a strategy for the dispersal of the genus (Kodahl et al., 2015); in addition, hard coats would protect seeds that can be dispersed over long distances. In other species, seeds were observed to have a thin and transparent coat, which is seemingly a common feature in Orchidaceae. Seeds from Orchidaceae have small sizes, and are called "dust seeds" (Swamy, 1949b; Arditti and Ghani, 2000). The rather small size observed in orchid seeds was traditionally thought to be an adaptation to long-distance wind dispersal events (Arditti and Ghani, 2000). However, recent molecular studies have shown discordant patterns that show the orchid seeds ability to reach long distances (Cozzolino et al., 2003; Trapnell and Hamrick, 2004). Many other species present dispersal patterns limited to a few meters (Chung et al., 2004; Chung et al., 2005; Ren et al., 2017).

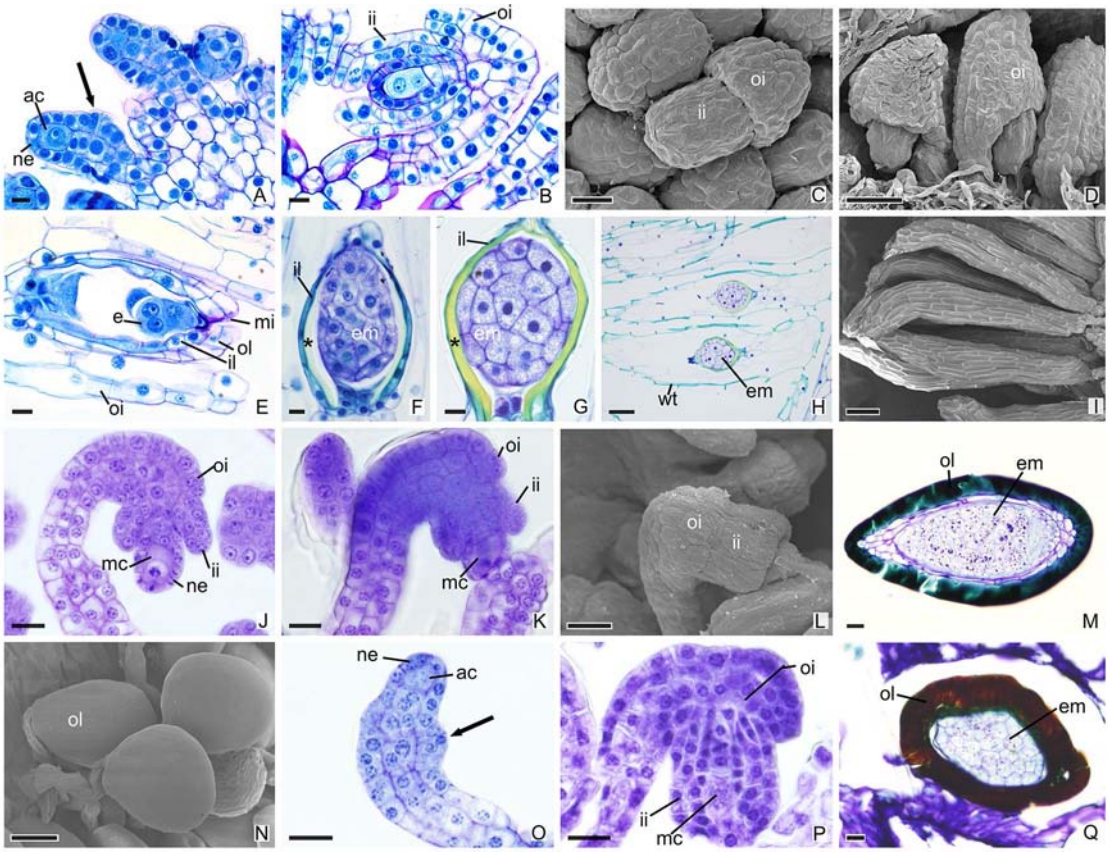

FIGURE 3 | Longitudinal sections of ovules and seeds of Vanilloideae species. **(A–I)** Ovules and seeds of *Cleistes libonii*. **(C**, **D**, **I)** Scanning microscopy electromyography. **(A)** Differentiation of the initial archesporial cell. Arrows indicate the initial formation of integuments. **(B)** Megaspore mother cell and formation of integuments. **(C**, **D)** Development of integuments. **(E)** Initial development of embryo. **(F–G)** Embryo. *indicate the extracellular exudate. **(H–I)** Seeds. **(J–N)** Ovules and seeds of *Vanilla planifolia.* **(L**, **N)** Scanning microscopy electromyography. **(J–K)** Megaspore mother cell and formation of integuments. **(L)** Development of integuments. **(M**, **N)** Seeds with hard dark-colored coat. **(O–Q)** Ovules and seed of *Vanilla palmarum*. **(O)** Differentiation of the initial archesporial cell. Arrows indicate the initial formation of integuments.(P) Megaspore mother cell and formation of integuments. Note the outer integument with three layers. **(Q)** Seed with hard dark-colored coat. ac, initial archesporial cell; em, embryo; f, funiculus; ii, inner integument; il, inner layer of the inner integument; mc, megaspore mother cell; mi, micropyle; ne, nucellar epidermis; oi, outer integuments; ol, out layer of the inner integument; wt, wall thickening. Scale bars A, B, E–G, J–M, O–Q = 20 μm; C = 50 μm; D, H, N = 100 μm; I = 200 μm.

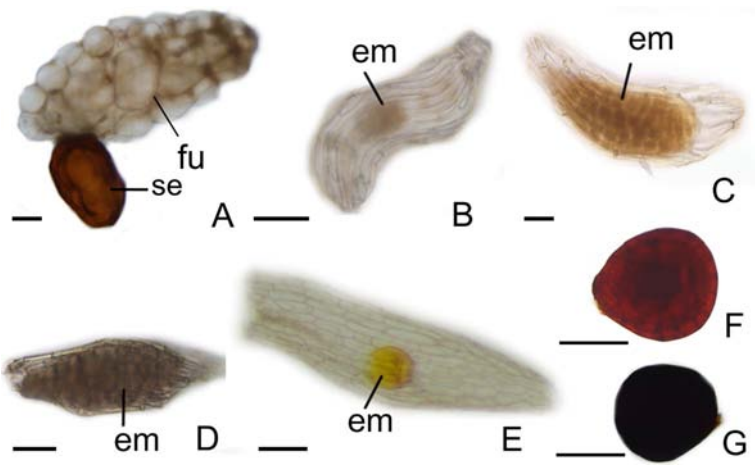

FIGURE 4 | Aspects of seeds. **(A)** Pogoniopsis schenckii. **(B)** Polystachya estrellensis. **(C)** Elleanthus brasiliensis. **(D)** Isochilus linearis. **(E)** Cleistes libonii. **(F)** Vanilla planifolia. **(G)** Vanilla palmarum. em, embryo; fu, funiculus; se, seed . Scale bars A, B, C, D, E = 150 μm; F, G = 75 μm.

Dark-colored hard seed coats, as observed in *P. schenckii*, *V. planifolia,* and *V. palmarum,* have already been described for *Apostasia* (Swamy, 1947). Occurrence of phytomelanin deposition in Asparagales seeds is described in the literature (Dahlgren et al., 1985). Phytomelanin is a dark and insoluble pigment that is found in different parts of plants and exhibit distinct transport load and structural stability (Nicolaus et al., 1964; Cordero and Casadevall, 2017). Phytomelanin's main function is to confer protection to different conditions, such as environmental variations, harmful radiation, extreme temperatures, and chemical and mechanical stress (Roulin, 2014; Cordero and Casadevall, 2017). The dark-colored integument in the species studied may result from phytomelanin deposition. However, studies are still needed to clarify this issue.

The results obtained show novelties in the development of the seed coat in Orchidaceae. *P. schenckii* has an ategmic ovule and has a hard seed coat that originates from the nucellar epidermis. Mycoheterotrophic plants have numerous modifications in their morphology, reproductive biology, and physiology (Leake, 1994; Bidartondo, 2005), the most prominent among loss of photosynthetic function and severe ruptures in the plastid genome (Graham et al., 2016). The genomic losses observed may be related not only to photosynthetic processes, but also to the absence of genes that present other functions, such as genes related to reproductive functions. Anatomical analyses show that there is no evidence of integument development in the ovules of *P. schenckii*. Thus, the reduction of the integuments found in the species may be due to the absence of gene expression, or even the absence of genes linked to the development of the integument; however, molecular studies are necessary to elucidate this issue.

DATA AVAILABILITY STATEMENT

The datasets generated for this study are available on request to the corresponding author.

AUTHOR CONTRIBUTIONS

MA carried the anatomical analysis, analysis of scanning and transmission microscopy, and writing the manuscript. FP supervised the work and writing the manuscript. MN carried anatomical analyses in *Cleistes libonii* and JM was responsible for collecting the material, carried anatomical analyses, writing the manuscript, and supervised the work.

FUNDING

This study was financed in part by the Coordenação de Aperfeiçoamento de Pessoal de Nível Superior - Brasil (CAPES) - Finance Code 001. Juliana Lischka Sampaio Mayer thank FAPESP (2015/26479-6), FAEPEX 0944/14, CNPq (447453/2014-9), and CNPQ (310184/2016-9) for funding support.

ACKNOWLEDGMENTS

We thank *The Espaço da Escrita - Pró-Reitoria de Pesquisa - UNICAMP - for the language services provided* and the access to equipment and assistance provided by the Electron Microscope Laboratory (LME/UNICAMP). We thank the Instituto Florestal (Parque Estadual da Serra do Mar, Núcleo Santa Virginia and Núcleo Picinguaba) for the development of the study on protected public land and Carlos Eduardo Pereira Nunes for his help in field activities.

SUPPLEMENTARY MATERIAL

The Supplementary Material for this article can be found online at: https://www.frontiersin.org/articles/10.3389/fpls.2019.01447/full#supplementary-material

SUPPLEMENTARY TABLE 1 | List of the type of integuments in species of Orchidaceae. Ateg = ategmic ovules; biteg = bitegmic ovules; uniteg = unitegmic ovules.

REFERENCES

Abe, K. (1972). Contributions to the embryology of the Family Orchidaceae. VI. Development of the embryo sac in 15 species of Orchids. *Sei Rep. Tohoku Univ. Ser. IV (Biol)* 36, 135–178.

Abe, K. (1976). A reinvestigation of the development of the Embryo Sac in *Gastrodia elata Blume* (Orchidaceae). *Ann. Bot.* 40, 99–102. doi: 10.1093/oxfordjournals.aob.a085119

Abe, K. (1977). Development of the Embryo Sac in *Amitostigma kinoshitae* (Makino) Schltr. (Orchidaceae). *Ann. Bot.* 41, 897–899. doi: 10.1093/oxfordjournals.aob.a085367

Arditti, J. (1992). *Fundamentals of orchid biology*. Arditti, J, editor. New York: John Wiley & Sons Inc.

Arditti, J., and Ghani, A. K. A. (2000). Tansley Review No. 110.: Numerical and physical properties of orchid seeds and their biological implications. *New Phytol.* 145, 367–421. doi: 10.1046/j.1469-8137.2000.00587.x

Arekal, G. D., and Karanth, K. A. (1981). The embryology of *Epipogium roseum* (Orchidaceae). *P1. Syst. Evol.* 138, 1–7. doi: 10.1007/bf00984604

Bencivenga, S., Simonini, S., Benkova, E., and Colombo, L. (2012). The transcription factors BEL1 and SPL are required for cytokinin and auxin signaling during ovule development in Arabidopsis. *Plant Cell* 24, 2886–2897. doi: 10.1105/tpc.112.100164

Bidartondo, M. I. (2005). The evolutionary ecology of mycoheterotrophy: Tansley review. *New Phytol.* 167, 335–352. doi: 10.1111/j.1469-8137.2005.01429.x

Boesewinkel, F. D., and Bouman, F. (1984). "Embryology of angiosperms," in *The seed structure*. Ed. Johri, B. M. (Verlag: Springer), 597–610.

Bouman, F. (1984). "Embryology of Angiosperms," in *The ovule*. Ed. Johri, B. M. (Verlag: Springer), 123–157.

Bouman, F., Cobb, L., Devente, N., Goethals, V., Maas, P. J. M., and Smets, E. (2002). "Gentianaceae systematics and natural history," in *The seeds of Gentianaceae*. Eds. L. Struwe, L., and Albert, V. A. (Cambridge: Cambridge University Press), 498–572.

Bozzola, J. J., and Russel, L. D. (1998). *Electron microscopy. principles and techniques for biologists*. Boston: Jones e Bartlett Publishers.

Brown, R. H., Nickrent, D. L., and Gasser, C. S. (2010). Expression of ovule and integument associated genes in reduced ovules of Santalales: ovule gene expression in Santalales. *Evol. Dev.* 12, 231–240. doi: 10.1111/j.1525-142X.2010.00407.x

Caetano, A. P. S., Basso-Alves, J. P., Cortez, P. A., Brito, V. L. G. D., Michelangeli, F. A., Reginato, M., et al. (2018). Evolution of the outer ovule integument and its systematic significance in Melastomataceae. *Bot. J. Linn. Soc* 186, 224–246. doi: 10.1093/botlinnean/box093

Chen, J. C., and Fang, S. C. (2016). The long pollen tube journey and *in vitro* pollen germination of *Phalaenopsis* orchids. *Plant Reprod.* 29, 179–188. doi: 10.1007/s00497-016-0280-z

Cheung, A. Y., and Wu, H. (2001). Pollen tube guidance — right on target. *Science* 293, 1441–1442. doi: 10.1126/science.1065051

Chung, M. Y., Nason, J. D., and Chung, M. G. (2004). Spatial genetic structure in populations of the terrestrial orchid *Cephalanthera longibracteata* (Orchidaceae). *Am. J. Bot.* 91, 52–57. doi: 10.3732/ajb.91.1.52

Chung, M. Y., Nason, J. D., and Chung, M. G. (2005). Spatial genetic structure in populations of the terrestrial orchid *Orchis cyclochila* (Orchidaceae). *Plant Syst. Evol.* 254, 209–219. doi: 10.1007/s00606-005-0341-5

Coen, O., and Magnani, E. (2018). Seed coat thickness in the evolution of angiosperms. *Cell. Mol. Life Sci.* 75, 2509–2518. doi: 10.1007/s00018-018-2816-x

Cordero, R. J. B., and Casadevall, A. (2017). Functions of fungal melanin beyond virulence. *Fungal Biol. Rev.* 31, 99–112. doi: 10.1016/j.fbr.2016.12.003

Cozzolino, S., Cofasso, D., Pellegrino, G., Masachhio, A., and Widmer, A. (2003). Fine-scale phylogeographical analysis of Mediterranean *Anacamptis palustris* (Orchidaeae) populations based on chloroplast minisatellite and microsatellite variation. *Mol. Ecol.* 12, 2783–2792. doi: 10.1046/j.1365-294x.2003.01958.x

Cozzolino, S., and Widmer, A. (2005). Orchid diversity: an evolutionary consequence of deception? *Trends Ecol. Evol.* 20, 487–494. doi: 10.1016/j.tree.2005.06.004

Cribb, P. J. (1999). "Genera Orchidacearum: Volume 1: General Introduction, Apostasioideae, Cypripedioideae," in *Morfology*. Eds. Pridgeon, A. M., Cribb, P. J., Chase, M. W., and Rasmussen, F. N. (Oxford: Oxford University Press Inc.), 13–23.

Dahlgren, R. M. T., Clifford, H. T., and Yeo, P. F. (1985). *The Families of the Monocotyledons*. Heidelberg: Springer-Verlag.

Dong-mei, L., Xiulin, Y., Chengye, L., and Xiaoying, H. (2006). Growth paths of pollen tubes in ovary of *Phaius tankervilliae* (Aiton) Bl. *J. Trop. Subtrop. Bot.* 14, 130–133. doi: 10.3969/j.issn.1005-3395.2006.2.007

Duarte, M. O., Oliveira, D. M. T., and Borba, E. L. (2019). Ontogenesis of ovary and fruit of *Acianthera johannensis* (Pleurothallidinae, Orchidaceae) reveals a particular female embryology. *Flora* 259, 151462. doi: 10.1016/j.flora.2019.151462

Endress, P. K. (1994). *Diversity and evolutionary biology of tropical flowers*. Cambridge: Cambridge University Press.

Endress, P. K. (2006). Angiosperm floral evolution: morphological developmental framework. *Adv. Bot. Res.* 44, 1–61. doi: 10.1016/S0065-2296(06)44001-5

Endress, P. K. (2011). Angiosperm ovules: diversity, development, evolution. *Ann. Bot.* 107, 1465–1489. doi: 10.1093/aob/mcr120

Endress, P. K. (2015). Patterns of angiospermy development before carpel sealing across living angiosperms: diversity, and morphological and systematic aspects: Angiospermy Development Across Living Angiosperms. *Bot. J. Linn. Soc.* 178, 556–591. doi: 10.1111/boj.12294

Fredrikson, M., Carlsson, K., and Franksson, O. (1988). Confocal scanning laser microscopy, a new technique used in an embryological study of *Dactylorhiza maculata* (Orchidaceae). *Nord. J. Bot.* 8, 369–374. doi: 10.1111/j.1756-1051.1988.tb00513.x

Fredrikson, M. (1990). Embryological study of *Herminium monorchis* (Orchidaceae) using confocal scanning laser microscopy. *Am. J. Bot.* 77, 123–127. doi: 10.1002/j.1537-2197.1990.tb13535.x

Fredrikson, M. (1992). The development of the female gametophyte of *Epipactis* (Orchidaceae) and its inference for reproductive ecology. *Am. J. Bot.* 79, 63–68. doi: 10.1002/j.1537-2197.1992.tb12624.x

Friis, E. M., Crane, P. R., and Pedersen, K. R. (2011). *Early flowers and angiosperm evolution*. Cambridge; New York: Cambridge University Press.

Gabriel, B. L. (1982). *Biological electron microscopy*. New York: Van Nostrand Reinhold Company.

Gerrits, P. O., and Smid, L. (1983). A new less toxic polymerization system for the embedding of soft tissues in glycol methacrylate and subsequent preparing of serial sections. *J. Microsc.* 132, 81–, 85. doi: 10.1111/j.1365-2818.1983.tb04711.x

Gomez, M. D., Ventimilla, D., Sacristan, R., and Perez-Amador, M. A. (2016). Gibberellins regulate ovule integument development by interfering with the transcription factor ATS. *Plant Physiol.* 172, 2403–2415. doi: 10.1104/pp.16.01231

Gonzalez, A., Sato, H., and Marazzi, B. (2019). Embryology in *Helosis cayennensis* (Balanophoraceae): structure of female flowers, fruit, endosperm and embryo. *Plants* 8, 74. doi: 10.3390/plants8030074

Gurudeva, M. R. (2011). Development of embryo sac in *Zeuxine gracilis* (Breda) bl. (orchidaceae). *J. Indian Bot. Soc* 90, 191–194.

Graham, S. W., Lam, V. K. Y., and Merckx, V. S. F. T. (2016). Plastomes on the edge: the evolutionary breakdown of mycoheterotroph plastid genomes. *New Phytol.* 214, 48–55. doi: 10.1111/nph.14398

Hanaich, T., Sato, T., Iwamoto, T., Malavasi, Y. J., Hoshiro, M., and Mizuno, N. A. (1986). Stable lead by modification of Sato method. *J. Electron. Microscrosc.* 35, 304–306. doi: 10.1093/oxfordjournals.jmicro.a050582

Herrero, M. (2001). Ovary signals for directional pollen tube growth. *Sex Plant Reprod.* 14, 3–7. doi: 10.1007/s004970100082

Kapil, R. N., and Tiwari, S. C. (1978). The integumentary tapetum. *Bot. Rev.* 44, 457–490. doi: 10.1007/BF02860847

Karnovsky, M. J. (1965). A formaldehyde-glutaraldehyde fixative o high osmolarity of use in eletron microscopy. *J. Cell Biol.* 27, 137–138.

Kodahl, N., Johansen, B. B., and Rasmussen, F. N. (2015). The embryo sac of *Vanilla imperialis* (Orchidaceae) is six-nucleate, and double fertilization and formation of endosperm are not observed: embryo sac of *Vanilla imperialis*. *Bot. J. Linn. Soc* 177, 202–213. doi: 10.1111/boj.12237

Krawczyk, E., Rojek, J., Kowalkowska, A. K., Kapusta, M., Znaniecka, J., and Minasiewicz, J. (2016). Evidence for mixed sexual and asexual reproduction in the rare European mycoheterotrophic orchid *Epipogium aphyllum*, Orchidaceae (ghost orchid). *Ann. Bot.* 118, 159–172. doi: 10.1093/aob/mcw084

Law, S. K., and Yeung, E. C. (1989). Embryology of *Calypso bulbosa*. I. Ovule development. *Am. J. Bot.* 76, 1668–1674. doi: 10.1002/j.1537-2197.1989.tb15151.x

Leake, J. R. (1994). The biology of myco-heterotrophic ('saprophytic') plants. *New Phytol.* 127, 171–216. doi: 10.1111/j.1469-8137.1994.tb04272.x

Lee, Y. I., Lee, N., Yeung, E. C., and Chung, M. C. (2005). Embryo development of *Cypripedium formosanum* in relation to seed germination in vitro. *J. Am. Soc Hortic. Sci.* 130, 747–753. doi: 10.21273/JASHS.130.5.747

Lee, Y. I., Yeung, E. C., Lee, N., and Chung, M. C. (2008). Embryology of *Phalaenopsis amabilis* var. *formosa:* embryo development. *Bot. Stud.* 49, 139–146.

Lee, Y. I., and Yeung, E. C. (2012). Embryology of the lady's slipper orchid, *Paphiopedilum delenatii*: ovule development. *Bot. Stud.* 53, 8.

Li, Y. Y., Chen, X.-M., Guo, S. X., and Lee, Y. I. (2016). Embryology of two mycoheterotrophic orchid species, *Gastrodia elata* and *Gastrodia nantoensis*: ovule and embryo development. *Bot. Stud.* 57, 18. doi: 10.1186/s40529-016-0137-7

Li, Y. X., Li, Z. H., Schuitman, A., Chase, M. W., Li, J. W., Huang, W. C., et al. (2019). Phylogenomics of Orchidaceae based on plastid and mitochondrial genomes. *Mol. Phylogenet. Evol.* 139, 1–11. doi: 10.1016/j.ympev.2019.106540

Liu, F., Tian, M., Wang, C. X., Maojiang, G., and Quanjan, L. (2012). Studies on fruit growth and embryo development of the endangered species *Cypripedium japonicum*. *J. Plant Resour. Environ.* 21, 28–35.

Lu-Han, W., Jyh-Shyan, T., and Hai-Shan, C. (2016). Embryological studies on *Spiranthes sinensis* (Pers.) Ames. *Flora Morphol. Distrib. Funct. Ecol. Plants* 224, 191–202. doi: 10.1016/j.flora.2016.07.019

Maas, P. J. M., and Ruyters, P. (1986). *Voyria* and *Voyriella* (Saprophytic Gentianaceae) [Monograph 41]. *Flora* 40/42, 1–93. www.jstor.org/stable/4393786.

Maheshwari, P., and Naraynaswami, S. (1951). Embryological studies on *Spiranthes australis* Lind1. *Bot. J. Linn. Soc* 53, 474–756. doi: 10.1111/j.1095-8339.1952.tb01558.x

Mayer, J. L. S., Carmello-Guerreiro, S. M., and Appezzato-da-Glória, B. (2011). Anatomical development of the pericarp and seed of *Oncidium flexuosum* Sims (ORCHIDACEAE). *Flora Morphol. Distrib. Funct. Ecol. Plants* 206, 601–609. doi: 10.1016/j.flora.2011.01.009

Mc Dowel, E. M., and Trump, B. (1976). Histological fixatives for diagnostic light and electron microscopy. *Arch. Pathol. Lab. Med.* 100, 517–527.

Merckx, V. F. S. T., Freudenstein, J. V., Kissling, J., Christenhusz, M. J. M., Stotler, R. E., Crandall-Stotler, B., et al. (2013). "Mycoheterotrophy," in *Taxonomy and classification*. Ed. Merckx, V. F. S. T. (New York: Springer), 19–102.

Mohana Rao, P. R., and Sood, S. K. (1979). Embryology of *Habenaria densa* (Orchidaceae). *Bot. Notiser* 132, 145–148.

Nicolaus, R. A., Piatelli, M., and Fattorusso, E. (1964). The structure of melanins and melanogenesis: IV. On some natural melanins. *Tetrahedron* 20, 1163–1172. doi: 10.1016/s0040-4020(01)98983-5

Nishimura, G., and Yukawa, T. (2010). Dark material accumulation and sclerotization during seed coat formation in *Vanilla planifolia* Jacks. ex Andrews (Orchidaceae). *Bull. Natl. Mus. Nat. Sci.* 36, 33–37.

Okuda, S., Tsutsui, H., Shiina, K., Sprunck, S., Takeuchi, H., Yui, R., et al. (2009). Defensin-like polypeptide LUREs are pollen tube attractants secreted from synergid cells. *Nature* 458, 357–361. doi: 10.1038/nature07882

Pace, L. (1907). Fertilization in *Cypripedium. Bot. Gaz.* 5, 353–374. doi: 10.1086/329378

Polli, A., Souza, L. A., and Almeida, O. J. G. (2016). Structural development of the fruits and seeds in three mistletoe species of *Phoradendron* (Visceae: Santalaceae). *Rodriguésia* 67, 649–659. doi: 10.1590/2175-7860201667309

Ren, M.-X., Cafasso, D., Cozzolino, S., and Pinheiro, F. (2017). Extensive genetic differentiation at a small geographical scale: reduced seed dispersal in a narrow endemic marsh orchid. *Anacamptis Robusta Bot. J. Linn. Soc* 183, 429–438. doi: 10.1093/botlinnean/bow017

Rodolphe, G., Severine, B., Michel, G., and Pascale, B. (2011). "The dynamical processes of biodiversity - case studies of evolution and spatial distribution," in *Biodiversity and evolution in the vanilla genus*. Ed. Grillo, O. (Croatia: InTech). doi: 10.5772/24567

Roulin, A. (2014). Melanin-based colour polymorphism responding to climate change. *Glob. Change Biol.* 20, 3344–3350. doi: 10.1111/gcb.12594

Sato, H. A., and Maria Gonzalez, A. (2016). Floral development and anatomy of pistillate flowers of *Lophophytum* (Balanophoraceae), with special reference to the embryo sac inversion. *Flora* 219, 35–47. doi: 10.1016/j.flora.2016.01.002

Sakai, W. S. (1973). Simple method for differential staining of paraffin embedded plant material using toluidine blue O. *Stain Technol.* 48, 247–249. doi: 10.3109/10520297309116632

Sharp, L. W. (1912). The orchid embryo sac. *Bot. Gaz.* 54, 372–385. doi: 10.1086/330930

Sood, S. K. (1985). Gametophytes, integuments initiation and embryogeny in *Microstylis cylindrostachya* (Orchidaceae, Epidendreae). *Proc. Indian Acad. Sci.* 6, 379–387. doi: 10.1007/bf03053676

Sood, S. K. (1986). Gametogenesis, integuments initiation and embryogeny in three species of *Habenaria* (Orchidaceae, Orchideae). *Proc. Indian Acad. Sci.* 6, 487–494. doi: 10.1007/bf03053543

Sood, S. K., and Mohana Rao, P. R. (1986). Gametophytes, embryogeny and pericarp of *Microstylis wallichii* lindl. (Orchidaceae). *Bot. Mag. Tokyo* 99, 351–359. doi: 10.1007/BF02488715

Sood, S. K. (1988). Development of gametophytes, embryogeny and pericarp in *Goodyera repens* (Orchidaceae, Neottieae). *Proc. lndian Acad. Sci.* 2, 149–156. doi: 10.1007/bf03053400

Sood, S. K., and Mohana Rao, P. R. (1988). Studies in the embryology of the diandrous orchid *Cypripedium cordigerum* (Cypripedieae, Orchidaceae). *Plant Syst. Evol.* 160, 159–168. doi: 10.1007/BF00936043

Sood, S. K. (1989). Embryology and systematic position of *Liparis* (Orchidaceae). *Plant Syst. Evol.* 166, 1–9. doi: 10.1007/BF00937871

Sood, S. K. (1992). Embryology of *Malaxis saprophyta*, with comments on the systematic position of *Malaxis* (Orchidaceae). *P1. Syst. Evol.* 179, 95–105. doi: 10.1007/bf00938022

Suaza-Gaviria, V., Pabón-Mora, N., and González, F. (2016). Development and Morphology of Flowers in Loranthaceae. *Int. J. Plant Sci.* 177, 559–578. doi: 10.1086/687280

Suetsugu, K. (2018). Seed dispersal in the mycoheterotrophic orchid *Yoania japonica*: further evidence for endozoochory by camel crickets. *Plant Biol.* 20, 707–712. doi: 10.1111/plb.12731

Swamy, B. G. L. (1945). Embryo sac and fertilization in *Cypripedium spectabile*. *Bot. Gaz.* 107, 291–295.

Swamy, B. G. L. (1946a). The embryology of *Zeuxine sulcata* Lindl. *New Phytol.* 45, 132–136. doi: 10.1111/j.1469-8137.1946.tb05050.x

Swamy, B. G. L. (1946b). Embryology of *Habenaria*. *Proc. Nat. Inst. Sci.* 12, 413–426.

Swamy, B. G. L. (1947). On the life-history of *Vanilla planifolia*. *Bot. Gaz.* 108, 449–456. doi: 10.1086/335429

Swamy, B. G. L. (1949a). Embryological Studies in the Orchidaceae. I. Gametophytes. *Am. Midl. Nat.* 41, 184. doi: 10.2307/2422025

Swamy, B. G. L. (1949b). Embryological studies in the orchidaceae. II. Embryogeny. *Am. Midl. Nat.* 41, 202. doi: 10.2307/2422026

Tobe, H. (2016). Embryology of *Cardiopteris* (Cardiopteridaceae, Aquifoliales), with emphasis on unusual ovule and seed development. *J. Plant Res.* 129, 883–897. doi: 10.1007/s10265-016-0845-9

Tohda, H. (1967). An embryological study of *Hetaeria skikokiana*, a saprophytic orchid in Japan. *Sei Rep. Tohoku Univ. Ser. IV (Biol)* 33, 83–95.

Trapnell, D. W., and Hamrick, J. L. (2004). Partitioning nuclear and chloroplast variation at multiple spatial scales in the neotropical epiphytic orchid *Laelia rubescens*. *Mol. Ecol.* 13, 2655–2666. doi: 10.1111/j.1365-294X.2004.02281.x4

Windsor, J. B., Symonds, V. V., Mendenhall, J., and Lloyd, A. M. (2000). *Arabidopsis* seed coat development: morphological differentiation of the outer integument. *Plant J.* 22, 483–493. doi: 10.1046/j.1365-313x.2000.00756.x

Wirth, M., and Withner, C. L. (1959). "The orchids: a scientific survey," in *Embryology and development in the Orchidaceae*. Ed. Withner, C. L. (New York: Ronald Press), 155–188.

Yang, C. K., and Lee, Y. I. (2014). The seed development of a mycoheterotrophic orchid, *Cyrtosia javanica* Blume. *Bot. Stud.* 55, 44. doi: 10.1186/s40529-014-0044-8

Yeung, E. (1996). Embryology of *Cymbidium sinense*: embryo development. *Ann. Bot.* 78, 105–110. doi: 10.1006/anbo.1996.0101

Yeung, E. C., and Law, S. K. (1989). Embryology of *Epidendrum ibaguense*. I. Ovule development. *Can. J. Bot.* 67, 2219–2226. doi: 10.1139/b89-283

Yeung, E. C., and Law, S. K., (1997). "Orchid biology reviews and perspectives, VII," in *Ovule and megagametophyte development in orchids*. Eds. Arditti, J., and Pridgeon, A. M. (New York: Springer Science), 31–68.

Zhang, X. S., and O'Neill, S. D. (1993). Ovary and gametophyte development are coordinately regulated by auxin and ethylene following pollination. *Plant Cell* 5, 403–418. doi: 10.1105/tpc.5.4.403

Zeng, S., Zhang, Y., Teixeira da Silva, J. A., Wu, K., Zhang, J., and Duan, J. (2014). Seed biology and *in vitro* seed germination of *Cypripedium*. *Crit. Rev. Biotechnol.* 34, 358–371. doi: 10.3109/07388551.2013.841117

Conflict of Interest: The authors declare that the research was conducted in the absence of any commercial or financial relationships that could be construed as a potential conflict of interest.

frontiers in Plant Science

ORIGINAL RESEARCH
published: 30 January 2020
doi: 10.3389/fpls.2019.01709

PeERF1, a SHINE-Like Transcription Factor, Is Involved in Nanoridge Development on Lip Epidermis of *Phalaenopsis* Flowers

Pei-Han Lai[1†], *Li-Min Huang*[1†], *Zhao-Jun Pan*[2], *Wann-Neng Jane*[3], *Mei-Chu Chung*[3], *Wen-Huei Chen*[4] and *Hong-Hwa Chen*[1,4,5*]

[1] Department of Life Sciences, National Cheng Kung University, Tainan, Taiwan, [2] Institute of Ecology and Evolutionary Biology, National Taiwan University, Taipei, Taiwan, [3] Institute of Plant and Microbial Biology, Academia Sinica, Taipei, Taiwan, [4] Orchid Research and Development Center, National Cheng Kung University, Tainan, Taiwan, [5] Institute of Tropical Plant Sciences, National Cheng Kung University, Tainan, Taiwan

OPEN ACCESS

Edited by:
Jen-Tsung Chen,
National University of Kaohsiung, Taiwan

Reviewed by:
Hirokazu Tanaka,
Meiji University, Japan
Chao Bian,
Beijing Genomics Institute (BGI), China

***Correspondence:**
Hong-Hwa Chen
hhchen@mail.ncku.edu.tw

[†]These authors have contributed equally to this work

Specialty section:
This article was submitted to Plant Development and EvoDevo, a section of the journal Frontiers in Plant Science

Received: 23 July 2019
Accepted: 04 December 2019
Published: 30 January 2020

Citation:
Lai P-H, Huang L-M, Pan Z-J, Jane W-N, Chung M-C, Chen W-H and Chen H-H (2020) PeERF1, a SHINE-Like Transcription Factor, Is Involved in Nanoridge Development on Lip Epidermis of Phalaenopsis Flowers. Front. Plant Sci. 10:1709. doi: 10.3389/fpls.2019.01709

Phalaenopsis orchids have a spectacular floral morphology with a highly evolved lip that offers a landing platform for pollinators. The typical morphological orchid lip features are essential for the special pollination mechanism of *Phalaenopsis* flowers. Previously, we found that in the lip, a member of the AP2/EREBP protein family was highly expressed. Here, we further confirmed its high expression and characterized its function during lip development. Phylogenetic analysis showed that AP2/EREBP belongs to the Va2 subgroup of ERF transcription factors. We named it PeERF1. We found that *PeERF1* was only expressed at stage 5, as flowers opened. This coincided with both thickening of the cuticle and development of nanoridges. We performed knockdown expression of *PeERF1* using CymMV-based virus-induced gene silencing in either the *AP2* conserved domain, producing *PeERF1_AP2*-silenced plants, or the *SHN* specific domain, producing *PeERF1_SHN*-silenced plants. Using cryo-SEM, we found that the number of nanoridges was reduced only in the *PeERF1_AP2*-silenced group. This change was found on both the abaxial and adaxial surfaces of the central lip lobe. Expression of *PeERF1* was reduced significantly in *PeERF1_AP2*-silenced plants. In cutin biosynthesis genes, expression of both *PeCYP86A2* and *PeDCR* was significantly decreased in both groups. The expression of *PeCYP77A4* was reduced significantly only in the *PeERF1_AP2*-silenced plants. Although *PeGPAT* expression was reduced in both silenced plants, but to a lesser degree. The expression of *PeERF1* was significantly reduced in the petal-like lip of a big-lip variant. *PeCYP77A4* and *PeGPAT* in the lip were also reduced, but *PeDCR was not*. Furthermore, heterologous overexpression of *PeERF1* in the genus *Arabidopsis* produced leaves that were shiny on the adaxial surface. Taken together, our results show that in *Phalaenopsis* orchids PeERF1 plays an important role in formation of nanoridges during lip epidermis development.

Keywords: AP2/EREBP, cutin biosynthesis genes, lip, nanoridge, orchid, *Phalaenopsis*, transcription factor

INTRODUCTION

Phalaenopsis orchids are renowned for their unique and elegant floral morphology and long florescence duration. Recently, they have become the model Orchidaceae research plants. Two databases for genetic information have been established, OrchidBase 3.0 and Orchidstra 2.0 (Fu et al., 2011; Su et al., 2013a; Tsai et al., 2013; Chao et al., 2017). The floral morphology of *Phalaenopsis* orchids includes three sepals, three petals, and one column. The column is formed by fusion of the style and a part of the androecium. The outer two perianth whorls are typically petaloid and are referred to as tepals. Instead of producing three uniform petals, *Phalaenopsis* flowers have a highly evolved, modified, and resupinated inner medium petal, the lip (Rudall and Bateman, 2002; Tsai et al., 2004; Tsai and Chen, 2006; Tsai et al., 2008; Pan et al., 2011; Pan et al., 2014). This lip is understood to play an important role both in pollination and evolution (Robinson and Burns-Balogh, 1982; Cozzolino and Widmer, 2005; Mondragón-Palomino and Theißen, 2008), as it provides a platform for pollinators.

Lip morphogenesis consists of five stages, from the embedded stage 1 to the open flower of stage 5. There is no division of the lip at stage 1. However, in stage 2, the lip divides quickly into three distinct parts. There are two lateral lobes, one central lobe, and one callus. The split lip forms a tunnel-like structure in the mature flower (**Figure 1A**, Li), a feature related to evolved pollination strategies (Cozzolino and Widmer, 2005). Although *Phalaenopsis* orchids exhibit unique floral morphological features, Cryo-scanning electron microscopy (Cryo-SEM) has revealed that the perianth lip epidermis has a unique functional morphology not found in sepals or petals (Pan et al., 2011; Hsieh et al., 2013a; Hsieh et al., 2013b; Pan et al., 2014; Hsu et al., 2015b). Heavy and dense nanoridges cover the lip epidermis. These undulated nanostructures, also called cuticular folds, are assumed to contain cuticular lipids (Koch et al., 2008; Koch et al., 2009a; Koch et al., 2009b).

Diverse perianth and floral epidermis adaptations have evolved in both eudicots and monocots. In many flowering plants, the epidermal surfaces of sepals and petals display a range of patterns in combination with diverse micro- and nanostructures (Kay et al., 1981; Whitney et al., 2009; Whitney et al., 2011b; Kourounioti et al., 2013). More than 75% of petal epidermal cells of angiosperms are conical or papillate, usually on the adaxial side where potential pollinators would be found (Kay et al., 1981; Whitney et al., 2009; Whitney et al., 2011a; Whitney et al., 2011b). Moreover, in many plants, sepal and petal epidermal cells are covered with various density and orientation of nanoridges (Jeffree, 2006). These structures on the surface of sepal and petal epidermal cells are believed to attract pollinators and enhance pollination success through visual signals (Whitney et al., 2009; Whitney et al., 2011b; Kourounioti et al., 2013; Moyroud et al., 2017) and act as tactile signals affecting pollinator movement (Prüm et al., 2011; Rands et al., 2011; Prüm et al., 2012; Prüm et al., 2013; Adachi et al., 2015). Moreover, cell surface cuticle structures can strengthen cells and thereby function many ways in plant development as well as survival and defense in unfavorable environments, such as under biotic or abiotic stress (e.g., dehydration, pathogens, UV light, frost, and insect attacks) (Koch et al., 2008; Koch et al., 2009a; Koch et al., 2009b).

The first identified transcription factors (TFs) that regulate cuticle biosynthesis are SHINEs/WAX INDUCERs (SHNs/WINs), members of the V group of the ethylene responsive factor (ERF) subfamily of the apetala2/ethylene response element binding protein (AP2/EREBP) TF family (Aharoni et al., 2004; Broun et al., 2004; Nakano et al., 2006). In *Arabidopsis SHINE* gain-of-function mutant (*shn*) and plants overexpressing *AtWIN1/SHN1*, *AtSHN2*, or *AtSHN3* have shiny leaves and increased accumulation of epidermal wax on the top of leaves as compared with wild type (Aharoni et al., 2004; Broun et al., 2004). By co-silencing all three AtSHN clade members, SHNs redundantly regulate the formation of petal surface nanoridges and also cell elongation, adhesion, and separation (Shi et al., 2011). Recently, increased number of SHN-like TFs that belong to the ERF-V group have been identified and they exhibit various functions during plant physiological processes.

The ERF-V group includes two subgroups: Va and Vb. The Va subgroup contains two conserved motifs of the conserved middle motif (CMV-1) and C-terminal motif (CMV-2), which the Vb subgroup does not contain (Nakano et al., 2006). The ERF-Va subgroup is further divided into two subgroups, Va1 and Va2, containing a complete or incomplete CMV-1 motif, respectively (Nakano et al., 2014). Functional characterization of genes in the Va1 subgroup from several plants indicates that they are involved in cuticle development. *Arabidopsis* AtSHNs regulate cuticle formation (Aharoni et al., 2004; Broun et al., 2004; Shi et al., 2011).

Similar research has been done with several plant species. In barley it was found that HvNud is involved in the lipid biosynthesis of the grain surface, which produces hulled caryopses (Taketa et al., 2008). Tomato SlSHINE3 is involved in cutin metabolism of fleshy fruit epidermal cells for patterning the epidermal surface (Shi et al., 2013) and SlSHN1 is involved in wax accumulation of leaf epidermal cells, which enhances drought tolerance (Al-Abdallat et al., 2014). Rice OsAP2/ERF-"N-22" is involved in wax biosynthesis and also enhances drought resistance (Mawlong et al., 2014), while wheat TdSHN1 is involved in the cuticle formation of leaf surfaces (Jäger et al., 2015). *Eucalyptus* EgrSHN1 and EgrSHN2 are involved in cell wall biosynthesis of flowers (Marques et al., 2013). Hence, the complete CMV-1 and CMV-2 motifs of ERF-Va1 genes are deemed the SHINE domains. SHINE domains are considered to be important in cuticle development. The subgroup Va1 is identified as the SHINE clade (Aharoni et al., 2004).

In contrast, the Va2 subgroup, with an incomplete CMV-1 motif, is involved in various physiological processes: *Arabidopsis* At5g25190 is induced by 1-aminocyclopropane-1-carboxylicacid (ACC) and salt (NaCl) and was named the ethylene- and salt-inducible ERF gene (*AtESE3*) (Zhang et al., 2011), but its

Abbreviations: AF, anticlinal field; CF, central field; Cryo-SEM, Cryo-scanning electron microscopy; ERF, ethylene responsive factor; RT-PCR, reverse transcription–polymerase chain reaction; SHN/WIN, SHINE/WAX INDUCER; TFs, transcription factors; VIGS, virus-induced gene silencing.

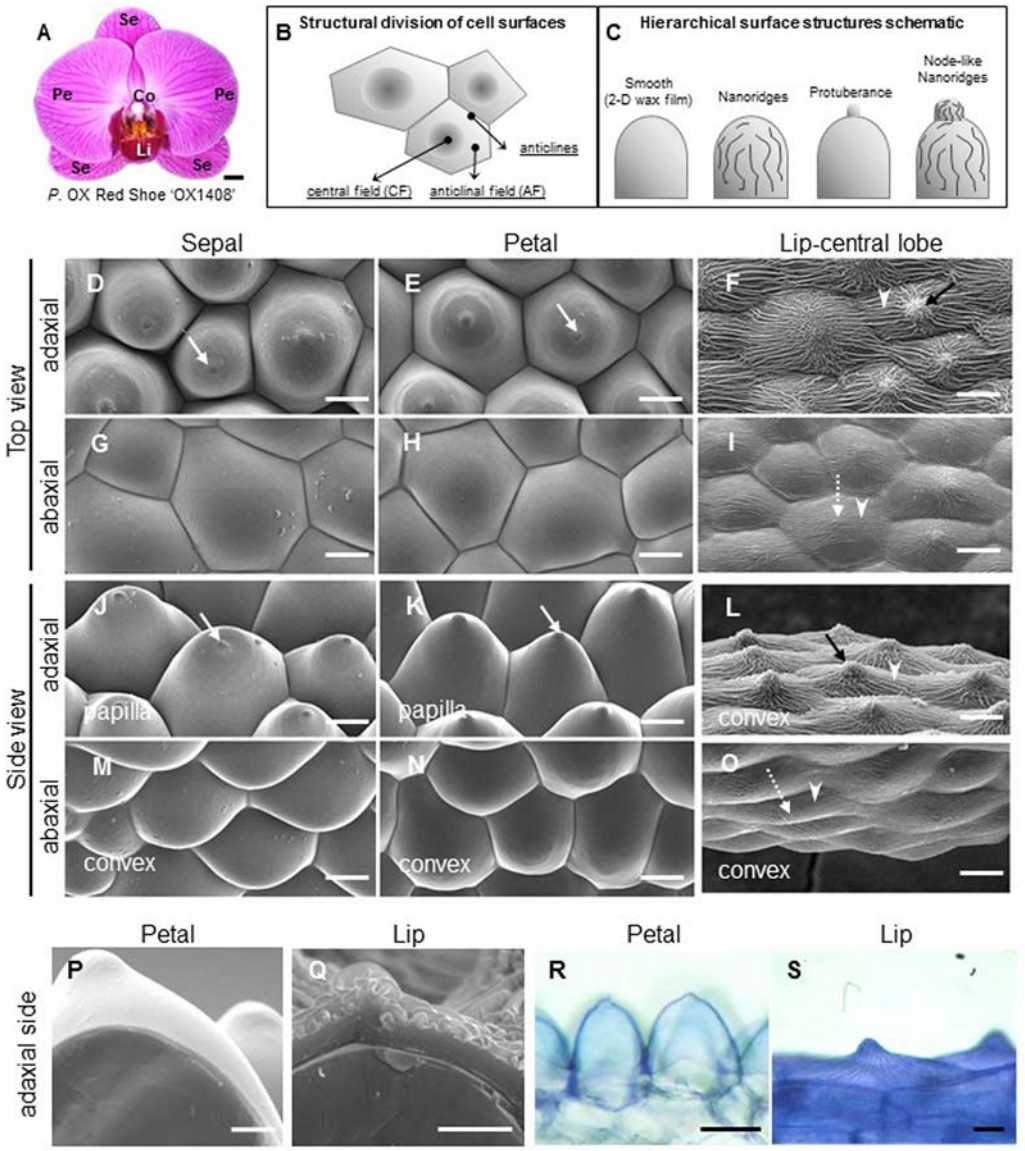

FIGURE 1 | Ultrastructure of floral epidermal cells in the cultivar *P.* OX Red Shoes "OX1408." **(A)** Floral morphology. Scale bar, 5 cm. Se, sepal; Pe, petal; Li, lip; Co, column. **(A)** Schematic diagrams of the cell structural division of a single cell surface. The central field (CF) is in the center middle of the cell surface and the anticline field (AF) is between the middle area and the boundary of the cell. Anticlines directly connected to the cell area (modified after Koch et al., 2009a). **(A)** Schematic diagrams of epidermis that built up the cell hierarchical structures with 2-D smooth wax films or decorated with protuberance, nanoridges, and node-like nanoridges. **(D–O)** Cyro-SEM top view and side view of epidermal cells of perianth organs. White arrows indicate a protuberance on the top of the cell. Black arrows indicate node-like nanoridges in the CF of the cell. White arrowheads indicate parallel nanoridges in the AF of the cell. Scale bars, 30 μm. **(P–Q)** Cross section of adaxial epidermal cells of petal and lip. Scale bars, 10 μm. **(R–S)** Lipophilic dye "Sudan Black B" staining on the adaxial epidermal cells of petal and lip. Scale bars, 100 μm.

overexpression confers no typical SHINE phenotype (Aharoni et al., 2004). Tomato LeERF1 regulates fruit ripening and softening (Li et al., 2007). *Populus* PtaERF003 is involved in lateral root formation (Trupiano et al., 2013). *Eucalyptus* Egr33m and Egr40m are involved in wood cell wall biosynthesis (Marques et al., 2013). Tomato SlERF52 regulates flower pedicel abscission (Nakano et al., 2014). Whereas, NvERF045 in berries regulates berry ripening and is also involved in cuticle development (Leida et al., 2016). Moreover, the Vb subgroup At5g19790 does not contain CMV-1 and CMV-2 motifs and is important in low potassium signaling (Kim et al., 2012).

Gene associated with cutin biosynthesis for epidermal nanoridge formation include CYP86A and CYP77A, members of a cytochrome P450 family, glycerol-3-phosphate

acyltransferase 6 (GPAT), and defective in cuticular ridges (DCR) (Kannangara et al., 2007; Li-Beisson et al., 2009; Panikashvili et al., 2009; Shi et al., 2011; Shi et al., 2013; Petit et al., 2016; Mazurek et al., 2017). GPAT6 and CYP77A6 are for the formation of floral cutin in *Arabidopsis thaliana* (Li-Beisson et al., 2009). *CYP86A4* has been reported as one of the downstream target genes *SHN* (Shi et al., 2011; Shi et al., 2013). It has been shown that *DCR*-deficient plants have defective cuticle formation with altered epidermal cell differentiation (Panikashvili et al., 2009). This defective formation in reproductive and vegetative tissues was correlated with low abundance of 9(10),16-dihydroxyhexadecanoic acid in the cutin polymer of *DCR* (*At5g23940*)-deficient plants (Panikashvili et al., 2009).

We previously identified several unigenes dominantly expressed in the *Phalaenopsis* lip (Hsiao et al., 2013). Among them, one member of the AP2 family, *P. equestris ethylene responsive factor 1* (*PeERF1*), was found to be most similar to the SHINE clade homolog At5g25190.

Here, to extend our understanding of the function of *PeERF1* in *Phalaenopsis* orchids, we analyzed its spatial and temporal gene expression; downregulated *PeERF1* expression by using CymMV-based virus-induced gene silencing (VIGS) in orchids; and examined heterologous overexpression of *PeERF1* in *Arabidopsis* for comparison. The abnormal phenotypes of nanoridge sculpture patterns of lip epidermal cells were observed in the somaclonal variant, *P.* "Join Big foot TH365" containing enlarged petal-like lip mutants. We further investigated the relationship of putative *Phalaenopsis* orthologs of known cutin biosynthetic genes with the cuticle formation in *Phalaenopsis* lips. These genes include two cytochrome P450s, *PeCYP86A2* and *PeCYP77A4*, and two putative acyltransferases, *PeGPAT* and *PeDCR*. We hope that these results will contribute to the understanding of transcriptional regulation of late-stage orchid lip formation during floral morphogenesis.

MATERIALS AND METHODS

Plant Materials

We conducted gene spatial expression analysis on specimens of *Phalaenopsis equestris* obtained from the Taiwan Sugar Corp. (Tainan, Taiwan), and both gene temporal expression and VIGS experiments on the commercial cultivar *P.* OX Red Shoes "OX1408" obtained from Oxen Biotechnology Corp. (Tainan, Taiwan).

The flower buds of *P.* OX Red Shoes "OX1408" were divided into five stages by size (**Figure 3C**). A single raceme spike inflorescence embraces 8–10 flowers. The smallest flower bud is embedded in the tip of an inflorescence and is stage 1 (< 0.5 cm), followed by successive stage 2 (0.5–1 cm), stage 3 (1–2 cm), stage 4 (2–3 cm), and blooming flowers are stage 5 (floral diameter of 12 cm) (**Figure 3C**). For comparison, we used wild-type flower and big-lip variant flower (petal-like lip) of *P.* hybrid "Join Big foot" (*P.* Yu Pin Easter Island x *P.* I- Hsin Diamond "Join White of Love"). These were provided by Join Orchids Incorporation (Tainan, Taiwan). For VIGS experiments, plants were kept in the greenhouse at the Tainan District Agricultural Research and Extension Station, Council of Agriculture, under a controlled temperature of 27°C/22°C (day/night). Other mature orchid plants were maintained in the greenhouse at National Cheng Kung University under natural light and controlled temperature from 23°C to 27°C.

Cryo-SEM

We examined changes in cellular morphology from the 1st to the 8th blooming flowers of silenced plants (stage 5, floral diameter of 12 cm) using Cryo-SEM. Sample preparation and Cryo-SEM examination follows previous research (Hsieh et al., 2013a; Pan et al., 2014). Fresh samples were dissected and loaded on the stub, which was subsequently frozen with liquid nitrogen slush, and then quickly transferred to a sample preparation chamber at -160°C for 5 min. After that time the temperature was raised to -85°C and sublimed for 15 min. Samples were then coated with platinum (Pt) at -130°C and transferred to the cryo-stage in an SEM chamber and observed at -160°C using Cryo scanning electron microscope (FEI Quanta 200 SEM/Quorum Cryo System PP2000TR FEI) with 20 kV.

Images were taken under a Cryo stage at < -160°C. We measured the nanoridge area on 40 flowers, 5 flowers from each of 8 plants using ImageJ (http://rsb.info.nih.gov/ij/). Mean data were compared by Duncan's multiple-range test, using SPSS v17.

Cloning and Characterization of *PeERF1*

Using TRIsure reagent (Bioline, UK) total RNA was extracted and then treated with RNase-free DNaseI (Invitrogen, USA) to remove residual DNA. We cloned the full-length cDNA of *PeERF1* (accession no. MG948436) using a SMART rapid amplification of cDNA ends (RACE) kit (Clontech, USA). We randomly selected 6 to 8 positive clones for sequencing. For gene expression analysis, quantitative real-time RT-PCR (qRT-PCR) was performed in triplicate and repeated independently three times as previously described (Hsu et al., 2015a). Primers for all the PCR and qRT-PCR experiments are in **Supplementary Table S1**.

For qRT-PCR, the cDNA template was mixed with 2X SYBR Green PCR master mix (Applied Biosystems, Norwalk, CT, USA) in an ABI 7300 instrument (Applied Biosystems) with three biological replicates. For gene quantification, qRT-PCR was performed at stage 5 flowers of *PeERF1*-silenced plants in triplicate, and repeated in three silenced plants independently. For PCR reaction, each sample was analyzed in triplicate. Reactions involved incubation at 50°C for 2 min, then 95°C for 10 min, and thermal cycling for 40 cycles (95°C for 15 s and 60°C for 1 min). The relative quantification was calculated according to the manufacturer's instructions (Applied Biosystems). To control the integrity of RNA and normalize target RNA copy numbers in gene-silenced and mock-treated flowers, the housekeeping gene *PeActin4* (AY134752) was recruited as an internal control for normalization (Chen et al., 2005).

Sequence Alignment and Phylogenetic Analysis

Multiple sequence alignment was generated by using AlignX (Vector NTI advance 11, Invitrogen). The protein sequences of SHN homologous TFs were obtained from the National Center for Biotechnology Information (NCBI) databases (http://www.ncbi.nlm.nih.gov/), and accession numbers are as follows: *A. thaliana* AtSHN1 (NP_172988), AtSHN2 (NP_196680), AtSHN3 (NP_851073), At5g25190 (NP_197901.1), and At5g19790 (NP_197480.1); tomato (*Solanum lycopersicum*) SlSHN1 (XP_004235965), SlSHN3 (XP_004240977), and SlERF52 (BAO18577); tomato (*Lycopersicon esculentum*) LeERF1 (AAL75809); berry (*Vitis vinifera*) VvERF045 (ANT73695); barley (*Hordeum vulgare L.*) HvNud (BAG12386); wheat (*Triticum aestivum L.*) TdSHN1 (ANY98960); rice (*Oryza sativa*) OsAP2/ERF-"N-22" (ACU44657), and *Populus* (*P. tremula*x *P. alba*) PtaERF003 (Potri.018G021900). *Eucalyptus grandis* SHN homologous TFs can be accessed in the Phytozome database (http://www.phytozome.net/cgi-bin/gbrowse/eucalyptus/): EgrSHN1 (Eucgr.C04221.1), EgrSHN2 (Eucgr.C01178.1), Egr33m (Eucgr.C02719.1), and Egr40m (Eucgr.C03947.1) (Marques et al., 2013). These sequences were used to construct phylogenetic trees by using MEGA5.0 (Tamura et al., 2011). Phylogenetic relationships were inferred by the neighbor-joining method and evolutionary distances were computed by the Poisson correction method. Bootstrap values were calculated with 1,000 replicates.

Virus-Induced Gene Silencing (VIGS)

VIGS experiments with *PeERF1* were performed as previously described (Hsieh et al., 2013a; Pan et al., 2014); 142-nt and 175-nt fragments for the conserved AP2 domain and the specific incomplete "SHINE domains," i.e., CMV-1 and CMV-2 motifs of *PeERF1*, respectively, were constructed into the pCymMV-Gateway plasmid (Lu et al., 2007). The constructed VIGS-silencing plasmids for producing the *PeERF1_AP2*-silenced and *PeERF1_SHN*-silenced plants were named pCymMVGateway-PeERF1_AP2 and pCymMV-Gateway-PeERF1_SHN, respectively. These plasmids were transformed into *Agrobacterium* (strain EHA105). For infiltration, *Agrobacterium tumefaciens* strain EHA105 containing pCymMVGateway-PeERF1_AP2 or mMV-Gateway-PeERF1_SHN were grown overnight at 28°C to OD_{600} = 1. After centrifugation, bacterial cell pellets were resuspended by adding 300 µl MS medium containing 100 µM acetosyringone and allowed to stand at room temperature for 0.5 h. Two methods of Agro-infiltration were used: inflorescence injection and leaf injection. For inflorescence injection, suspensions were injected into the stalk of the raceme with eight internodes and one visible floral bud (extruding out of its bract) by use of a 1-ml syringe with a needle in all silencing treatments. The raceme stalk usually emerges from the stem between the third and fourth leaves. For leaf injection, suspensions were injected into the leaf directly above the emerging inflorescence. Mock-treated plants were recruited as the negative control. They were handled the same and contained an empty vector of a *Cymbidium* mosaic virus infectious clone with a Gateway system vector. Transformed EHA105 was injected into both inflorescence spikes and the leaf directly above the emerging inflorescence. For VIGS, eight independent *PeERF1*_AP2-silenced and eight *PeERF1*_ SHN-silenced plants as well as eight mock control plants were generated, and repeated twice independently. qRT-PCR was used to examine the knockdown expression of cuticle biosynthesis-related genes in the 5th floral buds (stage 3, length of 1–2 cm) after agro-infiltration in triplicate and repeated three times independently; Cryo-SEM was used to examine the changes in cellular morphology from the 5th to the 8th blooming flowers of silenced plants (stage 5, floral diameter of 12 cm).

Ectopic Expression of *PeERF1* in *Arabidopsis*

A. thaliana ecotype Columbia was used for transformation experiments as previously described (Chen et al., 2012). Full-length cDNA of *PeERF1* was cloned into the pBI121 vector under the control of the constitutive *Cauliflower* mosaic virus (CaMV) 35S promoter, and the resulted plasmid was named pBI121-*PeERF1*. We then introduced pBI121-*PeERF1* plasmid into *Agrobacterium tumefaciens* (strain GV3101) and transformed into wild-type *Arabidopsis* by the floral dip method (Clough and Bent, 1998). In total, 60 kanamycin-resistant T1 seedlings were obtained and grown at 23°C in a growth chamber under long-day conditions (16-h light/8-h dark). A total of 457 T2 heterozygous seedlings were obtained with a segregation ratio of 3:1 as analyzed by chi-square test. For gene expression analysis, RNA samples of T1 heterozygous plants were extracted to confirm the successful expression by qRT-PCR in triplicate and repeated three times independently. The primers were listed in **Supplementary Table S1**.

RESULTS

Phalaenopsis Flowers Showed Unique Lip Cuticle Features Relative to Other Perianth Epidermal Morphology

To investigate the detailed ultrastructure of orchid floral epidermal cells, we first examined the floral epidermal morphology of a native species, *P. aphrodite* subsp. *formosana* (**Supplementary Figure S1**) and the commercial cultivar, *P.* OX Red Shoe "OX1408" (**Figure 1A**) by using Cryo-SEM. The schematic diagrams of different regions and hierarchical structures on the cell surface of *Phalaenopsis* flowers are shown in **Figures 1B**, **C**. The "central field" (CF) and "anticlinal field" (AF) represent the inner and outer parts of cells, respectively, and the boundaries of two perpendicular cell walls are "anticlines" (**Figure 1B**). The epidermal cells of the *Phalaenopsis* orchid perianth have a variety of cell morphology, including convex or papilla cell shapes. The cell surface of the perianth epidermal cells can be smooth, covered with 2-D wax films or decorated

with protuberances, nanoridges, or other node-like nanoridges (**Figure 1C**).

The adaxial epidermal cells of sepals and petals in *P.* OX Red Shoe "OX1408" flowers featured a papilla cell shape with a protuberance on the top (**Figures 1D**, **E**, **J**, **K**, white arrow), and the abaxial epidermal cells of sepals and petals had a convex cell shape with smooth 2-D wax films (**Figures 1G**, **H**, **M**, **N**). In contrast, heavy and dense nanoridges were found on the lip epidermis. The lip adaxial epidermal cells had convex cell shape with the appearance of node-like nanoridges in the CF (**Figures 1F**, **L**, black arrow) and parallel and radial nanoridges in the AF (**Figures 1F**, **L**, white arrowhead) of cell surfaces. The lip abaxial epidermal cells had a convex cell shape with parallel nanoridges in the CF (**Figures 1I**, **O**, white dashed arrow) and AF of cell surfaces (**Figures 1I**, **O**, white arrowhead). The same heavy nanoridges were also observed on the lip epidermis of *P. aphrodite* subsp. *formosana* (**Supplementary Figure S1D**).

Cross sections of petal and lip adaxial epidermal cells showed markedly different thickness of cuticles (**Figures 1P**, **Q**). The petal adaxial epidermal cells were covered with smooth 2-D wax films (**Figure 1P**) as compared with the complex and heavy nanoridges on the lip adaxial epidermal cells (**Figure 1Q**). Histochemistry staining with the lipophilic dye "Sudan Black B" revealed a lipid layer on the petal cuticle and lip adaxial epidermal cells (**Figures 1R**, **S**).

PeERF1 Displayed Lip Development-Associated Gene Expression Patterns

We analyzed and confirmed the spatial expression patterns of *PeERF1* in both vegetative (root, leaf, and stalk) and reproductive organs (pedicle, bud, sepal, petal, lip, and column) of *P. equestris* (**Figures 2A, B**) by qRT-PCR. *PeERF1* was highly expressed in reproductive organs (pedicle and flower bud) with lower expression in roots, and very low expression in leaf and stalk tissue. As expected, *PeERF1* was highly expressed in the lip and column, with threefold expression in lip as compared with sepals and petals (**Figure 2C**).

Development of Cuticles on Lip Epidermal Cells Concomitant With the *PeERF1* Gene Expression at Late Stage of Lip Morphogenesis

Temporal expression of *PeERF1* during lip morphogenesis was examined in five stages of lip development (**Figures 3A–C**). *PeERF1* showed low and increasing expression from stage 1 to stage 4, with a sharp increase at stage 5 (**Figure 3D**).

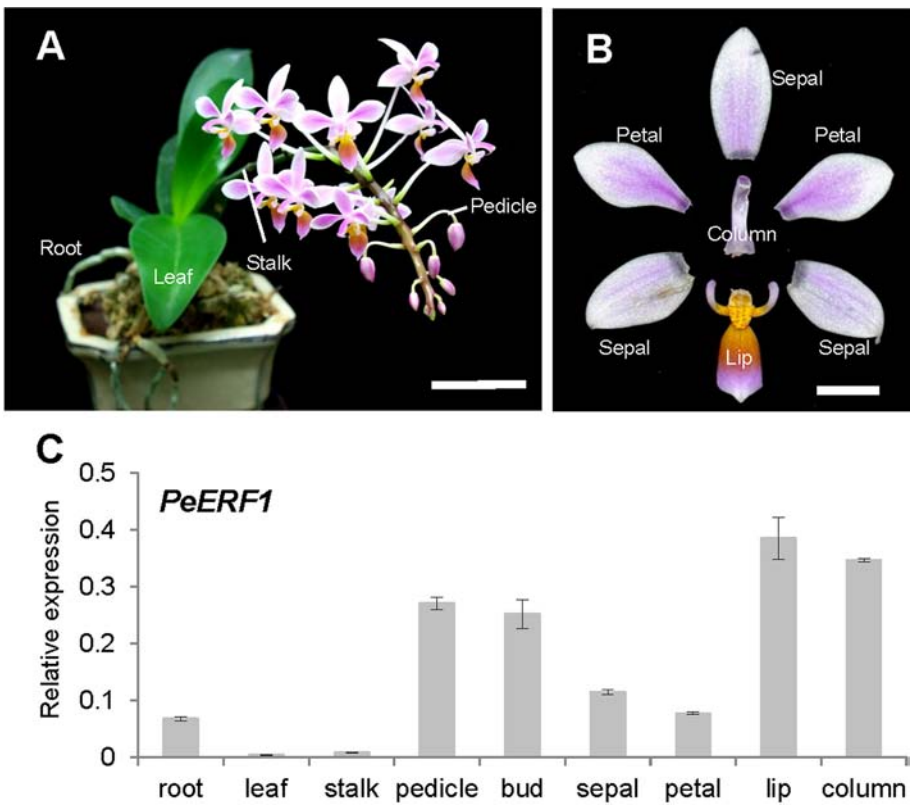

FIGURE 2 | Spatial expression patterns of *PeERF1* in the native species *P. equestris*. **(A)** Various vegetative and reproductive tissues were analyzed, including roots, leaves, pedicles, and stalks. Scale bar, 5 cm. **(B)** Flower organs were analyzed, including sepals, petals, lip, and column. Scale bar, 1 cm. **(C)** Spatial expression patterns of *PeERF1* in various organs. Total RNA were extracted from variant tissues in three independent plants. Three technical repeats were performed for each sample. Data are mean ± SD. Numbers above the bars are expression levels after normalization with the internal control (*PeActin4*) (Chen et al., 2005).

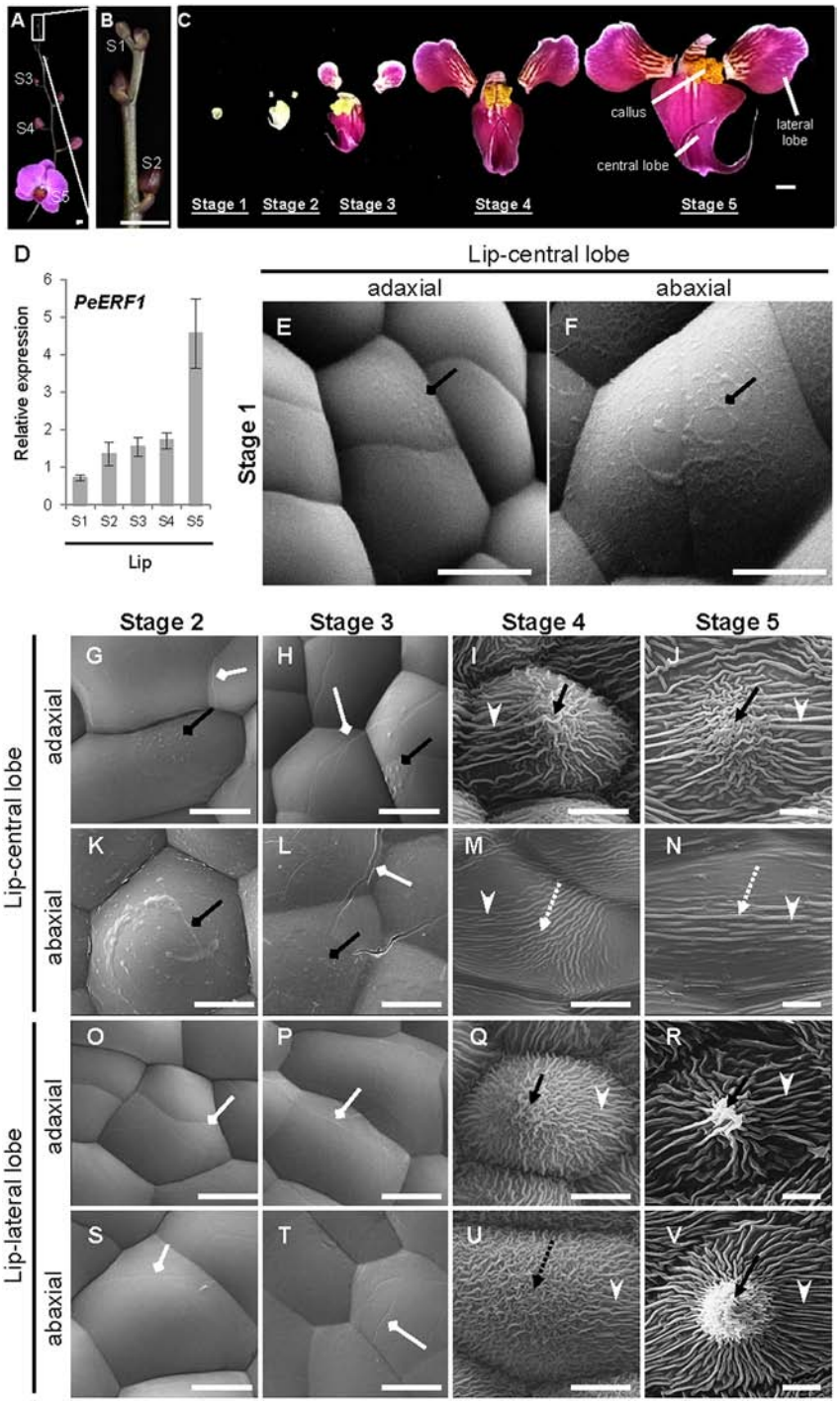

FIGURE 3 | Temporal expression patterns of *PeERF1* and the ultrastructure of lip epidermal cells during various developmental stages of *P.* OX Red Shoes "OX1408" flowers. **(A–C)** Various stages of lip development during floral morphogenesis. S1, stage 1, flower bud (0–0.5 cm); S2, stage 2, flower bud (0.5–1 cm); S3, stage 3, flower bud (1–2 cm); S4, stage 4, flower bud (2–3 cm); S5, stage 5, flowering. Scale bars, 2 cm **(A–B)** and 1 cm **(C)**. **(D)** Temporal expression patterns of *PeERF1* at various lip developmental stages. Total RNA were extracted from the various lip developmental stages in three independent plants. Three technical repeats were performed for each sample. Data are mean ± SD. Numbers above the bars are expression levels after normalization with the internal control (*PeActin4*). **(E–V)** Cyro-SEM of adaxial and abaxial sites of epidermal cells of different parts of lip organs during developmental stages. Black rhombus-head lines indicate the secreted bubble-like preliminary cuticle components. White rhombus-head lines indicate the traces of preliminary nanoridges. Black arrows indicate node-like nanoridges in the CF of the cell. Black dashed arrows indicate irregular nanoridges in the CF of the cell. White arrowheads indicate parallel nanoridges in the AF of the cell. Scale bars, 10 μm.

The ultrastructure of the lip epidermis during various developmental stages was examined under Cryo-SEM. Both adaxial and abaxial surfaces of epidermal cells in the lip-central lobe showed secreted bubble-like preliminary cuticle components and heavy cuticle layers from stages 1 to 3 (**Figures 3E, F, G, H, K, L**, black rhombus-head line). Traces of preliminary nanoridges started to form on the lip epidermis from stages 2 to 3 (**Figures 3G, H, L, O, P, S, T**, white rhombus-head line). These then thickened and the number of nanoridges increased from stages 4 to 5 (**Figures 3I, J, M, N, Q, R, U, V**).

The final mature forms of nanoridges varied in different parts of the lip. The adaxial epidermal cells of the central lobe showed anode-like nanoridges in the CF (**Figure 3J**, black arrow), and parallel and radial nanoridges in the AF (**Figure 3J**, white arrowhead). Similar nanoridges on adaxial epidermal cells of the central lobe were also found on the adaxial and abaxial epidermal cells of lateral lobes (**Figure 3R, V**). In contrast, the abaxial epidermal cells of the central lobe showed looser parallel nanoridges in the CF (**Figure 3N**, white dashed arrow) and AF (**Figure 3N**, white arrowhead). Thus, the typical lip epidermal features containing nanoridges are important markers of the lip morphological identity. These results suggest that *PeERF1* may have a correlation with nanoridge formation during lip morphogenesis.

PeERF1 is Phylogenetically Assigned to the Va2 Subgroup of the ERF Subfamily

Phylogenetic analysis showed that PeERF1 belongs to the Va2 subgroup of the ERF subfamily of the AP2/EREBP family (**Figure 4A**), and the sequence alignment indicated that PeERF1 contains incomplete "SHINE domains" (CMV-1 and CMV-2 motifs) (**Figure 4B**). Of note, the protein sequences of incomplete "SHINE domains" of PeERF1 are distinguished from other members of the ERF-Va2 subgroup, which results in a separate branch from the other ERF-Va2 members and closer to the ERF-Va1 subgroup (**Figure 4**).

Silencing of *PeERF1* Resulted in Abnormal Sculpture of Nanoridges on the Lip Epidermis

To assess the role of *PeERF1* in lip cuticle development, CymMV-based VIGS was used to silence its expression with a 142-nt conserved AP2 domain (139–281 nt) and the 175-nt incomplete "SHINE domains" (346–521 nt) in *P.* OX Red Shoes "OX1408." This resulted in plants that were *PeERF1_AP2*-silenced and *PeERF1_SHN*-silenced (**Supplementary Figure S2A**). Using Cryo-SEM we examined the perianth epidermis micro-morphology from *PeERF1_AP2*-silenced plants. Lip epidermis nanoridges showed continuously altered distribution of structures within one plant from the 1st to the 7th flowers. We also found more severely altered phenotypes, with looser, thinner, uneven, and hollowed distribution of nanoridge structures especially on the lip epidermis of the 6th and the 7th flowers (**Supplementary Figure S3**). Flowers on these silenced plants showed no obvious difference in floral morphology as compared with mock-treated plants (**Supplementary Figures S2B–D**).

The most severe phenotype was observed on the 7th blooming flowers in *PeERF1_AP2*-silenced plants (**Figure S3D**). This was concomitant with the expression of *PeERF1* at late stage of lip morphogenesis. We then further examined the cell surface on the lip epidermis of the 7th blooming flowers of both types of silenced plants (**Figures 5A–L**, top view; **Supplementary Figure S4**, side view). Looser and fewer nanoridges in the AF of adaxial and abaxial surfaces of central lobe epidermal cells were observed as compared with mock-treated plants (**Figures 5A–F**, white arrowhead). In addition, the AF showed uneven distribution of parallel and irregular nanoridges, which was hollow by reducing the coverage of nanoridges on adaxial and abaxial surfaces of lateral lobe epidermal cells (**Figures 5H, I, K, L**, white arrowhead; **Figure 5M**). Moreover, *PeERF1_AP2*-silenced plants showed unique, thicker, and extended nanoridges across anticlines of both the adaxial and abaxial surface of lip-lateral lobe epidermal cells (**Figures 5H, K**, black spherical-head line).

In contrast, the sepals and petals of all blooming flowers of *PeERF1*-silenced plants otherwise showed no obvious phenotypic changes in the adaxial and abaxial surface of epidermal cells (**Supplementary Figure S5**). *PeERF1* and cutin biosynthesis genes were downregulated in both silenced plants; however, these cells do not have cuticle on their cell surface (**Supplementary Figure S6**).

Off-Target Silencing Effects in VIGS Phenotype

Both *PeERF1*-silenced plants showed downregulation of *PeERF1* (**Figures 6A** and **S6A**). However, the transcript level of *PeSHN1* was much lower than that of *PeERF1* (**Figures 6A, B**). We speculate that the downregulation of *PeSHN1* was due to off-target effect since there are 71.8% and 47.1% identity between the AP2 and SHN domains of *PeERF1* and *PeSHN1* genes, respectively (**Supplementary Figure S7**). However, it is also possible that transcription of *PeSHN1* is regulated by PeERF1 to some extent (**Figures 6A, B** and **Supplementary Figure S6B**).

Reduced Expression of Cutin Biosynthesis Genes in the *PeERF1*-Silenced Plants

Next, we examined whether the expression of cuticle biosynthesis genes was altered upon the reduction of *PeERF1* expression in the VIGS plants. Expression of *PeERF1* in the lip was reduced significantly in *PeERF1_AP2*-silenced plants, but less so in *PeERF1_SHN*-silenced plants. *PeCYP86A2* and *PeCYP77A4*, *PeGPAT*, *PeGPAT*, and *PeDCR* are putative *Phalaenopsis* orthologs of known cutin biosynthetic genes, which contribute to the cuticle formation in *Phalaenopsis* lips. Similar to the reduced expression of *PeERF1* in the *PeERF1_SHN*-silenced plants, the expressions of *PeCYP86A2, PeDCR*, and *PeCYP77A4* were reduced significantly in *PeERF1_AP2*-silenced plants (**Figures 6C, D**). The expressions of *PeCYP86A2* and *PeDCR* were reduced, while the expression of *PeCYP77A4* was not affected in the *PeERF1_SHN*-silenced plants (**Figures 6C, D**). The expression of *PeGPAT* was reduced in both *PeERF1_AP2*-silenced and *PeERF1_SHN*-silenced plants, but to a less extent (**Figure 6F**). Therefore, both *PeCYP77A4* and

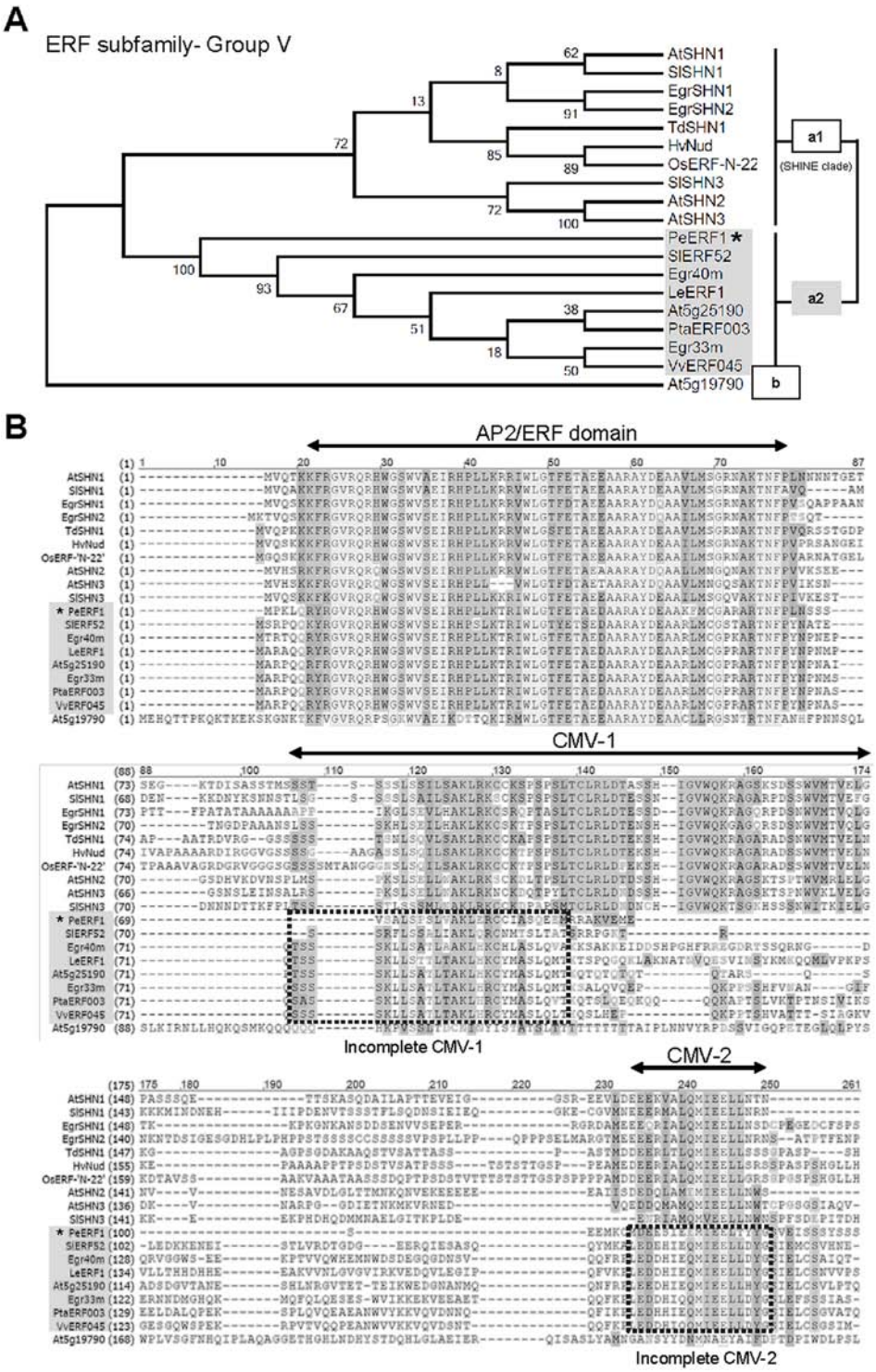

FIGURE 4 | Phylogenetic analysis and sequence alignment of PeERF1. **(A)** Phylogenetic analysis of PeERF1 with published ERF-V group proteins. Bootstrap values were calculated with 1,000 replicates. PeERF1 is highlighted with a star (*). **(B)** Multiple alignment of amino acid sequences of PeERF1 and ERF-V group proteins. According to the existence of "SHINE domains" (CMV-1 and CMV-2 motifs), the ERF-V group was classified into two groups: Va group, with SHINE domains, and Vb group, without SHINE domains. In addition, the Va group was further divided into two subgroups: Va1 subgroup, with complete SHINE domains (deemed as "SHINE clade"), and Va2 subgroup, with incomplete SHINE domains.

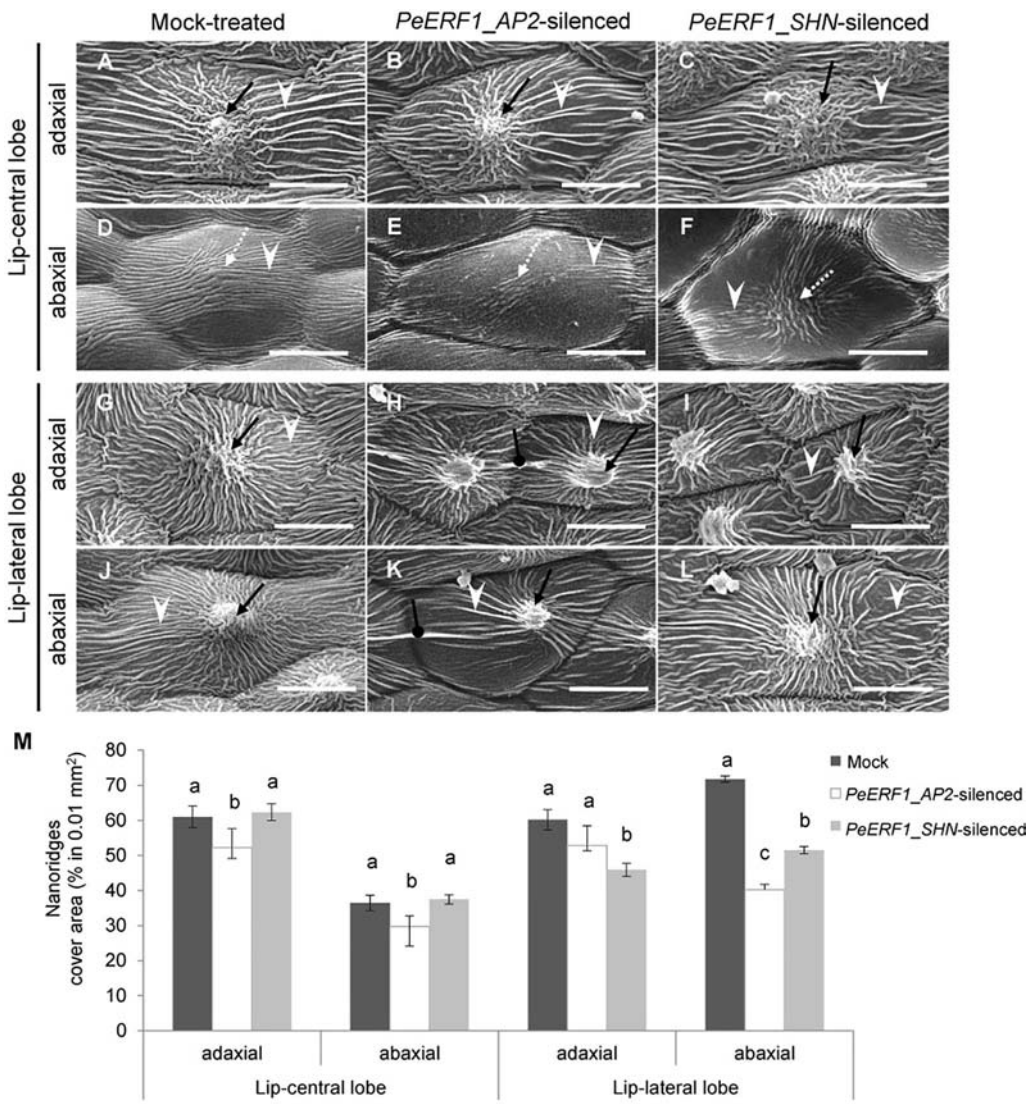

FIGURE 5 | Nanoridge characteristics of ultrastructure of lip epidermal cells from 7th blooming flowers of *PeERF1*-silenced *P.* OX Red Shoes "OX1408." **(A–L)** Cryo-SEM was used to examine the changes in cellular morphology from the 5th to the 8th blooming flowers of silenced plants (stage 5, floral diameter of 12 cm). Top view of adaxial and abaxial sites of lip central and lateral lobe epidermis in mock-treated, *PeERF1*_AP2-silenced, and *PeERF1*_SHN-silenced plants. Black arrows indicate node-like nanoridges in the CF of the cell. White dashed arrows indicate parallel nanoridges in the CF of the cell. White arrowheads indicate parallel nanoridges in the AF of the cell. Black spherical-head line indicates thicker and extended nanoridges across anticlines of cells. Scale bars, 30 μm. **(M)** The coverage of nanoridges on the top of adaxial and abaxial lip epidermal cells of mock-treated and *PeERF1*-silenced flowers. For Cryo-SEM examination, eight plants were injected with control, specific domain and conserved domain separately, and repeated twice. Data are mean ± SD (n = 15); the same letters above the bars indicate no statistical difference by Duncan's multiple range test ($P < 0.05$).

PeGPAT were found to be crucial for cuticle formation, and their expressions were regulated by other TFs in addition to PeERF1 or PeSHN1.

Nanoridges Disappeared in the Petal-Like Lip of the "Join Big Foot" Variant

From population of the *P.* hybrid "Join Big foot" grown from seedlings we selected two plants each with wild-type flower (normal split-lip organ) and with the big-lip enlarged petal-like lip flower. We observed these in order to confirm the association of *PeERF1* and cuticle formation during lip morphogenesis (**Figure 7A**). Cryo-SEM revealed that cell morphology and ultrastructure were severely changed in the petal-like lip epidermal cells of the big-lip variant as compared with wild type (**Figures 7B–Q**). In wild type, the epidermal cells of split-lip organs showed an abnormal, uneven, and hollowed distribution of parallel nanoridges in the AF of cells (**Figures 7B, D, F, H**). In the big-lip variant, all adaxial and abaxial surfaces of the lip epidermal cells displayed similar characteristics of petal adaxial epidermal cells with a papilla cell shape with smooth 2-D wax

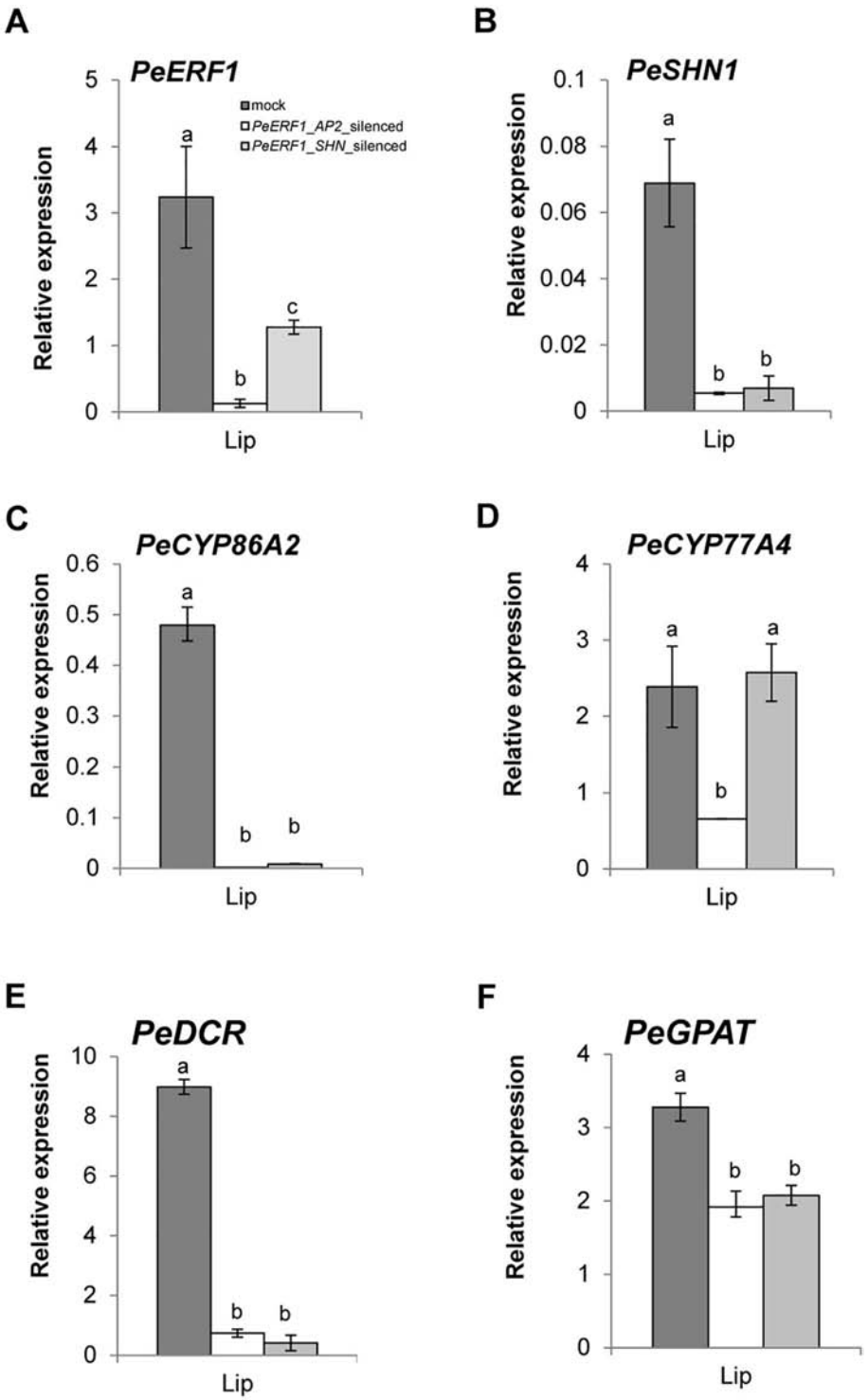

FIGURE 6 | Expression patterns of *PeERF1* and cuticle-associated genes in *PeERF1*-silenced plants. Transcript level of *PeERF1* **(A)**, *PeSHN1* **(B)**, and cutin metabolism-related genes (*PeCYP86A2*, *PeCYP77A4*, *PeGPAT*, and *PeDCR*) **(C–F)** in mock-treated and *PeERF1*-silenced flowers. Total RNA of sepal, petal, and lip were extracted from the 5th floral bud (stage 3, length of 1–2 cm) at 30 days post-inoculation. Three technical repeats and three biological repeats were performed for gene expression analysis in the *PeERF1*_silenced plants. Data are mean ± SD; the same letters above the bars indicate no statistical difference by Duncan's multiple range test ($P < 0.05$).

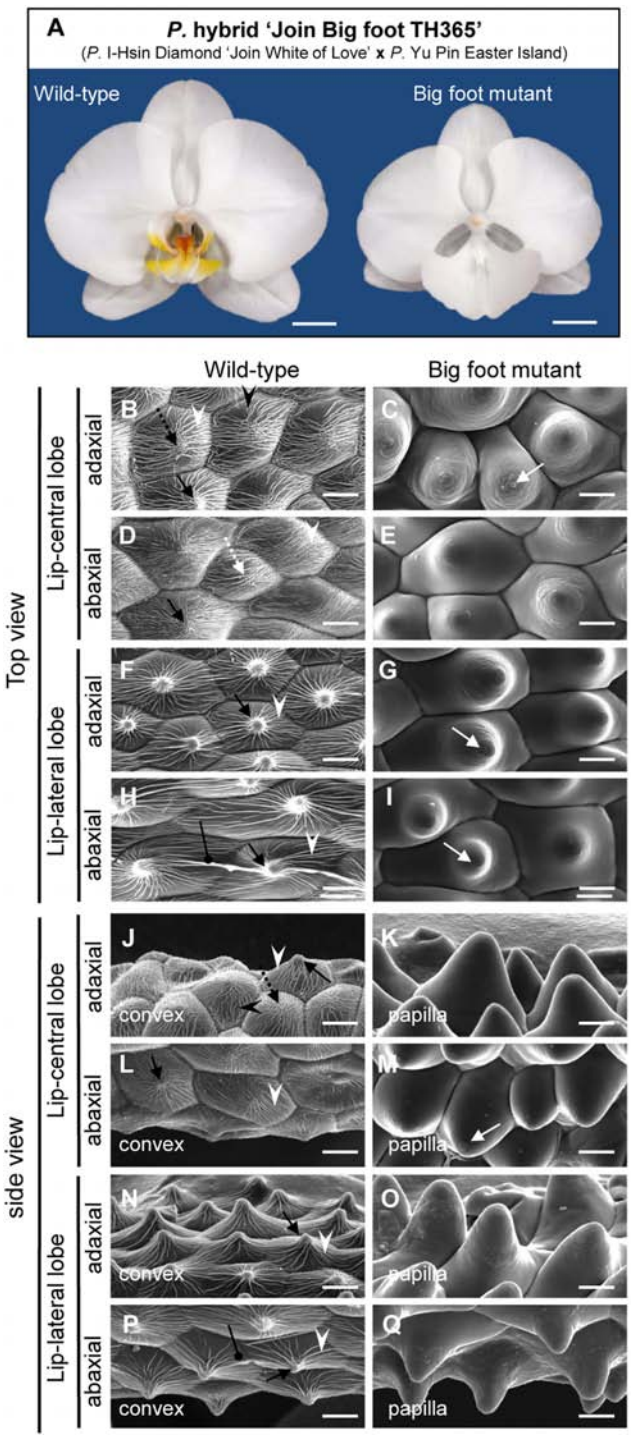

FIGURE 7 | Floral morphology and ultrastructure of lip epidermal cells of somaclonal variants with normal lip or enlarged petal-like lip mutants. **(A)** The flowers of somaclonal variants of *P.* hybrid "Join Big foot TH365" (*P.* I-Hsin Diamond "Join White of Love" x *P.* Yu Pin Easter Island). The lip morphology of "big foot mutant" flower showed morphological conversions to petal-like structure. Scale bars, 2 cm. **(B–Q)** Top view and side view of adaxial and abaxial sites of lip central and lateral lobe epidermis in "wild-type" and "big foot mutant" of somaclonal variants of *P.* "Join Big foot TH365" flowers. White arrows indicate a protuberance on the top of the cell. Black arrows indicate node-like nanoridges in the CF of the cell. White dashed arrows indicate parallel nanoridges in the CF of the cell. Black dashed arrows indicate irregular nanoridges in the CF of the cell. White arrowheads indicate parallel nanoridges in the AF of the cell. Black arrowheads indicate irregular nanoridges in the AF of the cell. Black spherical-head line indicates thicker and extended nanoridges across anticlines of the cells. Different cell shape types of floral epidermal cells are in the lower left corner of each panel. Scale bars, 30 μm.

films and a protuberance on the top of the cell (**Figures 7C, E, G, I, K, M, O, Q**; **Supplementary Figures S8** and **S9**). The phenotypic observations were done in three big-foot variant plants. Lip morphology was altered to various levels, from severe to mild, yet the phenotypic change for nanoridge formation was the same (data not shown).

Reduced Expression of *PeERF1* and Cutin Biosynthesis Genes Associated With Big-Foot Variant

To further understand the molecular mechanisms of petal-like lip formation, we investigated gene expression of cutin biosynthesis genes *PeERF1*, *PeSHN1* (*PeCYP86A2*, *PeCYP77A4*, *PeDCR*, and *PeGPAT*) (**Figure 8**), as well as expression of floral morphogenesis genes (B-class [*DEFICIENS* (*DEF*)/*APETALA3* (*AP3*)-like (*PeMADS2-5*) and GLOBOSA (GLO)/PISTILLATA (PI)-like (*PeMADS6*)], *AGAMOUS-LIKE6a* (*PeAGL6a*), and E-class [*SEPALLATA1-4* (*PeSEP1-4*)] MADS box genes) (**Supplementary Figure S10**).

Expression of *PeERF1* was significantly reduced in the lip of the big-foot variant as compared to the wild type. In addition, the expressions of *PeCYP77A4* and *PeGPAT* were reduced in the big-foot variant lip compared to that of the wild-type plant, while expression levels of *PeCYP86A2* and *PeDCR* were not significantly different between the big-foot variant and the wild type. Interestingly, expression of *PeSHN1* was nearly unaffected for petal-like lip in big-foot variant as compared to that of lip in wild-type plant. These results suggest that *PeERF1*, *PeCYP77A4*, and *PeGPAT* were involved in the nanoridge formation in the orchid lip.

For MADS box genes, highest expressions of *PeMADS3, 4 and 6*, and *PeAGL6a* were detected in the lip of "wild-type" flowers, whereas *PeMADS2* expressed higher in the petals (**Figure 8A**). In contrast, only *PeMADS2* and *PeMADS3* expressed higher in petal-like lip compared to the petal in the big-foot variant (**Supplementary Figure S10**). Intriguingly, we found little or no difference in transcriptional levels of *PeMADS4~6* between the petal-like lip and the petals of the big-foot variant (**Supplementary Figure S10**).

Ectopic Expression of *PeERF1* in *Arabidopsis* Resulted in a Typical SHINE Phenotype

To further characterize the biological function of *PeERF1,* we performed ectopic overexpression of *PeERF1* under the control of CaMV 35S promoter by *Agrobacterium*-mediated transformation in *Arabidopsis*. Two batches of overexpression were performed. In the first batch, a total of 60 T1 transgenic lines were generated, and in the second batch of overexpression, a total of 48 transgenic lines were generated. Most of overexpressing lines showed SHINE phenotypes. Three overexpressing lines (L24, L37, and L52) from the first batch and three overexpression lines (P12, P13, and P15) from the second batch were used for further analysis (**Figure 9**). These plants have enhanced brilliant, shiny green color and curved-down edges rosette leaves as compared to wild-type plants (**Figures 9A–C**). For seedlings of *35S:PeERF1* transgenic lines, the adaxial surface of the second pair of true leaves show a shiny surface with few trichomes as compared with the wild type (**Figures 9D**, **E**). At the cellular level, the adaxial surfaces of rosette leaf epidermal cells of *35S:PeERF1* transgenic plants showed ectopic nanoridge formation and wax deposition on the surface, in contrast to the wild-type leaf with a smooth surface (**Figures 9F–H**, black arrow).

In addition, qRT-PCR was performed to examine the gene expression in the two transgenic lines with obvious phenotype, P12 and P15 from the second batch of overexpression. Ectopic expression of *PeERF1* was accompanied by upregulation of cuticle biosynthesis genes, including *AtCYP86A4*, *AtDCR*, and *AtGPAT6* in two independent lines (**Figure 9I**). Furthermore, the ectopic overexpression of *PeERF1* in *Arabidopsis* did not disturb the expression of the three endogenous *AtSHNs* (*AtSHN1~AtSHN3*) as well as the *PeERF1* orthologous gene *At5g25190* in all ectopic overexpression lines except the expression of *At5g25190* in the line P12 (**Figure 9I**). These results suggest that *PeERF1*, with similar SHINE phenotypes, might be assigned to one of the SHINE-like TFs and can be ectopically overexpressed and functionally involved in leaf cuticle development in *Arabidopsis*.

DISCUSSION

PeERF1 Exhibits Partial SHINE Functions but Contains Incomplete SHINE Domains

ERF-Va2 subgroup genes are not known to have a typical SHINE phenotype; rather, they are involved in various developmental and physiological processes (Aharoni et al., 2004; Li et al., 2007; Marques et al., 2013; Trupiano et al., 2013; Nakano et al., 2014; Leida et al., 2016). Recently, berry VvERF045 SHINE domains were found to be involved in berry ripening and epidermal cuticle development. Transgenic grapevine lines overexpressing *VviERF045* show stunted growth, discolored, and smaller leaves, with reduced gene expression for epidermal wax decoration and wax biosynthesis. This indicates that VviERF045 is a potential repressor in epidermis patterning and cuticle development (Leida et al., 2016).

In this study, *PeERF1_AP2*-silenced plants showed significantly reduced expressions of *PeERF1* and *PeSHN1* with loose and uneven nanoridges on the lip epidermal surface, accompanied by drastically reduced expression of cutin biosynthesis genes including *PeCYP86A2*, *PeCYP77A4*, and *PeDCR*. Expression of *PeGPAT*, on the other hand, was affected only to a less extent (**Figure 6**). These results suggest that both *PeERF1* and *PeSHN1* are important for cuticle formation. Yet the expression level of *PeSHN1* was much lower than that of *PeERF1*. Similar to the reduced expression of *PeERF1* in the *PeERF1_SHN*-silenced plants, the expressions of *PeCYP86A2*, *PeDCR*, and *PeCYP77A4* were reduced significantly in *PeERF1_AP2*-silenced plants. The expression of *PeCYP77A4* was not affected in the *PeERF1_SHN*-silenced plants (**Figure 6D**). The expression of *PeGPAT* was reduced in both

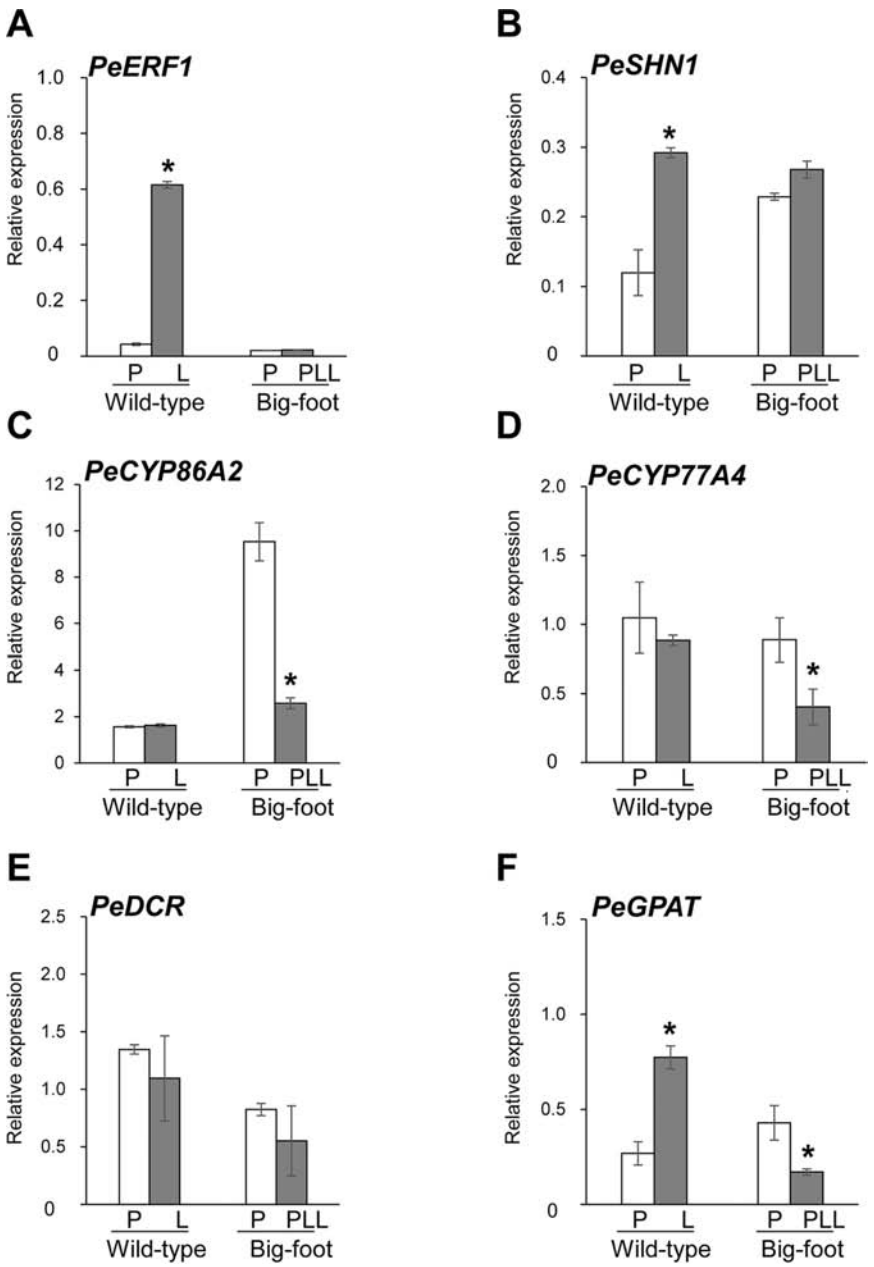

FIGURE 8 | Expression patterns of *PeERF1*, *PeSHN1*, cutin-biosynthetic genes in petal and lip of "wild-type" and "big foot mutant" flowers of *P.* hybrid "Join Big foot TH365." Transcript level of genes related to lip epidermis development *PeERF1* **(A)**, *PeSHN1* **(B)**, and cutin metabolism-related genes (*PeCYP86A2*, *PeCYP77A4*, *PeGPAT*, and *PeDCR*) **(C–F)** in flowers of "wild-type" and "big foot mutant" of *P.* "Join Big foot TH365" were examined. P, L, and PPL were represented as petal, lip, and petal-like lip, respectively. mRNA of petal and lip were extracted from the 2nd floral bud in three independent plants of big foot mutant and wild type. Three technical repeats were performed for each sample. Data are mean ± SD. Numbers above the bars are expression levels after normalization with internal control (*PeActin4*). *P < 0.05 by one-tailed t-test.

PeERF1_AP2-silenced and *PeERF1-SHN* plants, but to a lesser extent (**Figure 6F**). Therefore, it appears that *PeCYP77A4* and *PeGPAT* are regulated by PeERF1 and/or PeSHN1 and downregulation of these genes might explain the cuticle formation defects in the *PeERF1*-silenced plants. Based on our observations, it is also suggested that proper expression of *PeCYP77A4* and *PeGPAT* might involve additional TF(s). Thus, our results suggest that *PeERF1* as a SHN-like homolog is a potential activator in the lip epidermal cell patterning of *Phalaenopsis* flowers. Furthermore, transgenic *Arabidopsis* lines overexpressing *PeERF1* showed typical SHINE phenotypes similar to *AtSHN*-overexpressing *Arabidopsis* (**Figures 9A–C**).

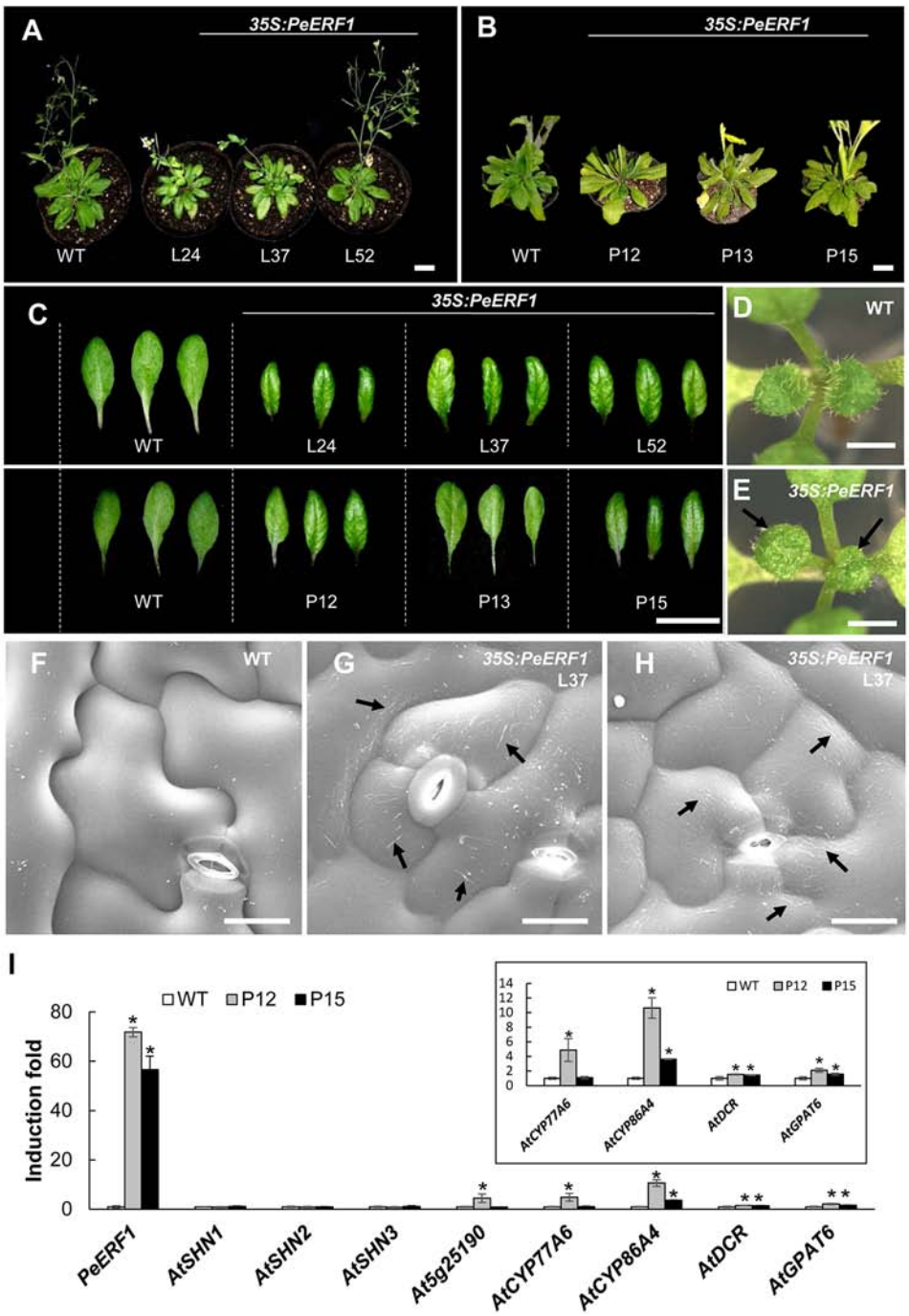

FIGURE 9 | Phenotype analysis and expression patterns of transgenic *Arabidopsis* plants ectopically expressing *PeERF1*. **(A)** Wild-type and *35S:PeERF1* transgenic lines (the first batch, L24, L37, and L52) at 45 days old, and **(B)** wild-type and *35S:PeERF1* transgenic lines (the second batch, P12, P13, and P15) at 60 days old. Scale bars, 5 cm. **(C)** Shiny and curved-down edges of the rosette leaves of 45-day-old wild-type and *35S:PeERF1* transgenic plants of L24, L37 and L52, and 60-day-old wild-type and *35S:PeERF1* transgenic plants of P12, P13, and P15. Scale bars, 2 cm. **(D–E)** Seedlings of wild-type and *35S:PeERF1* transgenic plants. Black arrow indicates the top view of the second pair of true leaves with a shiny surface. **(F–H)** Micrograph images of adaxial surface of rosette leaf epidermal cells of wild-type and *35S:PeERF1* transgenic line 37. Black arrow indicates ectopic wax deposition in the AF and anticlines of the cell. Scale bars, 10 μm. **(I)** Expression patterns of *PeERF1* and *Arabidopsis* cuticle-associated genes (*AtSHN1-3*, *At5g25190*, *AtCYP86A4*, *AtCYP77A6*, *AtGPAT6*, and *AtDCR6*) in wild type and *35S:PeERF1* overexpressing lines P12 and P15 were determined by qRT-PCR and normalized to the expression level of the *Actin* gene as an internal control. Fold induction of *PeERF1* and 8 genes associated with cuticle biosynthesis in *35S:PeERF1* transgenic plants and wild-type plants, as compared to control. Asterisks were used to indicate statistically significant difference compared with wild-type plants. Three technical replicates were performed for each overexpression line and repeated in two different overexpression lines independently. Data are mean ± SD. *P < 0.05 by one-tailed t-test.

The *PeERF1* overexpressing plants enhanced the expression of *AtCYP86A4*, *AtDCR*, and *AtGPAT6* without disturbance of the expression of endogenous *AtSHNs* and the homologous gene *At5g25190* except the expression of *At5g25190* in the line P12 was increased (**Figure 9I**). With the fact that *At5g25190* does not have the function for cuticle formation (Aharoni et al., 2004), the phenotype observed in the overexpressor P12 was due to the *PeERF1 per se*. Therefore, our results suggest that *PeERF1*, as a *SHINE*-like TF, increase the *Arabidopsis* cuticle-associated genes and result the shiny surface of rosette leaves.

Recent studies have indicated the importance of CMV-1 and CMV-2 motifs of SHINE domains. A highly conserved valine (V) residue in the complete CMV-1 motif in barley has been found to be associated with lipid biosynthesis of grain (Taketa et al., 2008). When V is changed to aspartic acid (D) in the complete CMV-1 motif, instead of the typical hulled caryopsis in barley, a naked one results. This is associated with lipid formation of caryopsis and hull adhesion (Taketa et al., 2008). In addition, the existence of a C-terminal 30-amino-acid region of the CMV-2 motif is also important for transcriptional activation of SlERF52 (Nakano et al., 2014). The protein sequences of PeERF1 were more distinguished from other members of the ERF-Va2 subgroup (**Figure 4**). We found that PeERF1 has a serine (S) residue at position 5 of the incomplete CMV-2 motif, whereas several members of the Va2 subgroup have a histidine (H) residue at the same position (**Figure 4B**).

PeERF1, PeSHN1, and Other TFs Together Regulate Cutin Biosynthesis Genes for Nanoridge Formation

Studies of SHINE genes modulating cuticle permeability and epidermal cell patterning have revealed the requirement of the downstream synthesis of cutin polyesters (Kannangara et al., 2007; Li-Beisson et al., 2009; Panikashvili et al., 2009; Shi et al., 2011; Shi et al., 2013; Petit et al., 2016; Mazurek et al., 2017). A recent model was formulated of the association between cutin biosynthesis and nanoridge formation of the petal cuticle (Mazurek et al., 2017). However, although several SHN putative downstream target genes related to cuticle formation have been reported, SHN TFs do not bind directly to most of their presumed targets. In fact, they require an interacting partner for SHN-mediated target regulation (Kannangara et al., 2007). So far, only the promoter regions of CYP86A cytochrome P450s (AtCYP86A4, AtCYP86A7, and SlCYP86A69) and GSDL-motif lipases (AtRXF26) have been found to be activated by SHNs in *Arabidopsis* and tomato (Shi et al., 2011; Shi et al., 2013).

When *PeERF1* was silenced, we found associated downregulation of cutin biosynthesis gene expressions and reduced numbers of nanoridges on lip abaxial and adaxial surfaces. However, even though the expressions of *PeCYP86A2* and *PeDCR* were significantly reduced, that of *PeGPAT* was only mildly reduced in lip epidermis in both *PeERF1*-silenced plants (**Figure 6**). Thus, *PeCYP86A2* and *PeDCR* may be downstream genes of *PeSHN1*, and PeCYP77A4 a downstream gene of *PeERF1*. *PeGPAT* was regulated by *PeERF1*, *PeSHN1*, and non-SHN like TFs. Hence, *PeERF1* as a SHN-like TF is involved in decorating the floral organ epidermal surface by regulating downstream cutin biosynthesis genes.

PeERF1, as a Downstream Target of Floral Morphogenesis Genes, is Involved in the Late Stage of Lip Morphogenesis

Recently, the roles of B- and E-class MADS-box genes were revealed for orchid tepal development (Tsai et al., 2004; Tsai et al., 2005; Lu et al., 2007; Hsieh et al., 2013a; Su et al., 2013b; Pan et al., 2014; Hsu et al., 2015b; Huang et al., 2015; Huang et al., 2016). We have shown that knock-down expression of E-class *PeSEP1-4* genes reduced the expression of *PeERF1*. *PeSEP1*-silenced plants had a changed ultrastructure in terms of nanoridge formation, of the floral epidermal cells (Pan et al., 2014). This result suggests that *PeERF1* could be a downstream gene of E-class MADS box genes.

In this study, we found that the expression of *PeERF1* was reduced to almost zero in the big-foot somaclonal variants with a petal-like lip, along with the loss of gene expression of B-class (*PeMADS4*, *PeMADS5*, and *PeMADS6*) and E-class (*PeAGL6a*) MADS box genes (**Supplementary Figure S10**). These results suggest that the developmental program of lip morphogenesis is very complex, and *PeERF1* is a downstream target gene of B- and E-class MADS box genes and is involved in lip morphogenesis.

The Timing for VIGS Phenotype and Off Target VIGS

Our previous VIGS results of MADS box silencing data showed the highest silencing efficiency at 4–7 weeks post-silencing with the first four flowers blooming after viral inoculation (Hsieh et al., 2013a; Hsieh et al., 2013b; Pan et al., 2014; Hsu et al., 2015a). This indicates that MADS box genes are induced in early floral morphogenesis.

PeSHN1 as an SHN ortholog contained the complete SHINE domains and was assigned to the ERF-Va1 subgroup (SHINE clade) (**Figure 4**). However, *PeERF1* was expressed at late stage lip morphogenesis so that VIGS phenotype was more distinct on the late emerged floral buds. The identity of *PeSHN1* with *PeERF1*_AP2-silenced and *PeERF1*_SHN-silenced regions were 71.8% and 47.1%, respectively. Yet, no contiguous matches were longer than 11 nt for the *PeSHN1* coding region and the VIGS fragment (**Supplementary Figure S7**). A nucleotide identity of less than 11 nt on target mRNA has previously been shown to reduce the chances of silencing induction (Senthil-Kumar and Mysore, 2011; Hsieh et al., 2013a). The off-target effects of *PeSHN1* silencing that occurred in all *PeERF1*-silenced plants may be due to sequence similarity. The combined effects of specific silencing of *PeERF1* and off-target silencing of *PeSHN1* together resulted in a change of nanoridge formation in lip epidermal cell patterning in the *PeERF1*-silenced plants, yet *PeSHN1* expressed much lower than *PeERF1* in the *Phalaenopsis* orchids.

Distinct Sculpture on the Lip Epidermal Surface Reveals the Special Deceit Pollination Strategy in *Phalaenopsis*

To contribute to successful sexual reproduction in higher plants, the perianth of flower creates various cues, such as tactile, visual, and olfactory signals, to reward or not reward (deceive) pollinators. In Orchidaceae, approximately one-third of orchid species have a deceit pollination strategy by using general floral signals without rewarding pollinators with nectar or pollen (Ackerman, 1986; Nilsson, 1992; Jersáková et al., 2006). Although numerous *Phalaenopsis* species are scentless, with a diversity of colorful perianths, floral morphology, and floral scents, bees are the major pollinators of *Phalaenopsis* flowers *via* food-deceptive pollination (Roman Kaiser, 1993; Hsiao et al., 2006; Tsai et al., 2008).

In this study, we examined the floral epidermal cell surfaces of *Phalaenopsis* species (**Figure 1**; **Supplementary Figure S1**); the tissues of sepals and petals had a papillae shape with a protuberance on the smooth epidermal surface, whereas the lip harbored numerous nanoridges on the epidermal surface. The biological function of nanoridges on the floral organs for pollinator attraction has been linked with the unique visual and tactile signals they produce (Whitney et al., 2009; Prüm et al., 2011; Rands et al., 2011; Whitney et al., 2011b; Prüm et al., 2012; Kourounioti et al., 2013; Prüm et al., 2013; Adachi et al., 2015; Moyroud et al., 2017).

We propose three steps of a special deceit pollination strategy in the scentless *Phalaenopsis* species. First, the papillae cell shape on the sepal and petal epidermis creates big brilliant visual cues to attract pollinators from a distance. Then, the convex cell shape with heavy nanoridges on the top of the lip epidermal cells generates more "flashy" visual cues (similar to guide lights on an aircraft runway) and direct pollinators to land on the lip instead of sepals and petals. Finally, the distinctive split lip with central lobes and lateral lobes creates a tunnel-like structure, and the nanoridges on the lip epidermis generate tactile cues that help pollinators walk and explore the area. During this process, because of the heavy and dense nanoridges on the top of the lip epidermis, the pollinators may slip toward the column and attach to the pollinia. While visiting subsequent flowers, successful pollination may occur when attached pollinia are placed into the stigmatic cavity underneath the column. The slippery quality of nanoridges for beetles has been reported (Prüm et al., 2011), and the slip-and-fall pollination mechanism related to the ultrastructural characterization of the floral lip was also shown for *Gongora bufonia* (Orchidaceae) (Adachi et al., 2015).

CONCLUSION

In conclusion, our results demonstrate that PeERF1, as an SHN-like TF, was involved in lip epidermal cell morphological formation at the last flowering stage by regulating lip nanoridge development in *Phalaenopsis* flowers. In addition, the heavy nanoridges on the lip epidermis, as typical lip features, may be essential for the pollination mechanism of *Phalaenopsis*. This study gives a better understanding of the transcriptional regulation of the late stage development of lip morphogenesis and the special pollination mechanism of *Phalaenopsis*.

DATA AVAILABILITY STATEMENT

The datasets generated for this study can be found in the PeERF1, MG948436; PeSHN1, XM_020736987.1; PeCYP86A2, XM_020732683.1; PeCYP77A4, XM_020725159.1; PeGPAT, XM_020727266.1; PeDCR, XM_020725429.1.

AUTHOR CONTRIBUTIONS

P-HL, W-HC, and H-HC conceived the research plans. P-HL performed most of the experiments, analyzed the data, and wrote the article with contributions from all the authors. L-MH assisted in the identification and expression analysis of cutin biosynthesis genes. Z-JP assisted with the performance of VIGS experiments. W-NJ and M-CC performed Cryo-SEM analysis and provided service for Cryo-scanning electron microscope.

FUNDING

This work was supported by grant no. MOST-107-2313-B-006-003-MY3 from the Ministry of Science and Technology, Taiwan.

ACKNOWLEDGMENTS

We thank Dr. Ming-Hsien Hsieh (Tainan District Agricultural Research and Extension Station, Council of Agriculture, Taiwan) for providing the greenhouse and for assistance with operating the VIGS experiment, and Dr. Shau-Ting Chiu (Biology Department, National Museum of Natural Science, Taichung, Taiwan) for helpful discussion of floral epidermal morphology. We also thank Oxen Biotechnology Corp. (Tainan, Taiwan) and Join Orchids Corp. (Tainan, Taiwan) for providing the plant materials for of *P.* OX Red Shoes "OX1408" and *P.* "Join Big foot TH365," respectively.

SUPPLEMENTARY MATERIALS

The Supplementary Material for this article can be found online at: https://www.frontiersin.org/articles/10.3389/fpls.2019.01709/full#supplementary-material

REFERENCES

Ackerman, J. D. (1986). Mechanisms and evolution of food-deceptive pollination systems in orchids. *Lindleyana* 1, 108–113.

Adachi, S. A., Machado, S. R., and Guimarães, E. (2015). Structural and ultrastructural characterization of the floral lip in Gongora bufonia (Orchidaceae): understanding the slip-and-fall pollination mechanism. *Botany* 93, 759–768. doi: 10.1139/cjb-2015-0114

Aharoni, A., Dixit, S., Jetter, R., Thoenes, E., van Arkel, G., and Pereira, A. (2004). The SHINE clade of AP2 domain transcription factors activates wax biosynthesis, alters cuticle properties, and confers drought tolerance when overexpressed in *Arabidopsis*. *Plant Cell* 16, 2463–2480. doi: 10.1105/tpc.104.022897

Al-Abdallat, A. M., Al-Debei, H. S., Ayad, J. Y., and Hasan, S. (2014). Over-expression of SlSHN1 gene improves drought tolerance by increasing cuticular wax accumulation in tomato. *Int. J. Mol. Sci.* 15, 19499–19515. doi: 10.3390/ijms151119499

Broun, P., Poindexter, P., Osborne, E., Jiang, C.-Z., and Riechmann, J. L. (2004). WIN1, a transcriptional activator of epidermal wax accumulation in *Arabidopsis*. *Proc. Natl. Acad. Sci. U.S.A.* 101, 4706–4711. doi: 10.1073/pnas.0305574101

Chao, Y. T., Yen, S. H., Yeh, J. H., Chen, W. C., and Shih, M. C. (2017). Orchidstra 2.0-A Transcriptomics Resource for the Orchid Family. *Plant Cell Physiol.* 58, e9–e9. doi: 10.1093/pcp/pcw220

Chen, Y. H., Tsai, Y. J., Huang, J. Z., and Chen, F. C. (2005). Transcription analysis of peloric mutants of *Phalaenopsis* orchids derived from tissue culture. *Cell Res.* 15, 639–657. doi: 10.1038/sj.cr.7290334

Chen, Y. Y., Lee, P. F., Hsiao, Y. Y., Wu, W. L., Pan, Z. J., Lee, Y. I., et al. (2012). C- and D-class MADS-box genes from *Phalaenopsis equestris* (Orchidaceae) display functions in gynostemium and ovule development. *Plant Cell Physiol.* 53, 1053–1067. doi: 10.1093/pcp/pcs048

Clough, S. J., and Bent, A. F. (1998). Floral dip: a simplified method for Agrobacterium-mediated transformation of *Arabidopsis thaliana*. *Plant J.* 16, 735–743. doi: 10.1046/j.1365-313x.1998.00343.x

Cozzolino, S., and Widmer, A. (2005). Orchid diversity: an evolutionary consequence of deception? *Trends In Ecol. Evol.* 20, 487–494. doi: 10.1016/j.tree.2005.06.004

Fu, C. H., Chen, Y. W., Hsiao, Y. Y., Pan, Z. J., Liu, Z. J., Huang, Y. M., et al. (2011). OrchidBase: a collection of sequences of the transcriptome derived from orchids. *Plant Cell Physiol.* 52, 238–243. doi: 10.1093/pcp/pcq201

Hsiao, Y. Y., Tsai, W. C., Kuoh, C. S., Huang, T. H., Wang, H. C., Wu, T. S., et al. (2006). Comparison of transcripts in *Phalaenopsis bellina* and *Phalaenopsis equestris* (Orchidaceae) flowers to deduce monoterpene biosynthesis pathway. *BMC Plant Biol.* 6, 14. doi: 10.1186/1471-2229-6-14

Hsiao, Y. Y., Huang, T. H., Fu, C. H., Huang, S. C., Chen, Y. J., Huang, Y. M., et al. (2013). Transcriptomic analysis of floral organs from *Phalaenopsis* orchid by using oligonucleotide microarray. *Gene* 518, 91–100. doi: 10.1016/j.gene.2012.11.069

Hsieh, M. H., Lu, H. C., Pan, Z. J., Yeh, H. H., Wang, S. S., Chen, W. H., et al. (2013a). Optimizing virus-induced gene silencing efficiency with Cymbidium mosaic virus in Phalaenopsis flower. *Plant Sci.* 201, 25–41. doi: 10.1016/j.plantsci.2012.11.003

Hsieh, M. H., Pan, Z. J., Lai, P. H., Lu, H. C., Yeh, H. H., Hsu, C. C., et al. (2013b). Virus-induced gene silencing unravels multiple transcription factors involved in floral growth and development in *Phalaenopsis* orchids. *J. Exp. Bot.* 64, 3869–3884. doi: 10.1093/jxb/ert218

Hsu, C. C., Chen, Y. Y., Tsai, W. C., Chen, W. H., and Chen, H. H. (2015a). Three R2R3-MYB transcription factors regulate distinct floral pigmentation patterning in *Phalaenopsis* spp. *Plant Physiol.* 168, 175–191. doi: 10.1104/pp.114.254599

Hsu, H. F., Hsu, W. H., Lee, Y. I., Mao, W. T., Yang, J. Y., Li, J. Y., et al. (2015b). Model for perianth formation in orchids. *Nat. Plants* 1, 15046. doi: 10.1038/nplants.2015.46

Huang, J. Z., Lin, C. P., Cheng, T. C., Chang, B. C. H., Cheng, S. Y., Chen, Y. W., et al. (2015). A de novo floral transcriptome reveals clues into *Phalaenopsis* orchid flower development. *PloS One* 10, e0123474. doi: 10.1371/journal.pone.0123474

Huang, J. Z., Lin, C. P., Cheng, T. C., Huang, Y. W., Tsai, Y. J., Cheng, S. Y., et al. (2016). The genome and transcriptome of *Phalaenopsis* yield insights into floral organ development and flowering regulation. *PeerJ J. Life Environ. Sci.* 4, e2017. doi: 10.7717/peerj.2017

Jäger, K., Miskó, A., Fábián, A., Deák, C., Kiss-Bába, E., Polgári, D., et al. (2015). Expression of a WIN/SHN-type regulator from wheat triggers disorganized proliferation in the Arabidopsis leaf cuticle. *Biol. Plantarum* 59, 29–36. doi: 10.1007/s10535-014-0471-0

Jeffree, C. E. (2006). *Annual Plant Reviews Volume 23: Biology of the Plant Cuticle* ed M. Riederer and C. Müller (Oxford, UK: Blackwell Publishing), 11–125.

Jersáková, J., Johnson, S. D., and Kindlmann, P. (2006). Mechanisms and evolution of deceptive pollination in orchids. *Biol. Rev. Cambridge Philos. Soc.* 81, 219–235. doi: 10.1017/S1464793105006986

Kannangara, R., Branigan, C., Liu, Y., Penfield, T., Rao, V., Mouille, G. G., et al. (2007). The transcription factor WIN1/SHN1 regulates cutin biosynthesis in *Arabidopsis thaliana*. *Plant Cell* 19, 1278–1294. doi: 10.1105/tpc.106.047076

Kay, Q. O. N., Daoud, H. S., and Stirton, C. H. (1981). Pigment distribution, light reflection and cell structure in petals. *Bot. J. Linn. Soc.* 83, 57–83. doi: 10.1111/j.1095-8339.1981.tb00129.x

Kim, M. J., Ruzicka, D., Shin, R., and Schachtman, D. P. (2012). The Arabidopsis AP2/ERF transcription factor RAP2. 11 modulates plant response to low-potassium conditions. *Mol. Plant* 5, 1042–1057. doi: 10.1093/mp/sss003

Koch, K., Bhushan, B., and Barthlott, W. (2008). Diversity of structure, morphology and wetting of plant surfaces. *Soft Mater.* 4, 1943–1963. doi: 10.1039/B804854A

Koch, K., Bhushan, B., and Barthlott, W. (2009a). Multifunctional surface structures of plants: an inspiration for biomimetics. *Prog. In Mater. Sci.* 54, 137–178. doi: 10.1016/j.pmatsci.2008.07.003

Koch, K., Bohn, H. F., and Barthlott, W. (2009b). Hierarchically sculptured plant surfaces and superhydrophobicity. *Langmuir* 25, 14116–14120. doi: 10.1021/la9017322

Kourounioti, R. L. A., Band, L. R., Fozard, J. A., Hampstead, A., Lovrics, A., Moyroud, E., et al. (2013). Buckling as an origin of ordered cuticular patterns in flower petals. *J. R. Soc. Interface* 10, 20120847. doi: 10.1098/rsif.2012.0847

Leida, C., Dal Rì, A., Dalla Costa, L., Gómez, M. D., Pompili, V., Sonego, P., et al. (2016). Insights into the role of the berry-specific ethylene responsive factor VviERF045. *Front. In Plant Sci.* 7, 1793. doi: 10.3389/fpls.2016.01793

Li, Y., Zhu, B., Xu, W., Zhu, H., Chen, A., Xie, Y., et al. (2007). LeERF1 positively modulated ethylene triple response on etiolated seedling, plant development and fruit ripening and softening in tomato. *Plant Cell Rep.* 26, 1999–2008. doi: 10.1007/s00299-007-0394-8

Li-Beisson, Y., Pollard, M., Sauveplane, V., Pinot, F., Ohlrogge, J., and Beisson, F. (2009). Nanoridges that characterize the surface morphology of flowers require the synthesis of cutin polyester. *Proc. Natl. Acad. Sci. U.S.A.* 106, 22008–22013. doi: 10.1073/pnas.0909090106

Lu, H. C., Chen, H. H., Tsai, W. C., Chen, W. H., Su, H. J., Chang, C. N., et al. (2007). Strategies for functional validation of genes involved in reproductive stages of orchids. *Plant Physiol.* 143, 558–569. doi: 10.1104/pp.106.092742

Marques, W. L., Salazar, M. M., Camargo, E. L. O., Lepikson-Neto, J., Tiburcio, R. A., do Nascimento, L. C., et al. (2013). Identification of four Eucalyptus genes potentially involved in cell wall biosynthesis and evolutionarily related to SHINE transcription factors. *Plant Growth Regul.* 69, 203–208. doi: 10.1007/s10725-012-9754-7

Mawlong, I., Ali, K., Kurup, D., Yadav, S., and Tyagi, A. (2014). Isolation and characterization of an AP2/ERF-type drought stress inducible transcription factor encoding gene from rice. *J. Plant Biochem. Biotechnol.* 23, 42–51. doi: 10.1007/s13562-012-0185-3

Mazurek, S., Garroum, I., Daraspe, J., De Bellis, D., Olsson, V., Mucciolo, A., et al. (2017). Connecting the molecular structure of cutin to ultrastructure and physical properties of the cuticle in petals of Arabidopsis. *Plant Physiol.* 173, 1146–1163. doi: 10.1104/pp.16.01637

Mondragón-Palomino, M., and Theißen, G. N. (2008). MADS about the evolution of orchid flowers. *Trends Plant Sci.* 13, 51–59. doi: 10.1016/j.tplants.2007.11.007

Moyroud, E., Wenzel, T., Middleton, R., Rudall, P. J., Banks, H., Reed, A., et al. (2017). Disorder in convergent floral nanostructures enhances signalling to bees. *Nature* 550, 469. doi: 10.1038/nature24285

Nakano, T., Suzuki, K., Fujimura, T., and Shinshi, H. (2006). Genome-wide analysis of the ERF gene family in *Arabidopsis* and rice. *Plant Physiol.* 140, 411–432. doi: 10.1104/pp.105.073783

Nakano, T., Fujisawa, M., Shima, Y., and Ito, Y. (2014). The AP2/ERF transcription factor SlERF52 functions in flower pedicel abscission in tomato. *J. Exp. Bot.* 65, 3111–3119. doi: 10.1093/jxb/eru154

Nilsson, L. A. (1992). Orchid pollination biology. *Trends In Ecol. Evol.* 7, 255–259. doi: 10.1016/0169-5347(92)90170-G

Pan, Z. J., Cheng, C. C., Tsai, W. C., Chung, M. C., Chen, W. H., Hu, J. M., et al. (2011). The duplicated B-class MADS-box genes display dualistic characters in orchid floral organ identity and growth. *Plant Cell Physiol.* 52, 1515–1531. doi: 10.1093/pcp/pcr092

Pan, Z. J., Chen, Y. Y., Du, J. S., Chen, Y. Y., Chung, M. C., Tsai, W. C., et al. (2014). Flower development of *Phalaenopsis* orchid involves functionally divergent SEPALLATA-like genes. *New Phytol.* 202, 1024–1042. doi: 10.1111/nph.12723

Panikashvili, D., Shi, J. X., Schreiber, L., and Aharoni, A. (2009). The Arabidopsis DCR encoding a soluble BAHD acyltransferase is required for cutin polyester formation and seed hydration properties. *Plant Physiol.* 151, 1773–1789. doi: 10.1104/pp.109.143388

Petit, J., Bres, C., Mauxion, J. P., Tai, F. W., Martin, L. B., Fich, E. A., et al. (2016). The glycerol-3-phosphate acyltransferase GPAT6 from tomato plays a central role in fruit cutin biosynthesis. *Plant Physiol.* 171, 894–913. doi: 10.1104/pp.16.00409

Prüm, B., Seidel, R., Bohn, H. F., and Speck, T. (2011). Plant surfaces with cuticular folds are slippery for beetles. *J. R. Soc. Interface*, rsif20110202. doi: 10.1098/rsif.2011.0202

Prüm, B., Seidel, R., Bohn, H. F., and Speck, T. (2012). Impact of cell shape in hierarchically structured plant surfaces on the attachment of male Colorado potato beetles (Leptinotarsa decemlineata). *Beilstein J. Nanotechnol.* 3, 57. doi: 10.3762/bjnano.3.7

Prüm, B., Bohn, H. F., Seidel, R., Rubach, S., and Speck, T. (2013). Plant surfaces with cuticular folds and their replicas: influence of microstructuring and surface chemistry on the attachment of a leaf beetle. *Acta Biomater.* 9, 6360–6368. doi: 10.1016/j.actbio.2013.01.030

Rands, S. A., Glover, B. J., and Whitney, H. M. (2011). Floral epidermal structure and flower orientation: getting to grips with awkward flowers. *Arthropod-Plant Interact.* 5, 279–285. doi: 10.1007/s11829-011-9146-3

Robinson, H., and Burns-Balogh, P. (1982). Evidence for a primitively epiphytic habit in Orchidaceae. *Syst. Bot.* 7, 353–358. doi: 10.2307/2418670

Roman Kaiser, G. R. (1993). *The scent of orchids: olfactory and chemical investigations* (Dübendorf, Switzerland, and Elsevier, Amsterdam: Amer Orchid Society).

Rudall, P. J., and Bateman, R. M. (2002). Roles of synorganisation, zygomorphy and heterotopy in floral evolution: the gynostemium and labellum of orchids and other lilioid monocots. *Biol. Rev. Cambridge Philos. Soc.* 77, 403–441. doi: 10.1017/S1464793102005936

Senthil-Kumar, M., and Mysore, K. S. (2011). New dimensions for VIGS in plant functional genomics. *Trends In Plant Sci.* 16, 656–665. doi: 10.1016/j.tplants.2011.08.006

Shi, J. X., Malitsky, S., De Oliveira, S., Branigan, C., Franke, R. B., Schreiber, L., et al. (2011). SHINE transcription factors act redundantly to pattern the archetypal surface of Arabidopsis flower organs. *PloS Genet.* 7, e1001388. doi: 10.1371/journal.pgen.1001388

Shi, J. X., Adato, A., Alkan, N., He, Y., Lashbrooke, J., Matas, A. J., et al. (2013). The tomato SlSHINE3 transcription factor regulates fruit cuticle formation and epidermal patterning. *New Phytol.* 197, 468–480. doi: 10.1111/nph.12032

Su, C. L., Chao, Y. T., Yen, S. H., Chen, C. Y., Chen, W. C., Chang, Y. C. A., et al. (2013a). Orchidstra: an integrated orchid functional genomics database. *Plant Cell Physiol.* 54, e11–e11. doi: 10.1093/pcp/pct004

Su, C. L., Chen, W. C., Lee, A. Y., Chen, C. Y., Chang, Y. C. A., Chao, Y. T., et al. (2013b). A modified ABCDE model of flowering in orchids based on gene expression profiling studies of the moth orchid *Phalaenopsis aphrodite*. *PloS One* 8, e80462. doi: 10.1371/journal.pone.0080462

Taketa, S., Amano, S., Tsujino, Y., Sato, T., Saisho, D., Kakeda, K., et al. (2008). Barley grain with adhering hulls is controlled by an ERF family transcription factor gene regulating a lipid biosynthesis pathway. *Proc. Natl. Acad. Sci. U.S.A.* 105, 4062–4067. doi: 10.1073/pnas.0711034105

Tamura, K., Peterson, D., Peterson, N., Stecher, G., Nei, M., and Kumar, S. (2011). MEGA5: molecular evolutionary genetics analysis using maximum likelihood, evolutionary distance, and maximum parsimony methods. *Mol. Biol. Evol.* 10, 2731–9. doi: 10.1093/molbev/msr121.

Trupiano, D., Yordanov, Y., Regan, S., Meilan, R., Tschaplinski, T., Scippa, G. S., et al. (2013). Identification, characterization of an AP2/ERF transcription factor that promotes adventitious, lateral root formation in Populus. *Planta* 238, 271–282. doi: 10.1007/s00425-013-1890-4

Tsai, W. C., and Chen, H. H. (2006). The orchid MADS-box genes controlling floral morphogenesis. *Sci. World J.* 6, 1933–1944. doi: 10.1100/tsw.2006.321

Tsai, W. C., Kuoh, C. S., Chuang, M. H., Chen, W. H., and Chen, H. H. (2004). Four DEF-like MADS box genes displayed distinct floral morphogenetic roles in *Phalaenopsis* orchid. *Plant Cell Physiol.* 45, 831–844. doi: 10.1093/pcp/pch095

Tsai, W. C., Lee, P. F., Chen, H. I., Hsiao, Y. Y., Wei, W. J., Pan, Z. J., et al. (2005). PeMADS6, a GLOBOSA/PISTILLATA-like gene in *Phalaenopsis equestris* involved in petaloid formation, and correlated with flower longevity and ovary development. *Plant Cell Physiol.* 46, 1125–1139. doi: 10.1093/pcp/pci125

Tsai, W. C., Hsiao, Y. Y., Pan, Z. J., Hsu, C. C., Yang, Y. P., Chen, W. H., et al. (2008). Molecular biology of orchid flowers: With emphasis on *Phalaenopsis*. *Adv. In Bot. Res.* 47, 99–145. doi: 10.1016/S0065-2296(08)00003-7

Tsai, W. C., Fu, C. H., Hsiao, Y. Y., Huang, Y. M., Chen, L. J., Wang, M., et al. (2013). OrchidBase 2.0: comprehensive collection of Orchidaceae floral transcriptomes. *Plant Cell Physiol.* 54, e7–e7. doi: 10.1093/pcp/pcs187

Whitney, H. M., Kolle, M., Andrew, P., Chittka, L., Steiner, U., and Glover, B. J. (2009). Floral iridescence, produced by diffractive optics, acts as a cue for animal pollinators. *Science* 323, 130–133. doi: 10.1126/science.1166256

Whitney, H. M., Bennett, K. M. V., Dorling, M., Sandbach, L., Prince, D., Chittka, L., et al. (2011a). Why do so many petals have conical epidermal cells? *Ann. Bot.* 108, 609–616. doi: 10.1093/aob/mcr065

Whitney, H. M., Glover, B. J., Walker, R., and Ellis, A. G. (2011b). The contribution of epidermal structure to flower colour in the South African flora. *Curtis's Bot. Mag.* 28, 349–371. doi: 10.1111/j.1467-8748.2011.01762.x

Zhang, L., Li, Z., Quan, R., Li, G., Wang, R., and Huang, R. (2011). An AP2 domain-containing gene, ESE1, targeted by the ethylene signaling component EIN3 is important for the salt response in *Arabidopsis*. *Plant Physiol.* 157, 854–865. doi: 10.1104/pp.111.179028

Conflict of Interest: The authors declare that the research was conducted in the absence of any commercial or financial relationships that could be construed as a potential conflict of interest.

frontiers in Plant Science

ORIGINAL RESEARCH
published: 21 February 2020
doi: 10.3389/fpls.2020.00022

Plastome Evolution and Phylogeny of Orchidaceae, With 24 New Sequences

*Young-Kee Kim[1], Sangjin Jo[1], Se-Hwan Cheon[1], Min-Jung Joo[1], Ja-Ram Hong[1], Myounghai Kwak[2] and Ki-Joong Kim[1]**

[1] Division of Life Sciences, Korea University, Seoul, South Korea, [2] Department of Plant Resources, National Institute of Biological Resources, Incheon, South Korea

In order to understand the evolution of the orchid plastome, we annotated and compared 124 complete plastomes of Orchidaceae representing all the major lineages in their structures, gene contents, gene rearrangements, and IR contractions/expansions. Forty-two of these plastomes were generated from the corresponding author's laboratory, and 24 plastomes—including nine genera (*Amitostigma*, *Bulbophyllum*, *Dactylorhiza*, *Dipodium, Galearis*, *Gymnadenia*, *Hetaeria*, *Oreorchis*, and *Sedirea*)—are new in this study. All orchid plastomes, except *Aphyllorchis montana, Epipogium aphyllum,* and *Gastrodia elata,* have a quadripartite structure consisting of a large single copy (LSC), two inverted repeats (IRs), and a small single copy (SSC) region. The IR region was completely lost in the *A. montana and G. elata* plastomes. The SSC is lost in the *E. aphyllum* plastome. The smallest plastome size was 19,047 bp, in *E. roseum,* and the largest plastome size was 178,131 bp, in *Cypripedium formosanum*. The small plastome sizes are primarily the result of gene losses associated with mycoheterotrophic habitats, while the large plastome sizes are due to the expansion of noncoding regions. The minimal number of common genes among orchid plastomes to maintain minimal plastome activity was 15, including the three subunits of *rpl* (14, 16, and 36), seven subunits of *rps* (2, 3, 4, 7, 8, 11, and 14), three subunits of *rrn* (5, 16, and 23), *trn*C-GCA, and *clp*P genes. Three stages of gene loss were observed among the orchid plastomes. The first was *ndh* gene loss, which is widespread in Apostasioideae, Vanilloideae, Cypripedioideae, and Epidendroideae, but rare in the Orchidoideae. The second stage was the loss of photosynthetic genes (*atp, pet*, *psa,* and *psb*) and *rpo* gene subunits, which are restricted to *Aphyllorchis, Hetaeria, Hexalectris,* and some species of *Corallorhiza* and *Neottia*. The third stage was gene loss related to prokaryotic gene expression (*rpl*, *rps*, *trn,* and others), which was observed in *Epipogium*, *Gastrodia*, *Lecanorchis,* and *Rhizanthella.* In addition, an intermediate stage between the second and third stage was observed in *Cyrtosia* (Vanilloideae). The majority of intron losses are associated with the loss of their corresponding genes. In some orchid taxa, however, introns have been lost in *rpl*16, *rps*16, and *clp*P(2) without their corresponding gene being lost. A total of 104 gene rearrangements were counted when comparing 116 orchid plastomes. Among them, many were concentrated near the IRa/b-SSC junction area. The plastome phylogeny of

OPEN ACCESS

Edited by:
Jen-Tsung Chen, National University of Kaohsiung, Taiwan

Reviewed by:
Aleksey Penin, Lomonosov Moscow State University, Russia
Kenji Suetsugu, Kobe University, Japan

***Correspondence:**
Ki-Joong Kim
kimkj@korea.ac.kr

Specialty section:
This article was submitted to Plant Systematics and Evolution, a section of the journal Frontiers in Plant Science

Received: *24 September 2019*
Accepted: *10 January 2020*
Published: *21 February 2020*

Citation:
Kim Y-K, Jo S, Cheon S-H, Joo M-J, Hong J-R, Kwak M and Kim K-J (2020) Plastome Evolution and Phylogeny of Orchidaceae, With 24 New Sequences. Front. Plant Sci. 11:22. doi: 10.3389/fpls.2020.00022

124 orchid species confirmed the relationship of {Apostasioideae [Vanilloideae (Cypripedioideae (Orchidoideae, Epidendroideae))]} at the subfamily level and the phylogenetic relationships of 17 tribes were also established. Molecular clock analysis based on the whole plastome sequences suggested that Orchidaceae diverged from its sister family 99.2 mya, and the estimated divergence times of five subfamilies are as follows: Apostasioideae (79.91 mya), Vanilloideae (69.84 mya), Cypripedioideae (64.97 mya), Orchidoideae (59.16 mya), and Epidendroideae (59.16 mya). We also released the first nuclear ribosomal (nr) DNA unit (18S-ITS1-5.8S-ITS2-28S-NTS-ETS) sequences for the 42 species of Orchidaceae. Finally, the phylogenetic tree based on the nrDNA unit sequences is compared to the tree based on the 42 identical plastome sequences, and the differences between the two datasets are discussed in this paper.

Keywords: Orchidaceae, plastome evolution, gene loss, IR contraction/expansion, genome rearrangement

INTRODUCTION

Orchidaceae is one of the most flourishing flowering plants and contains about 736 known genera and 28,000 species worldwide (Christenhusz and Byng, 2016). Recent studies recognize five subfamilies within Orchidaceae (Apostasioideae, Vanilloideae, Cypripedioideae, Orchidoideae, and Epidendroideae) as a monophyletic group (Chase et al., 2015). The most recently differentiated subfamily, Epidendroideae, includes about 505 genera and 20,600 species, and accounts for most of Orchidaceae (Chase et al., 2015). Orchidaceae is widely distributed throughout the world, and most members in temperate regions have terrestrial life forms, but orchids in tropical rainforests are known to have mainly epiphyte life forms (Givnish et al., 2015). Non-photosynthetic mycoheterotrophic orchids are found in a total of 43 genera and belong to three subfamilies: Vanilloideae, Orchidoideae, and Epidendroideae (Merckx et al., 2013).

Complete Orchidaceae plastomes have been reported in 38 genera and 118 species (NCBI GenBank, June 30, 2019). There are only five genera (*Corallorhiza*, 10 spp.; *Cymbidium,* 9 spp.; *Dendrobium,* 40 spp.; *Holcoglossum*, 11 spp.; and *Neottia*, 7 spp.) in which at least five plastomes per genus have been decoded (Logacheva et al., 2011; Barrett and Davis, 2012; Yang et al., 2013; Barrett et al., 2014; Feng et al., 2016; Niu et al., 2017b; Barrett et al., 2018; Kim et al., 2018). Among them, *Corallorhiza* and *Neottia* have been subjected to extensive evolutionary studies of their plastomes because both photosynthetic and non-photosynthetic species occur in a congeneric group (Barrett and Davis, 2012; Barrett et al., 2014; Feng et al., 2016; Barrett et al., 2018). In addition to the two genera, evolutionary studies have been carried out on the plastomes of some species of other orchid genera. For examples, extensive gene losses have been reported in several independent mycoheterotrophic orchid lineages—i.e., *Aphyllorchis* (Feng et al., 2016), *Cyrtosia* (Kim et al., 2019), *Epipogium* (Schelkunov et al., 2015), *Gastrodia* (Yuan et al., 2018), *Hexalectris* (Barrett and Kennedy, 2018) and *Rhizanthella* (Delannoy et al., 2011). In addition, *ndh* deletion and pseudogenization are assumed to be phenomena that occur independently in many orchid lineages such as *Apostasia* (Lin et al., 2017; Niu et al., 2017a), *Calypso* (Barrett et al., 2018), *Cattleya* (da Rocha Perini et al., 2016), *Cephalanthera* (Feng et al., 2016), *Cremastra* (Dong et al., 2018), *Cymbidium* (Yang et al., 2013; Kim et al., 2018; Wang et al., 2018), *Dendrobium* (Niu et al., 2017b), *Epipactis* (Dong et al., 2018), *Eulophia* (Huo et al., 2017), *Holcoglossum* (Li et al., 2019), *Limodorum* (Lallemand et al., 2019), *Liparis* (Krawczyk et al., 2018), *Neuwiedia* (Niu et al., 2017a), *Oncidium* (Wu et al., 2010; Kim et al., 2015a), *Paphiopedilum* (Niu et al., 2017b; Hou et al., 2018), *Phalaenopsis* (Chang et al., 2006), *Phragmipedium* (Kim et al., 2015a), *Platanthera* (Dong et al., 2018), *Vanilla* (Lin et al., 2015), and *Vanda* (Li et al., 2019). On the other hand, full *ndh* genes have been reported in members of *Anoectochilus* (Yu et al., 2016), *Calanthe* (Dong et al., 2018), *Cypripedium* (Kim et al., 2015b; Lin et al., 2015), *Habenaria* (Lin et al., 2015; Kim et al., 2017b), *Masdevallia* (Kim et al., 2015a), *Ophrys* (Roma et al., 2018), *Pleione* (Shi et al., 2018), and *Sobralia* (Kim et al., 2015a). Gene relocations within a plastome often occur in the reduced plastome of orchids such as *Cyrtosia* (Kim et al., 2019), *Hexalectris* (Barrett and Kennedy, 2018), and *Rhizanthella* (Delannoy et al., 2011). Similar gene rearrangement events within a plastome have been reported in Campanulaceae (Cosner et al., 1997), conifers (Hirao et al., 2008), Fabaceae (Cai et al., 2008), Geraniaceae (Chumley et al., 2006), and Oleaceae (Lee et al., 2007). Contractions of the small single copy (SSC) region similar to that of Geraniaceae were also reported in *Paphiopedilum* (Kim et al., 2015a; Niu et al., 2017b; Hou et al., 2018) and *Vanilla* (Lin et al., 2015; Amiryousefi et al., 2017).

Phylogenetic studies of Orchidaceae using entire plastomes are in a relatively early stage because of limited available plastome sequences (Givnish et al., 2015; Kim et al., 2015a; Lin et al., 2015; Niu et al., 2017b; Dong et al., 2018). But the relationships among major orchid lineages determined using whole plastomes agree well to the large-scale phylogenetic studies of Orchidaceae using two or three genes (Górniak

et al., 2010; Freudenstein and Chase, 2015). Therefore, several outstanding phylogenetic problems in Orchidaceae will be resolved if more plastome sequences are accumulated.

In this study we first completely decoded the plastomes of 24 taxonomic groups of Orchidaceae, including nine genera (*Amitostigma*, *Bulbophyllum*, *Dactylorhiza*, *Dipodium*, *Galearis*, *Gymnadenia*, *Hetaeria*, *Oreorchis*, and *Sedirea*) for which the plastomes had not yet been decoded previously. Second, this study re-annotated and compared the entire plastome sequences of 129 taxa comprising 124 Orchidaceae and five outgroups to investigate evolutionary directions in orchid plastomes, such as sizes, gene contents, gene losses, gene rearrangements, and inverted repeat (IR) expansions/contractions. Third, three stages of gene loss patterns were inferred from mycoheterotrophic orchids and the minimum genes required for plastid maintenance were inferred. Fourth, the phylogenetic trees of Orchidaceae were constructed using whole plastome sequences, and the times at which each taxonomic group differentiated were inferred. Among the 124 orchid plastomes completely decoded, 42 were produced by the NGS method in the laboratory of the corresponding author, and the nuclear ribosomal RNA gene unit (18S-ITS1-5.8S-ITS2-28S-NTS-ETS) was also annotated at the same time. Finally, the common features and differences among the 42 species were compared and explained by comparing their plastome trees and nrDNA gene unit trees.

MATERIALS AND METHODS

Plant Materials and DNA Extraction

Plant leaf materials used in this study and their voucher information are given in **Table 1**. Fresh leaf samples were ground into fine powder with liquid nitrogen in a mortar. Ground samples were used to extract genomic DNA using a G-spin™ II Genomic DNA Extraction Kit (Intron, Seoul, Korea). The quality of DNA was checked by a UVVIS spectrophotometer. Extracted DNAs were deposited into the Plant DNA Bank in Korea (PDBK) and voucher specimens were deposited into the Korea University (KUS) herbarium and National Institute of Biological Resources (NIBR) herbarium.

NGS Sequencing, Plastome Assembly, and Annotation

Four samples—*Calanthe bicolor*, *Dendrobium moniliforme*, *D. moniliforme* "Royal Dream," and *D. moniliforme* "Sangeum"—were sequenced by Illumina HiSeq 2000. Twenty other samples were sequenced by Illumina MiSeq. The resulting raw reads from HiSeq were trimmed by Geneious 6.1.8 (Kearse et al., 2012) with a 0.05 error probability limitation. *Dendrobium officinale* (NC024019) was used as a reference sequence to perform reference-guided assembly using a Geneious assembler. Contigs from the reference-guided assembly were used as reference

TABLE 1 | NGS data status and general features of the 24 newly sequenced Orchidaceae plastomes.

Subfamily	Tribe	Scientific Name	NGS Method	# of raw reads	# of trimmed reads	Coverages (X)	Length (bp)	Voucher specimen and/or DNA number
Epidendroideae	Collabieae	*Calanthe aristulifera*	MiSeq	10,977,664	555,650	851.4	158,204	NIBRVP0000709265
Epidendroideae	Collabieae	*Calanthe bicolor*	HiSeq	38,596,340	585,710	1,252.6	158,070	PDBK2012-1749
Epidendroideae	Cymbidieae	*Dipodium roseum*	MiSeq	23,515,448	871,246	1,733.7	141,209	PDBKTA2019-0006
Epidendroideae	Epidendreae	*Corallorhiza maculata* var. *maculata*	MiSeq	10,817,394	424,348	841.7	146,198	PDBK2017-1544
Epidendroideae	Epidendreae	*Cremastra unguiculata*	MiSeq	10,280,912	438,352	884.1	159,341	NIBRVP0000658615
Epidendroideae	Epidendreae	*Oreorchis patens*	MiSeq	8,530,614	553,290	363.8	158,542	PDBK2007-0151
Epidendroideae	Gastrodieae	*Gastrodia elata*	MiSeq	12,318,196	676,842	546.2	35,056	PDBK2017-1545
Epidendroideae	Malaxideae	*Bulbophyllum inconspicuum*	MiSeq	9,612,620	604,200	1,125.2	149,548	PDBK2012-0213
Epidendroideae	Malaxideae	*Dendrobium moniliforme*	HiSeq	8,745,236	614,130	869.0	151,711	PDBK2012-0008
Epidendroideae	Malaxideae	*Dendrobium moniliforme* 'Royal Dream'	HiSeq	20,728,340	616,358	1,211.9	151,695	PDBK2014-0012
Epidendroideae	Malaxideae	*Dendrobium moniliforme* 'Sangeum'	HiSeq	10,876,884	673,118	1277.4	151,711	PDBK2014-0009
Epidendroideae	Malaxideae	*Liparis auriculata*	MiSeq	8,360,832	686,628	1,353.2	153,460	NIBRVP0000703422
Epidendroideae	Malaxideae	*Liparis makinoana*	MiSeq	14,299,168	705,140	1,384.2	153,093	PDBK2012-0543
Epidendroideae	Neottieae	*Epipactis thunbergii*	MiSeq	21,093,888	897,388	706.4	159,279	PDBK2017-0509
Epidendroideae	Vandeae	*Sedirea japonica*	MiSeq	12,019,968	391,094	842.2	146,942	PDBK2019-0551
Orchidoideae	Cranichideae	*Goodyera rosulacea*	MiSeq	18,736,600	137,286	287.4	152,831	PDBK2012-0647
Orchidoideae	Cranichideae	*Hetaeria shikokiana*	MiSeq	10,227,090	105,074	540.2	130,934	PDBK2018-0672
Orchidoideae	Orchideae	*Amitostigma gracile*	MiSeq	8,563,894	137,432	220.4	156,120	PDBK2008-0404
Orchidoideae	Orchideae	*Dactylorhiza viridis* var. *coreana*	MiSeq	8,179,110	180,240	266.6	153,549	PDBK2011-0840
Orchidoideae	Orchideae	*Galearis cyclochila*	MiSeq	7,859,188	224,736	397.2	153,928	PDBK2000-0786
Orchidoideae	Orchideae	*Gymnadenia conopsea*	MiSeq	8,967,924	220,376	550.3	153,876	PDBK2011-0894
Orchidoideae	Orchideae	*Habenaria chejuensis*	MiSeq	8,865,896	359,614	576.0	153,896	PDBK2018-1246
Orchidoideae	Orchideae	*Habenaria flagellifera*	MiSeq	10,712,312	233,302	439.0	151,210	PDBK2018-1247
Orchidoideae	Orchideae	*Platanthera mandarinorum*	MiSeq	8,745,236	221,761	541.1	154,162	PDBK2013-0398

sequences to perform reference-guided assembly repeatedly until complete plastome sequences were obtained.

The resulting raw reads from MiSeq were trimmed by BBDuk 37.64, implemented in Geneious 11.1.5 (length: 27 kmer). BBNorm 37.64 was used to normalize trimmed reads (target coverage level: 30; minimum depth: 12). Normalized reads were used to perform *de-novo* assembly by Geneious assembler. Resulting *de-novo* assembly contigs were used as reference sequences to perform reference-guided assembly to obtain complete plastome sequences when the *de-novo* assembly did not produce complete plastome contigs. All complete plastome sequences were used as reference sequences to gather chloroplast reads from trimmed read sets. Gathered reads were reused to perform *de-novo* assembly and validate the level of completeness. Due to its unusual plastome structure, *Gastrodia elata* was assembled again by SPAdes 3.10.0 (Bankevich et al., 2012) using an error correction tool and assembly module. NGS results are given in **Table 1**.

Complete plastome sequences were annotated with BLASTn, tRNAscan-SE 2.0 (Lowe and Chan, 2016), ORF finder, and find annotation function in Geneious 11.1.5 (*Habenaria radiata* plastome sequences, NC035834, used as a reference). Alternative start codons—such as ACG and TTG—were also included in the ORF finder. Genes with many stop codons in the middle of sequences, uncorrectable frame shift mutations, and several large abnormal indels, were judged to have a pseudogene. Gene sequences with complete CDS or few (five or fewer) internal stop codons and for which RNA editing was possible were analyzed to have a gene. These criteria were based on a character reconstructions study of the gene status of *ndh* in Orchidaceae (Kim et al., 2015a). ORFs from the plastome sequence of four mixotrophic orchids (*Corallorhiza maculata* var. *maculata*, *Dipodium roseum*, *Gastrodia elata,* and *Hetaeria shikokiana*) were translated into protein sequences. The translated sequences were exported in the fasta format files to perform psi-blast (Altschul et al., 1997) based on several Orchidaceae plastome databases. Circular plastome maps were constructed using the OGdraw web server (Lohse et al., 2007). All downloaded NCBI plastome data used in our study were re-annotated because the published data contained many annotation errors. Finally, we manually edited some ambiguous annotation area using our comparative alignments of orchid sequences.

Phylogenetic Analysis

Ninety-nine plastome sequences were downloaded from the NCBI to perform phylogenetic analysis (**Table 2**; 94 Orchidaceae sequences, four Asparagales sequences, and one Liliales sequences). Eight to 79 CDS and two to four rRNA genes were extracted from plastome sequences. Each extracted region was aligned by MAFFT (Katoh et al., 2002) and all alignments were checked manually. Each aligned gene sequences were subjected to jModeltest (Darriba et al., 2012) in CIPRES Science Gateway (Miller et al., 2010) to obtain the best model. GTR-I-G-X or GTR-G-X were the best-fit models for all genes except *rrn*5 (short sequence), for which SYM-G was the best-fit model. Eighty-three alignments were concatenated to a length of 87,399 bp. Concatenated alignments were used to perform jModeltest (Darriba et al., 2012) in CIPRES Science Gateway (Miller et al., 2010) to obtain the best model. GTR+G+I was the best-fit model for concatenated data. Lost genes were treated as missing data because they do not affect the phylogenetic signals in the remaining genes (Lam et al., 2016). A maximum likelihood (ML) tree was constructed using RaxML-HPC2 on XSEDE in CIPRES Science Gateway with a GTR+G+I model and 100 bootstrap replicates (−672774.637133) of ML optimization likelihood. Concatenated alignment was also used to construct a Bayesian inference (BI) tree. MrBayes_CIPRES api (Miller et al., 2015) was used to construct a BI tree with a Markov chain Monte Carlo (MCMC) chain length of 1,000,000 and GTR +G+I model. The trees obtained were treated graphically using Treegraph2 (Stöver and Müller, 2010).

IRScope (Amiryousefi et al., 2018) was used to describe SC-IR junction regions among 41 plastome sequences generated in the laboratory (*Gastrodia elata* was excluded due to its lack of IR). The length information of 24 new plastome sequences was visualized by ggplot2 package in R (Wickham et al., 2016). Gene contents of 129 plastome sequences were displayed as a heatmap. The ProgressiveMauve algorithm (Darling et al., 2010) was used to check plastome rearrangements among 116 Orchidaceae plastome sequences, excluding non-photosynthetic orchids with an extremely short plastome (*Cyrtosia*, *Epipogium*, *Gastrodia*, *Lecanorchis,* and *Rhizanthella*). The resulting LCBs (locally collinear blocks) from ProgressiveMauve were extracted and numbered to visualize their features (**Tables S1** and **S2**).

The nuclear rDNA region—which contains 18S rRNA, internal transcribed spacers, 5.8S rRNA, 28S rRNA, NTS, and ETS—was generated in 42 Orchidaceae species (**Table 2**). Forty-two rDNA sequences were aligned by MAFFT (6,043 bp long). The alignment was tested with jModeltest in CIPRES Science Gateway. RaxML-HPC2 on XSEDE in CIPRES Science Gateway was used to construct an ML tree with a GTR+G+I model and 100 bootstrap replicates. The plastome sequence gene data of 42 species were also used to construct an ML tree. Eighty-three CDS and rRNA genes were extracted and aligned by MAFFT. Eighty-three alignments were concatenated into one (80,798 bp long). Concatenated alignments were used to perform jModeltest. An ML tree was constructed by RaxML-HPC2 on XSEDE with a GTR+G+I model with 100 bootstrap replicates. The trees obtained were treated by Treegraph2.

Divergence Time Estimation

The alignments used in the ML tree construction were also used to estimate divergence time. The GTR estimated model was selected to build a time divergence tree, following the results of PartifionFinder v2.1.1 (Lanfear et al., 2012). An XML file was prepared by BEAUti 2.5.2 (Bouckaert et al., 2019). The XML file was submitted to the CIPRES Science Gateway to perform BEAST2-XSEDE (Bouckaert et al., 2019). A relaxed clock log normal model (Drummond et al., 2006) and Yule model were chosen to perform MCMC with a chain length of 300,000,000. Logs and trees were collected every 5,000 generations, and three independent runs were performed. Three fossil data

TABLE 2 | Information on the sequences used in this study.

Subfamily	Tribe	Scientific name*	NCBI accession (nrDNA)	NCBI accession (Plastome)	Life style	Length (bp)	LSC (bp)	SSC (bp)	IR (bp)	GC %	# of coding genes	# of pseudo-genes	# of tRNAs
Epidendroideae	Arethuseae	*Bletilla ochracea*	–	NC029483	Terrestrial	157,431	85,810	17,949	26,836	37.3	74	9	30
Epidendroideae	Arethuseae	*Bletilla striata*	–	NC028422	Terrestrial	157,393	86,213	17,742	26,719	37.2	74	9	29
Epidendroideae	Arethuseae	*Pleione bulbocodioides*	–	NC036342	Terrestrial	159,269	87,121	18,712	26,718	37.2	83	0	30
Epidendroideae	Collabieae	*Calanthe aristulifera*	**MN221390**	**MN200378**	Terrestrial	158,204	86,889	18,369	26,473	36.7	83	0	30
Epidendroideae	Collabieae	*Calanthe bicolor*	**MN221391**	**MN200379**	Terrestrial	158,070	87,000	18,342	26,364	36.7	83	0	30
Epidendroideae	Collabieae	*Calanthe davidii*	–	NC037438	Terrestrial	153,629	86,045	15,672	25,956	36.9	83	0	30
Epidendroideae	Collabieae	*Calanthe triplicata*	–	NC024544	Terrestrial	158,759	87,305	18,460	26,497	36.7	83	0	30
Epidendroideae	Cymbidieae	*Cymbidium goeringii*	–	NC028524	Terrestrial	157,192	85,749	17,883	26,780	36.9	74	9	30
Epidendroideae	Cymbidieae	*Cymbidium lancifolium*	–	NC029712	Terrestrial	149,945	84,716	13,895	25,667	37.1	73	8	30
Epidendroideae	Cymbidieae	*Cymbidium macrorhizon*	MK333261	KY354040	Terrestrial	149,859	85,187	13,766	25,453	37.0	73	8	30
Epidendroideae	Cymbidieae	*Dipodium roseum*	**MN221399**	**MN200386**	Terrestrial	141,209	81,787	10,352	24,535	36.9	71	3	30
Epidendroideae	Cymbidieae	*Erycina pusilla*	–	NC018114	Epiphyte	143,164	83,733	11,675	23,878	36.7	71	6	29
Epidendroideae	Cymbidieae	*Eulophia zollingeri*	–	NC037212	Terrestrial	145,201	81,566	13,091	25,272	36.9	73	6	29
Epidendroideae	Cymbidieae	*Oncidium sphacelatum*	–	NC028148	Epiphyte	147,761	83,575	12,670	25,758	37.1	73	4	30
Epidendroideae	Epidendreae	*Calypso bulbosa* var. *occidentalis*	–	NC040980	Terrestrial	149,313	83,331	14,718	25,632	37.1	72	8	29
Epidendroideae	Epidendreae	*Cattleya crispata*	–	NC026568	Epiphyte	148,343	85,973	13,261	24,495	37.3	75	7	30
Epidendroideae	Epidendreae	*Cattleya liliputana*	–	NC032083	Epiphyte	147,092	85,945	13,149	24,304	37.4	75	7	30
Epidendroideae	Epidendreae	*Corallorhiza bulbosa*	–	NC025659	Terrestrial	148,643	82,851	12,368	26,712	37.1	72	7	29
Epidendroideae	Epidendreae	*Corallorhiza macrantha*	–	NC025660	Terrestrial	151,031	84,263	12,544	27,112	37.2	70	9	29
Epidendroideae	Epidendreae	*Corallorhiza maculata* var. *maculata* 1	**MN221392**	**MN200380**	Terrestrial	146,198	79,612	13,018	26,784	36.8	53	22	30
Epidendroideae	Epidendreae	*Corallorhiza maculata* var. *maculata* 2	–	KM390014	Terrestrial	146,886	80,395	12,885	26,803	36.8	55	25	29
Epidendroideae	Epidendreae	*Corallorhiza maculata* var. *mexicana*	–	KM390015	Terrestrial	151,506	84,347	12,671	27,244	37.1	71	8	29
Epidendroideae	Epidendreae	*Corallorhiza maculata* var. *occidentalis*	–	KM390016	Terrestrial	146,595	81,363	12,368	26,432	36.9	58	22	30
Epidendroideae	Epidendreae	*Corallorhiza mertensiana*	–	NC025661	Terrestrial	147,941	81,109	13,774	26,529	36.8	58	22	29
Epidendroideae	Epidendreae	*Corallorhiza odontorhiza*	–	NC025664	Terrestrial	147,317	82,257	13,508	25,776	37.0	71	8	29
Epidendroideae	Epidendreae	*Corallorhiza striata* var. *vreelandii*	–	JX087681	Terrestrial	137,505	72,631	12,388	26,243	36.4	46	30	29
Epidendroideae	Epidendreae	*Corallorhiza trifida*	–	NC025662	Terrestrial	149,384	83,092	14,420	25,936	37.2	72	9	29
Epidendroideae	Epidendreae	*Corallorhiza wisteriana*	–	NC025663	Terrestrial	146,437	76,350	17,743	26,172	37.1	71	8	29
Epidendroideae	Epidendreae	*Cremastra appendiculata*	–	NC037439	Terrestrial	155,320	87,098	15,478	26,372	37.2	76	5	30
Epidendroideae	Epidendreae	*Cremastra unguiculata*	**MN221393**	**MN200381**	Terrestrial	159,341	87,031	18,252	27,029	36.9	82	0	30
Epidendroideae	Epidendreae	*Hexalectris warnockii*	–	MH444822	Terrestrial	119,057	66,903	17,490	17,332	36.9	41	26	29
Epidendroideae	Epidendreae	*Masdevallia coccinea*	–	NC026541	Terrestrial	157,423	84,957	18,448	27,009	36.8	83	0	30
Epidendroideae	Epidendreae	*Masdevallia picturata*	–	NC026777	Epiphyte	156,045	84,948	18,029	26,534	36.9	83	0	29
Epidendroideae	Epidendreae	*Oreorchis patens*	**MN221415**	**MN200369**	Terrestrial	158,542	86,437	18,443	26,831	36.9	83	0	30

(Continued)

TABLE 2 | Continued

Subfamily	Tribe	Scientific name*	NCBI accession (nrDNA)	NCBI accession (Plastome)	Life style	Length (bp)	LSC (bp)	SSC (bp)	IR (bp)	GC %	# of coding genes	# of pseudo-genes	# of tRNAs
Epidendroideae	Gastrodieae	*Gastrodia elata* 2	–	NC037409	Terrestrial	35,304	(SC Only)	(SC Only)	-	34.2	23	2	5
Epidendroideae	Gastrodieae	*Gastrodia elata* 1	**MN221402**	**MN200389**	Terrestrial	35,056	(SC Only)	(SC Only)	-	26.7	23	2	5
Epidendroideae	Malaxideae	*Bulbophyllum inconspicuum*	**MN221389**	**MN200377**	Epiphyte	149,548	85,760	12,136	25,826	37.0	78	0	30
Epidendroideae	Malaxideae	*Dendrobium moniliforme* 2	–	NC035154	Epiphyte	148,778	84,867	11,945	25,983	37.5	70	5	30
Epidendroideae	Malaxideae	*Dendrobium moniliforme* 1	**MN221396**	**MN200384**	Epiphyte	151,711	84,773	14,352	26,293	37.5	73	7	30
Epidendroideae	Malaxideae	*Dendrobium moniliforme* 'Royal Dream'	**MN221397**	**MN200385**	Epiphyte	151,695	84,758	14,351	26,293	37.5	73	7	30
Epidendroideae	Malaxideae	*Dendrobium moniliforme* 'Sangeum'	**MN221398**	**MN200383**	Epiphyte	151,711	84,773	14,352	26,293	37.5	73	7	30
Epidendroideae	Malaxideae	*Dendrobium nobile*	–	NC029456	Epiphyte	153,660	85,686	14,654	26,660	37.5	73	7	30
Epidendroideae	Malaxideae	*Dendrobium officinale*	–	NC024019	Epiphyte	152,221	85,109	14,516	26,298	37.5	73	7	30
Epidendroideae	Malaxideae	*Liparis auriculata*	**MN221412**	**MN200365**	Terrestrial	153,460	83,785	17,731	25,972	36.9	83	0	30
Epidendroideae	Malaxideae	*Liparis loeselii*	-	MF374688	Terrestrial	153,687	84,596	17,673	25,709	36.9	74	9	29
Epidendroideae	Malaxideae	*Liparis makinoana*	**MN221413**	**MN200368**	Terrestrial	153,093	83,533	17,746	25,907	36.9	83	0	30
Epidendroideae	Malaxideae	*Oberonia japonica*	MN221414	NC035832	Epiphyte	142,996	81,669	10,969	25,179	37.4	72	2	30
Epidendroideae	Neottieae	*Aphyllorchis montana*	–	NC030703	Terrestrial	94,559	(SC Only)	(SC Only)	-	37.1	38	26	30
Epidendroideae	Neottieae	*Cephalanthera humilis*	–	NC030706	Terrestrial	157,011	86,908	15,133	27,485	37.3	71	10	30
Epidendroideae	Neottieae	*Cephalanthera longifolia*	–	NC030704	Terrestrial	161,877	88,806	19,187	26,942	37.2	83	0	30
Epidendroideae	Neottieae	*Epipactis mairei*	–	NC030705	Terrestrial	159,019	86,377	18,816	26,913	37.3	81	2	30
Epidendroideae	Neottieae	*Epipactis thunbergii*	**MN221400**	**MN200387**	Terrestrial	159,279	87,297	18,638	26,672	37.3	83	0	30
Epidendroideae	Neottieae	*Epipactis veratrifolia*	–	NC030708	Terrestrial	159,719	87,043	18,854	26,911	37.3	82	1	30
Epidendroideae	Neottieae	*Limodorum abortivum*	–	MH590355	Terrestrial	154,847	85,544	15,099	27,102	37.5	76	0	30
Epidendroideae	Neottieae	*Neottia acuminata*	–	NC030709	Terrestrial	83,190	51,145	5,371	13,337	36.6	31	20	30
Epidendroideae	Neottieae	*Neottia camtschatea*	–	NC030707	Terrestrial	106,385	52,960	9,273	22,076	37.2	38	29	30
Epidendroideae	Neottieae	*Neottia fugongensis*	–	NC030711	Terrestrial	156,536	85,357	18,311	26,434	31.6	83	0	30
Epidendroideae	Neottieae	*Neottia listeroides*	–	NC030713	Terrestrial	110,246	45,021	9,597	27,814	37.2	31	25	30
Epidendroideae	Neottieae	*Neottia nidus-avis*	–	NC016471	Terrestrial	92,060	36,422	7,822	23,908	34.4	29	8	27
Epidendroideae	Neottieae	*Neottia ovata*	–	NC030712	Terrestrial	156,978	85,433	18,071	26,737	37.6	83	0	30
Epidendroideae	Neottieae	*Neottia pinetorum*	–	NC030710	Terrestrial	155,959	84,449	18,104	26,703	37.5	82	1	30
Epidendroideae	Neottieae	*Palmorchis pabstii*	–	NC041190	Terrestrial	163,909	90,710	18,823	27,188	37.3	83	0	30
Epidendroideae	Nervilieae	*Epipogium aphyllum*	–	NC026449	Terrestrial	30,650	8,030	0	11,310	32.8	21	0	6
Epidendroideae	Nervilieae	*Epipogium roseum*	–	NC026448	Terrestrial	19,047	9,618	8,907	261	30.6	22	0	7
Epidendroideae	Sobralieae	*Elleanthus sodiroi*	–	NC027266	Terrestrial	161,511	88,425	18,880	27,103	37.1	83	0	30
Epidendroideae	Sobralieae	*Sobralia* aff. *bouchei* HTK-2015	–	NC028209	Terrestrial/ Epiphyte	161,543	88,684	18,835	27,012	37.1	83	0	30
Epidendroideae	Sobralieae	*Sobralia callosa*	–	NC028147	Terrestrial	161,430	88,666	18,794	26,985	37.1	83	0	30

(Continued)

TABLE 2 | Continued

Subfamily	Tribe	Scientific name*	NCBI accession (nrDNA)	NCBI accession (Plastome)	Life style	Length (bp)	LSC (bp)	SSC (bp)	IR (bp)	GC %	# of coding genes	# of pseudo-genes	# of tRNAs
Epidendroideae	Vandeae	*Gastrochilus fuscopunctatus*	MK317970	NC035830	Epiphyte	146,183	83,125	11,146	25,956	36.8	72	2	30
Epidendroideae	Vandeae	*Gastrochilus japonicus*	MK317969	NC035833	Epiphyte	147,697	84,695	11,174	25,914	36.8	72	2	30
Epidendroideae	Vandeae	*Holcoglossum amesianum*	–	NC041511	Epiphyte	148,074	84,250	12,026	25,899	36.6	72	4	30
Epidendroideae	Vandeae	*Holcoglossum flavescens*	–	NC041512	Epiphyte	146,863	83,288	11,959	25,808	36.7	72	4	30
Epidendroideae	Vandeae	*Holcoglossum lingulatum*	–	NC041465	Epiphyte	146,525	83,762	11,274	25,769	36.8	72	6	30
Epidendroideae	Vandeae	*Neofinetia falcata*	MK317968	KT726909	Epiphyte	146,491	83,802	11,775	25,457	36.6	72	4	30
Epidendroideae	Vandeae	*Neofinetia falcata* 'CheongSan'	MK317971	NC036372	Epiphyte	146,497	83,808	11,775	25,457	36.6	72	4	30
Epidendroideae	Vandeae	*Neofinetia richardsiana*	MK317967	NC036373	Epiphyte	146,498	83,809	11,775	25,457	36.6	72	4	30
Epidendroideae	Vandeae	*Pelatantheria scolopendrifolia*	MK317972	NC035829	Epiphyte	146,860	86,075	11,735	24,525	36.5	72	1	30
Epidendroideae	Vandeae	*Pendulorchis himalaica*	–	NC041513	Epiphyte	145,207	83,712	11,413	25,041	36.6	72	4	30
Epidendroideae	Vandeae	*Phalaenopsis aphrodite* subsp. *formosana*	–	NC007499	Epiphyte	148,964	85,957	11,543	25,732	36.7	71	3	30
Epidendroideae	Vandeae	*Phalaenopsis equestris*	–	NC017609	Epiphyte	148,959	85,967	11,300	25,846	36.7	71	8	30
Epidendroideae	Vandeae	*Phalaenopsis* 'Tiny Star'	–	NC025593	Epiphyte	148,918	85,885	11,523	25,755	36.7	71	7	31
Epidendroideae	Vandeae	*Sedirea japonica*	**MN221419**	**MN200373**	Epiphyte	146,942	84,882	10,568	25,746	32.2	72	2	30
Epidendroideae	Vandeae	*Thrixspermum japonicum*	MK317966	NC035831	Epiphyte	149,220	85,301	11,546	26,187	36.1	71	1	30
Epidendroideae	Vandeae	*Vanda brunnea*	–	NC041522	Epiphyte	149,216	85,783	11,713	25,860	36.7	72	7	30
Orchidoideae	Cranichideae	*Anoectochilus emeiensis*	–	NC033895	Terrestrial	152,650	82,670	17,342	26,319	36.9	80	0	31
Orchidoideae	Cranichideae	*Goodyera fumata*	–	NC026773	Terrestrial	155,643	84,077	18,342	26,612	37.3	83	0	30
Orchidoideae	Cranichideae	*Goodyera procera*	–	NC029363	Terrestrial	153,240	82,032	18,406	26,401	37.6	76	0	31
Orchidoideae	Cranichideae	*Goodyera rosulacea*	**MN221403**	**MN200390**	Terrestrial	152,831	82,041	17,720	26,535	36.8	83	0	30
Orchidoideae	Cranichideae	*Goodyera schlechtendaliana*	–	NC029364	Terrestrial	154,348	83,215	18,051	26,541	37.2	79	0	31
Orchidoideae	Cranichideae	*Goodyera velutina*	–	NC029365	Terrestrial	152,692	82,443	17,247	26,501	36.9	76	0	31
Orchidoideae	Cranichideae	*Hetaeria shikokiana*	**MN221408**	**MN200367**	Terrestrial	130,934	64,694	2,320	31,960	36.3	44	19	30
Orchidoideae	Cranichideae	*Kuhlhasseltia nakaiana*	MN221409	KY354041	Terrestrial	147,614	81,617	13,673	26,162	39.5	73	0	30
Orchidoideae	Cranichideae	*Ludisia discolor*	–	NC030540	Terrestrial	153,054	82,675	17,233	26,573	37.0	82	0	30
Orchidoideae	Diurideae	*Rhizanthella gardneri*	–	NC014874	Terrestrial	59,190	26,360	13,295	9,767	34.2	24	4	9
Orchidoideae	Orchideae	*Amitostigma gracile*	**MN221388**	**MN200376**	Terrestrial	156,120	85,171	18,165	26,392	36.4	83	0	30
Orchidoideae	Orchideae	*Dactylorhiza viridis* var. *coreana*	**MN221395**	**MN200382**	Terrestrial	153,549	82,715	17,728	26,553	31.9	83	0	30
Orchidoideae	Orchideae	*Galearis cyclochila*	**MN221401**	**MN200388**	Terrestrial	153,928	83,308	17,772	26,424	36.9	83	0	30
Orchidoideae	Orchideae	*Gymnadenia conopsea*	**MN221404**	**MN200391**	Terrestrial	153,876	83,142	17,702	26,516	38.6	83	0	29
Orchidoideae	Orchideae	*Habenaria chejuensis*	**MN221405**	**MN200392**	Terrestrial	153,896	83,732	17,026	26,569	36.6	82	0	30
Orchidoideae	Orchideae	*Habenaria flagellifera*	**MN221406**	**MN200366**	Terrestrial	151,210	81,072	17,110	26,514	36.7	83	0	30

(Continued)

TABLE 2 | Continued

Subfamily	Tribe	Scientific name*	NCBI accession (nrDNA)	NCBI accession (Plastome)	Life style	Length (bp)	LSC (bp)	SSC (bp)	IR (bp)	GC %	# of coding genes	# of pseudo-genes	# of tRNAs
Orchidoideae	Orchideae	*Habenaria pantlingiana*	–	NC026775	Terrestrial	153,951	83,641	17,370	26,470	36.6	83	0	30
Orchidoideae	Orchideae	*Habenaria radiata*	MN221407	NC035834	Terrestrial	155,353	84,833	17,718	26,401	36.5	83	0	30
Orchidoideae	Orchideae	*Ophrys fusca* subsp. *iricolor*	–	AP018716	Terrestrial	150,177	80,541	16,940	26,348	36.8	83	0	22
Orchidoideae	Orchideae	*Ophrys sphegodes*	–	AP018717	Terrestrial	146,754	80,471	16,177	25,053	36.9	83	0	22
Orchidoideae	Orchideae	*Platanthera japonica*	–	NC037440	Terrestrial	154,995	85,979	13,664	27,676	37.0	82	0	30
Orchidoideae	Orchideae	*Platanthera mandarinorum*	**MN221416**	**MN200370**	Terrestrial	154,162	83,325	17,757	26,540	36.8	83	0	30
Cypripedioideae	Cypripedioideae	*Cypripedium formosanum*	–	NC026772	Terrestrial	178,131	102,188	21,921	27,011	33.9	83	0	31
Cypripedioideae	Cypripedioideae	*Cypripedium japonicum*	–	NC027227	Terrestrial	174,417	97,322	21,911	27,592	34.5	82	1	30
Cypripedioideae	Cypripedioideae	*Paphiopedilum armeniacum*	–	NC026779	Terrestrial	162,682	91,734	3,666	33,641	35.4	72	5	30
Cypripedioideae	Cypripedioideae	*Paphiopedilum dianthum*	–	NC036958	Epiphyte	154,699	86,861	2,416	32,711	35.9	71	3	30
Cypripedioideae	Cypripedioideae	*Paphiopedilum niveum*	–	NC026776	Terrestrial	159,108	89,856	5,194	32,029	35.7	71	5	30
Cypripedioideae	Cypripedioideae	*Phragmipedium longifolium*	–	NC028149	Terrestrial	151,157	88,367	13,066	24,862	36.1	71	4	30
Vanilloideae	Pogonieae	*Pogonia japonica*	MN221417	MN200371	Terrestrial	158,200	87,447	5,387	32,683	36.4	72	4	30
Vanilloideae	Pogonieae	*Pogonia minor*	MN221418	MN200372	Terrestrial	158,170	87,457	5,375	32,669	36.4	72	4	30
Vanilloideae	Vanilleae	*Cyrtosia septentrionalis*	MN221394	MH615835	Terrestrial	96,859	58,085	10,414	17,946	34.8	41	0	25
Vanilloideae	Vanilleae	*Lecanorchis japonica*	MN221410	MN200364	Terrestrial	70,498	28,197	14,493	13,904	30.4	25	3	7
Vanilloideae	Vanilleae	*Lecanorchis kiusiana*	MN221411	MN200363	Terrestrial	74,084	30,824	14,118	14,571	30.0	25	2	8
Vanilloideae	Vanilleae	*Vanilla aphylla*	–	NC035320	Epiphyte	150,184	87,379	2,131	30,337	35.0	65	7	29
Vanilloideae	Vanilleae	*Vanilla madagascariensis*	MN221420	MN200374	Epiphyte	151,552	87,490	1,254	31,404	34.6	71	1	29
Vanilloideae	Vanilleae	*Vanilla planifolia* 2	–	NC026778	Epiphyte	148,011	86,358	2,037	29,808	35.4	72	1	30
Vanilloideae	Vanilleae	*Vanilla planifolia* 1	MN221421	MN200375	Epiphyte	147,714	86,061	2,037	29,808	35.4	72	1	30
Vanilloideae	Vanilleae	*Vanilla pompona*	–	NC036809	Epiphyte	148,009	86,358	2,037	29,807	35.4	72	1	30
Apostasioideae	Apostasioideae	*Apostasia odorata*	–	NC030722	Terrestrial	159,285	86,172	18,765	27,174	35.7	82	1	30
Apostasioideae	Apostasioideae	*Apostasia wallichii*	–	NC036260	Terrestrial	156,126	83,031	20,187	26,454	36.1	73	10	30
Apostasioideae	Apostasioideae	*Neuwiedia zollingeri* var. *singapureana*	–	LC199503	Terrestrial	161,068	88,910	18,056	27,051	36.0	73	10	29
Amarylidaceae (Outgroup)	Amarylidaceae (Outgroup)	*Allium cepa*	–	KM088013	Terrestrial	153,529	82,662	17,931	26,468	36.8	82	0	30
Asparagaceae (Outgroup)	Asparagaceae (Outgroup)	*Eustrephus latifolius*	–	NC025305	Terrestrial	159,736	82,403	13,607	31,863	38.1	78	2	30
Iridaceae (Outgroup)	Iridaceae (Outgroup)	*Iris gatesii*	–	NC024936	Terrestrial	153,441	82,702	18,371	26,184	37.9	83	0	29
Iridaceae (Outgroup)	Iridaceae (Outgroup)	*Iris sanguinea*	–	NC029227	Terrestrial	152,408	82,340	18,016	26,026	38.0	83	0	30
Liliales (Outgroup)	Liliales (Outgroup)	*Fritillaria hupehensis*	–	NC024736	Terrestrial	152,145	81,894	17,553	26,349	37.0	80	2	30

**Red scientific name indicates that the species is mixotroph or obligate (full) mycoheterotroph throughout its life cycle. The bold NCBI accession numbers for nrDNAs and plastomes indicate that the species' NGS data were generated in this study.*

(Asparagales, normal distribution, sigma 8.0, mean 105.3; *Dendrobium*, log-normal distribution, sigma 2.0, offset 23.2; and *Goodyera*, log-normal distribution, sigma 2.0, offset 15.0) were used to calibrate nodes (Ramírez et al., 2007; Conran et al., 2009; Gustafsson et al., 2010; Iles et al., 2015).

Three log and tree files were concatenated by Logcombiner v2.5.2 (Rambaut and Drummond, 2014) by discarding 20% of files. The concatenated log files were checked by Tracer v1.6 (Rambaut et al., 2014) to validate the effective sample size (ESS). Major parameters—including posterior, likelihood, and

the prior—exceeded an ESS of 100, and all other parameters exceeded an ESS of 50. The concatenated tree files were treated by Treeannotator (Rambaut and Drummond, 2007) in CIPRES Science Gateway with an option of 0.95 posterior probability. The concatenated maximum clade credibility tree generated by Treeannotator was treated by FigTree v1.4 (Rambaut, 2012) and "phytools" and "ape" packages in R.

RESULTS

General Features of 24 New Orchidaceae Plastomes

The taxonomic positions, NGS methods, raw read numbers, trimmed read numbers, plastome lengths, coverage depth, voucher information, etc. of the 24 new plastomes are summarized in **Table 1**. The coverage depths ranged from 220x (*Amitostigma gracile*) to 1,734x (*Dactylorhiza viridis* var. *coreana*), so that each plastome sequence was sequenced at least several hundred times.

Among the plastomes of the 24 newly decoded species, the length of the plastome of *Gastrodia elata*, a non-photosynthetic species, was the shortest at 35,056 bp and that of *Cremastra unguiculata*, a photosynthetic species, was the longest at 159,341 bp. *Gastrodia elata* is unique in that it only has a single copy of the plastome because the IR was lost. The plastomes of the remaining 23 species have quadripartite structures consisting of an large single copy (LSC), an SSC, and two IR regions. The total lengths of the plastomes and the relative lengths of the IR, SSC, and LSC of the 24 newly decoded species were compared, as shown in **Figure 1**.

Among the 24 species, the plastomes of 13 (*Amitostigma gracile*, *Calanthe aristulifera*, *C. bicolor, Dactylorhiza viridis* var. *coreana, Epipactis thunbergii, Galearis cyclochila, Goodyera rosulacea, Habenaria chejuensis, H. flagellifera, Liparis auriculata, L. makinoana, Oreorchis patens,* and *Platanthera mandarinorum*) had all the same genes as typical plant plastids. Various subunits of the *ndh* gene class were found to be pseudogenized or lost in eight species (*Bulbophyllum inconspicuum, Cremastra unguiculata, Dendrobium moniliforme, D. moniliforme* "Sangeum", *D. moniliforme* "Royal Dream", *Dipodium roseum, Gymnadenia conopsea*, and *Sedirea japonica*). In addition, *pet*L was lost in *Cremastra unguiculata, psb*D was pseudogenized in *Dipodium roseum*, and *trn*G-UCC was lost in *Gymnadenia conopsea*. In the case of the non-photosynthetic species *Corallorhiza maculata* var. *maculata*, *ccs*A, *cem*A, *ndh*B, *ndh*C, *ndh*D, *ndh*G, *ndh*H, *ndh*I, *ndh*J, *ndh*K, *pet*A, *pet*D, *pet*G, *psa*A, *psa*B, *psb*A, *psb*C, *rbc*L, *rpo*A, *rpo*B, *rpo*C1, and *ycf*1 existed as pseudogenes and *ndh*A, *ndh*E, *ndh*F, *psb*B, *psb*J, *psb*L, *psb*M, and *rpo*C2 were lost. In the case of *Hetaeria shikokiana*, another non-photosynthetic species, many genes were lost or pseudogenized. Among the genes, *cem*A,

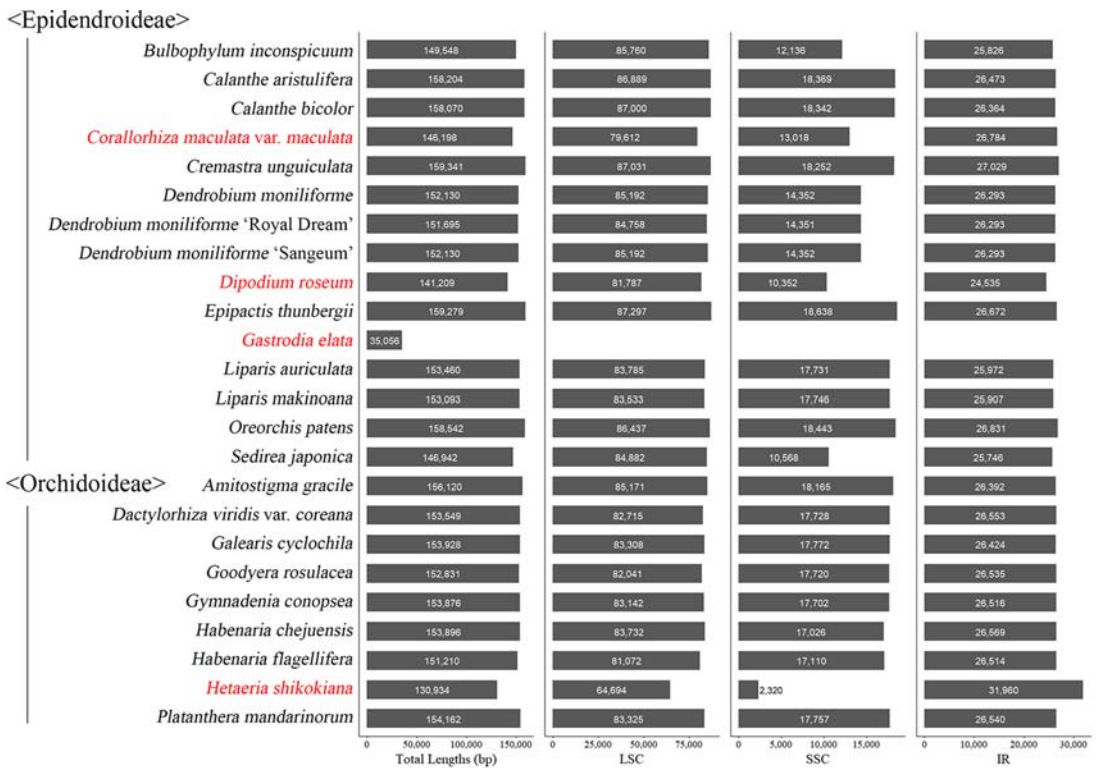

FIGURE 1 | Plastome length variation in 24 newly sequenced orchid species. The plastome of *Gastrodia elata* is 35,056 bp long and consists of only one single copy region. The species names in red indicate mycoheterotrophic species.

*ndh*A, *ndh*B, *ndh*C, *ndh*H, *pet*A, *pet*D, *pet*G, *pet*N, *psa*B, *psa*I, *psb*C, *psb*F, *psb*N, *rpo*A, *rpo*C1, *rpo*C2, *ycf*3, and *ycf*4 were pseudogenized, and *atp*A, *atp*B, *ccs*A, *ndh*D, *ndh*E, *ndh*F, *ndh*G, *ndh*I, *ndh*J, *pet*B, *psa*A, *psa*C, *psb*A, *psb*B, *psb*J, *psb*L, *psb*M, *rbc*L, *rpl*23, and *rpo*B were lost. *Gastrodia elata*, which has the shortest plastome of the 24 species examined, only had the following genes: *acc*D, *clp*P, *mat*K, *rpl*2, *rpl*14, *rpl*16, *rpl*20, *rpl*36, *rps*2, *rps*3, *rps*4, *rps*7, *rps*8, *rps*11, *rps*12, *rps*14, *rps*18, *rps*19, *rrn*5, *rrn*16, *rrn*23, *ycf*1, and *ycf*2. Two pseudogenes (*psa*I and *psb*K) remained, and all the other genes were lost.

Comparative Analyses of Orchidaceae Plastomes

The Orchidaceae plastomes that have been completely decoded and can be used in comparative studies comprise 60 genera, 142 species, and 146 accessions, including the 24 new plastomes (NCBI database, June 30, 2019). Since the main purpose of this study was to identify the evolutionary trends in plastomes of the entire Orchidaceae, there were three genera—*Cymbidium* (9 spp.), *Dendrobium* (40 spp.), and *Holcoglossum* (11 spp.)—for which the plastomes of many species were decoded, but only three species each were included in the comparative study. In the case of *Corallorhiza* (10 spp.) and *Neottia* (7 spp.), the plastomes of all species were included in the comparative study, even though the plastomes of many species were decoded, because these genera include both photosynthetic and non-photosynthetic species. In the case of the remaining genera, all available plastomes were included in the comparative study except for one species of *Cypripedium,* in which many problems were found in the re-annotation process. Therefore, five subfamilies, 17 tribes, 60 genera, 118 species, and 124 accessions were used in the comparative study in this paper. In addition, five outgroup plastomes were also used for comparison. Therefore, the GenBank accession numbers, taxonomic classification, habitats, plastome sizes, LSC lengths, IR lengths, SSC lengths, GC contents, and numbers of genes and pseudogenes of the 129 plastomes used in this study, along with whether or not their corresponding species is photosynthetic, are listed in **Table 2**. The plastomes of land plants usually have an AT-biased base composition. Furthermore, highly reduced plastomes have more AT-biased substitutions than typical plastomes because they experience relaxed selection. The average GC content of orchid plastomes in this study was 36.40 ± 1.71%. The three highly reduced orchid plastomes—*Epipogium aphyllum*, *E. roseum*, and *Rhizanthella*—had 32.8%, 30.6%, and 34.2% GC contents, respectively. The CDS of *E. aphyllum., E. roseum*, and *Rhizanthella* had 38.4%, 34.3%, and 38.1% GC contents, respectively. They showed 2–6% more AT-biased substitutions than general orchid plastomes. Extreme AT bias was reported in the plastome of *Rhopalocnemis phalloides*, which had a GC content of only 13.2% (Schelkunov et al., 2019). Among the 124 Orchidaceae plastomes used in the comparative study, 42 were decoded using the NGS method in the laboratory of the corresponding author. In addition to the plastomes, the base sequences of nuclear ribosomal RNA repeating unit DNA (nrDNA, 18S-ITS1-5.8S-ITS2-28S-NTS-ETS), which are present as tandem repeats, could also be assembled in these 42 species (**Figure 2**). Therefore, the GenBank accession numbers of these species are also published in **Table 2** for the first time. Consequently, these 42 species were used to compare nrDNA repeating unit-based trees and plastome-based trees.

Among the 124 Orchidaceae plastomes, 121 had an IR region. In the case of *Aphyllorchis montana*, the IR region was lost and the plastome existed only as a single copy (**Table 2**), similarly to *Gastrodia elata* 1 and 2. The plastome of *Aphyllorchis montana* is small at 94,559 bp. Another example of the SSC region being lost and the plastome consisting of the LSC and two IRs was reported in *Epipogium aphyllum* (**Figure 3**). These three species are examples of the quadripartite structure of a plastome not being maintained. The quadripartite structure was maintained in all the remaining species. *Epipogium aphyllum* is the only example in which the IRs appear consecutively without any SSC. However, in the case of *Epipogium roseum*, which is a related species, an SSC region, although short, existed at 890 bp, and the IR region was shortened to 261 bp (**Table 2**, **Figure 3**).

The largest plastome in Orchidaceae was 178,131 bp, in *Cypripedium formosanum,* and the smallest was 19,047 bp, in *Epipogium roseum* (**Figure 3**). The plastome sizes of all photosynthetic orchids were at least 140 kb. On the other hand, the plastome sizes of non-photosynthetic mycoheterotrophic orchids were mostly smaller than 150 kb and showed high positive correlations with gene numbers (**Figure 4A**). In addition, unlike the plastome sizes of epiphytic orchids, which were at least 140 kb, those of terrestrial orchids varied greatly because they include mycoheterotrophic species (**Figure 4B**). Although the plastome sizes of photosynthetic orchids mostly ranged from 145–160 kb, those of *Cypripedium* had a much larger derange; this was highly correlated with the expansion of the LSC region, and not correlated much with the expansion of IRs (**Figures 4C, D**). On the other hand, in the case of mycoheterotrophic species, plastome sizes showed high correlations with the size of both the LSC and IR.

FIGURE 2 | Diagram of nuclear ribosomal (nr) DNA repeat units consisting of 18S-ITS1-5.8S-ITS2-28S-NTS-ETS. The total length of the unit is approximately 10 kb, and it is arranged as a tandem repeat. The nrDNA repeat sequences of 42 orchid species were first reported in this paper.

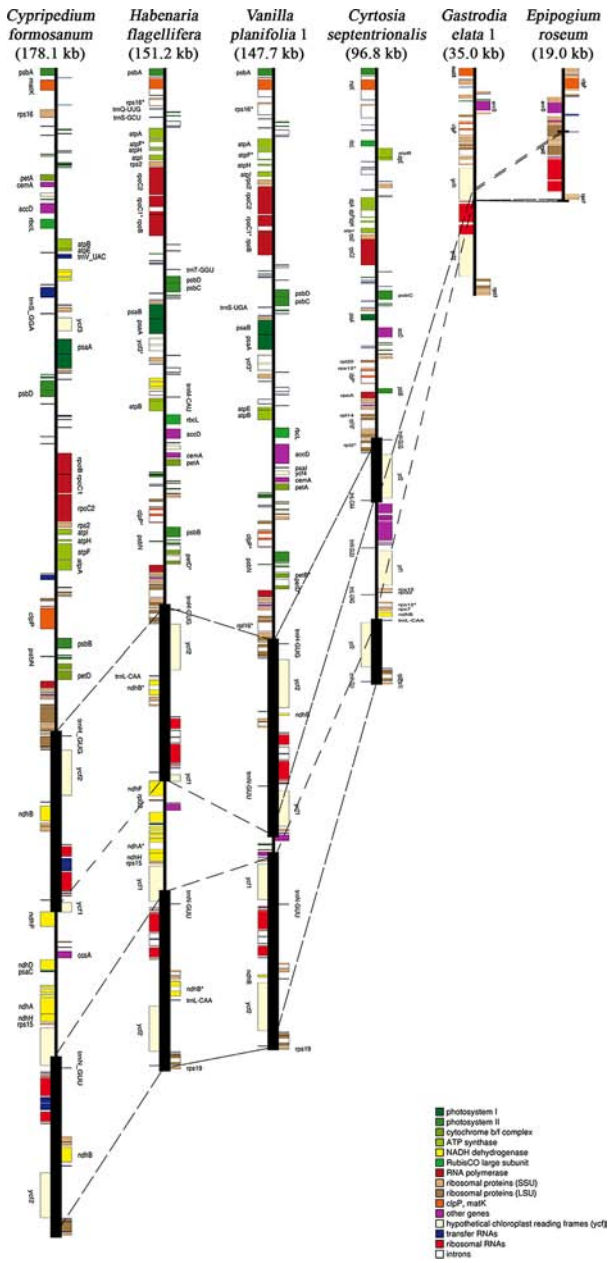

FIGURE 3 | Six representative plastomes of Orchidaceae. *Cypripedium formosanum* has the longest plastome (178.1 kb), while *Epipogium roseum* has the shortest. *Gastrodia elata* and *Epipogium roseum* hold 27 genes in their plastome, even though they have substantially different plastome sizes. The heavy vertical bars indicate inverted repeat (IR) regions and the broken lines among plastomes indicate the boundaries of IR and single copy regions.

Gene Content Evolution of Orchidaceae

The gene contents of the 124 orchid species showed high variation (**Figure 5**). A plastome usually contains a total of 113 genes, comprising 6 *atp*, 11 *ndh*, 6 *pet*, 9 *rpl*, 4 *rpo*, 12 *rps*, 4 *rrn*, 5 *psa*, 15 *psb*, 30 *trn*, and 11 ungrouped genes. Among the 124 species of Orchidaceae, 27 (22%) have all 113 genes existing in an active status. In eight species, one to three genes were pseudogenized or lost. These 35 species fall into the category of having plastomes with almost all their plastid genes, and they make up 28% of all 124 species in this study. There are 69 species where four to 11 of the 11 genes in the *ndh* gene class or all 11 *ndh* genes plus one or two other gene (s) do not function, indicating that the plastid *ndh* gene class does not function in 56% of all 124 species. Furthermore, *ndh* genes, photosynthesis light reaction genes (*pet, psa*, *psb*), and *rpo* gene were shown to be lost in 13 species. Such cases are also accompanied by the loss of *rpo* genes. Finally, in the case of *Lecanorchis* (two species), *Epipogium* (two species), *Gastrodia* (one species, two accs.), and *Rhizanthella* (one species), many housekeeping genes such as *rpl*, *rps*, and *trn* were also lost.

The presence of genes and pseudogenization in the 124 Orchidaceae and five outgroup species are set forth in **Figure 5** by subfamily, tribe, species, and gene class. In the case of photosynthetic orchids, up to 13 genes were lost. In most of these cases, 11 *ndh* genes and one or two other genes were lost. In an exceptional case with photosynthetic orchids, 19 genes were lost in *Vanilla aphylla* with epiphytic habitats. The lost genes seem to consist of 11 *ndh* genes and eight other pseudogenized genes. However, given that only 11 to 12 genes were lost from the plastids in other *Vanilla* species, it is inferred that the plastid gene annotation of this species is problematic. On the other hand, among the species known to be mycoheterotrophic species, the fewest genes were lost in *Limodorum abortivum*, where the loss of seven genes comprising *cem*A, five *ndh* genes, and *rpl*22 was observed. *Limodorum abortivum* was followed by *Cymbidium macrorhizon*, in which 10 *ndh* genes were lost, *Eulophia zollingeri*, where 11 *ndh* genes and *trn*G-UCC were lost, and *Dipodium roseum*, where 11 *ndh* genes and a *psb*D gene were lost. However, although these four species have the mycoheterotrophic nutritional mode, they also have chlorophyll, and are reported or observed to be orchids that carry out low levels of photosynthesis. In the case of *Corallorhiza*, both mycoheterotrophic and photosynthetic species exist, and the levels of photosynthesis vary according to variety or habitat, even in the same species. When seen based on the degree of gene loss, species in which 11 *ndh* genes and one to three other genes were lost are very likely to preserve photosynthetic activity. When the gene contents of the 124 orchid plastomes were compared, a large gap was found in the area where 14–25 genes were lost. Therefore, whether photosynthetic ability was lost or not can be divided around this range (**Figures 4** and **5**).

Among the plastomes that are classified into completely non-photosynthetic orchids because at least 25 genes were lost, two groups are recognized based on the numbers of lost genes and preserved genes. That is, they are a group of plastomes in which the number of preserved genes is similar to or larger than the number of lost genes (13 plastomes), and a group of plastomes in which the number of lost genes is overwhelmingly larger (seven plastomes). Among the 124 plastomes, the Orchidaceae species

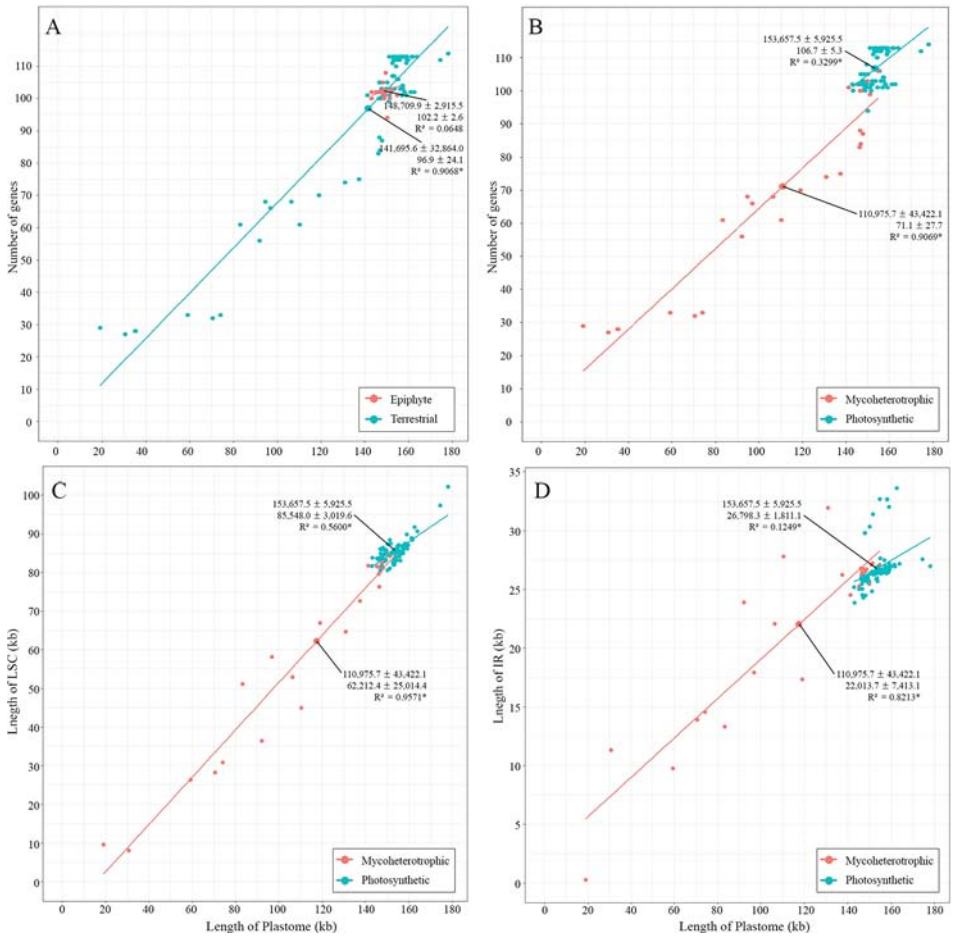

FIGURE 4 | Relationships between plastome lengths and gene numbers. **(A)**: Terrestrial orchids show a wider range of variation than epiphytic orchids. **(B)**: Mycoheterotrophic orchids show a wider range of variation than photosynthetic orchids. **(C, D)**: Plastome lengths are more strongly correlated with LSC lengths than IR lengths in both mycoheterotrophic and photosynthetic orchids.

that belong to the latter are *Epipogium aphyllum* (86 lost, 27 preserved), *Epipogium roseum* (84 lost, 29 preserved), *Gastrodia elata* 1 and 2 (85 lost, 28 preserved), *Lecanorchis kiusiana* (80 lost, 33 preserved), *Lecanorchis japonica* (81 lost, 32 preserved), and *Rhizanthella gardneri* (80 lost, 33 preserved). These seven plastomes have 27–33 genes preserved, and among them, 20 genes are common (**Table 3**). These 20 genes are inferred to be the minimum common plastid genes necessary to maintain non-photosynthetic plastids. However, among these 20 plastid genes, five are missing in any of the remaining 117 Orchidaceae plastomes. Therefore, 15 genes are common to all orchid plastids. The 15 genes comprise 14 housekeeping genes (*rpl*14, *rpl*16, *rpl*26, *rps*2, *rps*3, *rps*4, *rps*7, *rps*8, *rps*11, *rps*14, *rrn*5, *rrn*16, *rrn*23, and *trn*C-GGA) and *clp*P.

To determine the patterns of plastome gene loss over Orchidaceae evolution, we plotted the gene loss patterns on the ML phylogenetic trees using Bayesian estimation approaches (**Figure 6**). Apostasioideae, Vanilloideae, Cypripedioideae, and Orchidoideae are shown in **Figure 6A**, and Epidendroideae is shown in **Figure 6B**. In the case of the *ndh* gene class, gene loss or pseudogenization occurred independently in almost all lineages of Epidendroideae. On the other hand, in the case of the four remaining subfamilies, the loss of *ndh* genes, although relatively rare, was observed independently in at least five lineages. The loss of genes directly involved in the photosynthetic light reaction—such as *psa*, *psb*, and *pet*—was observed in six lineages of Epidendroideae, two lineages of Orchidoideae, and one lineage of Vanilloideae. The loss of housekeeping genes such as *rpl*, *rps*, and *trn* occurred independently in three lineages: *Gastrodia-Epipogium* of Epidendroideae, *Lecanorchis* of Vanilloideae, and *Rhizanthella* of Orchidoideae.

Sixteen genes in the typical land plant plastomes (*atp*F, *ndh*A, *ndh*B, *pet*B, *pet*D, *rpl*2, *rpl*16, *rpo*C1, *rps*12, *rps*16, *trn*A-UGC, *trn*G-UCC, *trn*I-GAU, *trn*K-UUU, *trn*L-UAA, and *trn*V-UAC) generally have one intron, and two genes (*clpP* and *ycf*3) have

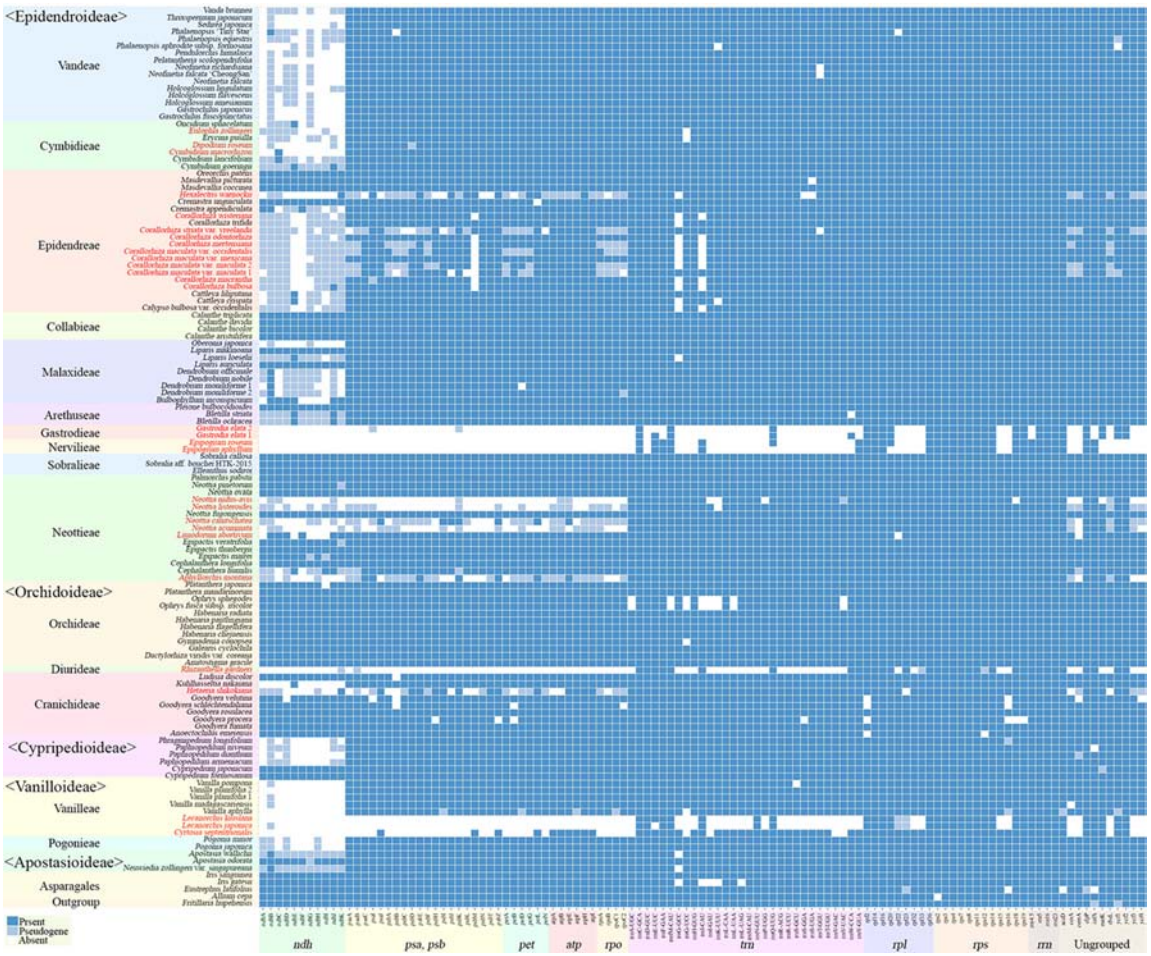

FIGURE 5 | Distribution patterns of gene loss in Orchidaceae. The dark blue, light blue, and white blocks indicate presence, pseudogene, and absence of each gene, respectively. The non-functionalization of 11 *ndh* genes are distributed widely across all taxonomic groups of Orchidaceae. This frequently occurs in Epidendroideae and Vanilloideae. The non-functionalization of *psa*, *psb*, *pet*, and *rpo* gene classes are confined to mycoheterotrophic lineages. In addition, the loss of housekeeping genes such as the *rps*, *rpl*, or *trn* gene classes occur independently in four genera, *Epipogium*, *Gastrodia*, *Lecanorchis,* and *Rhizanthella*. The species names in red indicate mycoheterotrophic orchids.

two introns. The absence or presence of these 20 introns are summarized (**Figure 7**). The majority of intron losses are associated with the loss of their corresponding gene; the exceptions are *rpl*16, *rps*16, and *clp*P(2), in which the introns were lost but the corresponding genes were not in some terminal clade of the tree.

To identify gene rearrangements among Orchidaceae plastomes, gene block analysis was carried out using MAUVE. Among the 124 Orchidaceae plastomes, only 116 taxonomic groups were analyzed; eight were excluded—*Cyrtosia septentrionalis*, *Epipogium roseum*, *Epipogium aphyllum*, *Gastrodia elata* 1, *G. elata* 2, *Lecanorchis kiusiana*, *L. japonica*, and *Rhizanthella gardneri*—because they had severe gene losses and were therefore meaningless in gene block analysis. A total of 134 gene blocks were identified. The aligned lengths (kb), gene regions, forward/reverse orientations, and names of taxa distributed in individual gene blocks are listed in **Tables S1** and **S2**. In addition, the orientations of the 134 gene block and distribution patterns by taxonomic group (**Figure 8A**), and the lengths of individual blocks and the number of shared taxonomic groups (**Figure 8B**), were set forth. Among the 134 blocks, 104 were identified as genome rearrangement blocks because they showed variations, and 30 were identified as constant blocks. In terms of plastome regions, 48 blocks were found in the LSC region and among them, 34 were identified as rearrangement blocks and 14 were identified as constant blocks. Only three blocks were found in the IR region, and they were rearranged blocks. Eighty-three blocks (~60%) were found in the SSC region and 24 small blocks were identified in the *ycf*1 gene region existing at the IR/SSC boundary.

Based on block length, 81 blocks shorter than 1 kb, 35 blocks 1 to 5 kb long, six blocks 5 to 10 kb long, and 12 blocks longer

TABLE 3 | Minimum genes required for seven orchid species with extremely degraded plastomes (*Epipogium aphyllum*, *E. roseum*, two *Gastrodia elata*, *Lecanorchis japonica*, *L. kiusiana,* and *Rhizanthella gardneri*).

Scientific Name Gene	*Epipogium aphyllum*	*Epipogium roseum*	*Gastrodia elata*	*Gastrodia elata*	*Lecanorchis japonica*	*Lecanorchis kiusiana*	*Rhizanthella gardneri*	Other Orchids	Notes
***acc*D**	+	+	+	+	+	+	+	116/117	*Vanilla aphylla* (Pseudogene)
clp*P	**+**	**+**	**+**	**+**	**+**	**+**	**+**	117	
***rpl*2**	+	+	+	+	+	+	+	113/117	*Anoectochilus emeiensis* (Absent), *Goodyera procera* (Absent), *G. schlechtendaliana* (Absent), *G. velutina* (Absent)
rpl*14	**+**	**+**	**+**	**+**	**+**	**+**	**+**	117	
rpl*16	**+**	**+**	**+**	**+**	**+**	**+**	**+**	117	
rpl*36	**+**	**+**	**+**	**+**	**+**	**+**	**+**	117	
rps*2	**+**	**+**	**+**	**+**	**+**	**+**	**+**	117	
rps*3	**+**	**+**	**+**	**+**	**+**	**+**	**+**	117	
rps*4	**+**	**+**	**+**	**+**	**+**	**+**	**+**	117	
rps*7	**+**	**+**	**+**	**+**	**+**	**+**	**+**	117	
rps*8	**+**	**+**	**+**	**+**	**+**	**+**	**+**	117	
rps*11	**+**	**+**	**+**	**+**	**+**	**+**	**+**	117	
rps*14	**+**	**+**	**+**	**+**	**+**	**+**	**+**	117	
***rps*18**	+	+	+	+	+	+	+	115/117	*Neottia nidus-avis* (Absent), *Goodyera procera* (Absent)
***rps*19**	+	+	+	+	+	+	+	116/117	*Goodyera procera* (Absent)
rrn*5	**+**	**+**	**+**	**+**	**+**	**+**	**+**	117	
rrn*16	**+**	**+**	**+**	**+**	**+**	**+**	**+**	117	
rrn*23	**+**	**+**	**+**	**+**	**+**	**+**	**+**	117	
trn*C-GCA	**+**	**+**	**+**	**+**	**+**	**+**	**+**	117	
***trn*fM-CAU**	**+**	**+**	**+**	**+**	**+**	**+**	**+**	115/117	*Ophrys fusca* subsp. *iricolor* (Absent) *Ophrys sphegodes* (Absent)

Bold gene name with an asterisk indicates that all 124 orchid species share the gene.

than 10 kb were found. The longest gene block is 52.63 kb in length, located between *pet*D-*rps*12 in the LSC region that has rearranged. This block was followed by *trn*E-UUC-*ycf*3 (40.6 kb, rearrangement), *rpo*C2-*rpo*B (29.49 kb, rearrangement), *trn*G-UUC-*rpo*C2 (22.42 kb, rearrangement), *psb*A-*trn*K-UUU (21.00 kb, rearrangement), *cem*A-trnP-UGG (18.15 kb, rearrangement), *trn*V-UAC-*atp*B (16.92 kb, rearrangement), *psb*B-*pet*D (16.64 kb, rearrangement), *trn*L-UAA-*ndh*J (14.42 kb rearrangement), *psa*J-*clp*P (14.42 kb, rearrangement), *rrn*16-*rrn*5 (13.19 kb, rearrangement), and *rps*16 (12.32 kb, rearrangement). Among the 12 gene blocks longer than 10 kb long, 10 are distributed in the LSC region and two in the IR region (**Figure 8B**).

In the gene block analysis, to compare structures in the vicinity of the IR/SSC junctions where many small rearrangements are concentrated, the SC-IR junctions of 42 species of Orchidaceae (including 24 new plastome sequences) decoded in this laboratory were schematized by taxonomic group and expressed as shown in **Figure S2**. Here, the IR of *Gastrodia elata* was deleted. All the LSC-IRb junctions of 19 taxonomic groups, not including non-photosynthetic taxonomic groups (*Cyrtosia*, *Hetaeria*, *Lecanorchis*), were formed in the vicinity of *rpl*22. The LSC-IRb junction of *Cyrtosia septentrionalis* was found in the vicinity of *rps*19, that of *Lecanorchis* was found in the vicinity of *rpl*2, and that of *Hetaeria shikokiana* was found in the vicinity of *rpl*2. As with LSC-IRb junctions, LSC-IRa junctions were identified to have been formed in the IGS before *psb*A in all taxonomic groups except for three non-photosynthetic taxonomic groups (*Hetaeria shikokiana, Lecanorchis kiusiana,* and *L. japonica*). The IRa-SSC and IRb-SSC junctions of the remaining taxonomic groups—except non-photosynthetic taxonomic groups, seven species of Vanilloideae (in *Cyrtosia*, *Lecanorchis*, *Pogonia*, and *Vanilla*) and one species of Orchidoideae (*Hetaeria*)—were located on *ndh*F and *ycf*1, respectively. Seven taxonomic groups belonging to Vanilloideae commonly showed a phenomenon of a shorter SSC and among them, in the case of non-photosynthetic taxonomic groups

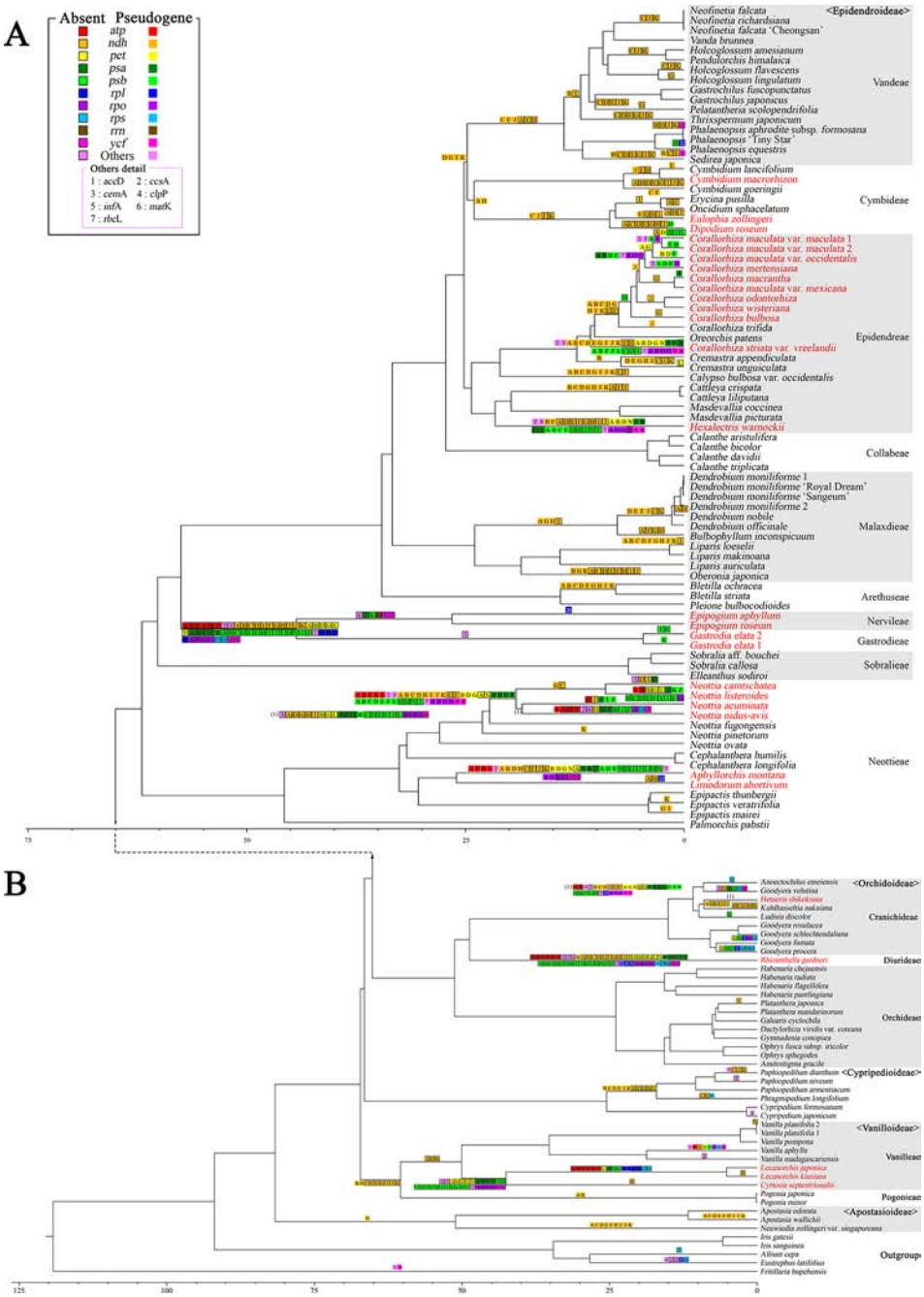

FIGURE 6 | Evolution of gene losses in the phylogenetic tree of Orchidaceae. A total of 129 taxa—124 Orchidaceae and five outgroup taxa—were the subject of tree reconstruction. The sequences of 83 protein coding genes were concatenated to a length of 87,399 bp. A maximum likelihood (ML) tree was constructed using RaxML-HPC2 with a GTR+G+I model (ML = −672774.637133 of ML optimization likelihood). All the genes were then plotted on the tree node using parsimony criteria under the condition of no parallel gains of the same gene. The species names in red indicate mycoheterotrophic orchids. **(A)**: The basal portion of the tree showing the subfamilies Apostasioideae, Vanilloideae, Cypripedioideae, and Orchidoideae. **(B)**: The upper portions of the tree showing the subfamily Epidendroideae.

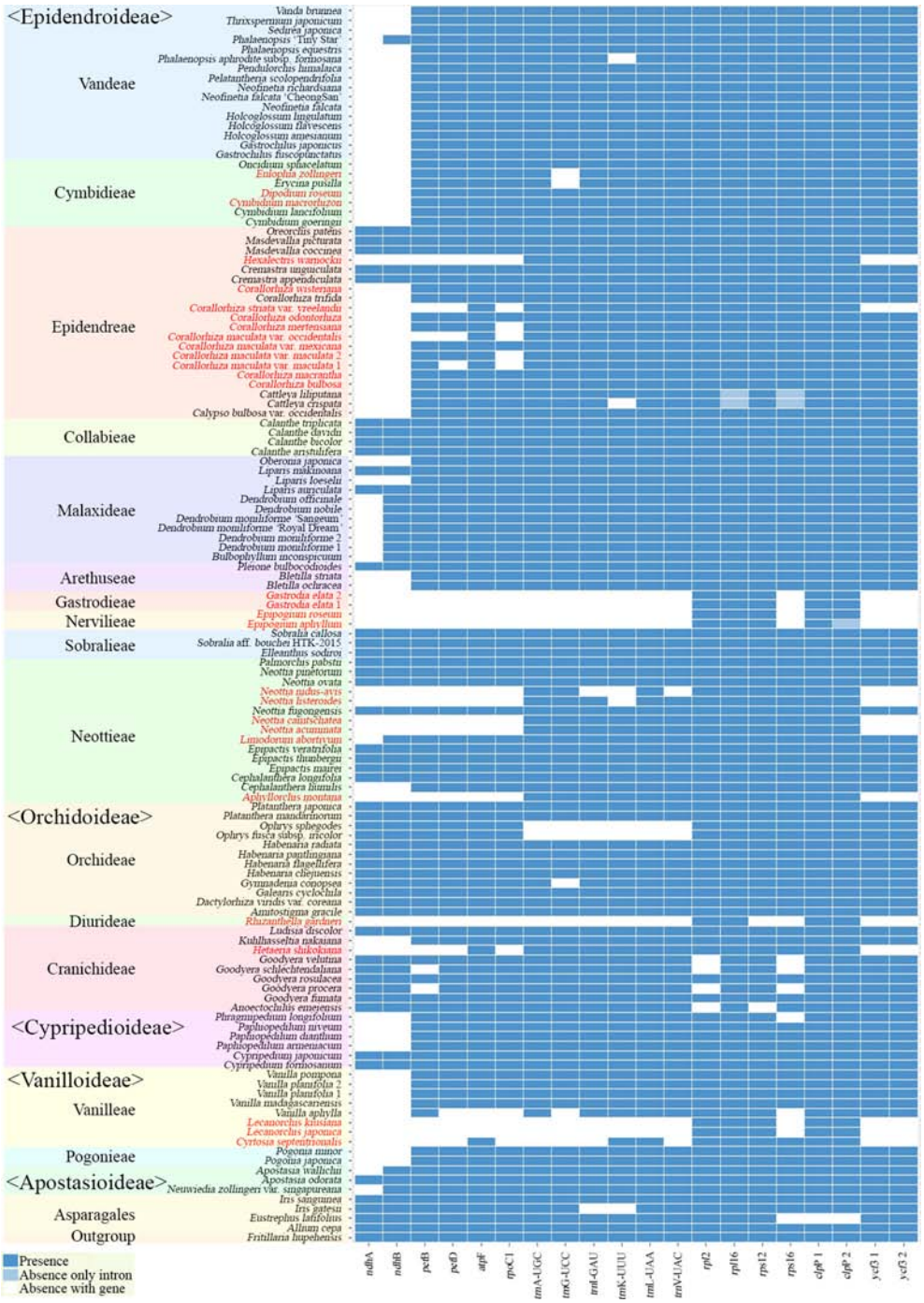

FIGURE 7 | Distribution patterns of the loss of 20 introns in Orchidaceae. The dark blue, light blue, and white blocks indicate intron presence, absence without corresponding gene loss, and absence with corresponding gene loss, respectively.

Cyrtosia and *Lecanorchis*, the rRNA genes generally present in the IR were relocated to the SSC. Although *Hetaeria shikokiana* belongs to Orchidoideae, it has a shortened SSC (2,320 bp), similar to the taxonomic groups of Vanilloideae (**Figure 1**).

Phylogenetic Relationships Among the Major Lineages of Orchidaceae

The phylogenetic relationships connected to Apostasioideae {Vanilloideae [Cypripedioideae (Orchidoideae, Epidendroideae)]}

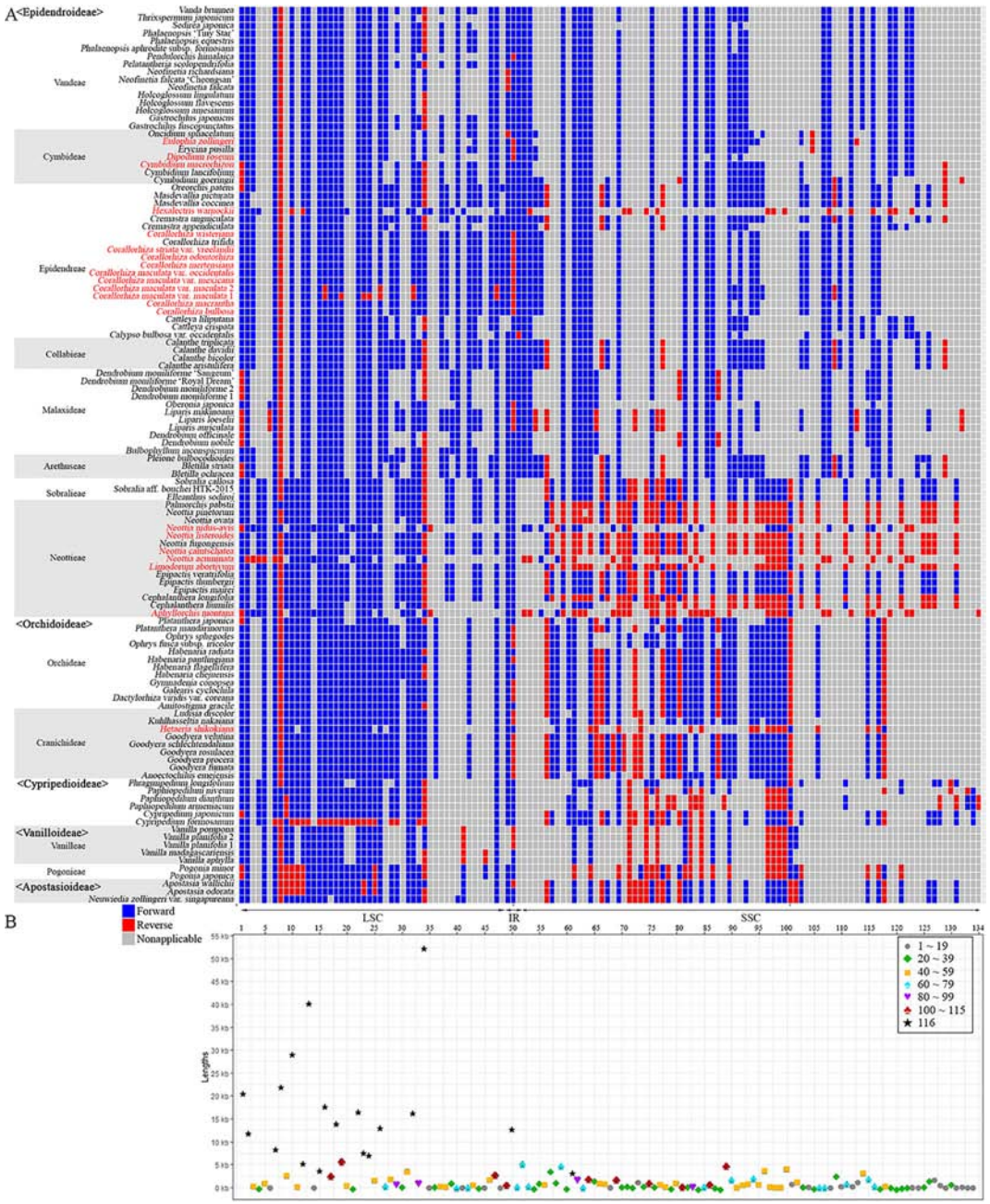

FIGURE 8 | Distribution of gene blocks. A total of 134 gene blocks were recognized in the 124 orchid plastomes. Thirty were constant blocks. 104 blocks show both forward (dark blue) and reverse (red) orientations and confirmed the block rearrangements. Blocks that are non-applicable because of gene losses or shifts are indicated in gray. All large rearrangements longer than 15 kb are located on the LSC. The species names in red indicate mycoheterotrophic orchids. **(A)**: Forward and reverse orientations of each gene block in the orchid species. **(B)**: Locations, lengths, and frequencies of 134 gene blocks.

were identified based on a ML tree made using 83 genes (**Figure S3**). Although bootstrap values were high at most nodes, those of the nodes of *Anoectochilus emeiensis* and *Goodyera velutina*, and *G. procera* and *G. fumata* of Cranichideae, were shown to be relatively low at 69.4% and 77.6%, respectively, as was the bootstrap value of the node dividing *Neottia camtschatea*, *N. listeroides,* and *N. nidus-avis* at 63.3%. The results of a BI tree made using the same data matrix are shown in **Figure S4**. The BI value of Cranichideae, which had low bootstrap values in the ML tree, showed a high

degree of support at 1.0, but the BI value of *Corallorhiza*'s branches showed a degree of support of 0.5. Despite the bootstrap and BI support problems in several sub-taxonomic groups, the relationships among the tribes (Pogonieae, Vanilleae, Cranichideae, Diurideae, Orchideae, Neottieae, Sobralieae, Nervilieae, Gastrodieae, Arethuseae, Malaxideae, Collabieae, Epidendreae, Cymbidieae, and Vandeae) represented by the data matrix used were identified to be strongly supported in both the ML and BI trees. In addition, both ML and BI trees had very long branch lengths leading to the taxa with highly reduced plastomes, such as *Epipogium*, *Gastrodia*, and *Rhizanthella* (**Figures S3** and **S4**).

Comparing Chloroplast and Nuclear Datasets

Among the 42 Orchidaceae species decoded in this laboratory, both plastome sequences and nrDNA units (18S-ITS1-5.8S-ITS2-28S) about 10 kb long exist (**Table 2**). Therefore, phylogenetic trees using the nrDNA regions and phylogenetic trees using the base sequences of the 83 plastid genes were made using the same method and compared (**Figure 9**). The best nrDNA tree was obtained at ML = −35673.363572 and the best plastid tree was obtained at ML = −332414.394814. These phylogenetic trees included only three subfamilies—Vanillioideae, Orchidoideae, and Epidendroideae—and the mutual relationships among the three subfamilies and the tree topologies in Vanilloideae and Orchidoideae were identical. However, differences between the two trees were found in the tree topologies in Epidendroideae. In particular, the phylogenetic positions of *Gastrodia elata*, *Bulbophyllum inconspicuum*, *Calanthe bicolor*, *C. aristulifera*, *Cremastra unguiculata*, *Corallorhiza maculata* var. *maculata*, *Oreorchis patens*, *Sedirea japonica*, and *Thrixspermum japonicum* differed between the two trees (**Figure 9**).

Time Estimation

A phylogenetic tree was constructed using 83 plastid genes in 124 Orchidaceae species and five outgroup species, and the divergence times of individual tree nodes were estimated using BEAST2. The results are shown in **Figure 10**. The inferred branching times of 21 main clades are set forth in **Table 4**. For easy comparison with existing studies, literature materials are also presented in **Table 4**. In this study, Orchidaceae was inferred to have diverged from other Asparagales at 99.20 (83.78–114.92) mya; Apostasioideae, which is a basal subfamily, was inferred to have diverged from other subfamilies at 79.91 (59.65–99.00) mya; and Vanilloideae was inferred to have diverged at 69.84 (52.59–89.63) mya. It was inferred that Pogonieae and Vanilleae of Vanilloideae diverged at 57.52 (37.88–77.68) mya, Cypripedioideae diverged at 64.97 (48.54–84.93) mya, and Orchidoideae diverged from

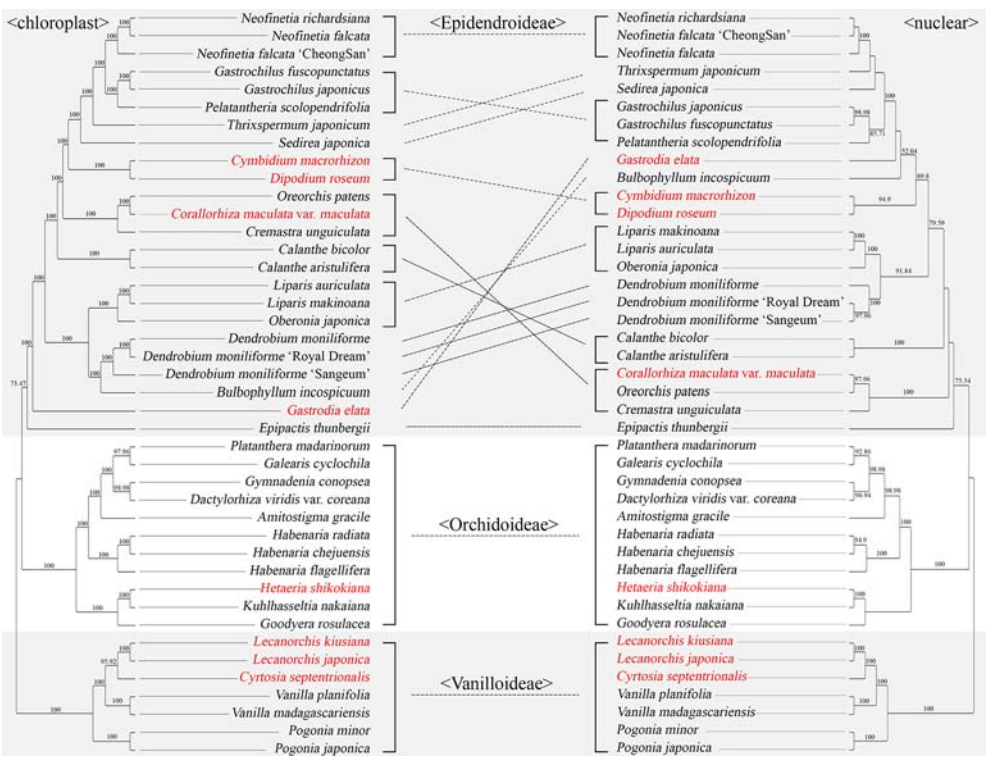

FIGURE 9 | Comparison of a plastid tree and nrDNA tree for the same 42 orchid species. The 83 aligned protein coding genes were 80,798 bp long. A maximum likelihood (ML) tree was constructed using RaxML-HPC2 with a GTR+G+I model with 100 bootstrap replicates. The best plastid tree was obtained with ML = −332414.394814. The nrDNA unit (18S-ITS1-5.8S-ITS2-28S) was approximately 10 kb long. The tree reconstruction methods for nrDNA were identical to those of the plastid tree. The species names in red indicate mycoheterotrophic orchids. The lines between the two trees indicate the topological differences between them.

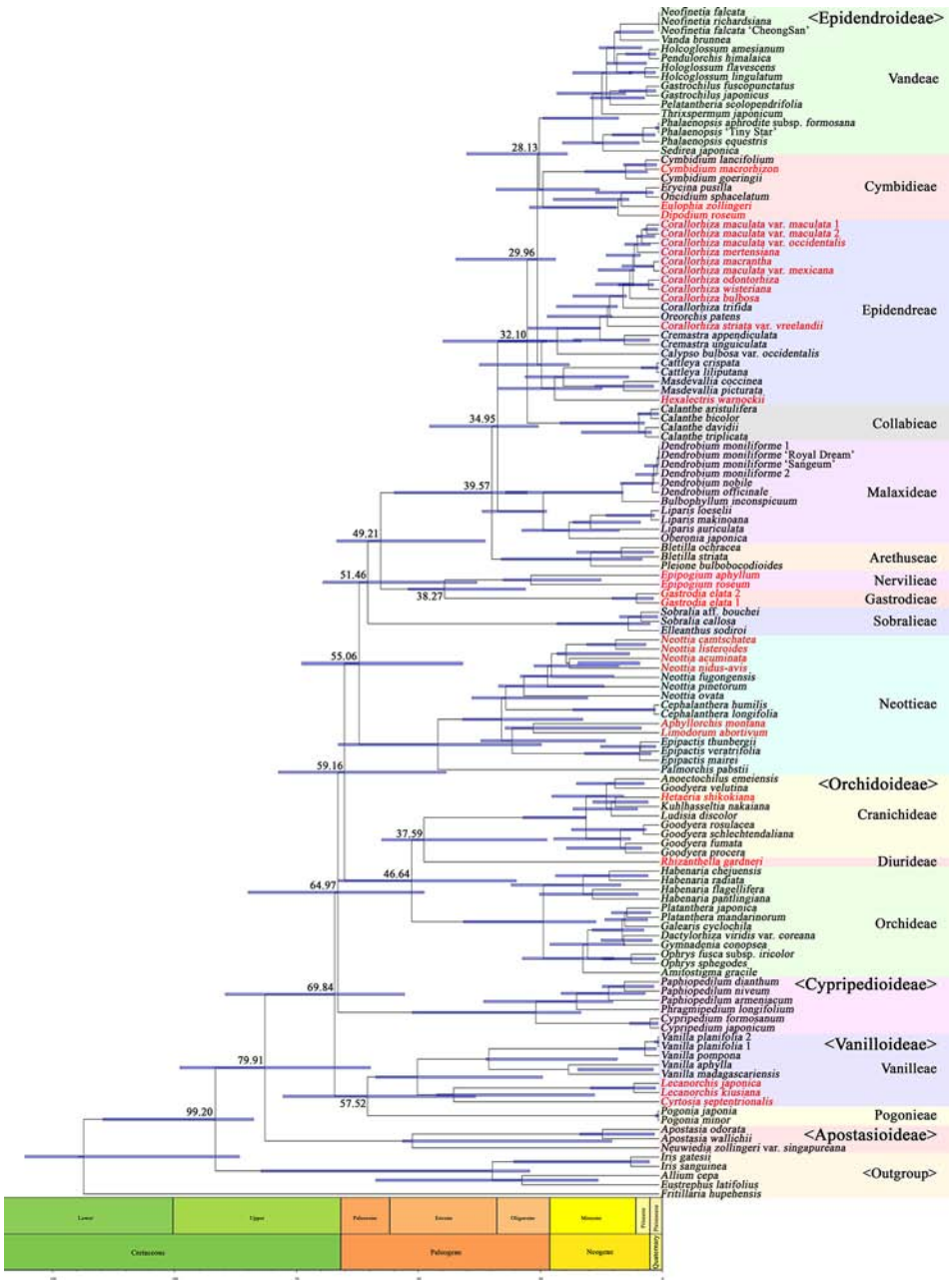

FIGURE 10 | Fossil data showing the estimated divergence time of each node. Three fossil data were used to calibrate nodes (Asparagales—mean 105.3 mya, *Dendrobium*—23.2 mya, and *Goodyera*—15.0 mya). Orchidaceae diverged from its sister family at 99.20 mya, and then five subfamilies subsequently diverged in the order of Apostasioideae (79.91 mya), Vanilloideae (69.84 mya), Cypripedioideae (64.97 mya), Orchidoideae (59.16 mya), and Epidendroideae (59.16 mya). However, several specious subtribes within the Epidendroideae diverged in relatively short time periods (39.57–28.13 mya). The species names in red indicate mycoheterotrophic orchids.

Epidendroideae at 59.16 (43.99–78.66) mya. Cranichideae of Orchidoideae diverged from Orchideae at 46.64 (29.49–66.26) mya and Diurideae diverged from Cranichideae at 37.59 (23.13–57.30) mya. Neottieae diverged at 55.06 (40.55–73.82) mya and other taxonomic groups of Epidendroideae and Sobralieae diverged at 51.46 (37.65–69.44) mya. In addition, Gastrodieae and Nervilleae diverged from other Epidendroideae at 49.21 (35.89–66.60) mya, and the two tribes diverged from each other at 38.27 (27.59–51.84) mya. Arethuseae diverged at 39.57 (27.20–54.68) mya, Malaxideae at 34.95 (24.93–47.40) mya, Collabieae at

TABLE 4 | Comparing time estimation results with two previous studies that used two and three genes for analysis.

Node		This study (mya)	Gustafsson et al., 2010 (Two genes, stem age, mya)	Givnish et al., 2015 (Three genes, stem age, mya)
Orchidaceae		99.20 (83.78–114.92)	104	111.38
Apostasioideae		79.91 (59.65–99.00)	77	89.46
	Vanilloideae	69.84 (52.59–89.63)	69	83.6
Vanilloideae	Pogonieae	57.52 (37.88–77.68)	57	77.81
	Vanilleae	57.52 (37.88–77.68)	57	77.81
Cypripedioideae		64.97 (48.54–84.93)	71	76.43
	Orchidoideae	59.16 (43.99–78.66)	61	63.99
	Orchideae	46.64 (29.49–66.26)	33	54.39
Orchidoideae	Diurideae	37.59 (23.13–57.30)	48	48.24
	Cranichideae	37.59 (23.13–57.30)	48	48.24
	Epidendroideae	59.16 (43.99–78.66)	61	63.99
	Neottieae	55.06 (40.55–73.82)	49	48.05
	Sobralieae	51.46 (37.65–69.44)	43	43.33
	Nervilieae	38.27 (27.59–51.84)	43	40.69
	Gastrodieae	38.27 (27.59–51.84)	N/A	N/A
Epidendroideae	Arethuseae	39.57 (27.20–54.68)	33	37.86
	Malaxideae	34.95 (24.93–47.40)	35	36.56
	Collabieae	32.10 (23.20–44.64)	33	33.76
	Epidendreae	29.96 (21.36–41.98)	35	34.08
	Cymbideae	28.13 (18.92–39.72)	35	32.67
	Vandeae	28.13 (18.92–39.72)	35	32.67

32.10 (23.20–44.64) mya, Epidendreae at 29.96 (21.36–41.98) mya, and Cymbideae and Vandeae at 28.13 (18.92–39.72) mya (**Figure 10**, **Table 4**).

DISCUSSION

Evolution of the Plastome Structure

Most plastomes of flowering plants have quadripartite structures consisting of LSC and SSC regions with two IR regions between the two SCs (Bock, 2007). The IR regions are generally known to play a role in the structural stability of plastomes (Palmer and Thompson, 1982), and Orchidaceae plastomes are no exception. When the 124 Orchidaceae plastomes were compared, all but *Aphyllorchis montana*, *Epipogium aphyllum,* and *Gastrodia elata* (2 accessions) had quadripartite structures (**Table 2**). *Gastrodia elata* (Epidendroideae-Gastrodieae) is a special case in which the plastome exists only as one single copy because the IR region was lost when the plastome contracted to about 35.1 kb (**Figure 1**). In the case of *Aphyllorchis montana* (Epidendroideae-Neottieae), the plastome also exists as only one single copy region because the IR region was lost when the plastome size decreased to 94.6 kb (Feng et al., 2016). In the case of *Epipogium aphyllum* (Epidendroideae-Nervilieae), the plastome has a tripartite structure consists of the SC and IR because the two IR regions were combined to head-to-head formation when the SSC region disappeared and the plastome contracted to 30.6 kb (Schelkunov et al., 2015). However, in the case of *Epipogium roseum* in the same genus, the SSC region exists at 890 bp (shorter than average) and the IR decreased to 261 bp (**Figure 3**). Although these structural variations are related to gene losses associated with mycoheterotrophic habitats, the phenomenon of broken quadripartite structures appears only in the three species mentioned above of the 28 mycoheterotrophic species compared. Plastomes exist as only SC regions due to the loss of IR in several gymnosperms (Wu et al., 2011), *Trifolium* (Fabaceae), *Medicago* (Fabaceae), and *Cicer* (Fabaceae) (Cai et al., 2008). However, all these are photosynthetic species, which are different from the Orchidaceae mentioned above.

Another feature that can be found frequently in Orchidaceae plastomes is IR expansion/shift toward the SSC region. Therefore, the SSC size has been greatly reduced. Due to this feature, which can be found in *Pogonia* and *Vanilla* of Vanilloideae, the lengths of IR became 29,808–32,683 bp because both IRa and IRb expanded toward the SSC (Lin et al., 2015; Amiryousefi et al., 2017). In contrast, the lengths of the SSC were shortened by as much as 1,254–5,387 bp. The similar SSC contractions were also found in three species of Cypripedioideae: *Paphiopedilum armeniacum*, *P. dianthum*, and *P. niveum* (**Table 2**). The same phenomenon was observed in the newly decoded plastome of *Hetaeria shikokiana*, and the length of the IR and the SSC were found to be 31,960 bp and 2,320 bp, respectively (**Figure 1**). Among the four genera in which SSC contraction occurred, *Paphiopedilum*, *Pogonia,* and *Vanilla* carry out photosynthesis, while *Hetaeria* does not. As for life forms, three genera (*Hetaeria*, *Paphiopedilum*, and *Pogonia*) have terrestrial life forms, while one genus (*Vanilla*) has an epiphytic life form. In all four genera, *ndh* genes were deleted in most cases. This is thought to be a widely occurring phenomenon in orchids due to parallel evolution and is not considered attributable to the direct effect of SSC contraction. Since *ndh* genes exist in the vicinity of IR-SSC—such as *ndh*A, *ndh*B, and *ndh*H in *Pogonia* and *Hetaeria*, which are pseudogenes—*ndh* genes are not a direct cause of SSC contraction. However, many small sequence block rearrangements appear in many Orchidaceae lineages near the IR-SSC boundary, indicating that the *ndh*F and *ycf*1 genes at the IR-SSC boundary may affected the stability of Orchidaceae

plastomes. This is a common phenomenon, especially in species that have lost their *ndh* gene class or the capacity for photosynthesis.

On the other hand, no IR shift toward the IR-LSC is observed in the Orchidaceae plastomes (**Figure S2**). The largest plastome size in Orchidaceae was 178,131 bp in *Cypripedium formosanum*, but there was no IR expansion toward the LSC in this case either. The increase in plastome sizes in photosynthetic plant species is mainly related to IR expansion (Chumley et al., 2006; Weng et al., 2014; Blazier et al., 2016). However, in the case of *Cypripedium*, the genome size increased due to scattered AT-rich repeats among IGS in the LSC region without IR expansion (**Figure S2**) (Kim et al., 2015b). Mycoheterotrophic orchids have plastome sizes below 150 kb and show high correlations between length of the LSC region and the IR length (R^2 = 0.9571 and R^2 = 0.8213, respectively). On the other hand, the plastome sizes of all photosynthetic orchids were at least 140 kb and showed a weak correlation with the length of the LSC region (R^2 = 0.5606), but little correlation with the IR length (R^2 = 0.1251) (**Figures 4C, D**). This means that, in mycoheterotrophic orchids, genome contraction occurs regardless of region, but genome size expansion is affected more by the expansion of the LSC region than the expansion of the IR region.

Gene block analysis was conducted using MAUVE to identify gene rearrangements among Orchidaceae plastomes and, according to the results, 104 out of 134 blocks had rearrangements in at least one taxonomic group (**Figure 8**, **Tables S1** and **S2**). Of the 104 rearrangements, 34 were distributed in the LSC region, three were distributed in the IR region, and the remaining 67 were concentrated on the SSC region. Among the LSC rearrangements, 11 were at least 10 kb long. On the other hand, the SSC rearrangements were mostly concentrated on *ndh*F and *ycf*1 in the IR/SSC boundary region, and most were short rearrangements that did not exceed 1 kb (**Figure 8**, **Table S2**). Many of the IRa-SSC junction rearrangements are assumed to be attributable to the unequal crossing over among repeats during the processes of pseudogenization and gene loss of *ndh*F and *ycf*1. In the IR region, IR shift occurred as the genes in the SSC region were lost and became smaller, and the region containing the *rrn*4.5-*rrn*23 gene moved to the SSC region. Their position changes have been reported in mycoheterotrophs with large gene losses, such as *Aphyllorchis montana*, *Cyrtosia septentrionalis*, *Hexalectris warnockii*, *Lecanorchis japonica*, *L. kiusiana,* and *Rhizanthella gardneri* (Delannoy et al., 2011; Feng et al., 2016; Barrett and Kennedy, 2018; Kim et al., 2019). Given that the relevant shift did not occur in other mycoheterotrophs (*Corallorhiza*, *Dipodium*, *Hetaeria*, or *Neottia*), this is considered to be an independent evolutionary phenomenon associated with gene loss.

Based on taxonomic groupings, although some species in the genera that include both photosynthetic and non-photosynthetic nutritional modes such as *Cephalanthera*, *Cymbidium*, *Epipactis*, and *Platanthera* (Merckx et al., 2013) shared rearrangements, species of other genera in the same category (e.g., *Cremastra*) did not share any rearrangements, indicating that the gene relocation in the plastome occurred after development of non-photosynthetic mycoheterotrophy. Therefore, the plastid gene rearrangements are judged to have developed independently in many orchid lineages, and this is supported by the fact that each of photosynthetic groups (*Apostasia*, *Bulbophyllum*, *Dendrobium*, *Elleanthus*, *Oberonia*, *Ophrys*, *Palmorchis*, *Pleione*, *Pogonia*, *Sobralia*, and *Vanilla*) has multiple rearrangements. Furthermore, since a number of rearrangements have been reported in *Aphyllorchis montana*, *Cyrtosia septentrionalis*, *Hexalectris warnockii*, *Lecanorchis japonica*, *L. kiusiana,* and *Rhizanthella gardneri*, which are mycoheterotrophs that reached stage 2 of gene loss, it is assumed that rearrangements played some role in gene loss. However, given that there is no gene rearrangement in mycoheterotrophs (*Corallorhiza*, *Hetaeria*, and *Neottia*) (Delannoy et al., 2011; Feng et al., 2016; Barrett and Kennedy, 2018; Kim et al., 2019), whose gene losses reached stage 1 or 2, further comparative studies are necessary to determine the relationships between gene relocation and gene loss.

Evolution of Mycoheterotrophy and Gene Loss in Orchidaceae

Almost all orchid species are initially mycoheterotrophs at an early stage of development, then subsequently develop into full autotrophs. Some orchids exhibit both autotrophic and mycoheterotrophic (mixotrophic) nutritional modes, even at adult stages. Finally, several orchid species maintain an obligate (full) mycoheterotrophic (non-photosynthetic) nutritional mode throughout their life cycle. Forty-three genera in Orchidaceae are known to include non-photosynthetic mycoheterotrophs (Merckx et al., 2013). Among them, 17 were used in this study (*Aphyllorchis*, *Cephalanthera*, *Corallorhiza*, *Cremastra*, *Cymbidium*, *Cyrtosia*, *Dipodium*, *Epipogium*, *Eulophia*, *Gastrodia*, *Hetaeria*, *Hexalectris*, *Lecanorchis*, *Limodorum*, *Neottia*, *Platanthera*, and *Rhizanthella*), and only photosynthetic species were analyzed in the case of three of these genera (*Cephalanthera*, *Cremastra*, and *Platanthera*). However, when the plastomes were checked, it was found that *Cymbidium macrorhizon*, *Eulophia zollingeri*, *Dipodium roseum*, and *Limodorum abortivum* only lost the *ndh* gene (**Figure 5**, **Figure S1**). In addition, after many literature reviews and firsthand observation by these researchers, it was found that, regarding these four species, chlorophylls exist in stems and flowers and low-level photosynthesis is carried out during a certain period in the life cycle (Blumenfeld, 1935; Girlanda et al., 2006; Kim et al., 2017a; Suetsugu et al., 2018). Therefore, it is reasonable to treat these four species as mixotrophs rather than obligate mycoheterotrophs. Among the species thought to be non-photosynthetic, *Corallorhiza*, which was studied the most extensively, is very likely to have photosynthetic capability if only *ndh* genes had been lost. In addition, cases have been reported in which members of the same species of *Corallorhiza* had different, mixotrophic nutritional modes depending on living environments (Barrett and Davis, 2012; Barrett et al., 2014; Barrett et al., 2018). The estimated divergence times of these mixotrophs are 7.44 (2.41–15.37) mya (*Cymbidium*), 17.34 (8.87–26.76) mya (*Dipodium* and *Eulophia*), and 17.77 (3.68–31.79) mya (*Limodorum*), and the evolution of these genera are

thought to be relatively recent events. Furthermore, the divergence times of the obligate mycoheterotrophic groups were also estimated as follows: 23.61 (16.05–33.12) mya (*Corallorhiza* and *Cremastra*), 21.56 (11.77–33.40) mya (*Hexalectris*), 38.27 (27.60–51.84) mya (*Gastrodia* and *Epipogium*), 28.11 (15.75–40.61) mya (*Aphyllorchis*, *Cephalanthera*, *Epipactis,* and *Neottia*), 5.32 (1.71–9.80) mya (*Platanthera*), 37.59 (23.13–57.30) mya (*Rhizanthella*), 7.48 (2.26–13.66) mya (*Hetaeria*), and 27.82 (13.31–45.95) mya (*Cyrtosia* and *Lecanorchis*) (**Figure 10**). It can be seen that, except for Gastrodieae (*Gastrodia*), Nervilleae (*Epipogium*), and Diurideae (*Rhizanthella*), all these species diverged more recently than 30 mya (**Figure 10**). When estimated based on the foregoing, there are two possibilities: the obligate mycoheterotrophic taxa are relatively recently evolved taxonomic groups within Orchidaceae, and information about the older obligate mycoheterotrophic taxonomic groups is not yet available. To test these, further studies should be conducted on other species in Gastrodieae and Nervilleae, whom are estimated to have diverged for long times ago.

While epiphytic orchids consisted only of photosynthetic species and all had genomes at least 140 kb long, terrestrial orchids showed a large variation in plastome sizes and had much different numbers of functional genes because they included non-photosynthetic species (**Figure 4A**). In addition, the correlation between genome size and the number of functional genes was high ($R^2 = 0.9069$) in mycoheterotrophs, and relatively low ($R^2 = 0.3320$) in photosynthetic species (**Figure 4B**). Also, mycoheterotrophs are distributed into three clusters: one with about 100 functional genes, one with 55–90 functional genes, and one with 25–30 functional genes (**Figures 4B** and **5**). This means that in the evolutionary process of mycoheterotrophic species, gene loss occurred step by step in three stages rather than on a continuous spectrum.

The first stage of gene loss was the pseudogenization or loss of the *ndh* gene class. There are 11 *ndh* gene subunits in each plastome. *ndh* gene losses are observed in all five subfamilies of Orchidaceae, and appear at especially high frequencies in Cypripedioideae, Epidendroideae, and Vanilloideae. On the other hand, the frequencies of non-functionalization are low in Apostasioideae and Orchidoideae. The *ndh* genes of the epiphytic orchids (*Bulbophyllum*, *Cattleya*, *Dendrobium*, *Erycina*, *Gastrochilus*, *Holcoglossum*, *Neofinetia*, *Oberonia*, *Phalaenopsis*, *Pelatantheria*, *Pendulorchis*, *Sedirea*, *Thrixspermum*, *Vanda*, and *Vanilla*) used in the analysis were lost or pseudogenized (**Figures 5** and **6**). Although the loss or pseudogenization of *ndh* genes was also observed in terrestrial taxonomic groups (*Apostasia*, *Calypso*, *Cephalanthera*, *Cremastra*, *Cymbidium*, *Epipactis*, *Goodyera*, *Kuhlhasseltia*, *Limodorum*, *Liparis*, *Neuwiedia*, *Oncidium*, *Paphiopedilum*, *Phragmipedium*, *Platanthera*, and *Pogonia*), the frequencies are low compared to epiphytes. Although the loss or pseudogenization of *ccs*A, *cem*A, and *inf*A is often observed in addition to *ndh* gene non-functionalization, but no clear trend has been found (Barrett et al., 2014; Kim et al., 2015a; Feng et al., 2016; Niu et al., 2017b; Hou et al., 2018). In the phylogenetic tree, the non-functionalization of *ndh* appears to occur gradually and independently in the process of pseudogenization in many independent lineages (**Figure 6**). However, given that most orchid species in which *ndh* gene non-functionalization occurred retain photosynthetic capacity, it is inferred that the function of this gene class may be affected by the nuclear or mitochondrial genomes. Of course, the gene function may be maintained by RNA editing after pseudogenization, but the possibility is low because most pseudogenization entail not only base changes but also indels. However, given that *ndh* genes were lost in all non-photosynthetic species, the loss of the *ndh* gene class is considered to be a precondition for the development of mycoheterotrophs.

The second stage of gene loss is the loss of functions of genes involved in the photosynthetic light reaction, such as *pet* (six genes), *psa* (five genes), and *psb* (15 genes). This includes the *rpo* (four genes) gene class, which includes housekeeping genes. Gene losses at this stage are shown to have progressed independently in at least 10 clades including six independent lineages of Epidendroideae (*Aphyllorchis, Corallorhiza*, *Epipogium*, *Gastrodia*, *Hexalectris,* and *Neottia*), two Orchidoideae clades (*Hetaeria* and *Rhizanthella*), and one Vanilloideae clade (*Cyrtosia* and *Lecanorchis*) (**Figure 6**). In particular, in the case of *Corallorhiza* and *Neottia*, gene losses progressed independently depending on species, even within the same genus, indicating that these are important taxonomic groups for understanding second stage gene losses. In addition, the plastomes of *Cyrtosia* and *Lecanorchis* of Vanilloideae degraded significantly so that *ccs*A, *cem*A, *rbc*L, *ycf*3, and *ycf*4 were commonly deleted in addition to *ndh*, *pet*, *psa*, *psb*, and *rpo*, and it was identified that some subunits of the housekeeping genes, such as *rpl* and *rps,* were also deleted from *Lecanorchis* (**Figure 6A**). The degradation of *Cyrtosia* and *Lecanorchis* of Vanilloideae is thought to be part of the transition process from plastome degradation stage 2–4 (Wicke et al., 2016). On the other hand, *Hetaeria shikokiana* of Orchidoideae and *Corallorhiza maculata* var. *maculata* of Epidendroideae correspond to plastome degradation stage 2 because some of their *ndh*, *psa*, *psb*, *pet,* and *rpo* genes were deleted or pseudogenized. However, since plastome degradation stages 2 and 3 (Wicke et al., 2013; Wicke et al., 2016) appeared to occur simultaneously in Orchidaceae, this stage was defined as the second stage of gene loss.

The third stage of gene loss in Orchidaceae includes cases where only 27 to 33 out of 113 unique plastome genes remain, meaning that further gene loss has occurred than in stage 2 cases. Since at least 55 genes are preserved in stage 2 and fewer than 33 genes are preserved in stage 3, a large gap exists between the two stages (**Figure 4B**). In stage 3, all the photosynthesis-related gene functions were lost and most housekeeping genes—such as *trn*, *rpl,* and *rps*—were also lost. In addition, the fact that pseudogenes do not exist or are limited to three or fewer is also a characteristic of stage 3. This stage is observed in a total of four lineages: two lineages of Epidendroideae (*Epipogium*, 27 to 29

conserved genes; *Gastrodia*, 28 conserved genes), one of Orchidoideae (*Rhizanthella*, 33 conserved genes), and one of Vanilloideae (*Lecanorchis*, 32–33 conserved genes) (**Figures 5** and **6**, **Table 2**). Regarding the number of genes, the 27 in *Epipogium aphyllum* are the minimum number of genes found in Orchidaceae plastomes. Furthermore, 20 genes that commonly exist in the four lineages of seven plastomes, which are in gene loss stage 3, were identified, comprising *rpl* (12, 14, 16, 36), *rps* (2, 3, 4, 7, 8, 11, 14, 18, 19), *rrn* (5, 16, 23), *trn*C-GCA, *trn*fM-CAU, *acc*D, and *clp*P (**Table 3**). The fact that the same 20 genes have been preserved even though the extremely contracted orchid plastomes evolved from four independent mycoheterotrophic lineages means that those genes selectively remained because they perform the minimum functions necessary to maintain the plastomes. Since five (*rpl*12, *rps*18, *rps*19, *trn*fM-CAU, and *acc*D) of these 20 genes were lost in one to four other orchid species (**Table 3**), it was concluded that there are 15 common orchid plastome genes.

Comparisons of Plastome and nrDNA Trees

Thus far, phylogenetic studies using a portion of the plastome genes have been common (Cameron et al., 1999; Givnish et al., 2015), and phylogenetic studies using the entire plastome genes have also progressed thanks to the development of NGS technology (Yang et al., 2013; Kim et al., 2015a; Feng et al., 2016). The use of chloroplast genes in phylogenetic studies has many advantages such as ease of use, but this has been pointed out to be vulnerable to lineage sorting and problems such as plastome capture due to hybridization because it only tracks maternal lineages. Although NGS technology and transcriptome analysis are developing, there are still cost limitations to using the entire nuclear genome for phylogenetic studies. Therefore, nuclear ribosomal ITS regions have been extensively used in studies of the relationships between species or allied genera. An advantage of the genome skimming NGS is that, for plastome sequences with high depths of coverage (see **Table 1**), it can decode about 10 kb of regions that exist as tandem repeats (18S-ITS1-5.8S-ITS2-28S-NTS-ETS) (**Figure 2**). Although it has difficulties in recovering entire NTS-ETS when the plastome coverage depth is below then 500x, genome skimming for NGS can easily recover the 6 kb region of the 18S-ITS1-5.8S-ITS2-28S region. Therefore, in this study, an attempt was made to compare phylogenetic trees constructed using all the same plastome genes and phylogenetic trees constructed using the nrDNA unit sequences. Orchid plastomes from 42 species, representing three subfamilies of Orchidaceae, were produced in the laboratory of the corresponding author and directly compared (**Figure 9**).

According to the results, the relationships among the three subfamilies were the same as (Vanilloideae (Orchidoideae, Epidendroideae)). Furthermore, the associations among the tribes and species in Vanilloideae and Orchidoideae were completely identical. However, the topologies of the two trees were different for the relationships among Epidendroideae taxa. In the Epidendroideae, there was no difference in generic or tribal grouping, but the positions of *Gastrodia,* in which the plastome reduced greatly, and *Bulbophyllum*, which is a photosynthetic species, were very different. In addition, clades with bootstrap support values of less than 50% had different topologies. However, it is not clear from this comparative analysis alone whether these differences are due to lineage sorting, ancient plastome capture, other evolutionary histories, or sampling issues. Although plastome data for diverse orchid species are currently known, the sequence data for nrDNA repeats for the 42 species in this study are presented for the first time. Although some nodes in Epidendroideae show discrepancies, major parts of the trees are generally identical to each other. In addition, these data are thought to be easily obtainable because nrDNA repeats can be recovered by simply carrying out additional data mining while conducting plastome sequencing using the genome skimming NGS method. If more data are accumulated for the same sample, then the evolution of orchids can be more easily understood.

Diversification of Major Lineages of Orchidaceae

The results of estimating the divergence times of major clades of Orchidaceae using all 83 genes in the plastome were similar to the findings of previous studies conducted using two or three genes at some points, and different at others (**Figure 10**, **Table 4**). First, in this study, the time of origin of orchids was estimated to be 99.20 (83.78–114.92) mya, which is similar to the previous estimate of 104 mya using two genes, and not significantly different from the 111.38 mya estimated using three genes (Gustafsson et al., 2010; Givnish et al., 2015). However, the finding in this study shows the divergence time of the basal taxonomic groups ranging from Orchidoideae and Cypripedioideae to Epidendroideae to be a little earlier than the previous finding estimated using two genes (1.84–6.03 mya differences), and a little more recent than the result using three genes. That is, the times estimated in the two previous studies are very different and the one in this study fell between the other two. However, the origin time of terminal tribes in Epidendroideae was inferred to be more recent by this study than the previous studies, which only used two or three genes.

Orchidoideae is estimated to consist of 198 genera and 4,931 species, and the Epidendroideae is estimated to consist of 505 genera and 20,606 species (Chase et al., 2015; Christenhusz and Byng, 2016). These two clades account for most of Orchidaceae and diverged 71.85 mya (**Figure 10**, **Table 4**). The divergence times of Arethuseae (25 genera, 723 species), Collabieae (20 genera, 453 species), Cymbideae (165 genera, 3,997 species), Epidendreae (99 genera, 6,935 species), Malaxideae (16 genera, 4,631 species), Podochileae (27 genera, 1,292 species), and Vandeae (136 genera, 2,340 species)—tribes of Epidendroideae consisting of many species—are later than 39.57 (27.20–54.68) mya, which is relatively recent. These data mean that many species differentiated in a short time. In studies that analyzed

diversification rates, the relevant tribes had higher rates compared to the basal lineage in most cases, thereby supporting the hypothesis that many species underwent evolutionary radiation in a short time (Givnish et al., 2015).

Perspective

Sixty genera, 140 species, 146 accessions of Orchidaceae plastomes have been completed decoded and can be used in comparative studies of plastomes, including the 24 plastomes newly reported in this study (NCBI database, June 30, 2019). In the present study, the evolutionary trends of plastomes were compared and analyzed to understand the evolutionary processes of orchid plastomes and mycoheterotrophic orchids. Only three different types of species were selected in the case of *Cymbidium* (9 spp.), *Dendrobium* (40 spp.), and *Holcoglossum* (11 spp.) because many species in these genera have been studied. Therefore, the plastomes of 60 genera, 118 species, and 124 accessions were analyzed. In addition, for the 42 species decoded in the corresponding author's laboratory, a plastome tree and nrDNA tandem repeat tree were compared to discuss evolution. Orchidaceae is known to include about 736 genera and 28,000 species. Therefore, those genera for which their plastomes have been decoded thus far make up approximately 8% of all the known genera of the Orchidaceae, and those species whose plastomes have been decoded thus far comprise less than 1% of all the known species of the Orchidaceae. There are 43 genera known to include non-photosynthetic mycoheterotrophs in Orchidaceae. In this study, plastome gene loss patterns of 17 genera that correspond to 40% of the foregoing genera were compared and analyzed to derive third-stage gene losses and 15 common genes. However, if further studies are conducted with more genera and species, Orchidaceae plastome gene losses can be understood better. In particular, genera such as *Corallorhiza* and *Neottia*, in which photosynthetic species coexist with non-photosynthetic mycoheterotrophs, should be intensively studied with all species, including several populations per species. Studies of the taxonomic groups in which many species were recently differentiated should be continuously conducted to elucidate the mechanism of evolutionary radiation. In this regard, the use of both plastid and nuclear genomes using NGS technology will increase for orchid evolution studies. If high-quality NGS data are accumulated by 50% at the genus level and 10% at the species level, then the evolution of orchids can be better understood.

DATA AVAILABILITY STATEMENT

The datasets generated for this study can be found in the National Center for Biotechnology Information (NCBI), please find accession numbers in **Table 2**.

AUTHOR CONTRIBUTIONS

K-JK and MK designed research. Y-KK, SJ, S-HC, J-RH, and MK collected the research materials. Y-KK and SJ performed research. Y-KK, SJ S-HC, J-RH, and M-JJ analyzed data and deposited the data to data libraries. Y-KK and K-JK wrote the manuscript. MK and K-JK secured the research funds.

FUNDING

This work was supported by the National Research Foundation of Korea (NRF) under grant no. NRF-2015M3A9B8030588 to K-JK and by the National Institute of Biological Resources (NIBR) under the genetic evaluation of vascular plants IV-1 (2018, grant no. NIBR201803102) to MK and K-JK.

ACKNOWLEDGMENTS

We thank to two anonymous reviewers for their helpful comments to improving the manuscript. We would like to thank Noah Last of Third Draft Editing for his English language editing. We also thank to Dr. Sanghun Oh of Daejeon University for the leaf materials of *Calanthe aristulifera* and Dr. Kyeongwon Kang of Babo Orchid Farm for the materials of *Habenaria chejuensis* and *H. flagellifera*. We thank the curator of the Korea University Herbarium (KUS) for voucher specimen preparation. The genomic and chloroplast DNAs are deposited in the Plant DNA Bank in Korea (PDBK).

SUPPLEMENTARY MATERIAL

The Supplementary Material for this article can be found online at: https://www.frontiersin.org/articles/10.3389/fpls.2020.00022/full#supplementary-material

REFERENCES

Altschul, S. F., Madden, T. L., Schäffer, A. A., Zhang, J., Zhang, Z., Miller, W., et al. (1997). Gapped BLAST and PSI-BLAST: a new generation of protein database search programs. *Nucleic Acids Res.* 25, 3389–3402. doi: 10.1093/nar/25.17.3389

Amiryousefi, A., Hyvönen, J., and Poczai, P. (2017). The plastid genome of Vanillon (*Vanilla pompona*, Orchidaceae). *Mitochondrial DNA Part B* 2, 689–691. doi: 10.1080/23802359.2017.1383201

Amiryousefi, A., Hyvo, J., and Poczai, P. (2018). Genome analysis IRscope: an online program to visualize the junction sites of chloroplast genomes. *Bioinformatics* 34, 3030–3031. doi: 10.1093/bioinformatics/bty220

Bankevich, A., Nurk, S., Antipov, D., Gurevich, A. A., Dvorkin, M., Kulikov, A. S., et al. (2012). SPAdes: a new genome assembly algorithm and its applications to single-cell sequencing. *J. Comput. Biol.* 19, 455–477. doi: 10.1089/cmb.2012.0021

Barrett, C. F., and Davis, J. I. (2012). The plastid genome of the mycoheterotrophic *Corallorhiza striata* (Orchidaceae) is in the relatively early stages of degradation. *Am. J. Bot.* 99, 1513–1523. doi: 10.3732/ajb.1200256

Barrett, C. F., and Kennedy, A. H. (2018). Plastid genome degradation in the endangered, mycoheterotrophic, North American orchid *Hexalectris warnockii*. *Genome Biol. Evol.* 10, 1657–1662. doi: 10.1093/gbe/evy107

Barrett, C. F., Freudenstein, J. V., Li, J., Mayfield-Jones, D. R., Perez, L., Pires, J. C., et al. (2014). Investigating the path of plastid genome degradation in an early-

transitional clade of heterotrophic orchids, and implications for heterotrophic angiosperms. *Mol. Biol. Evol.* 31, 3095–3112. doi: 10.1093/molbev/msu252

Barrett, C. F., Wicke, S., and Sass, C. (2018). Dense infraspecific sampling reveals rapid and independent trajectories of plastome degradation in a heterotrophic orchid complex. *New Phytol.* 218, 1192–1204. doi: 10.1111/nph.15072

Blazier, J. C., Jansen, R. K., Mower, J. P., Govindu, M., Zhang, J., Weng, M. L., et al. (2016). Variable presence of the inverted repeat and plastome stability in *Erodium*. *Ann. Bot.* 117, 1209–1220. doi: 10.1093/aob/mcw065

Blumenfeld, H. (1935). Beitrage zur Physiologie des Wurzepilzes von *Limodorum abortivum* (L.) Sw. Universitat Basel.

Bock, R. (2007). "Structure, function and inheritance of plastid genomes," in *Cell and molecular biology of plastids*. Ed. R. Bock (Berlin: Springer), 29–63. doi: 10.1007/978-3-642-12422-8_3

Bouckaert, R., Vaughan, T. G., Barido-Sottani, J., Duchêne, S., Fourment, M., Gavryushkina, A., et al. (2019). BEAST 2.5: an advanced software platform for Bayesian evolutionary analysis. *PloS Comput. Biol.* 15, e1006650. doi: 10.1371/journal.pcbi.1006650

Cai, Z., Guisinger, M., Kim, H. G., Ruck, E., Blazier, J. C., McMurtry, V., et al. (2008). Extensive reorganization of the plastid genome of *Trifolium subterraneum* (Fabaceae) is associated with numerous repeated sequences and novel DNA insertions. *J. Mol. Evol.* 67, 696–704. doi: 10.1007/s00239-008-9180-7

Cameron, K. M., Chase, M. W., Whitten, W. M., Kores, P. J., Jarrell, D. C., Albert, V. A., et al. (1999). A phylogenetic analysis of the Orchidaceae: evidence from *rbc*L nucleotide sequences. *Am. J. Bot.* 86, 208–224. doi: 10.2307/2656938

Chang, C. C., Lin, H. C., Lin, I. P., Chow, T. Y., Chen, H. H., Chen, W. H., et al. (2006). The chloroplast genome of *Phalaenopsis aphrodite* (Orchidaceae): comparative analysis of evolutionary rate with that of grasses and its phylogenetic implications. *Mol. Biol. Evol.* 23, 279–291. doi: 10.1093/molbev/msj029

Chase, M. W., Cameron, K. M., Freudenstein, J. V., Pridgeon, A. M., Salazar, G., van den Berg, C., et al. (2015). An updated classification of Orchidaceae. *Bot. J. Linn. Soc* 177, 151–174. doi: 10.1111/boj.12234

Christenhusz, M. J. M., and Byng, J. W. (2016). The number of known plants species in the world and its annual increase. *Phytotaxa* 261, 201–217. doi: 10.11646/phytotaxa.261.3.1

Chumley, T. W., Palmer, J. D., Mower, J. P., Fourcade, H. M., Calie, P. J., Boore, J. L., et al. (2006). The complete chloroplast genome sequence of *Pelargonium* × *hortorum*: organization and evolution of the largest and most highly rearranged chloroplast genome of land plants. *Mol. Biol. Evol.* 23, 2175–2190. doi: 10.1093/molbev/msl089

Conran, J. G., Bannister, J. M., and Lee, D. E. (2009). Earliest orchid macrofossils: early miocene *dendrobium* and *earina* (Orchidaceae: Epidendroideae) from New Zealand. *Am. J. Bot.* 96, 466–474. doi: 10.3732/ajb.0800269

Cosner, M. E., Jansen, R. K., Palmer, J. D., and Downie, S. R. (1997). The highly rearranged chloroplast genome of *Trachelium caeruleum* (Campanulaceae): multiple inversions, inverted repeat expansion and contraction, transposition, insertions/deletions, and several repeat families. *Curr. Genet.* 31, 419–429. doi: 10.1007/s002940050225

da Rocha Perini, V., Leles, B., Furtado, C., and Prosdocimi, F. (2016). Complete chloroplast genome of the orchid *Cattleya crispata* (Orchidaceae: Laeliinae), a neotropical rupiculous species. *Mitochondrial DNA Part A. Anal.* 27, 4075–4077. doi: 10.3109/19401736.2014.1003850

Darling, A. E., Mau, B., and Perna, N. T. (2010). progressiveMauve: multiple genome alignment with gene gain, loss and rearrangement. *PloS One* 5, e11147. doi: 10.1371/journal.pone.0011147

Darriba, D., Taboada, G. L., Doallo, R., and Posada, D. (2012). jModelTest 2: more models, new heuristics and parallel computing. *Nat. Methods* 9, 772. doi: 10.1038/nmeth.2106

Delannoy, E., Fujii, S., Colas Des Francs-Small, C., Brundrett, M., and Small, I. (2011). Rampant gene loss in the underground orchid *Rhizanthella Gardneri* highlights evolutionary constraints on plastid genomes. *Mol. Biol. Evol.* 28, 2077–2086. doi: 10.1093/molbev/msr028

Dong, W. L., Wang, R. N., Zhang, N. Y., Fan, W. B., Fang, M. F., and Li, Z. H. (2018). Molecular evolution of chloroplast genomes of orchid species: insights into phylogenetic relationship and adaptive evolution. *Int. J. Mol. Sci.* 19. doi: 10.3390/ijms19030716

Drummond, A. J., Ho, S. Y. W., Phillips, M. J., and Rambaut, A. (2006). Relaxed phylogenetics and dating with confidence. *PloS Biol.* 4, e88. doi: 10.1371/journal.pbio.0040088

Feng, Y. L., Wicke, S., Li, J. W., Han, Y., Lin, C. S., Li, D. Z., et al. (2016). Lineage-specific reductions of plastid genomes in an orchid tribe with partially and fully mycoheterotrophic species. *Genome Biol. Evol.* 8, 2164–2175. doi: 10.1093/gbe/evw144

Freudenstein, J. V., and Chase, M. W. (2015). Phylogenetic relationships in epidendroideae (Orchidaceae), one of the great flowering plant radiations: progressive specialization and diversification. *Ann. Bot.* 115, 665–681. doi: 10.1093/aob/mcu253

Górniak, M., Paun, O., and Chase, M. W. (2010). Phylogenetic relationships within Orchidaceae based on a low-copy nuclear coding gene, xdh: congruence with organellar and nuclear ribosomal DNA results. *Mol. Phylogenet. Evol.* 56, 784–795. doi: 10.1016/j.ympev.2010.03.003

Girlanda, M., Selosse, M. A., Cafasso, D., Brilli, F., Delfine, S., Fabbian, R., et al. (2006). Inefficient photosynthesis in the Mediterranean orchid *Limodorum abortivum* is mirrored by specific association to ectomycorrhizal Russulaceae. *Mol. Ecol.* 15, 491–504. doi: 10.1111/j.1365-294X.2005.02770.x

Givnish, T. J., Spalink, D., Ames, M., Lyon, S. P., Hunter, S. J., Zuluaga, A., et al. (2015). Orchid phylogenomics and multiple drivers of their extraordinary diversification. *Proc. R. Soc. B Biol. Sci.* 282, 20151553. doi: 10.1098/rspb.2015.1553

Gustafsson, A. L. S., Verola, C. F., and Antonelli, A. (2010). Reassessing the temporal evolution of orchids with new fossils and a Bayesian relaxed clock, with implications for the diversification of the rare South American genus *Hoffmannseggella* (Orchidaceae: Epidendroideae). *BMC Evol. Biol.* 10. doi: 10.1186/1471-2148-10-177

Hirao, T., Watanabe, A., Kurita, M., Kondo, T., and Takata, K. (2008). Complete nucleotide sequence of the *Cryptomeria japonica* D. Don. chloroplast genome and comparative chloroplast genomics: diversified genomic structure of coniferous species. *BMC Plant Biol.* 8, 1–20. doi: 10.1186/1471-2229-8-70

Hou, N., Wang, G., Zhu, Y., Wang, L., and Xu, J. (2018). The complete chloroplast genome of the rare and endangered herb *Paphiopedilum dianthum* (Asparagales: Orchidaceae). *Conserv. Genet. Resour.* 10, 709–712. doi: 10.1007/s12686-017-0907-x

Huo, X., Zhao, Y., Qian, Z., and Liu, M. (2017). Characterization of the complete chloroplast genome of *Eulophia zollingeri*, an endangered orchid in China. *Conserv. Genet. Resour.* 10, 817–819. doi: 10.1007/s12686-017-0938-3

Iles, W. J. D., Smith, S. Y., Gandolfo, M. A., and Graham, S. W. (2015). Monocot fossils suitable for molecular dating analyses. *Bot. J. Linn. Soc.* 178, 346–374. doi: 10.1111/boj.12233

Katoh, K., Misawa, K., Kuma, K., and Miyata, T. (2002). MAFFT: a novel method for rapid multiple sequence alignment based on fast Fourier transform. *Nucleic Acids Res.* 30, 3059–3066. doi: 10.1093/nar/gkf436

Kearse, M., Moir, R., Wilson, A., Stones-Havas, S., Cheung, M., Sturrock, S., et al. (2012). Geneious basic: an integrated and extendable desktop software platform for the organization and analysis of sequence data. *Bioinformatics* 28, 1647–1649. doi: 10.1093/bioinformatics/bts199

Kim, H. T., Kim, J. S., Moore, M. J., Neubig, K. M., Williams, N. H., Whitten, W. M., et al. (2015a). Seven new complete plastome sequences reveal rampant independent loss of the *ndh* gene family across orchids and associated instability of the inverted repeat/small single-copy region boundaries. *PloS One* 10. doi: 10.1371/journal.pone.0142215

Kim, J. S., Kim, H. T., and Kim, J.-H. (2015b). The largest plastid genome of monocots: a novel genome type containing AT residue repeats in the slipper orchid *Cypripedium japonicum*. *Plant Mol. Biol. Rep.* 33, 1210–1220. doi: 10.1007/s11105-014-0833-y

Kim, Y. K., Kwak, M. H., Chung, M. G., Kim, H. W., Jo, S., Sohn, J. Y., et al. (2017a). The complete plastome sequence of the endangered orchid *Cymbidium macrorhizon* (Orchidaceae). *Mitochondrial DNA Part B Resour.* 2, 725–727. doi: 10.1080/23802359.2017.1390411

Kim, Y. K., Kwak, M. H., Hong, J. R., Kim, H. W., Jo, S., Sohn, J. Y., et al. (2017b). The complete plastome sequence of the endangered orchid *Habenaria radiata* (Orchidaceae). *Mitochondrial DNA Part B Resour.* 2, 704–706. doi: 10.1080/23802359.2017.1390410

Kim, H. T., Shin, C. H., Sun, H., and Kim, J. H. (2018). Sequencing of the plastome in the leafless green mycoheterotroph *Cymbidium macrorhizon* helps us to understand an early stage of fully mycoheterotrophic plastome structure. *Plant Syst. Evol.* 304, 245–258. doi: 10.1007/s00606-017-1472-1

Kim, Y. K., Jo, S., Cheon, S. H., Joo, M. J., Hong, J. R., Kwak, M. H., et al. (2019). Extensive losses of photosynthesis genes in the plastome of a mycoheterotrophic orchid, *Cyrtosia septentrionalis* (Vanilloideae: Orchidaceae). *Genome Biol. Evol.* 11, 565–571. doi: 10.1093/gbe/evz024

Krawczyk, K., Wiland-Szymańska, J., Buczkowska-Chmielewska, K., Drapikowska, M., Maślak, M., Myszczyński, K., et al. (2018). The complete chloroplast genome of a rare orchid species *Liparis loeselii* (L.). *Conserv. Genet. Resour.* 10, 305–308. doi: 10.1007/s12686-017-0809-y

Lallemand, F., Logacheva, M., Clainche, I. L., Bérard, A., Zheleznaia, E., May, M., et al. (2019). Thirteen new plastid genomes from mixotrophic and autotrophic species provide insights into heterotrophy evolution in Neottieae orchids. *Genome Biol. Evol.* 11, 2457–2467. doi: 10.1093/gbe/evz170

Lam, V. K. Y., Merckx, V. S. F. T., and Graham., S. W. (2016). A few-gene plastid phylogenetic framework for mycoheterotrophic monocots. *Am. J. Bot.* 103, 692–708. doi: 10.3732/ajb.1500412

Lanfear, R., Calcott, B., Ho, S. Y. W., and Guindon, S. (2012). PartitionFinder: combined selection of partitioning schemes and substitution models for phylogenetic analyses. *Mol. Biol. Evol.* 29, 1695–1701. doi: 10.1093/molbev/mss020

Lee, H. L., Jansen, R. K., Chumley, T. W., and Kim, K. J. (2007). Gene relocations within chloroplast genomes of *Jasminum* and *Menodora* (Oleaceae) are due to multiple, overlapping inversions. *Mol. Biol. Evol.* 24, 1161–1180. doi: 10.1093/molbev/msm036

Li, Z. H., Ma, X., Wang, D. Y., Li, Y. X., Wang, C. W., and Jin, X. H. (2019). Evolution of plastid genomes of *Holcoglossum* (Orchidaceae) with recent radiation. *BMC Evol. Biol.* 19, 1–10. doi: 10.1186/s12862-019-1384-5

Lin, C. S., Chen, J. J. W., Huang, Y. T., Chan, M. T., Daniell, H., Chang, W. J., et al. (2015). The location and translocation of *ndh* genes of chloroplast origin in the Orchidaceae family. *Sci. Rep.* 5, 1–10. doi: 10.1038/srep09040

Lin, C. S., Chen, J. J. W., Chiu, C. C., Hsiao, H. C. W., Yang, C. J., Jin, X. H., et al. (2017). Concomitant loss of ndh complex-related genes within chloroplast and nuclear genomes in some orchids. *Plant J.* 90, 994–1006. doi: 10.1111/tpj.13525

Logacheva, M. D., Schelkunov, M. I., and Penin, A. A. (2011). Sequencing and analysis of plastid genome in mycoheterotrophic orchid *Neottia nidus-avis*. *Genome Biol. Evol.* 3, 1296–1303. doi: 10.1093/gbe/evr102

Lohse, M., Drechsel, O., and Bock, R. (2007). OrganellarGenomeDRAW (OGDRAW): a tool for the easy generation of high-quality custom graphical maps of plastid and mitochondrial genomes. *Curr. Genet.* 52, 267–274. doi: 10.1007/s00294-007-0161-y

Lowe, T. M., and Chan, P. P. (2016). tRNAscan-SE On-line: integrating search and context for analysis of transfer RNA genes. *Nucleic Acids Res.* 44, W54–W57. doi: 10.1093/nar/gkw413

Merckx, V. S. F. T., Freudenstein, J. V., Kissling, J., Christenhusz, M. J. M., Stotler, R. E., Crandall-Stotler, B., et al. (2013). *Taxonomy and Classification BT - Mycoheterotrophy: The Biology of Plants Living on Fungi*. Ed. V. Merckx (New York, NY: Springer New York), 19–101. doi: 10.1007/978-1-4614-5209-6_2

Miller, M. A., Pfeiffer, W., and Schwartz, T. (2010). "Creating the CIPRES Science Gateway for inference of large phylogenetic trees", in *2010 gateway computing environments workshop (GCE)*. (IEEE), 1–8.

Miller, M. A., Schwartz, T., Pickett, B. E., He, S., Klem, E. B., Scheuermann, R. H., et al. (2015). A RESTful API for access to phylogenetic tools *via* the CIPRES science gateway. *Evol. Bioinforma.* 11, EBO–S21501. doi: 10.4137/EBO.S21501

Niu, Z., Pan, J., Zhu, S., Li, L., Xue, Q., Liu, W., et al. (2017a). Comparative analysis of the complete plastomes of *Apostasia wallichii* and *Neuwiedia singapureana* (Apostasioideae) reveals different evolutionary dynamics of IR/SSC boundary among photosynthetic orchids. *Front. Plant Sci.* 8, 1–11. doi: 10.3389/fpls.2017.01713

Niu, Z., Xue, Q., Zhu, S., Sun, J., Liu, W., and Ding, X. (2017b). The complete plastome sequences of four orchid species: insights into the evolution of the Orchidaceae and the utility of plastomic mutational hotspots. *Front. Plant Sci.* 8, 1–11. doi: 10.3389/fpls.2017.00715

Palmer, J. D., and Thompson, W. F. (1982). Chloroplast DNA rearrangements are more frequent when a large inverted repeat sequence is lost. *Cell* 29, 537–550. doi: 10.1016/0092-8674(82)90170-2

Ramírez, S. R., Gravendeel, B., Singer, R. B., Marshall, C. R., and Pierce, N. E. (2007). Dating the origin of the Orchidaceae from a fossil orchid with its pollinator. *Nature* 448, 1042–1045. doi: 10.1038/nature06039

Rambaut, A., and Drummond, A. J. (2007). *TreeAnnotator in Computer Program and Documentation Distributed by the Author*. Available online at: https://www.beast2.org/

Rambaut, A., and Drummond, A. J. (2014). *LogCombiner v2.1.3 in Computer Program and Documentation Distributed by the Author*. Available online at: https://www.beast2.org/

Rambaut, A., Suchard, M. A., Xie, D., and Drummond, A. J. (2014). *Tracer 1.6 in Computer Program and Documentation Distributed by the Author*. Available online at: https://www.beast2.org/tracer-2/

Rambaut, A. (2012). *FigTree v1. 4. in Computer Program and Documentation Distributed by the Author*. Available online at: http://tree.bio.ed.ac.uk/software/figtree/

Roma, L., Cozzolino, S., Schlüter, P. M., Scopece, G., and Cafasso, D. (2018). The complete plastid genomes of *Ophrys iricolor* and *O. Sphegodes* (Orchidaceae) and comparative analyses with other orchids. *PloS One* 13, 1–15. doi: 10.1371/journal.pone.0204174

Schelkunov, M. I., Shtratnikova, V. Y., Nuraliev, M. S., Selosse, M. A., Penin, A. A., and Logacheva, M. D. (2015). Exploring the limits for reduction of plastid genomes: a case study of the mycoheterotrophic orchids *Epipogium aphyllum* and *Epipogium roseum*. *Genome Biol. Evol.* 7, 1179–1191. doi: 10.1093/gbe/evv019

Schelkunov, M. I., Nuraliev, M. S., and Logacheva, M. D. (2019). *Rhopalocnemis phalloides* has one of the most reduced and mutated plastid genomes known. *PeerJ* 7, e7500. doi: 10.7717/peerj.7500

Shi, Y., Yang, L., Yang, Z., and Ji, Y. (2018). The complete chloroplast genome of *Pleione bulbocodioides* (Orchidaceae). *Conserv. Genet. Resour.* 10, 21–25. doi: 10.1007/s12686-017-0753-x

Stöver, B. C., and Müller, K. F. (2010). TreeGraph 2: combining and visualizing evidence from different phylogenetic analyses. *BMC Bioinf.* 11, 1–9. doi: 10.1186/1471-2105-11-7

Suetsugu, K., Ohta, T., and Tayasu, I. (2018). Partial mycoheterotrophy in the leafless orchid *Cymbidium macrorhizon*. *Am. J. Bot.* 105, 1595–1600. doi: 10.1002/ajb2.1142

Wang, H., Park, S. Y., Lee, A. R., Jang, S. G., Im, D. E., Jun, T. H., et al. (2018). Next-generation sequencing yields the complete chloroplast genome of *C. goeringii* acc. smg222 and phylogenetic analysis. *Mitochondrial DNA Part B Resour.* 3, 215–216. doi: 10.1080/23802359.2018.1437812

Weng, M. L., Blazier, J. C., Govindu, M., and Jansen, R. K. (2014). Reconstruction of the ancestral plastid genome in geraniaceae reveals a correlation between genome rearrangements, repeats, and nucleotide substitution rates. *Mol. Biol. Evol.* 31, 645–659. doi: 10.1093/molbev/mst257

Wicke, S., Muller, K. F., de Pamphilis, C. W., Quandt, D., Wickett, N. J., Zhang, Y., et al. (2013). Mechanisms of functional and physical genome reduction in photosynthetic and nonphotosynthetic parasitic plants of the broomrape family. *Plant Cell* 25, 3711–3725. doi: 10.1105/tpc.113.113373

Wicke, S., Müller, K. F., dePamphilis, C. W., Quandt, D., Bellot, S., and Schneeweiss, G. M. (2016). Mechanistic model of evolutionary rate variation en route to a nonphotosynthetic lifestyle in plants. *Proc. Natl. Acad. Sci.* 113, 9045–9050. doi: 10.1073/pnas.1607576113

Wickham, H., Chang, W., and Wickham, M. H. (2016), Package 'ggplot2.' *Creat. Elegant Data Vis. Using Gramm. Graph.* Version 2. 1–189.

Wu, F.-H., Chan, M.-T., Liao, D.-C., Hsu, C.-T., Lee, Y.-W., Daniell, H., et al. (2010). Complete chloroplast genome of *Oncidium* Gower Ramsey and evaluation of molecular markers for identification and breeding in Oncidiinae. *BMC Plant Biol.* 10, 68. doi: 10.1186/1471-2229-10-68

Wu, C. S., Lin, C. P., Hsu, C. Y., Wang, R. J., and Chaw, S. M. (2011). Comparative chloroplast genomes of pinaceae: insights into the mechanism of diversified genomic organizations. *Genome Biol. Evol.* 3, 309–319. doi: 10.1093/gbe/evr026

Yang, J.-B., Tang, M., Li, H.-T., Zhang, Z.-R., and Li, D.-Z. (2013). Complete chloroplast genome of the genus *Cymbidium*: lights into the species identification, phylogenetic implications and population genetic analyses. *BMC Evol. Biol.* 13, 84. doi: 10.1186/1471-2148-13-84

Yu, C. W., Lian, Q., Wu, K. C., Yu, S. H., Xie, L. Y., and Wu, Z. J. (2016). The complete chloroplast genome sequence of *Anoectochilus roxburghii*. *Mitochondrial DNA* 27, 2477–2478. doi: 10.3109/19401736.2015.1033706

Yuan, Y., Jin, X., Liu, J., Zhao, X., Zhou, J., Wang, X., et al. (2018). The *Gastrodia elata* genome provides insights into plant adaptation to heterotrophy. *Nat. Commun.* 9, 1–11. doi: 10.1038/s41467-018-03423-5

Conflict of Interest: The authors declare that the research was conducted in the absence of any commercial or financial relationships that could be construed as a potential conflict of interest.

frontiers in Plant Science

CORRECTION
published: 20 March 2020
doi: 10.3389/fpls.2020.00322

Corrigendum: Plastome Evolution and Phylogeny of Orchidaceae, With 24 New Sequences

*Young-Kee Kim[1], Sangjin Jo[1], Se-Hwan Cheon[1], Min-Jung Joo[1], Ja-Ram Hong[1], Myounghai Kwak[2] and Ki-Joong Kim[1]**

[1] Division of Life Sciences, Korea University, Seoul, South Korea, [2] Department of Plant Resources, National Institute of Biological Resources, Incheon, South Korea

OPEN ACCESS

Approved by:
Frontiers Editorial Office,
Frontiers Media SA, Switzerland

***Correspondence:**
Ki-Joong Kim
kimkj@korea.ac.kr

Specialty section:
This article was submitted to Plant Systematics and Evolution, a section of the journal Frontiers in Plant Science

Received: 03 March 2020
Accepted: 04 March 2020
Published: 20 March 2020

Citation:
Kim Y-K, Jo S, Cheon S-H, Joo M-J, Hong J-R, Kwak M and Kim K-J (2020) Corrigendum: Plastome Evolution and Phylogeny of Orchidaceae, With 24 New Sequences. Front. Plant Sci. 11:322. doi: 10.3389/fpls.2020.00322

Keywords: Orchidaceae, plastome evolution, gene loss, IR contraction/expansion, genome rearrangement

A Corrigendum on

Plastome Evolution and Phylogeny of Orchidaceae, With 24 New Sequences
by Kim, Y.-K., Jo, S., Cheon, S.-H., Joo, M.-J., Hong, J.-R., Kwak, M., et al. (2020). Front. Plant Sci. 11:22. doi: 10.3389/fpls.2020.00022

In the original article, there was a mistake in the legend for Figure 4 as published. The word "**terrestrial**" at the end of the legend for Figure 4A should be "**epiphytic.**" The correct legend appears below.

Figure 4. Relationships between plastome lengths and gene numbers. **(A)**: Terrestrial orchids show a wider range of variation than epiphytic orchids. **(B)**: Mycoheterotrophic orchids show a wider range of variation than photosynthetic orchids. **(C,D)**: Plastome lengths are more strongly correlated with LSC lengths than IR lengths in both mycoheterotrophic and photosynthetic orchids.

The authors apologize for this error and state that this does not change the scientific conclusions of the article in any way. The original article has been updated.

frontiers in Plant Science

ORIGINAL RESEARCH
published: 27 February 2020
doi: 10.3389/fpls.2020.00126

Phylogeny and Historical Biogeography of *Paphiopedilum* Pfitzer (Orchidaceae) Based on Nuclear and Plastid DNA

Chi-Chu Tsai[1,2†], *Pei-Chun Liao*[3†], *Ya-Zhu Ko*[4†], *Chih-Hsiung Chen*[5] *and Yu-Chung Chiang*[4,6*]

[1] Kaohsiung District Agricultural Research and Extension Station, Pingtung, Taiwan, [2] Department of Biological Science and Technology, National Pingtung University of Science and Technology, Pingtung, Taiwan, [3] School of Life Science, National Taiwan Normal University, Taipei, Taiwan, [4] Department of Biological Sciences, National Sun Yat-sen University, Kaohsiung, Taiwan, [5] Department of Botany, National Museum of Natural Science, Taichung, Taiwan, [6] Department of Biomedical Science and Environment Biology, Kaohsiung Medical University, Kaohsiung, Taiwan

OPEN ACCESS

Edited by:
Jen-Tsung Chen,
National University of Kaohsiung, Taiwan

Reviewed by:
Allison Miller,
Saint Louis University, United States
Xun Gong,
Chinese Academy of Sciences, China

***Correspondence:**
Yu-Chung Chiang
yuchung@mail.nsysu.edu.tw

[†]These authors have contributed equally to this work

Specialty section:
This article was submitted to Plant Development and EvoDevo, a section of the journal Frontiers in Plant Science

Received: 23 July 2019
Accepted: 28 January 2020
Published: 27 February 2020

Citation:
Tsai C-C, Liao P-C, Ko Y-Z, Chen C-H and Chiang Y-C (2020) Phylogeny and Historical Biogeography of Paphiopedilum Pfitzer (Orchidaceae) Based on Nuclear and Plastid DNA. Front. Plant Sci. 11:126. doi: 10.3389/fpls.2020.00126

The phylogeny and biogeography of the genus *Paphiopedilum* were evaluated by using phylogenetic trees derived from analysis of nuclear ribosomal internal transcribed spacer (ITS) sequences, the plastid *trn*L intron, the *trn*L-F spacer, and the *atp*B-*rbc*L spacer. This genus was divided into three subgenera: *Parvisepalum*, *Brachypetalum*, and *Paphiopedilum*. Each of them is monophyletic with high bootstrap supports according to the highly resolved phylogenetic tree reconstructed by combined sequences. There are five sections within the subgenus *Paphiopedilum*, including *Coryopedilum*, *Pardalopetalum*, *Cochlopetalum*, *Paphiopedilum*, and *Barbata*. The subgenus *Parvisepalum* is phylogenetic basal, which suggesting that *Parvisepalum* is comprising more ancestral characters than other subgenera. The evolutionary trend of genus *Paphiopedilum* was deduced based on the maximum likelihood (ML) tree and Bayesian Evolutionary Analysis Sampling Trees (BEAST). Reconstruct Ancestral State in Phylogenies (RASP) analyses based on the combined sequence data. The biogeographic analysis indicates that *Paphiopedilum* species were firstly derived in Southern China and Southeast Asia, subsequently dispersed into the Southeast Asian archipelagoes. The subgenera *Paphiopedilum* was likely derived after these historical dispersals and vicariance events. Our research reveals the relevance of the differentiation of *Paphiopedilum* in Southeast Asia and geological history. Moreover, the biogeographic analysis explains that the significant evolutionary hotspots of these orchids in the Sundaland and Wallacea might be attributed to repeated migration and isolation events between the south-eastern Asia mainland and the Sunda Super Islands.

Keywords: *Paphiopedilum*, molecular phylogeny, biogeography, evolutionary trend, dispersal events

INTRODUCTION

The orchid genus *Paphiopedilum* Pfitzer belongs to the subfamily Cypripedioideae Lindley. This subfamily has been considered a distinct lineage since Lindley (1840) separated them from other orchids based on the characteristic of having two separated fertile anthers [see (Cribb, 1998)]. This subfamily includes only five genera: *Cypripedium*, *Mexipedium*, *Paphiopedilum*, *Phragmipedium,* and *Selenipedium*. *Mexipedium* and *Selenipedium* are monotypic genera (Albert and Chase, 1992), which was a finding supported by ITS sequence analysis (Cox et al., 1997). These five genera are distributed in separate and restricted geographical ranges (Cribb, 1998). *Paphiopedilum* is distinguished from genera *Cypripedium* and *Selenipedium* by its conduplicate coriaceous leaves, as opposed to the plicate persistent leaves of the latter two genera. Furthermore, *Paphiopedilum* differs from *Phragmipedium* and *Mexipedium*, as they display imbricate sepal vernation, different chromosome base numbers and a unilocular ovary (Albert and Chase, 1992; Albert, 1994).

The systematics of the genus *Paphiopedilum* proposed by Cribb (1997b) are largely consistent with Atwood (1984), except that Cribb placed the *Parvisepalum* group within subgenus *Brachypetalum*. Cribb (1997b) accepted the suggestion of Karasawa (1982) and Karasawa and Saito (1982) to promote the *Parvisepalum* group (e.g., *Parvisepalum delenatii*, *Parvisepalum armeniacum*, *Parvisepalum micranthum*, *Parvisepalum malipoense,* and *Parvisepalum emersonii*) to the subgeneric rank, since the two relatively new species (i.e., *P. malipoense* and *P. emersonii*) found in this group have been described. According to the classification of Cribb (1997b), the genus *Paphiopedilum* comprised of approximately 69 species worldwide. Cribb divided this genus into three subgenera, *Parvisepalum*, *Brachypetalum*, and *Paphiopedilum,* which are mainly based on the morphological characteristics of flower inflorescence, leaf type, floral morphology, and molecular data on ITS sequences (Cox et al., 1997). Recently, several new species and treatment have been described for this genus. The genus *Paphiopedilum* was described as containing approximately 98 species worldwide by the year 2000 (Koopowitz, 2000). In this genus, *Paphiopedilum* was divided into five sections: *Coryopedilum*, *Pardalopetalum*, *Cochlopetalum*, *Paphiopedilum,* and *Barbata*. Subgenera of the genus *Paphiopedilum* distribute in distinct geographic regions (Cribb, 1997b). The subgenera *Parvisepalum* and *Brachypetalum*, as well as the section *Paphiopedilum* of the subgenus *Paphiopedilum*, are found only in mainland Asia. The *Parvisepalum* subgenus is concentrated in southern China and Vietnam, the subgenus *Brachypetalum* is mostly found in Thailand (**Figure 1**). Among the subgenus *Paphiopedilum*, *Paphiopedilum* ranges from India to southern China, Thailand and Indo-China, and the species diversity found in southern China was the most concentrated. The section *Cochlopetalum* is restricted to the islands of Sumatra and Java. The section *Pardalopetalum* is widespread in Southeast Asia, the Malay Archipelago, as far east as Sulawesi, and Luzon in the Philippines. The enormous species diversity of the section *Coryopedilum* locates in Borneo, and this section range from the Philippines to Sulawesi in New Guinea. The section *Barbata* is widespread from eastern Nepal, across to Hong Kong and the Philippines, south to the Malay Archipelago, New Guinea, and the Solomon Islands (Cribb, 1998).

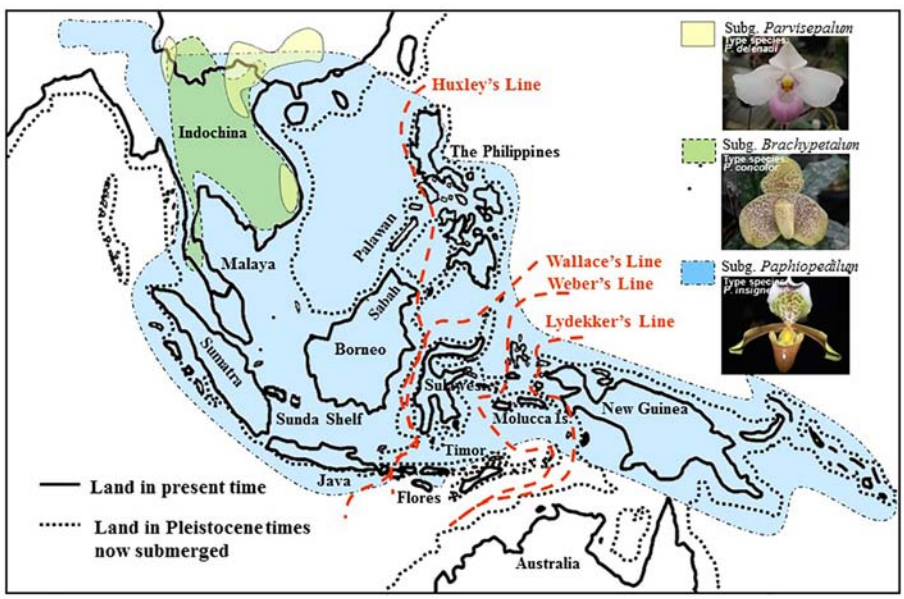

FIGURE 1 | Map of the geographical distribution of *Paphiopedilum* based on the phylogeny of Cribb (1998). Comparison of Southeast Asian landmasses between the Pleistocene era and the present. During the Pleistocene, Indochina, Malaya, Sumatra, Java, Borneo, and the Philippines were interconnected and were separated from Sulawesi by the Makassar Strait.

Paphiopedilum is a genus of tropical Asiatic origin, and its range extends eastward, reaching the Philippines, Southeast Asia, Borneo, and the Malay Archipelago, crossing Wallace's Line into Sulawesi, the Moluccas, New Guinea, and the Solomon Islands (Cribb, 1998). Tracking back to the geological history of Southeast Asian, the Palawan, Mindoro, Zamboanga, and the adjacent small islands are the older islands of the Southern Philippines. These regions are located on the border of the Eurasian Plate and have been shifting away from the mainland mass by tectonic collision since the early Miocene (~30 Mya) and the shell of the older plate was merged to Borneo until 5~10 Mya (Karig et al., 1986; Stephan et al., 1986; Hall, 1996). In contrast, most of the Philippine islands formed less than 5 Mya (Aurelio et al., 1991; Quebral et al., 1994). In addition, the Sundaland was comprised of the Malay Peninsula, Sumatra, Java, Sulawesi, and Borneo and merged with Bali, the Philippines, and even New Guinea/Australia into Sunda Superland interconnecting by land bridge during the last glacial period (0.01~1.8 Mya) (van Oosterzee, 1997). Since the last glacial period, species migrated forward and backwards between these regions and isolated after the last glacial maximum (LGM), causing the broken of Sunda Superland (Tsai et al., 2015).

The chloroplast primers for the *atp*B-*rbc*L, *trn*L-*trn*F spacer, and *trn*L intron are useful for phylogenetic studies at the intrageneric level. The primers for the *trn*L-*trn*F spacer and *trn*L intron developed by Taberlet et al. (1991) have been applied for inferring phylogenies at the intrageneric level (Goldblatt et al., 2002; Hodkinson et al., 2002; Mogensen, 1996; Van Raamsdonk et al., 2003), and have also been used successfully on Orchidaceae (Tsai et al., 2012). The *atp*B-*rbc*L regions are high length differences due to frequent occurrence of indels and are often used in combination with other primers to provide more information (Yoshinaga et al., 1992; Chiang et al., 1998; Von Konrat et al., 2010). Therefore, this study aims to further elucidate the phylogeny of *Paphiopedilum* through analysis ITS (internal transcribed spacer) sequences and three non-coding plastid DNA sequences (*trn*L intron, *trn*L-F, and *atp*B-*rbc*L spacers). In addition, the biogeography of this genus is clarified based on the phylogenetic tree derived from the molecular evidence.

MATERIALS AND METHODS

Plant Materials

Seventy-eight taxa of *Paphiopedilum* and two outgroups from genus *Phragmipedium* were used in this study (**Table 1**). All leaf materials were taken from living plants in the greenhouse of the Kaohsiung District Agricultural Improvement Station (KDAIS) in Taiwan.

DNA Extraction, PCR Amplification, and Sequencing

Total DNA was extracted from fresh etiolated leaves by using the cetyltrimethylammonium bromide (CTAB) method (Doyle and Doyle, 1987). Approximate DNA yields were determined by using the spectrophotometer (model U-2001, Hitachi).

The PCR reaction was used to amplify nuclear ribosomal ITS sequence and chloroplast (cp) DNA fragments *trn*L intron and the *trn*L-*trn*F spacer, *atp*B-*rbc*L spacer. ITS primers were designed from conserved regions of the 3' end of the 18S rRNA gene and the 5'end of the 26S rRNA gene using sequences from different species present in GenBank. Universal primers for *trn*L intron and the *trn*L-*trn*F spacer were referenced from Taberlet et al. (1991). Primer sequences for amplifying of the *atp*B-*rbc*L spacer were designed from the conserved regions of the 3' end of the *atp*B gene and the 5'end of the *rbc*L gene of chloroplast DNA using sequences of different species obtained from GenBank. Detailed amplification conditions and primer sequences are given in **Supplementary Table S1**. All PCR products were separated by agarose gel electrophoresis (1.0%, w/v in TBE) and were recovered using glassmilk (BIO 101, California).

PCR products were directly sequenced using the dideoxy chain-termination method on an ABI377 automated sequencer with the Ready Reaction Kit (PE Biosystems, California) of the BigDye™ Terminator Cycle Sequencing. The PCR reaction primer sequences were used as sequencing primers. Each sample was sequenced two or three times to confirm the sequences. Reactions were performed as recommended by the product manufacturers.

Sequence Alignment and Phylogenetic Reconstruction

The sequence alignment was determined using the ClustalW multiple alignment program in BioEdit (Hall, 1999), and four regions were combined for the following analysis. The alignment was checked, and apparent alignment errors were corrected by hand. Indels (insertion/deletions) were treated as missing data. For phylogenetic reconstruction, two *Phragmipedium* taxa treating as outgroups were sequenced to resolve whether all in-group taxa formed a monophyletic lineage. The best-fitting substitution model was selected (**Supplementary Table S2**) by a model test using MEGA 6.0 (Tamura et al., 2013). Tamura 3-parameter model (T92) using a discrete Gamma distribution (+G) was selected for following neighbor-joining (NJ) phylogenetic reconstruction. The general time reversible (GTR) using a discrete gamma distribution (+G) and considering the proportion of invariable sites (+I) were chosen for following divergence time estimation using the Yule model methods in BEAST 1.8.0 (Drummond and Rambaut, 2007; Drummond et al., 2012). The phylogenetic tree for the combined multiple sequence datasets used equally weighted characters. Moreover, because the sequence data of the four genera (*Mexipedium, Selenipedium*, *Cypripedium*, and *Goodyera*) in NCBI is limited, only two sets of fragment data (ITS: *Mexipedium xerophyticum*-MK161260.1; *Selenipedium aequinoctiale*-JF825977.1; *Cypripedium_macranthos*-KT338684.1; Goodyera_procera-MK451741.1and *trn*L-*trn*F spacer: *Mexipedium xerophyticum*-FR851215.1; *Selenipedium aequinoctiale*-JF825975.1; *Cypripedium_macranthos*-JF797026.1; Goodyera_procera-MK451782.1) are used as an additional analysis and compared with the data using only genus *Phragmipedium* as outgroup. The results of six outgroups are showed in **Supplementary Data**.

TABLE 1 | Names of specimens, geographical distribution, source, and GenBank accession numbers for sequences of the internal transcribed spacer (ITS) of ribosomal DNA (rDNA), the plastid *trn*L intron, the *trn*L-F spacer, and the *atp*B-*rbc*L spacer.

Taxa and systematic classification [a]	Geographical distribution	Voucher [b]	GenBank accession no.			
			ITS	*trn*L intron	*trn*L-F spacer	*atp*B-*rbc*L spacer
Genus *Paphiopedilum*						
Subgenus *Parvisepalum*						
Paphiopedilum armeniacum S.C. Chen & F.Y. Liu	Southwest China	C. C. Tsai 2021	EF156086	EF156001	EF156171	GQ850803
Paphiopedilum delenatii Guill.	Vietnam	C. C. Tsai 2073	EF156096	EF156011	EF156181	GQ850813
Paphiopedilum emersonii Koop. & P.J. Cribb	China	C. C. Tsai 2351	EF156099	EF156014	EF156184	GQ850816
Paphiopedilum hangianum Perner & Gruss	China	C. C. Tsai 2201	EF156109	EF156024	EF156194	GQ850826
Paphiopedilum jackii H.S. Hua	China, Vietnam	C. C. Tsai 2330	EF156118	EF156033	EF156203	GQ850832
Paphiopedilum malipoense S.C. Chen & Z.H. Tsi	China, Vietnam	C. C. Tsai 2024	EF156125	EF156040	EF156210	GQ850839
Paphiopedilum micranthum T. Tang & F. T. Wang	China, Vietnam	C. C. Tsai 2020	EF156128	EF156043	EF156213	GQ850842
Paphiopedilum micranthum var. *eburneum* Fowlie	China	No voucher	EF156127	EF156042	EF156212	GQ850841
Paphiopedilum vietnamense Perner & Gruss	Vietnam	C. C. Tsai 2110	EF156158	EF156073	EF156243	GQ850871
Subgenus *Brachypetalum*						
Paphiopedilum concolor (Bateman) Pfitzer	China, Burma, Thailand, Laos, Vietnam	C. C. Tsai 2307	EF156093	EF156008	EF156178	GQ850810
Paphiopedilum godefroyae (God.-Leb.) Stein	Thailand	C. C. Tsai 2321	EF156107	EF156022	EF156192	GQ850824
Paphiopedilum godefroyae var. *leucochilum* (Masters) Hallier	Thailand	C. C. Tsai 2031	EF156106	EF156021	EF156191	GQ850823
Paphiopedilum niveum (Rchb.f.) Stein	Southern Thailand, Malay peninsula	C. C. Tsai 2039	EF156130	EF156045	EF156215	GQ850844
Subgenus *Paphiopedilum*						
Section *Coryopedilum*						
Paphiopedilum adductum Asher	Philippines	C. C. Tsai 2025	EF156082	EF155997	EF156167	GQ850799
Paphiopedilum anitum Golamco	Philippines	C. C. Tsai 2295	EF156083	EF155998	EF156168	GQ850800
Paphiopedilum gigantifolium Braem, M.L. Baker & C.O. Baker	Sulawesi	No voucher	EF156103	EF156018	EF156188	GQ850821
Paphiopedilum kolopakingii Fowlie	Borneo	C. C. Tsai 2057	EF156121	EF156036	EF156206	GQ850835
Paphiopedilum ooii Koopowitz	Borneo	no voucher	EF156138	EF156046	EF156216	GQ850845
Paphiopedilum philippinense (Rchb.f.) Stein	Northeast Borneo, Philippines	C. C. Tsai 2007	EF156142	EF156050	EF156220	GQ850848
Paphiopedilum glanduliferum (Blume) Stein	New Guinea	C. C. Tsai 2040	EF156104	EF156019	EF156189	GQ850822
Paphiopedilum randsii fowlie	Mindanao, Philippines	C. C. Tsai 2297	EF156132	EF156053	EF156223	GQ850851
Paphiopedilum rothschildianum (Rchb.f.) Stein	Borneo	C. C. Tsai 2249	EF156135	EF156056	EF156226	GQ850853
Paphiopedilum sanderianum (Rchb.f.) Stein	Borneo	C. C. Tsai 2309	EF156136	EF156057	EF156227	GQ850854
Paphiopedilum stonei (Hook.) Stein	Borneo	C. C. Tsai 2310	EF156146	EF156061	EF156231	GQ850858
Paphiopedilum supardii Braem & Loeb	Borneo	C. C. Tsai 2189	GQ505309	GQ505312	GQ505315	GQ850860
Paphiopedilum wilhelminae L.O. Williams	New Guinea	C. C. Tsai 2205	GQ505310	GQ505313	GQ505316	GQ850875
Section *Pardalopetalum*						
Paphiopedilum dianthum T. Tang & F.T. Wang	China	C. C. Tsai 2085	EF156097	EF156012	EF156182	GQ850814
Paphiopedilum haynaldianum (Rchb.f.) Stein	Philippines	No voucher	EF156110	EF156025	EF156195	GQ850827
Paphiopedilum lowii (Lindl.) Stein	Peninsular Malaysia, Sumatra, Borneo, Sulawesi	C. C. Tsai 2285	EF156124	EF156039	EF156209	GQ850838
Paphiopedilum parishii (Rchb.f.) Stein	Southwest China, Burma, Thailand	C. C. Tsai 2276	EF156140	EF156048	EF156218	GQ850847
Paphiopedilum richardianum Asher & Beaman	Sulawesi	C. C. Tsai 2068	EF156133	EF156054	EF156224	GQ850852
Section *Cochlopetalum*						
Paphiopedilum victoria-regina (Sander) M.W. Wood	Sumatra	C. C. Tsai 2045	EF156157	EF156072	EF156242	GQ850870

(Continued)

TABLE 1 | Continued

Taxa and systematic classification [a]	Geographical distribution	Voucher [b]	GenBank accession no.			
			ITS	*trn*L intron	*trn*L-F spacer	*atp*B-*rbc*L spacer
Paphiopedilum liemianum (Fowlie) Karas. & Saito	Northern Sumatra	C. C. Tsai 2133	EF156123	EF156038	EF156208	GQ850837
Paphiopedilum moquetteanum (J.J. Smith) Fowlie	Southwest Java	C. C. Tsai 2314	EF156129	EF156044	EF156214	GQ850843
Paphiopedilum primulinum M.W. Wood & P. Taylor	Northern Sumatra	C. C. Tsai 2359	EF156143	EF156051	EF156221	GQ850849
Paphiopedilum victoria-mariae (Rolfe) Rolfe	Sumatra	No voucher	EF156156	EF156071	EF156241	GQ850869
Section *Paphiopedilum*						
Paphiopedilum barbigerum Tang & Wang	China, northern Vietnam	C. C. Tsai 2023	EF156088	EF156003	EF156173	GQ850805
Paphiopedilum charlesworthii (Rolfe) Pfitzer	Burma, northern Thailand, southwest China	C. C. Tsai 2192	EF156091	EF156006	EF156176	GQ850808
Paphiopedilum druryi (Bedd.) Stein	Southern India	C. C. Tsai 2093	EF156098	EF156013	EF156183	GQ850815
Paphiopedilum exul (Ridl.) Rolfe	Peninsular Thailand	C. C. Tsai 2083	EF156101	EF156016	EF156186	GQ850818
Paphiopedilum esquirolei Schltr.	China, India, Bhutan (Southeast Asia)	C. C. Tsai 2335	EF156100	EF156015	EF156185	GQ850817
Paphiopedilum fairrieanum (Lindl.) Stein	India, Bhutan	C. C. Tsai 2079	EF156102	EF156017	EF156187	GQ850819
Paphiopedilum gratrixianum (Masters) Guillaumin	Laos, Vietnam	C. C. Tsai 2155	EF156108	EF156023	EF156193	GQ850825
Paphiopedilum helenae Aver.	Northern Vietnam	C. C. Tsai 2053	EF156111	EF156026	EF156196	GQ850828
Paphiopedilum henryanum Braem	China, northern Vietnam	C. C. Tsai 2277	EF156112	EF156027	EF156197	GQ850829
Paphiopedilum herrmannii Fuchs & Reisinger	Northeast India	C. C. Tsai 2109	EF156113	EF156028	EF156198	GQ850880
Paphiopedilum hirsutissimum (Lindl. ex Hook.) Stein	China, India, Bhutan (Southeast Asia)	C. C. Tsai 2240	EF156114	EF156029	EF156199	GQ850830
Paphiopedilum spicerianum (Rchb.f.) Pfitzer	Northeast India	C. C. Tsai 2229	EF156145	EF156060	EF156230	GQ850857
Paphiopedilum tigrinum Koop. & N. Haseg.	China	C. C. Tsai 2218	EF156149	EF156064	EF156234	GQ850862
Paphiopedilum tranlienianum Gruss & Perner	Unknown	C. C. Tsai 2042	EF156151	EF156066	EF156236	GQ850864
Paphiopedilum villosum (Lindl.) Stein	India, Burma, Thailand (Southeast Asia)	C. C. Tsai 2216	EF156159	EF156074	EF156244	GQ850872
Section *Barbata*						
Paphiopedilum acmodontum Schoser ex M.W. Wood	Philippines	C. C. Tsai 2094	EF156081	EF155996	EF156166	GQ850879
Paphiopedilum appletonianum (Gower) Rolfe	China, Thailand, Cambodia, Laos, Vietnam (Southeast Asia)	C. C. Tsai 2153	EF156084	EF155999	EF156169	GQ850801
Paphiopedilum argus (Rchb.f.) Stein	Philippines	C. C. Tsai 2282	EF156085	EF156000	EF156170	GQ850802
Paphiopedilum braemii Mohr	Northern Sumatra, Indonesia	C. C. Tsai 2151	EF156089	EF156004	EF156174	GQ850806
Paphiopedilum barbatum (Lindl.) Pfitzer	Southern Thailand, peninsular Malaysia, Sumatra	C. C. Tsai 2227	EF156087	EF156002	EF156172	GQ850804
Paphiopedilum callosum (Rchb.f.) Stein	Thailand, Cambodia, Laos, Vietnam (south-east Asia)	C. C. Tsai 2267	EF156090	EF156005	EF156175	GQ850807
Paphiopedilum ciliolare (Rchb.f.) Stein	Philippines	C. C. Tsai 2078	EF156092	EF156007	EF156177	GQ850809
Paphiopedilum curtisii (Rchb. f.) Stein	Sumatra	C. C. Tsai 2107	EF156094	EF156009	EF156179	GQ850811
Paphiopedilum dayanum (Lindl.) Stein	Borneo	C. C. Tsai 2280	EF156095	EF156010	EF156180	GQ850812
Paphiopedilum fowliei Birk	Philippines	No voucher	GQ505311	GQ505314	GQ505317	GQ850820
Paphiopedilum hookerae (Rchb.f.) Stein	Borneo	C. C. Tsai 2089	EF156116	EF156031	EF156201	GQ850831
Paphiopedilum volonteanum (Sander) Stein	Borneo	No voucher	EF156115	EF156030	EF156200	GQ850873
Paphiopedilum javanicum (Reinw. ex Lindl.) Pfitzer	Borneo, southeast Sumatra, Java	C. C. Tsai 2326	EF156120	EF156035	EF156205	GQ850834
Paphiopedilum javanicum var. *virens* (Rchb. f.) Stein	North Borneo	No voucher	EF156119	EF156034	EF156204	GQ850833
Paphiopedilum lawrenceanum (Rchb.f.) Stein	Borneo	C. C. Tsai 2013	EF156122	EF156037	EF156207	GQ850836
Paphiopedilum mastersianum (Rchb.f.) Stein	Moluccas	C. C. Tsai 2341	EF156126	EF156041	EF156211	GQ850840
Paphiopedilum papuanum (Ridl.) Ridl.	New Guinea	No voucher	EF156139	EF156047	EF156217	GQ850846
Paphiopedilum purpuratum (Lindl.) Stein	China, Vietnam	C. C. Tsai 2049	EF156131	EF156052	EF156222	GQ850850
Paphiopedilum sangii Braem	Sulawesi	C. C. Tsai 2088	EF156137	EF156058	EF156228	GQ850855

(Continued)

TABLE 1 | Continued

Taxa and systematic classification [a]	Geographical distribution	Voucher [b]	GenBank accession no.			
			ITS	*trn*L intron	*trn*L-F spacer	*atp*B-*rbc*L spacer
Paphiopedilum schoseri Braem	Moluccas	No voucher	EF156144	EF156059	EF156229	GQ850856
Paphiopedilum sukhakulii Schoser & Senghas	Northern Thailand	C. C. Tsai 2226	EF156147	EF156062	EF156232	GQ850859
Paphiopedilum superbiens (Rchb.f.) Stein	Sumatra	C. C. Tsai 2082	EF156148	EF156063	EF156233	GQ850861
Paphiopedilum tonsum (Rchb.f.) Stein	Northern Sumatra, Indonesia	C. C. Tsai 2087	EF156150	EF156065	EF156235	GQ850863
Paphiopedilum urbanianum Fowlie	Philippines	C. C. Tsai 2161	EF156152	EF156067	EF156237	GQ850865
Paphiopedilum veniferum Koop. & Haseg	Unknown	C. C. Tsai 2253	EF156153	EF156068	EF156238	GQ850866
Paphiopedilum venustum (Wall. ex Sims) Pfitzer ex Stein	Bhutan, India, Nepal	C. C. Tsai 2032	EF156154	EF156069	EF156239	GQ850867
Paphiopedilum wardii Summerh	Burma, southwest China	C. C. Tsai 2139	EF156161	EF156076	EF156246	GQ850874
Genus *Phragmipedium*						
Phragmipedium pearcei Garay	Ecuador, Peru	C. C. Tsai 2009	EF156163	EF156078	EF156248	GQ850877
Phragmipedium longifolium Rchb. f. & Warsc	Costa Rica, Panama, Colombia, Ecuador	C. C. Tsai 2043	EF156165	EF156080	EF156250	GQ850876

[a]*The systematics of Phalaenopsis are based on Christenson (2001).*
[b]*Voucher specimens were deposited at the herbarium of the National Museum of Natural Science, Taiwan (TNM).*

Genetic relationships were determined using NJ in the MEGA 6.0 (Tamura et al., 2013), maximum parsimony (MP) in PHYLIP 3.68 (Felsenstein, 2004), and maximum likelihood (ML) in MEGA 6.0 (Tamura et al., 2013). Bootstrapping (1,000 replicates) was carried out to estimate the support for NJ, MP, and ML topologies (Felsenstein, 1985; Hillis and Bull, 1993). The strict consensus parsimonious tree was then constructed by using the MEGA 6.0 (Tamura et al., 2013).

Divergence Time Estimation

The combined chloroplast DNA (cpDNA) dataset was used to estimate the divergence times using the Bayesian Yule model methods (BEAST version 1.7.5). The characteristic of uniparental inheritance in cpDNA prevents the interference of recombination introgression on phylogenetic reconstruction (Drummond et al., 2012). The general-time reversible (GTR) model with estimates of invariant sites (+I) and gamma-distributed among site rate variation (+G) in all matrices without partitions model was determined by the nucleotide substitution model test, conducted in MEGA 6.0 (Tamura et al., 2013).

To estimate the divergence time, two strategies, the strict and relaxed clock models, were adopted. For the relaxed clock, the calibration point at the most recent common ancestor (MRCA) of *Paphiopedilum* and *Phragmipedium* for 22 Ma (Gustafsson et al., 2010) were used to calculate the divergence times of each node. However, since there is no suitable fossil record to correct the calibration of divergence times for the ingroup, we recalculate the divergence time by strict clock model for consistency. For the strict clock, the mean substitution rate of 1.82×10^{-9} subs/site/year with the lower and upper limits 1.11×10^{-9} subs/site/year and 2.53×10^{-9} subs/site/year, respectively, were used for the cpDNA spacers in *Phalaenopsis amabilis* complex (Tsai et al., 2015).

We conducted four independent runs of a Yule prior and four Markov Chain Monte Carlo (MCMC) chains with a different starting seed. The first 10% simulations were discarded (burn-in) in a total of 10^8 generations. For thinning, one tree was reserved every 10,000 trees, and finally, 10,000 trees were left to calculate the posterior probability of each node. The effective sample size (ESS) > 200 was used as a criterion to check whether the sampling (simulations) is proper and is reaching a stationary distribution by Tracer v1.6 (Rambaut et al., 2018). Four independent-runs results, including the log file and tree file, were combined with the assistance of LogCombiner 1.6.1 (Drummond and Rambaut, 2007). TreeAnnotator 1.6.1 (Drummond and Rambaut, 2007) was used to summarize a consensus tree with a criterion of the maximum clade reliability using the mean heights option. The final consensus tree was drawn by FigTree 1.3.1 (Rambaut, 2009).

Biogeographic Inference Using Reconstruct Ancestral State in Phylogenies

The Statistical dispersal–vicariance analysis was used to assess the biogeographic patterns of *Paphiopedilum* species [Statistical Dispersal-Vicariance Analysis (S-DIVA), (Yu et al., 2010)]. Bayes–Lagrange Statistical dispersal–extinction–cladogenesis (S-DEC) model (Ree and Smith, 2008) was performed in Reconstruct Ancestral State in Phylogenies (RASP) 3.2 (Yu et al., 2015) to distinguish the events of vicariance, dispersal, and extinction. Five geographic areas were determined mainly according to Myers et al. (2000) with a little modification to illuminate the vicariance, dispersal and extinction events of *Paphiopedilum* species. The hotspot areas in South-Central China and Indo-Burma with the Malay Peninsula were combined as area A, consisting of China, Nepal, India, Bhutan, Burma, Thailand, Malaysia, Cambodia, Vietnam, and Laos. The hotspot "Sundaland" including Borneo, Java, and Sumatra were set as the area B. We move the Malay Peninsula from the area "Sundaland" to area A due to the integrity of the current landmass. The hotspots "Wallacea" (include Sulawesi and Moluccas) and "Philippines" were set as area C and area E.

Respectively, islands of New Guinea eastern from the Wallacea are defined as area D. Species of outgroup were all defined as the area I. These two outgroup species are distributed in Ecuador, Peru, Costa Rica, Panama, and Colombia. The real distribution of outgroups is too far from the areas of the species in this study. Therefore, the ranges of outgroups are assigned to a new area in which none of the ingroup species occurs (Yu et al., 2014). The ML tree topologies were used in S-DIVA analysis.

RESULTS

Sequence Alignment and Characteristics

The lengths of the ITS sequences obtained from the *Paphiopedilum* and outgroup samples were similar to those reported for a broad example of angiosperms (Baldwin, 1992; Baldwin et al., 1995). The alignment length of the ITS sequence is 735 nucleotides, of which 343 were identified as variable sites with 235 potentially parsimony informative sites. The average genetic distance between the 78 *Paphiopedilum* samples was 0.039 in ITS, and the average genetic distance between the 78 *Paphiopedilum* species was 0.01 in cpDNA. The alignment of combined plastid DNA fragments contained a total of 2,409 characters, of which 872 were identified as variable sites with 588 potentially parsimony informative sites. Since the sequences of three samples of every species are the same within species, only one sequence per species was used for the analyses and deposited in NCBI GenBank. The accession numbers of the nuclear ribosomal ITS sequences and the three fragments of plastid DNA from the 78 *Paphiopedilum* taxa and the two outgroup samples (from the genus *Phragmipedium*) are shown in **Table 1**.

Phylogeny Reconstruction

Both NJ and MP trees revealed a monophyletic relationship of 78 *Paphiopedilum* taxa with high bootstrap supports (**Figure 2**). Moreover, the use of six outgroups for phylogeny reconstruction showed similar bootstrap supports (**Supplementary Figure S1**). In the *Paphiopedilum* monophyletic clade, three subgenera *Parvisepalum*, *Brachypetalum*, and *Paphiopedilum* formed independent monophyletic clades with 100/100/100, 98/91/84, and 61/59/86% bootstrap supporting values in NJ/MP/ML trees, in which subgenus *Parvisepalum* was diverged firstly from other lineages (**Figure 2**, **Supplementary Figure S1**). In subgenus *Paphiopedilum*, sections *Barbata*, *Cochlopetalum*, *Pardalopetalum,* and *Coryopedilum* are monophyletic with 94/96/100, 79/81/94, 100/100/100, and 100/100/100% bootstrap supporting values in NJ, MP, and ML trees. Additionally, the use of six outgroups for phylogeny reconstruction showed similar patterns (**Supplementary Figure S1**). However, section *Paphiopedilum* showed a low support [56/51/54% bootstrap values (**Supplementary Figure S2**); 59% bootstrap values (**Supplementary Figure S1**)] for the monophyly.

In addition, the molecular data demonstrates that a newly described variety, *P. micranthum* var. *eburneum*, is closely related to *P. malipoense* based on the plastid DNA within subgenus *Parvisepalum*, which is inconsistent with the inference by nuclear ITS and combined data. In ITS tree, *P. micranthum* var. *eburneum* is sister with *P. micranthum* var. *micranthum* (**Figures 2** and **3**). Therefore, we infer a hybridization event between the ancestor of *P. micranthum* and *P. malipoense* that lead to a plastid capture in *P. micranthum* var. *eburneum*.

Divergence Time Estimates

The coalescence time of the genus *Paphiopedilum* was estimated to be 7.09 Mya with 95% confidence intervals (95% CI) of 5.88–8.41 Mya (**Figure 4**) according to the substitution rate referenced from Tsai et al. (2015). If calibrating by relaxed clock referring to Gustafsson et al. (2010), the estimated coalescence time of the genus *Paphiopedilum* was 5.72 Mya (**Figure 4**). In the genus *Paphiopedilum*, the coalescence times estimated by strict clock were 4.30 Mya (95% CI: 3.50–5.18 Mya), 2.47 Mya (95% CI: 1.73–3.33 Mya), and 4.08 Mya (95% CI: 3.39–4.86 Mya) for subgenera *Parvisepalum*, *Brachypetalum*, and *Paphiopedilum*, respectively (**Figure 4**). After re-calibrating by a relaxed clock, the coalescence time was estimated to be 3.3 Mya, 2.24, and 3.38 Mya Mya for subgenera *Parvisepalum*, *Brachypetalum*, and *Paphiopedilum*, respectively (**Figure 4**). In addition, the strict clock suggested that the coalescence times were tracked back to 2.19 Mya (95% CI: 0.17–2.77 Mya), 1.54 Mya (95% CI: 0.93–2.27 Mya), 3.12 Mya (95% CI: 2.49–3.81 Mya), 2.48 (95% CI: 1.86–3.17 Mya), and 1.60 Mya (95% CI: 1.10–2.18 Mya) for clades of subgenera *Barbata*, *Cochlopetalum*, *Paphiopedilum*, *Coryopedilum,* and *Pardalopetalum* of subgenus *Paphiopedilum*, respectively. By relaxed clock, the coalescence time was estimated to be 1.94, 1.3, 2.59, 1.81, and 1.08 Mya for clades of subgenera *Barbata*, *Cochlopetalum*, *Paphiopedilum*, *Coryopedilum,* and *Pardalopetalum* of subgenus *Paphiopedilum*, respectively. Additionally, the use of six outgroups for divergence time estimation also showed similar supports (**Supplementary Figure S2**). In short, the estimates of the coalescence times by strict and relaxed clocks are similar, but the time calculated is slightly shorter by relaxed clocks. Regardless, the coalescence time of the genus *Paphiopedilum* will not be earlier than Upper Miocene.

Demographic History and Historical Biogeography Inference

Complicated evolutionary processes of continuous and episodic dispersal, vicariance, and extinctions determined the current geographic distribution of genus *Paphiopedilum*. Since the most probable ancestral areas located on continental Asia (area A in **Figure 5**), dispersal events seem to determine the extant distributions of subgenera largely. The results supported vicariance events on nodes 159, 146, and 109 shown in **Table 2** and **Figure 5**, and on nodes 163, and 132 (**Supplementary Table S3** and **Figure S3**). The node 147 revealed dispersal events among section *Coryopedilum/Pardalopetalum* of *Paphiopedilum* and other sections of *Paphiopedilum* causing by migration route from area A (China, Nepal, India, Bhutan, Burma, Thailand, Malaysia, Cambodia, Vietnam, and Laos) to B area (Sumatra, Borneo, and Java). Meanwhile, the nodes 145, 129, 114, and 102 also revealed dispersal events from north to south, according to Sundaland and Sunda Super Islands.

Furthermore, the use of six outgroups for dynamic historical inference showed similar patterns (**Supplementary Table S3** and

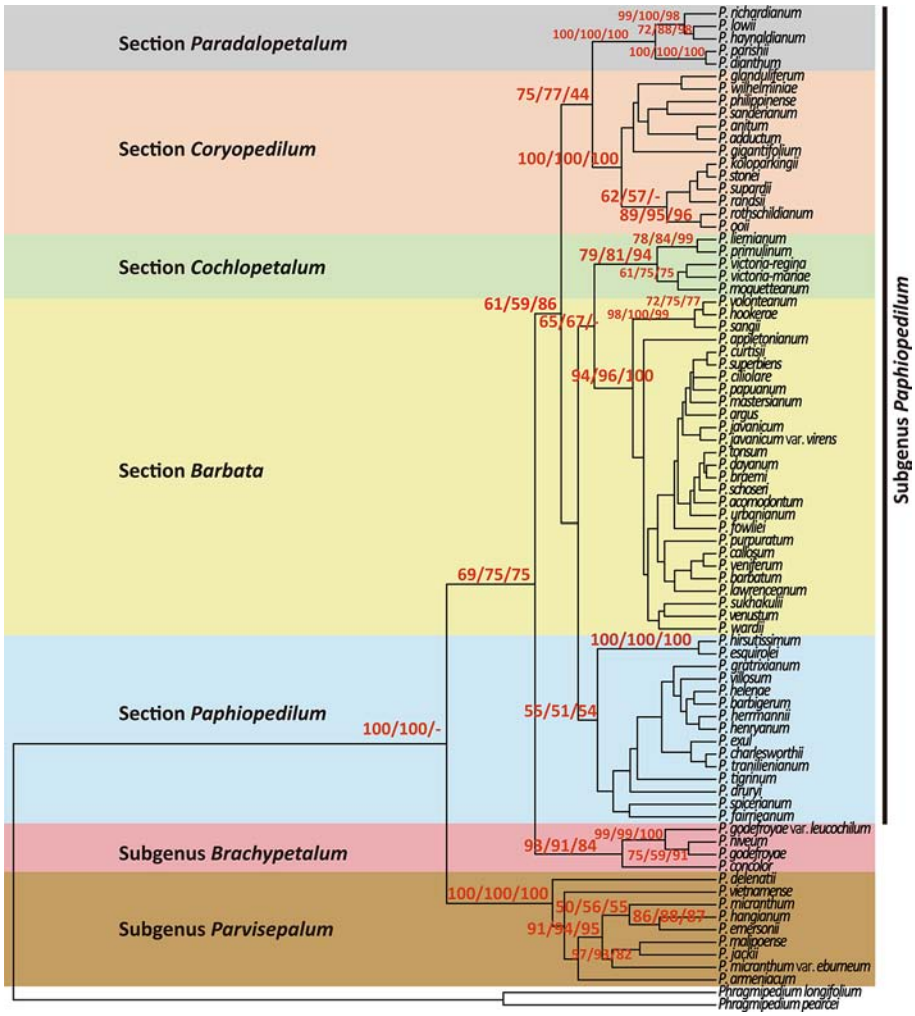

FIGURE 2 | Phylogenetic relationships using neighbor-joining (NJ), maximum parsimony (MP), and maximum likelihood (ML) resulting from analysis of the combined data matrix (nuclear ribosomal ITS, plastid *trn*L intron, *trn*L-F spacer, and *atp*B-*rbc*L spacer) from 78 *Paphiopedilum* and 2 outgroup species. Only the strict consensus of all most parsimonious trees (MP trees) are showed in this figure, and the bootstrap values > 50% are shown on each branch for NJ/MP/ML between major lineage.

Figure S3). Only the nodes 146 and 109 were detected vicariance event causing by the geological separation between Indochina and Sumatra/Borneo/Java. In addition, in subgenus *Paphiopedilum*, 2 vicariance and 10 dispersal events were detected, which suggesting a significant dispersal process affected biogeographical patterns in shaping the current distribution in the subgenus *Paphiopedilum*. Areas A and B might be the two possible ancestral areas and likely shaped by several complicated dispersal events in the subgenus *Paphiopedilum*.

DISCUSSION

Systematics Revision of Genus *Paphiopedilum*

In general, our phylogenetic inference is mostly congruent with that of Cox et al. (1997), Cribb (1997b), and Guo et al. (2015). In the genus *Paphiopedilum*, tessellated leaves, single flowers with broad elliptic to subcircular petals, and a sizeable thin-textured lip characterize subgenus *Parvisepalum* in southwest China and Vietnam (Cribb, 1998). Within this subgenus, the phylogenetic topography and the divergence time of at least 4.30 Mya rejected the previous hypothesis of the sister-species relationship between *P. armeniacum* and *P. delenatii* (Cribb, 1983) (**Figure 4**). The geographical distribution of these two species is also separated (Yunnan, China for *P. armeniacum*, and Vietnam for *P. delenatii*) (Cribb, 1998).

Furthermore, a newly described variety, *P. micranthum* var. *eburneum*, is phylogenetically close to *P. malipoense* in maternal-inherited plastid DNA but close to *P. micranthum* in biparental-inherited nuclear ITS sequences (**Figure 5**), suggesting that *P. micranthum* var. *eburneum* is a natural hybrid between the maternal parent *P. malipoense* and the paternal parent *P. micranthum* and experienced the event of chloroplast

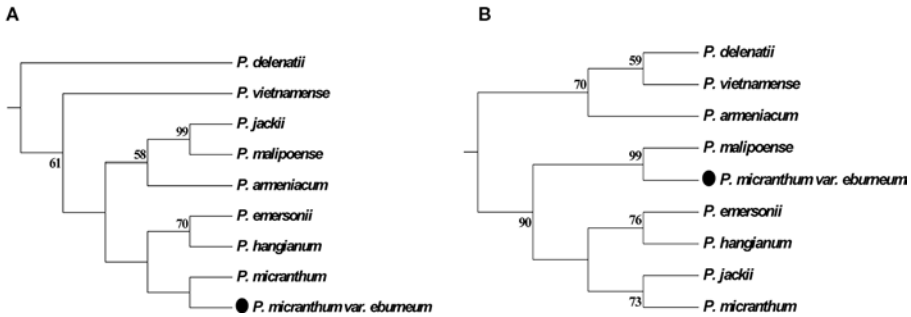

FIGURE 3 | Parsimonious phylogenetic tree of the *Paphiopedilum* subgenus *Parvisepalum* derived from ITS sequences of nuclear ribosomal DNA (nrDNA) **(A)** and plastid DNA **(B)**. The solid circle (.) represents a putative natural hybrid (based on molecular evidence).

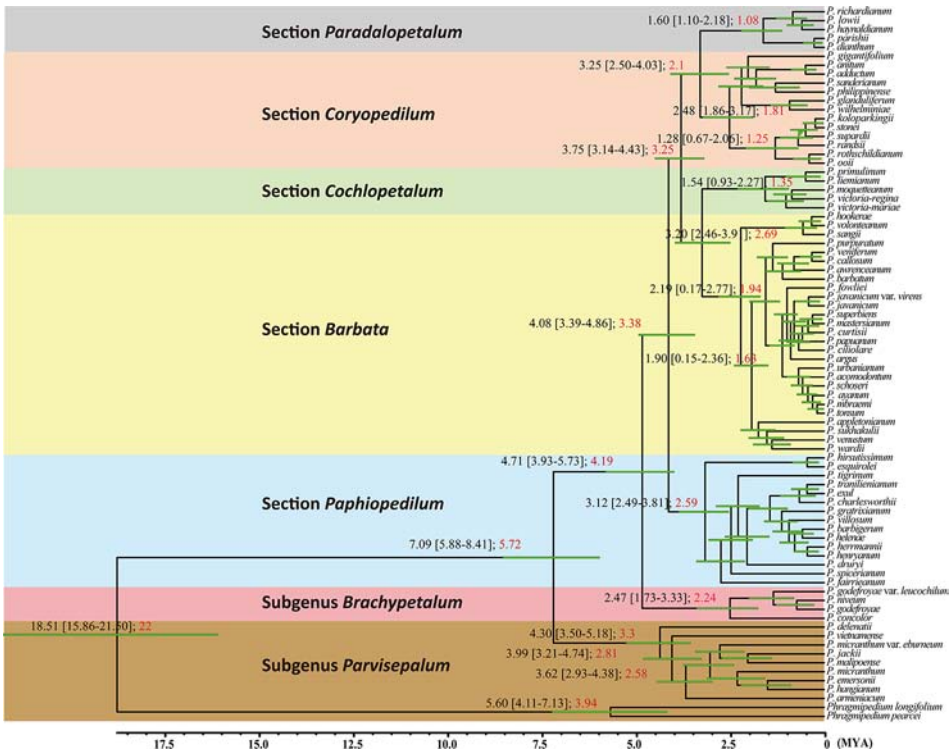

FIGURE 4 | Results of calescence time estimations performed with BEAST 1.8.0 for the from 78 *Paphiopedilum* taxa based on the combined data matrix (nuclear ribosomal ITS, plastid *trn*L intron, *trn*L-F spacer, and *atp*B-*rbc*L spacer). The black numbers in each node are using the mean rate of 1.82 × 10–9 subs/site/year, with the lower and upper limits 1.11 × 10–9 subs/site/year and 2.53 × 10–9 subs/site/year (Tsai et al., 2015). The red numbers in each node are using the Gustafsson et al. (2010) fossil calibration time data to calibrate the divergence time.

capture. The overlap of the geographical distribution of these three taxa also supports this hypothesis (Cribb, 1998). In addition, ITS sequences are usually concertedly evolved *via* unequal crossing-over (Schlotterer and Tautz, 1994) and biased gene conversion (Hillis et al., 1991), which results in sequence homogeneity between paralogs (Maynard, 1989).

The monophyly of subgenus *Brachypetalum* inferred in this study is congruent with the inference by Cox et al. (1997). The subgenus *Brachypetalum* is geographically confined to Southeast Asia (Cribb, 1998). Albeit overlapping distribution with subgenus *Parvisepalum* (Cribb, 1998), subgenus *Brachypetalum* is phylogenetically separated, consistent with the distinguishable leaf anatomy between these two subgenera (Cribb, 1998). Both molecular and morphological evidences support the independent taxonomic treatment between subgenera *Brachypetalum* and *Parvisepalum* (Karasawa, 1982; Karasawa and Saito, 1982; Cribb, 1997b), but object with Atwood's (1984) opinion of taking the subgenus *Parvisepalum* as a synonym of *Brachypetalum*.

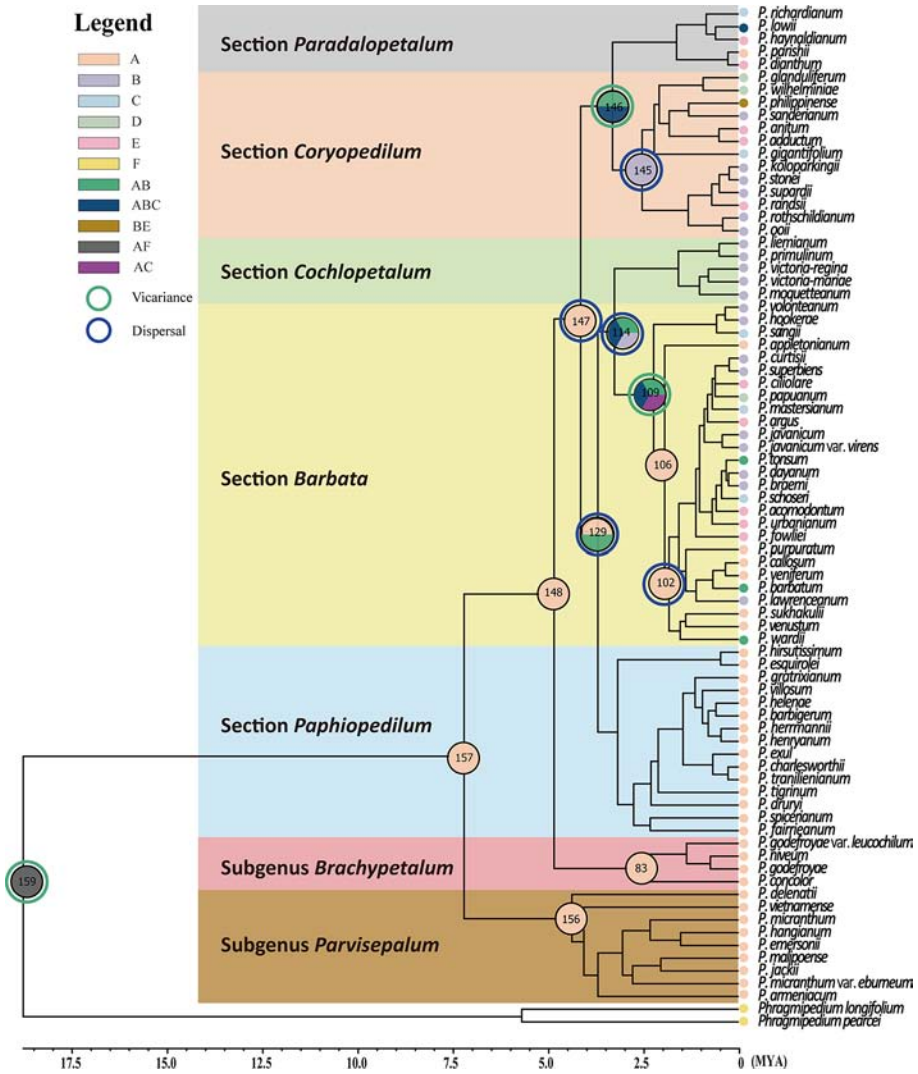

FIGURE 5 | Ancestral distributions reconstructed by the Statistical dispersal–vicariance analysis [S-DIVA, (Yu et al., 2010)] and Bayes–Lagrange Statistical dispersal–extinction–cladogenesis (S-DEC) model (Ree and Smith, 2008) performed in Reconstruct Ancestral State in Phylogenies (RASP) 3.2 (Yu et al., 2015). Phylogenetic relationships of the 78 *Paphiopedilum* species, plus the two outgroups *Phragmipedium pearcei* and *Ph. longifolium*, obtained from sequence judgments of the combined sequence and generated by BEAST. The distribution areas of extant the 78 *Paphiopedilum* species are marked in capitals A–E and I [(A) China, Nepal, India, Bhutan, Burma, Thailand, Malaysia, Cambodia, Vietnam, and Laos; (B) Sumatra, Borneo and Java; (C) Sulawesi and Moluccas; (D) New Guinea; (E) Philippines; and (I) outgroup], respectively. The green and blue circles indicate the vicariance and dispersal events obtained from the RASP analysis, respectively.

The monophyletic subgenus *Paphiopedilum* can be morphologically and phylogenetically subdivided into five sections: *Coryopedilum*, *Pardalopetalum*, *Cochlopetalum*, *Paphiopedilum*, and *Barbata* (Cox et al., 1997; Cribb, 1997b). Section *Coryopedilum* is characterized by its plain green, strap-like leaves, and multi-flowered inflorescences, which flowers are blooming simultaneously (Cribb, 1998). This section distributes throughout Borneo, Sulawesi, New Guinea, and the Philippines (Cribb, 1998). Except placing *Paphiopedilum parishii* and *Paphiopedilum dianthum* into section *Pardalopetalum* from section *Coryopedilum*, Cribb (1997b) agreed with Atwood (1984) that section *Pardalopetalum* is independent from section *Coryopedilum* taxonomically, according to the ITS analysis (Cox et al., 1997) and similar green strap-like leaves and staminodes (Cribb, 1997b), which is consistent with our phylogenetic inference. However, the only character that separates sections of *Pardalopetalum* and *Coryopedilum* is the morphology of staminode. Whether this single character is sufficient to characterize them as separating sections should be re-evaluated with more evidence.

Unlike the simultaneous bloom of section *Coryopedilum*, section *Cochlopetalum* flower in succession, and their flowers bear elliptic bracts, linear, spirally twisted, spreading, ciliate petals, and a pot-shaped spotted lip (Cribb, 1998). Section

Cochlopetalum distributes in Sumatra and Java only (Cribb, 1998). The extensive section *Barbata* is the sister of section *Cochlopetalum*, also characterized by a solitary flower with a lip and prominent incurved side-lobes, but the leaf tessellated (Cribb, 1998). The morphological dissimilarity and reciprocally monophyletic relationship indicate that, despite recently diverged, these two sections should be independent taxonomically.

Biogeography and Evolutionary Trends

The clade of genus *Paphiopedilum* is coalesced to 7.09 or 5.72 Mya, similar to the estimate of 7.62 Mya by Guo et al. (2015). The flower morphology of subgenus *Parvisepalum* is intermediate between other subgenera of *Paphiopedilum* and *Cypripedium* (Chen and Tsi, 1984), which could be explained by the earlier divergence of subgenus *Parvisepalum* in genus *Paphiopedilum* (Guo et al., 2012). Presently, the genus *Cypripedium* is distributed throughout worldwide temperate zones (Cox et al., 1997), with China as a center for species diversity (Cribb, 1997a). Therefore, genera *Paphiopedilum* and *Cypripedium* have most likely diverged in mainland Asia (Chen and Tsi, 1984).

However, genus *Paphiopedilum* was suggested as the sister with two American genera *Phragmipedium* and *Mexipedium* according to morphology, plastid *rbc*L (Albert, 1994), ITS (Cox et al., 1997), and both nuclear and plastid genes (Guo et al., 2012). These inferences are conflict to the hypothesis of the divergence between *Paphiopedilum* and *Cypripedium* in China, but implied the divergence of *Paphiopedilum* from the group of *Phragmipedium* + *Mexipedium*, by which the slipper orchids (Cypripedioideae) were hypothesized widespread throughout North America and Asia in the past (Atwood, 1984; Albert, 1994; Cox et al., 1997).

Subgenus *Parvisepalum* in southwest China and Vietnam diverged earlier from the other subgenera of genus *Paphiopedilum*. The coalescence time of subgenera *Parvisepalum*, *Brachypetalum,* and *Paphiopedilum* were tracking back to the Upper Miocene (Guo et al., 2015). Subgenus *Brachypetalum* in mainland Southeast Asia was descended from the subgenus *Parvisepalum* inferred by S-DIVA (**Figure 5**), which agrees with other disjunctions at the Southern China and Indochina (Guo et al., 2015) or Sunda Shelf and New Guinea/Australia (Tougard, 2001; Lohman et al., 2011; Tsai et al., 2015).

The subgenus *Paphiopedilum* is further descended and evolved quickly in the Sunda Shelf. A land bridge might connect Mindoro, Palawan, Borneo, the Malay Peninsula, Borneo, Sumatra, Java, Bali, and various parts of the Philippines when sea levels falling during Pleistocene (about 0.01~1.8 Mya) (van Oosterzee, 1997) (**Figure 1**). Surfaced land bridge connected these regions and was beneficial to the interisland and continent-island dispersal in Southeast and South Asia (van Oosterzee, 1997). The clade of *Coryopedilum* + *Pardalopetalum* was the first derived in subgenus *Paphiopedilum* based on the phylogenetic tree, which reflects in the sympatric distribution of subgenus *Brachypetalum* and section *Pardalopetalum* (**Figure 6**). Following this clade formation, sections *Paphiopedilum* and *Barbata* were subdivided and dispersed throughout Southeast Asian archipelagoes across the land bridge during the glacials. The southward expansion from continental Asia into the Greater Sunda Islands through the Indochina and Malay Peninsulas were also reported in other taxa, e.g., *Lithocarpus* (Fagaceae) (Yang et al., 2018). Such colonization events between continental Asia and the Greater Sunda Islands mostly occurred during Miocene and Plio-Pleistocene (de Bruyn

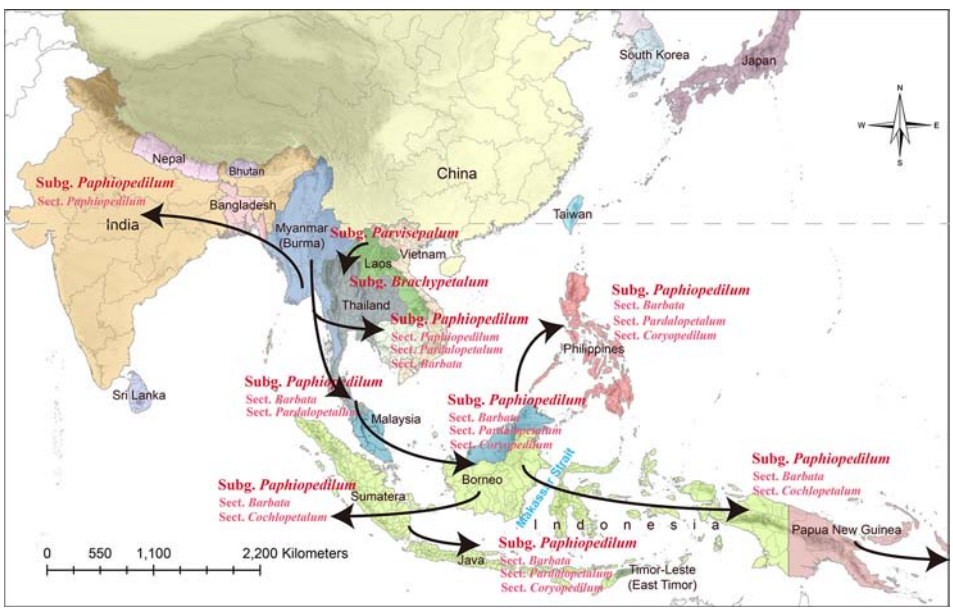

FIGURE 6 | The possible evolutionary routes of the genus *Paphiopedilum*.

TABLE 2 | The ancestral areas and dispersal–vicariance analysis inferred through Reconstruct Ancestral State in Phylogenies (RASP). Ancestral areas for the node and the number of dispersal (Dis), vicariance (Vic), and extinction (Ext) events are shown.

Node	Ancestral areas	RASP ROUTE	Dis	Vic	Ext	Prob
159	[AF]	AF- > A|F	0	1	0	1.00
157	[A]	A- > A^A- > A|A	0	0	0	1.00
156	[A]	A- > A^A- > A|A	0	0	0	1.00
148	[A]	A- > A^A- > A|A	0	0	0	1.00
147	[A]	A- > A^A^B- > ABC^A^B- > AB|ABC	3	0	0	0.99
146	[ABC|AB]	ABC- > AC|B	0	1	0	1.00
145	[B]	B- > B^B- > BDE^B- > BDE|B	2	0	0	0.91
129	[AB|A]	AB- > AB^A- > ABC^A- > A|ABC	2	0	0	0.74
114	[ABC|AB|B]	ABC- > ABC^B- > B|ABC	1	0	0	0.60
109	[ABC|AC|AB]	ABC- > BC|A	0	1	0	1.00
106	[A]	A- > A^A- > A|A	0	0	0	0.89
102	[A]	A- > A^A- > ABE^A- > A|ABE	2	0	0	0.99
83	[A]	A- > A^A- > A|A	0	0	0	1.00

et al., 2014). As a "corridor," Indochina reveals high flora diversity and the high species richness, which facilitates the *in situ* speciation (de Bruyn et al., 2014).

Another flora diversity hotspot is Borneo (de Bruyn et al., 2014), which is also important for the genus *Paphiopedilum*. The section *Cochlopetalum*, which is found only in Sumatra and Java, might represent a group derived from Borneo. The S-DIVA inferred multiple times dispersal events sourced from Borneo with two vicariances to illustrate the current distribution of the five sections within subgenus *Paphiopedilum* (**Figure 5** and **Table 2**). The Borneo is the second original center of *Paphiopedilum*. The tropical forests and rugged topography harbor diversified niches opened to the speciation of organisms. The repeated submergence and emergence of land bridges could promote repeated genetic isolation and gene flow between closed related taxa. During the Plio-Pleistocene glacial oscillations. This process accelerates the diversification rates in the Sunda Super Islands.

Dispersal and vicariance events that exposed geographic isolation among taxa might be due to the land bridge submergence (Chiang et al., 2009; Chiang et al., 2013; Ge et al., 2012; Ge et al., 2015; Hsu et al., 2013) in Sunda Shelf and Sunda Super Island during the Pleistocene (**Figure 5** and **Table 2**) (Guo et al., 2015; Tsai et al., 2015). Cenozoic collision accompanied by a cyclical climate (glacial oscillations) caused by the fragmentation of the Sunda Super Islands (de Bruyn et al., 2014). The Borneo, Java, Sumatra, and the southern Philippines belong to the Sunda plate, Sulawesi is composed of broken plates, and the Moluccas and New Guinea belong to the Australian plate (Hall, 1998). The deep trenches between these plates cause segregation of species between Sundaland and the islands in the east. Because of the seed germination relies on symbiotic fungi, the geographical isolation maybe not only influences orchid itself but also in symbiotic fungi. However, these inferences still need further verification.

CONCLUSIONS

In summary, the origin and coalescence time of genus *Paphiopedilum* tracked back to Southern China/Eastern Indochina since late Miocene and early Pliocene, while the range expansion and species divergence were related to sea-level fluctuations during the Plio-Pleistocene glacial cycles. Historical geological barriers shaped a pattern of vicariance among disjunct distributed subgenera after isolated ancestral populations. The ancestral taxa of subgenus *Paphiopedilum* migrated from Southern China/Eastern Indochina to south which developed quickly in the Sunda Shelf. Due to the submergence of the Sunda Shelf and Sunda Super Island, species of subgenus *Paphiopedilum* dispersed with isolation between islands as well as subsequent *in situ* speciation within islands from other taxa within section or subgenus, which accelerated species divergence in subgenus *Paphiopedilum*. *Paphiopedilum* distributes in four of 25 biodiversity hotspots (Myers et al., 2000), the Indo-Burma, Sundaland, Wallacea, and Philippines, where are also the "major evolutionary hotspots" (de Bruyn et al., 2014). It is suggests that rich and fascinating historical biogeographic events have created rich species diversity there, such as the case of *Paphiopedilum*. However, deforestation has caused the so-called "empty forest syndrome" (de Bruyn et al., 2014). We hope that these areas will not become extinction hotspots, even though they are almost now.

DATA AVAILABILITY STATEMENT

The datasets generated for this study are available on request to the corresponding author.

AUTHOR CONTRIBUTIONS

Conceived and designed the experiments: C-CT and Y-CC. Performed the experiments: C-CT, P-CL, Y-ZK, C-HC, and Y-CC. Analyzed the data: C-CT, P-CL, Y-ZK, C-HC, and Y-CC. Contributed reagents/materials/analysis tools: C-CT, P-CL, Y-ZK, C-HC, and Y-CC. Wrote the paper: C-CT, P-CL, and Y-CC. Conceived of the study, edited the manuscript, and approved the final manuscript: C-CT, P-CL, Y-ZK, C-HC, and Y-CC.

FUNDING

This research was supported by funding from the Ministry of Science and Technology, Taiwan (MOST 105-2621-B-110-003-MY3 and MOST 105-2621-B-110-001) to Y-CC and by partial financing (the Higher Education Sprout Project) of NSYSU.

ACKNOWLEDGMENTS

The achievement of this study is dedicated to the memory of the scientific contributions of the first author C-CT, who died of a

stroke on November 05, 2015. We are grateful to Dr. F. H. Lin for his valuable comments and helpful discussion in the course of the study.

SUPPLEMENTARY MATERIAL

The Supplementary Material for this article can be found online at: https://www.frontiersin.org/articles/10.3389/fpls.2020.00126/full#supplementary-material

SUPPLEMENTARY FIGURE S1 | Phylogenetic relationships using Maximum Likelihood resulting from analysis of the combined data matrix (nuclear ribosomal ITS, and trnL-F spacer) from 78 Paphiopedilum and 6 outgroup species.

SUPPLEMENTARY FIGURE S2 | Results of calescence time estimations performed with BEAST 1.8.0 for the from 78 Paphiopedilum taxa and 6 outgroup species based on the combined data matrix (nuclear ribosomal ITS, and trnL-F spacer).

SUPPLEMENTARY FIGURE S3 | Ancestral distributions reconstructed by the Statistical dispersal–vicariance analysis (S-DIVA, Yu et al., 2010) and Bayes–Lagrange Statistical dispersal–extinction–cladogenesis (S-DEC) model (Ree and Smith, 2008) performed in RASP 3.2 (Yu et al., 2015). Phylogenetic relationships of the 78 Paphiopedilum species, plus the six outgroups, obtained from sequence judgments of the combined sequence and generated by BEAST. The distribution areas of extant the 78 Paphiopedilum species species are marked in capitals A–E and I ((A) China, Nepal, India, Bhutan, Burma, Thailand, Malaysia, Cambodia, Vietnam, and Laos; (B) Sumatra, Borneo and Java; (C) Sulawesi and Moluccas; (D) New Guinea; (E) Philippines; and (I) outgroup), respectively. The green and blue circles indicate the vicariance and dispersal events obtained from the RASP analysis, respectively.

REFERENCES

Albert, V. A., and Chase, M. A. (1992). Mexipedium: a new genus of slipper orchid (Cypripedioideae: Orchidaceae). *Lindleyana* 7, 172–176.

Albert, V. A. (1994). Cladistic relationships of the slipper orchids (Cypripedioideae: Orchidaceae) from congruent morphological and molecular data. *Lindleyana* 9, 115–132.

Atwood, J. T. (1984). The relationships of the slipper orchids (subfamily Cypripediodeae), Orchidaceae. *Selbyana* 7, 129–247.

Aurelio, M. A., Barrier, E., Rangin, C., and Muller, C. (1991). The philippine fault in the late cenozoic tectonic evolution of the bondoc-masbate-N. leyte area, central philippines. *J. Southeast Asian Earth Sci.* 6, 221–238. doi: 10.1016/0743-9547(91)90069-A

Baldwin, B. G., Sanderson, M. J., Wojciechowski, M. F., Campbell, C. S., and Donoghue, M. J. (1995). The ITS region of nuclear ribosomal DNA-a valuable source of evidence on angiosperm phylogeny. *Ann. Missouri Bot. Garden* 82, 247–277. doi: 10.2307/2399880

Baldwin, B. G. (1992). Phylogenetic utility of the internal transcribed sequences of nuclear ribosomal DNA in plants: an example from the Compositae. *Mol. Phylogenet. Evol.* 1, 3–16. doi: 10.1016/1055-7903(92)90030-K

Chen, S. C., and Tsi, Z. H. (1984). On Paphiopedilum malipoense sp. nov.-an intermediate from between and Cypripedium. *Acta Phytotaxonomica Sin.* 22, 119–124.

Chiang, T. Y., Schaal, B. A., and Peng, C. I. (1998). Universal primers for amplification and sequencing a noncoding spacer between the *atp*B and *rbc*L genes of chloroplast DNA. *Bot. Bull. Academia Sin.* 39, 245–250.

Chiang, Y. C., Hung, K. H., Moore, S. J., Ge, X. J., Huang, S., Hsu, T. W., et al. (2009). Paraphyly of organelle DNAs in *Cycas* Sect. Asiorientales due to ancient ancestral polymorphisms. *BMC Evol. Biol.* 9, 161. doi: 10.1186/1471-2148-9-161

Chiang, Y. C., Huang, B. H., Chang, C. W., Wan, Y. T., Lai, S. J., Huang, S., et al. (2013). Asymmetric introgression in the horticultural living fossil *Cycas* Sect, Asiorientales using a genome-wide scanning approach. *Int. J. Mol. Sci.* 14, 8228–8251. doi: 10.3390/ijms14048228

Cox, A. V., Pridgeon, A. M., Albert, V. A., and Chase, M. W. (1997). Phylogenetics of the slipper orchids (Cypripediodeae: Orchidaceae); Nuclear rDNA sequences. *Plant Syst. Evol.* 208, 197–223. doi: 10.1007/BF00985442

Cribb, P. (1983). A synopsis of the genus *Paphiopedilum*. *Plantsman* 4, 193–212.

Cribb, P. (1997a). *The Genus Cypripedium* (Portland, Oregon: Timber Press).

Cribb, P. (1997b). *The Genus Paphiopedilum* (Portland, Oregon: Timber Press).

Cribb, P. (1998). *The Genus Paphiopedilum*. *2nd ed.* (Kota Kinabalu, Sabah, Malaysia: Natural History Publications (Borneo) in association with Royal Botanic Gardens, Kew), 427.

de Bruyn, M., Stelbrink, B., Morley, R. J., Hall, R., Carvalho, G. R., Cannon, C. H., et al. (2014). Borneo and Indochina are major evolutionary hotspots for Southeast Asian biodiversity. *Syst. Biol.* 63, 879–901. doi: 10.1093/sysbio/syu047

Doyle, J. J., and Doyle, J. L. (1987). A rapid DNA isolation procedure for small quantities of fresh leaf tissue. *Phytochem. Bull.* 19, 11–15.

Drummond, A. J., and Rambaut, A. (2007). BEAST: Bayesian evolutionary analysis by sampling trees. *BMC Evol. Biol.* 7, 214–221. doi: 10.1186/1471-2148-7-214

Drummond, A. J., Suchard, M. A., Xie, D., and Rambaut, A. (2012). Bayesian phylogenetics with BEAUti and the BEAST 1.7. *BMC Evol. Biol.* 29, 1969–1973. doi: 10.1093/molbev/mss075

Felsenstein, J. (1985). Confidence limits on phylogenies: an approach using the bootstrap. *Evolution* 39, 783–791. doi: 10.1111/j.1558-5646.1985.tb00420.x

Felsenstein, J. (2004). *PHYLIP (Phylogeny Inference Package) Version 3.6* (Seattle: Department of Genome Sciences, University of Washington).

Ge, X. J., Hsu, T. W., Hung, K. H., Lin, C. J., Huang, C. C., Huang, C. C., et al. (2012). Inferring multiple refugia and phylogeographical patterns in *Pinus massoniana* based on nucleotide sequence variation and fingerprinting. *PLoS One* 7, e43717. doi: 10.1371/journal.pone.0043717

Ge, X. J., Hung, K. H., Ko, Y. Z., Hsu, T. W., Gong, X., Chiang, T. Y., et al. (2015). Genetic divergence and biogeographical patterns in *Amentotaxus argotaenia* species complex. *Plant Mol. Biol. Rep.* 33 (2), 264–280. doi: 10.1007/s11105-014-0742-0

Goldblatt, P., Savolainen, V., Porteous, O., Sostaric, I., Powell, M., Reeves, G., et al. (2002). Radiation in the Cape flora and the phylogeny of Racock irises *Moraea* (Iridaceae) based on four plastid DNA regions. *Mol. Phylogenet. Evol.* 25, 341–360. doi: 10.1016/S1055-7903(02)00235-X

Guo, Y. Y., Luo, Y. B., Liu, Z. J., and Wang, X. Q. (2012). Evolution and biogeography of the slipper orchids: eocene vicariance of the conduplicate genera in the old and new world tropics. *PLoS One* 7 (6), e38788. doi: 10.1371/journal.pone.0038788

Guo, Y. Y., Luo, Y. B., Liu, Z. J., and Wang, X. Q. (2015). Reticulate evolution and sea-level fluctuations together drove species diversification of slipper orchids (*Paphiopedilum*) in South-East Asia. *Mol. Ecol.* 24, 2838–2855. doi: 10.1111/mec.13189

Gustafsson, A. L. S., Verola, C. F., and Antonelli, A. (2010). Reassessing the temporal evolution of orchids with new fossils and a Bayesian relaxed clock, with implications for the diversification of the rare South American genus *Hoffmannseggella* (Orchidaceae: Epidendroideae). *BMC Evol. Biol.* 10, 177. doi: 10.1186/1471-2148-10-177

Hall, R. (1996). "Reconstructing Cenozoic SE Asia," in *Tectonic Evolution of SE Asia*. Eds. R. Hall and D. J. Blundell (London, UK: Geological Society of London Special Publication No. 106), 153–184.

Hall, R. (1998). "The plate tectonics of Cenozoic SE Asia and the distribution of land and sea," in *Biogeography and Geological Evolution of SE Asia*. Eds. R. Hall and J. D. Holloway (Leiden, The Netherlands: Backhuys Publishers), 99–131.

Hall, T. A. (1999). BioEdit: a user-friendly biological sequence alignment editor and analysis program for windows 95/98/NT. *Nucleic Acids Symp. Ser.* 41, 95–98.

Hillis, D. M., and Bull, J. J. (1993). An empirical test of bootstrapping as a method for assessing confidence in phylogenetic analysis. *Syst. Biol.* 42, 182–192. doi: 10.1093/sysbio/42.2.182

Hillis, D. M., Moritz, C., Porter, C. A., and Baker, R. J. (1991). Evidence for biased gene conversion in concerted evolution of ribosomal DNA. *Science* 251, 308–310. doi: 10.1126/science.1987647

Hodkinson, T. R., Chase, M. W., Lledo, M. D., Salamin, N., and Renvoize, S. A. (2002). Phylogenetics of *Miscanthus*, *Saccharum* and related genera (*Saccharinate*, *Andropogoneae*, Poaceae) based on the DNA sequences from ITS nuclear ribosomal DNA and plastid *trn*L intron and *trn*L-F intergenic spacer. *J. Plant Res.* 115, 381–392. doi: 10.1007/s10265-002-0049-3

Hsu, T. W., Shih, H. C., Kuo, C. C., Chiang, T. Y., and Chiang, Y. C. (2013). Characterization of 42 microsatellite markers from poison ivy, *Toxicodendron radicans* (Anacardiaceae). *Int. J. Mol. Sci.* 214, 20414–20426. doi: 10.3390/ijms141020414

Karasawa, K., and Saito, K. (1982). A revision of the genus *Paphiopedilum* (Orchidaceae). *Bull. Hiroshima Bot. Garden* 5, 1–69.

Karasawa, K. (1982). *The Genus Paphiopedilum* (Karasawa, Hiroshima, Japan: Seibundo Shinkosha Publisher).

Karig, D. E., Sarewitz, D. R., and Iiaeck, G. D. (1986). Role of strike-slip faulting in the evolution of allochthonous terraces in the Philippines. *Geology* 14, 852–855. doi: 10.1130/0091-7613(1986)14<852:ROSFIT>2.0.CO;2

Koopowitz, H. (2000). A revised checklist of the genus *Paphiopedilum*. *Orchid Digest* 64, 155–179.

Lindley, J. (1840). *The genera and species of orchidaceous plants* (Pp554. Ridgways, Piccadilly, London: printed by W. Nicoi., 60, Pali Mall).

Lohman, D. J., de Bruyn, M., Page, T., von Rintelen, K., Hall, R., Ng, P. K. L., et al. (2011). Biogeography of the Indo-Australian Archipelago. *Annu. Rev. Ecol. Evol. Syst.* 42, 205–226. doi: 10.1146/annurev-ecolsys-102710-145001

Maynard, S. (1989). *Evolutionary Genetics* (Oxford, UK: Oxford University Press), 325.

Mogensen, H. L. (1996). The hows and whys of cytoplasmic inheritance in seed plants. *Am. J. Bot.* 83, 383–404. doi: 10.1002/j.1537-2197.1996.tb12718.x

Myers, N., Mittermeier, R. A., Mittermeier, C. G., da Fonseca, G. A. B., and Kent, J. (2000). Biodiversity hotspots for conservation priorities. *Nature* 403, 853–858. doi: 10.1038/35002501

Quebral, R. D., Pubellier, M., and Rangin, C. (1994). The Mindanao: a transition from collision to strike-slip environment. *Tectonics* 15, 713–726. doi: 10.1029/95TC00480

Rambaut, A., Drummond, A. J., Xie, D., Baele, G., and Suchard, M. A. (2018). Posterior summarisation in Bayesian phylogenetics using Tracer 1.7. *Syst. Biol.* 67, 901–904. doi: 10.1093/sysbio/syy032

Rambaut, A. (2009). *FigTree version 1.3.1* (University of Edinburgh: Institute of Evolutionary Biology). [http://tree.bio.ed.ac.uk/software/FigTree/].

Ree, R. H., and Smith, S. A. (2008). Maximum likelihood inference of geographic range evolution by dispersal, local extinction, and cladogenesis. *Syst. Biol.* 57, 4–14. doi: 10.1080/10635150701883881

Schlotterer, C., and Tautz, D. (1994). Chromosomal homogeneity and *Drosophila* ribosomal DNA arrays suggests intrachromosomal exchanges drive concerted evolution. *Curr. Biol.* 4, 777–783. doi: 10.1016/S0960-9822(00)00175-5

Stephan, J. F., Blanchet, R., Rangin, C., Pelletir, B., Letouzey, J., and Muller, C. (1986). Geodynamic evolution of the Taiwan-Luzon-Mindoro belt since the Late Eocene. *Tectonophysics* 125, 245–268. doi: 10.1016/0040-1951(86)90017-X

Taberlet, P., Gielly, L., Pautou, G., and Bouvet, J. (1991). Universal primers for amplification of three non-coding regions of chloroplast DNA. *Plant Mol. Biol.* 17, 1105– 1109. doi: 10.1007/BF00037152

Tamura, K., Stecher, G., Peterson, D., Filipski, A., and Kumar, S. (2013). MEGA6: Molecular evolutionary genetics analysis Version 6.0. *Mol. Biol. Evol.* 30, 2725–2729. doi: 10.1093/molbev/mst197

Tougard, C. (2001). Biogeography and migration routes of large mammal faunas in south-east asia during the late middle pleistocene: focus on the fossil and extant faunas from thailand. *Palaeogeogr Palaeoclimatol. Palaeoecol.* 168, 337–358. doi: 10.1016/S0031-0182(00)00243-1

Tsai, C. C., Chiang, Y. C., Lin, Y. S., Liu, W. L., and Chou, C. H. (2012). Plastid *trn*L intron polymorphisms among *Phalaenopsis* species used for identifying the plastid genome type of *Phalaenopsis* hybrids. *Sci. Hortic.* 142, 84–91. doi: 10.1016/j.scienta.2012.05.004

Tsai, C. C., Chou, C. H., Wang, H. V., Ko, Y. Z., Chiang, T. Y., and Chiang, Y. C. (2015). Biogeography of the P*halaenopsis amabilis* species complex inferred from nuclear and plastid DNAs. *BMC Plant Biol.* 15, 202. doi: 10.1186/s12870-015-0560-z

van Oosterzee, P. (1997). *Where Worlds Collide: The Wallace Line* (Ithaca, NY: Cornell Univ. Press).

Van Raamsdonk, L. M., Ensink, W., Van Heusden, A. W., Vrielink-Van Ginkel, M., and Kik, C. (2003). Biodiversity assessment based on cpDNA and crossability analysis in selected species of *Allium* subgenus *Rhizirideum*. *Theor. Appl. Genet.* 107, 1048–1058. doi: 10.1007/s00122-003-1335-8

Von Konrat, M., Shaw, A. J., and Renzaglia, K. S. (2010). Bryophytes: The closest living relatives of early land plants. *Phytotaxa* 9, 1–278. doi: 10.11646/phytotaxa.9.1.1

Yang, C. K., Chiang, Y. C., Huang, B. H., Ju, L. P., and Liao, P. C. (2018). Nuclear and chloroplast DNA phylogeography suggests an early miocene southward expansion of *Lithocarpus* (Fagaceae) on the Asian continent and islands. *Bot. Stud.* 59, 27. doi: 10.1186/s40529-018-0244-8

Yoshinaga, K., Kubota, Y., Ishii, T., and Wada, K. (1992). Nucleotide sequence of *atp*B, *rbc*L, *trn*R, *ded*B and *psa*L chloroplast genes from a fern *Angiopteris lygodiifolia*: a possible emergence of Spermatophyta lineage before the separation of Bryophyta and Pteridophyta. *Plant Mol. Biol.* 18, 79–82. doi: 10.1007/BF00018458

Yu, Y., Harris, A. J., and He, X. J. (2010). S-DIVA (statistical dispersal–vicariance analysis): a tool for inferring biogeographic histories. *Mol. Phylogenet. Evol.* 56, 848–850. doi: 10.1016/j.ympev.2010.04.011

Yu, Y., Harris, A. J., and He, X. J. (2014). *A rough guide to RASP 2.1 (Beta)* (Brazil: University of Sao Paulo).

Yu, Y., Harris, A. J., Blair, C., and He, X. (2015). RASP (Reconstruct Ancestral State in Phylogenies): a tool for historical biogeography. *Mol. Phylogenet. Evol.* 87, 46–49. doi: 10.1016/j.ympev.2015.03.008

Conflict of Interest: The authors declare that the research was conducted in the absence of any commercial or financial relationships that could be construed as a potential conflict of interest.

Advantages of publishing in Frontiers

OPEN ACCESS
Articles are free to read for greatest visibility and readership

FAST PUBLICATION
Around 90 days from submission to decision

HIGH QUALITY PEER-REVIEW
Rigorous, collaborative, and constructive peer-review

TRANSPARENT PEER-REVIEW
Editors and reviewers acknowledged by name on published articles

Frontiers
Avenue du Tribunal-Fédéral 34
1005 Lausanne | Switzerland

Visit us: www.frontiersin.org
Contact us: info@frontiersin.org | +41 21 510 17 00

REPRODUCIBILITY OF RESEARCH
Support open data and methods to enhance research reproducibility

DIGITAL PUBLISHING
Articles designed for optimal readership across devices

FOLLOW US
@frontiersin

IMPACT METRICS
Advanced article metrics track visibility across digital media

EXTENSIVE PROMOTION
Marketing and promotion of impactful research

LOOP RESEARCH NETWORK
Our network increases your article's readership